Factorization and Resummation at Subleading Powers

Sebastian E. Jaskiewicz

Dissertation

Physik–Department T31
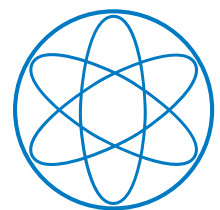Technische Universität München

Factorization and Resummation at Subleading Powers

Sebastian Eryk Jaskiewicz

Factorization and Resummation at Subleading Powers

Faktorisierung und Resummation zu höherer Potenz

Sebastian E. Jaskiewicz

Abstract

In this work, we investigate subleading power effects in Drell-Yan and Higgs production processes. We discuss the emergence of collinear functions, a critical new ingredient to factorization at next-to-leading power. We derive the factorization theorem valid near the kinematic threshold of the partonic processes in the diagonal and off-diagonal channels. We calculate the collinear functions and the soft functions at one and two loops, respectively. Using renormalization group methods, we perform leading logarithmic resummation for the diagonal channels.

Zusammenfassung

In dieser Arbeit untersuchen wir Effekte höherer Potenz zu Drell-Yan und Higgsproduktionsprozessen. Wir diskutieren das Auftreten von kollinearen Funktionen, ein entscheidender neuer Baustein bei der Faktorisierung zu NLP. Wir leiten ein Faktorisierungstheorem gültig in der Nähe des kinematischen Schwellenwerts für partonische Prozesse in mehreren Kanälen her. Desweiteren berechnen wir die kollinearen und soften Funktionen zur Ein-, respektive Zwei-Schleifenordnung. Unter Anwendung von Renormierungsgruppenmethoden resummieren wir die führenden Logarithmen in den diagonalen Kanälen.

Contents

Part I

1

Introduction

Particle physics is tasked with the noble goal of understanding the fundamental constituents of Nature and their interactions. Considering the current status of this field of research, it is difficult to imagine a time filled with more anticipation. On the one side stands a tremendously successful field-theoretic description known as the Standard Model (SM) of particle physics [1, 2, 3, 4], completed in 2012 with the discovery of the Higgs Boson by the ATLAS and CMS groups based at the Large Hadron Collider (LHC) accelerator complex at CERN [5, 6]. On the other side lies a heap of observational data which hints at the existence of physics beyond the SM, such as the gravitationally detected presence of dark matter (DM), no sign of which has as of yet been measured at collider experiments. The field remains delicately poised in this way and eagerly awaits the completion of the High Luminosity upgrade of the LHC (HL-LHC). Over its lifetime, the HL-LHC will deliver a ten-fold increase in the total integrated luminosity achieved thus far [7], making the experimental measurements of fundamental interactions ever more precise. The technological advancement in experimental observations challenges the status of theoretical predictions and makes it critically important to understand better the components which form the SM. It is crucial to increase the precision of theoretical predictions in order to be able to draw meaningful conclusions in comparison of the results of the calculations within the SM to experimental data. Only this interplay between precise experimental measurements and theoretical calculations can enable us to discover signs of New Physics beyond the SM at the particle level in colliders.

The SM is made up of the electroweak (EW) and strong sectors, with Quantum Chromodynamics (QCD) describing the strong interactions. Since the LHC collides protons made up of quarks and gluons at very high energies ($\sim$13TeV), a large part of the effort to increase the precision of theoretical predictions is devoted to improving the understanding of QCD processes which inevitably feature in the experiments. Due to the phenomenon of Asymptotic Freedom [8, 9], the strong coupling α_s becomes weak for processes involving large momentum transfers. Concretely, α_s becomes perturbative already at a few GeV [10]. Therefore, theoretical calculations can be organised in a perturbative series and systematically improved by computations of higher and higher order corrections in the α_s expansion.

Naturally, the calculation of the higher order corrections becomes increasingly more complex. However, with the value of the strong coupling at $\alpha_s \sim 0.1$, the first order correction, so-called next-to-leading order (NLO), is around 10% of the leading order

value. The next-to-next-to-leading order (NNLO) $\sim 1\%$, and so on. Therefore, the key point is that precise predictions can be obtained through calculation of the first few orders in perturbation theory, as these already describe the physical processes well. It is therefore not surprising that the calculation of high fixed-order predictions has evolved into a whole rich research field of its own. We do not provide here a reference guide to the many research works that can be found in literature. For us it suffices to note that the current state-of-the-art predictions for inclusive cross-sections are available at the next-to-next-to-next-to leading order (N^3LO) for certain phenomenologically relevant process such as Higgs boson production via gluon-gluon fusion [11, 12] and via vector boson fusion [13], and Drell-Yan production [14, 15]. These processes require as input amplitudes exhibiting a $2 \to 1$ topology at leading order. Recently, for the first time, four-point amplitudes at N^3LO have been reported [16]. Many observables relevant for LHC phenomenology are known at NNLO, see [17] and [18] for recent reviews.

Despite the clear success of the fixed-order calculations approach, there exist noteworthy drawbacks. It is a well-known fact that fixed-order perturbation theory is unreliable in application to processes which involve widely separated scales. Examples of such processes include production of particles near kinematic threshold or with small (or large) transverse momentum. In such regions of phase space, close to singular limits of the theory, the higher-order corrections are supplemented by large logarithms of the scale ratios. We denote a sample scale ratio by ζ. These large logarithms multiply the small coupling constant which is a priori the expansion parameter of the theory. This leads to a dangerous situation that threatens the convergence of the perturbatvie series on which the predictive power of the theoretical calculations is based. Namely, the coupling constant α_s is no longer a reliable expansion parameter. Rather, we should consider $\alpha_s \ln(\zeta) \sim \mathcal{O}(1)$ or $\alpha_s \ln^2(\zeta) \sim \mathcal{O}(1)$, depending on the process, as such a combination appears at every order in the calculation. In a setting of this type, it is apparent that each next order in the perturbative expansion is numerically as important as the previous one. Hence, to make a reliable theoretical prediction we must capture the all-order behaviour of these terms.

The solution to this issue is to divide the problem into pieces which each depend only on one physical scale. This is known as derivation of a *factorisation* theorem. The all-order expressions can then be obtained using scale evolution by solving the renormalization group equations (RGEs) for each of the pieces appearing in the factorisation formula. This step is known as *resummation*. Pioneering results on factorisation were derived using traditional diagrammatic techniques [19]. In order to better understand the landscape of applicability of the various all-order results, we consider as an example the schematic expansion of the cross-section for the Drell-Yan (DY) process $A + B \to \gamma^*(Q) + X$ near the threshold regime $z = Q^2/\hat{s} \to 1$, where $\hat{s}$ is the centre-of-mass energy squared. The cross-section has the following form

$$\hat{\sigma}_{ab}(z) = \sum_{n=0}^{\infty} \alpha_s^n \left[c_n \delta(1-z) + \sum_{m=0}^{2n-1} \left(c_{nm} \left[\frac{\ln^m(1-z)}{1-z} \right]_+ + d_{nm} \ln^m(1-z) \right) + \dots \right]. \quad (1.1)$$

We see that the most singular terms in the $z = 1$ limit are ones with the coefficients c_n, c_{nm}. These contributions are known as the *leading power* (LP) singular terms. For the purposes of resummation, instead of counting orders in α_s as is done in fixed-order calculations where we discuss LO, NLO, NNLO and so on, we count which towers of

logarithms are included in the all order result. For instance, the terms c_0 and $c_{n(2n-1)}$ constitute the *leading logarithms* (LL). Terms suppressed by one power in the logarithmic counting, $c_{n(2n-2)}$, are known as the *next-to-leading logarithms* (NLL), and so on. The first all-order summation of the LP logarithms has been obtained in [20, 21]. Equivalent results have later been derived using soft-collinear effective field theory (SCET) methods [22, 23, 24], and the current state-of-art is the resummation of LP threshold logarithms up to next-to-next-to-next-to-leading logarithmic (N^3LL) accuracy [24, 25]. SCET is an *effective field theory* of QCD in which the work presented here is grounded. We give an introduction to this formalism in chapter 2.

Similarly, to DY, the deep-inelastic scattering (DIS) process has been resummed at LP first using traditional diagrammatic techniques [26], and later in SCET [27], up to N^3LL accuracy. Indeed, large logarithms appearing in many other relevant observables have been resummed at leading power to date [28, 29, 30].

We now focus on the terms with the d_{nm} coefficients in equation (1.1) which are suppressed by one power of $(1 - z)$ with respect to the leading power terms that we have discussed above. These terms are referred to as the *next-to-leading power* (NLP) contributions. The leading logarithmic series at NLP is given by the logarithms with $d_{n(2n-1)}$ coefficients, where $n = 1, 2, \ldots$ to all orders.

The next-to-leading power logarithms are less singular than their leading power counterparts, and historically have received far less attention in the literature. Consequently, the structure of factorisation and resummation at NLP is not as well understood. It is precisely the investigation of these terms within the soft-collinear effective field theory that we are concerned with in this work.

We chose to investigate the NLP effects in the Drell-Yan process as it is one of the simplest hadron-hadron collision processes. Several fixed-order calculations have also explored the subleading power effects in this setting. For example, explicit computations of partonic cross-sections at NLP up to NNLO, and partly beyond, were performed by employing the expansion-by-regions method in [31, 32] and diagrammatic factorisation techniques in [33, 34, 35, 36, 37, 38, 39].

The leading logarithmic resummation of the Drell-Yan and Higgs production processes was first achieved in [40, 41]. We describe the SCET methods used in [40, 41] in this work. A confirmation of the result in the diagrammatic framework was obtained later in [42, 43]. In addition to the threshold region, the analysis of subleading power corrections for Drell-Yan and single Higgs production has been investigated at fixed-order for resolution variables such as N-jettiness [44, 45, 46, 47, 48, 49] and the q_T of the lepton pair or the Higgs boson [50, 51]. The q_T resummation of fiducial power corrections has been achieved in [52]. NLP threshold effects were also recently studied for processes such as prompt photon production [53]. The resummation of NLP leading logarithms for an event shape has been reported in [54, 55]. Factorisation theorem for Higgs production or decay through light-quark loops has been given in [56, 57]. Corresponding resummation was performed at LL in [58, 59, 60] and in [61, 62] up to NLL. Power-enhanced QED corrections to $B_q \to \mu^+\mu^-$ were summed in [63, 64].

The resummation of NLP leading logarithms [40, 41] is dependent on the general factorisation formula derived in [65]. We discuss the derivation of the factorisation formula with additional details in this work. The all order factorisation formula is also a necessary

for taking the non-trivial step beyond the NLP leading logarithmic resummation, which we discuss here.

The factorisation formula, which achieves the separation of scales through operator definitions of the relevant functions, and its check against the known NNLO NLP results from the expansion-by-regions approach, are one of the key results presented in this work. We consider the diagonal channel as in [65], and additionally present results for the off-diagonal gluon-antiquark channel.

The factorisation theorem must be regarded as a formal result, because it applies to bare regularized quantities. As will be explored in detail, when one attempts to renormalize these quantities by subtracting the divergent parts, the convolution of the various factors becomes itself divergent. This complicates the resummation of NLP logarithms beyond the LL accuracy with renormalization group methods in the standard paradigm of SCET. An attempt at understanding divergent convolutions in the effective field theory framework has been reported in [66].

Another important result discussed in this work, which has been extensively explored in [65] and used in [40, 41], is the identification of *NLP collinear functions* or radiative jet functions at the amplitude level in the factorisation formula at NLP. We discuss their origin, the reason why they do not appear in the well-known LP factorisation formula with explicit one-loop examples, and provide their precise operator definition in SCET. We also calculate the collinear functions at $\mathcal{O}(\alpha_s)$ for both diagonal and off-diagonal channels, which illustrates the concept at the practical level and is required for the NNLO comparison mentioned above.

We have so far motivated the consideration of NLP terms in factorisation theorems with phenomenological arguments. Indeed, these terms do impact precision calculations. However, the extension of calculations to next-to leading power (NLP) brings with it non-trivial conceptual challenges which are interesting to purse in their own right as a way of gaining insight into the intricate structure of gauge theories at high perturbative orders beyond what is known so far at leading power. These effects are interesting study from the field theoretic point of view, since new physical effects and conceptual challenges emerge.

Many of the results regarding factorisation and resummation at next-to-leading power in this thesis have been included in existing publications

- M. Beneke, A. Broggio, M. Garny, S. Jaskiewicz, R. Szafron, L. Vernazza et al., *Leading-logarithmic threshold resummation of the Drell-Yan process at next-to-leading power*, *JHEP* **03** (2019) 043, [1809.10631]

- M. Beneke, M. Garny, S. Jaskiewicz, R. Szafron, L. Vernazza and J. Wang, *Leading-logarithmic threshold resummation of Higgs production in gluon fusion at next-to-leading power*, *JHEP* **01** (2020) 094, [1910.12685]

- M. Beneke, A. Broggio, S. Jaskiewicz and L. Vernazza, *Threshold factorization of the Drell-Yan process at next-to-leading power*, *JHEP* **07** (2020) 078, [1912.01585]

and conference proceedings

- S. Jaskiewicz, *Next-to-leading power threshold factorization for Drell-Yan production*, in *Proceedings, 14th International Symposium on Radiative Corrections: Application*

of Quantum Field Theory to Phenomenology (RADCOR 2019): Avignon, France, September 8-13, 2019, 2019, `1912.08882`, DOI.

Moreover, chapter 6 contains material to be published

- A. Broggio, S. Jaskiewicz and L. Vernazza, in preparation .

1.1 Outline

The contents of this work are organised as follows. In chapter 2, we discuss the soft-collinear effective field theory framework on which our investigations are grounded. We briefly review important leading power concepts and provide a more extensive look at general next-to-leading power features.

In chapter 3, the focus is on the threshold Drell-Yan process. We put the framework discussed in chapter 2 to use and derive formal all order factorisation formulas for the diagonal and off-diagonal channels before specialising to next-to-leading power. Much emphasis is placed on new objects appearing in factorisation formulas for the first time at next-to-leading power. These are the NLP collinear functions, subsequently computed to next-to-leading order accuracy in chapter 4, and generalised soft functions, which are discussed in chapter 5. We find that the calculation of complete NNLO generalised soft functions is far from trivial and we dedicate chapter 6 to the discussion of the techniques we applied to arrive at the results.

In chapter 7, the separate ingredients calculated in preceding chapters are brought together according to the factorisation formulas to obtain results at fixed order in the α_s expansion. Comparison with results found in literature serves to verify the correctness of the derived factorisation formulas.

In chapter 8, we specify the factorisation formula for the diagonal channel in Drell-Yan production to leading logarithmic accuracy and preform resummation to all orders in perturbation theory using renormalization group equations and scale evolution. A related process of threshold Higgs production via gluon-gluon fusion is investigated in chapter 9. We conclude and provide an outlook in chapter 10.

The appendices are a collection of useful auxiliary results and expressions to which we point in the relevant places in the main text. Appendix A contains list of NLP Lagrangian terms, helpful spin and colour relations, and useful integrals. Appendix B contains results for the power-suppressed one-loop one-soft emission Drell-Yan amplitude. Appendix C provides more details on the one-soft-particle-reducible contributions which are first discussed in section 4.1.1.

2

Nanos gigantum humeris insidentes

The work contained in this thesis is rooted in the framework of soft-collinear effective field theory (SCET) [69, 70, 71, 72, 73]. SCET describes low energy degrees of freedom in processes with energetic particles. This effective field theory originates from efforts to resum large logarithms which appear in heavy meson decays, for example $B \to X_u \ell \nu$ and $B \to X_s \gamma$ where X_u and X_s are clusters of collinear quarks and gluons, in cases where the phase space of the final state is restricted [74, 75, 76, 77, 78]. Since this time, SCET has been applied to a plethora of processes which involve energetic particles in a variety of contexts such as inclusive hadron-collider cross-sections, event shapes, jet physics, electroweak Sudakov logarithms, and even gravity. For a more complete review of applications of SCET see for example chapter 9 of [79].

Needless to say, the literature on SCET is by now extremely extensive and here we do not aim to provide a complete overview nor discuss all the intricacies that can arise in SCET in the various contexts to which it has been applied. Instead, we introduce the necessary key concepts required to follow the discussion of the developments presented in this work. In particular, we focus on highlighting some of the novel features of SCET emergent only beyond the well-understood leading power regime. For extra information regarding SCET we refer to lecture notes [80, 81, 82, 83, 84] and books [79, 85] in addition to the original publications cited above.

2.1   Soft-collinear effective field theory

SCET describes the dynamics of collinear and soft partons. Collinear partons are characterized by a large momentum component along one light-like direction, and suppressed momentum components along the remaining directions. In order to describe the dynamics, it is therefore convenient to choose light-like reference vectors n_{i-}^{μ} and n_{i+}^{μ} for each collinear direction i. These vectors are given by

$$n_{i-}^{\mu} = (1, \vec{n}_i), \qquad n_{i+}^{\mu} = (1, -\vec{n}_i). \tag{2.1}$$

The $\vec{n}_i$ is a three-vector, and the light-like reference vectors satisfy $n_{i-} \cdot n_{i+} = 2$ and $n_{i-}^2 = n_{i+}^2 = 0$. Using these reference vectors, the metric tensor is decomposed in the following way

$$g^{\mu\nu} = n_{i+}^{\mu} \frac{n_{i-}^{\nu}}{2} + n_{i-}^{\mu} \frac{n_{i+}^{\nu}}{2} + g_{i\perp}^{\mu\nu} \tag{2.2}$$

which defines $g_{i\perp}^{\mu\nu}$. This leads to the realisation that a general four-vector can be written in terms of its light-cone components

$$p^\mu = p_\nu g^{\nu\mu} = (n_{i+}p)\frac{n_{i-}^\mu}{2} + (n_{i-}p)\frac{n_{i+}^\mu}{2} + p_{i\perp}^\mu, \qquad p^\mu = (n_{i+}p, n_{i-}p, p_{i\perp}), \qquad (2.3)$$

where we have also written the four-vector utilising the component notation. It follows that the scalar product of the vector p^μ with itself (and with another arbitrary vector q^μ) is given by

$$p^2 = (n_{i+}p)(n_{i-}p) + p_{i\perp}^2 \qquad \left(p \cdot q = \frac{1}{2}(n_{i+}p)(n_{i-}q) + \frac{1}{2}(n_{i-}p)(n_{i+}q) + p_{i\perp} \cdot q_{i\perp}\right). \qquad (2.4)$$

The power-counting parameter λ is identified by the perpendicular, $\perp$, component of the collinear momenta, $p_{i\perp} \sim Q\lambda$, where Q is a generic large scale in the process, whose virtuality is $\mathcal{O}(\lambda^2)$. In this work we concern ourselves with physical processes for which the virtuality of the collinear modes in any of the collinear directions, i, is of the same order, $\mathcal{O}(\lambda^2)$, and which is parametrically larger than the virtuality of the soft mode which is $\mathcal{O}(\lambda^4)$, as all of the component of the soft momentum scale as $Q\lambda^2$. This set up leads to a version of the soft-collinear effective field theory known as SCET$_\text{I}$. The Lagrangian for this theory with power suppressed interactions out up to $\mathcal{O}(\lambda^2)$ has been worked out in [73]. The subleading power interactions between collinear and soft fields given here play a central role in much of the considerations presented in this work, and we will return to discuss them in far greater detail. However, we first intend to start from the beginning and show how the expansion-by-regions method simplifies loop calculations of Feynman diagrams with a hierarchy of scales present. We then discuss the leading power effective field theory construction, which gives the expanded integrals directly, that is, SCET$_\text{I}$ at leading power. After this discussion, we introduce the framework which extends these considerations from leading power to subleading powers. This framework was developed in a formal setting for the calculation of anomalous dimensions of subleading-power N-jet operators in a series of papers [86, 87, 88] to which we refer the interested reader for all the technical details. Below we aim to introduce the concepts necessary in the analysis that follows and to set up the notation.

2.2   Expansion-by-regions method

The technique of expansion-by-regions [89, 90] is a method that enables asymptotic expansion of loop integrals in dimensional regularization around different kinematic limits. As will be demonstrated here for a simple example, the idea is that a given integral is separated into different regions. The integrand can then be expanded in an appropriate kinematic limit for each individual region. This yields simpler intermediate integrals, and we recover the result for the original integral once the results for different regions are recombined. The expansion-by-regions method is a useful technique that allows one to obtain results for Feynman diagrams which are too difficult for direct evaluation, for example, if a large number of disparate scales are involved. This by itself is a very useful tool in fixed-order perturbative calculations. However, the expansion-by-regions technique forms the foundation of even more powerful methods if we interpret the non-vanishing

on-shell regions as contributing propagating degrees of freedom to an effective field theory. Within the effective field theory framework, the different contributing regions are described by different sets of fields, and the expanded integrals are in one-to-one correspondence with the Feynman diagrams of the effective field theory in dimensional regularization. Importantly, the concept of scale separation is built-in to the constructed effective field theory. This facilitates the derivation of factorisation theorems which give access to results valid to all orders in perturbation theory via solutions of systems of renormalization group equations.

Moreover, the effective field theory Lagrangian, unlike individual Feynman diagrams, is manifestly gauge invariant and allows for the systematic inclusion of subleading power corrections. The expansion-by-regions method underpins all of the above important concepts. Therefore we dedicate this section to a short example of this method at work.

As the example, we choose a one-loop vertex correction considered in detail in chapter 2 of [79] since the contributing modes found here are also relevant for the discussion presented in the following chapters. The integral which we consider is given by

$$I = i\,\pi^{-d/2}\mu^{4-d}\,\int d^d k \frac{1}{(k^2 + i\delta)} \frac{1}{[(k+l)^2 + i\delta]} \frac{1}{[(k+p)^2 + i\delta]}\,, \tag{2.5}$$

which corresponds to the propagator structure of the diagram depicted in figure 2.1. We ignore here the Dirac spin structure for simplicity as it does not alter the contributing momentum regions. In order to apply the expansion-by-regions method the problem must exhibit a hierarchy of scales, therefore we insist that the external quark lines carry large momenta l and p, but their respective invariant masses are small, such that $L^2, P^2 \ll Q^2$, where $L^2 = -l^2 - i\delta$, $P^2 = -p^2 - i\delta$, and $Q^2 = -(l-p)^2 - i\delta$. For convenience we introduce a small expansion parameter defined by

$$\lambda^2 \sim \frac{P^2}{Q^2} \sim \frac{L^2}{Q^2}. \tag{2.6}$$

The integral in (2.5) is in fact finite in $d = 4$ and can be evaluated directly. The full result is a complicated function of polylogarithms which we do not write here. To leading order in the λ expansion, it is given by

$$I = \frac{1}{Q^2}\left(\ln\left(\frac{Q^2}{P^2}\right)\ln\left(\frac{Q^2}{L^2}\right) + \frac{\pi^2}{3} + \mathcal{O}(\lambda)\right). \tag{2.7}$$

We reiterate that the aim of the expansion-by-regions method is to identify modes which give a non-zero contribution to the integral in (2.5). If we identify these modes correctly, they will conspire to reproduce the result in (2.7).

We begin the investigation by parametrising the momenta. In this example there are only two directions of large momentum flow, therefore we can use the basis of light-like reference vectors given in (2.1) and drop the i subscript by choosing a back-to-back configuration such that we work in the frame where $\vec{Q} = 0$. The directions of large momentum flow are $p^\mu \approx Q n_-^\mu/2$ and $l^\mu \approx Q n_+^\mu/2$. The components of the external momenta scale in the following way

$$p^\mu \sim Q(1, \lambda^2, \lambda), \qquad l^\mu \sim Q(\lambda^2, 1, \lambda), \tag{2.8}$$
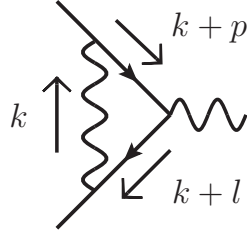
Figure 2.1: *One-loop $e\bar{e}\gamma$ vertex correction. The external fermion legs are kept slightly off-shell, $p^2 \neq 0$ and $l^2 \neq 0$. The discussion in the text focuses on the scalar propagators and we neglect the Dirac structures in the numerators.*

which satisfies $p^2 \sim l^2 \sim \lambda^2 Q^2$ in (2.6). We must now find which modes of the loop momentum, k in the diagram in figure 2.1, contribute to the integral. To this end, we first parametrise each component of the loop momentum with the expansion parameter λ raised to an arbitrary power $k^\mu \sim Q(\lambda^a, \lambda^b, \lambda^c)$. It turns out that only combinations satisfying $a + b = 2c$ are relevant. If $c > 0$, these modes describe to particles which are on-shell in the $\lambda \to 0$ limit and which correspond to the propagating degrees of freedom in the effective field theory, as eluded to above. As will become evident momentarily, four regions give non-zero contributions to the integral. In the first region, the components of the loop momentum scale with $a = b = c = 0$, which gives $k^\mu \sim Q(1, 1, 1)$. This is known as a *hard* region. Next we have regions *collinear* to p^μ and l^μ. These take on $k^\mu \sim Q(1, \lambda^2, \lambda)$ and $k^\mu \sim Q(\lambda^2, 1, \lambda)$ scaling respectively. The final contributing region with loop momentum scaling as $k^\mu \sim Q(\lambda^2, \lambda^2, \lambda^2)$ is known as the *soft* region.

To demonstrate that these regions indeed reproduce the result in equation (2.7), we now consider each region separately and expand the integrand accordingly. We begin with the *hard* region where $k^2 \sim \lambda^0 Q^2$. Writing the scalar products in component form as in equation (2.4), we expand the integrand in λ and keep only the leading terms. This yields the following integral

$$I^{\text{hard}} = i\,\pi^{-d/2}\mu^{4-d} \int d^d k \frac{1}{(k^2 + i\delta)} \frac{1}{[k^2 + (n_- l)(n_+ k) + i\delta]} \frac{1}{[k^2 + (n_+ p)(n_- k) + i\delta]}\,. \quad (2.9)$$

Note that in this region $(n_+ p)(n_- k) \sim \lambda^0 Q^2$, whereas $p_\perp \cdot k_\perp \sim \lambda Q^2$ and $(n_- p)(n_+ k) \sim \lambda^2 Q^2$. Hence, the latter two scalar products are suppressed with respect to the first and are therefore omitted in the integrand above. An analogous analysis yields the propagator with the momentum l^μ. We can integrate (2.9) which gives the following result

$$I^{\text{hard}} = \frac{1}{(n_- l)(n_+ p)} \frac{1}{\epsilon^2} \left(\frac{(n_- l)(n_+ p)}{\mu^2} \right)^{-\epsilon} \frac{\Gamma[1+\epsilon]\Gamma[1-\epsilon]^2}{\Gamma[1-2\epsilon]}\,. \quad (2.10)$$

Next, we begin with the integral in (2.5) again and find that in the region of loop momentum k^μ collinear to p^μ the integrand is expanded as

$$I^{\text{collinear}} = i\,\pi^{-d/2}\mu^{4-d} \int d^d k \frac{1}{(k^2 + i\delta)} \frac{1}{[(n_- l)(n_+ k) + i\delta]} \frac{1}{[(k+p)^2 + i\delta]}\,, \quad (2.11)$$

again to leading order in λ, which yields

$$I^{\text{collinear}} = \frac{1}{(n_-l)(n_+p)} \frac{1}{\epsilon^2} \left(\frac{P^2}{\mu^2} \right)^{-\epsilon} \frac{\Gamma[1+\epsilon]\Gamma[1-\epsilon]^2}{\Gamma[1-2\epsilon]} . \tag{2.12}$$

Similarly, in the region collinear to l^μ, which we call *anticollinear* in order to distinguish it from the region collinear to p^μ, the expanded integrand takes the form

$$I^{\text{collinear}} = i\,\pi^{-d/2}\mu^{4-d} \int d^d k \frac{1}{(k^2+i\delta)} \frac{1}{[(k+l)^2+i\delta]} \frac{1}{[(n_+p)(n_-k)+i\delta]} , \tag{2.13}$$

for which we obtain

$$I^{\text{anticollinear}} = \frac{1}{(n_-l)(n_+p)} \frac{1}{\epsilon^2} \left(\frac{L^2}{\mu^2} \right)^{-\epsilon} \frac{\Gamma[1+\epsilon]\Gamma[1-\epsilon]^2}{\Gamma[1-2\epsilon]} . \tag{2.14}$$

Finally, we consider the soft region where the integral is given by

$$I^{\text{soft}} = i\,\pi^{-d/2}\mu^{4-d} \int d^d k \frac{1}{(k^2+i\delta)} \frac{1}{[(n_-p)(n_+k)+l^2+i\delta]} \frac{1}{[(n_+p)(n_-k)+p^2+i\delta]} , \tag{2.15}$$

and the result is

$$I^{\text{soft}} = \frac{1}{(n_-l)(n_+p)} \frac{1}{\epsilon^2} \left(\frac{L^2 P^2}{(n_-l)(n_+p)\mu^2} \right)^{-\epsilon} \Gamma[1+\epsilon]\Gamma[1-\epsilon]^2 . \tag{2.16}$$

We now expand all of the above results in ϵ to expose explicitly the pole and logarithm structure contained in the individual regions

$$I^{\text{hard}} = \frac{\Gamma[1+\epsilon]}{Q^2} \left(\frac{1}{\epsilon^2} + \frac{1}{\epsilon}\ln\left(\frac{\mu^2}{Q^2}\right) + \frac{1}{2}\ln^2\left(\frac{\mu^2}{Q^2}\right) - \frac{\pi^2}{6} + \mathcal{O}(\lambda) \right), \tag{2.17}$$

$$I^{\text{collinear}} = \frac{\Gamma[1+\epsilon]}{Q^2} \left(-\frac{1}{\epsilon^2} - \frac{1}{\epsilon}\ln\left(\frac{\mu^2}{P^2}\right) - \frac{1}{2}\ln^2\left(\frac{\mu^2}{P^2}\right) + \frac{\pi^2}{6} + \mathcal{O}(\lambda) \right), \tag{2.18}$$

$$I^{\text{anticollinear}} = \frac{\Gamma[1+\epsilon]}{Q^2} \left(-\frac{1}{\epsilon^2} - \frac{1}{\epsilon}\ln\left(\frac{\mu^2}{L^2}\right) - \frac{1}{2}\ln^2\left(\frac{\mu^2}{L^2}\right) + \frac{\pi^2}{6} + \mathcal{O}(\lambda) \right), \tag{2.19}$$

$$I^{\text{soft}} = \frac{\Gamma[1+\epsilon]}{Q^2} \left(\frac{1}{\epsilon^2} + \frac{1}{\epsilon}\ln\left(\frac{\mu^2 Q^2}{P^2 L^2}\right) + \frac{1}{2}\ln^2\left(\frac{\mu^2 Q^2}{P^2 L^2}\right) + \frac{\pi^2}{6} + \mathcal{O}(\lambda) \right), \tag{2.20}$$

where we have used $(n_-l)(n_+p) = Q^2$. We see that each region depends on a single scale, such that the logarithms can be made small by a suitable choice of μ in each region. Moreover, individual regions contain divergences in ϵ. However, upon summation of all the different regions these poles cancel and in the end we obtain a result for the integral (2.5) in the limit $P^2 \sim L^2 \ll Q^2$. Concretely, we recover the result in (2.7) which is accurate to leading power in the λ expansion. The effective field theory framework is then construcuted to give each of the contributing regions directly, we outline this construction in the following sections.

The example presented here is only meant to illustrate the expansion-by-regions method in one of the simplest possible scenarios. In general, this method allows for systematic inclusion of terms suppressed by powers of λ. Indeed, power corrections are the central theme of the work presented here. In the sections that follow, we describe SCET at leading power and how subleading power corrections are included in this effective field theory. In appendix B.2 we present results for a full (including the numerator structure) amplitude for the Drell-Yan process valid up to next-to-leading power in λ expansion. We obtain the results using the SCET framework and find agreement with the results obtained by the means of expansion-by-regions method.

2.3   SCET at leading power

In this section we introduce the soft-collinear effective field theory framework at leading power in the λ expansion. We focus on the construction of SCET with modes found to contribute to the example integral above, this is the so-called SCET$_\mathrm{I}$ field theory. An important remark is that different versions of SCET may be applicable to different processes, for example the so-called SCET$_\mathrm{II}$ is the appropriate effective field theory construction for proceses where the contributing "soft" region has the same virtuality as the collinear, $k^\mu \sim Q(\lambda, \lambda, \lambda)$.

2.3.1   SCET$_\mathrm{I}$: field decomposition and the Lagrangian

We consider SCET in a general case where there exist N collinear directions. The quark and gluon fields are split into N-collinear and a soft parts

$$\psi(x) \;\rightarrow\; \underbrace{\psi_1(x) + \cdots + \psi_N(x)}_{N\text{ collinear fermion fields}} + q(x), \qquad (2.21)$$

$$A^\mu(x) \;\rightarrow\; \underbrace{A_1^\mu(x) + \cdots + A_N^\mu(x)}_{N\text{ collinear gluon fields}} + A_s^\mu(x), \qquad (2.22)$$

where q is the soft part of the fermion field and A_s^μ is the soft part of the gauge field. Note that no fields corresponding to the hard modes are included in the above splitting of the full theory fields. Contributions from the hard regions are included in the effective field theory framework through matching coefficients, named Wilson coefficients, of operators constructed from the collinear and soft fields. This is where SCET differs from traditional effective field theories, here we integrate out a *mode* of the full theory rather than a full heavy field.

The fermion field in each collinear sector is further split into two components

$$\psi_i(x) \equiv \xi_i(x) + \eta_i(x), \qquad (2.23)$$

where the $\xi_i(x)$ and $\eta_i(x)$ fields are defined using projection operators in the following way

$$\xi_i(x) = \frac{\slashed{n}_{i-}\slashed{n}_{i+}}{4}\psi_i(x), \qquad \eta_i(x) = \frac{\slashed{n}_{i+}\slashed{n}_{i-}}{4}\psi_i(x). \qquad (2.24)$$

The above definitions enable us to determine the power in λ with which the different components of the SCET fermion field scale. This is achieved using the two-point correlators in QCD

$$\langle 0|\mathbf{T}\left[\xi_i(x)\bar{\xi}_i(0)\right]|0\rangle = \frac{\not{n}_{i-}\not{n}_{i+}}{4}\left[\int \frac{d^4p}{(2\pi)^4}\frac{i}{p^2+i\delta}e^{-ip\cdot x}\not{p}\right]\frac{\not{n}_{i+}\not{n}_{i-}}{4} = \lambda^2, \tag{2.25}$$

where we have used decomposition in equation (2.3) to write p^μ in terms of light-like components before contracting it with a γ_μ and using the fact that $\not{n}_{i-}\not{n}_{i-} = \not{n}_{i+}\not{n}_{i+} = 0$, such that

$$\frac{\not{n}_{i-}\not{n}_{i+}}{4}\not{p}\frac{\not{n}_{i+}\not{n}_{i-}}{4} = (n_{i+}p)\frac{\not{n}_{i-}}{2} \sim \lambda^0\,. \tag{2.26}$$

Hence, from (2.25) we see that the $\xi_i(x)$ field scales as $\xi_i \sim \lambda$. A similar analysis reveals that the $\eta_i(x)$ field scales as $\eta_i \sim \lambda^2$, and the soft field $q(x)$ scales as $q \sim \lambda^3$. The gauge field scales like its momentum, hence $A_c^\mu(x) \sim p_c^\mu$ and $A_s^\mu(x) \sim p_s^\mu$, where the momenta p_c^μ and p_s^μ are some collinear and soft momenta. For this reason only the n_-A_s component is not power suppressed with respect its counterpart within the collinear gluon field $A_c^\mu(x)$. The suppressed component of the collinear field $\eta_i(x)$ is integrated out using equations of motion.

We will shortly present the leading power Lagrangian. However, we must first make two important remarks regarding the interaction terms of the SCET Lagrangian. Firstly, the fields belonging to different collinear directions do not directly interact with each other as this is forbidden by momentum conservation – only soft exchanges are permitted between the collinear sectors. Secondly, each interaction term which is permitted by momentum conservation and which contains a mixture of collinear and soft fields must be multipole expanded to achieve homogeneous power counting [72]. We elaborate on the latter remark by considering a Fourier transform of an interaction term in the Lagrangian, schematically we have

$$\int d^dx\,\bar{\xi}_c(x)\,A_s^\mu(x)\,\xi_c(x) = \int d^dx \int \frac{d^dp_1}{(2\pi)^d}\frac{d^dp_2}{(2\pi)^d}\frac{d^dp_s}{(2\pi)^d}\bar{\tilde{\xi}}_c(p_1)\,\tilde{A}_s^\mu(p_s)\,\tilde{\xi}_c(p_2)$$
$$\times e^{-i(p_1+p_2+p_s)\cdot x}, \tag{2.27}$$

where momenta p_1, p_2 are collinear and momentum p_s is soft. Focusing on the exponent, we note that sum of momenta p_1, p_2, and p_s scales as $p_1^\mu + p_2^\mu + p_s^\mu \sim Q(1, \lambda^2, \lambda)$ which implies that the position variable x^μ scales as $x^\mu \sim (1/Q)(1/\lambda^2, 1, 1/\lambda)$. With this, we can see that all components of the collinear modes by construction contribute equally. However, if we consider now the scalar product of x^μ with a soft momentum, we find that not all components contribute equally

$$p_s \cdot x = \frac{1}{2}\underbrace{(n_-p_s)(n_+x)}_{\mathcal{O}(\lambda^0)}+\frac{1}{2}\underbrace{(n_+p_s)(n_-x)}_{\mathcal{O}(\lambda^2)}+\underbrace{p_{s\perp}\cdot x_\perp}_{\mathcal{O}(\lambda^1)} \tag{2.28}$$

where we have denoted that the first term is dominant, $(n_-p_s)(n_+x) \sim \lambda^0$, and the remaining terms are power suppressed with respect to the $(n_-p_s)(n_+x)$ term. Therefore, the

soft field in contact with collinear fields must be Taylor expanded around $x_-^\mu = (n_+ x) n_-^\mu / 2$. This yields

$$
\begin{aligned}
\int d^d x \, \bar{\xi}_c(x) \, A_s^\mu(x) \, \xi_c(x) &= \int d^d x \, \bar{\xi}_c(x) \left[A_s^\mu(x_-) + \underbrace{x_\perp \cdot \partial_\perp A_s^\mu(x_-)}_{\mathcal{O}(\lambda)} + \mathcal{O}(\lambda^2) \right] \xi_c(x) \\
&= \int d^d x \, \bar{\xi}_c(x) \, A_s^\mu(x_-) \xi_c(x) + \mathcal{O}(\lambda) \,.
\end{aligned}
\tag{2.29}
$$

Hence, soft fields multiplying collinear fields in the SCET Lagrangian are evaluated at a position x_-^μ, rather than a full x^μ position. Importantly, we evaluate the soft fields at x_-^μ *after* the derivatives are taken.

The soft-collinear effective field theory Lagrangian for QCD is separated into a soft and N collinear parts as follows

$$
\mathcal{L}_{\mathrm{SCET_I}} = \mathcal{L}_s + \sum_{i=1}^{N} \mathcal{L}_i,
\tag{2.30}
$$

where each of the collinear sectors is systematically power expanded in the small power counting parameter λ

$$
\mathcal{L}_i = \underbrace{\mathcal{L}_i^{(0)}}_{\mathcal{O}(\lambda^0)} + \underbrace{\mathcal{L}_i^{(1)}}_{\mathcal{O}(\lambda^1)} + \underbrace{\mathcal{L}_i^{(2)}}_{\mathcal{O}(\lambda^2)} + \ldots
\tag{2.31}
$$

The first term in the expansion, $\mathcal{L}_i^{(0)}$, is known as the *leading power* contribution, and the remaining terms denote the power corrections. The number in the superscript in terms on the right-hand side of (2.31) denotes the relative power suppression in λ with respect to the leading power term. The soft Lagrangian is given by

$$
\mathcal{L}_s = \bar{q}_s i \slashed{D}_s q_s - \frac{1}{4} \left(F_{\mu\nu}^{s,A} \right)^2
\tag{2.32}
$$

where A is the adjoint colour index and the soft covariant derivative is defined as

$$
i D_\mu^s(x) = i \partial_\mu + g_s A_\mu^s(x),
\tag{2.33}
$$

in terms of which we define the soft field strength tensor

$$
i g_s F_{\mu\nu}^s = \left[i D_\mu^s, i D_\nu^s \right].
\tag{2.34}
$$

The different collinear sectors in (2.30) have identical structure, here we give the leading power contribution to the i-th collinear sector

$$
\mathcal{L}_i^{(0)} = \bar{\xi}_i \frac{\slashed{n}_{i+}}{2} \left[i n_{i-} D_i + + g_s n_{i-} A_s(x_{i-}) + i \slashed{D}_{i\perp} \frac{1}{i n_{i+} D_i} i \slashed{D}_{i\perp} \right] \xi_i - \frac{1}{4} \left(F_i^{\mu\nu,A} \right)^2,
\tag{2.35}
$$

where we have made the dependence on $n_{i-} A_s(x_{i-})$ explicit. The covariant derivative is given by

$$
i D_i^\mu(x) = i \partial^\mu + g_s A_i^\mu(x) \,.
\tag{2.36}
$$

As emphasised above, the position argument of the soft field in (2.35) is only the component x_-^μ. The collinear fields are evaluated at x^μ. The field strength in equation (2.35) is defined by

$$ig_s F_i^{\mu\nu} = \left[iD_i^\mu + g_s n_{i-} A^s(x_{i-}) \frac{n_+^\mu}{2}, iD_i^\nu + g_s n_{i-} A^s(x_{i-}) \frac{n_+^\mu}{2} \right], \tag{2.37}$$

where D_i^μ is decomposed as

$$D_i^\mu = (n_{i-} D_i) \frac{n_{i+}^\mu}{2} + (n_{i+} D_i) \frac{n_{i-}^\mu}{2} + D_{i\perp}^\mu \tag{2.38}$$

according to (2.3).

At leading power, soft gluons couple to collinear partons through eikonal vertices, this is explicit in the leading power Lagrangian of SCET in (2.35).

Gauge transformations

Manifest gauge invariance built into the Lagrangian and non-local operators, which we introduce below, is one of the key features of SCET. It enables us to make all-order statements and predictions. We discuss it briefly here and remark that a detailed study of gauge transformation properties of the non-abelian SCET Lagrangian has been performed in [73].

The gauge transformations of QCD must be expanded so that the scaling of the soft and collinear fields in the SCET Lagrangian is not altered by gauge transformations. The soft and i-collinear gauge transformations are defined by

$$V_s(x) = \exp\left[i\,\alpha_s^A(x)\mathbf{T}^A\right], \qquad V_i(x) = \exp\left[i\,\alpha_i^A(x)\mathbf{T}^A\right], \tag{2.39}$$

where the gauge functions $\alpha_s^A(x)$ and $\alpha_i^A(x)$ have a soft and collinear scaling respectively.

Under a soft gauge transformation, the soft fields transform in the standard way, see for example [91]. However, the i-collinear fields transform according to

$$\xi_i(x) \quad\to\quad V_s(x_{i-})\,\xi_i(x), \tag{2.40}$$

$$A_i^\mu(x) \quad\to\quad V_s(x_{i-})\,A_i^\mu(x)\,V_s^\dagger(x_{i-}). \tag{2.41}$$

Note that the soft gauge transformation here is expanded and depends only on the x_{i-}^μ component to keep a homogeneous power counting.

Next we consider the i-collinear gauge transformations. The soft fields do not transform under these transformations since this would alter their power counting. The i-collinear fields transform as

$$\xi_i(x) \quad\to\quad V_i(x)\,\xi_i(x), \tag{2.42}$$

$$A_i^\mu(x) \quad\to\quad V_i(x)\,A_i^\mu(x)\,V_i^\dagger(x) + \frac{1}{g_s}V_i(x)\left[i\partial^\mu + g_s\,\frac{n_{i+}^\mu}{2}n_{i-}A_s(x_{i-}), V_i^\dagger(x)\right]. \tag{2.43}$$

To summarise, the fermion fields transform according to

$$\psi \to V_{s/i}\psi \tag{2.44}$$

and all covariant derivatives transform as

$$D^\mu \to V_{s/i} D^\mu V_{s/i}^\dagger \,, \tag{2.45}$$

with the arguments replaced $x^\mu \to x_{i-}^\mu$ in the correct places. The Lagrangian in (2.35) is manifestly invariant under both soft and collinear gauge transformations separately. Manifest gauge invariance can be systematically included in the subleading power Lagrangian, as is carried out in detail in [73].

Wilson lines

Wilson lines are objects which play a critical role in ensuring gauge invariance of SCET. We define the i-collinear Wilson line with the large component of the associated gauge field in the exponent

$$W_i(x) = [x, -\infty n_{i+}] = \mathbf{P} \exp\left[ig_s \int_{-\infty}^0 ds\, n_{i+} A_i(x + sn_{i+})\right], \tag{2.46}$$

and the soft Wilson lines with the $n_{i-} A_s$ component of the soft gauge field [1]

$$Y_{i+}(x) \;=\; \mathbf{P} \exp\left[ig_s \int_{-\infty}^0 ds\, n_{i-} A_s(x + sn_{i-})\right]. \tag{2.47}$$

The symbol $\mathbf{P}$ in both of the above equations denotes a path ordering operator such that gauge fields with a larger s are placed to the left of those with a smaller s. The limits of the integrals in the exponents of equations (2.46) and (2.47), namely from $-\infty$ to 0, arise due to the fact that for concreteness we are considering *incoming* particles. In Wilson lines describing *outgoing* particles the limits extend from 0 to ∞. Explicit expressions for Wilson lines describing QED and QCD particles and antiparticles can be found in equations (A.16) – (A.23) of [64].

The usefulness of Wilson lines in the construction of SCET becomes apparent upon consideration of the behaviour of these objects under gauge transformations. Namely, taking as an example the collinear gauge transformations we find that the Wilson lines transform as follows

$$W_i(x) \to V_i(x) W_i(x) V_i^\dagger(-\infty n_{i+})\,. \tag{2.48}$$

If we then consider gauge functions which vanish at infinity, such that $V_i^\dagger(-\infty n_{i+}) = 1$, then the following building blocks are collinear-gauge invariant [92]

$$\psi_i(x) \in \begin{cases} \chi_i(x) = W_i^\dagger(x)\xi_i(x) & i\text{-collinear quark} \\[2mm] \mathcal{A}_{i\perp}^\mu(x) = W_i^\dagger(x)\left[iD_{i\perp}^\mu W_i(x)\right] & i\text{-collinear gluon} \end{cases} \tag{2.49}$$

Using the scaling of the fields which make up the building blocks, as discussed below equation (2.25), we see that the scaling of each collinear building block is $\mathcal{O}(\lambda)$ [72].

---

[1]When there are only two, back-to-back, collinear directions present, we will use the soft Wilson line $Y_\pm(x) \;=\; \mathbf{P} \exp\left[ig_s \int_{-\infty}^0 ds\, n_\mp A_s(x + sn_\mp)\right]$, where the + and − correspond to soft Wilson lines for the collinear and anticollinear directions.

Since Wilson lines appear ubiquitously in SCET, we briefly comment on their contribution to calculation of Feynman diagrams. A Wilson line may source any number of gluons by keeping higher orders in the expansion of the exponential in equations (2.46) and (2.47). The higher number of emissions are suppressed by corresponding powers of g_s. For illustration, we consider the $\mathcal{O}(g_s)$ term. The momentum-space Feynman rule can be obtained Fourier transforming the gauge field and performing the ds integral. By requiring that the Wilson line is well-behaved at infinity, we can fix the $i\delta$ prescription. For example, considering the soft Wilson line in equation (2.47) and expanding to first order we find the following

$$Y_{i+}(x) = 1 + \int \frac{d^4k}{(2\pi)^4} e^{-ik\cdot x} \left[-g_s \frac{n_{i-}^\mu}{n_{i-}k - i\delta} \mathbf{T}^A \right] \tilde{A}_{s,\mu}^A(k) + \mathcal{O}(g_s^2), \qquad (2.50)$$

where the term in the square bracket is the momentum-space Feynman rule. This Feynman rule has an eikonal form as expected, namely, it contains a *linear* dependence on the momentum.

We note that the appearance of eikonal propagators is common within soft-collinear effective field theory since it deals with the kinematic situation where the soft momentum is parametrically smaller than other momenta in the process and a consistent expansion can be performed. This linear dependence on momentum is in contrast to the momentum squared behaviour usually encountered in the propagators in calculations using full, unexpanded, QCD.

2.3.2 Decoupling transformation

An important feature of the SCET Lagrangian is that the soft-collinear interactions can be completely removed at leading power. This is achieved by the so-called decoupling transformation [71] which is defined by the field redefinition below. For simplicity, we focus on one collinear direction, *c*. However, the decoupling transformation can be applied to every collinear sector present in a given problem. The decoupling transformation is given by

$$\xi_c(x) \rightarrow Y_+(x_-)\,\xi_c^{(0)}(x)\,, \qquad (2.51)$$

$$A_c^\mu(x) \rightarrow Y_+(x_-)A_c^{(0)\mu}(x)Y_+^\dagger(x_-)\,. \qquad (2.52)$$

Corresponding decoupling transformations for outgoing particles are given in equation (A.15) of [64].

Focusing on the fermion piece of the leading power Lagrangian given in (2.35), we see that the soft-collinear interactions arise only due to the presence of the soft gauge field, A_s, in the $in_- D$ piece. Therefore, considering this term in the Lagrangian, and performing the decoupling transformation we see that

$$\bar{\xi}_c\left(in_- D_c + g_s n_- A_s\right) \frac{\slashed{n}_+}{2}\xi_c = \bar{\xi}_c^{(0)}\, in_- D_c^{(0)}\, \frac{\slashed{n}_+}{2}\,\xi_c^{(0)}\,, \qquad (2.53)$$

where the right-hand side of this equation, written in terms of the decoupled collinear fields, does not contain any soft fields. Effectively, the field redefinitions in equations (2.51) and (2.52) remove all soft-collinear interactions from the leading power Lagrangian in (2.35).

Alternatively, we can write the decoupled leading power Lagrangian in terms of the decoupled collinear gauge-invariant fields introduced in (2.49). In this case, the interaction term takes the following form

$$\bar{\xi}_c \left(in_-D_c + g_s n_-A_s\right) \frac{\slashed{n}_+}{2} \xi_c = \bar{\chi}_c^{(0)} \left(in_-\partial + n_-\mathcal{A}_c^{(0)}\right) \frac{\slashed{n}_+}{2} \chi_c^{(0)} , \qquad (2.54)$$

where $\mathcal{A}_c^\mu = W_c^\dagger \left[iD_c^\mu W_c\right]$ according to the second line of (2.49). The superscript (0) on the decoupled fields is customarily dropped after the field redefinition is performed. This convention is followed in this work, unless for clarity we make this superscript explicit in which case this will be noted.

2.3.3   Matching procedure

In equations (2.21) and (2.22) we have specified how the full QCD fields decompose into effective field theory fields and remarked that hard modes are contained in the so-called Wilson, hard-matching, coefficients. In this section we outline how this procedure is performed in practice. To construct the effective field theory, we write down all possible operators compatible with the symmetries of the theory and assign a matching coefficient to each operator – the Wilson coefficients. We then compute identical quantities in the full and effective theories, and adjust the value of the Wilson coefficient such that the two results match. In SCET, the Lagrangian is not modified by the matching corrections. The hard-matching corrections are received only by operators which contain at least two collinear fields in separate directions. As an example we consider the matching of the QED vector current to the SCET fields. This quantity will become useful in the following chapters.

The matching of the vector current requires only two back-to-back collinear directions. Therefore they can be described by one set of light-like vectors $n_\pm^\mu$. As usual, the $(n_{1+}p) = (n_+p)$ component of the momentum p is large in the first sector which we call collinear, and in the second sector, which we call anticollinear, the large component is (n_-p), where $(n_{2+}p) = (n_-p)$.

We construct the leading power current operator using the collinear gauge-invariant fields given in (2.49). It is important that we include all possible operators in the effective field theory. With this in mind, we note that derivatives of a field with respect to its large component are not power suppressed, $n_+\partial \chi_c(x) \sim \lambda^0 \chi_c(x)$. Hence, we have to keep an arbitrary number of these derivatives in the current operators. This is achieved by considering the expansion of the collinear field in the direction of the large momentum flow

$$\chi_c(x + tn_+) = \sum_{k=0}^\infty \frac{t^k}{k!} \left(n_+\partial\right)^k \chi_c(x) , \qquad (2.55)$$

which implies that the inclusion of any number of unsuppressed derivatives acting on the collinear field is equivalent to making the field non-local along the collinear direction. Sometimes this is referred to as "smearing" along the light-cone.

The matching of the vector current in the full theory onto the SCET fields at leading power is described by the following equation

$$\bar{\psi}\,\gamma^\rho\psi(0) \;=\; \int dt\,d\bar{t}\,\widetilde{C}^{A0,A0}(t,\bar{t})\bar{\chi}_{\bar{c}}(\bar{t}n_-)\,\gamma_\perp^\rho\chi_c\,(tn_+) , \qquad (2.56)$$
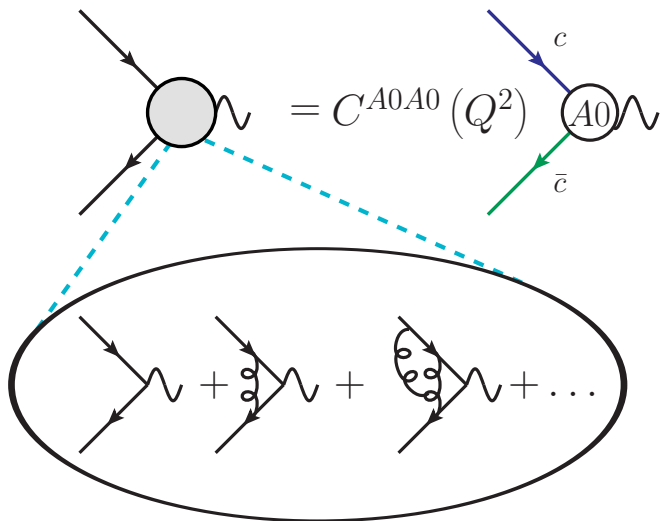
Figure 2.2: *Momentum-space pictorial representation of the hard matching relation given in equation (2.56). Hard fluctuations in full theory diagrams appear on the left-hand side of the matching equation. On the right-hand side we find SCET fields and the Wilson coefficient, C^{A0}, for the leading power DY current operator. The value of C^{A0} is found by the requirement that the two sides of the matching equation are equal.*

where we have used the $\chi_c, \bar{\chi}_{\bar{c}}$ fields which are *not* decoupled. Here we use the "bar" notation to denote variables which account for the anticollinear direction, $\bar{t}$, and we keep this convention in the following chapters. The physical interpretation of this equation is that the hard fluctuations in the full theory, on the left-hand side, are integrated out and contained in the matching, Wilson, coefficient $\widetilde{C}^{A0,A0}(t,\bar{t})$ in the effective field theory, on the right-hand side. The $A0$ notation will be explained in section 2.4.1. A pictorial representation of the matching equation in (2.56) is presented in momentum space in figure 2.2, where we have used the Fourier transform of the Wilson coefficient defined by

$$C^{A0,A0}(n_+p, n_-\bar{p}) = \int dt\, d\bar{t}\, e^{-i\,(n_+p)\,t - i\,(n_-\bar{p})\,\bar{t}}\; \widetilde{C}^{A0,A0}(t,\bar{t})\,. \tag{2.57}$$

The operator matching equation given in (2.56) is valid to all orders in perturbation theory. In practical applications, information about the Wilson coefficient is required up to a certain accuracy in α_s. Currently, it is known up to three loops [93, 94]. In the present work, we use the d-dimensional hard matching coefficient at the one-loop order. The result for this quantity can be found in equation (2.23) of [95]

$$\begin{aligned}
C^{A0,A0}(n_+p, n_-\bar{p}) &= 1 + \frac{\alpha_s}{4\pi} C_F \left(\frac{-Q^2}{\mu^2}\right)^{-\epsilon} \left(-\frac{2}{\epsilon^2} - \frac{3}{\epsilon} - 8 + \frac{\pi^2}{6}\right.\\
&\quad \left. + \epsilon\left(\frac{\pi^2}{4} + \frac{14\zeta(3)}{3} - 16\right) + \mathcal{O}(\epsilon^2)\right) + \mathcal{O}(\alpha_s^2)\,, \tag{2.58}
\end{aligned}$$

where $Q^2 = (n_+p)(n_-\bar{p})$ and we keep terms up to $\mathcal{O}(\epsilon)$. For later purposes, we define the H function which is given by the product of the hard matching coefficient and its

complex conjugate, $H = |C^{A0,A0}|^2$. Taking care to treat the imaginary part correctly, up to one-loop accuracy the hard function is given by

$$
\begin{aligned}
H(Q^2) \;=\; & 1 + \frac{\alpha_s C_F}{4\pi}\left(-\frac{4}{\epsilon^2} - \frac{1}{\epsilon}\left(4\ln\left(\frac{\mu^2}{Q^2}\right) + 6 \right) \right. \\
& -\left(2\ln^2\left(\frac{\mu^2}{Q^2}\right) + 6\ln\left(\frac{\mu^2}{Q^2}\right) - \frac{7\pi^2}{3} + 16 \right) \\
& +\epsilon\left(-\frac{2}{3}\ln^3\left(\frac{\mu^2}{Q^2}\right) - 3\ln^2\left(\frac{\mu^2}{Q^2}\right) + \left(\frac{7}{3}\pi^2 - 16\right)\ln\left(\frac{\mu^2}{Q^2}\right)\right. \\
& \left.\left. +\frac{28}{3}\zeta(3) + \frac{7}{2}\pi^2 - 32 \right) + \mathcal{O}(\epsilon^2) \right) + \mathcal{O}(\alpha_s^2)\,.
\end{aligned}
\tag{2.59}
$$

As discussed in section 2.3.2, the decoupling of soft-collinear interactions is an important property of the leading power Lagrangian. The decoupling transformation can also be applied to the SCET fields present in the hard matching equation. We state again here the field redefinition for the collinear-gauge-invariant collinear quark building block for the incoming particles which we consider in this work

$$
\chi_c(x) \;\rightarrow\; Y_+(x_-)\,\chi_c^{(0)}(x).
\tag{2.60}
$$

Application of the decoupling transformation in (2.60) to the SCET current in equation (2.56) has the following effect

$$
\bar{\psi}\,\gamma^\rho\psi(0) \;=\; \int dt\, d\bar{t}\,\widetilde{C}^{A0,A0}(t,\bar{t})\,\bar{\chi}_{\bar{c}}(\bar{t}n_-)\,Y_-^\dagger(0)\gamma_\perp^\rho Y_+(0)\chi_c\,(tn_+)\,,
\tag{2.61}
$$

where on the right-hand side of the equation we now use the *decoupled* fields, but have already dropped the superscript (0). The consequence of this field redefinition we depict in the two diagrams in figure 2.3. The soft interactions are now governed by the Wilson lines as can be seen on the right panel of figure 2.3 and there are no soft-collinear interactions, in contrast to the non-decoupled theory presented in the left panel. The leading power Wilson coefficient is represented by the circle connecting collinear and anticollinear directions labelled *A0*.

2.4   SCET at next-to-leading power

Since its inception, the formalism of the soft-collinear effective field theory has been applied to many processes and by now many relevant LHC observables are resummed to a high logarithmic accuracy at leading power. The subleading power corrections have received comparatively less attention, although the first studies of next-to-soft emissions from amplitudes using diagrammatic techniques date back to the work of Low [96] and Burnett and Kroll [97] in the late 1950s and 1960s. The effective field theory framework is ideally suited to investigations beyond the leading power as systematic power expansion and gauge invariance are built into the formalism. Indeed, exploration of power corrections in various contexts by the means of SCET has received increased interest in recent times. On
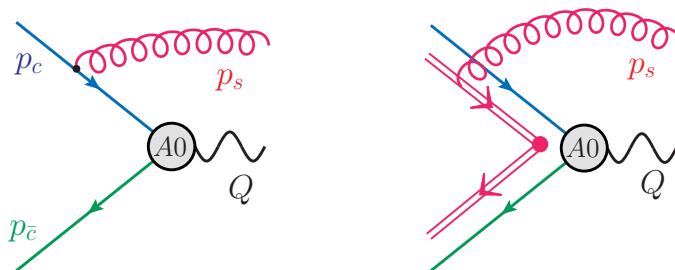
Figure 2.3: *The left panel depicts the QED vector current matched onto SCET fields prior to the application of the decoupling transformation. The right panel corresponds to the same object after the decoupling transformation, in equation (2.60), has been applied.*

the one hand, the motivation is to improve the accuracy of phenomenological predictions, and on the other hand, purely to advance our understanding of gauge theories beyond leading power to all orders in perturbation theory. There exist interesting field theoretic phenomena and intricate structures to study.

It is noteworthy that some of the ingredients necessary for computations beyond leading power have been worked out some time ago, for instance the non-abelian SCET Lagrangian has been presented as early as 2002 in [73] and power corrections in $1/m_B$ have been studied in the context of B-physics in [75]. The basis for subleading N-jet operators, on which the work presented here is grounded, has been introduced by M. Beneke, M. Garny, R. Szafron, and J. Wang in [86, 87] along with a first complete computations of the soft-anomalous dimensions at subleading power. There exist specific cases for which the subleading power anomalous dimensions were computed earlier, such as the heavy-to-light current [98, 99] and the power suppressed tree-level currents relevant for the production of two jets in electron-positron collisions [100, 101]. Moreover, formal insights and investigations of properties of subleading currents and divergent operators were discussed aforementioned authors in [88]. We direct the interested reader to these references for the many technical details and considerations in the position-space formalism which we now introduce in a practical manner.[2]

2.4.1 Basis for subleading N-jet operators

We begin the discussion by writing down the Lagrangian of SCET up to $\mathcal{O}(\lambda^2)$ in the power expansion. We do this in full since the Lagrangian will be extensively used throughout this work and it makes clear the structure of subleading power Feynman rules that we discuss in section 2.4.2. The Lagrangian is invariant under N collinear gauge transformations and a soft gauge transformation. We have briefly discussed the manifest gauge invariance of the SCET Lagrangian at leading power in section 2.3.1, the extension beyond leading power is intricate and was developed for the non-abelian case in [73].

The full SCET Lagrangian, given schematically in (2.30), is constructed from the soft

---

[2]An operator basis at next-to-leading power in the momentum-space SCET formulation can be found in [102, 103, 104, 105].

Lagrangian, $\mathcal{L}_s$, and N copies of the collinear Lagrangian, $\mathcal{L}_i$. To avoid cluttering of the expressions with additional indices, we focus on a single collinear direction and drop the corresponding index i distinguishing between the different collinear directions. Then, using the notation in (2.31) the Lagrangian up to $\mathcal{O}(\lambda^2)$ is given by [73]

$$\mathcal{L} = \mathcal{L}^{(0)} + \mathcal{L}_\xi^{(1)} + \mathcal{L}_\xi^{(2)} + \mathcal{L}_{\xi q}^{(1)} + \mathcal{L}_{\xi q}^{(2)} + \mathcal{L}_{\rm YM}^{(1)} + \mathcal{L}_{\rm YM}^{(2)}, \tag{2.62}$$

where $\mathcal{L}^{(0)}$ is written in equation (2.35), and for completeness the subleading power terms are explicitly given by

$$\mathcal{L}_\xi^{(1)} = \bar{\xi}\left(x_\perp^\mu n_-^\nu W_c\, g_s F_{\mu\nu}^s W_c^\dagger\right)\frac{\slashed{n}_+}{2}\xi, \tag{2.63}$$

$$\mathcal{L}_\xi^{(2)} = \mathcal{L}_{\xi,\rm I}^{(2)} + \mathcal{L}_{\xi,\rm II}^{(2)} + \mathcal{L}_{\xi,\rm III}^{(2)} \tag{2.64}$$

$$= \frac{1}{2}\bar{\xi}\left((n_-x)n_+^\mu n_-^\nu W_c\, g_s F_{\mu\nu}^s W_c^\dagger\right)\frac{\slashed{n}_+}{2}\xi + \frac{1}{2}\bar{\xi}\left(x_\perp^\mu x_\perp^\eta n_-^\nu W_c\left[D_\eta^s, g_s F_{\mu\nu}^s\right]W_c^\dagger\right)\frac{\slashed{n}_+}{2}\xi$$

$$+ \frac{1}{2}\bar{\xi}\left(i\slashed{D}_{c\perp}\frac{1}{in_+D_c}x_\perp^\mu\gamma_\perp^\nu W_c\, g_s F_{\mu\nu}^s W_c^\dagger + x_\perp^\mu\gamma_\perp^\nu W_c\, g_s F_{\mu\nu}^s W_c^\dagger\frac{1}{in_+D_c}i\slashed{D}_{c\perp}\right)\frac{\slashed{n}_+}{2}\xi, \tag{2.65}$$

$$\mathcal{L}_{\xi q}^{(1)} = \bar{q}\, W_c^\dagger i\slashed{D}_{c\perp}\xi - \bar{\xi}\, i\overleftarrow{\slashed{D}}_{c\perp}W_c^\dagger q \tag{2.66}$$

$$\mathcal{L}_{\xi q}^{(2)} = \bar{q}\, W_c^\dagger\left(in_-D + i\slashed{D}_{c\perp}\frac{1}{in_+D_c}i\slashed{D}_{c\perp}\right)\frac{\slashed{n}_+}{2}\xi + \bar{q}\, x_{\perp\mu}\overleftarrow{D}_s W_c^\dagger\, i\slashed{D}_{c\perp}\xi$$

$$- \bar{\xi}\frac{\slashed{n}_+}{2}\left(in_-\overleftarrow{D} + i\overleftarrow{\slashed{D}}_{c\perp}\frac{1}{in_+\overleftarrow{D}_c}i\overleftarrow{\slashed{D}}_{c\perp}\right)W_c\, q - \bar{\xi}\, i\overleftarrow{\slashed{D}}_{c\perp}W_c\, x_{\perp\mu}D_s^\mu\, q, \tag{2.67}$$

$$\mathcal{L}_{\rm YM}^{(1)} = \mathrm{Tr}\left(n_+^\mu F_{\mu\nu_\perp}^c W_c\, i\left[x_\perp^\rho n_-^\sigma F_{\rho\sigma}^s, W_c^\dagger\left[iD_c^{\nu_\perp}W_c\right]\right]W_c^\dagger\right)$$

$$- \mathrm{Tr}\left(n_{+\nu}F_c^{\mu\nu_\perp}W_c\, n_-^\rho F_{\rho\nu_\perp}^s W_c^\dagger\right), \tag{2.68}$$

$$\mathcal{L}_{\rm YM}^{(2)} = \frac{1}{2}\mathrm{Tr}\left(n_+^\mu F_{\mu\nu_\perp}^c W_c\, i\left[n_-x\, n_+^\rho n_-^\sigma\, F_{\rho\sigma}^s + x_\perp^\rho x_{\perp\omega}n_-^\sigma\left[D_s^\omega, F_{\rho\sigma}^s\right], W_c^\dagger\left[iD_c^{\nu_\perp}W_c\right]\right]W_c^\dagger\right)$$

$$- \frac{1}{2}\mathrm{Tr}\left(n_+^\mu F_{\mu\nu_\perp}^c W_c\, i\left[x_\perp^\rho\, F_{\rho\nu_\perp}^s, W_c^\dagger\, in_-D\, W_c\, in_-D_s\right]W_c^\dagger\right)$$

$$+ \mathrm{Tr}\left(F_c^{\mu_\perp\nu_\perp}W_c\, i\left[x_\perp^\rho\, F_{\rho\mu_\perp}^s, W_c^\dagger\left[iD_{c\nu_\perp}W_c\right]\right]W_c^\dagger\right)$$

$$+ \frac{1}{2}\mathrm{Tr}\left(n_+^\mu n_+^\nu F_{\mu\nu}^c W_c n_+^\rho n_+^\sigma F_{\rho\sigma}^s W_c^\dagger\right) - \mathrm{Tr}\left(F_c^{\mu_\perp\nu_\perp}W_c F_{\mu_\perp\nu_\perp}^s W_c^\dagger\right)$$

$$- \mathrm{Tr}\left(n_{+\mu}F_c^{\mu\nu_\perp}W_c n_-^\rho x_{\perp\sigma}\left[D_s^\sigma, F_{\rho\nu_\perp}^s\right]W_c^\perp\right). \tag{2.69}$$

In the above expressions, just as in the leading power Lagrangian, the soft fields are evaluated at position x_-, we do not write this explicitly to avoid cumbersomeness.

We recall that the number in brackets in the superscript of $\mathcal{L}$ denotes the power suppression of the term with respect to the leading power expression. We demonstrate the counting briefly using the power counting of the fields given in equation (2.25) for the collinear fields, and discussed below this equation for the soft fields. The leading power action is $\mathcal{O}(\lambda^0)$, and now we consider the action for the $\mathcal{L}_\xi^{(1)}$ Lagrangian term in (2.63)

$$\int d^4x\, \mathcal{L}_\xi^{(1)} = \int \underbrace{d^4x}_{\sim 1/\lambda^4}\underbrace{\bar{\xi}}_{\sim\lambda}\left(\underbrace{x_\perp^\mu}_{\sim 1/\lambda}n_-^\nu W_c\, g_s\underbrace{F_{\mu\nu}^s}_{\sim\lambda^4}W_c^\dagger\right)\frac{\slashed{n}_+}{2}\underbrace{\xi}_{\sim\lambda} \sim \mathcal{O}(\lambda), \tag{2.70}$$

as required.

The form of this Lagrangian can seem intimidating at first, especially the appearance of explicit position arguments which arise as a consequence of multipole expansion. In momentum space, these give rise to derivatives that act on delta functions which ensure momentum conservation at every vertex in a Feynman diagram. This is not a standard feature in the usual QCD Feynman diagram calculation, and a point which we will return to in section 2.4.2, where we present how these rules can nonetheless be worked out and applied consistently in a calculation.

An important feature of the SCET Lagrangian is that explicit homogenous power counting is manifest in each term, this fact makes the SCET framework ideally suited to deriving all order factorisation theorems.

Another important observation is that there are no purely collinear subleading interactions as every term in equations (2.63) – (2.69) contains a soft field. This remains true even *after* the decoupling transformation is performed as will be shown in section 2.4.3. This feature leads to new physical effects at subleading powers and has profound consequences for the structure of factorisation beyond leading power. This fact we mention now without a proper explanation or example, however, we will return to this discussion in far greater detail in our case study of the factorisation in the Drell-Yan process and Higgs production at threshold in chapters 3 and 9 respectively.

Having written down the Lagrangian up to $\mathcal{O}(\lambda^2)$, we proceed to outline the construction of a complete basis for subleading power N-jet operators as described in [86]. In chapter 3 we specialise to a particular number of jet directions, $N = 2$, for the Drell-Yan process. However, for the purposes of the construction of the N-jet basis we keep the discussion general.

The structure of an N-jet operator is captured by [86]

$$J = \int \left[\prod_{ik} dt_{i_k} \right] C(\{t_{i_k}\}) \, J_s(0) \prod_{i=1}^{N} J_i(t_{i_1}, t_{i_2}...) \tag{2.71}$$

where $C(\{t_{i_k}\})$ is a generalised Wilson coefficient, J_s is a soft operator, and J_i is a product of n_i collinear-gauge-invariant collinear building blocks associated to a particular collinear direction n_{i+}

$$J_i(t_{i_1}, t_{i_2}...) = \prod_{k=1}^{n_i} \psi_{i_k}(t_{i_k} n_{i+}). \tag{2.72}$$

The elementary collinear-gauge-invariant collinear building blocks we have already given above in the context of the leading power discussion in equation (2.49).

As the starting point for the construction, we consider the leading power N-jet operator to which only a single building block contributes in each direction. In the expressions, this means that we take $n_i = 1$ for every direction $i = 1, 2, ...N$. This is labelled by a superscript $A0$, and explicitly, we write

$$J_i^{A0}(t_i) = \psi_i(t_i n_{i+}), \tag{2.73}$$

for every i. We have depicted the leading power N-jet operator in the top-left diagram of figure 2.4.

We proceed to consider the contributions which are suppressed by $\mathcal{O}(\lambda)$. As explained in [86], there are effectively two ways in which power suppression in the N-jet operator can arise up to and including $\mathcal{O}(\lambda^2)$.

The first way is through derivatives, $\partial_{i\perp}$, acting on the building blocks ψ_{i_k}. Up to and including order $\mathcal{O}(\lambda^2)$, the basis is given by

$$
\begin{align}
J_i^{A1}(t_i) &= i\partial_{i\perp}^{\mu} J_i^{A0}(t_i) & \mathcal{O}(\lambda), \tag{2.74}\\
J_i^{A2}(t_i) &= i\partial_{i\perp}^{\mu} i\partial_{i\perp}^{\nu} J_i^{A0}(t_i) & \mathcal{O}(\lambda^2). \tag{2.75}
\end{align}
$$

Within the label "An" in the superscript, A means that there is only one field present in the current, and n gives the order of the power suppression in λ. Such operators are depicted in the top-right and bottom-left diagrams of figure 2.4.

The second way of inducing power suppression in the N-jet operator is by introducing another i-collinear building block in a particular collinear direction, since each building block scales as $\mathcal{O}(\lambda)$. These operators are labelled by J^{Bn}, with the letter B indicating that there are two fields present in one collinear direction. We have the following possibilities at $\mathcal{O}(\lambda)$ [86]

$$
J_i^{B1}(t_{i_1}, t_{i_2}) = \psi_{i_1}(t_{i_1} n_{i+})\psi_{i_2}(t_{i_2} n_{i+}) \in
\begin{cases}
\chi_i(t_{i_1} n_{i+})\chi_i(t_{i_2} n_{i+})\\
\mathcal{A}_{i\perp}^{\mu}(t_{i_1} n_{i+})\chi_i(t_{i_2} n_{i+})\\
\mathcal{A}_{i\perp}^{\mu}(t_{i_1} n_{i+})\mathcal{A}_{i\perp}^{\nu}(t_{i_2} n_{i+})\\
\chi_i(t_{i_1} n_{i+})\bar{\chi}_i(t_{i_2} n_{i+})
\end{cases}
\tag{2.76}
$$

and the conjugate operators. As an illustration, a J^{B1} operator in the i-th direction is present in the bottom-left diagram of figure 2.4, alongside a J^{A1} operator in the j-th direction.

We can also envisage that derivatives acting on the J^{B1} operators will give rise to operators of type J^{B2}, where there is still one extra field present in a particular collinear direction with respect to the leading power, and a $\partial_{i\perp}$ derivative is acting on the building blocks. The possibilities are [86]

$$
J_i^{B2}(t_{i_1}, t_{i_2}) \in
\begin{cases}
\psi_{i_1}(t_{i_1} n_{i+}) i\partial_{i\perp}\psi_{i_2}(t_{i_2} n_{i+})\\
i\partial_{i\perp}\left[\psi_{i_1}(t_{i_1} n_{i+})\psi_{i_2}(t_{i_2} n_{i+})\right]
\end{cases}
\tag{2.77}
$$

where any of the J^{B1} currents can make up the $\psi_{i_1}(t_{i_1} n_{i+})\psi_{i_2}(t_{i_2} n_{i+})$ combination.

At $\mathcal{O}(\lambda^2)$ another type of power suppressed current is possible, namely, one where two extra collinear building blocks are included in a particular direction, on top of the leading power building block. In accordance with the labelling scheme we follow here, the operator of this type is labelled J^{C2} as it is made up by a total three fields in one collinear direction, and it is given by [86]

$$
J_i^{C2}(t_{i_1}, t_{i_2}) = \psi_{i_1}(t_{i_1} n_{i+})\psi_{i_2}(t_{i_2} n_{i+})\psi_{i_3}(t_{i_3} n_{i+}). \tag{2.78}
$$

A J^{C2} operator is depicted to be present in the ith direction in the bottom-right diagram of figure 2.4.

To summarise the above discussion, we have thus far considered two ways of including power suppression in the current operators in a particular collinear direction, that is, through inclusion of derivatives on the building blocks, and the addition of extra building blocks themselves.

As discussed in [86], there exists a third way that power suppression can enter the subleading power operator basis, and that is through appearance of completely new types of operators such as contributions to the pure soft building block, J_s. However, it has been shown in [86] that any new type of collinear building block can be recast in the basis already given above, and the pure soft contributions start at $\mathcal{O}(\lambda^3)$. We refer to the discussion in [86] for more details. Here we only give examples of the pure soft building blocks for concreteness, since the formal factorisation theorem derived in chapter 3 is an all order and all power expression which does contain J_s, but the calculations we perform are at the next-to-leading power, $\mathcal{O}(\lambda^2)$, level. The covariant, pure soft, building blocks which can make up J_s are for example

$$q(x) \sim \mathcal{O}(\lambda^3), \qquad F_s^{\mu\nu}(x) \sim \mathcal{O}(\lambda^4), \qquad iD_s^\mu\, q(x) \sim \mathcal{O}(\lambda^5). \qquad (2.79)$$

Note that the fields retain the full x dependence in the purely soft sector. The covariant derivative, which acts only on soft building blocks, is $iD_s^\mu(x) = i\partial^\mu + g_s A_s^\mu(x)$, and the soft field strength tensor is given by $ig_s F_s^{\mu\nu} = \left[iD_s^\mu, iD_s^\nu\right]$ as in equations (2.33) and (2.34) respectively. Note that in equation (2.71) $J_s(x)$ appears with the argument $x = 0$ on the grounds that when the purely soft building block appears in a product with operators in N collinear directions, the multipole expansion must be carried out in each of the collinear directions effectively requiring that $x = 0$ in $J_s(x)$.

This concludes the discussion of how power suppression can be included in each leg of an N-jet scattering process. It is then easy to see how the total power suppression for the N-jet operator in (2.71) is obtained. One simply has to sum all the possible combinations which give rise to power suppression. For example, at $\mathcal{O}(\lambda^2)$ the power suppression could be induced by a J^{A2}, J^{B2}, or J^{C2} operator on a single leg, with $N-1$ directions remaining at leading power, or by two J^{A1} or J^{B1} operators on two separate i-collinear legs and $N-2$ directions kept at leading power. One could also consider a mixture of J^{A1} and J^{B1} currents on two separate legs. We show these examples in several panels of figure 2.4. Such an investigation is systematically performed in chapter 3 for the Drell-Yan process up to $\mathcal{O}(\lambda^2)$.

These considerations do not yet yield a full picture regarding N-jet operator basis in SCET. We continue to follow the framework introduced in [86] and adopt the interaction picture. This means that it is understood that all operator matrix elements are evaluated with the leading-power SCET Hamiltonian and that we treat the subleading SCET Lagrangian insertions as perturbations. The basis of subleading power N-jet operators then contains further operators which are "non-local" and are built from time-ordered products of the current operators J defined above with terms from the subleading SCET Lagrangian, given here in equations (2.63) – (2.69). At $\mathcal{O}(\lambda)$ these time-ordered product operators take the following form

$$J_i^{T1}(t_i) = i \int d^d x\, T\left\{ J_i^{A0}(t_i)\, \mathcal{L}_i^{(1)}(x) \right\}, \qquad (2.80)$$
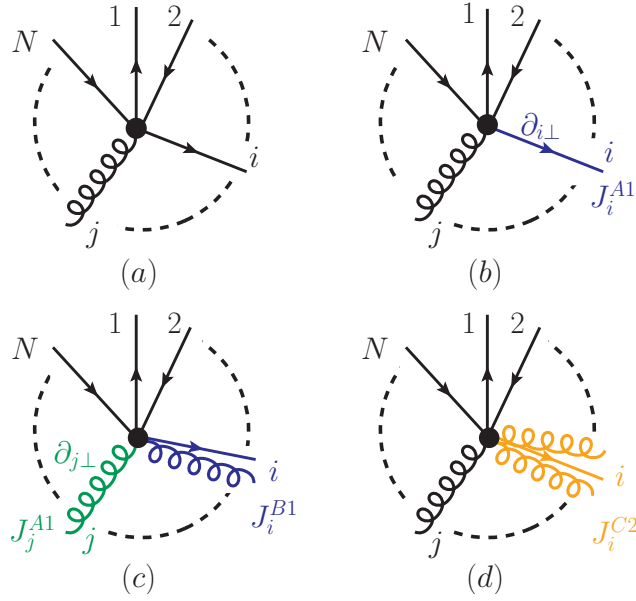
Figure 2.4:   *Sample contributions to the N-jet scattering process. In panel (a) we have schemat-
ically drawn a leading power N-jet operator with one collinear field present in each
of the N collinear directions. Panels (b), (c), and (d) show possible power correc-
tions to the leading power process in (a). We have coloured the collinear sectors
which receive power corrections. Panel (b) contains $\mathcal{O}(\lambda)$ contribution where the
power suppression is provided by a $\partial_\perp$ derivative acting on the fermion field in the
i-th collinear direction. The remaining legs are kept at leading power. Panels (c)
and (d) show an overall λ^2 suppressed N-jet operator. In panel (c), the $\mathcal{O}(\lambda^2)$
suppression comes from two different collinear sectors, i and j in this example.
The $\mathcal{O}(\lambda)$ power suppression in the i-th collinear sector is provided by the presence
of an additional field in that direction and the power suppression of the same order
is provided in the j-th collinear sector by a $\partial_\perp$ derivative. In panel (d), the $\mathcal{O}(\lambda^2)$
suppression originates in the i-th sector with two additional collinear fields present,
with respect to the leading power case. Many more other possible combinations
exist.*

where $\mathcal{L}_i^{(1)}(x)$ are terms of the subleading power Lagrangian in the relevant collinear
sector $\mathcal{L}_i^{(1)}(x) = \mathcal{L}_{i\xi}^{(1)}(x) + \mathcal{L}_{i\xi q}^{(1)}(x) + \mathcal{L}_{i\mathrm{YM}}^{(1)}(x)$ given in equations (2.63), (2.66), and (2.68)
respectively. At higher powers, the basis includes single and multiple higher-power
Lagrangian insertions $\mathcal{L}^{(n)}$ in time-ordered products with power-suppressed currents, such
as J_i^{A1}, J_i^{B1}, J_i^{A2} and so on, as well as the leading power J^{A0} current. We stress here that
the time-ordered product operators do contain soft fields, through the subleading power
Lagrangian terms. This is in stark contrast to the operators of the A, B, $C \ldots$ - type,
which, as discussed above, contain only the derivatives on collinear building blocks or
additional building blocks in any particular direction.

2.4.2 Feynman rules

Explicit calculation of the NLP collinear functions at one-loop order, carried out in chapter 4, is one of the main new contributions of the work presented here. For this reason, and since the next-to-leading power SCET Feynman rules are more involved than QCD Feynman rules, we now discuss how they are derived and how they can be used in calculations. We also give explicitly the subleading SCET Feynman rules which are extensively used in this work. For a full set of Feynman rules up to $\mathcal{O}(\lambda^2)$ we point to appendix A of [87].

To avoid unnecessary clutter in the expressions, we now focus on one collinear sector and set $n_{i\pm}^\mu \to n_\pm^\mu$. As stated above, we work in the interaction picture where the subleading SCET Lagrangian terms are used as perturbations. To find the Feynman rules we consider the interaction part of the action, in particular, for the purpose of this example, we concentrate on the first term in $\mathcal{L}_\xi^{(2)}$ in equation (2.65) which we name $\mathcal{L}_{\xi,\mathrm{I}}^{(2)}$:

$$\mathcal{L}_{\xi,\mathrm{I}}^{(2)} = \frac{1}{2}\bar{\xi}\left((n_-x)n_+^\rho n_-^\nu W_c\, g_s F_{\rho\nu}^s W_c^\dagger\right)\frac{\slashed{n}_+}{2}\xi\,. \tag{2.81}$$

The matrix element of this Lagrangian term with an incoming quark and soft gluon, and an outgoing quark, carrying momenta p, k, and p' respectively, is given by

$$\langle\bar{q}(p')|i\int d^dx\, \mathcal{L}_{\xi,\mathrm{I}}^{(2)}(x)|q(p)\, g^A(k)\rangle = \langle\bar{q}(p')|i\int d^dx\, \frac{1}{2}\bar{\xi}(x)\left((n_-x)n_+^\rho n_-^\nu W_c\, g_s F_{\rho\nu}^s W_c^\dagger\right)$$
$$\times\frac{\slashed{n}_+}{2}\xi(x)|q(p)\, g^A(k)\rangle, \tag{2.82}$$

where A is the adjoint colour index of the soft gluon.

Using standard mode decomposition and taking the derivatives which appear in the soft field strength tensor gives the following expression

$$\langle\bar{q}(p')|i\int d^dx\, \mathcal{L}_{\xi,\mathrm{I}}^{(2)}(x)|q(p)\, g^A(k)\rangle = \frac{1}{2}\bar{v}(p')i\int d^dx\,(n_-x)n_+^\rho n_-^\nu\left(-ik_\rho\epsilon_\nu(k)+ik_\nu\epsilon_\rho(k)\right)$$
$$\times\frac{\slashed{n}_+}{2}\, g_s\mathrm{T}^A\, u(p)e^{ip'\cdot x}e^{-ip\cdot x}e^{-ik\cdot x_-}, \tag{2.83}$$

where we have set the (conjugate)collinear Wilson lines, $W_c(W_c^\dagger)$, to unity, and we suppress spin and fundamental colour indices. We stress that here, since we consider subleading power terms of the SCET Lagrangian, due to multipole expansion the derivatives acting on the soft fields here are performed before the position is set to $x^\mu = x_-^\mu$, where $x_-^\mu = (n_+x)\, n_-^\mu/2$. Only after the derivative acting on the soft field A_s is performed, can x^μ be set to x_-^μ as we have done in the argument of the exponential $e^{-ik\cdot x_-}$. Therefore, the n_+k component of the soft momentum survives in the numerator of equation (2.83), although it is not conserved in the momentum-conserving delta function which we show below.

In the standard derivation of Feynman rules, the next step after reaching the analogue of (2.83) would be to perform the d-dimensional integral over the position of the interaction vertex which yields the momentum conserving delta function. At subleading powers, as in (2.83), this step cannot be directly performed due to (n_-x) component appearing in

the expression. We first replace this term with a derivative with respect to the incoming momentum p acting on $e^{-ip\cdot x}$, $(n_- x)e^{-ip\cdot x} = in_-^\mu \frac{\partial}{\partial p_\mu} e^{-ip\cdot x}$. Then the $\int d^d x$ integral can be performed and we obtain

$$\langle \bar{q}(p')|i \int d^d x \, \mathcal{L}^{(2)}_{\xi,\mathrm{I}}(x)|q(p)\, g^A(k)\rangle \;=\; \frac{1}{2} ig_s \mathrm{T}^A \, \bar{v} \, (n_- Z) n_+^\rho n_-^\nu \Big(k_\rho \epsilon_\nu - k_\nu \epsilon_\rho\Big) \frac{\displaystyle{\not{n}}_+}{2}\, u. \tag{2.84}$$

On the right-hand side $\bar{v} \equiv \bar{v}(p')$, $u \equiv u(p)$, $\epsilon_{\nu(\rho)} \equiv \epsilon_{\nu(\rho)}(k)$, and

$$Z^\mu = \frac{\partial}{\partial p_\mu} (2\pi)^d \, \delta^{(d)}\Big(p + k_+ - p'\Big), \tag{2.85}$$

where $k_+^\mu = (n_- k)\, n_+^\mu / 2$ in the argument of the delta function. Finally, in the last step, to obtain the Feynman rule for this power suppressed interaction we strip off the polarisation vector and the spinors. The result, along with the Feynman rules for the remaining terms in $\mathcal{L}^{(2)}_\xi(x)$, will be given shortly. We first remark two important features of the above result.

First, perhaps the most non-standard feature, is the derivative in (2.85) which acts on the momentum conserving delta function. Because of this fact, momentum conservation cannot be naively imposed at the subleading power interaction vertices in Feynman diagrams. In practice, in a Feynman diagram calculation, the above result means that we first have to integrate by parts, such that this derivative acts on the rest of the expression, and only after this derivative is evaluated can the momentum conservation at the subleading power vertex be imposed using the delta function in (2.85). Standard Feynman rules often have the momentum conserving delta function stripped off, as it is implied that momentum is conserved at every vertex, and this is often implemented as soon as one draws the Feynman diagram. Here, the momentum conserving delta function remains in the Feynman rules explicitly and it has to be dealt with carefully as will be shown in chapter 4 in a concrete calculation. For example, see the discussion between equations (4.31) and (4.33).

The second crucial feature that we point out is already present at leading power, however, it is nonetheless important from the point of view of constructing a consistent effective field theory framework. It is namely the fact it is only the $(n_- k)$ component of the soft momentum which enters the momentum conserving delta function, as can be seen in (2.85). This is a consequence of multipole expansion which guarantees homogeneous power counting. This component is of the same order as the small component of the collinear momentum, $\mathcal{O}(\lambda^2)$, hence it remains after the multipole expansion is performed. This is in contrast to $n_+ k$ and $k_\perp$ components of the soft momentum which are power suppressed with respect to the corresponding components of the collinear momentum in $\mathrm{SCET_I}$ as explained below equation (2.4) and which therefore do not enter the momentum conserving delta function. To illustrate this point explicitly, consider a Feynman graph where there is a collinear quark propagator attached to the above soft-collinear interaction. Due to the interaction, soft momentum is injected into the collinear propagator (given below in equation (2.87)), however only the k_+^μ component survives[3]

$$\int \frac{d^d p}{(2\pi)^d} \frac{i(n_+ p)}{p^2} \frac{\displaystyle{\not{n}}_-}{2}(2\pi)^d \, \delta^{(d)}\Big(p + k_+ - p'\Big) = \frac{i(n_+ p')}{(p' - k_+)^2} \frac{\displaystyle{\not{n}}_-}{2}. \tag{2.86}$$

---

[3]We take a simple example where the derivative described in detail above is taken to be acting on another part of the amplitude and not on the nearest propagator which we write here.

We stress that this does *not* mean that we set (n_+k) component to zero in the Feynman rule for the subleading soft-collinear interaction like the one which we have derived above in (2.84), the soft momentum appearing there keeps all the components as explained above. Similarly to the previous remark, for an explicit example we direct the reader to chapter 4 and specifically the expression in equation (4.33).

We have now presented a detailed example of next-to-leading power Feynman rule derivation. Moreover, having discussed its important features, which are also more generally present at subleading powers, we now for ease of access and completeness give most relevant Feynman rules for the work presented here. In line with our presentation thus far, we continue to focus on one collinear direction, however of course the form of these Feynman rules is the same in each collinear sector.

We begin with writing down the collinear quark propagator which takes the following form

$$\frac{i(n_+p)}{p^2 + i\delta}\frac{\slashed{n}_-}{2}. \tag{2.87}$$

The collinear gluon propagator on the other hand takes the standard form. In Feynman gauge it is given by $-ig_{\mu\nu}/(p^2 + i\delta)$. Similarly, the soft quark propagator also takes the standard form: $i\slashed{k}/(k^2 + i\delta)$.

For the introduction of the subleading power SCET Feynman rules, it is also necessary to generalise Z which is given in (2.85) for the specific case we considered. We now change the label to X in accordance with [87] and define the following structures

$$X^\mu = \partial^\mu\left[(2\pi)^d\delta^{(d)}\left(\sum p_{\text{in}} - \sum p_{\text{out}}\right)\right], \tag{2.88}$$

$$X^\mu X^\nu = \partial^\mu\partial^\nu\left[(2\pi)^d\delta^{(d)}\left(\sum p_{\text{in}} - \sum p_{\text{out}}\right)\right], \tag{2.89}$$

where the partial derivative $\partial^\mu = \partial/\partial p_{\text{in}\mu}$ if the derivative acts on any of the incoming momenta (this can be freely chosen), or $\partial^\mu = -\partial/\partial p_{\text{out}\mu}$ if the derivative instead acts on any of the outgoing momenta.

The collinear-quark soft-gluon interaction vertex is given by

$$ig_s\mathbf{T}^a \begin{cases} \dfrac{\slashed{n}_+}{2}n_{-\mu} & \mathcal{O}(\lambda^0) \\[2mm] \dfrac{\slashed{n}_+}{2}X_\perp^\rho n_-^\nu(k_\rho g_{\nu\mu} - k_\nu g_{\rho\mu}) & \mathcal{O}(\lambda) \\[2mm] S^{\rho\nu}(k,p,p')\dfrac{\slashed{n}_+}{2}(k_\rho g_{\nu\mu} - k_\nu g_{\rho\mu}) & \mathcal{O}(\lambda^2) \end{cases} \tag{2.90}$$

where
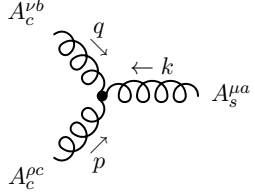
$$S^{\rho\nu}(k,p,p') \equiv \frac{1}{2}\left[\underbrace{(n_-X)n_+^\rho n_-^\nu}_{\text{I}} + \underbrace{(kX_\perp)X_\perp^\rho n_-^\nu}_{\text{II}} + \underbrace{X_\perp^\rho\left(\frac{\slashed{p}_\perp'}{n_+p'}\gamma_\perp^\nu + \gamma_\perp^\nu\frac{\slashed{p}_\perp}{n_+p}\right)}_{\text{III}}\right]. \tag{2.91}$$

We note that, as the underlying low-energy physics dictates, the very first term in (2.90), $\mathcal{O}(\lambda^0)$, is simply the eikonal vertex. The eikonal soft-collinear coupling is explicit in the leading power SCET Lagrangian (2.35).

The Feynman rule for the $\mathcal{O}(\lambda)$ suppressed soft-collinear interaction derives from the Lagrangian term $\mathcal{L}_\xi^{(1)}$ given in (2.63).

The three terms of $S^{\rho\nu}(k, p, p')$ in equation (2.91) of the $\mathcal{O}(\lambda^2)$ vertex in the last entry of (2.90) correspond directly to the three terms in the power-suppressed SCET Lagrangian written down in (2.64),(2.65) (originally given in equation (28) of [73]). We have underbraced the three contributions and labelled them with Roman numerals, I, II, and III, in light of the discussion presented in chapter 4. The first Feynman rule labelled by I is due to the first Lagrangian term in (2.64), (2.65), which we call $\mathcal{L}_{\xi,\mathrm{I}}^{(2)}$ (as defined in (2.81)). Analogously the second and third Feynman rules come from $\mathcal{L}_{\xi,\mathrm{II}}^{(2)}$ and $\mathcal{L}_{\xi,\mathrm{III}}^{(2)}$ respectively. We also see that we have agreement for the Feynman rule given by the Lagrangian term $\mathcal{L}_{\xi,\mathrm{I}}^{(2)}$, which we have derived with identical conventions for incoming and outgoing partons in (2.84) and which is given here in the first term, I, in equation (2.91).

For the purposes of the calculations performed in chapter 4 we find it useful to also present explicitly the collinear-soft three-gluon interaction vertex. In equation (A.45) of [87] we find

$$
\frac{1}{2} g_s f^{abc} \begin{cases} V_{\mu\nu\rho}^{(0)}(k, q, p) & \mathcal{O}(\lambda^0) \\ V_{\mu\nu\rho}^{(1)}(k, q, p) & \mathcal{O}(\lambda) \\ \sum_{i=1}^{6} V_{\mu\nu\rho}^{(2),i}(k, q, p) & \mathcal{O}(\lambda^2) \end{cases}
\tag{2.92}
$$

where, in the Feynman gauge, the leading power interaction is given by

$$
V_{\mu\nu\rho}^{(0)}(k, q, p) \equiv -2g_{\nu\rho}(n_+ p)\, n_{-\mu} \, .
\tag{2.93}
$$

The interaction at $\mathcal{O}(\lambda)$ is given by

$$
V_{\mu\nu\rho}^{(1)}(k, q, p) \equiv V_{\nu\rho}^{(1),\lambda_\perp}(q, p) f_{\mu\lambda_\perp}^-(k) \, ,
\tag{2.94}
$$

where

$$
f_\mu^{\pm\nu_\perp}(k) = n_\pm^\kappa g_\perp^{\nu\sigma}(k_\kappa g_{\mu\sigma} - g_{\mu\kappa} k_\sigma) \, ,
\tag{2.95}
$$

and

$$
V_{\nu\rho}^{(1),\lambda_\perp}(q, p) \equiv f_\nu^{+\sigma_\perp}(q) f_{\rho\sigma_\perp}^+(p) \left(\frac{1}{n_+ q} - \frac{1}{n_+ p} \right) X_\perp^\lambda + H_{\nu\rho}^{+\lambda_\perp}(q, p) \, .
\tag{2.96}
$$

The $H_{\nu\rho}^{+\lambda_\perp}(q, p)$ term in (2.96) is given by

$$
H_{\nu\rho}^{+\lambda_\perp}(q, p) \equiv f_\nu^{+\lambda_\perp}(q) \frac{n_{+\rho}}{n_+ p} - f_\rho^{+\lambda_\perp}(p) \frac{n_{+\nu}}{n_+ q} - n_+^\sigma (g_{\sigma\nu} g_{\kappa\rho} - g_{\sigma\rho} g_{\kappa\nu}) g_\perp^{\kappa\lambda} \, .
\tag{2.97}
$$

The two terms on the right-hand side of equation (2.96) originate from the two terms of $\mathcal{L}_{\mathrm{YM}}^{(1)}$ given in equation (2.68).

The interaction at $\mathcal{O}(\lambda^2)$ is most involved. It is made up of the following six contributions

$$
V_{\mu\nu\rho}^{(2),1}(k, q, p) \equiv V_{\nu\rho}^{(2),1}(q, p) \left(-n_- X f_\mu^{+-}(k) + k X_\perp X_\perp^\lambda f_{\mu\lambda_\perp}^-(k) \right) \, ,
$$

$$
\begin{aligned}
V^{(2),2+3}_{\mu\nu\rho}(k,q,p) &\equiv V^{(2),2+3,\lambda_\perp}_{\nu\rho}(q,p)X^\kappa_\perp f_{\mu\kappa_\perp\lambda_\perp}(k)\,, \\
V^{(2),4}_{\mu\nu\rho}(k,q,p) &\equiv V^{(2),4}_{\nu\rho}(q,p)f^{+-}_\mu(k)\,, \\
V^{(2),5}_{\mu\nu\rho}(k,q,p) &\equiv V^{(2),5,\lambda_\perp\sigma_\perp}_{\nu\rho}(q,p)f_{\mu\lambda_\perp\sigma_\perp}(k)\,, \\
V^{(2),6}_{\mu\nu\rho}(k,q,p) &\equiv V^{(2),6,\lambda_\perp}_{\nu\rho}(q,p)kX_\perp f^{-}_{\mu\lambda_\perp}(k)\,,
\end{aligned}
\tag{2.98}
$$

These six vertex factors correspond directly to the six terms of the $\mathcal{L}^{(2)}_{\mathrm{YM}}$ Lagrangian which we write in equation (2.69). The number of the precise term to which each Feynman rule corresponds to is indicated in the superscript. The $f^{+-}_\mu(k)$ and $f^{\rho_\perp\nu_\perp}_\mu(k)$ terms are defined as

$$
f^{+-}_\mu(k) = n^\kappa_+ n^\sigma_- (k_\kappa g_{\mu\sigma} - g_{\mu\kappa}k_\sigma) = (n_+ k)n_{-\mu} - (n_- k)n_{+\mu}\,, \tag{2.99}
$$

$$
f^{\rho_\perp\nu_\perp}_\mu(k) = g^{\rho\kappa}_\perp g^{\nu\sigma}_\perp (k_\kappa g_{\mu\sigma} - g_{\mu\kappa}k_\sigma) = k^\rho_\perp \delta^\nu_{\perp\mu} - k^\nu_\perp \delta^\rho_{\perp\mu}, \tag{2.100}
$$

respectively, and the coefficients on the right-hand sides of the Feynman rules in (2.98) are given by

$$
\begin{aligned}
V^{(2),1}_{\nu\rho}(q,p) &\equiv \frac{1}{2}f^{+\sigma_\perp}_\nu(q)f^+_{\rho\sigma_\perp}(p)\left(\frac{1}{n_+ q} - \frac{1}{n_+ p}\right) \\
V^{(2),2+3,\lambda_\perp}_{\nu\rho}(q,p) &\equiv (q-p)^\lambda_\perp g_{\nu\rho} + \frac{pq}{n_+ p}(n_{+\rho}\delta^\lambda_{\perp\nu} + n_{+\nu}\delta^\lambda_{\perp\rho}) - q_\rho\delta^\lambda_{\perp\nu} + p_\nu\delta^\lambda_{\perp\rho} \\
&\quad - \frac{q^\lambda_\perp p_\nu n_{+\rho} + p^\lambda_\perp q_\rho n_{+\nu}}{n_+ p}\,, \\
V^{(2),4}_{\nu\rho}(q,p) &\equiv \frac{1}{2}\frac{n_{+\nu}n_{+\rho}}{n_+ p}\,n_-(p+q)\,, \\
V^{(2),5,\lambda_\perp\sigma_\perp}_{\nu\rho}(q,p) &\equiv \left(p^\lambda_\perp \frac{n_{+\nu}\delta^\sigma_{\perp\rho} - n_{+\rho}\delta^\sigma_{\perp\nu}}{n_+ p} + \delta^\lambda_{\perp\rho}\delta^\sigma_{\perp\nu}\right) - (\lambda \leftrightarrow \sigma)\,, \\
V^{(2),6,\lambda_\perp}_{\nu\rho}(q,p) &\equiv -\frac{n_{+\nu}n_{+\rho}}{n_+ p}(p+q)^\lambda_\perp\,.
\end{aligned}
\tag{2.101}
$$

It should be noted that in the derivation of the above contributions, except for the first line, $n_+(p+q) = 0$ has been used. Moreover, for terms without $X_\perp$, $(p+q)_\perp = 0$ has been used in simplifications of the Feynman rules.

2.4.3 Decoupling transformation

We have seen how a priori in the leading power Lagrangian soft-collinear interactions are present and give rise to eikonal vertices. We have also seen how an application of a field redefinition, the decoupling transformation, separates the soft and collinear sectors completely at leading power, this is detailed in section 2.3.2. Although the structure of the soft fields in the subleading Lagrangian terms in equations (2.63) - (2.69) is more complicated, one might wonder whether a similar feat could be achieved for these terms. As we will now show through the explicit application of the decoupling transformation this is not the case [75, 40, 54].

To illustrate the fact that soft-collinear interactions persist at subleading powers even after the decoupling transformation is performed, we begin with the lowest order, $\mathcal{O}(\lambda)$,

power suppressed term in the quark Lagrangian, $\mathcal{L}_\xi^{(1)}$, given in (2.63). For convenience we write $\mathcal{L}_\xi^{(1)}$ again here

$$\mathcal{L}_\xi^{(1)} = \bar{\xi}\left(x_\perp^\mu n_-^\nu W_c\, g_s F_{\mu\nu}^s W_c^\dagger\right)\frac{\not{n}_+}{2}\xi = \bar{\chi}\left(x_\perp^\mu n_-^\nu\, g_s F_{\mu\nu}^s\right)\frac{\not{n}_+}{2}\chi, \qquad (2.102)$$

where in the second step we have used (2.49) to write the collinear fields in terms of the collinear-gauge-invariant collinear building blocks. Now performing the decoupling transformation as defined in (2.60) yields the following result

$$\mathcal{L}_\xi^{(1)} = \bar{\chi}^{(0)}\, x_\perp^\mu n_-^\nu\, g_s Y_+^\dagger F_{\mu\nu}^s Y_+ \frac{\not{n}_+}{2}\chi^{(0)}. \qquad (2.103)$$

Note that in this section we keep the (0) superscript on the decoupled fields to emphasise that the field redefinition has been applied. We now define $F_{\mu\nu}^+ = Y_+^\dagger F_{\mu\nu}^s Y_+$ and make use of the following relation

$$ig_s n_-^\nu F_{\mu\nu}^+ = \left[-in_-\partial\mathcal{B}_\mu^+\right], \qquad (2.104)$$

where on the right-hand side the square brackets remind that the $n_-\partial$ derivative acts only on the introduced soft gluon building block, $\mathcal{B}^+$, which is built from a soft covariant derivative and soft Wilson lines. In fact, in what follows we will use two sets of soft gluon and soft quark building blocks which are defined as

$$\mathcal{B}_\pm^\mu = Y_\pm^\dagger\left[i\, D_s^\mu\, Y_\pm\right], \qquad (2.105)$$
$$q^\pm = Y_\pm^\dagger q_s. \qquad (2.106)$$

Using the above relations, the $\mathcal{L}_\xi^{(1)}$ Lagrangian term in (2.103) becomes

$$\mathcal{L}_\xi^{(1)} = \bar{\chi}^{(0)}\, ix_\perp^\mu\left[in_-\partial\mathcal{B}_\mu^+\right]\frac{\not{n}_+}{2}\chi^{(0)}. \qquad (2.107)$$

We recall that, as in the Lagrangian given above in equation (2.62), the soft field is evaluated at the multipole-expanded position, x_-^μ. In this result, we draw attention to the fact that the collinear fields present here are *decoupled*. We see that even after the decoupling transformation is performed, soft-collinear interactions persist at subleading power. The vast implications of this observation for the description of physical processes at subleading powers will be explored in detail in chapter 3.

Following the above considerations leads to the same results at further subleading powers. For example, we focus again on the $\mathcal{L}_{\xi,\mathrm{I}}^{(2)}$ term found in (2.81), which we have used in the explicit Feynman rule derivation in the previous subsection. By analogy with $\mathcal{L}_\xi^{(1)}$ in (2.102) we can simply write down the result since the field content of both terms is identical. Explicitly we have

$$\mathcal{L}_{\xi,\mathrm{I}}^{(2)} = \frac{1}{2}\bar{\xi}(n_-x)n_+^\rho n_-^\nu W_c g_s F_{\rho\nu}^s W_c^\dagger\frac{\not{n}_+}{2}\xi = \frac{1}{2}\bar{\chi}^{(0)}(in_-x)n_+^\rho\left[in_-\partial\mathcal{B}_\rho^+\right]\frac{\not{n}_+}{2}\chi^{(0)} = \mathcal{L}_{1\xi}^{(2)}. \quad (2.108)$$

In the last step we introduce notation from [40], which we will often use to refer to the decoupled Lagrangian. The manipulations become more cumbersome for the remaining

terms in the subleading power SCET Lagrangian. The $\mathcal{L}_{\xi,\mathrm{II}}^{(2)}$ Lagrangian term splits into two parts in the decoupled basis $\mathcal{L}_{\xi,\mathrm{II}}^{(2)} = \mathcal{L}_{2\xi}^{(2)} + \mathcal{L}_{3\xi}^{(2)}$ which are given by

$$\mathcal{L}_{2\xi}^{(2)} = \frac{1}{2}\bar{\chi}_c^{(0)} x_\perp^\mu x_\perp^\nu \left[i\partial_\nu in_-\partial \mathcal{B}_\mu^+ \right] \frac{\slashed{n}_+}{2}\chi_c^{(0)}, \tag{2.109}$$

$$\mathcal{L}_{3\xi}^{(2)} = \frac{1}{2}\bar{\chi}_c^{(0)} x_\perp^\mu x_\perp^\nu \left[\mathcal{B}_\nu^+, in_-\partial \mathcal{B}_\mu^+ \right] \frac{\slashed{n}_+}{2}\chi_c^{(0)}, \tag{2.110}$$

Similarly, $\mathcal{L}_{\xi,\mathrm{III}}^{(2)}$ Lagrangian term splits into $\mathcal{L}_{\xi,\mathrm{III}}^{(2)} = \mathcal{L}_{4\xi}^{(2)} + \mathcal{L}_{5\xi}^{(2)}$ which are given by

$$\mathcal{L}_{4\xi}^{(2)} = \frac{1}{2}\bar{\chi}_c^{(0)} \left(i\slashed{\partial}_\perp + \mathcal{A}_{c\perp}^{(0)} \right) \frac{1}{in_+\partial} ix_\perp^\mu \gamma_\perp^\nu \left[i\partial_\nu \mathcal{B}_\mu^+ - i\partial_\mu \mathcal{B}_\nu^+ \right] \frac{\slashed{n}_+}{2}\chi_c^{(0)} + \text{h.c.}, \tag{2.111}$$

$$\mathcal{L}_{5\xi}^{(2)} = \frac{1}{2}\bar{\chi}_c^{(0)} \left(i\slashed{\partial}_\perp + \mathcal{A}_{c\perp}^{(0)} \right) \frac{1}{in_+\partial} ix_\perp^\mu \gamma_\perp^\nu \left[\mathcal{B}_\nu^+, \mathcal{B}_\mu^+ \right] \frac{\slashed{n}_+}{2}\chi_c^{(0)} + \text{h.c.}, \tag{2.112}$$

The $\mathcal{A}_{c\perp}^{(0)}$ is the decoupled collinear-gluon field. For completeness we also write down here the terms of the fermion Lagrangian which contains the soft quark. After the decoupling transformation these terms are given by

$$\mathcal{L}_{\xi q}^{(1)} = \bar{q}_+ \mathcal{A}_{c\perp}^{(0)} \chi_c^{(0)} + \text{h.c.}, \tag{2.113}$$

$$\mathcal{L}_{\xi q}^{(2)} = \bar{q}_+ \left[in_-\partial + n_-\mathcal{A}_c^{(0)} + \left(i\slashed{\partial}_\perp + \mathcal{A}_{c\perp}^{(0)} \right) \frac{1}{in_+\partial} \left(i\slashed{\partial}_\perp + \mathcal{A}_{c\perp}^{(0)} \right) \right] \frac{\slashed{n}_+}{2}\chi_c^{(0)}$$

$$+ \bar{q}_+ \left(i\overleftarrow{\partial}^\mu + \mathcal{B}_+^\mu \right) x_{\perp\mu} \left(i\slashed{\partial}_\perp + \mathcal{A}_{c\perp}^{(0)} \right) \chi_c^{(0)} + \text{h.c.} \,. \tag{2.114}$$

In what follows, the (0) superscripts will not be made explicit to keep the notation as light as possible. The Yang-Mills Lagrangian in the decoupled basis is provided in appendix A.1.

2.4.4 Matching beyond leading power

The formal N-jet operator basis we have described above in section 2.4.1. In this subsection, we find it instructive to illustrate features of the matching procedure beyond leading power using the example of hard matching of the vector current which we have considered at leading power and given the results for, up to $\mathcal{O}(\alpha_s)$, in section 2.3.3. We write down the possible basis of operators following the formal discussion above, and explicitly perform tree-level matching in momentum space for the subleading SCET currents at $\mathcal{O}(\lambda)$. In this example we focus on $\mathcal{O}(\lambda)$ contributions as the size of the basis of subleading operators remains manageable and suitable for an introductory discussion.

As in section 2.3.3, we restrict the discussion to only two collinear directions which are back-to-back. In a general setting, the total power suppression of an N-jet operator is given by summation of the power suppression in each i-collinear sector. At $\mathcal{O}(\lambda)$, the power suppression can arise in one sector only, with the second sector remaining at leading power. Moreover, the only two possible types of power suppressed building blocks are J_i^{A1} and J_i^{B1} given in equations (2.74) and (2.76) respectively. The hard matching of the vector current at $\mathcal{O}(\lambda)$ is given by

$$\bar{\psi}\gamma_\rho\psi(0)|_{\mathcal{O}(\lambda)} = \int dt d\bar{t}\, \tilde{C}^{A0,A1}(t,\bar{t})\, J_\rho^{A0,A1}(t,\bar{t}) + \int dt_1 dt_2 d\bar{t}\, \tilde{C}^{A0,B1}(t_1,t_2,\bar{t})\, J_\rho^{A0,B1}(t_1,t_2,\bar{t})$$

$$+ \int dt\, d\bar{t}\, \tilde{C}^{A1,A0}(t,\bar{t})\, J_\rho^{A1,A0}(t,\bar{t}) + \int dt\, d\bar{t}_1 d\bar{t}_2\, \tilde{C}^{B1,A0}(t,\bar{t}_1,\bar{t}_2)\, J_\rho^{B1,A0}(t,\bar{t}_1,\bar{t}_2)$$
$$+ c \leftrightarrow \bar{c}, \tag{2.115}$$

where

$$J_\rho^{A0,A1}(t,\bar{t}) = \bar{\chi}_{\bar{c}}(\bar{t}n_-)\, \Gamma_{\rho\,\mu}^{A0,A1}\, i\partial_\perp^\mu \chi_c(tn_+), \tag{2.116}$$

$$J_\rho^{A0,B1}(t_1,t_2,\bar{t}) = \bar{\chi}_{\bar{c}}(\bar{t}n_-)\, \Gamma_{\rho\,\mu}^{A0,B1}\, \mathcal{A}_{c\perp}^\mu(t_2 n_+)\chi_c(t_1 n_+), \tag{2.117}$$

$$J_\rho^{A1,A0}(t,\bar{t}) = \bar{\chi}_{\bar{c}}(\bar{t}n_-)\, i\overleftarrow{\partial}^\mu{}_\perp\, \Gamma_{\rho\,\mu}^{A1,A0}\, \chi_c(tn_+), \tag{2.118}$$

$$J_\rho^{B1,A0}(t,\bar{t}_1,\bar{t}_2) = \bar{\chi}_{\bar{c}}(\bar{t}_1 n_-)\, \mathcal{A}_{\bar{c}\perp}^\mu(t_2 n_-)\Gamma_{\rho\,\mu}^{B1,A0}\, \chi_c(t_1 n_+). \tag{2.119}$$

We see that placing power suppression in the anticollinear sector takes the same form as in the collinear one, hence without loss of generality we next focus on the case where the power suppression arises in the collinear sector. The purpose of the current discussion is two-fold. Firstly, we discuss the possible spinor and Lorentz structure which can make up the $\Gamma_{\rho\,\mu}^{A0,A1}$ and $\Gamma_{\rho\,\mu}^{A0,B1}$ structures. Secondly we compute tree-level matching coefficients $C^{A0,A1}$ and $C^{A0,B1}$ in momentum space. In general, the Fourier transform of the hard matching Wilson coefficients is given by

$$\tilde{C}\left(\{t_k\},\{\bar{t}_{\bar{k}}\}\right) = \int \left\{\frac{dn_+ p_k}{2\pi}\right\} \left\{\frac{dn_- \bar{p}_{\bar{k}}}{2\pi}\right\}\, e^{i\,(n_+ p_k)\,t_k} e^{i\,(n_- \bar{p}_{\bar{k}})\,\bar{t}_{\bar{k}}}\, C(\{n_+ p_k\},\{n_- \bar{p}_{\bar{k}}\}), \tag{2.120}$$

where we have suppressed the superscript labels and we see that for this example the sets are either $\{t_k\} = \{t\}$ for the J_c^{A1} current, or $\{t_k\} = \{t_1,t_2\}$ for the J_c^{B1} and we always keep $\{\bar{t}_{\bar{k}}\} = \{\bar{t}\}$. In the exponents we use Einstein's summation convention. As noted in section 2.3.3, the unbarred positions and momenta refer to the collinear direction, and the barred to the anticollinear.

The structures which could make up $\Gamma_{\rho\,\mu}^{A0,A1}$ and $\Gamma_{\rho\,\mu}^{A0,B1}$ are constrained by symmetries of QCD, since we know that helicity and chirality must be preserved. This for example excludes the γ_5, $\gamma_{\perp\rho}\gamma_{\perp\mu}$, and $\sigma_{\rho\mu}$ spin structures from the basis. It is clear that the allowed structures must carry two Dirac and two Lorentz indices, and not vanish due to projection properties of the (anti)collinear fermion fields sandwiching the Γ structures. Another constraint is that the μ index is contracted with a $\perp$ structure, $\partial_\perp^\mu$ or $\mathcal{A}_\perp^\mu$ in equations (2.116) and (2.117) respectively. This for example excludes $\gamma_{\perp\rho}n_{\pm\mu}$. In the end, the only structures which fulfil the requirements for both of the $\mathcal{O}(\lambda)$ suppressed currents are $n_{\pm\rho}\gamma_{\perp\mu}$.

To find the exact coefficients we now perform the subleading hard matching in momentum space. We restrict our calculation to tree-level. The matching coefficients can be obtained by appropriately selecting matrix elements of the operator matching equation in (2.115).

To this end, we first target the C'^{A0A1} coefficient of the $J_\rho^{A0,A1}(t,\bar{t})$ operator. Choosing the matrix element with an initial state made up of a collinear quark with momentum p and an anticollinear antiquark with momentum l gives the tree-level amplitudes written below. This situation corresponds to the equation written in terms of momentum-space diagrams in figure 2.5. We find

$$\bar{v}_{\bar{c}}(l)\, i\gamma_\rho\, \frac{1}{(n_+ p)}\slashed{p}_\perp\, \frac{\slashed{n}_+}{2}\, u_c(p) = C_{\text{tree}}^{A0A1}\, \bar{v}_{\bar{c}}(l)\, i\Gamma_{\rho\,\mu}^{A0,A1} p_\perp^\mu\, u_c(p), \tag{2.121}$$
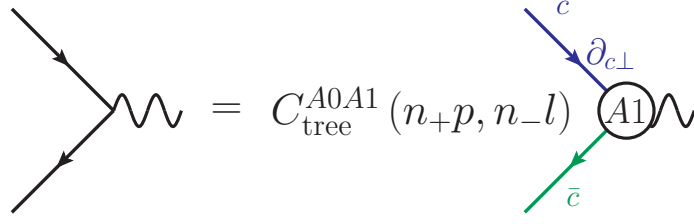
Figure 2.5: *Momentum-space representation of the tree-level matrix elements of the hard matching operator equation* (2.115). *Initial state is made up of a collinear quark with momentum p and an anticollinear antiquark with momentum l.*

where the expanded QCD result is on left-hand side and the SCET expression is presented on the right-hand side. We keep only the $\mathcal{O}(\lambda)$ term for QCD amplitude. Using projection properties of the spinors, we simplify the QCD expression on the left-hand side and find

$$-\bar{v}_{\bar{c}}(l)\, in_{+\rho}\, \frac{1}{(n_+ p)}\slashed{p}_\perp\, u_c(p) = C^{A0A1}_{\text{tree}}\, \bar{v}_{\bar{c}}(l)\, i\Gamma^{A0,A1}_{\rho\mu}p^\mu_\perp\, u_c(p), \qquad (2.122)$$

which implies that

$$C^{A0A1}_{\text{tree}} = -\frac{1}{(n_+ p)}, \qquad \Gamma^{A0,A1}_{\rho\mu} = n_{+\rho}\gamma_{\perp\mu}. \qquad (2.123)$$

Next, we target the C^{A0B1} coefficient of the $J^{A0,B1}_\rho(t_1,t_2,\bar{t})$ operator. The investigation follows the same steps as for the example above. This time we consider a different matrix element of the operator matching equation in (2.115) such that we can tag the $J^{A0,B1}_\rho(t_1,t_2,\bar{t})$ contribution. The operator $J^{A0,B1}_\rho(t_1,t_2,\bar{t})$ contains an additional gluon field in the collinear direction on top of the collinear quark field. Hence, we choose to calculate the matrix element with a collinear quark and gluon with momenta p and q respectively, and an anticollinear antiquark with momentum l. The corresponding amplitudes, in momentum-space, are given in figure 2.6. As can be seen in the figure, the situation is complicated by the fact that the $J^{A0,B1}_\rho(t_1,t_2,\bar{t})$ operator is not the only $\mathcal{O}(\lambda)$ operator which has a non-zero contribution to the matrix element we have chosen to calculate. Indeed, the $J^{A0,A1}_\rho(t,\bar{t})$ has two possible contributions. A collinear gluon can be attached to the collinear Wilson line which is used in defining the collinear gauge-invariant building block, see equation (2.49). A collinear gluon can also attach directly to the collinear quark via a leading power interaction. Fortunately, we have calculated the C^{A0A1}_{tree} coefficient above, and therefore the only unknown variable in our matching calculation is the value of the C^{A0B1}_{tree} coefficient for which we can solve the equation.

We spare the details of this calculation and give directly the result. We find that there are in fact two $\Gamma^{A0,B1}_{\rho\mu}$ contributions to the $J^{A0,B1}_\rho(t_1,t_2,\bar{t})$ operator in (2.117) each with its own matching coefficient. We find

$$C^{A0B1}_{\text{tree}+} = \frac{1}{n_+(p+q)}, \qquad \Gamma^{A0,B1}_{\rho\mu,+} = n_{+\rho}\gamma_{\perp\mu}, \qquad (2.124)$$
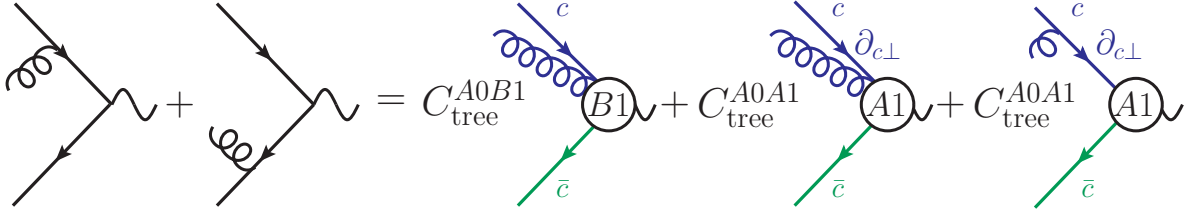
Figure 2.6: *Similar to figure 2.5, we again present the momentum-space tree-level matrix element of the hard matching operator equation in (2.115). However, for a different initial state. The initial state here is made up of a collinear quark with momentum p and a collinear gluon with momentum q, along with an anticollinear antiquark with momentum l. The QCD diagrams have to be expanded to $\mathcal{O}(\lambda)$.*

$$C_{\text{tree}-}^{A0B1} = -\frac{1}{(n_-l)}, \qquad \Gamma_{\rho\mu,-}^{A0,B1} = n_{-\rho}\gamma_{\perp\mu}. \tag{2.125}$$

The matching coefficients for operators suppressed in the anticollinear direction can be found in an analogous manner.

Part II

Threshold factorisation at subleading powers

3

Drell-Yan: factorisation theorem

Massive lepton-pair production in hadron-hadron collisions was first studied in 1970 by S.D. Drell and T.M. Yan [106]. The process - named the Drell-Yan (DY) process after the authors - is schematically written as

$$A(p_A) + B(p_B) \rightarrow \text{DY}(Q^2)[\rightarrow \ell(l_1)\bar{\ell}(l_2)] + X(p_X), \qquad (3.1)$$

where A(B) denotes the incoming hadron with momentum $p_A(p_B)$, $\text{DY}(Q^2)$ is an uncoloured intermediate state with a large invariant mass Q^2 which decays into the two leptons $\ell, \bar{\ell}$ with momenta l_1 and l_2 respectively, and X is the unobserved QCD radiation with momentum p_X. The hadronic centre-of-mass energy squared is given by $s = (p_A + p_B)^2$. The Drell-Yan process in the centre-of-mass frame is shown in figure 3.1.

The Drell-Yan process has played an incredibly important role in shaping the understanding of the nature of particles and their interactions, both theoretically and experimentally. The study of the behaviour of time-like photons in reactions of the type given in (3.1) and the search for new particles which decay into e^+e^- and $\mu^+\mu^-$ pairs has formed a large experimental program since 1970 [107]. The resonance searches performed in this program have been fruitful and already in 1974 have led to the discovery of J/Ψ meson at the Brookhaven National Laboratory [108] and at the Stanford Linear Accelerator Center [109]. The two respective independent research groups were led by Ting and Richter who were later awarded the 1976 Nobel Prize in Physics. The same philosophy led to the confirmation of the existence of $W^\pm$ and Z bosons postulated by the electroweak theories at the CERN Super Proton Synchrotron using proton-antiproton ($p\bar{p}$) collisions [110, 111, 112, 113].

Because of its clean final-state experimental signature, the Drell-Yan process continues to be important in the precision phenomenology program at the LHC. For instance, it is a key ingredient in the extraction of parton distribution functions (PDFs) from LHC measurements, which are subsequently used to make theoretical predictions for other processes. It also plays a role in searches for New Physics beyond the Standard Model. This heavy experimental use of the Drell-Yan process is one motivation for the advancement in the theoretical understanding of the process over the years. Since the 1970s, there exists a practical, phenomenologically motivated, need to obtain precise theoretical predictions and have a clear understanding of the perturbative uncertainties. Consequently, the theoretical predictions for the Drell-Yan process at next-to-leading order in strong coupling have been obtained already in 1978 [114, 115]. The complete next-to-next-to-leading
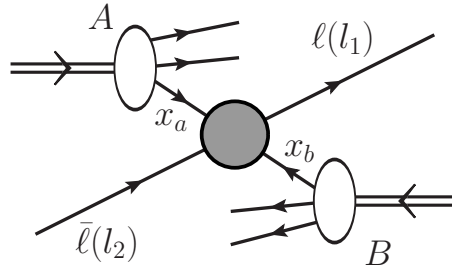
Figure 3.1: *Schematic representation of the Drell-Yan process in the centre-of-mass frame. Partons with momentum fractions x_a and x_b are drawn from their respective PDFs, A and B, and interact to produce a lepton-antilepton pair, $\ell(l_1)\bar{\ell}(l_2)$, in the final state.*

order results were published in 1991 [116] (partial results were already presented earlier in [117, 118, 119, 120] and see also [121, 122] for complete results), and the current state-of-the-art at fixed α_s order is the calculation at N³LO recently obtained in [14] for a neutral current and [15] for the charged current. In addition to the QCD corrections, the electroweak (EW) corrections were studied in [123, 124], and recently [125, 126] have considered the mixed QCD-EW corrections.

Similar to the advancement of fixed-order computations, the Drell-Yan process has served an important role in the development of resummation techniques. This procedure is necessary in certain kinematic configurations, for example in the threshold region where the invariant mass of the pair of leptons squared is close to the centre-of-mass energy squared, since the perturbative expansion of the cross-section develops large logarithms and can not be trusted unless these are under control to all orders in α_s. Again, this is on the one hand of phenomenological importance, because even if in the reactions at hadron colliders the lepton pair production does not occur close to the threshold regime in practice, the parton luminosity dynamically enhances the contribution of the partonic threshold region as observed in [24]. On the other hand, it is important from a theoretical perspective, since the Drell-Yan process shares features with other phenomenologically relevant processes studied at the LHC, such as Higgs boson production via gluon fusion, it provides a physically relevant case study to advance the accuracy of resummation and develop new techniques, which can then be applied on other processes, such as Higgs production. This will be evident in chapter 9.

The first summation of enhanced logarithms has been first achieved in seminal publications [20, 21]. With the advent modern of effective field theories and resummation using renormalization group techniques, this process was again considered within the framework of SCET [22, 23, 24] , and at leading power in the threshold expansion is now known to a very high logarithmic accuracy, N³LL [24, 25].

As we have established, the Drell-Yan process is an excellent test ground. Investigations away from strict threshold have been considered recently in [127]. Yet another direction where the exploration of the Drell-Yan process can provide insights into the structure of field theories is the investigation beyond leading power in the threshold expansion.

As mentioned in the introduction, the DY process was previously studied at NLP

at fixed order using expansion-by-regions method and diagrammatic techniques. These studies aimed at extension of the Low-Burnett-Kroll (LBK) theorem for amplitudes by introducing the concept of a radiative jet functions. We discuss the relation to our formalism in section 4.3.

The effective field theory approach to this problem is where the contents of this work are relevant. The SCET framework is designed with the view of resummation as it possesses manifestly gauge-invariant Lagrangian and systematic power counting. With the threshold resummation at leading power already obtained to a very high logarithmic accuracy, the next-to-leading power factorisation and resummation is the next natural challenge. The first resummation of the threshold DY process at next-to-leading power and leading logarithmic accuracy has been achieved in [40]. The relevant all order theorem factorisation has been presented in [65] and forms the core of this work. Here we construct the foundation for resummation beyond leading logarithms through a derivation of factorisation theorem in the effective field theory framework. We present both, formal all-power factorisation formula, and the specification of it to next-to-leading power.

This chapter proceeds as follows. In section 3.1 we specify the effective field theory framework introduced above to the case of the Drell-Yan process and discuss its kinematic set up at threshold. We review the leading power factorisation and discuss the emergence of collinear functions at subleading powers in detail. At the end of this section, we provide formal definitions for these new objects. Section 3.2 is dedicated to the derivation of the subleading power factorisation formula for the diagonal, $q\bar{q}$-channel, of the Drell-Yan process. We obtain a formal all-power expression before specifying to the next-to-leading power case and provide operatorial definitions for the objects which enter the factorisation formulas. We also investigate the form of the factorisation formula at fixed next-to-next-to leading order. In section 3.3 we follow a similar pattern and derive the subleading power factorisation formula for the off-diagonal, $q\bar{q}$-channel, of the Drell-Yan process. We again first perform an all-power derivation before also presenting the result at next-to-leading power.

3.1 Preliminaries, dynamics, and collinear functions

The focus of this work is the investigation of the partonic version of the process given in (3.1). For simplicity, the DY(Q^2) particle in equation (3.1) is chosen to be a highly virtual photon, γ^*. Conceretly, we consider the partonic Drell-Yan channel initiated by a $q\bar{q}$ pair

$$q(x_a p_A)\bar{q}(x_b p_B) \rightarrow \gamma^*(Q^2)\left[\rightarrow \ell(l_1)\bar{\ell}(l_2)\right] + X(p_X), \qquad (3.2)$$

for which the factorisation theorem is derived in section 3.2, and the partonic Drell-Yan channel initiated by $g\bar{q}$

$$g(x_a p_A)\bar{q}(x_b p_B) \rightarrow \gamma^*(Q^2)\left[\rightarrow \ell(l_1)\bar{\ell}(l_2)\right] + X(p_X), \qquad (3.3)$$

which is explored in section 3.3. Diagrams representing these channels of the Drell-Yan process at the cross-section level are depicted in figure 3.2.
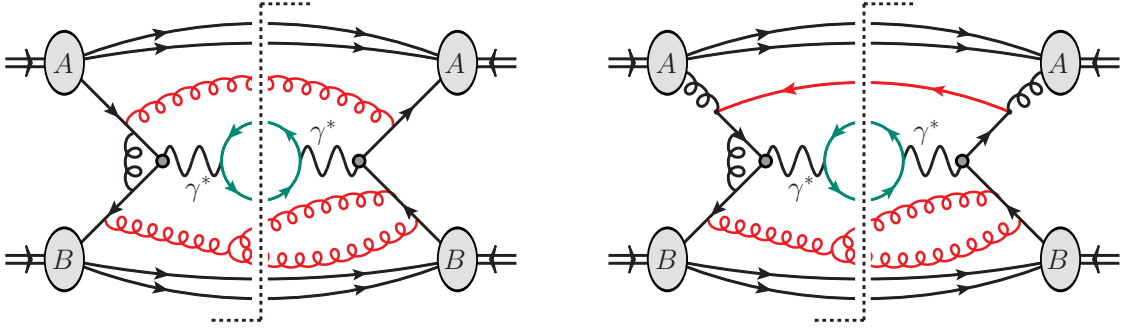
Figure 3.2: *Schematic representations of the Drell-Yan process cross-section in the $q\bar{q}$-channel (left) and $g\bar{q}$-channel (right). The grey ovals labelled A and B represent colliding protons. In each diagram, two partons drawn from their respective parton distribution functions interact to create a virtual photon, γ^*, which then decays to pair of leptons. We have also included additional QCD radiation, the red coloured lines represent soft partons at threshold. Only these are permitted to enter the final state at threshold.*

The machinery set up in section 2.1 enables the treatment of N-jet processes beyond leading power. For the specific case of the Drell-Yan production we require two back-to-back directions and hence need to specify only two light-like vectors

$$n_-^{\mu} = (1,0,0,1), \qquad n_+^{\mu} = (1,0,0,-1). \tag{3.4}$$

The momenta are decomposed in this case as in equation (2.3) with the index i dropped. As discussed above, the effective field theory framework is best suited to the study of the Drell-Yan process in the kinematic threshold region. We make this precise here. The partonic kinematic threshold corresponds to the case where almost all of the energy in the interaction between the two incoming partons is carried away by the intermediate boson, γ^*. This in turns means that the kinematic phase space for the unobserved radiation X is highly constrained as it can only be made up of very low energy radiation, also known as soft radiation. The partonic centre-of-mass energy squared is given by $\hat{s} = x_a x_b s$, where x_a and x_b are the momentum fractions of the incoming partons as prescribed in (3.2) and (3.3) and s is the hadronic centre-of-mass energy squared as given below (3.1). We define the kinematic variable $z = Q^2/\hat{s}$, using which the kinematic threshold region discussed here is captured by the limit $z \to 1$. Using this variable, the small power counting parameter λ, in terms of which the power expansion of the Lagrangian has been carried out in chapter 2, is defined as $\lambda = \sqrt{1-z} \ll 1$. The relevant momentum regions are given by [24]

$$
\begin{aligned}
p_h &\sim Q(1,1,1), & p_s &\sim Q(\lambda^2, \lambda^2, \lambda^2), \\
p_c &\sim Q(1, \lambda^2, \lambda), & p_{\bar{c}} &\sim Q(\lambda^2, 1, \lambda).
\end{aligned}
\tag{3.5}
$$

The hard fluctuations are integrated out and encoded in hard matching Wilson coefficients as explained in sections 2.3.3 and 2.4.4. Hence the remaining free degrees of freedom in the effective field theory are (anti)collinear and soft. We stress that in the threshold configuration the threshold-(anti)collinear virtuality, $p_c(p_{\bar{c}}) \sim Q^2\lambda^2$, is too large to enter

the final state X. However, there is enough energy available such that the soft radiation $p_s \sim Q^2\lambda^4$ is permitted in the final state X.

In addition to the threshold-collinear modes written above, at the hadronic level the effective field theory description contains (anti)collinear-PDF modes which have the scaling

$$p_{X_c^{\text{PDF}}} \sim (Q, \Lambda^2/Q, \Lambda), \qquad p_{X_{\bar{c}}^{\text{PDF}}} \sim (\Lambda^2/Q, Q, \Lambda), \tag{3.6}$$

where Λ is the strong interaction scale. It is assumed that the strong interaction scale is parametrically smaller than the threshold-collinear scale $\Lambda \ll Q\lambda = Q(1-z)^{1/2}$ and as such, the modes with $(\bar{c})c$-PDF scaling *can* be radiated into the hadronic final state. The standard parton distribution functions (PDFs) are defined in terms of these modes. The work here concerns power corrections in the threshold-collinear scale λ, and we work at leading power in the Λ/Q expansion, the latter is also known as the leading-twist approximation.

Having described the relevant mode structure, we begin the derivation of the factorisation theorem beyond leading power by writing down the standard expression of the d-dimensional cross-section which, in the centre-of-mass frame, reads

$$\begin{aligned}
d\sigma &= \frac{1}{2s}d^dq \int \frac{d^{d-1}l_1}{(2\pi)^3 2E_1} \frac{d^{d-1}l_2}{(2\pi)^3 2E_2} \delta^{(d)}(l_1 + l_2 - q) \\
&\times \sum_X |\langle \ell\bar{\ell}\, X|A\,B\rangle|^2 \, (2\pi)^d\, \delta^{(d)}(p_A + p_B - q - p_X),
\end{aligned} \tag{3.7}$$

where $p_X = p_{X_s} - p_{X_c^{\text{PDF}}} - p_{X_{\bar{c}}^{\text{PDF}}}$ since, as discussed above, the soft and $(\bar{c})c$-PDF modes can be radiated into final state, hence we write them here explicitly.

We do not consider corrections to the electromagnetic interaction between the off-shell photon and the final state leptons, hence the hadronic and leptonic parts of the amplitude factorise. Evaluating the phase-space for the final state leptons in, $d = 4$ since it is finite, results in the transverse lepton tensor and the expression for the cross-section in terms of the hadronic tensor $W_{\mu\rho}$, which is kept in d-dimensions, is as follows

$$d\sigma = \frac{4\pi\alpha_{\text{em}}^2}{3s\,q^2} \frac{d^dq}{(2\pi)^d} \left(-g^{\mu\rho}W_{\mu\rho} \right), \tag{3.8}$$

where

$$\begin{aligned}
g^{\mu\rho}W_{\mu\rho} &= \int d^dx\, e^{-iq\cdot x} \langle A(p_A)B(p_B)|J^{\dagger\rho}(x)J_\rho(0)|A(p_A)B(p_B)\rangle \\
&= \sum_X (2\pi)^d \delta^{(d)}\left(p_A + p_B - q - p_{X_s} - p_{X_c^{\text{PDF}}} - p_{X_{\bar{c}}^{\text{PDF}}}\right) \\
&\times \langle A(p_A)B(p_B)|J_\rho^\dagger(0)|X\rangle\langle X|J^\rho(0)|A(p_A)B(p_B)\rangle,
\end{aligned} \tag{3.9}$$

and the electromagnetic quark current is given by $J^\rho = \sum_q e_q\bar{\psi}_q\gamma^\rho\psi_q$. In order to not obscure the considerations at subleading powers through an overloading of the notation, we work with a single quark flavour with charge $e_q = 1$. In the threshold configuration, where the unobserved QCD final state X is forced to only contain soft radiation, the hard matching to SCET fields can be performed at amplitude level, since there are no contributions to the hadronic tensor where the currents at positions 0 and x are

connected by hard partons. Therefore, for the derivation of the factorisation theorem for the Drell-Yan process at threshold it is sufficient to consider the hard matching of the electromagnetic quark current as presented in leading-power and subleading-power examples in sections 2.3.3 and 2.4.4 respectively, and by extending it to all powers. This line of investigation is pursued in sections 3.2 for the $q\bar{q}$ and 3.3 for the $g\bar{q}$ channels.

For the moment however, following the pedagogical presentation in [65] we review the leading power considerations which gives us the opportunity to introduce the concept of *amplitude-level collinear functions* which are new objects that emerge and play an important role in factorisation at subleading powers.

3.1.1   Factorisation and collinear functions at leading power

We begin with the leading power hard matching equation before the decoupling transformation has been performed. This is given in (2.56) and we write it here again for convenience

$$\bar{\psi}\gamma_\rho\psi(0) = \int dt\, d\bar{t}\, \widetilde{C}^{A0,A0}(t,\bar{t})\, J_\rho^{A0,A0}(t,\bar{t}) \tag{3.10}$$

where in the notation for N-jet operators described above

$$J_\rho^{A0,A0}(t,\bar{t}) = \bar{\chi}_{\bar{c}}(\bar{t}n_-)\gamma_{\perp\rho}\chi_c(tn_+)\,. \tag{3.11}$$

The fields χ_c are the collinear-gauge-invariant collinear quark fields as discussed in section 2.1, and the corresponding momentum-space coefficient is related to the position-space matching coefficient by the Fourier transform defined in equation (2.57).

The first step in the derivation is to perform the field redefinition which decouples the soft-collinear interactions. This is given in equation (2.61). We consider here the matrix element of the resulting operator as dictated by (3.9)

$$
\begin{aligned}
\langle X|\bar{\psi}\,\gamma^\rho\psi(0)|A(p_A)B(p_B)\rangle &= \int dt\, d\bar{t}\, \widetilde{C}^{A0,A0}(t,\bar{t}) \\
&\times\ \langle X|\bar{\chi}_{\bar{c}}(\bar{t}n_-)\,Y_-^\dagger(0)\gamma_\perp^\rho Y_+(0)\chi_c\,(tn_+)\,|A(p_A)B(p_B)\rangle\,.
\end{aligned} \tag{3.12}
$$

Here, since the field redefinition which decouples the soft and collinear fields has already been performed and the final state is only composed of soft and $(\bar{c})c$-PDF collinear radiation due to kinematic constraints, it also factorises $\langle X| = \langle X_s|\langle X_{\bar{c}}^{\text{PDF}}|\langle X_c^{\text{PDF}}|$. It follows that at leading power the matrix element for Drell-Yan production factorises into a soft matrix element, composed of soft Wilson lines only, times the two matrix elements which each contain solely the (anti)collinear physics

$$
\begin{aligned}
\langle X|\bar{\psi}\,\gamma^\rho\psi(0)|A(p_A)B(p_B)\rangle &= \int dt\, d\bar{t}\, \widetilde{C}^{A0,A0}(t,\bar{t})\, \langle X_{\bar{c}}^{\text{PDF}}|\bar{\chi}_{\bar{c}}\,(\bar{t}n_-)|B(p_B)\rangle\,\gamma_\perp^\rho \\
&\times\ \langle X_c^{\text{PDF}}|\chi_c\,(tn_+)\,|A(p_A)\rangle\,\langle X_s|\mathbf{T}\left[Y_-^\dagger(0)Y_+(0)\right]|0\rangle\,.
\end{aligned} \tag{3.13}
$$

We draw attention to the fact that the final states of the (anti)collinear matrix elements are $(\bar{c})c$-PDF collinear whereas the fields appearing in those matrix elements, $\chi_c\,(tn_+)(\bar{\chi}_{\bar{c}}\,(\bar{t}n_-))$,
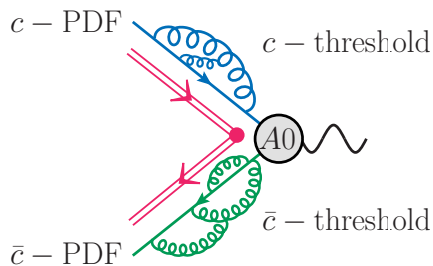
Figure 3.3: *Leading twist depiction of separated sectors in a Drell-Yan scattering amplitude after the decoupling transformation has been performed. Marked in the diagram are the $c(\bar{c})$-PDF collinear modes of the incoming (anti)quark and the purely threshold-(anti)collinear loops which are scaleless and zero in dimensional regularization. The red double lines represent the soft Wilson lines which are present due to the field redefinition which decouples the soft and collinear sectors. For clarity we do not include virtual loops with soft scaling which also vanish in dimensional regularization.*

are threshold-collinear. Therefore, a matching between the fields with these different modes must be performed. At leading power, this matching is trivial and takes the form

$$\chi_c(tn_+) = \int du\, \tilde{J}(t, u)\, \chi_c^{\text{PDF}}(un_+), \tag{3.14}$$

with a similar relation for the anticollinear direction up to a $n_- \leftrightarrow n_+$ replacement. The matching coefficient, $\tilde{J}(t, u)$, which we call the collinear function, is a delta function to all orders in perturbation theory $\tilde{J}(t, u) = \delta(t - u)$ and for this reason it is usually omitted in the discussion of leading power factorisation. Nonetheless, we find it instructive to investigate precisely how this result is obtained at leading power, as this will allow us to contrast this case with next-to-leading power considerations.

We begin by noting again that the decoupling transformation has already been performed. Therefore, since all the sectors are decoupled, only purely threshold-(anti)collinear loop corrections to the Drell-Yan process can occur at amplitude level[1]. This is shown schematically in figure 3.3. We remark that by "purely" threshold-(anti)collinear it is meant that there are no soft attachments. Taking the initial (anti)collinear partons on-shell, such loop corrections lead only to scaleless integrals, which are zero in dimensional regularization. Hence, at this level it is easy to see that indeed the leading power collinear function is simply given by a delta function to all orders in α_s which converts the threshold-(anti)collinear fields to $(\bar{c})c$-PDF collinear fields.

In order to show the consistency of this approach, we consider now the theory prior to the application of the decoupling transformation. In this case, at leading power the soft-collinear interactions do occur, albeit solely through eikonal vertices as discussed in section 2.1. Consequently, in the calculation of the Drell-Yan amplitude diagrams with threshold-collinear corrections such as the one presented in figure 3.4 are present. Since

---

[1]Purely soft loop corrections can occur as well, but the same conclusion will be drawn for the virtual soft corrections as for the purely threshold-collinear loops. Only soft real radiation contributes to the soft function at the cross-section level.
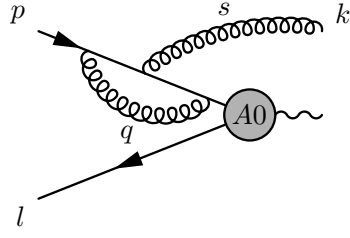
Figure 3.4: *Example of a leading power diagram with a threshold-collinear loop and a leading power (eikonal) soft emission. This diagram yields a non-zero result.*
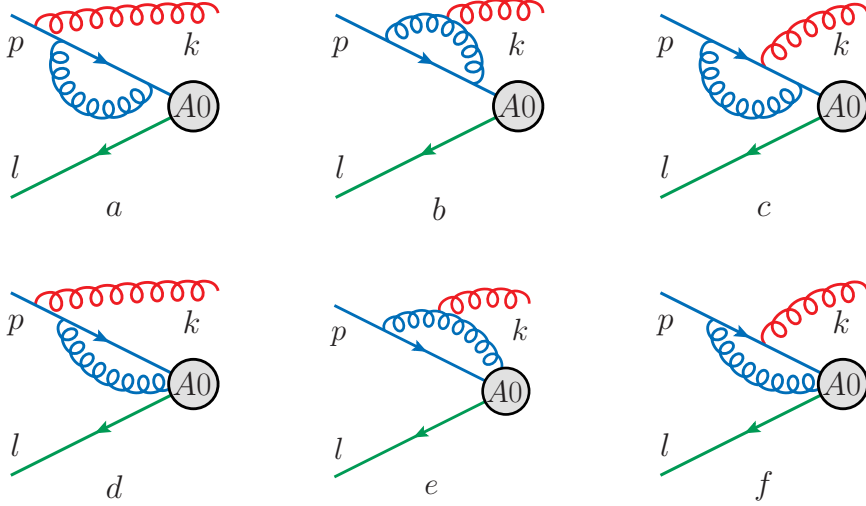
Figure 3.5: *Collinear loop contributions to the Drell-Yan scattering amplitude with one soft emission. The blue(green) colour denotes the (anti)collinear momentum flow. The incoming momentum is p(l). The red line represents the outgoing soft gluon with a soft momentum labelled by k. In the second row of the figure, the emission of the collinear gluon from the J^{A0} current comes from the collinear Wilson line present in the definition of the collinear-gauge-invariant collinear building block as defined in (2.49).*

there is an external soft attachment to the threshold-collinear leg, the loop correction is no longer scaleless, but rather, in dimensional regularization, it is proportional to the collinear invariant $[\mu^2/(n_-k)(n_+p)]^\epsilon$, where the threshold-collinear and soft momenta p and k are labelled in the figure and $(n_-k)(n_+p) \sim \lambda^2$. Considering therefore, a single diagram it seems that an object resembling the collinear function appears already at leading power and has non-vanishing loop corrections. This is seemingly in clear contradiction with the conclusions we have reached when considering the decoupled theory. However, the picture is saved when we include all the possible diagrams with a threshold-collinear loop. These are shown in figure 3.5. The external partons are on-shell, $p^2 = l^2 = k^2 = 0$, and the incoming (anti)collinear (anti)quark carries only its largest momentum component, $p^\mu = (n_+p, 0, 0)$ ($l^\mu = (0, n_-l, 0)$). As example, diagram a is explicitly calculated in appendix B.1. The results for each of the diagrams, labelled a - f as in figure 3.5, are given by

$$\mathcal{M}_a^{\text{LP}} \quad = \quad -\bar{v}_{\bar{c}}(l)i\gamma_\perp^\rho \frac{\alpha_s}{4\pi}g_s \mathbf{T}^B C_F \frac{n_{-\nu}}{(n_-k)}\left[\frac{(n_+p)(n_-k)}{\mu^2}\right]^{-\epsilon}\frac{(1-\epsilon)}{\epsilon}\mathfrak{f}[\epsilon]u_c(p), \qquad (3.15)$$

$$\mathcal{M}_b^{\mathrm{LP}} = \bar{v}_{\bar{c}}(l)i\gamma_\perp^\rho \frac{\alpha_s}{4\pi} g_s \mathbf{T}^B \frac{C_A}{2} \frac{n_{-\nu}}{(n_-k)} \left[\frac{(n_+p)(n_-k)}{\mu^2}\right]^{-\epsilon} \frac{(1-\epsilon)}{\epsilon} \mathfrak{f}[\epsilon] u_c(p), \tag{3.16}$$

$$\mathcal{M}_c^{\mathrm{LP}} = \bar{v}_{\bar{c}}(l)i\gamma_\perp^\rho \frac{\alpha_s}{4\pi} g_s \mathbf{T}^B \left(C_F - \frac{C_A}{2}\right) \frac{n_{-\nu}}{(n_-k)} \left[\frac{(n_+p)(n_-k)}{\mu^2}\right]^{-\epsilon} \frac{(1-\epsilon)}{\epsilon} \mathfrak{f}[\epsilon] u_c(p), \tag{3.17}$$

$$\mathcal{M}_d^{\mathrm{LP}} = \bar{v}_{\bar{c}}(l)i\gamma_\perp^\rho \frac{\alpha_s}{4\pi} g_s \mathbf{T}^B C_F \frac{n_{-\nu}}{(n_-k)} \left[\frac{(n_+p)(n_-k)}{\mu^2}\right]^{-\epsilon} \frac{2(1-\epsilon)}{\epsilon^2} \mathfrak{f}[\epsilon] u_c(p), \tag{3.18}$$

$$\mathcal{M}_e^{\mathrm{LP}} = -\bar{v}_{\bar{c}}(l)i\gamma_\perp^\rho \frac{\alpha_s}{4\pi} g_s \mathbf{T}^B C_A \frac{n_{-\nu}}{(n_-k)} \left[\frac{(n_+p)(n_-k)}{(\mu)^2}\right]^{-\epsilon} \frac{(1-\epsilon)}{\epsilon^2} \mathfrak{f}[\epsilon] u_c(p), \tag{3.19}$$

$$\mathcal{M}_f^{\mathrm{LP}} = -\bar{v}_{\bar{c}}(l)i\gamma_\perp^\rho \frac{\alpha_s}{4\pi} g_s \mathbf{T}^B \left(2C_F - C_A\right) \frac{n_{-\nu}}{(n_-k)} \left[\frac{(n_+p)(n_-k)}{\mu^2}\right]^{-\epsilon} \frac{(1-\epsilon)}{\epsilon^2} \mathfrak{f}[\epsilon] u_c(p), \tag{3.20}$$

where in all of the above expressions we have defined a factor containing a finite combination of Γ functions and the Euler-Mascheroni constant γ_E

$$\mathfrak{f}[\epsilon] \equiv \frac{e^{\epsilon\gamma_E}\Gamma[1+\epsilon]\Gamma[1-\epsilon]^2}{\Gamma[2-2\epsilon]}. \tag{3.21}$$

The index ρ belongs to the external photon, γ^*, and we have omitted polarisation $\epsilon^{*\nu}(k)$ for the soft emitted gluon, which also carries the colour index B. It is also noteworthy that in obtaining these results, we have used neither the on-shell, $k^2 = 0$, nor the transversality, $k \cdot \epsilon^*(k) = 0$, conditions for the emitted soft gluon. We see that the sum of $\mathcal{M}_a^{\mathrm{LP}}$ in (3.15) and $\mathcal{M}_b^{\mathrm{LP}}$ in (3.16) gives the negative of $\mathcal{M}_c^{\mathrm{LP}}$ in (3.17). Similarly, the sum of $\mathcal{M}_d^{\mathrm{LP}}$ in (3.18) and $\mathcal{M}_e^{\mathrm{LP}}$ in (3.19) results in the negative of $\mathcal{M}_f^{\mathrm{LP}}$ in (3.20). Therefore, indeed it is clear that individually these diagrams are not scaleless and in general are non-zero, however, when summed they vanish to all orders in ϵ. We have shown this through explicit calculation at one-loop order, but the same must hold to all orders in the α_s expansion. It is a consequence of the decoupling of the soft-collinear interactions at leading power in the threshold expansion. Therefore, we can consider the theory before decoupling transformation, and same conclusions about the leading power collinear functions are reached.

It should be noted that here we have focused on the threshold-collinear correction to the DY *amplitude*, and not directly the collinear function, however, these two objects are closely related. In what follows, this description will be refined and the threshold-collinear fluctuation will indeed be identified with another object at subleading powers, but the physical origin of this cancellation is identical here. Statement that leading power collinear functions vanish is equivalent to one that the amplitudes with a threshold-collinear loop vanish at leading power, as the same physics is captured. The former gives a clearer physical picture due to factorisation.

After the matching in equation (3.14) is performed for the (anti)collinear fields appearing in (3.13), the derivation of the leading power factorisation follows the usual steps. The matrix element in (3.13), now with $(\bar{c})c$-PDF fields, is combined with its conjugate that is translated to position x according to (3.9). This procedure yields standard PDFs $f_{a/A}(x_a)$ and $f_{b/B}(x_b)$ from the collinear matrix element

$$\langle A(p_A)|\bar{\chi}_{c,\eta i}^{\mathrm{PDF}}(x + g'n_+)\chi_{c,\beta b}^{\mathrm{PDF}}(gn_+)|A(p_A)\rangle$$

$$= \frac{\delta_{bi}}{N_c} \left(\frac{\slashed{n}_-}{4}\right)_{\beta\eta} (n_+ p_A) \int_0^1 dx_a \, e^{i(x + g' n_+ - g n_+) \cdot p_A x_a} f_{a/A}(x_a), \quad (3.22)$$

and the anticollinear matrix element

$$\langle B(p_B)| \bar{\chi}^{\mathrm{PDF}}_{\bar{c},\alpha a}(\bar{g} n_-) \chi^{\mathrm{PDF}}_{\bar{c},\delta j}(x + \bar{g}' n_-)|B(p_B)\rangle$$
$$= -\frac{\delta_{ja}}{N_c} \left(\frac{\slashed{n}_+}{4}\right)_{\delta\alpha} (n_- p_B) \int_0^1 dx_b \, e^{-i(\bar{g} n_- - \bar{g}' n_- - x) \cdot p_B x_b} f_{b/B}(x_b), \quad (3.23)$$

respectively. We have explicitly written the spin, $\alpha, \beta, \delta, \eta$, and fundamental colour, a, b, i, j, indices for concreteness. After performing the remaining integrals over the positions, simplifying the result, and combining the hadronic tensor with the leptonic one according to (3.8) one arrives at

$$\frac{d\sigma}{dQ^2} = \frac{4\pi\alpha_{\mathrm{em}}^2}{3N_c Q^4} \int d^d x \int_0^1 dx_a dx_b \, f_{a/A}(x_a) f_{b/B}(x_b) \frac{d^{d-1}\vec{q}\,(1-\epsilon)}{(2\pi)^{d-1} 2\sqrt{Q^2 + \vec{q}\,'^2}} \frac{1}{(2\pi)} Q^2$$
$$\times \quad e^{i(x_a p_A + x_b p_B - q)\cdot x}|C(-\hat{s})|^2 \frac{1}{N_c} \mathrm{Tr}\langle 0|\bar{\mathbf{T}}\left[Y_+^\dagger(x) Y_-(x)\right] \mathbf{T}\left[Y_-^\dagger(0) Y_+(0)\right]|0\rangle, \, (3.24)$$

where we have used for hard Wilson matching coefficients $C^{*A0}\left(x_a(n_+ p_A), x_b(n_- p_B)\right)$ $C^{A0}\left(x_a(n_+ p_A), x_b(n_- p_B)\right) = |C(-\hat{s})|^2$. The minus in the argument of $C(-\hat{s})$ is conventional. We also note the non-standard factor of $(1-\epsilon)$ appearing in the above equation. The derivation performed here is for the bare partonic cross-section $\hat{\sigma}$ and contains d-dimensional quantities. Therfore, care has to be taken when these are evaluated. For example, the lepton trace appearing here already at leading power when evaluated in d-dimensions yields a factor $\mathrm{Tr}\left[\left(\frac{\slashed{n}_-}{4}\right)\gamma_{\perp\rho}\left(\frac{\slashed{n}_+}{4}\right)\gamma_\perp^\rho\right] = -(1-\epsilon)$, which is the origin of the extra $(1-\epsilon)$ factor in equation (3.24) compared with standard derivations which use $d = 4$.

The next step in the derivation of the factorisation formula is the expansion of the phase space. In general, the phase space is process specific and does not have a homogeneous power counting unlike the terms in the SCET Lagrangian. For the moment we focus on leading power contribution, however, power corrections can generally arise from expansion of the phase space as will be shown explicitly at next-to-leading power in section 3.2.2. Note that in equation (3.24) the Wilson lines in the anti time-ordered product contain full x dependence. However, since the derivation is performed in the partonic centre-of-mass frame where $x_a \vec{p}_A + x_b \vec{p}_B = 0$, it follows that the three-momentum of the DY boson must to be balanced by the soft radiation, $\vec{q} = -\vec{p}_{X_s}$. Expanding the soft radiation energy in powers of λ gives the following

$$\left(x_a p_A + x_b p_B - q\right)^0 = p_{X_s}^0 = \sqrt{\hat{s}} - \sqrt{Q^2 + \vec{q}\,'^2} = \frac{\Omega_*}{2} - \frac{\vec{q}\,'^2}{2Q} + \mathcal{O}(\lambda^6), \quad (3.25)$$

where Ω_* is further expanded in powers of $(1-z)$,

$$\Omega_* = \frac{2Q(1 - \sqrt{z})}{\sqrt{z}} = Q(1-z) + \frac{3}{4}Q(1-z)^2 + \mathcal{O}(\lambda^6). \quad (3.26)$$

As can be seen from this expansion, power corrections to the DY partonic cross-section at a given order in λ can arise from a lower power matrix element contribution, multiplied

by the power suppressed phase space terms. As mentioned above, this will be obtained explicitly at next-to-leading power in what follows, however, this statement holds at general subleading powers. At leading power we keep only the first term in this power expansion, which means that we can then perform the integral over $\vec{q}$ which yields a $\delta^{(d-1)}(x)$ delta function, which upon evaluation sets the dependence of the soft matrix element to the x^0 component rather than on the full x coordinate. We then arrive at the following result

$$\frac{d\sigma_{\text{DY}}}{dQ^2} = \frac{4\pi\alpha_{\text{em}}^2}{3N_cQ^4} \sum_{a,b} \int_0^1 dx_a dx_b \, f_{a/A}(x_a) f_{b/B}(x_b) \, z \, \frac{\hat{\sigma}_{ab}(z)}{z} \, . \tag{3.27}$$

We have inserted a factor of $1 = z/z$ into the formula since the results in literature, for example in the full next-to-next-to leading order computation in [116], are often written for the quantity $\hat{\sigma}_{ab}(z)/z$. The partonic cross-section $\hat{\sigma}_{ab}(z)$ is factorised into a hard function, given by $H(\hat{s}) = |C(-\hat{s})|^2 = H(Q^2) + \mathcal{O}(\lambda^2)$, and a soft function:

$$\hat{\sigma}(z) = H(Q^2) \, Q S_{\text{DY}}(Q(1-z)) \, , \tag{3.28}$$

where we have for the moment set $d = 4$, and the objects appearing here are understood to be renormalized, as this is the leading power factorisation formula for Drell-Yan used for resummation and the aim here is to make contact with the known leading power result in literature. The soft function for Drell-Yan at leading power is given by [128]

$$S_{\text{DY}}(\Omega) = \int \frac{dx^0}{4\pi} \, e^{i\Omega\, x^0/2} \, \widetilde{S}_0\left(x^0\right) \, , \tag{3.29}$$

where the leading power position-space soft function is

$$\widetilde{S}_0(x) \;=\; \frac{1}{N_c} \text{Tr} \, \langle 0| \bar{\mathbf{T}} \left[Y_+^\dagger(x) Y_-(x) \right] \mathbf{T} \left[Y_-^\dagger(0) Y_+(0) \right] |0\rangle \, . \tag{3.30}$$

The soft function is defined at amplitude squared level, with scale supplied by the energy of the partons crossing the cut denoted by Ω in (3.29). Recent investigations of this object and its relation to other soft functions have been reported in [129].

In figure 3.6 we present a schematic picture of factorisation at leading power encapsulated by the expression in equation (3.27). The PDFs are depicted by the black ovals labelled A and B connected by solid lines, and the partonic picture is contained within the yellow frame. Only two ingredients make up the partonic cross-section. The first is the hard function, $H(Q^2)$ in equation (3.28), which is built from the hard Wilson matching coefficient and its conjugate. The matching coefficients are represented by the purple circles labelled $A0$ on the left and right-hand sides of the cut in figure 3.6. The second element are the double red lines which represent soft Wilson lines, the vacuum matrix element of which yields the soft function $S_{\text{DY}}(\Omega)$ in (3.28), as defined by equations (3.29) and (3.30).

We note that in equation (3.27) we have also included the contribution to the cross-section from the SCET current where it is the incoming quark that is anticollinear, and the antiquark that is collinear.

It is worth mentioning here that at next-to-leading power, the factorisation theorem which will be derived below must be understood as a formal result containing regularized
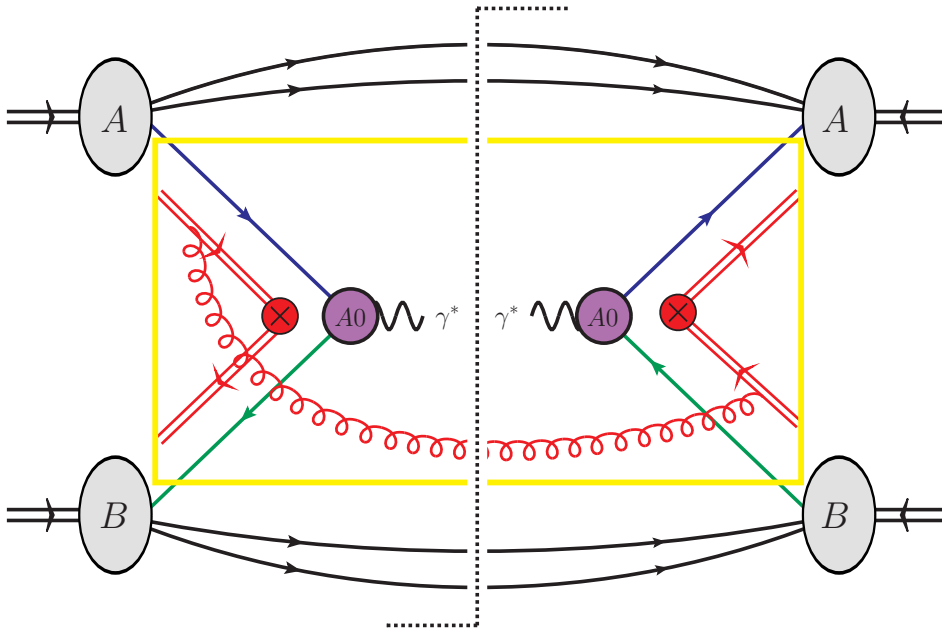
Figure 3.6:   *Schematic representation of factorisation of the Drell-Yan cross-section at leading power. The corresponding equation is given in (3.27) with the partonic cross-section $\hat{\sigma}(z)$, contained within the yellow frame here, in (3.28). The soft emissions are sourced by soft Wilson lines drawn in red. Here, for clarity, we show only one soft gluon emission, however the soft function in (3.29) captures the emissions to all orders.*

quantities, that is, we work with d-dimensional soft, hard, and collinear functions. Therefore, in order to compare with literature we find it convenient to define the quantity $\Delta(z)$, which is given by

$$\Delta(z) = \frac{1}{(1-\epsilon)} \frac{\hat{\sigma}(z)}{z} \, . \tag{3.31}$$

This corresponds to the object Δ for which results are given in [117, 116], with the extra factor of $(1 - \epsilon)$ divided out. This step is convenient due to the fact that we evaluate the leptonic spin trace in d-dimensions as explained above, contrary to setting $d = 4$ as is done conventionally [117, 116]. We will again remind of this fact in the relevant sections to avoid confusion.

Only once we reach chapter 8, where the leading logarithmic resummation is carried out at next-to-leading power, will we renormalize the quantities which appear in the formal factorisation in section 3.2.2 and not encounter divergent convolutions, which does not hold for next-to-leading power resummations beyond the leading logarithmic accuracy. These statements will be clarified in due course, at the moment we simply aim to put the considerations of the above discussion in a broader context of the contents presented in this work.

3.1.2 Collinear functions at subleading powers

Having discussed and outlined the well-known derivation of the factorisation formula for the Drell-Yan process near the kinematic threshold at leading power, and in particular, having highlighted the existence of trivial collinear functions, we promptly advance the discussion to subleading powers. The crucial ingredient present in the discussion of factorisation carried out in sections 3.2 and 3.3 is the concept of subleading power, amplitude level, collinear functions which are non-trivial starting from next-to-leading power. This subsection aims to show the origin of these new objects through a pedagogical example contrasting against the leading power discussion presented in the previous subsection. After we motivate the existence of the collinear functions, we provide formal definitions valid to any order in the power expansion. These definitions are used in the derivation of the factorisation formulas in sections 3.2 and 3.3 and in the calculation of the collinear functions themselves in chapter 4.

The critical observation is that the new physical ingredients in factorisation formulas at subleading power, the collinear functions, arise from soft-collinear interactions present in the power-suppressed Lagrangian. Recall that these were absent in the leading power discussion after the decoupling transformation was performed. The soft-collinear interactions at next-to-leading power technically appear as a consequence of Lagrangian insertions in time-ordered product operators. As an illustrative example, we consider the insertion of the next-to-leading power soft-collinear interaction Lagrangian $\mathcal{L}_{2\xi}^{(2)}$ after the decoupling transformation has been performed which is given in (2.109) and which we write here again for convenience

$$\mathcal{L}_{2\xi}^{(2)}(x) = \frac{1}{2} \bar{\chi}_c(x)\, x_\perp^\mu x_\perp^\nu \left[i\partial_\nu\, in_- \partial \mathcal{B}_\mu^+(x_-) \right] \frac{\slashed{n}_+}{2} \chi_c(x). \tag{3.32}$$

In contrast to section 2.4.3, we have here already dropped the (0) superscript, however it is understood that the fields present in the above Lagrangian term are decoupled. The $\mathcal{B}_\pm$ field is a soft building block built from a soft covariant derivative and soft Wilson lines as defined in equation (2.105). We stress that despite the application of the decoupling transformation, the soft-collinear interactions remain in the Lagrangian term. Following the construction presented in [86], as explained in section 2.4.1, and in particular below equation (2.80), the basis of subleading power operators contains ones built from time-ordered products of current operators with terms from the subleading SCET Lagrangian. The Lagrangian insertions are treated as perturbations and appear in the non-local operators with an integral over the position of the insertion, for instance, in this particular example we have

$$J_c^{T2}(t) = i \int d^d x\, \mathbf{T}\left[\chi_c(tn_+)\, \mathcal{L}_{2\xi}^{(2)}(x) \right], \tag{3.33}$$

where the field $\chi_c(tn_+)$ is taken from the leading power $J^{A0,A0}$ current. We illustrate this situation in figure 3.7. It is important to note that whereas the collinear fields in (3.32) depend on all components of the x coordinate, the soft $\mathcal{B}_\pm(x_-)$ field only depends on the $x_-^\mu = (n_+x)\frac{n^\mu}{2}$ component due to multipole expansion. This dependence links the collinear and soft fields in (3.33), leading to a collinear invariant for collinear loop integrals. The existence of such invariant is in stark contrast to the situation at leading power, where
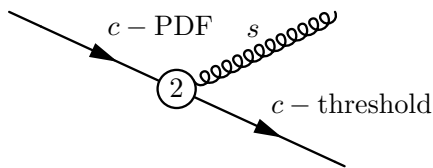
Figure 3.7: *A collinear quark line with an insertion of the power-suppressed Lagrangian term* $\mathcal{L}_{2\xi}^{(2)}$.

after the application of the decoupling transformation the $(\bar{c})c$-threshold loops were all scaleless, as depicted in figure 3.3. In order to make our statements more concrete, we now consider the matrix element of the electromagnetic current matched to SCET fields with an insertion of the Lagrangian in (3.32),

$$
\begin{aligned}
\langle X|\bar{\psi}\gamma^\rho\psi(0)|A(p_A)B(p_B)\rangle &= \int dt\, d\bar{t}\, \widetilde{C}^{A0,A0}(t,\bar{t})\, \langle X_{\bar{c}}^{\mathrm{PDF}}|\bar{\chi}_{\bar{c},\alpha a}(\bar{t}n_-)|B(p_B)\rangle\gamma^\rho_{\perp,\alpha\gamma}\\
&\times i\int d^d x\, \langle X_c^{\mathrm{PDF}}|\frac{1}{2}x_\perp^\nu x_\perp^\mu (in_-\partial_x)^2\, \mathbf{T}\left[\chi_{c,\gamma f}\,(tn_+)\,\bar{\chi}_c\,(x)\,\mathbf{T}^A\frac{\slashed{n}_+}{2}\chi_c\,(x)\right]|A(p_A)\rangle\\
&\times \langle X_s|\mathbf{T}\left(\left[Y_-^\dagger(0)Y_+(0)\right]_{af}\frac{i\partial_\perp^\mu}{in_-\partial}\mathcal{B}_{\perp\nu}^{+A}\,(x_-)\right)|0\rangle\,. \qquad (3.34)
\end{aligned}
$$

We have made use of the fact that the insertion of the subleading power Lagrangian terms is treated as a perturbation. Hence the states are eigenstates of the leading power Hamiltonian and therefore factorise in the same way as in the leading power computation in the previous section, $\langle X| = \langle X_s|\langle X_{\bar{c}}^{\mathrm{PDF}}|\langle X_c^{\mathrm{PDF}}|$. Comparing (3.34) to the leading power expression given in (3.13), we first note that there are additional threshold collinear fields in the c-PDF matrix element. Secondly, there is a convolution in x_- between the collinear and soft matrix elements. Momentum with a soft scaling is injected into the collinear matrix element due to the presence of this extra convolution, which in turn induces a scale and leads to the emergence of collinear functions. Another difference is present in the soft matrix element itself. Namely, written here in the last line, it now contains an explicit gauge field insertion in addition to the Wilson lines. This soft matrix element will form a part of the *generalised* soft function. There are no changes to the anticollinear matrix element compared to the leading power result since we consider placing the power suppression only in the collinear sector in this illustrative example. The anticollinear matrix element, after trivial leading power matching, will form part of a PDF at cross-section level.

   We now concentrate on the collinear matrix element, which is written in the second line of (3.34). As mentioned above, due to threshold kinematics, the threshold-collinear modes cannot radiate into the final state. At leading power in the Λ/Q expansion, also known as the leading twist expansion, the threshold-collinear fields present in the collinear matrix element must be integrated out and matched to c-PDF mode operators consisting of a single quark (or gluon) field. After squaring the amplitude, the matrix elements of c-PDF fields will form the standard PDFs. Below we refine this picture and provide formal matching equations. However, a prototype for this matching step is the equation

$$
i\int d^d x\, \mathbf{T}\left[\{\psi_c(tn_+)\}\mathcal{L}_c^{(2)}(x)\right] = 2\pi\int du\int dx_-\,\tilde{J}(t,u;x_-)\,\chi_c^{\mathrm{PDF}}(un_+)\,, \qquad (3.35)
$$

where $\mathcal{L}_c^{(2)}(x)$ contains only the collinear pieces of a Lagrangian insertion. The perturbative matching coefficient $\tilde{J}(t, u; z_-)$ is the *collinear function*. The *amplitude* level collinear physics is contained in $\tilde{J}(t, u; z_-)$. We emphasise once more that it first appears in a non-trivial way in power-suppressed corrections to the Drell-Yan process. The equation in (3.35) provides an operator definition for the concept of the "radiative jet amplitude" [130, 36, 37]. We note now that in a general case we must perform the matching in the presence of soft structures which, acting as projectors, define independent collinear functions. The soft structure is omitted in the above example as we only consider a single Lagrangian insertion. However, we must include all possible Lagrangian insertions in an all-order derivation of factorisation, and there exist relations between them. Formal definitions of this matching procedure are given in section 3.1.3 below.

We now continue with the representative example and calculate the tree-level contribution to a subleading power collinear function due to the fields in the second line of (3.34). For this purpose, it is useful to introduce the momentum-space operator which contains only collinear fields,

$$
\mathcal{J}_{\gamma, f}^{\mu\nu, A}(n_+ p, \omega) \equiv \int dt\, e^{i\,(n_+ p)\,t}\, i \int d^d x\, e^{i\omega(n_+ x)/2}
$$
$$
\times \frac{1}{2} x_\perp^\nu x_\perp^\mu (in_- \partial_x)^2 \, \mathbf{T}\left[\chi_{c,\gamma f}(tn_+)\, \bar{\chi}_c(z)\, \mathbf{T}^A \frac{\slashed{n}_+}{2}\chi_c(x)\right]. \tag{3.36}
$$

In order to calculate the perturbative threshold-collinear matching coefficient defined in (3.35), instead of the hadronic matrix element in (3.34) we consider its partonic analogue. This amounts to exchanging the incoming hadron by an incoming quark, and the vacuum state replaces the PDF-collinear final state. The incoming quark carries momentum q and fundamental colour index e. Hence, we have at this point

$$
\langle 0|\mathcal{J}_{\gamma, f}^{\mu\nu, A}(n_+ q_a, \omega)\,|q(q)_e\rangle = \int dt\, e^{i(n_+ q_a)\,t}\, i \int d^d x\, \left[(in_- \partial_x)^2 e^{i\omega\,(n_+ x)/2}\right]
$$
$$
\times \frac{1}{2} x_\perp^\nu x_\perp^\mu\, \langle 0|\mathbf{T}\left[\chi_{c,\gamma f}(tn_+)\, \bar{\chi}_c(x)\, \mathbf{T}^A \frac{\slashed{n}_+}{2}\chi_c(x)\right]|q(q)_e\rangle
$$
$$
= -\frac{1}{2} i\omega^2\,(2\pi) \int \frac{d^d k}{(2\pi)^d}\, \delta\,(n_+ q_a - n_+ k) \int d^d x\, \left[\frac{\partial}{\partial k_{\perp\nu}} \frac{\partial}{\partial k_{\perp\mu}} \frac{i(n_+ k)}{k^2}\right]
$$
$$
\times e^{i\omega\,(n_+ x)/2} e^{ik\cdot x}\, \mathbf{T}_{fe}^A\, u_{c,\gamma}(q)\, e^{-i\,x\cdot q}, \tag{3.37}
$$

where in the step between the two equations we have contracted two of the collinear fields to form the collinear quark propagator according to

$$
\overbrace{\chi_c(y)\bar{\chi}_c}(z) = \int \frac{d^d k}{(2\pi)^d}\, \frac{i(n_+ k)}{(k)^2 + i\delta}\, \frac{\slashed{n}_-}{2}\, e^{-ik\cdot(y-z)}, \tag{3.38}
$$

we have performed the $in_- \partial_x$-derivatives and the integral over dt, we have also used the following relation

$$
\chi_{c,\gamma d}(x)|q(q)_e\rangle = \delta_{de}\, u_{c,\gamma}(q) e^{-ix\cdot q}\,|0\rangle \tag{3.39}
$$

for the incoming quark with momentum q. The d in the subscript is a fundamental colour index. The momentum derivatives and the d-dimensional x-integral can be performed next.

The latter yields delta functions which remove the remaining integral over the momentum k. Then we find

$$\langle 0| \mathcal{J}^{\mu\nu,\,A}_{\gamma,f}\left(n_+q_a,\omega\right)|q(q)_e\rangle \;\;=\;\; (2\pi) J^{\mu\nu,\,A}_{2\xi,\gamma\beta,fe}\left(n_+q_a, n_+q;\,\omega\right) u_{c,\beta}(q)\,, \qquad (3.40)$$

where

$$J^{\mu\nu,\,A}_{2\xi,\gamma\beta,fe}\left(n_+q_a, n_+q;\,\omega\right) \equiv \delta\left(n_+q_a - n_+q\right)\frac{-g^{\nu\mu}_\perp}{(n_+q)}\,\mathbf{T}^A_{fe}\,\delta_{\gamma\beta} \qquad (3.41)$$

This matching coefficient defines the momentum-space tree-level collinear function. Although we have so far only explicitly obtained a tree-level result for a single Lagrangian insertion, the appearance of collinear functions beyond leading power is generic and constitutes a key concept in next-to-leading power investigations. Importantly, in this section we have argued that the soft-collinear interactions persist at subleading powers even after the application of the decoupling transformation, which changes the physical picture of factorisation in Drell-Yan production at threshold. We observed the emergence of new objects, the collinear functions, and in chapter 4 we explicitly calculate the one-loop corrections to these functions.

Before we continue, we draw attention to the fact that in this subsection, we have considered only the time-ordered product operator type of power correction. We recall from section 2.4.1 that the suppressed operator basis includes also type A, B, $C...$ operators which provide power suppression by including derivatives and additional fields in a particular collinear direction. Crucially, they do not include soft-collinear interactions. One may argue that power suppression in the Drell-Yan amplitude, and eventually cross-section, can arise from these operators alone, without the need for insertions of power suppressed SCET Lagrangian terms. However, without time-ordered product operators, performing the decoupling transformation achieves the same result as at leading power. Namely, the soft and collinear sectors become separated. With the calculation restricted to leading-twist—that is leading order in Λ/Q—the additional threshold fields must form loops at amplitude level as the threshold collinear modes also cannot be radiated into the final state since their virtuality is too large. The matching is then trivially null since, in the same way as at leading power in the threshold expansion, the threshold collinear loops are scaleless. This is shown in figure 3.8 for J^{B2}_c and J^{C2}_c operators. Therefore, we clearly see that soft-collinear interactions that enter through time-ordered products operators with subleading SCET Lagrangian terms are critical to factorisation at next-to-leading power. We exploit this fact in the derivation of subleading power factorisation formula in sections 3.2 and 3.3.

3.1.3   Collinear matching: formal definitions

The collinear functions are important new objects appearing in the factorisation theorem beyond leading power. Having now motivated the existence of the collinear functions, we find it useful to write down here the formal, generic collinear matching equations. We will use these in much of what follows and having understood the physics behind these new objects, it is helpful to have the definitions collected before diving into the technical derivation of the factorisation theorem itself.
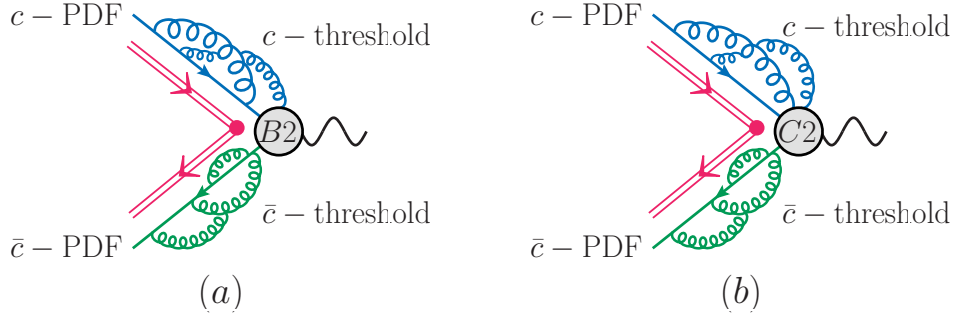
Figure 3.8: *The anticollinear leg is kept at leading power, and the label in the hard interaction refers to the power suppressed current in the collinear direction, J_c^{B2} and J_c^{C2} in panels (a) and (b) respectively.*

Suppressing the indices, we have for a general collinear matching in the $q\bar{q}$ - channel the following equation

$$i^m \int \{d^d z_j\}\, \mathbf{T} \left[\{\psi_c(t_k n_+)\} \times \left\{\mathcal{L}^{(l)}(z_j)\right\} \right]$$
$$= 2\pi \sum_i \int du \int \{dz_{j-}\}\, \tilde{J}_i\left(\{t_k\}, u; \{z_{j-}\}\right) \chi_c^{\mathrm{PDF}}(un_+)\, \mathfrak{s}_i(\{z_{j-}\}), \qquad (3.42)$$

and for the case where the incoming parton is a gluon, we define the following general collinear matching equation

$$i^m \int \{d^d z_j\}\, \mathbf{T} \left[\{\psi_c(t_k n_+)\} \times \left\{\mathcal{L}^{(l)}(z_j)\right\} \right]$$
$$= 2\pi \sum_i \int du \int \{dz_{j-}\}\, \tilde{G}_i\left(\{t_k\}, u; \{z_{j-}\}\right) \mathcal{A}_{c\perp}^{\mathrm{PDF}}(un_+)\, \mathfrak{s}_i(\{z_{j-}\}). \qquad (3.43)$$

Since the above equations are general, they are rather notation heavy, consequently we take a moment to go through and explain each piece:

- $\{z_{j-}\}$ denotes the set of m positions at which the insertions of the soft building blocks are located.

- $\{d^d z_j\} = \prod_{j=0}^{m} d^d z_j$ and $\{dz_{j-}\} = \prod_{j=0}^{m} dn_+ z_j/2$. The upper limit in both products originates from the total number of the Lagrangian insertions.

- $\left\{\mathcal{L}^{(l)}(z_j)\right\}$ denotes a set of m Lagrangian insertions suppressed by a power of order λ^l, where l can be different for each insertion.

- $\{\psi_c(t_k n_+)\}$ is a set of n fields chosen from the elementary collinear-gauge-invariant collinear building blocks given in equation (2.49). Each building block is dependent on a variable from the set $\{t_k\}$ which is also of size n. We write again the building blocks from for convenience

$$\psi_i(t_i n_{i+}) \in \begin{cases} \chi_i(t_i n_{i+}) \equiv W_i^\dagger \xi_i & \text{collinear quark} \\ \mathcal{A}_{i\perp}^\mu(t_i n_{i+}) \equiv W_i^\dagger\, [i\, D_{i\perp}^\mu\, W_i] & \text{collinear gluon} \end{cases} \qquad (3.44)$$

for a collinear quark and gluon field in the i-th direction, respectively.

- $\mathfrak{s}_i(\{z_{j-}\})$ is a soft operator. The sum with index i runs over a basis of the soft structures,

$$
\mathfrak{s}_i(\{z_{j-}\}) \quad \in \quad \left\{ \mathbb{1}, \frac{i\partial_\perp^\mu}{in_-\partial}\mathcal{B}_{\mu_\perp}^+(z_{1-}), \frac{i\partial_{[\mu_\perp}}{in_-\partial}\mathcal{B}_{\nu_\perp]}^+(z_{1-}), \right. \tag{3.45}
$$
$$
\frac{1}{(in_-\partial)^2}\left[\mathcal{B}^{+\,\mu_\perp}(z_{1-}), \left[in_-\partial\mathcal{B}_{\mu_\perp}^+(z_{1-})\right]\right] \ , \frac{1}{(in_-\partial)}\left[\mathcal{B}_{\mu_\perp}^+(z_{1-}), \mathcal{B}_{\nu_\perp}^+(z_{1-})\right],
$$
$$
\left. \mathcal{B}_{\mu_\perp}^+(z_{1-})\mathcal{B}_{\nu_\perp}^+(z_{2-}), \frac{1}{(in_-\partial_{z_1})(in_-\partial_{z_2})}q_{+\sigma}(z_{1-})\bar{q}_{+\lambda}(z_{2-}), \dots \right\}.
$$

Here $[\mu, \nu]$ denotes antisymmetrisation $\mu\nu - \nu\mu$. The presence of the soft structures in the collinear matching equation may seem out of place at first. However, the soft structures play an essential role in defining *independent* collinear functions as coefficients of *independent* soft structures. The ellipses in (3.45) include all possible *independent* soft structures. We emphasise the word "independent" as there exist relations between the soft structures which link the individual insertions of power suppressed Lagrangian terms. It is understood that the set of soft structures in (3.45) is written after the application of the equation of motion

$$
n_+\mathcal{B}^+(z_-) \quad = \quad -2\frac{i\partial_\perp^\mu}{in_-\partial}\mathcal{B}_{\mu_\perp}^+(z_-) - 2\frac{1}{(in_-\partial)^2}\left[\mathcal{B}^{+\,\mu_\perp}(z_-), \left[in_-\partial\mathcal{B}_{\mu_\perp}^+(z_-)\right]\right]
$$
$$
-2\frac{g_s^2}{(in_-\partial)^2}\mathbf{T}^A\,\bar{q}_+(z_-)\mathbf{T}^A\,\slashed{n}_-q_+(z_-). \tag{3.46}
$$

In appendix B.2, we explicitly show an example where this definition of collinear functions, belonging to particular soft structures, is imperative. We discuss how failing to take into account the relations between the soft structures can lead to an inconsistent description. Specifically, see equations (B.13) – (B.23) and the explanations there. It should be noted that for our convenience, the list in (3.45) is still partially redundant. In particular, the two-gluon soft structures in the second line can be considered as special cases of the bi-local structure $\mathcal{B}_{\mu_\perp}^+(z_{1-})\mathcal{B}_{\nu_\perp}^+(z_{2-})$.

The formal all-order and all-power matching in equation (3.42) will be used extensively in the following sections. We appreciate that even with detailed explanations, it can still appear abstract. Therefore, in order to make it more transparent, a graphical illustration is provided in figure 3.9.

3.2   Quark-antiquark channel

With the description of the theoretical framework of subleading power operators in SCET completed, and having reviewed leading power factorisation and introduced the concept of collinear functions we now turn our attention to one of the main results of this work. Namely, the derivation of factorisation formula for the Drell-Yan process near threshold beyond leading power in the $(1-z)$ expansion.

We remind the reader that the derivation of the factorisation formula in SCET at leading power [24] involves matching the electromagnetic current to the leading power
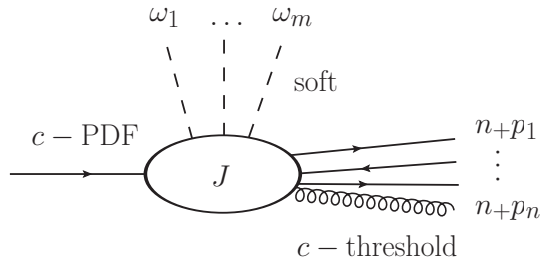
Figure 3.9: *A momentum-space pictorial representation of the matching equation (3.42). The oval labelled J is a collinear function. The ω_i variables are conjugate to the respective positions of the insertions of subleading-power Lagrangian terms. It is permitted that many threshold-collinear fields join to the (possibly power-suppressed) SCET currents of the $A, B, C...$ - type. However, there is only a single c-PDF field at leading twist in the Λ/Q expansion.*

SCET current as written in equation (3.10). We give the leading power current before the application of the decoupling transformation in equation (3.11). The matching coefficient in position space is related to the momentum-space matching coefficient by equation (2.57).

In order to derive the factorisation formula valid beyond the leading power in the $(1-z)$ expansion, we must alter the matching equation (3.10) to include higher orders in the λ expansion as discussed in section 2.4.4. We accomplish this first in general, by including all possible combinations of power-suppressed currents, which extends the $\mathcal{O}(\lambda)$ example in equation (2.115). It is also necessary to include insertions of subleading Lagrangian terms into the general power-suppressed currents. We make use of the formalism discussed in section 2.4.1. In section 3.2.1 we obtain a general factorisation formula valid to all powers. This is a formal result. To show the consistency of the approach, in section 3.2.2, we specialise the general result to next-to-leading power accuracy. For this case, we give explicit results for objects constituting the factorisation formula in the following sections. These are then used to cross-check the SCET computation against known QCD results directly up to the NNLO order.

3.2.1 Factorisation at general subleading powers

In this section we present the derivation of the formal factorisation formula beyond leading power. Since in the threshold kinematic configuration only soft radiation is permitted to enter the final state, the hard matching is done at amplitude level. In general, power suppressed contributions at any order in λ can arise in the collinear, anticollinear, or both sectors. As presented in section 2.4.1, the power suppression can come from power suppressed currents of type $A, B, C...$ in the (anti)collinear direction, and from time-ordered products of currents with terms from the subleading power SCET Lagrangian. Therefore, in a general, all power, hard matching of the vector current we must sum over all the possibilities. Omitting the index structure, such general matching equation is given by specifying (2.71) to two directions

$$\bar{\psi}\gamma_\rho\psi(0) = \sum_{m_1,m_2} \int \{dt_k\}\,\{d\bar{t}_{\bar{k}}\}\,\widetilde{C}^{\,m_1,m_2}\left(\{t_k\}, \{\bar{t}_{\bar{k}}\}\right)\,J_s(0)\,J_\rho^{m_1,m_2}\left(\{t_k\}, \{\bar{t}_{\bar{k}}\}\right). \quad (3.47)$$

The equation is written in a compact form, which we now unpack. The sizes of the sets $\{dt_k\}$ and $\{t_k\}$ depend on the type of collinear current present in a particular term on the right-hand side of the matching equation. In the same way, sizes of $\{d\bar{t}_{\bar{k}}\}$ and $\{\bar{t}_{\bar{k}}\}$ correspond to anticollinear currents present in each term. The indices m_1 and m_2 label the basis of SCET operators according to the building blocks out of which each current is constructed and their corresponding short-distance matching coefficients $\widetilde{C}^{m_1 m_2}$. We use the formalism and notation developed in [86, 87], which we have already described in detail in section 2.4.1. The simplest example is the leading power case, as is written in equation (3.10) where $m_1 = A0$ and $m_2 = A0$. The sum over the indices m_1 and m_2 accounts for the inclusion of all possible contributions.

As already mentioned, the collinear and anticollinear directions can both support sources of power suppression. Therefore, the SCET currents in (3.47) are built in the following way

$$J_\rho^{m_1, m_2}\left(\{t_k\}, \{\bar{t}_{\bar{k}}\}\right) = J_{\bar{c}}^{m_1}\left(\{\bar{t}_{\bar{k}}\}\right)\, \Gamma_\rho^{m_1, m_2}\, J_c^{m_2}\left(\{t_k\}\right). \tag{3.48}$$

The $J_c^{m_2}\left(\{t_k\}\right)$ is constructed using collinear-gauge-invariant collinear building blocks given in equation (2.49) and derivatives acting on these building blocks, as discussed in section 2.4.1. We recall from section 2.4.1 that the letter A, B, C, ... which labels the operator J^{An}, J^{Bn}, J^{Cn}, ... denotes the number of fields in a particular collinear direction. The number $n = 0, 1, 2$, etc. gives the overall power of λ of the current with respect to the leading power. Explicit examples of J^{A1}, J^{A2}, J^{B1}, J^{B2}, and J^{C2} are given in (2.74), (2.75), (2.76), (2.77), and (2.78), respectively. Identical operators exist for the anticollinear direction, and the total power suppression of $J_\rho^{m_1, m_2}\left(\{t_k\}, \{\bar{t}_{\bar{k}}\}\right)$ is given by the sum of power suppression in $J_{\bar{c}}^{m_1}\left(\{\bar{t}_{\bar{k}}\}\right)$ and $J_c^{m_2}\left(\{t_k\}\right)$. $\Gamma_\rho^{m_1, m_2}$ in (3.48) stands for the appropriate spinor and Lorentz structure of the operator. We have already encountered the expression for the leading power case $\Gamma_\rho^{A0, A0} = \gamma_{\perp\rho}$ in (3.11). We have also discussed the more involved case at $\mathcal{O}(\lambda)$ in section 2.4.4. We have found that $\Gamma_\rho^{A0, A1} = n_{+\rho}$ and $\Gamma_\rho^{A0, B1} = n_{\pm\rho}$. We remark that in the construction presented here, the Γ^{m_1, m_2} structure carries only the index of the vector boson, ρ, which is common to all operators participating in the matching. However, this way of proceeding is slightly different to the one presented in the example in section 2.4.4. In particular, in equations (2.116) – (2.119) we have defined Γ^{m_1, m_2} to carry also the leftover indices of the corresponding currents used in the matching. That is, currents J^{A1} and J^{B1} in equations (2.74) and (2.76). The reason for this choice is that the general basis of subleading power operators keeps open any indices which appear. In section 2.4.4 we found what structures are contracted with these indices such that the only remaining open index is one of the vector boson. Here, in order to keep the derivation general but also transparent, we choose to move any such structures into the definition of $J_{\bar{c}}^{m_1}$ and $J_c^{m_2}$ since we consider arbitrarily power suppressed currents and the specific spinor and Lorentz structure can in general be found by explicit matching at any one power. We note that in what follows, we give the complete basis at the next-to-leading power.

In addition to the SCET subleading currents, as discussed in section 2.4.1, there exist time-ordered products of the currents with terms from the subleading SCET Lagrangian. Following [86] we denote these operators by Tn, where n indicates the order of power suppression. An example for an i-collinear direction at $\mathcal{O}(\lambda)$ is given in equation (2.80).

For a collinear direction at $\mathcal{O}(\lambda^2)$ we have for instance

$$J_c^{T2}(t) = i \int d^d z \, \mathbf{T} \left[J_c^{A0}(t) \, \mathcal{L}^{(2)}(z) \right] . \tag{3.49}$$

Similarly to (2.80), here $\mathcal{L}^{(2)} = \mathcal{L}_\xi^{(2)} + \mathcal{L}_{\xi q}^{(2)} + \mathcal{L}_{\mathrm{YM}}^{(2)}$ are the power-suppressed terms in the SCET Lagrangian [73] given here in section 2.4.1.

We stress here again, as was done already in section 3.1.2, that the time-ordered product operators are crucial ingredients of the factorisation of the Drell-Yan process at next-to-leading power. To yield a non-zero subleading power amplitude at least one leg must have such a time-ordered product. The underlying reason for this fact is that as shown in section 2.4.3, the decoupling transformation does not remove the soft-collinear interactions in the subleading SCET Lagrangian terms, and as illustrated in section 3.1.2, the injection of soft momentum into collinear loops is necessary to form non-vanishing collinear functions.

Following the construction of subleading power operator basis presented in [86], we also have in the generalised Drell-Yan matching equation (3.47), as in equation (2.71) for the general N-jet case, the purely soft building blocks, $J_s(0)$. As discussed in section 2.4.1, the purely soft building blocks start contributing to the current operator, in addition to the collinear fields, from $\mathcal{O}\left(\lambda^3\right)$. We keep $J_s(0)$ in the derivation of the formal fractionation theorem for arbitrary powers. The soft fields will form a part of generalised soft functions.

We focus now on the (anti)collinear pieces. As we have discussed in detail in section 3.1.2, only the $(\bar{c})c$-PDF modes are permitted to radiate into the final state in the $z \to 1$ threshold kinematic region. The virtuality of the threshold collinear modes is too large. Therefore, a second collinear matching onto $\bar{c}$-PDF and c-PDF fields has to be performed using equation (3.42) for the threshold (anti)collinear modes appearing in equation (3.48). The time-ordered product of the collinear fields, denoted by $J_c^{m_2}(\{t_k\})$, of a general SCET operator in equation (3.48) with terms from the subleading power SCET Lagrangian makes up the top line of (3.42). Hence, we apply the general matching in (3.42) both to the collinear and anticollinear sectors, which then yields the following for the Drell-Yan matrix element of the generalised matching in (3.47)

$$\begin{aligned}
\langle X|\bar{\psi}\gamma_\rho\psi(0)|A(p_A)B(p_B)\rangle &= \sum_{m_1,m_2} \sum_{i,\bar{i}} \int \{dt_k\} \{d\bar{t}_{\bar{k}}\} \, \widetilde{C}^{m_1,m_2}\left(\{t_k\},\{\bar{t}_{\bar{k}}\}\right) \\
&\times 2\pi \int d\bar{u} \int \{d\bar{z}_{\bar{j}+}\} \, \bar{\tilde{J}}_{\bar{i}}^{m_1}\left(\{\bar{t}_{\bar{k}}\},\bar{u};\{\bar{z}_{\bar{j}+}\}\right) \langle X_{\bar{c}}^{\mathrm{PDF}}|\bar{\chi}_{\bar{c}}^{\mathrm{PDF}}(\bar{u}n_-)|B(p_B)\rangle \\
&\times 2\pi \int du \int \{dz_{j-}\} \, \tilde{J}_i^{m_2}\left(\{t_k\},u;\{z_{j-}\}\right) \langle X_c^{\mathrm{PDF}}|\chi_c^{\mathrm{PDF}}(un_+)|A(p_A)\rangle \\
&\times \Gamma_\rho^{m_1,m_2} \langle X_s| \mathbf{T}\left(\bar{\mathfrak{s}}_{\bar{i}}(\{\bar{z}_{\bar{j}+}\})\left[Y_-^\dagger J_s Y_+\right](0) \, \mathfrak{s}_i(\{z_{j-}\})\right)|0\rangle .
\end{aligned} \tag{3.50}$$

We take a moment to go through the notation used in this equation. The index k $(\bar{k})$ counts the number of collinear (anticollinear) building block fields within each current, and a sum over all possible currents is performed. The number of insertions of the subleading power Lagrangian terms into the collinear (anticollinear) sector is indexed by j $(\bar{j})$, and the sum is again over all possibilities. As we have stressed in section 3.1.2, a non-vanishing subleading-power amplitude can only arise when at least one subleading power Lagrangian insertion is included. Finally, the $\tilde{J}_i$ $(\bar{\tilde{J}}_{\bar{i}})$ are the collinear (anticollinear) functions and

$\mathfrak{s}_i(\{z_{j-}\})$ $(\bar{\mathfrak{s}}_{\bar{\imath}}(\{\bar{z}_{\bar{\jmath}+}\}))$ are constructed with explicit $\mathcal{B}^+$, q_+ $(\mathcal{B}^-$, $q_-)$ field products and their derivatives. The possible structures are listed in (3.45). It is understood that at leading power, or when a single time-ordered product is present on one leg only, both or one of the collinear functions are trivial, and the corresponding soft build block is unity. We point out that in the above equation, and throughout the text, the barred notation $(\bar{\ })$ is used to denote the anticollinear direction, and the tilde $(\tilde{\ })$ refers to the quantities with dependence on the position arguments such as $t, \bar{t}$. This notation, which we also use for indices, is meant to help keep track of the origin of the many different contributions to the factorisation theorem.

In the next steps of the derivation of the general factorisation formula, we require the Fourier transform of the generalised hard matching Wilson coefficients written in (2.120), and for the c-PDF and (c)-PDF fields, which are given by

$$\chi_c^{\mathrm{PDF}}(un_+) = \int \frac{d(n_+p_a)}{2\pi} e^{-i(n_+p_a)\,u}\, \hat{\chi}_c^{\mathrm{PDF}}(n_+p_a)\,, \tag{3.51}$$

$$\bar{\chi}_{\bar{c}}^{\mathrm{PDF}}(\bar{u}n_-) = \int \frac{d(n_-p_b)}{2\pi} e^{+i(n_-p_b)\,\bar{u}}\, \hat{\bar{\chi}}_{\bar{c}}^{\mathrm{PDF}}(n_-p_b)\,. \tag{3.52}$$

Moreover, remembering that $z_{j-} = n_+z_j/2$ $\left(\bar{z}_{\bar{\jmath}+} = n_-z_{\bar{\jmath}}/2\right)$ we make the following definition for the collinear (anticollinear) functions

$$\int \{dt_k\} \int du\, \tilde{J}_i^{m_2}\left(\{t_k\}, u; \{z_{j-}\}\right)\, e^{i\,(n_+p_k)\,t_k}\, e^{-i(n_+p_a)\,u}$$
$$= \int \left\{\frac{d\omega_j}{2\pi}\right\}\, e^{-i\omega_j\,z_{j-}}\, J_i^{m_2}\left(\{n_+p_k\}, n_+p_a; \{\omega_j\}\right)\,, \tag{3.53}$$

$$\int \{d\bar{t}_{\bar{k}}\} \int d\bar{u}\, \tilde{\bar{J}}_{\bar{\imath}}^{m_1}\left(\{\bar{t}_{\bar{k}}\}, \bar{u}; \{\bar{z}_{\bar{\jmath}+}\}\right)\, e^{i(n-\bar{p}_{\bar{k}})\,\bar{t}_{\bar{k}}} e^{+i(n_-p_b)\,\bar{u}}$$
$$= \int \left\{\frac{d\bar{\omega}_{\bar{\jmath}}}{2\pi}\right\}\, e^{-i\bar{\omega}_{\bar{\jmath}}\bar{z}_{\bar{\jmath}+}}\, \bar{J}_{\bar{\imath}}^{m_1}\left(\{n_-\bar{p}_{\bar{n}}\}, -n_-p_b; \{\bar{\omega}_{\bar{\jmath}}\}\right). \tag{3.54}$$

With $\{\omega_j\}$ $(\{\bar{\omega}_{\bar{\jmath}}\})$ we have labelled the set of variables conjugate to $\{z_{j-}\}$ $(\{\bar{z}_{\bar{\jmath}+}\})$, we use Einstein's summation convention in the exponents, and $\left\{\frac{d\omega_j}{2\pi}\right\} = \frac{d\omega_1}{2\pi} \times ... \times \frac{d\omega_m}{2\pi}$ $\left(\left\{\frac{d\bar{\omega}_{\bar{\jmath}}}{2\pi}\right\} = \frac{d\bar{\omega}_{\bar{1}}}{2\pi} \times ... \times \frac{d\bar{\omega}_{\bar{m}}}{2\pi}\right)$. The variables $\{\omega_j\}$ $(\{\bar{\omega}_{\bar{\jmath}}\})$ have a soft scaling. Implementing equations (2.120) and (3.51) – (3.54) in (3.50) yields the following result

$$\langle X|\bar{\psi}\gamma_\rho\psi(0)|A(p_A)B(p_B)\rangle = \sum_{m_1,m_2} \sum_{i,\bar{\imath}} \int \left\{\frac{dn_+p_k}{2\pi}\right\} \left\{\frac{dn_-\bar{p}_{\bar{k}}}{2\pi}\right\}$$
$$\times \int d(n_+p_a)\, d(n_-p_b)\, C^{m_1,m_2}(\{n_+p_k\}, \{n_-\bar{p}_{\bar{k}}\})$$
$$\times \int \left\{\frac{d\bar{\omega}_{\bar{\jmath}}}{2\pi}\right\}\, \bar{J}_{\bar{\imath}}^{m_1}\left(\{n_-\bar{p}_{\bar{k}}\}, -n_-p_b; \{\bar{\omega}_{\bar{\jmath}}\}\right)\, \langle X_{\bar{c}}^{\mathrm{PDF}}|\hat{\bar{\chi}}_{\bar{c}}^{\mathrm{PDF}}(n_-p_b)|B(p_B)\rangle$$
$$\times \int \left\{\frac{d\omega_j}{2\pi}\right\}\, J_i^{m_2}\left(\{n_+p_k\}, n_+p_a; \{\omega_j\}\right)\, \langle X_c^{\mathrm{PDF}}|\hat{\chi}_c^{\mathrm{PDF}}(n_+p_a)|A(p_A)\rangle$$

$$\times \Gamma_\rho^{m_1,m_2} \int \{d\bar{z}_{\bar{j}+}\} \int \{dz_{j-}\} \, e^{-i\bar{\omega}_{\bar{j}} \bar{z}_{\bar{j}+}} \, e^{-i\omega_j z_{j-}}$$

$$\times \langle X_s | \, \mathbf{T} \left(\bar{\mathfrak{s}}_{\bar{i}} (\{\bar{z}_{\bar{j}+}\}) \left[Y_-^\dagger J_s Y_+ \right] (0) \, \mathfrak{s}_i (\{z_{j-}\}) \right) | 0 \rangle \,. \tag{3.55}$$

The next steps in the derivation of the factorisation formula involve squaring the amplitude, which results in the hadronic tensor $W_{\mu\rho}$ defined in (3.9), and introducing the PDFs using the definitions in (3.22) and (3.23). For these reasons, it is useful to inverse Fourier transform the c-PDF and $\bar{c}$-PDF fields into position space. This yields the following for the amplitude and its conjugate,

$$
\begin{aligned}
\langle X | \bar{\psi} \gamma_\rho \psi(0) | A(p_A) B(p_B) \rangle &= \sum_{m_1,m_2} \sum_{i,\bar{i}} \int \left\{ \frac{dn_+ p_k}{2\pi} \right\} \left\{ \frac{dn_- \bar{p}_{\bar{k}}}{2\pi} \right\} \\
&\times \int d(n_+ p_a) \, d(n_- p_b) \int dg \, d\bar{g} \, e^{i(n_+ p_a)g} e^{-i(n_- p_b)\bar{g}} \, C^{m_1,m_2}(\{n_+ p_k\}, \{n_- \bar{p}_{\bar{k}}\}) \\
&\times \int \left\{ \frac{d\bar{\omega}_{\bar{j}}}{2\pi} \right\} \bar{J}_{\bar{i}}^{m_1} \left(\{n_- \bar{p}_{\bar{k}}\}, -n_- p_b; \{\bar{\omega}_{\bar{j}}\} \right) \langle X_{\bar{c}}^{\mathrm{PDF}} | \bar{\chi}_{\bar{c}}^{\mathrm{PDF}} (\bar{g} \, n_-) | B(p_B) \rangle \\
&\times \int \left\{ \frac{d\omega_j}{2\pi} \right\} J_i^{m_2} \left(\{n_+ p_k\}, n_+ p_a; \{\omega_j\} \right) \langle X_c^{\mathrm{PDF}} | \chi_c^{\mathrm{PDF}} (g \, n_+) | A(p_A) \rangle \\
&\times \Gamma_\rho^{m_1,m_2} \times \int \{d\bar{z}_{\bar{j}+}\} \int \{dz_{j-}\} \, e^{-i\bar{\omega}_{\bar{j}} \bar{z}_{\bar{j}+}} \, e^{-i\omega_j z_{j-}} \\
&\times \langle X_s | \mathbf{T} \left(\bar{\mathfrak{s}}_{\bar{i}} (\{\bar{z}_{\bar{j}+}\}) \left[Y_-^\dagger J_s Y_+ \right] (0) \, \mathfrak{s}_i (\{z_{j-}\}) \right) | 0 \rangle \,,
\end{aligned}
\tag{3.56}
$$

and

$$
\begin{aligned}
\langle A(p_A) B(p_B) | \psi \gamma_\mu \bar{\psi}(0) | X \rangle &= \sum_{m_1',m_2'} \sum_{i',\bar{i}'} \int \left\{ \frac{d(n_+ p_{k'}')}{2\pi} \right\} \left\{ \frac{d(n_- \bar{p}_{\bar{k}'}')}{2\pi} \right\} \\
&\times \int d(n_+ p_a') \, d(n_- p_b') \int dg' d\bar{g}' \, e^{-i(n_+ p_a')g'} \, e^{+i(n_- p_b')\bar{g}'} \, C^{*\, m_1',m_2'} (\{n_+ p_{k'}'\}, \{n_- \bar{p}_{\bar{k}'}'\}) \\
&\times \int \left\{ \frac{d\bar{\omega}_{\bar{j}'}'}{2\pi} \right\} \bar{J}_{\bar{i}'}^{*\, m_1'} \left(\{n_- \bar{p}_{\bar{k}'}'\}, -n_- p_b'; , \{\bar{\omega}_{\bar{j}'}'\} \right) \langle B(p_B) | \chi_{\bar{c}}^{\mathrm{PDF}} (\bar{g}' \, n_-) | X_{\bar{c}}^{\mathrm{PDF}} \rangle \\
&\times \int \left\{ \frac{d\omega_{j'}'}{2\pi} \right\} J_{i'}^{*\, m_2'} \left(\{n_+ p_{k'}'\}, n_+ p_a'; \{\omega_{j'}'\} \right) \langle A(p_A) | \bar{\chi}_c^{\mathrm{PDF}} (g' \, n_+) | X_c^{\mathrm{PDF}} \rangle \\
&\times \bar{\Gamma}_\mu^{m_1',m_2'} \times \int \{d\bar{z}_{\bar{j}'+}'\} \int \{dz_{j'-}'\} e^{+i\bar{\omega}_{\bar{j}'}' \bar{z}_{\bar{j}'+}'} e^{+i\omega_{j'}' z_{j'-}'} \\
&\times \langle 0 | \bar{\mathbf{T}} \left(\bar{\mathfrak{s}}_{i'}' (\{z_{j'-}'\}) \left[Y_+^\dagger J_s^\dagger Y_- \right] (0) \, \mathfrak{s}_{\bar{i}'}' (\{\bar{z}_{\bar{j}'+}'\}) \right) | X_s \rangle \,,
\end{aligned}
\tag{3.57}
$$

respectively. The expressions become cumbersome at this point and beyond, in particular since the next step involves bringing together the above two expressions according to (3.9). Therefore, to keep the size of the expressions manageable we define the following coefficient function which contains both, the collinear, anticollinear, and hard matching functions at the amplitude level,

$$
\begin{aligned}
D_{i\bar{i}\,\rho}^{m_1,m_2} (n_+ p_a, -n_- p_b; \{\omega_j\}, \{\bar{\omega}_{\bar{j}}\}) &= (2\pi)^2 \int \left\{ \frac{dn_+ p_k}{2\pi} \right\} \left\{ \frac{dn_- \bar{p}_{\bar{k}}}{2\pi} \right\} \\
&\times C^{m_1,m_2}(\{n_+ p_k\}, \{n_- \bar{p}_{\bar{k}}\}) \, \bar{J}_{\bar{i}}^{m_1}(\{n_- \bar{p}_{\bar{k}}\}, -n_- p_b; \{\bar{\omega}_{\bar{j}}\})
\end{aligned}
$$

$$\times \Gamma_\rho^{m_1,m_2}\; J_i^{m_2}(\{n_+p_k\}, n_+p_a; \{\omega_j\})\,, \tag{3.58}$$

$$
\begin{aligned}
D^{*\,m_1',m_2'}_{i'\,\bar{i}'\,\mu}(n_+p_a', -n_-p_b'; \{\omega_{j'}'\}, \{\bar{\omega}_{\bar{j}'}'\}) \;&=\; (2\pi)^2 \int \left\{\frac{d(n_+p_{k'}')}{2\pi}\right\} \left\{\frac{d(n_-\bar{p}_{\bar{k}'}')}{2\pi}\right\} \\
&\times C^{*\,m_1',m_2'}(\{n_+p_{k'}'\}, \{n_-\bar{p}_{\bar{k}'}'\}) \bar{J}^{*\,m_1'}_{\bar{i}'}\left(\{n_-\bar{p}_{\bar{k}'}'\}, -n_-p_b'; \{\bar{\omega}_{\bar{j}'}'\}\right) \\
&\times \bar{\Gamma}^{m_1',m_2'}_\mu J^{*\,m_2'}_{i'}\left(\{n_+p_{k'}'\}, n_+p_a'; \{\omega_{j'}'\}\right)\,. \tag{3.59}
\end{aligned}
$$

As mentioned above, we now square the amplitude, which gives the hadronic tensor $W_{\mu\rho}$ defined in (3.9). The hadronic tensor is related to the d-dimensional cross-section as dictated by equation (3.8).

Many simplifications can be made at this stage. The c-PDF and $\bar{c}$-PDF matrix elements, with corresponding fields written in coordinate space, are identified with the PDFs, which are given in equations (3.22) and (3.23) for the derivation of factorisation formula at leading power. We perform integrations over the auxiliary variables $g, \bar{g}, g'$, and $\bar{g}'$. This gives delta functions which are then used in evaluation of integrals over n_+p_a, n_-p_b, n_+p_a', and n_-p_b'. When the dust settles, we end up with an all-power version of equation $(3.24)^2$. Extracting then the convolution with the PDFs from the hadronic Drell-Yan spectrum as given in (3.27), we obtain the expression

$$
\begin{aligned}
\hat{\sigma} \;=\; & \sum_{\substack{m_1',m_2' \\ m_1,m_2}} \sum_{\substack{i',\bar{i}' \\ i,\bar{i}}} \int \left\{\frac{d\bar{\omega}_{\bar{j}'}'}{2\pi}\right\} \left\{\frac{d\omega_{j'}'}{2\pi}\right\} \left\{\frac{d\bar{\omega}_{\bar{j}}}{2\pi}\right\} \left\{\frac{d\omega_j}{2\pi}\right\} \\
& \times (-Q^2) \left[\left(\frac{\slashed{n}_-}{4}\right) D^{*\,m_1',m_2'\,\rho}_{i'\,\bar{i}'}(x_a n_+p_A, x_b n_-p_B; \{\omega_{j'}'\}, \{\bar{\omega}_{\bar{j}'}'\})\right. \\
& \qquad\qquad \left. \times \left(\frac{\slashed{n}_+}{4}\right) D^{m_1,m_2}_{i\,\bar{i}\,\rho}(x_a n_+p_A, x_b n_-p_B; \{\omega_j\}, \{\bar{\omega}_{\bar{j}}\})\right] \\
& \times \int \frac{d^{d-1}\vec{q}}{(2\pi)^{d-1}\,2\sqrt{Q^2+\vec{q}^{\,2}}}\,\frac{1}{2\pi}\int d^d x\, e^{i(x_a p_A + x_b\, p_B - q)\cdot x} \\
& \times \widetilde{S}_{i\,\bar{i}\,i'\,\bar{i}'}(x; \{\omega_j\}, \{\bar{\omega}_{\bar{j}}\}, \{\omega_{j'}'\}, \{\bar{\omega}_{\bar{j}'}'\}) \tag{3.60}
\end{aligned}
$$

for the most general form of the power-suppressed $q\bar{q}$-induced partonic cross-section near threshold. We remind the reader that the barred and tilde notation is used to refer to the anticollinear direction and objects which depend on the coordinate-space arguments, respectively. The complex conjugate amplitude contributions to the factorisation formula are marked throughout the text with a prime ($'$) symbol. We note that this use of notation also applies to the indices and can be mixed, in such a way that for example $\bar{i}'$ denotes the contribution from the anticollinear piece of the complex conjugate amplitude.

In the last line of the above equation we have introduced the generalised multi-local soft function, $\widetilde{S}_{i\,\bar{i}\,i'\,\bar{i}'}(x; \{\omega_j\}, \{\bar{\omega}_{\bar{j}}\}, \{\omega_{j'}'\}, \{\bar{\omega}_{\bar{j}'}'\})$, which is given by

$$\widetilde{S}_{i\,\bar{i}\,i'\,\bar{i}'}(x; \{\omega_j\}, \{\bar{\omega}_{\bar{j}}\}, \{\omega_{j'}'\}, \{\bar{\omega}_{\bar{j}'}'\})$$

---

[2]Except for the fact that here we do not evaluate the lepton trace since we keep $\Gamma_\rho^{m_1,m_2}$ and $\bar{\Gamma}^{m_1',m_2'\,\rho}$ structures general.

$$
= \int \{d\bar{z}'_{\bar{j}'+}\} \int \{dz'_{j'-}\} \int \{d\bar{z}_{\bar{j}+}\} \int \{dz_{j-}\} \; e^{+i\bar{\omega}'_{\bar{j}'}\bar{z}'_{\bar{j}'+}} \, e^{+i\omega'_{j'}z'_{j'-}} \; e^{-i\bar{\omega}_{\bar{j}}\bar{z}_{\bar{j}+}} \; e^{-i\omega_j z_{j-}}
$$

$$
\times \frac{1}{N_c} \mathrm{Tr} \, \langle 0 | \bar{\mathbf{T}} \left(\bar{\mathfrak{s}}'_{i'} \left(\{x + z'_{j'-}\} \right) \left[Y^\dagger_+ \, J^\dagger_s \, Y_- \right](x) \, \mathfrak{s}'_{\bar{i}'} \left(\{x + \bar{z}'_{\bar{j}'+}\} \right) \right)
$$

$$
\times \mathbf{T} \left(\bar{\mathfrak{s}}_{\bar{i}} \left(\{\bar{z}_{\bar{j}+}\} \right) \left[Y^\dagger_- \, J_s \, Y_+ \right](0) \, \mathfrak{s}_i \left(\{z_{j-}\} \right) \right) | 0 \rangle . \tag{3.61}
$$

With this we conclude the derivation of the general factorisation formula for the Drell-Yan cross-section in the $z \to 1$ limit including power corrections in $(1-z)$. These results have appeared in equations (2.1) and (2.2) of [40] without a derivation, which is carried out here as in [65] with additional details and explicit intermediate equations. We remark here that up to this point no phase space expansion has been carried out. This is in contrast to the result for the leading power factorisation formula in equation (3.28) with the soft function given in (3.29), where the spatial $d^{d-1}q$ and $d^{d-1}x$ integrals were performed leaving behind dependence only on the energy component of the soft radiation crossing the cut. The phase space is not homogeneous in the λ power counting, which is manifested in equations (3.25) and (3.26). To these type of power corrections, originating in the expansion of the phase space, we will refer to as *kinematic power corrections*. Power corrections due to subleading power currents and insertions of subleading Lagrangian terms are named *dynamical power corrections*. At leading power only the lowest orders in both kinematic and dynamic power corrections is kept hence we can unambiguously write down the result as in (3.28) with the soft function in (3.29). However, at any given higher order in the power expansion, one has to account for all possible contributions due to interference from these two types of power corrections. Since the formula in equation (3.60) is general and accurate to all powers, we keep the phase space unexpanded.

3.2.2 Factorisation at next-to-leading power

In this section we restrict the discussion general subleading power effects to only the next-to-leading power. At this level, we can make certain simplifications in the general formula given in equation (3.60).

The first observation we make is that the total number of ω variables at next-to-leading power is highly constrained. This is due to the fact that the ω variables are connected to the soft emissions from collinear functions, which means that they originate in time-ordered product insertions of subleading-power Lagrangian terms. On the one hand, at least one ω variable must appear since at least one time-ordered product operator must be present in the SCET amplitude to induce a threshold-collinear scale. Otherwise, as we have discussed in section 3.1.2, all of the threshold-collinear corrections to the $(\bar{c})c$-PDF matrix element are scaleless and a trivial null result is obtained. On the other hand, the total power suppression at next-to-leading power is $\mathcal{O}(\lambda^2)$. Therefore, no more than two separate ω variables can be present. These would correspond to two $\mathcal{L}^{(1)}$ insertions, each providing $\mathcal{O}(\lambda)$ suppression. The limit on the total number of subleading power soft-collinear interactions also constrains the total number of soft structures $\mathfrak{s}_i$ from the set (3.45), that are required at next-to-leading power.

Another simplification occurs due to the fact that in the position-space SCET framework, as we discussed in section 2.4.1, the purely soft building blocks start contributing to the current operator only from $\mathcal{O}(\lambda^3)$ [86]. Therefore, at next-to-leading power the purely soft

part $J_s(0)$ does not appear in the factorisation formula. The soft structures originate only from single insertions of the $\mathcal{O}(\lambda^2)$ SCET Lagrangian terms, $\mathcal{L}_\xi^{(2)}$ and $\mathcal{L}_{\text{YM}}^{(2)}$, in equations (2.65) and (2.69), and double insertions of the single power-suppressed Lagrangian terms, $\mathcal{L}_\xi^{(1)}$, $\mathcal{L}_{\xi q}^{(1)}$, and $\mathcal{L}_{\text{YM}}^{(1)}$, in equations (2.63), (2.66), and (2.68), respectively.

We next consider the kinematic set up of the process itself. In the centre-of-mass frame, the kinematic set up does not support power suppression induced by an operator with $\mathcal{O}(\lambda)$ scaling on the collinear or anticollinear leg. This simplification arises because the incoming collinear (anticollinear) momentum may be chosen to carry only its large component, $p^\mu = (n_+p, 0, 0)$ $(l^\mu = (0, n_-l, 0))$ with $n_+p \sim Q$ $(n_-l \sim Q$ for the anticollinear leg), as we have chosen in section 3.1.1 for the calculation of the amplitude with one collinear loop at leading power. We recall also that the components of the soft momentum all scale as $\mathcal{O}(\lambda^2)$. The key observation is that in order for the collinear (anticollinear) leg to carry $\mathcal{O}(\lambda)$ suppression, it would necessarily have to be proportional to $p_\perp^\mu(l_\perp^\mu) \sim Q\lambda$, the transverse component of the collinear (anticollinear) momentum. This is because there exists no other momentum component in the threshold kinematics which has a $\mathcal{O}(\lambda)$ scaling. However, the transverse momentum component of both the collinear and anticollinear momenta vanishes. This, therefore, implies that the $\mathcal{O}(\lambda^2)$ power suppression cannot arise due to two separate insertions of $\mathcal{L}_\xi^{(1)}$ (or $\mathcal{L}_{\text{YM}}^{(1)}$) Lagrangian terms on two different legs of a diagram. The above arguments also imply that in the $q\bar{q}$ channel a non-vanishing $\mathcal{O}(\lambda)$ *amplitude* does not exist. It should be noted however, that this does not mean that a non-vanishing $\mathcal{O}(\lambda)$ cannot contribute in general. Indeed, the emission of a soft quark does give rise to an amplitude with such scaling, however this forms a part of the (anti)quark-gluon (qg, $\bar{q}g$) channel and will be explored in more detail in section 3.3.

In consequence, at cross-section level at next-to-leading power, the $\mathcal{O}(\lambda^2)$ power correction must arise in the amplitude which is then interfered with the leading power amplitude as dictated by (3.9). This yields the next-to-leading power, $\mathcal{O}(\lambda^2)$ suppressed, cross-section. There still exist numerous possibilities for the generation of $\mathcal{O}(\lambda^2)$ suppression in the amplitude. One of the types of possibilities is a time-ordered product operator, such as $J^{T2}(t)$, built from a $\mathcal{L}^{(1)}$ insertion and a subleading current of type J^{A1} or J^{B1}. We have discussed the $\mathcal{O}(\lambda)$ power suppressed currents in the example matching in section 2.4.4. For convenience, we write the two possible types of currents here, including explicitly the Γ_ρ structure

$$J_\rho^{A0,A1}(t, \bar{t}) \;\; = \;\; \bar{\chi}_{\bar{c}}(\bar{t}n_-) \, n_{+\rho} \, i\partial\!\!\!/_\perp \chi_c(tn_+), \tag{3.62}$$

$$J_\rho^{A0,B1}(t_1, t_2, \bar{t}) \;\; = \;\; \bar{\chi}_{\bar{c}}(\bar{t}n_-) \, n_{\pm\rho} \, A\!\!\!/_{c\perp}(t_2 n_+)\chi_c(t_1 n_+), \tag{3.63}$$

There also exist the corresponding power suppressed currents with the power suppression in the anticollinear direction, which we do not write explicitly here. The most significant aspect of the two $\mathcal{O}(\lambda)$ currents is that both are proportional to $n_{\pm\rho}$. This is an important feature because at the cross-section level the amplitude in which the J^{A1} and J^{B1} currents could appear, is interfered with the leading power amplitude. As can be seen in (3.11), the latter is proportional to $\gamma_{\perp\rho}$. The contraction of $n_{\pm\rho}$ and $\gamma_{\perp\rho}$ yields a null result. Therefore, a potential contribution of this type vanishes at cross-section level to all orders in perturbation theory. This is a major simplification in the type and number of contributions possible at next-to-leading power in the general factorisation formula derived

in section 3.2.1. At next-to-leading power, the sum over the indices in $m_{1,2}$ in the formula in equation (3.60) contains only the J^{A0}-type current, along with the time-ordered product operators built from the leading power J^{A0} current and insertions of subleading power SCET Lagrangian terms. This also implies that in the next-to-leading power factorisation formula, the only the hard matching coefficient of the leading power current, $C^{A0,A0}$, appears.

The consequence of the above considerations is that the soft structures which are relevant at next-to-leading power are the explicitly presented terms in (3.45) and the ellipsis is dropped. This statement holds after the equation of motion, written in (3.46), is used to eliminate the soft structure $n_+ \mathcal{B}^+$, which is redundant.

The above discussion of the simplifications which occur at next-to-leading power, but may not necessarily apply beyond that accuracy, allows us to present a more compact, next-to-leading power, version of the general subleading-power factorisation formula given in equation (3.60). Specifically, up to and including $\mathcal{O}(\lambda^2)$ the general formula in (3.60) simplifies to the following

$$
\begin{aligned}
\hat{\sigma}(z) \;=\; & \sum_{i,i'=0}^{5} \int \left\{ \frac{d\omega_j}{2\pi} \right\} \left\{ \frac{d\omega'_{j'}}{2\pi} \right\} \mathrm{Tr} \left[\left(\frac{\not{n}_-}{4} \right) D_{i'}^{*\rho}(x_a n_+ p_A, x_b n_- p_B; \{\omega'_{j'}\}) \right. \\
& \times \left. \left(\frac{\not{n}_+}{4} \right) D_{i\rho}(x_a n_+ p_A, x_b n_- p_B; \{\omega_j\}) \right] \\
& \times (-Q^2) \int \frac{d^{d-1}\vec{q}}{(2\pi)^{d-1} 2\sqrt{Q^2 + \vec{q}^2}} \frac{1}{2\pi} \int d^d x \, e^{i(x_a p_A + x_b p_B - q)\cdot x} \widetilde{S}_{ii'}(x; \{\omega_j\}, \{\omega'_{j'}\}) \\
& + \bar{c}\text{-terms}\,,
\end{aligned}
\tag{3.64}
$$

The set notation, namely $\{\omega_j\} = \{\omega_1, \omega_2\}$, is necessary only for the $i = 4, 5$ terms. These correspond to contributions where the soft structures are made up of insertions of the fields at different positions. This can be verified by considering the explicit expressions written below. The remaining terms require only a single ω variable. An exception to this statement is the leading power position space soft function, written above in equation (3.30), which naturally does not require any ω variables as it is solely made up of products of Wilson lines.

In equation (3.64), the terms, where the power suppression is placed on the anticollinear leg, are denoted by "$\bar{c}$-terms". This is done both for the amplitude and its conjugate. We do not write these terms explicitly to keep the expressions as concise as possible. Eventually, these terms contribute a factor of 2 to the power-suppressed terms in the formula in the above equation.

We have argued in detail above, that at next-to-leading power only the $J^{A0,A0}$ current is required in formation of time-ordered products with subleading-power Lagrangian insertions in the matching to the Drell-Yan vector current. This implies that the general structure Γ^ρ which is defined in equation (3.48) in simply given by $\gamma_\perp^\rho$ at next-to-leading power. Moreover, the anticollinear functions $\bar{J}_{\bar{i}}^{m_1}(\{n_- \bar{p}_{\bar{k}}\}, -n_- p_b; \{\bar{\omega}_{\bar{j}}\})$ in the general definition (3.58) are in fact delta functions in $D_{i\rho}(x_a n_+ p_A, x_b n_- p_B; \{\omega_j\})$ since the power suppression in $D_{i\rho}(x_a n_+ p_A, x_b n_- p_B; \{\omega_j\})$ is placed on the collinear leg. This means that the $D_{i\rho}(x_a n_+ p_A, x_b n_- p_B; \{\omega_j\})$ coefficient function simplifies to

$$
D_{i\rho}(x_a n_+ p_A, x_b n_- p_B; \{\omega_j\}) \;=\; \int d(n_+ p)\, d(n_- \bar{p})\, C^{A0,A0}(n_+ p, n_- \bar{p})
$$

$$\times\, \delta(n_-\bar{p} - x_b\, n_- p_B)\, \gamma_{\perp\rho}\, J_i\left(n_+ p, x_a\, n_+ p_A; \{\omega_j\}\right) . \tag{3.65}$$

In order to keep the expression general and notation not too cumbersome, we have chosen the index i, that is summed over in (3.64), to stand in place of all necessary indices—Dirac, Lorentz, and colour—that are needed by each separate term depending on the specific soft structure that acts as a projector in the collinear matching given in equation (3.42). We point out that in the evaluation of this factorisation formula, one must contract these indices before the spin trace is performed in equation (3.64). The reason for this is that particular soft functions, such as S_5 which we write explicitly below, can contain open spin indices that connect it to the collinear function. There also exists a similar expression to one given in equation (3.65) for the conjugate amplitude $D_{i'}^{*\rho}$ with variables $\{\omega_j\}$ replaced by $\{\omega'_{j'}\}$. It should also be noted that at leading power, both the collinear and anticollinear functions are simply delta functions as we have seen in section 3.1.1 with the trivial matching example. In this case, the $D_{i\rho}$ reduces to $\gamma_{\perp\rho}\, C^{A0,A0}$.

In the same way as in equation (3.60) for the general factorisation formula, the final-state phase-space integral over the lepton-pair momentum $\vec{q}$ is still contained in equation (3.64) in its exact form. As we have discussed in section 3.2.1, equations (3.25) and (3.26) indicate that the phase-space integral also adheres to a threshold power expansion in $(1 - z)$. Therefore, in addition to the dynamical power corrections originating through time-ordered product insertions into the amplitude, there exist also kinematic power corrections where the amplitudes are kept at leading power in λ and it is the integration over the phase space that provides the power correction. This type of correction we denote by $\Delta_{\text{NLP}}^{kin}(z)$ making use of the definition in (3.31) and it will be discussed in more detail below.

Before we proceed to explore the factorisation formula in (3.64) further, we focus on the appearing collinear functions themselves. We already discussed that in the next-to-leading power factorisation only the leading power hard current $J^{A0,A0}$ is required to form the time-ordered product operators with insertions of subleading-power Lagrangian terms. This leads us to the conclusion that in the next-to-leading power case the set $\{\psi_c(t_k n_+)\}$ in the general collinear matching equation (3.42) is in fact made up of only a single quark or antiquark collinear field. Moreover, the set $\{\mathcal{L}^{(l)}(z_j)\}$ of Lagrangian insertions is either formed by only $\mathcal{O}(\lambda^2)$ insertions $\{\mathcal{L}^{(2)}(z)\}$ or two $\mathcal{O}(\lambda)$ insertions $\{\mathcal{L}^{(1)}(z_1), \mathcal{L}^{(1)}(z_2)\}$. Making use of the momentum-space collinear functions which were defined in (3.53), leads us to conclude that the collinear matching equation at next-to-leading power is either given by

$$i \int d^d z\, \mathbf{T}\left[\chi_{c,\gamma f}\left(t n_+\right) \mathcal{L}^{(2)}(z)\right] \quad = 2\pi \sum_i \int \frac{d\omega}{2\pi} \int \frac{dn_+ p}{2\pi}\, e^{-i(n_+ p)\, t} \int \frac{dn_+ p_a}{2\pi}$$

$$\times J_{i;\gamma\beta,\mu,fbd}\left(n_+ p, n_+ p_a; \omega\right)\, \hat{\chi}_{c,\beta b}^{\text{PDF}}(n_+ p_a) \int dz_-\, e^{-i\,\omega\, z_-}\, \mathfrak{s}_{i;\mu,d}(z_-) \tag{3.66}$$

for the $\mathcal{L}^{(2)}(z)$ insertions, or

$$i^2 \int d^d z_1 \int d^d z_2\, \mathbf{T}\left[\chi_{c,\gamma f}\left(t n_+\right) \mathcal{L}^{(1)}(z_1) \mathcal{L}^{(1)}(z_2)\right] \quad = 2\pi \sum_i \int \frac{d\omega_1}{2\pi} \frac{d\omega_2}{2\pi} \int \frac{dn_+ p}{2\pi}\, e^{-i(n_+ p)\, t}$$

$$\times \int \frac{dn_+ p_a}{2\pi}\, J_{i;\gamma\beta,\mu,fbd}\left(n_+ p, n_+ p_a; \omega_1, \omega_2\right)\, \hat{\chi}_{c,\beta b}^{\text{PDF}}(n_+ p_a)$$

$$\times \int dz_{1-} dz_{2-} \, e^{-i\,\omega_1\,z_{1-}} e^{-i\,\omega_2\,z_{2-}} \, \mathfrak{s}_{i;\mu,d}(z_{1-}, z_{2-}) \tag{3.67}$$

for the double $\mathcal{L}^{(1)}(z_1)\mathcal{L}^{(1)}(z_2)$ insertions. The indices μ and d connecting the J_i and $\mathfrak{s}_i$ structures stand for the collective Lorentz and colour indices suitable for the particular soft structure. As we have mentioned previously, and as can be seen on the right-hand side of equations (3.66) and (3.67), for each independent soft structure $\mathfrak{s}_i$ we have a corresponding collinear function J_i.

In the following steps, we further simplify the factorisation formula in equation (3.64). In order to avoid confusion, we discuss the kinematic and dynamical next-to-leading power corrections separately. Before we continue, we recall the discussion in the vicinity of equation (3.31). The important remark there is that the next-to-leading power factorisation formula we have derived and written in equation (3.64) is for the bare partonic cross-section $\hat{\sigma}$. Care has to be taken when dealing with this d-dimensional quantity. For example, the collinear singularities are still contained in $\hat{\sigma}$. These are usually subtracted by PDF renormalization. Moreover, the spin trace gives the following in d-dimensions $\mathrm{Tr}\left[\left(\frac{\not{n}_-}{4}\right)\gamma_{\perp\rho}\left(\frac{\not{n}_+}{4}\right)\gamma_{\perp}^\rho\right] = -(1-\epsilon)$ as we have already discussed in section 3.1.1. Therefore, in order to conveniently be able to compare the results obtained here with literature such as [117, 116], in what follows we consider the quantity Δ as defined in equation (3.31). The $1/(1-\epsilon)$ factor accounts for the fact that we work in d-dimensions, and the $1/z$ factor is also conventional in literature [117, 116].

NLP kinematic correction $\Delta_{\mathrm{NLP}}^{kin}(z)$

As explained above, contributions to the next-to-leading power cross-section can originate in expanding the kinematic factors to next-to-leading power accuracy, while keeping the soft and hard functions at leading power (recall that collinear functions are trivial at leading power). We now investigate these kinematic corrections to the Drell-Yan cross-section. The starting point is to take the leading power soft function term in (3.64). Noting that at leading power no time-ordered product insertions appear in the factorisation formula, such that the D coefficients can simplified as explained below equation (3.65), we begin to classify the kinematic corrections from the following expression

$$\Delta_{\mathrm{LP+NLP}}^{kin}(z) = \ H(\hat{s}) \frac{1}{z} \frac{Q}{4\pi} \int \frac{d^{d-1}\vec{q}}{(2\pi)^{d-1}} \int d^d x \, e^{i(\Omega_*/2)x^0 - i(\vec{q}^{\,2}/(2Q))x^0 - i\vec{q}\cdot\vec{x}} \, \widetilde{S}_0\left(x\right), \tag{3.68}$$

where $H(\hat{s}) = |C^{A0,A0}(x_a n_+ p_A, x_b n_- p_B)|^2$. We have also already used the fact that the energy of the soft hadronic final state can be expanded as in equation (3.25). A number of kinematic corrections can be identified in the above expression. It is understood that in this discussion while we consider a certain source of power corrections, the remaining factors which could give power suppression must be taken at leading power in order to yield overall power suppression for the cross-section at next-to-leading power and not beyond.

The first kinematic correction, which we label "$K1$", arises due to the power suppression provided by the second term in the exponent in equation (3.68). Performing Taylor expansion of the exponent, writing $\vec{q}$ in terms of spatial derivatives, and evaluating the

$d^{d-1}\vec{q}$ and $d^{d-1}\vec{x}$ integrals, we find the approximation

$$\Delta^{K1}_{\text{LP+NLP}}(\Omega) = H\!\left(Q^2\right)\frac{Q}{4\pi}\int dx^0\, e^{ix^0\Omega/2}\left(\underbrace{1}_{\text{LP}} + \underbrace{\frac{ix^0\partial_{\vec{x}}^2}{2Q}}_{\text{NLP}} + \mathcal{O}\!\left(\lambda^4\right)\right)\widetilde{S}_0(x)\Big|_{\vec{x}=0} \qquad (3.69)$$

valid to next-to-leading power. The unity in the bracket is in fact the leading power term and should be ignored as it does not form part of the kinematic correction, we have kept it here for clarity regarding the Taylor expansion. The next-to-leading power kinematic correction $\Delta^{K1}_{\text{NLP}}(\Omega)$ constitutes the second term in the bracket in (3.69), which we have underbraced for clarity. As is usually done, the $\vec{x}=0$ is set only after the spatial derivatives are performed. This result is general, and the derivative can in principle act on any soft function. However, since we work up to next-to-leading power, the kinematic correction needs to only be applied to the leading power soft function.

The second kinematic correction, labelled "$K2$", originates in the expansion of Ω_* in the first exponent in (3.68). The power expansion of Ω_* itself can be found in equation (3.26). We proceed in the same way as above, perform the Taylor expansion of the exponent and evaluate the $d^{d-1}\vec{q}$ and $d^{d-1}\vec{x}$ integrals

$$\Delta^{K2}_{\text{LP+NLP}}(\Omega) = H\!\left(Q^2\right)\frac{Q}{4\pi}\int dx^0\, e^{ix^0\Omega/2}\left(\underbrace{1}_{\text{LP}} + \underbrace{\frac{3i}{8Q}x^0\,\Omega^2}_{\text{NLP}} + \mathcal{O}\!\left(\lambda^4\right)\right)\widetilde{S}_0(x)\Big|_{\vec{x}=0}. \qquad (3.70)$$

Similarly to $\Delta^{K1}_{\text{NLP}}(\Omega)$ in (3.69), $\Delta^{K2}_{\text{NLP}}(\Omega)$ is in fact given only by the second term in the bracket. The first term is the leading power contribution which does not form a part of $\Delta^{K2}_{\text{NLP}}(\Omega)$. In both $\Delta^{K1}_{\text{NLP}}(\Omega)$ and $\Delta^{K2}_{\text{NLP}}(\Omega)$, the linear x^0 term can be replaced by a derivative with respect to Ω and taken out of the integral, the terms which remain form the momentum-space leading power Drell-Yan soft function $S_{\text{DY}}(\Omega)$ which can be found in (3.29).

The third kinematic correction, labelled "$K3$", comes from the expansion of the $1/z$ factor in (3.68). Straightforwardly, we find

$$\Delta^{K3}_{\text{LP+NLP}}(\Omega) = H\!\left(Q^2\right)\frac{1}{4\pi}\left(\underbrace{Q}_{\text{LP}} + \underbrace{\Omega}_{\text{NLP}} + \mathcal{O}\!\left(\lambda^4\right)\right)\int dx^0\, e^{ix^0\Omega/2}\widetilde{S}_0(x)\Big|_{\vec{x}=0}. \qquad (3.71)$$

Here, similarly to above, the first term in the bracket belongs to the leading power result and should be dropped.

The fourth kinematic correction, labelled "$K4$", is due to the expansion of the argument of the hard function $H(\hat{s})$ itself. Incorporating the expansion of the hard matching coefficient, $H(\hat{s}) = H(Q^2) + Q^2(1-z)H'(Q^2) + \mathcal{O}(\lambda^4)$, into (3.68) gives

$$\Delta^{K4}_{\text{LP+NLP}}(\Omega) = \left(\underbrace{H(Q^2)}_{\text{LP}} + \underbrace{Q^2\Omega H'(Q^2)}_{\text{NLP}} + \mathcal{O}(\lambda^4)\right)\frac{1}{4\pi}\int dx^0\, e^{ix^0\Omega/2}\widetilde{S}_0(x)\Big|_{\vec{x}=0}. \qquad (3.72)$$

Again the first term in the expansion of the hard function forms part of the leading power result.

For concreteness, we drop the leading power terms which were pointed out as the leading terms in the above expansions, and write again the four kinematic corrections at next-to-leading power. These are given by the following

$$\Delta^{K1}_{\text{NLP}}(\Omega) \;=\; H\!\left(Q^2\right)\frac{\partial}{\partial\Omega}\,\partial^2_{\vec{x}}\,S_{\text{DY}}(\Omega,\vec{x})|_{\vec{x}=0} \;=\; H\!\left(Q^2\right)S_{K1}(\Omega), \tag{3.73}$$

$$\Delta^{K2}_{\text{NLP}}(\Omega) \;=\; H\!\left(Q^2\right)\frac{3}{4}\,\Omega^2\frac{\partial}{\partial\Omega}S_{\text{DY}}(\Omega,\vec{x})|_{\vec{x}=0} \;=\; H\!\left(Q^2\right)S_{K2}(\Omega), \tag{3.74}$$

$$\Delta^{K3}_{\text{NLP}}(\Omega) \;=\; H\!\left(Q^2\right)\Omega\,S_{\text{DY}}(\Omega,\vec{x})|_{\vec{x}=0} \;=\; H\!\left(Q^2\right)S_{K3}(\Omega), \tag{3.75}$$

$$\Delta^{K4}_{\text{NLP}}(\Omega) \;=\; H'\!\left(Q^2\right)Q^2\,\Omega\,S_{\text{DY}}(\Omega,\vec{x})|_{\vec{x}=0} \;=\; H'\!\left(Q^2\right)Q^2\,S_{K3}(\Omega). \tag{3.76}$$

As we have mentioned, $S_{\text{DY}}(\Omega,\vec{x})$ is the leading power soft function defined in (3.29), with a difference that the x^0 argument is generalised to contain a non-zero spatial contribution $\vec{x}$. The sum of the above four terms, gives the full next-to-leading power kinematic correction, which we denote by $\Delta^{kin}_{\text{NLP}}(z)$. We explicitly evaluate these formulas with the relevant ingredients and present the results up to NNLO in chapter 7.

For the purposes of leading logarithmic resummation at next-to-leading power developed in chapter 8, in equations (3.73), (3.74), and (3.75) we have implicitly defined the three kinematic soft functions

$$S_{K1}(\Omega) \;=\; \frac{\partial}{\partial\Omega}\,\partial^2_{\vec{x}}\,S_{\text{DY}}(\Omega,\vec{x})|_{\vec{x}=0}\,, \tag{3.77}$$

$$S_{K2}(\Omega) \;=\; \frac{3}{4}\,\Omega^2\frac{\partial}{\partial\Omega}S_{\text{DY}}(\Omega,\vec{x})|_{\vec{x}=0}\,, \tag{3.78}$$

$$S_{K3}(\Omega) \;=\; \Omega\,S_{\text{DY}}(\Omega,\vec{x})|_{\vec{x}=0}\,. \tag{3.79}$$

The role of the kinematic corrections in the next-to-leading power resummation is discussed in section 8.2. Next, we consider contributions to the next-to-leading power cross-section from a different source.

Dynamical NLP power correction $\Delta^{dyn}_{\text{NLP}}(z)$

In this section we consider the contribution to the next-to-leading power cross-section where the phase space kinematics are kept at leading power, and the power suppression originates in the insertions of subleading-power Lagrangian terms. This means that, in the same manner as in section 3.1.1, we keep only the first term in the expansions given in equations (3.25) and (3.26). We can again perform the $d^{d-1}\vec{q}$ integral which yields a delta function for the spatial part of x, which then allows us to evaluate the $d^{d-1}\vec{x}$ integral and set $\vec{x}=0$ in the soft functions. Following these steps in equation (3.64) and remembering to switch to $\Delta^{dyn}_{\text{NLP}}(z)$ which is defined in equation (3.31) yields the following

$$\Delta^{dyn}_{\text{NLP}}(z) \;=\; -\frac{1}{(1-\epsilon)}Q\sum_{i,i'=0}^{5}\int\left\{\frac{d\omega_j}{2\pi}\right\}\left\{\frac{d\omega'_{j'}}{2\pi}\right\}\text{Tr}\left[\left(\frac{\slashed{n}_-}{4}\right)D^{*\rho}_{i'}(x_a n_+ p_A, x_b n_- p_B;\{\omega'_{j'}\})\right.$$

$$\times \left(\frac{\slashed{n}_+}{4}\right) D_{i\rho}(x_a n_+ p_A, x_b n_- p_B; \{\omega_j\}) \Bigg] \int \frac{dx^0}{4\pi}\, e^{i\Omega\, x^0}\, \widetilde{S}_{ii'}\left(x^0; \{\omega_j\}, \{\omega'_{j'}\}\right)$$

$$+\, \bar{c}\text{-terms}\,, \tag{3.80}$$

where $\Omega = Q(1-z)$.

In contrast to the case of the kinematic correction, the collinear functions which appear in the dynamical power correction are non-trivial. We recall that the collinear functions are tied to a particular soft function and they will carry the same indices. Moreover, in addition to the indices which connect the collinear function to its soft structure, the collinear functions have two Dirac and two colour indices, $\gamma\beta$ and fb, from the threshold-collinear and c-PDF fields in the matching equation (3.66). It is understood that the various collinear functions, J_i, in equation (3.80) have their indices dictated by matching equations (3.66) and (3.67). As an example we can consider the first soft structure in the set in (3.45). This soft structure contains one $\mathcal{B}^+$ field and hence carries in addition one adjoint index A through which it is connected to the collinear function. This implies that J_1 carries one adjoint index which is tied to the colour generator. We make this example concrete by writing the $J_1\left(n_+ p, x_a n_+ p_A; \omega\right)$ in (3.80) with the indices that it carries explicitly, which is then $J^A_{1;\gamma\beta,fb}\left(n_+ p, x_a n_+ p_A; \omega\right)$.

The $\Delta^{dyn}_{\mathrm{NLP}}(z)$ part of the factorisation formula in (3.80) can be simplified further through decomposition of the collinear functions into all allowed colour and spinor structures. We accomplish this in what follows. To continue the example case studied above, we consider the $J^A_{1;\gamma\beta,fb}\left(n_+ p, x_a n_+ p_A; \omega\right)$ collinear function again. This collinear function must be proportional to the colour generator $\mathbf{T}^A_{fb}$ as this is the only structure which has one adjoint A, and two fundamental, fb, colour indices. Taking advantage of this fact, we can now define a scalar collinear function which is multiplied by the colour generator $\mathbf{T}^A_{fb}$. At which point, we are free to move the colour factor into the soft function where it forms of the trace over the colour indices. In much the same fashion, the colour factors belonging to the other collinear functions can be absorbed by their corresponding soft functions. In this way, we can simplify the dynamical next-to-leading power part of the factorisation formula in (3.80) which gives the following result

$$\Delta^{dyn}_{\mathrm{NLP}}(z) \;=\; -\frac{2}{(1-\epsilon)}\, Q\left[\left(\frac{\slashed{n}_-}{4}\right)\gamma_{\perp\rho}\left(\frac{\slashed{n}_+}{4}\right)\gamma^\rho_\perp\right]_{\beta\gamma}$$

$$\times \int d(n_+ p)\, C^{A0,A0}\left(n_+ p, x_b n_- p_B\right) C^{*A0A0}\left(x_a n_+ p_A, x_b n_- p_B\right)$$

$$\times \sum_{i=1}^{5} \int \{d\omega_j\}\, J_{i,\gamma\beta}\left(n_+ p, x_a n_+ p_A; \{\omega_j\}\right)\, S_i(\Omega; \{\omega_j\}) + \text{h.c.}\,, \tag{3.81}$$

where as above $\Omega = Q(1-z)$.

As in (3.80) and as explained below equation (3.64), the double-valued set $\{\omega_j\} = \{\omega_1, \omega_2\}$, is only necessary for terms $i = 4, 5$. We have also discussed below equation (3.65) that care is needed for the case of the $i = 5$ structure, since as well as the Dirac indices $\beta\gamma$ which are written explicitly, J_5 and S_5 carry further Dirac indices contracted among them. This can be explicitly seen in the definition of S_5 below. The factor of 2 in the top line is attributed to the $\bar{c}$-terms in the last line of (3.80). Another simplification is realised when we make use of the fact that power suppression at $\mathcal{O}(\lambda^2)$ is always generated

in one of the amplitudes and that an $\mathcal{O}(\lambda)$ amplitude does not exist in the $q\bar{q}$-channel as we have discussed above. Therefore, one of the coefficient functions, D_ρ or $D^{*\rho}$, is always reduced to the leading power expression, $\gamma_{\perp\rho} C^{A0,A0}$ or $\gamma_\perp^\rho C^{*\,A0,A0}$ respectively. We emphasise here once more, that the main and crucial difference with respect to the leading power factorisation formula in equation (3.28), is the appearance of convolutions between the collinear jet functions and the generalised, multi-local, soft functions. We would also like to draw attention to the fact that the aforementioned structure resembles the power suppressed corrections in $1/m_b$ in the SCET description of the semi-leptonic B decay in the so-called shape function region [75, 131, 132].

In the factorisation formula written in equation (3.81) we have used the generalised, multi-local, soft functions in momentum space as the Fourier transforms defined in the following way,

$$S_i(\Omega; \{\omega_j\}) = \int \frac{dx^0}{4\pi} e^{i\Omega x^0/2} \int \left\{ \frac{dz_{j-}}{2\pi} \right\} e^{-i\omega_j z_{j-}} S_i(x_0; \{z_{j-}\}), \qquad (3.82)$$

where the position-space soft functions, $S_i(x_0; \{z_{j-}\})$, which contribute at the next-to-leading power are given by

$$S_1(x^0; z_-) = \frac{1}{N_c} \text{Tr}\langle 0|\bar{\mathbf{T}} \left[Y_+^\dagger(x^0) Y_-(x^0) \right] \mathbf{T} \left(\left[Y_-^\dagger(0) Y_+(0) \right] \frac{i\partial_\perp^\nu}{in_-\partial} \mathcal{B}_{\nu\perp}^+ (z_-) \right) |0\rangle, \quad (3.83)$$

$$S_{2;\mu\nu}(x^0; z_-) = \frac{1}{N_c} \text{Tr}\langle 0|\bar{\mathbf{T}} \left[Y_+^\dagger(x^0) Y_-(x^0) \right]$$
$$\times \mathbf{T} \left(\left[Y_-^\dagger(0) Y_+(0) \right] \frac{1}{(in_-\partial)} \left[\mathcal{B}_{\mu\perp}^+(z_-), \mathcal{B}_{\nu\perp}^+(z_-) \right] \right) |0\rangle, \qquad (3.84)$$

$$S_3(x^0; z_-) = \frac{1}{N_c} \text{Tr}\langle 0|\bar{\mathbf{T}} \left[Y_+^\dagger(x^0) Y_-(x^0) \right]$$
$$\times \mathbf{T} \left(\left[Y_-^\dagger(0) Y_+(0) \right] \frac{1}{(in_-\partial)^2} \left[\mathcal{B}^{+\,\mu_\perp}(z_-), \left[in_-\partial \mathcal{B}_{\mu\perp}^+(z_-) \right] \right] \right) |0\rangle, \qquad (3.85)$$

$$S_{4;\mu\nu,bf}^{AB}(x^0; z_{1-}, z_{2-}) = \frac{1}{N_c} \text{Tr}\langle 0|\bar{\mathbf{T}} \left[Y_+^\dagger(x^0) Y_-(x^0) \right]_{ba}$$
$$\times \mathbf{T} \left(\left[Y_-^\dagger(0) Y_+(0) \right]_{af} \mathcal{B}_{\mu\perp}^{+A}(z_{1-}) \mathcal{B}_{\nu\perp}^{+B}(z_{2-}) \right) |0\rangle, \qquad (3.86)$$

$$S_{5;bfgh,\sigma\lambda}(x^0; z_{1-}, z_{2-}) = \frac{1}{N_c} \langle 0|\bar{\mathbf{T}} \left[Y_+^\dagger(x^0) Y_-(x^0) \right]_{ba}$$
$$\times \mathbf{T} \left(\left[Y_-^\dagger(0) Y_+(0) \right]_{af} \frac{g_s^2}{(in_-\partial_{z_1})(in_-\partial_{z_2})} q_{+\sigma g}(z_{1-}) \bar{q}_{+\lambda h}(z_{2-}) \right) |0\rangle. \quad (3.87)$$

We recall from the discussion of the list in (3.45) that the NLP soft functions S_2 and S_3 are redundant and could in principle be eliminated by relating them to S_4.

At this point, we would like to point out that in principle, there could exist another soft function,

$$\widetilde{S}_{6;bf,\mu\nu}^A(x; \omega) = \int dz_- e^{-i\omega z_-} \frac{1}{N_c} \langle 0|\bar{\mathbf{T}} \left[Y_+^\dagger(x) Y_-(x) \right]_{ba}$$

$$\times \mathbf{T}\left(\left[Y_-^\dagger(0)Y_+(0)\right]_{af} \frac{i\partial_{[\mu_\perp}}{in_-\partial}\mathcal{B}_{\nu_\perp]}^{+A}(z_-)\right)|0\rangle\,, \qquad (3.88)$$

with the defining soft structure given by the second term (3.45). Indeed, this soft structure is needed to obtain the complete result for the next-to-leading power one-soft-gluon emission amplitude, as can be seen in appendix B.2 where the results are presented. However, the soft function with the $\frac{i\partial_{[\mu_\perp}}{in_-\partial}\mathcal{B}_{\nu_\perp]}^{+A}(z_-)$ soft structure does not contribute at the cross-section level at any order in perturbation theory. The reason for this is as follows. The soft functions, as can be seen in (3.83) – (3.87), are vacuum matrix elements of Wilson lines and the soft field insertions. Therefore, the only possible structure which could carry the Lorentz indices of the anti-symmetric soft building block $\frac{i\partial_{[\mu_\perp}}{in_-\partial}\mathcal{B}_{\nu_\perp]}^{+A}(z_-)$ in $\widetilde{S}_{6;bf,\mu\nu}^A(x;\omega)$ is the epsilon tensor. However, the epsilon tensor, by parity conservation, is excluded in QCD. Hence, we conclude that required in the factorisation formula at next-to-leading power are only the five soft functions given in equations (3.83) to (3.87), along with their corresponding collinear functions.

The all-order formulation of next-to-leading power threshold factorisation given above, and the operator definitions of the contributing collinear jet and soft functions, is one of the principal results of this work.

3.2.3   Expansion up to next-to-next-to-leading order

The next-to-leading power factorisation formula is verified in chapter 7 through the comparison of the results obtained using the factorisation formula and its elements to the existing fixed-order $\mathcal{O}(\alpha_s)$ and $\mathcal{O}(\alpha_s^2)$ results in the literature. In order to facilitate the comparison carried out in chapter 7, we now expand the factorisation formula in equation (3.81) to obtain the terms which arise up to and including the next-to-next-to-leading order in α_s.

The objects which appear in the factorisation formula in equation (3.81), a hard Wilson matching coefficient $C^{A0,A0}(n_+p, n_-\bar{p})$, the collinear functions $J_i(n_+p, x_a\,n_+p_A; \{\omega_j\})$, the soft functions $\widetilde{S}_i(x; \{\omega_j\})$, each have a perturbative expansion in the strong coupling α_s. At next-to-leading power, the generalised soft functions are made up of at least one explicit soft field insertion and its derivatives, instead of containing solely the soft Wilson lines as in the leading power case. Therefore, the lowest order at which the generalised soft functions can contribute to the cross-section is $\mathcal{O}(\alpha_s)$. On the other hand, the hard and the collinear functions can have tree-level contributions $\mathcal{O}(\alpha_s^0)$. Hence, to obtain the NLO result from the factorisation formula, only one possible combination of the contributing functions is possible. Namely, we require tree-level hard and collinear functions and a NLO soft function. Then, one order higher in α_s, to obtain the NNLO fixed order results, we must consider three possible contributing combinations. These are: (1) A tree-level hard function along with one-loop collinear function and a NLO soft function, (2) one-loop hard function, a tree-level collinear function and a NLO soft function, and lastly (3) tree-level hard and collinear functions, together with the NNLO, $\mathcal{O}(\alpha_s^2)$, soft functions.

Before we proceed, we make an important observation regarding the structure of collinear functions. It is the fact that since the kinematic set-up only allows for soft radiation into the final state, the large component (n_+p) of the incoming c-PDF momentum has to be the same as the sum of the large components of the outgoing threshold collinear momenta of
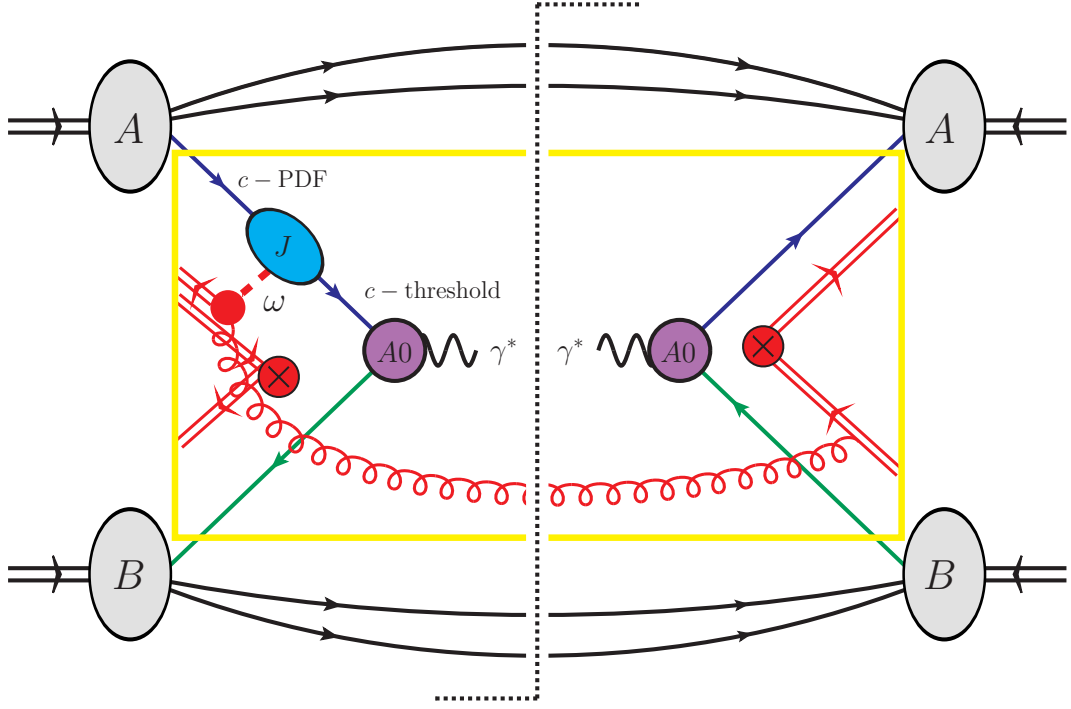
Figure 3.10: *This diagram is the next-to-leading power version of the diagram presented in figure 3.6. It is worth to compare and contrast the two. Since we work at leading twist, the parton distribution functions remain the same in both cases. The next-to-leading power cross-section, $\Delta_{\mathrm{NLP}}^{dyn}(z)$ in (3.81), is schematically drawn inside the golden frame. We have picked a representative contribution of the sum in the third line of equation (3.81). We immediately see that the structure of the factorisation beyond leading power is more intricate than the leading power result. We note the appearance of collinear functions originating in the matching of threshold-collinear fields to c-PDF fields. These are connected to generalised soft functions via a variable ω with a soft scaling. Explicit soft gauge field insertions into the soft function, denoted by large red dot, mean that the soft function contains at least one soft gluon emission and therefore starts at order α_s. As at leading power, only the J^{A0A0} hard current contributes to the next-to-leading power cross-section.*

a particular collinear function. Next, we note that for the J^{A0} current we require only one outgoing collinear momentum from the collinear function. Therefore, the collinear functions at the next-to-leading power must be proportional to $\delta(n_+p - x_a n_+ p_A)$. However, on top of the collinear function being proportional to the delta function in momenta $\delta(n_+p - x_a n_+ p_A)$, due to the fact that $n_- z$ components appear in the soft-collinear interactions, which in momentum space translate to $n_+ p$ derivatives, the momentum-space collinear functions may also contain derivatives of the momentum-conserving delta function. This is for example the case for the $J_1(n_+p, x_a\, n_+ p_A; \omega)$ collinear function. It is also diagonal in the Dirac indices, hence we can write the $J_1(n_+p, x_a\, n_+ p_A; \omega)$ collinear function in terms of two scalar components in the following way:

$$J_{1;\gamma\beta}\left(n_+p, x_a\, n_+ p_A; \omega\right) \;=\; \delta_{\gamma\beta}\left[J_{1,1}\left(x_a n_+ p_A; \omega\right)\delta\left(n_+p - x_a n_+ p_A\right)\right.$$

$$+ J_{1,2}\left(x_a n_+ p_A; \omega\right) \frac{\partial}{\partial(n_+ p)} \delta(n_+ p - x_a n_+ p_A) \Bigg]. \tag{3.89}$$

We can now make use of this decomposition in the factorisation formula. Namely, using integration by parts this derivative is moved to act on the amplitude hard-scattering coefficient. Therefore, the derivative collinear-function term, $J_{1,2}\left(x_a n_+ p_A; \omega\right)$, only contributes to the cross-section when the hard Wilson matching coefficient has momentum dependence. This happens only from the first loop order, $\mathcal{O}(\alpha_s)$ for $C^{A0,A0}$. Once we perform the derivative on the hard Wilson matching coefficient, one can evaluate the remaining $d(n_+ p)$ integral using the delta function in the second line of (3.89), which after these manipulations does not have a derivative acting on it.

Considering the list of soft functions in equations (3.83) – (3.87), the only soft function in this list which begins at the lowest, next-to-leading α_s order is S_1. The remaining soft functions are made from at least two explicit insertions of soft fields. Therefore, the leading contribution from these soft functions to the cross-section is at next-to-next-to-leading order. Hence, keeping only the contributions to next-to-leading order, we have

$$\Delta_{\mathrm{NLP}}^{dyn\,(1)}(z) \;=\; 4Q\, H^{(0)}(Q^2) \int d\omega\, J_{1,1}^{(0)}\left(x_a n_+ p_A; \omega\right) S_1^{(1)}(\Omega; \omega), \tag{3.90}$$

where the spin trace, $\mathrm{Tr}\left[\left(\frac{\slashed{n}_-}{4}\right) \gamma_{\perp\rho} \left(\frac{\slashed{n}_+}{4}\right) \gamma_\perp^\rho\right]$, has already been evaluated to yield a factor of $-(1-\epsilon)$.

Moreover, here and below in this section, the Ω variable is related to the threshold variable $1-z$ by $\Omega = Q(1-z)$. We may greatly simplify equation (3.90) by substituting in the tree-level result for the hard coefficient $H^{(0)}(Q^2) = 1$, and the tree-level collinear function, which we write below in equation (4.19):

$$\Delta_{\mathrm{NLP}}^{dyn\,(1)}(z) \;=\; -4 \int d\omega\, S_1^{(1)}(\Omega; \omega). \tag{3.91}$$

We now continue our considerations at the next-to-next-to-leading order. Above we have discussed the three possible types of contributions, they take the following expressions respectively:

- Collinear: tree-level hard function, one-loop collinear function, and a NLO soft function

$$\Delta_{\mathrm{NLP-coll}}^{dyn\,(2)}(z) \;=\; 4Q\, H^{(0)}\!\left(Q^2\right) \int d\omega\, J_{1,1}^{(1)}\left(x_a n_+ p_A; \omega\right) S_1^{(1)}(\Omega; \omega). \tag{3.92}$$

- Hard: one-loop hard function, tree-level collinear function, and a NLO soft function

$$\begin{aligned}
\Delta_{\mathrm{NLP-hard}}^{dyn\,(2)}(z) \;=\; & 2Q \int d\omega\, S_1^{(1)}(\Omega; \omega) \left(H^{(1)}\!\left(Q^2\right) J_{1,1}^{(0)}\left(x_a n_+ p_A; \omega\right) \right. \\
& - C^{*A0\,(0)}\left(x_a n_+ p_A,\, x_b n_- p_B\right) J_{1,2}^{(0)}\left(x_a n_+ p_A; \omega\right) \\
& \left. \times \frac{\partial}{\partial x_a(n_+ p_A)} C^{A0\,(1)}(x_a n_+ p_A, x_b n_- p_B) \right) + \mathrm{h.c.} \tag{3.93}
\end{aligned}$$

- Soft: tree-level hard function, tree-level collinear function, and NNLO soft functions

$$\Delta^{dyn\,(2)}_{\text{NLP}-\text{soft}}(z) \;=\; -\frac{4}{(1-\epsilon)}\,Q\left[\left(\frac{\slashed{n}_-}{4}\right)\gamma_{\perp\rho}\left(\frac{\slashed{n}_+}{4}\right)\gamma^\rho_\perp\right]_{\beta\gamma}H^{(0)}\!\left(Q^2\right)$$

$$\times\sum_{i=1}^{5}\int\{d\omega_j\}\,J^{(0)}_{i,\gamma\beta}\left(x_a\,n_+p_A;\{\omega_j\}\right)S^{(2)}_i\left(\Omega;\{\omega_j\}\right). \quad (3.94)$$

In $\Delta^{dyn\,(2)}_{\text{NLP}-\text{soft}}(z)$ the derivative terms in the collinear functions do not contribute, since the hard function takes its tree-level value which is a constant, and hence vanishes when the derivatives are applied.

The above expressions can be simplified by making use of the tree-level values for the relevant contributing objects. Specifically, since $H^{(0)}(Q^2) = 1$, we have

$$\Delta^{dyn\,(2)}_{\text{NLP}-\text{coll}}(z) \;=\; 4Q\int d\omega\, J^{(1)}_{1,1}(x_a\,n_+p_A;\omega)\,S^{(1)}_1(\Omega;\omega) \quad (3.95)$$

for the collinear term.

Next we consider the simplifications to the hard contribution $\Delta^{dyn\,(2)}_{\text{NLP}-\text{hard}}(z)$ in (3.93). $\Delta^{dyn\,(2)}_{\text{NLP}-\text{hard}}(z)$ is simplified by using tree-level values for the collinear functions in (4.19) and (4.20). We remind the reader that since this expression refers to d-dimensional regularized objects, care has to be taken when dealing with this quantity. In particular, the one-loop d-dimensional hard matching coefficient depends on $Q^2 = x_a x_b n_+ p_A n_- p_B$ only through an overall multiplicative factor $(-Q^2/\mu^2)^{-\epsilon}$. Therefore, performing the derivative yields the hard matching coefficient again, now multiplied by a factor of $-\epsilon/Q$. Along with the hermitian conjugate term in (3.93), from the derivative term we obtain the following: $-\epsilon/Q \times (C^{*A0(0)}C^{A0(1)} + C^{*A0(1)}C^{A0(0)}) = -\epsilon\,H^{(1)}/Q$. Then $\Delta^{dyn\,(2)}_{\text{NLP}-\text{hard}}(z)$ in equation (3.93) simplifies to

$$\Delta^{dyn\,(2)}_{\text{NLP}-\text{hard}}(z) = -4\,(1-\epsilon)\,H^{(1)}(Q^2)\int d\omega\, S^{(1)}_1\left(\Omega;\,\omega\right). \quad (3.96)$$

The soft contribution to the cross-section $\Delta^{dyn\,(2)}_{\text{NLP}-\text{soft}}(z)$ in equation (3.94) can also be simplified through the use of tree-level collinear functions. However, we do not present it here.

This concludes our discussion of the power corrections to the diagonal $q\bar{q}$-channel of the Drell-Yan process at threshold. In chapters 4, 5, and 6 we compute the relevant collinear and soft functions, before putting them together in chapter 7 to obtain explicit results up to next-to-next-to-leading order accuracy. In chapter 8, we again pick up discussion of the next-to-leading power factorisation formula, given here in equation (3.81), where after specifying the formula to the leading logarithmic accuracy we perform resummation at next-to-leading power.

3.3 Gluon-antiquark channel

In this section we consider the off-diagonal channel contribution to the Drell-Yan partonic cross-section at threshold as given in equation (3.3) and shown schematically in the right

panel of figure 3.2. For the process $g(x_a p_A)\,\bar{q}(x_b p_B)\ \to\ \gamma^*(Q^2)\,[\to \ell(l_1)\bar{\ell}(l_2)\,] + X(p_X)$ to take place in the $z \to 1$ limit, the incoming c-PDF gluon must be converted to a threshold collinear quark through the emission of a soft antiquark. The threshold-collinear quark retains almost all of the momentum of the incoming c-PDF gluon. The soft-quark interaction with collinear fields is inherently a subleading power effect. This can be deduced from the fact that soft quarks only appear in the soft term, $\bar{q}_s i \slashed{D}_s q_s$, in the leading power Lagrangian written in (2.35), and the soft quarks first appear in soft-collinear interaction terms at $\mathcal{O}(\lambda)$ in, $\mathcal{L}_{\xi q}^{(1)}$, in equation (2.66). Therefore, unlike in the case of the $q\bar{q}$-channel discussed in section 3.2, the contribution to the Drell-Yan cross-section from the $g\bar{q}$-channel does not begin at leading power as this process vanishes. Rather, the process is first realised at next-to-leading power through time-ordered product insertions of $\mathcal{L}_{\xi q}^{(1)}$ Lagrangian terms into the amplitudes. The cross-section is then obtained by interference of two such amplitudes.

The layout of this section resembles one of section 3.2, we first outline the derivation of the general factorisation formula for the $g\bar{q}$-channel of the partonic Drell-Yan process, before specifying the formula to the next-to-leading power accuracy.

3.3.1   Factorisation at general subleading powers

The derivation of the formal factorisation formula beyond leading power for the $g\bar{q}$-channel follows closely the derivation presented in section 3.2.1 for the $q\bar{q}$-channel. Here we follow the structure of section 3.2.1 and draw attention to the differences for the $g\bar{q}$-channel.

Following the formalism described in section 2.4.1, the general, all power, hard matching of the vector current is given in equation (3.47) with the SCET currents written in (3.48). As discussed above, in addition to the SCET subleading power currents, there exist non-local time-ordered products of the subleading currents with subleading power Lagrangian terms. Of particular importance for the $g\bar{q}$-channel are the $\mathcal{L}_{\xi q}^{(l)}$ insertions, which can convert the incoming c-PDF gluon into a threshold collinear quark through the emission of a soft antiquark.

As for the $q\bar{q}$-channel, the threshold kinematics still forbids the radiation of threshold collinear modes into the final state. Therefore, in the same way as in section 3.2.1, we perform a second collinear matching of the threshold collinear fields appearing in the generalised SCET currents and their time-ordered products with subleading SCET Lagrangian terms, onto c-PDF and $\bar{c}$-PDF fields. The matching for the anticollinear leg, with an incoming antiquark, uses equation (3.42) as for the diagonal channel case. In the matching of the threshold collinear fields to the c-PDF gluon building block, we use the general matching equation written in (3.43).

Performing these steps, we arrive at the following result for the Drell-Yan matrix element of the generalised matching for the $g\bar{q}$-channel, which is the analogue of the diagonal channel expression in (3.50)

$$
\begin{aligned}
\langle X|\bar{\psi}\gamma_\rho\psi(0)|A(p_A)B(p_B)\rangle \;=\; & \sum_{m_1,m_2}\sum_{i,\bar{i}} \int \{dt_k\}\,\{d\bar{t}_{\bar{k}}\}\,\widetilde{C}^{\,m_1,m_2}\left(\{t_k\},\{\bar{t}_{\bar{k}}\}\right) \\
& \times 2\pi \int d\bar{u}\int \{d\bar{z}_{\bar{j}+}\}\,\bar{\widetilde{J}}_{\bar{i}}^{\,m_1}\left(\{\bar{t}_{\bar{k}}\},\bar{u};\{\bar{z}_{\bar{j}+}\}\right)\,\langle X_{\bar{c}}^{\mathrm{PDF}}|\bar{\chi}_{\bar{c}}^{\mathrm{PDF}}(\bar{u}n_-)|B(p_B)\rangle
\end{aligned}
$$

$$\times\, 2\pi \int du \int \{dz_{j-}\}\, \tilde{G}_i^{m_2}\left(\{t_k\}, u; \{z_{j-}\}\right) \langle X_c^{\mathrm{PDF}}|\mathcal{A}_{c\perp}^{\mathrm{PDF}}(un_+)|A(p_A)\rangle$$

$$\times\, \Gamma_\rho^{m_1, m_2}\, \langle X_s|\, \mathbf{T}\left(\bar{\mathfrak{s}}_{\bar{\imath}}\left(\{\bar{z}_{\bar{\jmath}+}\}\right)\left[Y_-^\dagger\, J_s\, Y_+\right](0)\, \mathfrak{s}_i\left(\{z_{j-}\}\right)\right)|0\rangle. \tag{3.97}$$

Explicit Dirac, Lorentz, and colour indices are suppressed and the notation used here is the same as in equation (3.50). Namely, we use the index k ($\bar{k}$) to count the number of collinear (anticollinear) building block fields in a given current, and we sum over all of the possible currents. The index j ($\bar{\jmath}$) counts the number of insertions of the subleading power Lagrangians into each collinear (anticollinear) sector, and again we sum over all of the occurrences. At least one subleading power Lagrangian insertion is necessary to give a non-vanishing subleading-power amplitude, as discussed in section 3.1.2. Moreover, as discussed above, already at $\mathcal{O}(\lambda^2)$ in the $g\bar{q}$-channel an insertion of $\mathcal{L}_{\xi q}^{(1)}$ is needed at tree-level to yield a non-vanishing amplitude. In the anticollinear direction the matching is performed on the $\bar{c}$-PDF antiquark field as in the $q\bar{q}$-channel case and the anticollinear functions are denoted in the same way, $\bar{\bar{J}}_{\bar{\imath}}$. In the collinear direction we match to the c-PDF gluon field and $\tilde{G}_i$ are the collinear functions. The soft structures $\mathfrak{s}_i(\{z_{j-}\})$ ($\bar{\mathfrak{s}}_{\bar{\imath}}\left(\{\bar{z}_{\bar{\jmath}+}\}\right)$) are built from products of $\mathcal{B}^+$, q_+ ($\mathcal{B}^-$, q_-) fields and their derivatives. The list of possible structures is given (3.45).

Next, we use (3.52) for the Fourier transform of the $\bar{c}$-PDF field and for the c-PDF gluon field we use

$$\mathcal{A}_{c\perp}^{\mathrm{PDF}}(un_+) = \int \frac{dn_+p_a}{2\pi}\, e^{-i(n_+p_a)u}\, \hat{\mathcal{A}}_{c\perp}^{\mathrm{PDF}}(n_+p_a). \tag{3.98}$$

Similarly, to rewrite the anticollinear functions $\bar{\bar{J}}_{\bar{\imath}}$ in momentum space we use the definition given in equation (3.54). For the collinear functions we make an analogous definition to one in equation (3.53) by replacing $\tilde{J}_i \to \tilde{G}_i$

$$\int \{dt_k\} \int du\, \tilde{G}_i^{m_2}\left(\{t_k\}, u; \{z_{j-}\}\right)\, e^{i(n_+p_k)\, t_k}\, e^{-i(n_+p_a)\, u}$$

$$= \int \left\{\frac{d\omega_j}{2\pi}\right\}\, e^{-i\omega_j z_{j-}}\, G_i^{m_2}\left(\{n_+p_k\}, n_+p_a; \{\omega_j\}\right). \tag{3.99}$$

As before, the set $\{\omega_j\}$ denotes the variables with a soft scaling that are conjugate to $\{z_{j-}\}$ and in the exponents Einstein's summation convention is used. Also $\left\{\frac{d\omega_j}{2\pi}\right\} = \frac{d\omega_1}{2\pi} \times \ldots \times \frac{d\omega_m}{2\pi}$.

We now make use of equations (2.120), (3.52), (3.98), (3.54), and (3.99) in the general Drell-Yan matrix element written in (3.97) which leads us to the following expression

$$\langle X|\bar{\psi}\gamma_\rho\psi(0)|A(p_A)B(p_B)\rangle \;\; = \;\; \sum_{m_1, m_2}\, \sum_{i,\bar{\imath}} \int \left\{\frac{dn_+p_k}{2\pi}\right\}\left\{\frac{dn_-\bar{p}_{\bar{k}}}{2\pi}\right\}$$

$$\times \int d(n_+p_a)\, d(n_-p_b)\, C^{m_1, m_2}(\{n_+p_k\}, \{n_-\bar{p}_{\bar{k}}\})$$

$$\times \int \left\{\frac{d\bar{\omega}_{\bar{\jmath}}}{2\pi}\right\}\, \bar{J}_{\bar{\imath}}^{m_1}\left(\{n_-\bar{p}_{\bar{k}}\}, -n_-p_b; \{\bar{\omega}_{\bar{\jmath}}\}\right)\, \langle X_{\bar{c}}^{\mathrm{PDF}}|\hat{\bar{\chi}}_{\bar{c}}^{\mathrm{PDF}}(n_-p_b)|B(p_B)\rangle$$

$$\times \int \left\{\frac{d\omega_j}{2\pi}\right\}\, G_i^{m_2}\left(\{n_+p_k\}, n_+p_a; \{\omega_j\}\right)\, \langle X_c^{\mathrm{PDF}}|\hat{\mathcal{A}}_{c\perp}^{\mathrm{PDF}}(n_+p_a)|A(p_A)\rangle$$

$$\times \, \Gamma_\rho^{m_1,m_2} \int \{d\bar{z}_{\bar{j}+}\} \int \{dz_{j-}\} \, e^{-i\bar{\omega}_{\bar{j}}\,\bar{z}_{\bar{j}+}} \, e^{-i\omega_j\, z_{j-}}$$

$$\times \langle X_s | \, \mathbf{T} \left(\bar{\mathfrak{s}}_{\,\bar{i}} (\{\bar{z}_{\bar{j}+}\}) \left[Y_-^\dagger J_s Y_+ \right] (0)\, \mathfrak{s}_i(\{z_{j-}\}) \right) |0\rangle . \qquad (3.100)$$

In the next step, we obtain the hadronic tensor $W_{\rho\mu}$ by taking the square of the amplitude according to equation (3.9) and combining it with the final state leptons as in (3.8). Therefore, we define the following amplitude level coefficient functions in order to render the expressions handleable. For an amplitude we have

$$
\begin{aligned}
\mathcal{D}_{i\bar{i}}^{m_1,m_2\,\rho}(n_+p_a, -n_-p_b; \{\omega_j\}, \{\bar{\omega}_{\bar{j}}\}) \;=\;& (2\pi)^2 \int \left\{ \frac{dn_+p_k}{2\pi} \right\} \left\{ \frac{d(n_-\bar{p}_{\bar{k}})}{2\pi} \right\} \\
& \times C^{m_1,m_2}(\{n_+p_k\}, \{n_-\bar{p}_{\bar{k}}\}) \times \bar{J}_{\bar{i}}^{m_1}\left(\{n_-\bar{p}_{\bar{k}}\}, -n_-p_b; \{\bar{\omega}_{\bar{j}}\} \right) \\
& \times \Gamma^{m_1,m_2\,\rho}\, G_i^{m_2}\left(\{n_+p_k\}, n_+p_a; \{\omega_j\} \right) ,
\end{aligned}
\qquad (3.101)
$$

and for use in the conjugate amplitude we define

$$
\begin{aligned}
\mathcal{D}_{i'\bar{i}'\,\rho}^{*\,m_1',m_2'}(n_+p_a', -n_-p_b'; \{\omega_{j'}'\}, \{\bar{\omega}_{\bar{j}'}'\}) \;=\;& (2\pi)^2 \int \left\{ \frac{d(n_+p_{k'}')}{2\pi} \right\} \left\{ \frac{d(n_-\bar{p}_{\bar{k}'}')}{2\pi} \right\} \\
& \times C^{*\,m_1',m_2'}(\{n_+p_{k'}'\}, \{n_-\bar{p}_{\bar{k}'}'\}) \times \bar{J}_{\bar{i}'}^{*\,m_1'}\left(\{n_-\bar{p}_{\bar{k}'}'\}, -n_-p_b'; \{\bar{\omega}_{\bar{j}'}'\} \right) \\
& \times \bar{\Gamma}_\rho^{m_1',m_2'}\, G_{i'}^{*\,m_2'}\left(\{n_+p_{k'}'\}, n_+p_a'; \{\omega_{j'}'\} \right) .
\end{aligned}
\qquad (3.102)
$$

We next write the general amplitude expression and its conjugate in terms of these coefficient functions. Also the $(\bar{c})c$-PDF fields are inverse Fourier transformed, in which case we obtain

$$
\begin{aligned}
\langle X | \bar{\psi}\gamma^\rho\psi(0) | A(p_A)B(p_B) \rangle \;=\;& \frac{1}{(2\pi)^2} \sum_{m_1,m_2} \sum_{i,\bar{i}} \int d(n_+p_a)\, d(n_-p_b) \int \left\{ \frac{d\bar{\omega}_{\bar{j}}}{2\pi} \right\} \int \left\{ \frac{d\omega_j}{2\pi} \right\} \\
& \times \int dg\, d\bar{g}\; e^{i(n_+p_a)g} e^{-i(n_-p_b)\bar{g}}\, \mathcal{D}_{i\bar{i}}^{m_1,m_2\,\rho}(n_+p_a, -n_-p_b; \{\omega_j\}, \{\bar{\omega}_{\bar{j}}\}) \\
& \times \langle X_{\bar{c}}^{\text{PDF}} | \bar{\chi}_{\bar{c}}^{\text{PDF}}(\bar{g}\, n_-) | B(p_B) \rangle \, \langle X_c^{\text{PDF}} | \mathcal{A}_{c\perp}^{\text{PDF}}(g\, n_+) | A(p_A) \rangle \\
& \times \int \{d\bar{z}_{\bar{j}+}\} \int \{dz_{j-}\}\, e^{-i\bar{\omega}_{\bar{j}}\,\bar{z}_{\bar{j}+}}\, e^{-i\omega_j\, z_{j-}} \\
& \times \langle X_s | \mathbf{T}\left(\bar{\mathfrak{s}}_{\,\bar{i}}(\{\bar{z}_{\bar{j}+}\}) \left[Y_-^\dagger J_s Y_+ \right](0)\, \mathfrak{s}_i(\{z_{j-}\}) \right) |0\rangle
\end{aligned}
\qquad (3.103)
$$

for the amplitude in (3.100), and

$$
\begin{aligned}
\langle A(p_A)B(p_B) | \psi\gamma_\mu\bar{\psi}(0) | X \rangle \;=\;& \frac{1}{(2\pi)^2} \sum_{m_1',m_2'} \sum_{i',\bar{i}'} \int d(n_+p_a')\, d(n_-p_b') \int \left\{ \frac{d\bar{\omega}_{\bar{j}'}'}{2\pi} \right\} \int \left\{ \frac{d\omega_{j'}'}{2\pi} \right\} \\
& \times \int dg'\, d\bar{g}'\; e^{-i(n_+p_a')g'} e^{+i(n_-p_b')\bar{g}'}\, \mathcal{D}_{i'\bar{i}'\,\mu}^{*\,m_1',m_2'}(n_+p_a', -n_-p_b'; \{\omega_{j'}'\}, \{\bar{\omega}_{\bar{j}'}'\}) \\
& \times \langle B(p_B) | \chi_{\bar{c}}^{\text{PDF}}(\bar{g}'\, n_-) | X_{\bar{c}}^{\text{PDF}} \rangle \, \langle A(p_A) | \mathcal{A}_{c\perp}^{\text{PDF}}(g'\, n_+) | X_c^{\text{PDF}} \rangle \\
& \times \int \{d\bar{z}_{\bar{j}'+}'\} \int \{dz_{j'-}'\} e^{+i\bar{\omega}_{\bar{j}'}'\,\bar{z}_{\bar{j}'+}'}\, e^{+i\omega_{j'}'\, z_{j'-}'}
\end{aligned}
$$

$$\times \langle 0 | \bar{\mathbf{T}} \left(\bar{\mathbf{s}}'_{i'}(\{z'_{j'-}\}) \left[Y_+^\dagger J_s^\dagger Y_- \right] (0) \, \mathbf{s}'_{\bar{i}'}(\{\bar{z}'_{\bar{j}'+}\}) \right) |X_s\rangle, \qquad (3.104)$$

for its conjugate. We now interfere the amplitudes and combine the hadronic tensor with the leptonic part according to equations (3.9) and (3.8) respectively. At this point, we use equation (3.23) to rewrite the $\bar{c}$-PDF matrix element in terms of PDFs, and for the c-PDF matrix element we use the following relation from appendix A of [133]:

$$\langle A(p_A)|\mathcal{A}_{c\perp\eta'}^{A',\,\mathrm{PDF}}(x + g'n_+)\mathcal{A}_{c\perp\eta}^{A,\,\mathrm{PDF}}(gn_+)|A(p_A)\rangle = \frac{-g_{\perp\eta\eta'}}{(d-2)}\frac{\delta^{AA'}}{(N_c^2-1)}$$
$$\times \int_0^1 \frac{dx_a}{x_a} f_{g/A}(x_a) e^{ix_a(x+g'n_+-gn_+)\cdot p_A}. \quad (3.105)$$

We remark that the we do not make indices explicit in this general derivation, it is understood however, that the indices appearing in (3.105) are absorbed by the collinear functions. Finally, we perform the integrations over auxiliary variables $g, \bar{g}, g'$, and $\bar{g}'$ and the momenta n_+p_a, n_+p_b, $n_+p'_a$, and $n_+p'_b$ which gives the following for the Drell-Yan cross-section in the $g\bar{q}$-channel

$$\frac{d\sigma}{dQ^2} = \frac{4\pi\alpha_{\mathrm{EM}}^2}{3N_cQ^4} \int_0^1 \frac{dx_a}{x_a} f_{a/A}(x_a) \int_0^1 dx_b \, f_{b/B}(x_b) \, \hat{\sigma}_{ab} \qquad (3.106)$$

where $a = g$, $b = \bar{q}$, and

$$\hat{\sigma}_{g\bar{q}} = \sum_{\substack{m'_1,m'_2, \\ m_1,m_2}} \sum_{\substack{i',\bar{i}' \\ i,\bar{i}}} \int \left\{ \frac{d\bar{\omega}'_{\bar{j}'}}{2\pi} \right\} \left\{ \frac{d\omega'_{j'}}{2\pi} \right\} \left\{ \frac{d\bar{\omega}_{\bar{j}}}{2\pi} \right\} \left\{ \frac{d\omega_j}{2\pi} \right\}$$
$$\times \frac{1}{2(d-2)} \left[\mathcal{D}_{i\bar{i}}^{m_1,m_2\,\rho}(x_an_+p_A, x_bn_-p_B; \{\omega_j\}, \{\bar{\omega}_{\bar{j}}\}) \left(\frac{\slashed{n}_+}{4} \right) \right.$$
$$\left. \times \mathcal{D}_{i'\bar{i}'\,\rho}^{*\,m'_1,m'_2}(x_an_+p_A, x_bn_-p_B; \{\omega'_{j'}\}, \{\bar{\omega}'_{\bar{j}'}\}) \right]$$
$$\times \int \frac{d^{d-1}\vec{q}}{(2\pi)^3 2\sqrt{Q^2+\vec{q}^2}} \frac{1}{2\pi} Q \int d^dx\, e^{i(p_Ax_a+p_Bx_b-q)\cdot x}$$
$$\times \widetilde{S}_{g\bar{q};\,i\,\bar{i}\,i'\,\bar{i}'}(x; \{\omega_j\}; \{\bar{\omega}_{\bar{j}}\}; \{\omega'_{j'}\}; \{\bar{\omega}'_{\bar{j}'}\}). \qquad (3.107)$$

This is the result for the general form of the power-suppressed $g\bar{q}$-induced partonic cross-section in the $z \to 1$ limit. The notation with bars ($\bar{}$) and tildes ($\tilde{}$) is used here in the same way as in the derivation of the $q\bar{q}$-induced partonic cross-section. They refer to the anticollinear direction and objects with dependence on the coordinate variables respectively. Also, the contributions from the complex conjugate amplitude are denoted with a prime ($'$) symbol.

In the last line of equation (3.107) the generalised multi-local soft function for the $g\bar{q}$-channel was introduced. It is given by

$$\widetilde{S}_{g\bar{q};\,i\,\bar{i}\,i'\,\bar{i}'}(x; \{\omega_j\}; \{\bar{\omega}_{\bar{j}}\}; \{\omega'_{j'}\}; \{\bar{\omega}'_{\bar{j}'}\}) = \int\{d\bar{z}'_{\bar{j}'+}\} \int\{dz'_{j'-}\} \int\{d\bar{z}_{\bar{j}+}\} \int\{dz_{j-}\}$$
$$\times e^{+i\left(\bar{\omega}'_{\bar{j}'}\bar{z}'_{\bar{j}'+}\right)} e^{+i\left(\omega'_{j'}z'_{j'-}\right)} e^{-i\left(\bar{\omega}_{\bar{j}}\bar{z}_{\bar{j}+}\right)} e^{-i(\omega_jz_{j-})}$$

$$\times \frac{1}{C_F\, C_A} \langle 0| \bar{\mathbf{T}} \left(\bar{\mathfrak{s}}'_{i'}(\{x + z'_{j'-}\}) \left[Y^\dagger_+(x) J^\dagger_s Y_-(x) \right] \mathfrak{s}'_{\bar{i}'}(\{x + \bar{z}'_{\bar{j}'+}\}) \right)$$

$$\times \mathbf{T} \left(\bar{\mathfrak{s}}_{\bar{i}}(\{\bar{z}_{\bar{j}+}\}) \left[Y^\dagger_-(0) J_s Y_+(0) \right] \mathfrak{s}_i(\{z_{j-}\}) \right) |0\rangle . \tag{3.108}$$

We recall that in the same fashion as the $q\bar{q}$-channel result in equation (3.60), the result in equation (3.107) is a formal d-dimensional result with regularized quantities.

3.3.2   Factorisation at next-to-leading power

In this section we specify the general subleading power result in (3.107) to the case of next-to-leading power. We follow the steps of the analysis performed in section (3.2.2) for the $q\bar{q}$-channel.

   As we will describe in what follows, the main simplification arises due to the required change in fermion number between the initial c-PDF gluon and the field content of the vector current onto which the first hard matching step is performed in (3.47). Since in the threshold kinematics the collinear quarks cannot enter the final state, due to their large virtuality, the necessary change in fermion number must be realised through an emission of a soft quark into the final state. In general, this could be achieved through insertions of subleading-power Lagrangian terms, such as $\mathcal{L}^{(1)}_{\xi q}$ and $\mathcal{L}^{(2)}_{\xi q}$ in (2.66) and (2.67) respectively, in time-ordered products with current operators, and using soft quark fields in the purely soft building block $J_s(0)$ in equation (3.47). However, as discussed in section 2.4.1, and shown explicitly in (2.79), the purely soft building block $J_s(0)$ in position-space formulation of SCET does not contribute below $\mathcal{O}(\lambda^3)$ and therefore can be ignored in the next-to-leading power considerations. At $\mathcal{O}(\lambda^2)$ at the cross-section level, we can also ignore all subleading power Lagrangian terms $\mathcal{L}^{(l)}_{\xi q}$ with $l \geq 3$. Additionally, the aforementioned $\mathcal{L}^{(2)}_{\xi q}$ Lagrangian insertion can also be dropped as the amplitude with the $\mathcal{L}^{(2)}_{\xi q}$ Lagrangian insertion would have to be interfered with a leading power amplitude in order to yield $\mathcal{O}(\lambda^2)$ power suppressed cross-section. However, such contribution vanishes. With this, we conclude that in the $g\bar{q}$-amplitude the power suppression must originate via the emission of a soft quark through a time-ordered product insertion of a $\mathcal{L}^{(1)}_{\xi q}$ Lagrangian term with the J^{A0} current.

   Having established that there exists only one possibility of generating power suppression up to $\mathcal{O}(\lambda^2)$ at cross-section level, we now for concreteness give the collinear matching equation specified to the needed next-to-leading power case with explicit indices. Using the Fourier transforms in equations (3.98) and (3.99) we write the collinear function in momentum space

$$i \int d^d z\, \mathbf{T} \left[\chi_{c,\gamma f}\,(tn_+)\, \mathcal{L}^{(1)}(z) \right] = 2\pi \int \frac{d\omega}{2\pi} \int \frac{dn_+ p}{2\pi}\, e^{-i(n_+ p)t} \int \frac{dn_+ p_a}{2\pi}$$

$$\times G^{\eta, A}_{\xi q; \gamma\alpha, fa}(n_+ p, n_+ p_a; \omega)\, \hat{\mathcal{A}}^{\mathrm{PDF}\, A}_{c\perp\eta}(n_+ p_a) \int dz_-\, e^{-i\omega z_-}\, \mathfrak{s}_{\xi q;\alpha, a}(z_-), \tag{3.109}$$

where α is a Dirac index, η is a Lorentz index, and a and A are a fundamental and adjoint colour indices respectively. This is an analogue of equations (3.66) and (3.67) used in the $q\bar{q}$-channel next-to-leading power derivation. Here we do not sum over possible structures as the only the $\mathcal{L}^{(1)}_{\xi q}$ insertion gives rise to a soft structure, which is the soft

quark. Therefore, here we have

$$\mathfrak{s}_{\xi q;\alpha,a}(z_-) = \frac{g_s}{in_-\partial_z}q^+_{\alpha,a}(z_-)\,.\tag{3.110}$$

In order to simplify the next-to-leading power factorisation formula as much as possible, we make use of generic properties of the collinear function $G^{\eta,A}_{\xi q;\gamma\alpha,fa}(n_+p, n_+p_a; \omega)$ in the matching equation (3.109). Firstly, as discussed in section (3.2.3), this collinear function must be proportional to the delta function in the collinear momenta, $\delta(n_+p - n_+p_a)$, since the kinematic set-up does not allow for threshold collinear radiation into the final state. Therefore the incoming c-PDF momentum is the same as the outgoing threshold collinear momentum. Additional simplification for the $g\bar{q}$-case is the fact that no n_-z components appear in the $\mathcal{L}^{(1)}(z)$. Hence, momentum-space derivatives will not act on the collinear momentum delta function. Moreover, $G^{\eta,A}_{\xi q;\gamma\alpha,fa}(n_+p, n_+p_a; \omega)$ carries one adjoint colour index A and two fundamental colour indices fa, therefore we can extract a $\mathbf{T}^A_{fa}$ colour generator and transfer it into the definition of the soft function. The collinear function also carries a single Lorentz index η and two Dirac indices $\gamma\alpha$. From the matching equation in (3.109) we deduce that the Lorentz index is contracted with a $\perp$ structure. Therefore, in the collinear function a $\gamma^\eta_\perp$ must appear, as only other possible single Lorentz index carrying structures are $n^\eta_\pm$ which would vanish upon contraction with $\hat{\mathcal{A}}^{\mathrm{PDF}\,A}_{c\perp\eta}$. We define the scalar collinear function as

$$G^{\eta,A}_{\xi q,\gamma\alpha,fa}(n_+p, n_+p_a; \omega_1) = G_{\xi q}(n_+p; \omega_1)\,\delta((n_+p) - (n_+p_a))\,\mathbf{T}^A_{fa}\left[\slashed{n}_-\gamma^\eta_\perp\right]_{\gamma\alpha}\,.\tag{3.111}$$

We also note that similarly to the $q\bar{q}$-case, the $\Gamma^{m_1,m_2\,\rho}$ and $\bar{\Gamma}^{m'_1,m'_2}_\rho$ structures in (3.101) and (3.102) reduce to $\gamma^\rho_\perp$ and $\gamma_{\perp\rho}$ as again only the leading power hard matching current appears in the next-to-leading power factorisation formula. At this point we consider the spin structure in the second and third lines of equation (3.107). Namely, the $\mathcal{D}^\rho\left(\frac{\slashed{n}_+}{4}\right)\mathcal{D}^*_\rho$ terms for which the spin structures take the form

$$\left[\gamma_{\perp\eta}\slashed{n}_-\right]_{\sigma\beta}(\gamma_{\perp\rho})_{\beta\delta}\left(\frac{\slashed{n}_+}{4}\right)_{\delta\lambda}(\gamma^\rho_\perp)_{\lambda\gamma}\left[\slashed{n}_-\gamma^\eta_\perp\right]_{\gamma\alpha} = 4\frac{\slashed{n}_{-\sigma\alpha}}{4}(d-2)^2\,.\tag{3.112}$$

The factor of $\slashed{n}_{-\sigma\alpha}/4$ is absorbed into the definition of the soft function which we give below.

Another major simplification for the $g\bar{q}$-channel Drell-Yan cross-section at next-to-leading power occurs due to the fact that, as discussed at the beginning of this section, the leading power amplitude for the process $g\bar{q} \to \gamma^* + X$ vanishes. Therefore, the so-called kinematic correction considered in section 3.2 for the $q\bar{q}$ induced cross-section does not exist for the $g\bar{q}$-channel. Here, at $\mathcal{O}(\lambda^2)$ accuracy, it is only necessary to keep the leading power contribution to the phase-space kinematics. This implies that we take the first term in the power expansion of equation (3.68) (explicitly, the first term in (3.69)), and we can perform the $d^{d-1}\vec{q}$ integral in equation (3.107). This yields a delta function in $\vec{x}$ which is subsequently evaluated with the $d^{d-1}\vec{x}$ integral setting the $\vec{x}$ dependence to $\vec{x} = 0$. Only the x^0 dependence remains in the soft function.

Taking into consideration all of the above simplifications and making use of the definition of Δ in equation (3.31), we start from (3.107) and write down the factorisation

formula for the $g\bar{q}$-channel of the Drell-Yan partonic cross-section at next-to-leading power accuracy

$$
\Delta_{g\bar{q}} = 4H(Q^2) \int d\omega_1 \, d\omega_2
$$
$$
\times \, G^*_{\xi q}(x_a n_+ p_A; \omega_2) G_{\xi q}(x_a n_+ p_A; \omega_1) S(\Omega, \omega_1, \omega_2) \,. \tag{3.113}
$$

We have used the expanded hard function $H(\hat{s}) = |C^{A0,A0}(x_a n_+ p_A, x_b n_- p_B)|^2 = H(Q^2) + \mathcal{O}(\lambda^2)$, and the soft function $S(\Omega, \omega_1, \omega_2)$ is given by

$$
S_{g\bar{q}}(\Omega, \omega_1, \omega_2) = \int \frac{dx^0}{4\pi} \int \frac{dz_{1-}}{2\pi} \int \frac{dz_{2-}}{2\pi} e^{-i\omega_1 z_{1-}} e^{+i\omega_2 z_{2-}} e^{+i\,\Omega x^0/2}
$$
$$
\times \frac{1}{C_F \, C_A} \langle 0|\bar{\mathbf{T}}\Big(\frac{g_s}{in_- \partial_{z_2}} \bar{q}_+(x^0 + z_{2-}) \, \mathbf{T}^A \left\{ Y^\dagger_+(x^0) Y_-(x^0) \right\} \Big)
$$
$$
\times \frac{\slashed{n}_-}{4} \mathbf{T}\Big(\left\{ Y^\dagger_-(0) Y_+(0) \right\} \mathbf{T}^A \frac{g_s}{in_- \partial_{z_1}} q_+(z_{1-}) \Big)|0\rangle \,. \tag{3.114}
$$

The $\mathcal{L}^{(1)}_{\xi q}$ insertion in the amplitude is at position z_{1-} whereas in the conjugate amplitude we place the same insertion at position z_{2-}. The conjugate variables to these coordinate-space variables are ω_1 and ω_2 respectively. We note that the factorisation formula in equation (3.113), in the same way as the results for the $q\bar{q}$-channel Drell-Yan cross-section, is a d-dimensional formal result with regularized quantities. The objects appearing in the factorisation formula, $J_{\xi q}(x_a n_+ p_A; \omega_1)$, $J^*_{\xi q}(x_a n_+ p_A; \omega_2)$, and $S_{g\bar{q}}(\Omega, \omega_1, \omega_2)$, should not be treated as renormalized objects as the convolution linking the collinear and soft functions must be performed in d-dimensions. We compute these objects up to next-to-leading order in the following two chapters, and verify the validity of the factorisation formula at the fixed next-to-leading order in section 7.2, and discuss the consequences for leading logarithmic resummation in section 8.5.

Part III

Fixed-order next-to-leading power considerations

4

Drell-Yan: NLP collinear functions

The appearance of collinear functions in the next-to-leading power Drell-Yan partonic cross-section is one of the main findings of this work. We dedicate this section to the further exploration of the collinear functions through the direct computation of these objects to one-loop accuracy. We will use the one-loop collinear functions results in chapter 7 to verify the next-to-leading power factorisation formula derived in the previous section up to next-to-next-to-leading order in α_s.

We begin with the computation of collinear functions relevant for the $q\bar{q}$-channel factorisation formula considered in section 3.2 and in the following section we calculate the collinear functions relevant for the $g\bar{q}$-channel of the Drell-Yan process obtained in section 3.3.

In general, the collinear functions are defined by the operator matching equations given in (3.42) and (3.43). The left-hand side of each matching equation contains the threshold-collinear fields which come from the time-ordered products of hard matching currents with subleading-power Lagrangian terms. In the set-up of the problem we assume that the collinear scale is much greater than the scale of strong interactions, $Q^2(1-z) \gg \Lambda^2$. Therefore the collinear functions, $\tilde{J}_i(\{t_k\}, u; \{z_{j-}\})$ and $\tilde{G}_i(\{t_k\}, u; \{z_{j-}\})$, are perturbatively calculable short-distance coefficients in the matching equations (3.42) and (3.43). The collinear functions can be extracted from these operator matching equations by taking appropriate matrix elements between relevant partonic states. We perform these steps in detail in the following sections for the $q\bar{q}$ and $g\bar{q}$ channels at next-to-leading power.

4.1   Quark-antiquark channel

The relevant next-to-leading power matching equations are given in (3.66) and (3.67) for the single and double insertions of the subleading-power Lagrangian terms respectively. In order to keep the discussion clear, we introduce the following abbreviations

$$\tilde{\mathcal{T}}^{\mathfrak{a}}_{\gamma f}(t) \equiv i \int d^4 z\, \mathbf{T}\Big[\chi_{c,\gamma f}\,(tn_+)\,\mathcal{L}^{(2)}(z)\Big], \tag{4.1}$$

$$\tilde{\mathcal{T}}^{\mathfrak{b}}_{\gamma f}(t) \equiv i^2 \int d^d z_1 \int d^d z_2\, \mathbf{T}\Big[\chi_{c,\gamma f}\,(tn_+)\,\mathcal{L}^{(1)}(z_1)\mathcal{L}^{(1)}(z_2)\Big], \tag{4.2}$$

for the left-hand sides of equations (3.66) and (3.67) respectively. The Fourier transforms of these objects are given by

$$\mathcal{T}^{\mathfrak{a}}_{\gamma f}(n_+ q) = \int dt \, e^{i(n_+ q)\,t} \, \tilde{\mathcal{T}}^{\mathfrak{a}}_{\gamma f}(t) \,, \tag{4.3}$$

$$\mathcal{T}^{\mathfrak{b}}_{\gamma f}(n_+ q) = \int dt \, e^{i(n_+ q)\,t} \, \tilde{\mathcal{T}}^{\mathfrak{b}}_{\gamma f}(t) \,. \tag{4.4}$$

We also apply the Fourier transform to the right-hand sides of equations (3.66) and (3.67), and with this obtain the momentum-space matching equations as follows

$$
\begin{aligned}
\mathcal{T}^{\mathfrak{a}}_{\gamma f}(n_+ q) \;=\;& 2\pi \sum_i \int \frac{dn_+ p_a}{2\pi} \int du \, e^{i\,(n_+ p_a)\,u} \int \frac{d\omega}{2\pi} \\
& \times J_{i;\gamma\beta,\mu,fbd}\,(n_+ q, n_+ p_a; \omega) \; \chi^{\mathrm{PDF}}_{c,\beta b}(u n_+) \int dz_- \, e^{-i\omega z_-} \, \mathfrak{s}_{i;\mu,d}(z_-)
\end{aligned} \tag{4.5}
$$

for the single insertion, and

$$
\begin{aligned}
\mathcal{T}^{\mathfrak{b}}_{\gamma f}(n_+ q) \;=\;& 2\pi \sum_i \int \frac{dn_+ p_a}{2\pi} \int du \, e^{i\,(n_+ p_a)\,u} \int \frac{d\omega_1}{2\pi} \frac{d\omega_2}{2\pi} \\
& \times J_{i;\gamma\beta,\mu,fbd}\,(n_+ q, n_+ p_a; \omega_1, \omega_2) \; \chi^{\mathrm{PDF}}_{c,\beta b}(u n_+) \\
& \times \int dz_{1-} dz_{2-} \, e^{-i\,\omega_1 z_{1-}} e^{-i\,\omega_2 z_{2-}} \, \mathfrak{s}_{i;\mu,d}(z_{1-}, z_{2-})
\end{aligned} \tag{4.6}
$$

for the double insertions of power-suppressed Lagrangian terms.

In order to obtain the perturbative collinear functions $J_{i;\gamma\beta,\mu,fbd}\,(n_+ q, n_+ p_a; \omega)$ and $J_{i;\gamma\beta,\mu,fbd}\,(n_+ q, n_+ p_a; \omega_1, \omega_2)$ we choose appropriate partonic matrix elements of the matching equations above. For example, for the case of a collinear matching where only a single external soft gluon is present, the simplest partonic matrix element that we can consider is one with a soft gluon and a c-PDF quark, $\langle g(k)|...|q(p)\rangle$. Having made this choice, we calculate both sides of the relevant matching equation with the leading power collinear Lagrangian where the soft fields have been decoupled. In this case, the soft fields on both sides of the matching equation are external. Therefore, the soft matrix element $\langle g(k)|\mathfrak{s}_{i;\mu,d}(z_-)|0\rangle$ must take its tree-level value, as only soft loops can contribute to α_s corrections of the soft matrix element and these are not present in the collinear matching. The c-PDF matrix element, $\langle 0|\chi^{\mathrm{PDF}}_{c,\beta b}(u n_+)|q(p)\rangle$, also takes its tree-level value because here the loop corrections are scaleless as discussed in section 3.1.2.

To perform the calculation, we use momentum-space Feynman rules for the soft-collinear interaction vertices, such as the collinear-quark soft-gluon interaction vertex in (2.90), complete list of which is given in appendix A of [87]. The Feynman rules originate from the the power-suppressed SCET Lagrangian terms (2.63) – (2.69). An important feature of the next-to-leading power Feynman rules is the appearance of momentum-conservation delta functions with derivatives acting on them. As described in section 2.4.2, these derivatives acting on momentum-conserving delta functions arise due to the explicit presence of position-space arguments, x^μ, in the subleading-power SCET Lagrangian terms owing to multipole expansion [72]. In this section, we show explicitly how to deal with this complication, by first integrating by parts such that the derivatives act on the rest of the amplitude *before* momentum conservation is imposed.

4.1.1 Tree-level collinear functions

For the $q\bar{q}$-channel of the Drell-Yan process, we only require insertions of the quark-gluon subleading SCET Lagrangian terms to obtain the collinear functions at tree level. In order to include the Yang-Mills subleading power terms, at least one collinear gluon loop would be necessary such that a $\mathcal{L}_{\text{YM}}^{(l)}$ Lagrangian insertion could be connected to the diagram via a triple-gluon interaction. Contributions of this type are considered explicitly in the section 4.1.2. We divide the computation of the tree-level collinear functions for the $q\bar{q}$-channel into two sections. First, we calculate the collinear functions connected to single soft gluon structures, and in the second part, we consider the collinear functions connected to soft structures which support the emission of at least two soft partons.

Single soft gluon structures

Considering the quark-gluon subleading SCET Lagrangian given in equations (2.107) – (2.114), we find that only two soft gluon building blocks can support a tree-level single-gluon matrix element at next-to-leading power, $\mathcal{O}(\lambda^2)$. These structures are

$$\mathfrak{s}_1^A(z_-) = \frac{i\partial_\perp^\mu}{in_-\partial}\mathcal{B}_{\mu_\perp}^{+A}(z_-) \qquad \text{and} \qquad \mathfrak{s}_6^A(z_-) = \frac{i\partial_{[\mu_\perp}}{in_-\partial}\mathcal{B}_{\nu_\perp]}^{+A}(z_-). \tag{4.7}$$

Therefore, the sum over i in the operator matching equation given in (4.5) is reduced to contain only two contributions, $i = 1, 6$. Explicitly, taking the $\langle g(k)|...|q(p)\rangle$ matrix element of the collinear matching equation in (4.5) yields the following expression

$$\begin{aligned}
\langle g^K(k)|\mathcal{T}_{\gamma f}^{\mathfrak{a},1g}(n_+q)|q(p)_e\rangle &= 2\pi \int \frac{dn_+p_a}{2\pi}du\, e^{i(n_+p_a)u} \int \frac{d\omega}{2\pi} \int dz_-\, e^{-i\omega z_-} \\
&\times \Bigg(J_{1;\gamma\beta,fb}^A(n_+q, n_+p_a; \omega)\, \langle 0|\chi_{c,\beta b}^{\text{PDF}}(un_+)|q(p)_e\rangle\, \langle g^K(k)|\mathfrak{s}_1^A(z_-)|0\rangle \\
&\quad + J_{6;\gamma\beta,fb}^{\mu\nu,A}(n_+q, n_+p_a; \omega)\, \langle 0|\chi_{c,\beta b}^{\text{PDF}}(un_+)|q(p)_e\rangle\, \langle g^K(k)|\mathfrak{s}_{6;\mu\nu}^A(z_-)|0\rangle \Bigg), \tag{4.8}
\end{aligned}$$

where K is the adjoint colour index and e is the fundamental colour index of the external state. We have also added another label, $1g$, to the operator to remind that we are taking a soft gluon matrix element of this operator. The soft structure does contain soft Wilson lines and so in principle many more emissions could be considered. We choose the simplest case. We next evaluate the separate pieces making up (4.8) beginning with the c-PDF collinear matrix element $\langle 0|\chi_{c,\beta b}^{\text{PDF}}(un_+)|q(p)_e\rangle$ on the right-hand side which becomes

$$\langle 0|\chi_{c,\beta b}^{\text{PDF}}(un_+)|q(p)_e\rangle = \delta_{be}\sqrt{Z_{q,\text{PDF}}}\, u_{c,\beta}(p)\, e^{-i(n_+p)u}. \tag{4.9}$$

The $\sqrt{Z_{q,\text{PDF}}}$ is the on-shell wave renormalization factor of the c-PDF field. We turn our attention to the soft matrix elements $\langle g^K(k)|\mathfrak{s}_1^A(z_-)|0\rangle$ and $\langle g^K(k)|\mathfrak{s}_{6;\mu\nu}^A(z_-)|0\rangle$, which are found to yield

$$\langle g^K(k)|\frac{i\partial_\perp^\nu}{in_-\partial}\mathcal{B}_{\nu_\perp}^{+A}(z_-)|0\rangle = \delta^{AK}\frac{g_s}{(n_-k)}\left[k_\perp^\eta - \frac{k_\perp^2}{(n_-k)}n_-^\eta\right]\epsilon_\eta^*(k)\, e^{iz_-k} + \mathcal{O}(\alpha_s), \tag{4.10}$$

$$\langle g^K(k)|\frac{i\partial_{[\mu_\perp}}{in_-\partial}\mathcal{B}^{+A}_{\nu_\perp]}(z_-)|0\rangle \;=\; \delta^{AK}\,\frac{g_s}{(n_-k)}\left[k^\mu_\perp\,g^{\nu\eta}_\perp - k^\nu_\perp\,g^{\mu\eta}_\perp\right]\epsilon^*_\eta(k)\,e^{iz_-k} + \mathcal{O}(\alpha_s)\,. \quad (4.11)$$

We now insert the results in (4.9), (4.10), and (4.11) into equation (4.8), for which we then obtain

$$
\begin{aligned}
\langle g^K(k)|\mathcal{T}^{\mathfrak{a},1g}_{\gamma f}(n_+q)|q(p)_e\rangle \;=\;\; & 2\pi\,\frac{g_s}{(n_-k)}\left(J^K_{1;\gamma\beta,fe}\,(n_+q,n_+p;n_-k)\left[k^\eta_\perp - \frac{k^2_\perp}{(n_-k)}n^\eta_-\right]\right.\\
& \left.+\,J^{\mu\nu,K}_{6;\gamma\beta,fe}\,(n_+q,n_+p;n_-k)\left[k^\mu_\perp\,g^{\nu\eta}_\perp - k^\nu_\perp\,g^{\mu\eta}_\perp\right]\right)\sqrt{Z_{q,\mathrm{PDF}}}\,u_{c,\beta}(p)\epsilon^*_\eta(k)\,. \quad (4.12)
\end{aligned}
$$

This expression is the final result for our chosen partonic matrix element of the right-hand side of the operator matching equation given in (4.5) for soft structures supporting single gluon emissions. As we have explained above, we do not require loop corrections to the *c*-PDF and soft matrix elements in equations (4.9), (4.10), and (4.11) since the *c*-PDF and soft fields act only as external fields on both sides of the matching equation, which means that the expression in (4.12) is exact to all orders in perturbation theory.

We next compute the left-hand side of the matching equation (4.5) by considering the same matrix element $\langle g^K(k)|...|q(p)_e\rangle$ as we have used in obtaining the expression in (4.12) for the right-hand side.

Since the Yang-Mills and soft quark subleading power Lagrangian terms cannot contribute to the tree-level collinear function tied to a single soft gluon emissions structure, the only relevant terms in $\mathcal{L}^{(2)}$ in (4.1) are terms with one soft gauge field in $\mathcal{L}^{(2)}_{\xi,\mathrm{I}}$, $\mathcal{L}^{(2)}_{\xi,\mathrm{II}}$, and $\mathcal{L}^{(2)}_{\xi,\mathrm{III}}$, as given in (2.65). These terms give rise to the next-to-leading power soft-gluon vertex given in equation (2.91). The calculation at tree-level accuracy yields the following expression

$$
\begin{aligned}
\langle g^K(k)|\mathcal{T}^{\mathfrak{a},1g}_{\gamma f}(n_+q)|q(p)_e\rangle \;=\;\; & 2\pi\,\frac{g_s}{(n_-k)}\mathbf{T}^K_{fe}\left\{\vphantom{\frac{k^2_\perp}{(n_-k)}}\right.\\
& -\left[k^\eta_\perp - \frac{k^2_\perp}{(n_-k)}n^\eta_-\right]\frac{1}{n_+p}\delta(n_+q - n_+p)\delta_{\gamma\beta}\\
& -\left[(n_-k)n^\eta_+ - (n_+k)n^\eta_-\right]\frac{\partial}{\partial n_+q}\delta(n_+q - n_+p)\delta_{\gamma\beta}\\
& -\left[k^\mu_\perp g^{\nu\eta}_\perp - k^\nu_\perp g^{\mu\eta}_\perp\right]\frac{1}{2}\frac{1}{n_+p}\delta(n_+q - n_+p)\left[\gamma^\mu_\perp\gamma^\nu_\perp\right]_{\gamma\beta}\left.\vphantom{\frac{k^2_\perp}{(n_-k)}}\right\}\\
& \times\,\epsilon^*(k)_\eta\,\sqrt{Z_{q,c}}|_{\mathrm{tree}}\,u_{c,\beta}(p) + \mathcal{O}(\alpha_s)\,. \quad (4.13)
\end{aligned}
$$

In the effective field theory, including the threshold-collinear mode, the tree-level value of the on-shell wave function renormalization factor of the quark field is given by $\sqrt{Z_{q,c}}|_{\mathrm{tree}} = 1$.

The expression in equation (4.13) has been calculated directly using the next-to-leading power Feynman rule in (2.91). We note that this gives rise to three separate contributions, each proportional to a different soft structure. Inspection of (4.12) reveals only two soft structures onto which terms in equation (4.13) can be matched. The observation that must
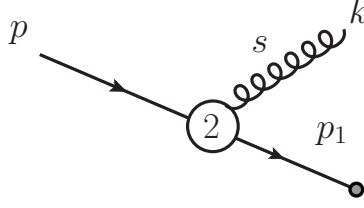
Figure 4.1: *Diagram contributing to the tree level collinear functions. Through calculation of this diagram using Feynman rules from [87] we can obtain the J_1 and J_6 tree-level collinear functions, corresponding to insertions of $\mathcal{L}_{1\xi}^{(2)}$ and $\mathcal{L}_{2\xi}^{(2)}$, and $\mathcal{L}_{4\xi}^{(2)}$, respectively.*

be made, is that the soft structures appearing in the direct calculation in equation (4.13) are not independent. In fact, they are connected by the equation-of-motion identity given in equation (3.46). Considering now the emitted gluon, we can use the transversality and on-shell conditions $k \cdot \epsilon^* = 0$ and $k^2 = 0$, respectively. These relations have not yet been applied in the calculation leading to the result in equation (4.13). To make use of these relations, we first rewrite $k \cdot \epsilon^* = 0$ in light-cone components which gives the following

$$(n_+ k)(n_- \epsilon^*) = 2\left(-\frac{(n_- k)(n_+ \epsilon^*)}{2} - k_\perp \cdot \epsilon_\perp^* \right). \tag{4.14}$$

This relation allows us to express the second soft structure in the curly bracket of (4.13) in terms of the first,

$$\left[(n_- k) n_+^\nu - (n_+ k) n_-^\nu \right] \epsilon_\nu^*(k) = -2 \left[k_\perp^\nu - \frac{k_\perp^2}{(n_- k)} n_-^\nu \right] \epsilon_\nu^*(k). \tag{4.15}$$

This result should not come as a surprise, since it is known that the two soft structures, $n_+ \mathcal{B}^+(z_-)$ and $\frac{i\partial_\perp^\mu}{in_-\partial} \mathcal{B}_{\mu_\perp}^+(z_-)$, are connected via the equation-of-motion identity in (3.46). Therefore, the two Lagrangian insertions which are built from these two soft structures, $\mathcal{L}_{1\xi}^{(2)}$ and $\mathcal{L}_{2\xi}^{(2)}$ respectively, must contribute to the same collinear function, J_1.

Finally, we insert the relation written in equation (4.14) into the tree-level computation result in (4.13) and arrive at the following

$$\langle g^K(k)|\mathcal{T}_{\gamma f}^{a,1g}(n_+q)|q(p)_e\rangle = 2\pi \frac{g_s}{(n_- k)} \mathbf{T}_{fe}^K \left\{ \vphantom{\frac{\partial}{\partial}} \right.$$

$$\left[k_\perp^\eta - \frac{k_\perp^2}{(n_- k)} n_-^\eta \right] \left(-\frac{1}{n_+ p} \delta(n_+ q - n_+ p) + 2 \frac{\partial}{\partial n_+ q} \delta(n_+ q - n_+ p) \right) \delta_{\gamma\beta}$$

$$\left. - \left[k_\perp^\mu g_\perp^{\nu\eta} - k_\perp^\nu g_\perp^{\mu\eta} \right] \frac{1}{2} \frac{1}{n_+ p} \delta(n_+ q - n_+ p) \left[\gamma_\perp^\mu \gamma_\perp^\nu \right]_{\gamma\beta} \right\}$$

$$\times \epsilon^*(k)_\eta \sqrt{Z_{q,c}}|_{\text{tree}} u_{c,\beta}(p) + \mathcal{O}(\alpha_s). \tag{4.16}$$

At this point we can compare the result for the left-hand side of the matching equation in (4.16), to the right-hand side given in (4.12), through which we obtain the tree-level

collinear functions

$$
J^{K(0)}_{1;\gamma\beta,fe}(n_+q, n_+p; \omega) \;\; = \;\; \mathbf{T}^K_{fe}\delta_{\beta\gamma}\left(-\frac{1}{n_+p}\delta(n_+q - n_+p) + 2\,\frac{\partial}{\partial n_+q}\delta(n_+q - n_+p)\right), \tag{4.17}
$$

$$
J^{\mu\nu,K(0)}_{6;\gamma\beta,fe}(n_+q, n_+p; \omega) \;\; = \;\; -\frac{1}{2}\frac{1}{n_+p}\mathbf{T}^K_{fe}\left[\gamma^\mu_\perp\gamma^\nu_\perp\right]_{\gamma\beta}\delta(n_+q - n_+p)\,. \tag{4.18}
$$

We note here the factor of -2 which appears in the second term of (4.17) in relation to the first term. This factor was not present the result prior to the use of on-shell and transversality relations given in equation (4.13). The origin of the factor of -2 can be traced all the way back to the equation-of-motion relation in (3.46), as the soft fields in the two terms which induce this contribution are connected by the equation-of-motion relation precisely with this weight.

We recall the scalar collinear function, J_1, decomposition which we introduced in (3.89). This decomposition we now apply to the result in equation (4.17) which implies

$$
J^{(0)}_{1,1}(n_+p; \omega) \;\; = \;\; -\frac{1}{n_+p}\,, \tag{4.19}
$$

$$
J^{(0)}_{1,2}(n_+p; \omega) \;\; = \;\; 2\,. \tag{4.20}
$$

We also note again that, as described in section 3.2.2, the collinear function J_6 does not contribute to the Drell-Yan partonic cross-section at any order in α_s.

Double soft parton structures

We now turn our attention to calculation of the collinear functions which multiply soft structures that contain at least two soft fields, for example $\frac{1}{(in_-\partial)}\left[\mathcal{B}^+_{\mu_\perp}(z_{1-}), \mathcal{B}^+_{\nu_\perp}(z_{1-})\right]$ and $\frac{1}{(in_-\partial_{z_1})(in_-\partial_{z_2})}q_{+\sigma}(z_{1-})\bar{q}_{+\lambda}(z_{2-})$ from the set in (3.45). Focusing on the graphical representation of the general collinear function presented in figure 3.9, these collinear functions are given by diagrams with a single external quark to the left and right, the c-PDF and threshold-collinear quarks respectively, and two external soft gluons or a soft quark-antiquark pair attached to the collinear function J. Here we perform the collinear matching computation at tree-level accuracy, for which the relevant diagrams are shown in figure 4.2. For concreteness, we state that the required subleading power Lagrangian insertions are single insertions of the $\mathcal{L}^{(2)}_{3\xi}$ and $\mathcal{L}^{(2)}_{5\xi}$ Lagrangian terms, and the double insertions of $\mathcal{L}^{(1)}_{\xi}$ and $\mathcal{L}^{(1)}_{\xi q}$ Lagrangian terms. The explicit forms of these terms are given in equations (2.110), (2.112), (2.107), and (2.113) respectively.

On top of the contributions due to Lagrangian insertions mentioned above, which explicitly contain at least two soft fields, we must also consider contributions due to one-soft-particle-reducible diagrams for the $\mathcal{L}^{(2)}_{1\xi}$ Lagrangian insertion. These contributions are shown in the last diagram in the top and bottom rows of figure 4.2. The reason for the inclusion of these diagrams as part of the contribution to the collinear functions with two soft partons is that in the derivation of the factorisation formula, specifically in the step where we perform the collinear matching, the $n_+\mathcal{B}^+$ has been eliminated from the list of soft structures using the equation-of-motion relation in (3.46). We see
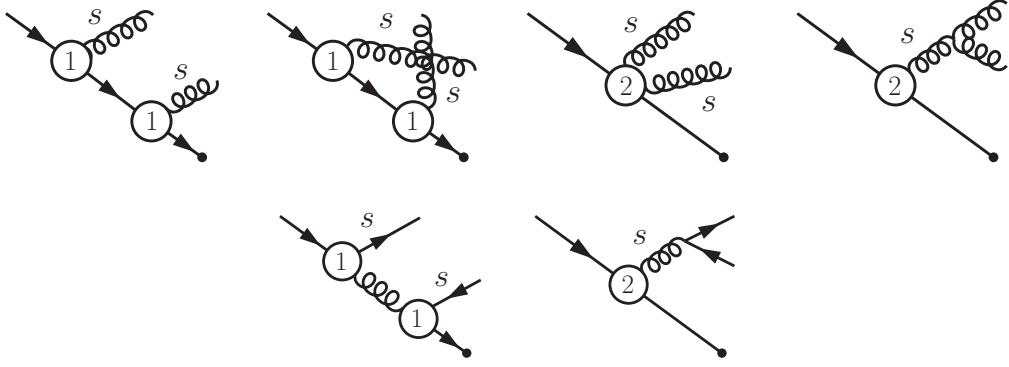
Figure 4.2: *Diagrams contributing to the matching of the two soft parton collinear functions. The soft lines are labelled with an "s". As described in the main text (and appendix C), the contributions from the one-soft-particle reducible diagrams, when the internal gluon originates from $n_+ \mathcal{B}^+$ term in $\mathcal{L}^{(2)}$, are reproduced by the two parton terms in the equation-of-motion relation (3.46) applied to (4.13).*

in the equation-of-motion relation in (3.46) that the $n_+ \mathcal{B}^+$ structure is proportional to another single gluon structure $\frac{i\partial_\perp^\mu}{in_- \partial} \mathcal{B}_{\mu_\perp}^+ (z_-)$, but also the two parton soft structures. The one-soft-particle-reducible diagrams must reproduce precisely those contributions. We discuss this in greater detail below, and show explicit computation in appendix C.

We begin the discussion by considering the collinear functions which are connected to soft structures that support two soft gluon emission at the same coordinate z_-. We start with the collinear functions which are induced by time-ordered product insertions of Lagrangian terms $\mathcal{L}_{3\xi}^{(2)}$ and $\mathcal{L}_{5\xi}^{(2)}$. These are calculated in the same manner as the collinear functions in the case of a single soft gluon emission. The right-hand side of the matching equation is a generalisation of (4.8) to the two-parton case. This is achieved by considering the $\mathfrak{s}_i$ structures given by third and fourth terms in (3.45), $\frac{1}{(in_-\partial)^2} \left[\mathcal{B}^{+\,\mu_\perp}(z_{1-}), \left[in_-\partial \mathcal{B}_{\mu_\perp}^+ (z_{1-}) \right] \right]$ and $\frac{1}{(in_-\partial)} \left[\mathcal{B}_{\mu_\perp}^+ (z_{1-}), \mathcal{B}_{\nu_\perp}^+ (z_{1-}) \right]$. We note that both of these terms are made from $\mathcal{B}_{\mu_\perp}^+$ building blocks only. Hence, the extraction of collinear functions is simplified by the choice of $\perp$ polarisations for the external soft gluons in the calculation.

We next turn our attention to the left-hand side of the matching equation. The results for this part are obtained by the computation of the third diagram in figure 4.2 with the $\mathcal{L}_{3\xi}^{(2)}$ and $\mathcal{L}_{5\xi}^{(2)}$ Lagrangian insertions. The collinear function J_3, as defined by (3.81) with the soft function written in equation (3.85), is given by

$$
\begin{aligned}
J_{3;\gamma\beta} \left(n_+ p, x_a\, n_+ p_A; \omega \right) = \delta_{\gamma\beta} \Big[& J_{3,1} \left(x_a n_+ p_A; \omega \right) \delta(n_+ p - x_a n_+ p_A) \\
& + J_{3,2} \left(x_a n_+ p_A; \omega \right) \frac{\partial}{\partial (n_+ p)} \delta(n_+ p - x_a n_+ p_A) \Big]
\end{aligned}
\tag{4.21}
$$

with $J_{3,1}$ and $J_{3,2}$ still to be determined.

We now inspect closer the relevant subleading-power SCET Lagrangian terms. Considering first the terms $\mathcal{L}_{3\xi}^{(2)}$ and $\mathcal{L}_{5\xi}^{(2)}$ in equations (2.110) and (2.112) respectively, we

notice that after the soft fields are stripped off, the leftover collinear pieces of $\mathcal{L}_{3\xi}^{(2)}$ are identical to the collinear pieces of $\mathcal{L}_{2\xi}^{(2)}$ in (2.109), and the leftover collinear pieces of $\mathcal{L}_{5\xi}^{(2)}$ are identical to those of $\mathcal{L}_{4\xi}^{(2)}$ in equation (2.111). This fact leads to the conclusion that the collinear functions induced by Lagrangian insertions of $\mathcal{L}_{3\xi}^{(2)}$ and $\mathcal{L}_{5\xi}^{(2)}$ are the same as those induced by terms $\mathcal{L}_{2\xi}^{(2)}$ and $\mathcal{L}_{4\xi}^{(2)}$ respectively. Namely, $J_{3,1}$ is equal to $J_{1,1}$, and J_2 to J_6. As briefly discussed above, we must also take care of the one-soft-particle reducible diagrams, due to the fact that the $n_+\mathcal{B}^+$ soft field was eliminated from the basis of soft structures. The already determined single-soft-gluon emission collinear function $J_{1,2}$ only partly reproduced the one-soft-particle reducible diagram. Namely, in terms of the equation-of-motion relation in (3.46), only the first term $\frac{i\partial_\perp^\mu}{in_-\partial}\mathcal{B}_{\mu_\perp}^+(z_-)$ is accounted for so far. There exist a number of ways to determine the as of yet unaccounted for pieces of this diagram. It could for example be obtained by explicit matching, or by using the single-gluon matrix element in equation (4.13) prior to the application of the on-shell and transversality relations on the external soft gluon. Following the latter way of working, we replace the n_+^η by the operator $n_+\mathcal{B}^+$. We then employ the operator equation-of-motion identity given in equation (3.46), which results in a term that is proportional to the two-soft gluon structure $\mathfrak{s}_3$. This term originates in the second term on the right-hand side of (3.46). At this point we make the deduction that $J_{3,2}$ in (4.21) must be equal to $J_{1,2}$ calculated earlier for the single-soft-gluon collinear function. Another way of obtaining the same result is to use the equation-of-motion identity in (3.46) directly in $\mathcal{L}_{1\xi}^{(2)}$. This leads to $\mathcal{L}_{1\xi}^{(2)}$ containing identical soft-gluon structure as $\mathcal{L}_{3\xi}^{(2)}$. We can then obtain $J_{3,2}$ from the newly generated $q\bar{q}gg$ vertex. More details and explicit calculations regarding the contribution of one-soft-particle reducible diagrams are given in appendix C.

The only contributions which are left to consider come from double insertions of $\mathcal{O}(\lambda)$ Lagrangian terms $\mathcal{L}^{(1)}$ at two different positions. The relevant collinear matching operator equation for double insertions of subleading-power Lagrangian terms is given in equation (3.67), which for convenience we give here again with the χ_c^{PDF} field written in coordinate space

$$i^2 \int d^4 z_1 \, d^4 z_2 \, \mathbf{T}\left[\chi_{c,\gamma f}(tn_+) \, \mathcal{L}^{(1)}(z_1)\mathcal{L}^{(1)}(z_2)\right] \quad = 2\pi \sum_i \int \frac{dn_+p_a}{2\pi} du \, e^{i(n_+p_a)u}$$

$$\times \int \frac{d\omega_1}{2\pi} \, dz_{1-} \, e^{-i\omega_1 z_{1-}} \int \frac{d\omega_2}{2\pi} \, dz_{2-} \, e^{-i\omega_2 z_{2-}} \int \frac{dn_+p}{2\pi} e^{-i(n_+p)t}$$

$$\times J_{i;\gamma\beta,\mu,fbd}(n_+p, n_+p_a; \omega_1, \omega_2) \, \chi_{c,\beta b}^{\text{PDF}}(un_+) \, \mathfrak{s}_{i;\mu,d}(z_{1-}, z_{2-}) \, . \tag{4.22}$$

To obtain the collinear function tied to the soft structure with two soft gluons emitted from two different positions we calculate the $\langle g(k_1)g(k_2)|...|q(p)\rangle$ partonic matrix element of the above operator matching equation. The right-hand side of the matrix element of the matching equation is then given by

$$\langle g(k_1)^{K_1} g(k_2)^{K_2}|\mathcal{T}_{\gamma f}^{\mathfrak{b},2g}(n_+q)|q(p)_e\rangle \;\; = \;\; 2\pi \int \frac{dn_+p_a}{2\pi} du \, e^{i(n_+p_a)u} \int \frac{d\omega_1}{2\pi} \, dz_{1-} \, e^{-i\omega_1 z_{1-}}$$

$$\times \int \frac{d\omega_2}{2\pi} \, dz_{2-} \, e^{-i\omega_2 z_{2-}} \left(J_{4;\gamma\beta,fb}^{\mu\nu,AB}(n_+q, n_+p_a; \omega_1, \omega_2) \right.$$

$$\left. \times \langle 0|\chi_{c,\beta b}^{\text{PDF}}(un_+)|q(p)_e\rangle \, \langle g(k_1)^{K_1} g(k_2)^{K_2}|\mathfrak{s}_{4;\mu\nu}^{AB}(z_{1-}, z_{2-})|0\rangle \right), \tag{4.23}$$

The left-hand side of the matching equation in (4.22), with $\mathcal{L}_\xi^{(1)}$ in (2.107) in place of the two $\mathcal{L}^{(1)}$ insertions in the time-ordered product, is calculated using subleading-power Feynman rules in the same manner as for the single soft gluon case above. The diagrams which we need to compute are the first two in the first line of figure 4.2. After obtaining the result, we equate both sides of the matching equation and arrive at the following result for the collinear function

$$
\begin{aligned}
J_{4;\gamma\beta,fb}^{\mu\nu,AB\,(0)}\left(n_+q, n_+p; \omega_1, \omega_2\right) &= \frac{2g_\perp^{\mu\nu}}{n_+p\,(\omega_1+\omega_2)^2}\left(\omega_1\,\mathbf{T}^A\mathbf{T}^B + \omega_2\,\mathbf{T}^B\mathbf{T}^A\right)_{fb} \\
&\times \delta_{\gamma\beta}\,\delta(n_+q - n_+p)\,.
\end{aligned}
\tag{4.24}
$$

It now remains to calculate the tree-level collinear function tied to the soft quark-antiquark pair soft structure. This computation proceeds in the same way as the two soft gluon calculation above after we replace the $\mathcal{L}^{(1)}$ in (4.22) with $\mathcal{L}_{\xi q}^{(1)}$ from equation (2.113). Taking the $\langle q(k_1)_{k_1}\bar{q}(k_2)_{k_2}|...|q(p)\rangle$ partonic matrix element of (4.22) with the double $\mathcal{L}_{\xi q}^{(1)}$ Lagrangian insertion yield the following for the right-hand side of the matching equation

$$
\begin{aligned}
\langle q(k_1)_{k_1}\bar{q}(k_2)_{k_2}|\mathcal{T}_{\gamma f}^{\mathfrak{b},2q}(n_+q)|q(p)_e\rangle &= 2\pi\int\frac{dn_+p_a}{2\pi}du\,e^{i\,(n_+p_a)u}\int\frac{d\omega_1}{2\pi}\,dz_{1-}\,e^{-i\omega_1 z_{1-}} \\
&\times\int\frac{d\omega_2}{2\pi}\,dz_{2-}\,e^{-i\omega_2 z_{2-}}\bigg(\,J_{5;\gamma\sigma\lambda\beta}^{fghb}\left(n_+q, n_+p_a; \omega_1, \omega_2\right) \\
&\times\langle 0|\chi_{c,\beta b}^{\mathrm{PDF}}(un_+)|q(p)_e\rangle\,\langle q(k_1)_{k_1}\bar{q}(k_2)_{k_2}|\mathfrak{s}_{5;\sigma\lambda,gh}(z_{1-}, z_{2-})|0\rangle\bigg)\,.
\end{aligned}
\tag{4.25}
$$

The left-hand side of the matching equation is captured by the first diagram in the second line of figure 4.2. Moreover, the one-soft-particle reducible diagram in the same figure where the emitted soft gluon splits into two soft quarks also contributes to the collinear function J_5. This is because in the quark-antiquark case we have used a non-redundant basis of soft structures with the single bi-local term $\mathfrak{s}_5$. The piece which is unaccounted for is the single emission from $n_+\mathcal{B}$ followed by a purely soft interaction, and this is recovered here in the same way as the two-gluon contribution. Namely, from the quark-antiquark term in the operator equation-of-motion identity given in (3.46). More explicit details are presented in appendix C. We combine both contributions, which yields the final result

$$
\begin{aligned}
J_{5;\gamma\sigma\lambda\beta}^{fk_1k_2e\,(0)}\left(n_+q, n_+p; \omega_1, \omega_2\right) &= -\mathbf{T}_{fk_2}^A\mathbf{T}_{k_1e}^A\frac{1}{n_+p}\frac{\omega_2}{(\omega_1+\omega_2)}\frac{\slashed{n}_{-\gamma\eta}}{2}\gamma_{\perp,\eta\sigma}^\mu\gamma_{\perp\mu,\lambda\beta}\,\delta(n_+q-n_+p) \\
&+ 2\,\mathbf{T}_{fe}^K\mathbf{T}_{k_1k_2}^K\frac{\omega_1\omega_2}{(\omega_1+\omega_2)^2}\slashed{n}_{-\lambda\sigma}\delta_{\gamma\beta}\frac{\partial}{\partial n_+q}\delta(n_+q-n_+p)\,.
\end{aligned}
\tag{4.26}
$$

4.1.2 One-loop collinear functions

Calculation of the one-loop collinear functions for the $q\bar{q}$-channel of the Drell-Yan process within SCET is one of the key results in this work. Obtaining the one-loop results for the collinear functions enables us to demonstrate the consistency of the concept of collinear functions and establish validity of the SCET framework.

In this section we compute the collinear functions J_1 and J_6 to one-loop accuracy. As can be seen in equation (3.95), the J_1 collinear function is needed at $\mathcal{O}(\alpha_s)$ in order to
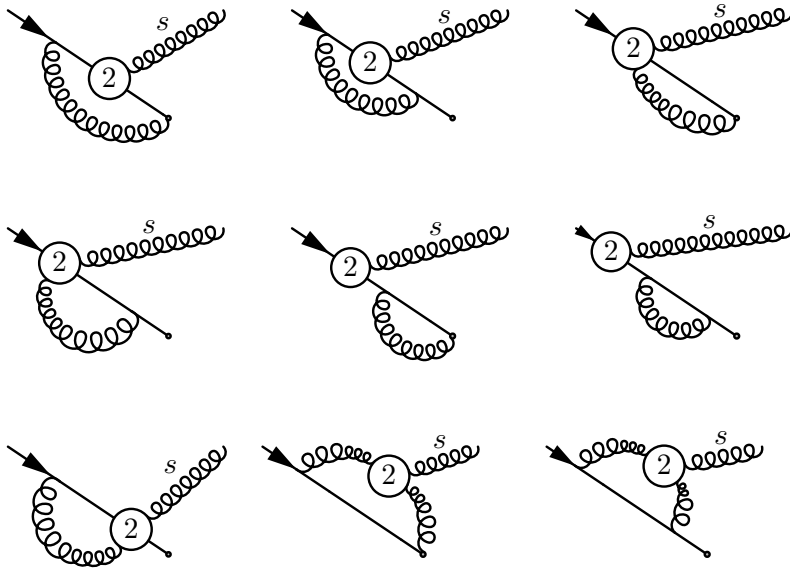
Figure 4.3:   *One-loop collinear diagrams with one external soft gluon which is labelled "s". The dot at the right end of the solid quark line denotes the χ_c field from the leading power current. The collinear gluon in the loop can attach to either the collinear quark or the collinear Wilson line in the definition of the χ_c field.*

verify the next-to-leading power factorisation formula in the comparison with the fixed next-to-next-to-leading order results in existing literature. We do not explicitly calculate the $\mathcal{O}(\alpha_s)$ corrections to the collinear functions corresponding to soft structures with two soft emitted partons. Corrections of this order would constitute a next-to-next-to-next-to-leading order effect at the cross-section level which is beyond the scope of this work.

In equation (4.12) we have already obtained the right-hand side of the matching equation that is valid to all orders in perturbation theory. We keep in mind that we must also obtain the on-shell wave function renormalization factor with $\mathcal{O}(\alpha_s)$ accuracy. However, since the calculation is carried out with dimensional regularization employed to treat ultraviolet and infrared divergences, the on-shell wave function renormalization factor is unity to all orders in perturbation theory, $\sqrt{Z_{q,\mathrm{PDF}}} = 1$, as the loops are scaleless. The same argument holds true for the $\sqrt{Z_{q,c}}$ factor appearing on the left-hand side of the matching equation. The coupling renormalization is also identical on the right- and left-hand sides of the matching equation, and cancels out at $\mathcal{O}(\alpha_s)$.

Keeping in mind the above considerations, in this section we perform the $\mathcal{O}(\alpha_s)$ calculation of the $\langle g^K(k)|\mathcal{T}^{\mathfrak{a},1g}_{\gamma f}(n_+q)|q(p)_e\rangle$ matrix element appearing on the left-hand side of (4.5). This computation requires the calculation of the Feynman diagrams with one collinear loop and a single soft emission. The soft emission is power-suppressed and enters the diagrams through insertions of the power-suppressed Lagrangian. The diagrams which are necessary in SCET are given in figure 4.3. All of the vertices appearing in the diagrams are taken to be interactions at leading-power, aside from the circled vertex which indicates the insertion of a subleading-power SCET Lagrangian term.
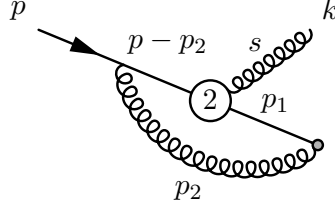
Figure 4.4: *One of the diagrams contributing to the one-loop collinear functions. Through calculation of this diagram using NLP Feynman rules we can obtain the J_1 and J_6 collinear functions, corresponding to insertions of $\mathcal{L}_{1\xi}^{(2)}$ and $\mathcal{L}_{2\xi}^{(2)}$, and $\mathcal{L}_{4\xi}^{(2)}$, respectively.*

Detailed computation

As mentioned in the discussion of the next-to-leading power Feynman rules in section 2.4.2, unfamiliar features, such as derivatives on delta functions which conserve momentum at vertices, arise during calculation of the diagrams in the effective theory at subleading powers. In order to highlight the differences to a usual QCD Feynman diagram calculation, we first compute the top-left diagram in figure 4.3 in considerable detail. The diagram with labelled momenta is shown in figure 4.4.

Applying the relevant NLP Feynman rules to the diagram in figure 4.4 and keeping track of all the indices explicitly gives the following expression

$$
\begin{aligned}
\langle g^K(k)|\mathcal{T}_{\gamma f}^{\mathfrak{a},1g}(n_+q)|q(p)_e\rangle_{\text{fig4.4}} &= (2\pi)\int \frac{d^dp_1}{(2\pi)^d}\int \frac{d^dp_2}{(2\pi)^d}\,\delta(n_+q - n_+p_1 - n_+p_2)\\
&\times g_s \mathbf{T}_{fa}^A \frac{n_{+\mu}}{(n_+p_2)}\frac{i(n_+p_1)}{p_1^2}\frac{\slashed{n}_{-\gamma\alpha}}{2}\\
&\times ig_s \mathbf{T}_{ab}^K S_{\alpha\beta}^{\sigma\delta}(-k,p-p_2,p_1)\frac{\slashed{n}_{+\beta\zeta}}{2}\Big(-k_\sigma g_{\delta\nu} + k_\delta g_{\sigma\nu}\Big)\frac{in_+(p-p_2)}{(p-p_2)^2}\frac{\slashed{n}_{-\zeta\lambda}}{2}\\
&\times ig_s \mathbf{T}_{be}^A C^\mu(p-p_2,p)\frac{\slashed{n}_{+\lambda\tau}}{2}\times \frac{-i}{p_2^2}\times u_{c\tau}(p)\,\epsilon^{*\nu}(k)
\end{aligned}
\tag{4.27}
$$

where the indices γ, α, β, ζ, λ, and τ are Dirac indices, f, a, b, and e are fundamental colour indices, A, K are adjoint colour indices, and μ, σ, δ, and ν are Lorentz indices. The leading power $C^\mu(p-p_2,p)$ vertex is given by

$$
C^\mu(p-p_2,p) = n_-^\mu + \frac{\slashed{p}_\perp - \slashed{p}_{2\perp}}{(n_+(p-p_2))}\gamma_\perp^\mu + \gamma_\perp^\mu \frac{\slashed{p}_\perp}{(n_+p)} - \frac{\slashed{p}_\perp - \slashed{p}_{2\perp}}{(n_+(p-p_2))}n_+^\mu \frac{\slashed{p}_\perp}{(n_+p)}.
\tag{4.28}
$$

We recall that in the chosen kinematics the incoming collinear momentum carries only its large component, $p^\mu = (n_+p)\frac{n_-^\mu}{2}$. Therefore, the leading power vertex $C^\mu(p-p_2,p)$ reduces to

$$
C^\mu(p-p_2,p) = n_-^\mu - \frac{\slashed{p}_{2\perp}}{(n_+(p-p_2))}\gamma_\perp^\mu.
\tag{4.29}
$$

In the starting expression in (4.27), the leading power vertex $C^\mu(p-p_2,p)$ is contracted with the gluon absorbed by the Wilson line in the hard current with index μ. This is

denoted by a dot on in the diagram in figure 4.4. Therefore only the n_-^μ term in 4.29 contributes. We use projection properties for the collinear spinnor

$$\frac{\slashed{n}_- \slashed{n}_+}{4}\, u_c(p) = u_c(p) \tag{4.30}$$

and manipulate the colour generator as given in (A.40). We then arrive at a simplified version of the expression in equation (4.27)

$$
\langle g^K(k)|\mathcal{T}_{\gamma f}^{\mathfrak{a},1g}(n_+ q)|q(p)_e\rangle_{\text{fig4.4}} = -2(2\pi)ig_s^3\left(C_F - \frac{1}{2}C_A\right)\mathbf{T}_{fe}^K \int \frac{d^d p_1}{(2\pi)^d}\int \frac{d^d p_2}{(2\pi)^d}
$$
$$
\times\, \delta(n_+ q - n_+ p_1 - n_+ p_2)\frac{1}{(n_+ p_2)}\frac{n_+ p_1}{p_1^2}\frac{n_+(p - p_2)}{(p - p_2)^2}\frac{1}{p_2^2}
$$
$$
\times \left[S^{\sigma\delta}(-k, p - p_2, p_1)u_c(p)\right]_\gamma\left(-k_\sigma g_{\delta\nu} + k_\delta g_{\sigma\nu}\right)\epsilon^{*\nu}(k). \tag{4.31}
$$

The subleading power vertex, based on (2.91), is given by

$$
S^{\sigma\delta}(-k, p - p_2, p_1) = \frac{1}{2}\Bigg[\underbrace{\left(n_- X\right)n_+^\sigma n_-^\delta}_{\text{I}} + \underbrace{\left(-kX_\perp\right)X_\perp^\sigma n_-^\delta}_{\text{II}}
$$
$$
+ \underbrace{X_\perp^\sigma\left(\frac{\slashed{p}_{1\perp}}{n_+ p_1}\gamma_\perp^\delta + \gamma_\perp^\delta\frac{\slashed{p}_\perp - \slashed{p}_{2\perp}}{n_+(p - p_2)}\right)}_{\text{III}}\Bigg], \tag{4.32}
$$

where we have also indicated which of the three subleading-power Lagrangian terms in (2.64) induces each piece of the Feynman rule. We remind the reader that the X^μ and $X^\mu X^\nu$ terms, given in equations (2.88) and (2.89) respectively, contain derivatives with respect to outgoing momentum p_1 acting on the momentum conservation delta function $\delta^{(d)}(p - p_2 - k_+ - p_1)$.

   In the next step of the calculation, we substitute in the expression for $S^{\sigma\delta}(-k, p - p_2, p_1)$ from (4.32). We then integrate by parts the momentum derivatives with respect to p_1 which are present in the X^μ and $X^\mu X^\nu$ terms. Once this integration is performed, these derivatives act on the rest of the integrand including the $\delta(n_+ q - n_+ p_1 - n_+ p_2)$ delta function in second line of (4.31). After this point, the momentum conservation delta function $\delta^{(d)}(p - p_2 - k_+ - p_1)$ present at the subleading-power interaction vertex can be evaluated with the integral over $d^d p_1$. This imposes momentum conservation and identifies $p_1^\mu = p^\mu - p_2^\mu - k_+^\mu$. We then arrive at the following expression

$$
\langle g^K(k)|\mathcal{T}_{\gamma f}^{\mathfrak{a},1g}(n_+ q)|q(p)_e\rangle_{\text{fig4.4}} = -(2\pi)ig_s^3\left(C_F - \frac{1}{2}C_A\right)\mathbf{T}_{fe}^K \int \frac{d^d p_2}{(2\pi)^d}
$$
$$
\times\, \frac{1}{(n_+ p_2)}\frac{n_+(p - p_2)}{(p - p_2)^2}\frac{1}{p_2^2}\left(-k_\sigma g_{\delta\nu} + k_\delta g_{\sigma\nu}\right)\epsilon^{*\nu}(k)
$$
$$
\times \Bigg\{n_- \cdot \frac{\partial}{\partial p_1}\left(\delta(n_+ q - n_+ p_1 - n_+ p_2)\frac{n_+ p_1}{p_1^2}\right)n_+^\sigma n_-^\delta\, u_{c,\gamma}(p)
$$
$$
- \left(k_\perp \cdot \frac{\partial}{\partial p_{1\perp}}\right)\frac{\partial}{\partial p_{1\perp\sigma}}\left(\delta(n_+ q - n_+ p_1 - n_+ p_2)\frac{n_+ p_1}{p_1^2}\right)n_-^\delta\, u_{c,\gamma}(p)
$$

$$+ \frac{\partial}{\partial p_{1\perp\sigma}} \left[\left(\delta(n_+ q - n_+ p_1 - n_+ p_2) \frac{n_+ p_1}{p_1^2} \right) \right.$$

$$\left. \times \left(\frac{\slashed{p}_{1\perp}}{n_+ p_1} \gamma_\perp^\delta - \gamma_\perp^\delta \frac{\slashed{p}_{2\perp}}{n_+(p - p_2)} \right)_{\gamma\beta} \right] u_{c,\beta}(p) \right\} \Bigg|_{p_1 = p - p_2 - k_+}. \qquad (4.33)$$

The third line in the above expression corresponds to the contribution labelled by I in (4.32), the fourth line to term II, and the fifth and sixth lines correspond to the term III. In what follows, in order to keep track of the details of the computation and expressions manageable, we separate the expression for the diagram in figure 4.4 in equation (4.33) into the three parts labelled I, II, and III in (4.32).

We begin with part I which is defined by

$$\langle g^K(k)|\mathcal{T}_{\gamma f}^{a,1g}(n_+ q)|q(p)_e\rangle_{\text{fig}4.4}^{\text{part I}} = -(2\pi)ig_s^3\left(C_F - \frac{1}{2}C_A\right)\mathbf{T}_{fe}^K \int \frac{d^d p_2}{(2\pi)^d}$$

$$\times \frac{1}{(n_+ p_2)} \frac{n_+(p - p_2)}{(p - p_2)^2} \frac{1}{p_2^2} \left(-k_\sigma g_{\delta\nu} + k_\delta g_{\sigma\nu} \right) \epsilon^{*\nu}(k)$$

$$\times n_- \cdot \frac{\partial}{\partial p_1} \left(\delta(n_+ q - n_+ p_1 - n_+ p_2) \frac{n_+ p_1}{p_1^2} \right) n_+^\sigma n_-^\delta u_{c,\gamma}(p) \} \Bigg|_{p_1 = p - p_2 - k_+}. \qquad (4.34)$$

We apply the product rule and simplify the expression. In the case of the derivative $n_- \cdot \frac{\partial}{\partial p_1}$ acting on the propagator we use the following

$$n_- \cdot \frac{\partial}{\partial p_1} \frac{(n_+ p_1)}{p_1^2} = \frac{2}{p_1^2} - \frac{2(n_+ p_1)(n_- p_1)}{p_1^4}$$

$$\overset{p_1 = p - p_2 - k_+}{=} \frac{2}{(p - k_+ - p_2)^2} + \frac{2(n_+(p - p_2))(n_-(k + p_2))}{(p - k_+ - p_2)^4}, \qquad (4.35)$$

where in the second line we have imposed momentum conservation at the power-suppressed vertex $p_1 = p - p_2 - k_+$, and (4.34) becomes

$$\langle g^K(k)|\mathcal{T}_{\gamma f}^{a,1g}(n_+ q)|q(p)_e\rangle_{\text{fig}4.4}^{\text{part I}} = 2(2\pi)ig_s^3\left(C_F - \frac{1}{2}C_A\right)\mathbf{T}_{fe}^K\left((n_+ k)n_{-\nu} - (n_- k)n_{+\nu}\right)$$

$$\times \int \frac{d^d p_2}{(2\pi)^d} \left(\frac{(n_+(p - p_2))}{(n_+ p_2)} \right) \frac{1}{(p - p_2)^2} \frac{1}{p_2^2} \left\{ -\frac{(n_+(p - p_2))}{(p - k_+ - p_2)^2} \frac{\partial}{\partial n_+ q} \delta(n_+ q - n_+ p) \right.$$

$$\left. +\delta(n_+ q - n_+ p)\left[\frac{1}{(p - k_+ - p_2)^2} + \frac{(n_+(p - p_2))(n_-(k + p_2))}{(p - k_+ - p_2)^4} \right] \right\} u_{c,\gamma}(p)\, \epsilon^{*\nu}(k). \quad (4.36)$$

As expected, two types of terms appear in this expression. One piece which is proportional to the derivative of the $\delta(n_+ q - n_+ p)$ delta function, and another proportional to the $\delta(n_+ q - n_+ p)$ delta function itself. Moreover, we note that because of the momentum derivative $n_- \cdot \frac{\partial}{\partial p_1}$ acting on the internal propagators of the diagram, we now encounter terms with double propagators $\sim 1/(p - k_+ - p_2)^4$.

It now remains to carry out the integration over loop momentum in this contribution to the diagram. We perform one of the necessary integrals in detail as an example. All

the rest of the integrals that we need were performed using the same techniques and are listed in appendix A.5.

The integral which we consider here as an example is

$$A(p,k) = g_s^2 \int \frac{d^d p_2}{(2\pi)^d} \frac{1}{(p - k_+ - p_2)^2} \frac{1}{(p - p_2)^2} \frac{1}{p_2^2} \frac{1}{(n_+ p_2)}. \tag{4.37}$$

We perform the integral over the loop momentum using contour integral methods. For this purpose we expand the propagators, restore the $i\delta$ prescription, and for conciseness use component notation where $p_- = n_+ p$ and $k_+ = n_- k$. Note that this should not be confused with the vector $k_+^\mu = (n_- k) n_+^\mu / 2$ which appears in the first propagator of (4.37). We have

$$\begin{aligned} A(p,k) &= g_s^2 \frac{1}{2} \int dp_{2+} dp_{2-} \frac{d^{d-2} p_{2\perp}}{(2\pi)^d} \frac{1}{p_{2-}} \left(p_{2-} p_{2+} + p_{2\perp}^2 + p_{2-} k_+ - p_{2+} p_- - p_- k_+ + i\delta \right)^{-1} \\ &\quad \times \left(p_{2-} p_{2+} + p_{2\perp}^2 - p_- p_{2+} + i\delta \right)^{-1} \left(p_{2-} p_{2+} + p_{2\perp}^2 + i\delta \right)^{-1}, \end{aligned} \tag{4.38}$$

where we have also rewritten the integral measure in component form

$$\int \frac{d^d p_2}{(2\pi)^d} = \frac{1}{2} \int dp_{2+} dp_{2-} \frac{d^{d-2} p_{2\perp}}{(2\pi)^d}. \tag{4.39}$$

We first make use of the Residue theorem to integrate over the p_{2+} component. For this purpose we rearrange the integrand in the following way

$$\begin{aligned} A(p,k) &= g_s^2 \frac{1}{2} \int dp_{2+} dp_{2-} \frac{d^{d-2} p_{2\perp}}{(2\pi)^d} \frac{1}{(p_{2-} - p_-)^2} \left(p_{2+} + \frac{p_{2\perp}^2}{(p_{2-} - p_-)} + \frac{i\delta}{(p_{2-} - p_-)} \right)^{-1} \\ &\quad \times \left(p_{2+} + \frac{p_{2\perp}^2}{(p_{2-} - p_-)} + \frac{p_{2-} k_+}{(p_{2-} - p_-)} - \frac{p_- k_+}{(p_{2-} - p_-)} + \frac{i\delta}{(p_{2-} - p_-)} \right)^{-1} \\ &\quad \times \frac{1}{(p_{2-})^2} \left(p_{2+} + \frac{p_{2\perp}^2}{p_{2-}} + \frac{i\delta}{p_{2-}} \right)^{-1}. \end{aligned} \tag{4.40}$$

We now analyse the range of integration over the component p_{2-}. There are three separate cases to consider. First, we look at the region where $p_{2-} < 0$. In this case all of the poles are above the real p_{2+} axis. Therefore, we can close the contour in the lower half plane which yields zero. Second, we consider the region where $p_{2-} > p_-$. Here, similarly to above, all three poles are below the real p_{2+} axis. Hence, closing the contour in the upper half plane again gives zero for the integral. Third, we consider the case where $0 < p_{2-} < p_-$. This is the only contributing region since the poles now appear above and below the real p_{2+} axis. We choose to close the contour in the lower half plane. This gives an additional minus sign due to the clockwise path. After some minor simplifications and rearrangements the integral in (4.40) becomes

$$A(p,k) = g_s^2 \frac{(-2\pi i)}{(2\pi)^2} \frac{1}{2} \int_0^{p_-} dp_{2-} \int \frac{d^{d-2} p_{2\perp}}{(2\pi)^{d-2}} \frac{1}{(p_-)^2} \left(p_{2\perp}^2 \right)^{-1} \left(p_{2\perp}^2 + \frac{p_{2-} k_+ (p_{2-} - p_-)}{p_-} \right)^{-1}. \tag{4.41}$$

Next, we make use of the fact that there is no dependence on angles between $\perp$ vectors in the above integral. Therefore, we can perform all the angular integrals in the $\perp$-plane immediately. This amounts to using the following d-dimensional result

$$\int \frac{d^{d-2}p_{2\perp}}{(2\pi)^{d-2}} = \frac{2\pi^{(d-2)/2}}{\Gamma[(d-2)/2]} \int_0^\infty \frac{dp_{2T}\, p_{2T}^{d-3}}{(2\pi)^{d-2}} \,. \tag{4.42}$$

Substitution of this result into the integral in (4.41) yields

$$
\begin{aligned}
A(p,k) &= g_s^2 \frac{(-i)}{4\pi} \int_0^{p_-} dp_{2-} \frac{2\pi^{(d-2)/2}}{\Gamma[(d-2)/2]} \int_0^\infty \frac{dp_{2T}\, p_{2T}^{d-3}}{(2\pi)^{d-2}} \left(-p_{2T}^2\right)^{-1} \\
&\quad \times \left(-p_{2T}^2 + \frac{k_+ p_{2-}(p_{2-} - p_-)}{p_-}\right)^{-1} \frac{1}{(p_-)^2}\,,
\end{aligned}
\tag{4.43}
$$

where we have also switched to the three vector notation $p_{2\perp}^2 = -p_{2T}^2$. We next simplify the integrand and change the radial integration measure to $dp_{2T} = dp_{2T}^2/2p_{2T}$. Also defining $M^2 = k_+ p_{2-}(p_- - p_{2-})/p_-$ allows us to write (4.43) in the following way

$$A(p,k) = g_s^2 \frac{(-i)}{4\pi} \int_0^{p_-} dp_{2-} \frac{(p_-)^{-2}}{\Gamma[(d-2)/2]} \int_0^\infty \frac{dp_{2T}^2 \left[p_{2T}^2\right]^{(d-6)/2}}{(4\pi)^{(d-2)/2}} \left(1 + \frac{p_{2T}^2}{M^2}\right)^{-1} M^{-2}. \tag{4.44}$$

In the next step, we rescale the transverse integration variable $p_{2T}^2 = p_{2T}^{\prime 2} M^2$, drop the $'$ on the rescaled $p_{2T}^{\prime 2}$, and choose the dimension $d = 4 - 2\epsilon$

$$A(p,k) = -g_s^2 \frac{i}{4\pi} \int_0^{p_-} dp_{2-} \frac{(p_-)^{-2}}{\Gamma[1-\epsilon]} \int_0^\infty \frac{dp_{2T}^2 \left[p_{2T}^2\right]^{-1-\epsilon}}{(4\pi)^{(1-\epsilon)}} \left(1 + p_{2T}^2\right)^{-1} M^{-2-2\epsilon}\,. \tag{4.45}$$

For the integration over the transverse component dp_{2T}^2 we use the integral representation of the Beta function, $B(-\epsilon, 1+\epsilon)$, given in equation (A.3). We also render the coupling dimensionless and arrive at

$$A(p,k) = -\frac{i\alpha_s\, e^{\epsilon\gamma_E}}{4\pi} \left[\frac{1}{\mu^2}\right]^{-\epsilon} \int_0^{p_-} dq_- \frac{(p_-)^{-2}}{\Gamma[1-\epsilon]} \frac{\Gamma[1+\epsilon]\Gamma[-\epsilon]}{\Gamma[1]} M^{-2-2\epsilon}\,. \tag{4.46}$$

Using the expression for M^2, $M^2 = k_+ p_{2-}(p_- - p_{2-})/p_-$, and rescaling $p_{2-} = p_{2-}'p_-$ after which we drop the $'$ on p_{2-}', the expression for the integral in (4.46) becomes

$$A(p,k) = -\frac{i\alpha_s e^{\epsilon\gamma_E}}{4\pi} \left[\frac{p_- k_+}{\mu^2}\right]^{-\epsilon} \frac{1}{(n_- k)} \int_0^1 dp_{2-} \frac{\Gamma[1+\epsilon]\Gamma[-\epsilon]}{\Gamma[1-\epsilon]} \left(1 - p_{2-}\right)^{-1-\epsilon} \frac{(p_{2-})^{-1-\epsilon}}{(p_-)^2}\,. \tag{4.47}$$

In the last step, we identify the Beta function $B(-\epsilon, -\epsilon)$ using the integral representation in (A.2). After some simplification we arrive at

$$A(p,k) = \frac{i\alpha_s e^{\epsilon\gamma_E}}{4\pi} \left[\frac{(n_+ p)(n_- k)}{\mu^2}\right]^{-\epsilon} \frac{1}{(n_+ p)^2(n_- k)} \Gamma[\epsilon] \frac{\Gamma[-\epsilon]^2}{\Gamma[-2\epsilon]} \tag{4.48}$$

In this way we have obtained the result for the needed integral in (4.37), which we write here explicitly and give again in equation (A.74) of appendix A.5 along with the rest of the necessary integrals

$$
g_s^2 \int \frac{d^d p_2}{(2\pi)^d} \frac{1}{(p-k_+-p_2)^2} \frac{1}{(p-p_2)^2} \frac{1}{p_2^2} \frac{1}{(n_+p_2)} = \frac{i\alpha_s}{4\pi} \left[\frac{(n_+p)(n_-k)}{\mu^2} \right]^{-\epsilon} \frac{2(1-2\epsilon)}{(n_-k)(n_+p)^2}
$$
$$
\times \frac{e^{\epsilon\gamma_E}\Gamma[\epsilon]\Gamma[-\epsilon]\Gamma[1-\epsilon]}{\Gamma[2-2\epsilon]} . \qquad (4.49)
$$

In appendix A.5 we provide all the integrals needed for the one-loop collinear functions computation. In particular, the results for integrals that are needed to obtain the final integrated expression for the calculation of the matrix element $\langle g^K(k)|\mathcal{T}_{\gamma f}^{\mathfrak{a},1g}(n_+q)|q(p)_e\rangle_{\text{fig4.4}}^{\text{part I}}$ in (4.36) can be found in (A.69), (A.75), (A.76), (A.77), (A.78), (A.79), (A.80), and (A.81). Making use of all the necessary integral results, the expression in (4.36) for $\langle g^K(k)|\mathcal{T}_{\gamma f}^{\mathfrak{a},1g}(n_+q)|q(p)_e\rangle_{\text{fig4.4}}^{\text{part I}}$ takes the following form

$$
\langle g^K(k)|\mathcal{T}_{\gamma f}^{\mathfrak{a},1g}(n_+q)|q(p)_e\rangle_{\text{fig4.4}}^{\text{part I}} = 2(2\pi)\frac{\alpha_s}{4\pi} g_s \mathbf{T}_{fe}^K \left(C_F - \frac{1}{2}C_A \right) \left[\frac{(n_+p)(n_-k)}{\mu^2} \right]^{-\epsilon}
$$
$$
\times \left(\frac{1}{(n_+p)}\delta(n_+q-n_+p) - \frac{\partial}{\partial n_+q}\delta(n_+q-n_+p)\frac{(1-\epsilon)}{\epsilon^2} \right)
$$
$$
\times \frac{e^{\epsilon\gamma_E}\Gamma[1+\epsilon]\Gamma[1-\epsilon]^2}{\Gamma[2-2\epsilon]} \left(\frac{(n_+k)}{(n_-k)}n_{-\nu} - n_{+\nu} \right) u_{c,\gamma}(p)\epsilon^{*\nu}(k). \quad (4.50)
$$

This result is valid to all orders in ϵ and we have not made use of on-shell, $k^2 = 0$, or transversality conditions, $k \cdot \epsilon^*(k) = 0$. We now continue, and in the same manner obtain results for part II and part III of the expression in (4.33). Part II is defined as

$$
\langle g^K(k)|\mathcal{T}_{\gamma f}^{\mathfrak{a},1g}(n_+q)|q(p)_e\rangle_{\text{fig4.4}}^{\text{part II}} = (2\pi)ig_s^3 \left(C_F - \frac{1}{2}C_A \right) \mathbf{T}_{fe}^K \int \frac{d^d p_2}{(2\pi)^d}
$$
$$
\times \frac{1}{(n_+p_2)} \frac{n_+(p-p_2)}{(p-p_2)^2} \frac{1}{p_2^2} \left(-k_\sigma g_{\delta\nu} + k_\delta g_{\sigma\nu} \right) n_-^\delta \, u_{c,\gamma}(p) \, \epsilon^{*\nu}(k)
$$
$$
\times \left(k_\perp \cdot \frac{\partial}{\partial p_{1\perp}} \right) \frac{\partial}{\partial p_{1\perp\sigma}} \left(\delta(n_+q-n_+p_1-n_+p_2)\frac{n_+p_1}{p_1^2} \right)\Bigg|_{p_1=p-p_2-k_+} . \quad (4.51)
$$

Here the $\perp$ derivatives yield zero when acting on the $\delta(n_+q-n_+p_1-n_+p_2)$ delta function. Hence the result for this part is only proportional to $\delta(n_+q-n_+p)$ and not its derivatives. Taking the derivatives, simplifying the resultant expression, and using integrals in (A.76), (A.77), (A.78) and (A.109) yields the following result

$$
\langle g^K(k)|\mathcal{T}_{\gamma f}^{\mathfrak{a},1g}(n_+q)|q(p)_e\rangle_{\text{fig4.4}}^{\text{part II}} = (2\pi)\frac{\alpha_s}{4\pi} g_s \mathbf{T}_{fe}^K \left(C_F - \frac{1}{2}C_A \right) \left[\frac{(n_+p)(n_-k)}{\mu^2} \right]^{-\epsilon}
$$
$$
\times \frac{1}{(n_+p)}\delta(n_+q-n_+p) \, 2(1+\epsilon)\frac{1}{\epsilon^2}\left(\frac{-1+3\epsilon-\epsilon^2}{(1-\epsilon)} \right)
$$

$$\times \frac{e^{\epsilon\gamma_E}\Gamma[1+\epsilon]\Gamma[1-\epsilon]^2}{\Gamma[2-2\epsilon]}\left(\frac{k_\perp^2 n_{-\nu}}{(n_-k)^2} - \frac{k_{\perp\nu}}{(n_-k)}\right) u_{c,\gamma}(p)\epsilon^{*\nu}(k) \quad (4.52)$$

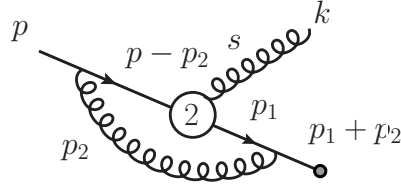Part III of the expression in (4.33) is defined as

$$\langle g^K(k)|\mathcal{T}_{\gamma f}^{\mathfrak{a},1g}(n_+q)|q(p)_e\rangle_{\text{fig4.4}}^{\text{part III}} = -(2\pi)ig_s^3\left(C_F - \frac{1}{2}C_A\right)\mathbf{T}_{fe}^K \int \frac{d^d p_2}{(2\pi)^d}$$

$$\times \frac{1}{(n_+p_2)}\frac{n_+(p-p_2)}{(p-p_2)^2}\frac{1}{p_2^2}\left(-k_\sigma g_{\delta\nu} + k_\delta g_{\sigma\nu}\right)\epsilon^{*\nu}(k)$$

$$\times \frac{\partial}{\partial p_{1\perp\sigma}}\left[\left(\delta(n_+q - n_+p_1 - n_+p_2)\frac{n_+p_1}{p_1^2}\right)\right.$$

$$\left.\times\left(\frac{\slashed{p}_{1\perp}}{n_+p_1}\gamma_\perp^\delta - \gamma_\perp^\delta\frac{\slashed{p}_{2\perp}}{n_+(p-p_2)}\right)_{\gamma\beta}\right]u_{c,\beta}(p)\Bigg|_{p_1=p-p_2-k_+} . \quad (4.53)$$

As in the calculation of parts I and II, we take the derivative with respect to the p_1 momentum, simplify the expression, and this time use results for integrals given in (A.74) and (A.69) upon which we arrive at the following result

$$\langle g^K(k)|\mathcal{T}_{\gamma f}^{\mathfrak{a},1g}(n_+q)|q(p)_e\rangle_{\text{fig4.4}}^{\text{part III}} = (2\pi)\frac{\alpha_s}{4\pi}g_s\mathbf{T}_{fe}^K\left(C_F - \frac{1}{2}C_A\right)\left[\frac{(n_+p)(n_-k)}{\mu^2}\right]^{-\epsilon}$$

$$\times\frac{1}{(n_+p)}\delta(n_+q - n_+p)\frac{1}{\epsilon^2}(1-2\epsilon)$$

$$\times\frac{e^{\epsilon\gamma_E}\Gamma[1+\epsilon]\Gamma[1-\epsilon]^2}{\Gamma[2-2\epsilon]}\frac{\left[\slashed{k}_\perp,\gamma_{\perp\nu}\right]_{\gamma\beta}}{(n_-k)}u_{c,\beta}(p)\epsilon^{*\nu}(k) . \quad (4.54)$$

We now collect the results for the three parts, I, II, and III, which make up the expression in (4.33) for the diagram in figure 4.4. The final expressions, given in (4.50), (4.52), and (4.54) respectively, are valid to all orders in ϵ. Upon putting the results together, we expand in ϵ for illustrative purposes

$$\langle g^K(k)|\mathcal{T}_{\gamma f}^{1g}(n_+q)|q(p)_e\rangle_{\text{fig4.4}} = (2\pi)\frac{g_s\alpha_s}{4\pi}\left(C_F - \frac{1}{2}C_A\right)\frac{\mathbf{T}_{fe}^K}{(n_+p)}\left[\frac{(n_+p)(n_-k)}{\mu^2}\right]^{-\epsilon}$$

$$\times\left\{\delta(n_+q - n_+p)\left[2\delta_{\gamma\beta}\left(\frac{(n_+k)}{(n_-k)}n_-^\nu - n_+^\nu\right)\right.\right.$$

$$+ \delta_{\gamma\beta}\left(\frac{k_\perp^2 n_-^\nu}{(n_-k)^2} - \frac{k_\perp^\nu}{(n_-k)}\right)\left(-\frac{2}{\epsilon^2} - \frac{2}{\epsilon} + 2 + \frac{\pi^2}{6}\right)$$

$$+ \frac{\left[\gamma_\perp^\nu,\slashed{k}_\perp\right]_{\gamma\beta}}{(n_-k)}\left(-\frac{1}{\epsilon^2} + \frac{\pi^2}{12}\right) + \mathcal{O}(\epsilon)\Bigg]$$

$$+ (n_+p)\frac{\partial}{\partial n_+q}\delta(n_+q - n_+p)\delta_{\gamma\beta}\left(\frac{(n_+k)}{(n_-k)}n_-^\nu - n_+^\nu\right)$$

$$\left.\times\left(-\frac{2}{\epsilon^2} - \frac{2}{\epsilon} - 4 + \frac{\pi^2}{6} + \mathcal{O}(\epsilon)\right)\right\}u_{c,\beta}(p)\epsilon_\nu^*(k) . \quad (4.55)$$

Figure 4.5: *Similar to figure 4.4 but now the collinear loop does not end at the field from the hard current Wilson line, but rather attached to the collinear quark before.*

We stress that in obtaining (4.55), the transversality $k \cdot \epsilon^*(k) = 0$ and on-shell $k^2 = 0$ conditions for the emitted gluon have not been used. We point out the presence of $1/\epsilon^2$ poles in the final result for this individual diagram. We discuss the implications of the appearance $1/\epsilon^2$ poles in the collinear functions in greater detail in section 8. Here, it suffices to note that the double ϵ poles in the collinear function would produce leading (double) logarithmic contributions from the collinear functions to the cross-section, and as we see in equation (4.55), $1/\epsilon^2$ poles do appear and multiply a number of terms in a NLP diagram.

Results

Without further details of the computations, we now give the results for the remaining diagrams in figure 4.3. The results are separated in a similar manner to the above example, according to the subleading-power Lagrangian insertion which produces the power suppression in each contribution to the diagram. In order to keep the expressions as concise as possible, we define the following renormalization scale dependent loop factor

$$\mathfrak{K}[\mu] = \left[\frac{(n_+ p)(n_- k)}{\mu^2} \right]^{-\epsilon}, \tag{4.56}$$

and the ϵ dependent factor containing Γ functions which we have defined in the context of leading power amplitude calculation in (3.21). We state it here again for convenience

$$\mathfrak{f}[\epsilon] = \frac{e^{\epsilon \gamma_E} \Gamma[1+\epsilon] \Gamma[1-\epsilon]^2}{\Gamma[2-2\epsilon]}. \tag{4.57}$$

We begin with the results for the second diagram in the top line of figure 4.3. We draw this diagram again with labelled momenta in figure 4.5. The results for parts I, II, and III associated with $\mathcal{L}_{1\xi}^{(2)}$, $\mathcal{L}_{2\xi}^{(2)}$, and $\mathcal{L}_{4\xi}^{(2)}$ Lagrangian insertions respectively are as follows

$$
\begin{aligned}
\langle g^K(k) | \mathcal{T}_{\gamma f}^{a,1g}(n_+ q) | q(p)_e \rangle_{\text{fig4.5}}^{\text{part I}} &= (2\pi) \frac{\alpha_s}{4\pi} g_s \mathbf{T}_{fe}^K \left(C_F - \frac{1}{2} C_A \right) \mathfrak{K}[\mu] \mathfrak{f}[\epsilon] \\
&\times \left(\frac{1}{(n_+ p)} \delta(n_+ q - n_+ p) \frac{1}{\epsilon} \left(-1 + 2\epsilon - \epsilon^2 \right) + \frac{\partial}{\partial n_+ q} \delta(n_+ q - n_+ p) \frac{1}{\epsilon} (1 - \epsilon) \right) \\
&\times \left(\frac{(n_+ k)}{(n_- k)} n_{-\nu} - n_{+\nu} \right) u_{c,\gamma}(p) \epsilon^{*\nu}(k)
\end{aligned}
\tag{4.58}
$$
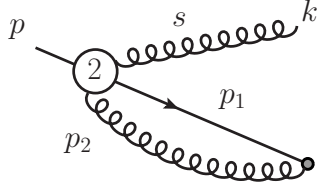
Figure 4.6: *Diagram corresponding to equation (4.61).*
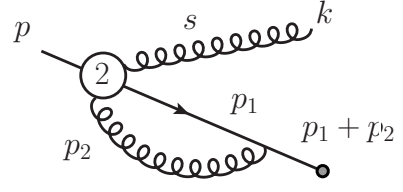
Figure 4.7: *Diagram corresponding to equation (4.62).*

for part I,

$$\langle g^K(k)|\mathcal{T}_{\gamma f}^{\mathfrak{a},1g}(n_+q)|q(p)_e\rangle_{\text{fig4.5}}^{\text{part II}} = -(2\pi)\frac{\alpha_s}{4\pi}g_s\mathbf{T}_{fe}^K\left(C_F - \frac{1}{2}C_A\right)\mathfrak{K}[\mu]\mathfrak{f}[\epsilon]$$

$$\times\frac{1}{(n_+p)}\delta(n_+q - n_+p)\frac{1}{\epsilon}(3 - \epsilon + \epsilon^2)\left(\frac{k_\perp^2}{(n_-k)^2}n_{-\nu} - \frac{k_{\perp\nu}}{(n_-k)}\right)u_{c,\gamma}(p)\epsilon^{*\nu}(k) \quad (4.59)$$

for part II, and for part III we have

$$\langle g^K(k)|\mathcal{T}_{\gamma f}^{\mathfrak{a},1g}(n_+q)|q(p)_e\rangle_{\text{fig4.5}}^{\text{part III}} = (2\pi)\frac{\alpha_s}{4\pi}g_s\mathbf{T}_{fe}^K\left(C_F - \frac{1}{2}C_A\right)\mathfrak{K}[\mu]\mathfrak{f}[\epsilon]$$

$$\times\frac{1}{(n_+p)}\delta(n_+q - n_+p)\frac{(3 + 2\epsilon)}{2\epsilon}\frac{\left[\slashed{k}_\perp, \gamma_{\perp\nu}\right]_{\gamma\beta}}{(n_-k)}u_{c,\beta}(p)\epsilon^{*\nu}(k). \quad (4.60)$$

Next, we consider the third diagram in the first row of figure 4.3. We draw the diagram with labelled momenta in figure 4.6. This contribution is identically zero, because the contraction of the terms in the Feynman rules directly with a collinear gluon originating from the Wilson line in the hard current vanishes. Hence,
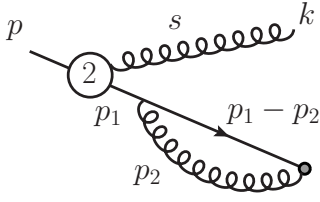
$$\langle g^K(k)|\mathcal{T}_{\gamma f}^{\mathfrak{a},1g}(n_+q)|q(p)_e\rangle_{\text{fig4.6}} = 0. \quad (4.61)$$

A contribution which does not vanish is one originating from the first diagram in the second row of figure 4.3. It is depicted once more in figure 4.7 with labelled momenta. The contribution to part I is given by
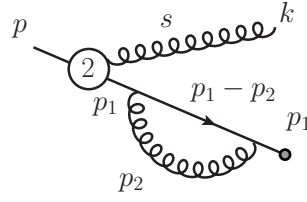
$$\langle g^K(k)|\mathcal{T}_{\gamma f}^{\mathfrak{a},1g}(n_+q)|q(p)_e\rangle_{\text{fig4.7}}^{\text{part I}} = (2\pi)\frac{\alpha_s}{4\pi}g_s\mathbf{T}_{fe}^K C_A\mathfrak{K}[\mu]\mathfrak{f}[\epsilon]$$

$$\times\left(\frac{1}{(n_+p)}\delta(n_+q - n_+p)\frac{1}{\epsilon}(1 - \epsilon) + \frac{\partial}{\partial n_+q}\delta(n_+q - n_+p)\frac{1}{\epsilon^2}(1 - \epsilon)\right)$$

$$\times\left(\frac{(n_+k)}{(n_-k)}n_{-\nu} - n_{+\nu}\right)u_{c,\gamma}(p)\epsilon^{*\nu}(k). \quad (4.62)$$

This result is very similar to result for $\langle g^K(k)|\mathcal{T}_{\gamma f}^{\mathfrak{a},1g}(n_+q)|q(p)_e\rangle_{\text{fig4.8}}^{\text{part I}}$ in equation (4.65). In fact, it is related by the replacement $C_F \to C_A/2$. For Part II of the same diagram we find the following

$$\langle g^K(k)|\mathcal{T}_{\gamma f}^{\mathfrak{a},1g}(n_+q)|q(p)_e\rangle_{\text{fig4.7}}^{\text{part II}} = (2\pi)\frac{\alpha_s}{4\pi}g_s\mathbf{T}_{fe}^K C_A\mathfrak{K}[\mu]\mathfrak{f}[\epsilon]$$

Figure 4.8: *Diagram corresponding to equation (4.65).*

Figure 4.9: *Diagram corresponding to equations (4.68), (4.69).*

$$\times \frac{1}{(n_+p)} \delta(n_+q - n_+p) \frac{1}{\epsilon^2} (1 - \epsilon^2) \left(\frac{k_\perp^2}{(n_-k)^2} n_{-\nu} - \frac{k_{\perp\nu}}{(n_-k)} \right) u_{c,\gamma}(p) \epsilon^{*\nu}(k) . \quad (4.63)$$

We note that this result is very similar to $\langle g^K(k)|\mathcal{T}_{\gamma f}^{\mathfrak{a},1g}(n_+q)|q(p)_e\rangle_{\text{fig4.8}}^{\text{part II}}$ in equation (4.66). Indeed, the only adjustment we are required to make is the replacement $C_F \to C_A/2$. Next, we consider Part III

$$\langle g^K(k)|\mathcal{T}_{\gamma f}^{\mathfrak{a},1g}(n_+q)|q(p)_e\rangle_{\text{fig4.7}}^{\text{part III}} = (2\pi)\frac{\alpha_s}{4\pi} g_s \mathbf{T}_{fe}^K \mathfrak{K}[\mu]\mathfrak{f}[\epsilon] \frac{1}{(n_+p)} \delta(n_+q - n_+p)$$

$$\times \left(-\frac{1}{\epsilon} C_F - \frac{1}{2\epsilon^2} (1 - 2\epsilon) C_A \right) \frac{\left[\slashed{k}_\perp, \gamma_{\perp\nu} \right]_{\gamma\beta}}{(n_-k)} u_{c,\beta}(p) \epsilon^{*\nu}(k) . \quad (4.64)$$

We next focus on the diagram in figure 4.8. Part I is given by

$$\langle g^K(k)|\mathcal{T}_{\gamma f}^{\mathfrak{a},1g}(n_+q)|q(p)_e\rangle_{\text{fig4.8}}^{\text{part I}} = (2\pi)\frac{\alpha_s}{4\pi} g_s \mathbf{T}_{fe}^K C_F \mathfrak{K}[\mu]\mathfrak{f}[\epsilon]$$

$$\times \left(\frac{1}{(n_+p)} \delta(n_+q - n_+p) \frac{2(1 - \epsilon)}{\epsilon} + \frac{\partial}{\partial n_+q} \delta(n_+q - n_+p) \frac{2(1 - \epsilon)}{\epsilon^2} \right)$$

$$\times \left(\frac{(n_+k)}{(n_-k)} n_{-\nu} - n_{+\nu} \right) u_{c,\gamma}(p) \epsilon^{*\nu}(k) . \quad (4.65)$$

Part II takes the following form

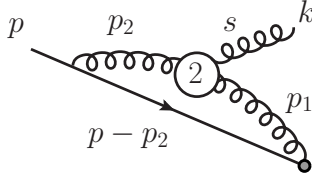$$\langle g^K(k)|\mathcal{T}_{\gamma f}^{\mathfrak{a},1g}(n_+q)|q(p)_e\rangle_{\text{fig4.8}}^{\text{part II}} = (2\pi)\frac{\alpha_s}{4\pi} g_s \mathbf{T}_{fe}^K C_F \mathfrak{K}[\mu]\mathfrak{f}[\epsilon]$$

$$\times \frac{1}{(n_+p)} \delta(n_+q - n_+p) \frac{2(1 - \epsilon^2)}{\epsilon^2} \left(\frac{k_\perp^2}{(n_-k)^2} n_{-\nu} - \frac{k_{\perp\nu}}{(n_-k)} \right) u_{c,\gamma}(p) \epsilon^{*\nu}(k) , \quad (4.66)$$

with part III being

$$\langle g^K(k)|\mathcal{T}_{\gamma f}^{\mathfrak{a},1g}(n_+q)|q(p)_e\rangle_{\text{fig4.8}}^{\text{part III}} = -(2\pi)\frac{\alpha_s}{4\pi} g_s \mathbf{T}_{fe}^K C_F \mathfrak{K}[\mu]\mathfrak{f}[\epsilon]$$

$$\times \frac{1}{(n_+p)} \delta(n_+q - n_+p) \frac{(1 - \epsilon)}{\epsilon^2} \frac{\left[\slashed{k}_\perp, \gamma_{\perp\nu} \right]_{\gamma\beta}}{(n_-k)} u_{c,\beta}(p) \epsilon^{*\nu}(k) . \quad (4.67)$$

We now give the results for the diagram in figure 4.9. Part I is given by

$$\langle g^K(k)|\mathcal{T}_{\gamma f}^{\mathfrak{a},1g}(n_+q)|q(p)_e\rangle_{\text{fig4.9}}^{\text{part I}} = -(2\pi)\frac{\alpha_s}{4\pi} g_s \mathbf{T}_{fe}^K C_F \mathfrak{K}[\mu]\mathfrak{f}[\epsilon]$$

Figure 4.10: *Diagram corresponding to equation (4.71).*

Figure 4.11: *Diagram corresponding to equation (4.72).*

$$\times \left(\frac{1}{(n_+p)}\delta(n_+q - n_+p)(1 - \epsilon) + \frac{\partial}{\partial n_+q}\delta(n_+q - n_+p)\frac{(1-\epsilon)}{\epsilon} \right)$$

$$\times \left(\frac{(n_+k)}{(n_-k)}n_{-\nu} - n_{+\nu} \right) u_{c,\gamma}(p)\epsilon^{*\nu}(k). \tag{4.68}$$
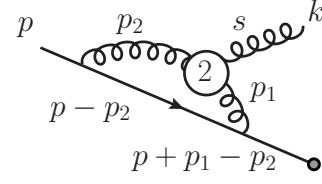
Part II takes the form

$$\langle g^K(k)|\mathcal{T}_{\gamma f}^{\mathfrak{a},1g}(n_+q)|q(p)_e\rangle_{\text{fig4.9}}^{\text{part II}} = -(2\pi)\frac{\alpha_s}{4\pi}g_s\mathbf{T}_{fe}^K C_F \mathfrak{K}[\mu]\mathfrak{f}[\epsilon]$$

$$\times \frac{1}{(n_+p)}\delta(n_+q - n_+p)\frac{(1-\epsilon^2)}{\epsilon}\left(\frac{k_\perp^2}{(n_-k)^2}n_{-\nu} - \frac{k_{\perp\nu}}{(n_-k)} \right) u_{c,\gamma}(p)\epsilon^{*\nu}(k), \tag{4.69}$$

and lastly we write part III

$$\langle g^K(k)|\mathcal{T}_{\gamma f}^{\mathfrak{a},1g}(n_+q)|q(p)_e\rangle_{\text{fig4.9}}^{\text{part III}} = (2\pi)\frac{\alpha_s}{4\pi}g_s\mathbf{T}_{fe}^K C_F \mathfrak{K}[\mu]\mathfrak{f}[\epsilon]$$

$$\times \frac{1}{(n_+p)}\delta(n_+q - n_+p)\frac{(1-\epsilon)}{2\epsilon}\frac{\left[\slashed{k}_\perp, \gamma_{\perp\nu}\right]_{\gamma\beta}}{(n_-k)}u_{c,\beta}(p)\epsilon^{*\nu}(k). \tag{4.70}$$

Comparing the results in equations (4.65), (4.66), and (4.67) to (4.68), (4.69), and (4.70) we note that at one-loop accuracy the contribution to the $\langle g^K(k)|\mathcal{T}_{\gamma f}^{\mathfrak{a},1g}(n_+q)|q(p)_e\rangle_{\text{fig4.8}}$ matrix element is proportional to $\langle g^K(k)|\mathcal{T}_{\gamma f}^{\mathfrak{a},1g}(n_+q)|q(p)_e\rangle_{\text{fig4.9}}$. Namely, we see that $\langle g^K(k)|\mathcal{T}_{\gamma f}^{\mathfrak{a},1g}(n_+q)|q(p)_e\rangle_{\text{fig4.8}} = (-2/\epsilon)\langle g^K(k)|\mathcal{T}_{\gamma f}^{\mathfrak{a},1g}(n_+q)|q(p)_e\rangle_{\text{fig4.9}}$.

We carry on and consider the leftmost diagram in the last row of figure 4.3 which yields a vanishing contribution.

The last two diagrams left to consider are the second and third diagrams in the third row of figure 4.3. As for the diagrams with a power-suppressed quark-gluon interaction considered above, we present the results for the diagrams with a power-suppressed three-gluon interaction according to the Feynman rule used in the computation of each piece. These Feynman rules can be traced back to particular power-suppressed Lagrangian terms in (2.69) as we discussed in section 2.4.2.

We now focus on the second diagram in the last row of figure 4.3. This is drawn again with labelled momenta in figure 4.10. The contribution due to the first term in the $\mathcal{O}(\lambda^2)$ Feynman rule in (2.92) vanishes

$$\langle g^K(k)|\mathcal{T}_{\gamma f}^{\mathfrak{a},1g}(n_+q)|q(p)_e\rangle_{\text{fig4.10}}^{\text{term 1}} = 0. \tag{4.71}$$

The $V_{\mu\nu\rho}^{(2),2+3}(k,q,p)$ piece in equation 2.98 gives a non-zero contribution

$$\langle g^K(k)|\mathcal{T}_{\gamma f}^{\mathfrak{a},1g}(n_+q)|q(p)_e\rangle_{\text{fig4.10}}^{\text{term 2+3}} = (2\pi)\frac{\alpha_s}{4\pi}g_s\mathbf{T}_{fe}^K C_A \mathfrak{K}[\mu]\mathfrak{f}[\epsilon]$$

$$\times \frac{1}{(n_+p)}\delta(n_+q - n_+p)\frac{1}{4\epsilon}\frac{\left[\slashed{k}_\perp,\gamma_{\perp\nu}\right]_{\gamma\beta}}{(n_-k)}u_{c,\beta}(p)\epsilon^{*\nu}(k). \quad (4.72)$$

The rest of the contributions, due to $V_{\mu\nu\rho}^{(2),4}(k,q,p)$, $V_{\mu\nu\rho}^{(2),5}(k,q,p)$, and $V_{\mu\nu\rho}^{(2),6}(k,q,p)$ in (2.98), all vanish

$$\langle g^K(k)|\mathcal{T}_{\gamma f}^{\mathfrak{a},1g}(n_+q)|q(p)_e\rangle_{\text{fig4.10}}^{\text{term 4}} = 0, \quad (4.73)$$

$$\langle g^K(k)|\mathcal{T}_{\gamma f}^{\mathfrak{a},1g}(n_+q)|q(p)_e\rangle_{\text{fig4.10}}^{\text{term 5}} = 0, \quad (4.74)$$

$$\langle g^K(k)|\mathcal{T}_{\gamma f}^{\mathfrak{a},1g}(n_+q)|q(p)_e\rangle_{\text{fig4.10}}^{\text{term 6}} = 0. \quad (4.75)$$

The final diagram left to consider is the third one in the last row of figure 4.3. It is presented again in figure 4.11 with labelled momenta. The results are again divided according to the terms in (2.92). The first term we split into two parts according to the soft structure and we find

$$\langle g^K(k)|\mathcal{T}_{\gamma f}^{\mathfrak{a},1g}(n_+q)|q(p)_e\rangle_{\text{fig4.11}}^{\text{term 1 part I}} = (2\pi)\frac{\alpha_s}{4\pi}g_s\mathbf{T}_{fe}^K C_A \mathfrak{K}[\mu]\mathfrak{f}[\epsilon]$$

$$\times \left(\frac{1}{(n_+p)}\delta(n_+q - n_+p)\frac{(2-\epsilon)}{2\epsilon(1+\epsilon)}(1-\epsilon)^2 + \frac{\partial}{\partial n_+q}\delta(n_+q - n_+p)\left(-\frac{2}{\epsilon^2} + \frac{5}{2\epsilon} - \frac{1}{2}\right)\right)$$

$$\times \left(\frac{(n_+k)}{(n_-k)}n_{-\nu} - n_{+\nu}\right)u_{c,\gamma}(p)\epsilon^{*\nu}(k) \quad (4.76)$$

for term 1 part I, and

$$\langle g^K(k)|\mathcal{T}_{\gamma f}^{\mathfrak{a},1g}(n_+q)|q(p)_e\rangle_{\text{fig4.11}}^{\text{term 1 part II}} = (2\pi)\frac{\alpha_s}{4\pi}g_s\mathbf{T}_{fe}^K C_A \mathfrak{K}[\mu]\mathfrak{f}[\epsilon]\frac{1}{(n_+p)}\delta(n_+q - n_+p)\frac{1}{(1+\epsilon)}$$

$$\times \frac{(-1)}{2\epsilon^2}\left(4 - 5\epsilon - 2\epsilon^2 - 4\epsilon^3 + \epsilon^4\right)\left(\frac{k_\perp^2}{(n_-k)}n_{-\nu} - k_{\perp\nu}\right)u_{c,\gamma}(p)\epsilon^{*\nu}(k) \quad (4.77)$$

for term 1 part II. Next, we have the following

$$\langle g^K(k)|\mathcal{T}_{\gamma f}^{\mathfrak{a},1g}(n_+q)|q(p)_e\rangle_{\text{fig4.11}}^{\text{term 2+3}} = (2\pi)\frac{\alpha_s}{4\pi}g_s\mathbf{T}_{fe}^K C_A \mathfrak{K}[\mu]\mathfrak{f}[\epsilon]$$

$$\times \frac{1}{(n_+p)}\delta(n_+q - n_+p)\frac{(-1)}{\epsilon}\frac{\left[\slashed{k}_\perp,\gamma_{\perp\nu}\right]_{\gamma\beta}}{(n_-k)}u_{c,\beta}(p)\epsilon^{*\nu}(k). \quad (4.78)$$

For term 4 we find

$$\langle g^K(k)|\mathcal{T}_{\gamma f}^{\mathfrak{a},1g}(n_+q)|q(p)_e\rangle_{\text{fig4.11}}^{\text{term 4}} = (2\pi)\frac{\alpha_s}{4\pi}g_s\mathbf{T}_{fe}^K C_A \mathfrak{K}[\mu]\mathfrak{f}[\epsilon]$$

$$\times \frac{1}{(n_+p)}\delta(n_+q - n_+p)\frac{(1-\epsilon)(1-2\epsilon)}{2\epsilon^2(1+\epsilon)}\left(\frac{(n_+k)}{(n_-k)}n_{-\nu} - n_{+\nu}\right)u_{c,\gamma}(p)\epsilon^{*\nu}(k). \quad (4.79)$$

Term 5 yields

$$\langle g^K(k)|\mathcal{T}^{\mathfrak{a},1g}_{\gamma f}(n_+q)|q(p)_e\rangle^{\text{term 5}}_{\text{fig4.11}} = (2\pi)\frac{\alpha_s}{4\pi}g_s\mathbf{T}^K_{fe}C_A\mathfrak{K}[\mu]\mathfrak{f}[\epsilon]$$

$$\times \frac{1}{(n_+p)}\delta(n_+q - n_+p)(2-\epsilon)\frac{1}{2\epsilon^2}\frac{[\not{k}_\perp, \gamma_{\perp\nu}]_{\gamma\beta}}{(n_-k)}u_{c,\beta}(p)\epsilon^{*\nu}(k), \tag{4.80}$$

and lastly for term 6 we find

$$\langle g^K(k)|\mathcal{T}^{\mathfrak{a},1g}_{\gamma f}(n_+q)|q(p)_e\rangle^{\text{term 6}}_{\text{fig4.11}} = (2\pi)\frac{\alpha_s}{4\pi}g_s\mathbf{T}^K_{fe}C_A\mathfrak{K}[\mu]\mathfrak{f}[\epsilon]$$

$$\times \frac{1}{(n_+p)}\delta(n_+q - n_+p)(1-\epsilon)\frac{(1-2\epsilon)}{\epsilon^2(1+\epsilon)}\left(\frac{k_\perp^2}{(n_-k)^2}n_{-\nu} - \frac{k_{\perp\nu}}{(n_-k)}\right)u_{c,\gamma}(p)\epsilon^{*\nu}(k). \tag{4.81}$$

This concludes the diagram-by-diagram presentation of the results for one-collinear-loop contributions to the collinear functions connected to soft structures which support a single soft gluon emission. The sum of these diagrams constitutes the one-loop result for the $\langle g^K(k)|\mathcal{T}^{\mathfrak{a},1g}_{\gamma f}(n_+q)|q(p)_e\rangle$ matrix element appearing on left-hand side of the matching equation in (4.5). We denote this quantity by $\langle g^K(k)|\mathcal{T}^{\mathfrak{a},1g}_{\gamma f}(n_+q)|q(p)_e\rangle^{(1)}$. Prior to the use of on-shell $k^2 = 0$ and transversality $k \cdot \epsilon(k) = 0$ conditions for the emitted soft gluon, it is given by

$$\langle g^K(k)|\mathcal{T}^{\mathfrak{a},1g}_{\gamma f}(n_+q)|q(p)_e\rangle^{(1)} = (2\pi)\frac{\alpha_s}{4\pi}g_s\mathbf{T}^K_{fe}\mathfrak{K}[\mu]\mathfrak{f}[\epsilon]\frac{1}{n_+p}\delta(n_+q - n_+p)\Bigg\{$$

$$\left(\frac{(n_+k)}{(n_-k)}n_-^\eta - n_+^\eta\right)\left(C_F\frac{(1+\epsilon)}{\epsilon} - C_A\frac{1}{2\epsilon^2}\frac{(-1-2\epsilon+6\epsilon^2+\epsilon^3)}{(1+\epsilon)}\right)\delta_{\gamma\beta}$$

$$-\left(\frac{k_\perp^\eta}{(n_-k)} - \frac{k_\perp^2}{(n_-k)^2}n_-^\eta\right)\left(C_F\frac{(2-7\epsilon+\epsilon^2)}{\epsilon(-1+\epsilon)} - C_A\frac{(1-3\epsilon^2)}{\epsilon^2(-1+\epsilon)}\right)\delta_{\gamma\beta}$$

$$+\frac{[k_\perp^\mu g_\perp^{\nu\eta} - k_\perp^\nu g_\perp^{\mu\eta}]}{(n_-k)}\frac{1}{2}(C_F - C_A)[\gamma_\perp^\mu\gamma_\perp^\nu]_{\gamma\beta}\Bigg\}\epsilon_\eta^*(k)\,u_{c,\beta}(p). \tag{4.82}$$

We note that remarkably the derivative delta function $\frac{\partial}{\partial n_+q}\delta(n_+q - n_+p)$ vanishes in the sum of all diagrams. Therefore, an $\mathcal{O}(\alpha_s)$ correction of this type is absent in equation (4.82). We also draw attention to the fact that so far, even in the sum of diagrams, the double ϵ poles do not vanish in coefficients of each soft structure. We now apply the on-shell and transversality relations for the emitted gluon which relates the second and third lines of the above equation. The relation is written in equation (4.15). The soft structure in the fourth line is not connected to the second and third lines, and we see that this term does not in fact contain any poles in ϵ. After the application of (4.15) we find

$$\langle g^K(k)|\mathcal{T}^{\mathfrak{a},1g}_{\gamma f}(n_+q)|q(p)_e\rangle^{(1)}$$

$$= 2\pi\frac{g_s\alpha_s}{4\pi}\mathbf{T}^K_{fe}\left[\frac{k_\perp^\eta}{(n_-k)} - \frac{k_\perp^2 n_-^\eta}{(n_-k)^2}\right]\epsilon_\eta^*(k)\,u_{c,\gamma}(p)\frac{\delta(n_+q - n_+p)}{n_+p}\left(\frac{n_-k\,n_+p}{\mu^2}\right)^{-\epsilon}$$

$$\times \left(C_F\left(-\frac{4}{\epsilon} + 3 + 8\epsilon + \epsilon^2\right) - C_A\left(-5 + 8\epsilon + \epsilon^2\right)\right)\frac{e^{\epsilon\gamma_E}\Gamma[1+\epsilon]\Gamma[1-\epsilon]^2}{(-1+\epsilon)(1+\epsilon)\Gamma[2-2\epsilon]}$$

$$+ 2\pi \, \frac{g_s \alpha_s}{4\pi} \, \mathbf{T}^K_{fe} \left[\frac{k^\mu_\perp \epsilon^{*\nu}_\perp(k)}{n_- k} - \frac{k^\nu_\perp \epsilon^{*\mu}_\perp(k)}{n_- k} \right] u_{c,\beta}(p) \, \frac{\delta(n_+ q - n_+ p)}{n_+ p} \left(\frac{n_- k \, n_+ p}{\mu^2} \right)^{-\epsilon}$$

$$\times \left[\gamma^\mu_\perp \gamma^\nu_\perp \right]_{\gamma\beta} (C_F - C_A) \, \frac{e^{\epsilon \gamma_E} \, \Gamma[1 + \epsilon] \Gamma[1 - \epsilon]^2}{2 \, \Gamma[2 - 2\epsilon]} \, . \tag{4.83}$$

We have here written explicitly the factors of $\mathfrak{K}[\mu]$ and $\mathfrak{f}[\epsilon]$ which can be found in equations (4.56) and (4.57) respectively. The result in equation (4.83) is our final expression for the one-loop accurate left-hand side of matching equation (4.5). In other words, $\langle g^K(k) | \mathcal{T}^{\mathfrak{a}, 1g}_{\gamma f}(n_+ q) | q(p)_e \rangle^{(1)}$ is the one-loop extension of the tree-level result given in (4.16). We draw attention to the fact that the expression in equation (4.83), which is the final result *after* application of (4.15), does not contain $1/\epsilon^2$ poles. The coefficient of the C_F term does contain a single pole in ϵ. Moreover, both the double and single poles in the coefficient of the C_A term present in (4.82) cancel, leaving the C_A coefficient in (4.83) finite.

We now compare the one-loop accurate result for the left-hand side of the matching equation, with the right-hand side given in (4.12). With this, we obtain the one-loop corrections to the collinear functions J_1 and J_6. We now first state the d-dimensional results, followed by the expansion of the results in $\epsilon = (4 - d)/2$. We have

$$J^{K\,(1)}_{1,1;\gamma\beta,fe}(n_+ q, n_+ p; \omega) = \frac{\alpha_s}{4\pi} \delta_{\gamma\beta} \mathbf{T}^K_{fe} \frac{1}{(n_+ p)} \left(\frac{n_+ p \, \omega}{\mu^2} \right)^{-\epsilon} \frac{e^{\epsilon \gamma_E} \Gamma[1 + \epsilon] \Gamma[1 - \epsilon]^2}{(-1 + \epsilon)(1 + \epsilon)\Gamma[2 - 2\epsilon]}$$

$$\times \left(C_F \left(-\frac{4}{\epsilon} + 3 + 8\epsilon + \epsilon^2 \right) - C_A \left(-5 + 8\epsilon + \epsilon^2 \right) \right) \delta(n_+ q - n_+ p) \tag{4.84}$$

$$= \frac{\alpha_s}{4\pi} \frac{1}{(n_+ p)} \delta_{\gamma\beta} \mathbf{T}^K_{fe} \left(C_F \left(\frac{4}{\epsilon} + 5 - 4 \ln \left(\frac{n_+ p \, \omega}{\mu^2} \right) \right) - 5 \, C_A \right) \delta(n_+ q - n_+ p)$$

$$+ \mathcal{O}(\epsilon) \, , \tag{4.85}$$

$$J^{K\,(1)}_{1,2;\gamma\beta,fe}(n_+ q, n_+ p; \omega) = 0 \, , \tag{4.86}$$

$$J^{\mu\nu, K\,(1)}_{6;\gamma\beta,fe}(n_+ q, n_+ p; \omega) = \frac{\alpha_s}{4\pi} \frac{1}{(n_+ p)} \left[\gamma^\mu_\perp \gamma^\nu_\perp \right]_{\gamma\beta} \mathbf{T}^K_{fe} \left(\frac{n_+ p \, \omega}{\mu^2} \right)^{-\epsilon}$$

$$\times \frac{e^{\epsilon \gamma_E} \Gamma[1 + \epsilon] \Gamma[1 - \epsilon]^2}{2 \, \Gamma[2 - 2\epsilon]} (C_F - C_A) \, \delta(n_+ q - n_+ p) \tag{4.87}$$

$$= \frac{\alpha_s}{4\pi} \frac{1}{2} \frac{1}{(n_+ p)} \left[\gamma^\mu_\perp \gamma^\nu_\perp \right]_{\gamma\beta} \mathbf{T}^K_{fe} (C_F - C_A) \, \delta(n_+ q - n_+ p) + \mathcal{O}(\epsilon) \, . \tag{4.88}$$

As we have pointed our earlier in the text, the collinear functions $J^{K\,(1)}_{1,2;\gamma\beta,fe}$ and $J^{K\,(1)}_{6;\gamma\beta,fe}$ do not contribute to the Drell-Yan cross-section at next-to-next-to-leading order .

4.2 Gluon-antiquark channel

In this section we follow the steps of the calculation performed in the section above for the collinear functions appearing at tree and one-loop level in the $q\bar{q}$-channel now for the

case of the $g\bar{q}$-channel. The relevant next-to-leading power matching equation is given in (3.109). We introduce the short-hand notation

$$\tilde{\mathcal{T}}_{\gamma f}^{\mathfrak{c}}(t) \equiv i \int d^4 z \, \mathbf{T}\Big[\chi_{c,\gamma f}(tn_+)\,\mathcal{L}^{(1)}(z)\Big], \tag{4.89}$$

for the left-hand side of (3.109). The Fourier transform of this quantity is defined in the following way

$$\mathcal{T}_{\gamma f}^{\mathfrak{c}}(n_+ q) = \int dt \, e^{i(n_+ q)\,t}\,\tilde{\mathcal{T}}_{\gamma f}^{\mathfrak{c}}(t). \tag{4.90}$$

Similarly to the considerations in the $q\bar{q}$-channel, we now also perform the Fourier transform of the right-hand side of the matching equation (3.109), which yields the matching equation in momentum space

$$\begin{aligned}\mathcal{T}_{\gamma f}^{\mathfrak{c}}(n_+ q) &= 2\pi \int \frac{dn_+ p_a}{2\pi} \int du\, e^{i\,(n_+ p_a)\,u} \int \frac{d\omega}{2\pi} \\ &\times G_{\xi q;\gamma\alpha,fa}^{\eta,A}(n_+ q, n_+ p_a;\omega)\,\mathcal{A}_{c\perp\eta}^{\mathrm{PDF}\,A}(un_+) \int dz_-\, e^{-i\omega\,z_-}\,\mathfrak{s}_{\xi q;\alpha,a}(z_-).\end{aligned} \tag{4.91}$$

We now extract the perturbative collinear functions $G_{\xi q;\gamma\alpha,fa}^{\eta,A}(n_+ q, n_+ p_a;\omega)$ by considering suitable partonic matrix elements of the operator matching equation in the same way as in the $q\bar{q}$-channel. Here the relevant matrix element is one with an incoming c-PDF gluon and an outgoing soft quark $\langle q_+(k)|...|g(p)\rangle$. We then proceed to compute both sides of the matching equation with the leading power decoupled Lagrangian. As in the $q\bar{q}$ case, the soft fields are external. Hence, the soft matrix element $\langle q_+(k)|\mathfrak{s}_{\xi q;\alpha,a}(z_-)|0\rangle$ retains its tree-level value. Similarly, for the c-PDF matrix element $\langle 0|\mathcal{A}_{c\perp\eta}^{\mathrm{PDF}\,A}(un_+)|g(p)\rangle$ the loop corrections are scaleless and $\langle 0|\mathcal{A}_{c\perp\eta}^{\mathrm{PDF}\,A}(un_+)|g(p)\rangle$ takes its tree-level value.

   We again use the momentum-space Feynman rules given in appendix A of [87] to carry out the calculation of the left-hand side of the matching equation. However, in comparison to the calculation of the collinear functions relevant for the $q\bar{q}$-channel, the computation performed here is far more straightforward. The reasons are twofold. First, since an emission of a soft quark in a time-ordered product insertion is necessary, there exists only one single soft structure which needs to be considered at next-to-leading power accuracy. Namely the $\mathfrak{s}_{\xi q;\alpha,a}(z_-) = \frac{g_s}{in_-\partial_z}q_{\alpha,a}^+(z_-)$ given in (3.110). Second, the Lagrangian insertion which induces the power suppression, $\mathcal{L}_{\xi q}^{(1)}$ in equation (2.66), does not contain any explicit position variables. This means that, in momentum space, no derivatives on the momentum-conservation delta functions appear at subleading power soft-collinear interaction vertices. This reduces drastically the number of terms one has to compute per diagram and the number of integrals involved in the calculation.

4.2.1 Tree-level collinear function

We begin with the tree-level computation of the collinear function for the $g\bar{q}$-channel. First we consider the right-hand side, so explicitly taking the relevant matrix element of equation (4.91) gives

$$\langle q_b^+(k)|\mathcal{T}_{\gamma f}^{\mathfrak{c}}(n_+ q)|g^B(p)\rangle = 2\pi \int \frac{dn_+ p_a}{2\pi} \int du\, e^{i\,(n_+ p_a)\,u} \int \frac{d\omega}{2\pi} \int dz_-\, e^{-i\omega\,z_-}$$
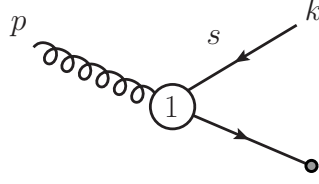
Figure 4.12:   *Tree-level effective field theory diagram in the $g\bar{q}$-channel.*

$$\times G^{\eta,A}_{\xi q;\gamma\alpha,fa}\left(n_+q, n_+p_a; \omega\right)\, \langle 0|\mathcal{A}^{\mathrm{PDF}\,A}_{c\perp\eta}(un_+)|g^B(p)\rangle\, \langle q_b^+(k)|\mathfrak{s}_{\xi q;\alpha,a}(z_-)|0\rangle\,, \quad (4.92)$$

where B is the adjoint colour index and b is the fundamental colour index of the external final state. The c-PDF matrix element in (4.92) is evaluates to the following

$$\langle 0|\mathcal{A}^{\mathrm{PDF}\,A}_{c\perp\eta}(un_+)|g^B(p)\rangle = \delta^{AB}\,\sqrt{Z_{g,\mathrm{PDF}}}\,\epsilon_{\perp\eta}(p)\,e^{-i(n_+p)u}. \quad (4.93)$$

The factor $\sqrt{Z_{g,\mathrm{PDF}}}$ is the on-shell renormalization factor of the c-PDF gluon field. The soft matrix element on the right-hand side of (4.92) becomes

$$\langle q_b^+(k)|\mathfrak{s}_{\xi q;\alpha,a}(z_-)|0\rangle = \langle q_b^+(k)|\frac{g_s}{in_-\partial_z}q^+_{\alpha,a}(z_-)|0\rangle = \delta_{ba}\,\frac{(-g_s)}{(n_-k)}\,v_\alpha(k)\,e^{iz_-k}\,. \quad (4.94)$$

In the second step we have used the form of the soft structure as given in (3.110). Using now the evaluated matrix elements given equations (4.93) and (4.94) in (4.92) yields

$$
\begin{aligned}
\langle q_b^+(k)|\mathcal{T}^{\mathfrak{c}}_{\gamma f}(n_+q)|g^B(p)\rangle &= (2\pi)\frac{(-g_s)}{(n_-k)}\,G^{\eta,B}_{\xi q;\gamma\alpha,fb}\left(n_+q, n_+p; n_-k\right) \\
&\quad \times v_\alpha(k)\,\sqrt{Z_{g,\mathrm{PDF}}}\,\epsilon_{\perp\eta}(p)\,,
\end{aligned}
\quad (4.95)
$$

This result constitutes our final expression for matrix element with the chosen partonic external states of the right-hand side of the matching equation in (4.91). Since the matrix elements in (4.93) and (4.94) have no loop corrections, the expression in (4.95) is valid to all orders in α_s.

Having obtained an expression for the right-hand side of the matching equation, we now compute the $\langle q_b^+(k)|...|g^B(p)\rangle$ matrix element of the left-hand side of (4.91). As discussed above, the only subleading-power Lagrangian term needed in (4.89), which is the left-hand side of (4.91), is the $\mathcal{L}^{(1)}_{\xi q}$ Lagrangian term in (2.66). This term gives rise to the Feynman rule given in equation (A.36) of [87]. Using this Feynman rule in computation of the tree-level diagram in figure 4.12 yields the following result

$$
\begin{aligned}
\langle q_b^+(k)|\mathcal{T}^{\mathfrak{c}}_{\gamma f}(n_+q)|g^B(p)\rangle &= (2\pi)\delta(n_+q - n_+p)\frac{1}{(n_-k)}\,g_s\mathbf{T}^B_{fb} \\
&\quad \times \left(\frac{\slashed{n}_-}{2}\gamma_{\perp\eta}\right)_{\gamma\alpha}v_\alpha(k)\sqrt{Z_{g,c}}|_{\mathrm{tree}}\epsilon^\eta_\perp(p) + \mathcal{O}(\alpha_s). \quad (4.96)
\end{aligned}
$$

The tree-level value of the on-shell wave function renormalization factor of the gluon field is $\sqrt{Z_{g,c}}|_{\mathrm{tree}} = 1$ in the effective field theory.
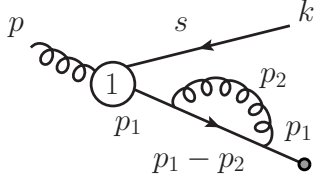
Figure 4.13: *Diagram corresponding to equation* (4.99).
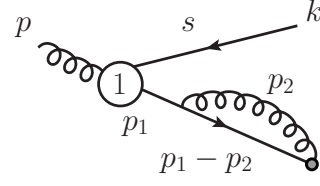
Figure 4.14: *Diagram corresponding to equation* (4.100).

Since at next-to-leading power in the $g\bar{q}$-channel only a single soft structure is relevant, no additional manipulations relating to the use of equation-of-motion identity, or on-shell and transversality conditions are necessary here. This is in contrast to the considerations presented for the collinear functions in the $q\bar{q}$-channel. At this point, we simply compare the result for the left-hand side of the matching equation given in (4.96) to the right-hand side in (4.95) and read off the tree-level result for the collinear function

$$G^{\eta,B}_{\xi q;\gamma\alpha,fb}\left(n_+q, n_+p; \omega_1\right) = -\delta(n_+q - n_+p)\, \mathbf{T}^B_{fb} \left(\frac{\slashed{n}_-}{2}\gamma_{\perp\eta}\right)_{\gamma\alpha} + \mathcal{O}(\alpha_s)\,. \tag{4.97}$$

Using the decomposition introduced in (3.111) we can extract the scalar collinear function $G_{\xi q}(n_+p; \omega_1)$ which appears in the factorisation formula in (3.113). Namely, we find

$$G^{(0)}_{\xi q}(n_+p; \omega_1) = -\frac{1}{2}\,, \tag{4.98}$$

where the superscript (0) denotes the fact that this is a tree-level result.

4.2.2 One-loop collinear function

Having obtained the tree-level value for the collinear function appearing in the factorisation theorem for the $g\bar{q}$-channel of the Drell-Yan partonic cross-section, we next consider the $\mathcal{O}(\alpha_s)$ corrections.

For the right-hand side of the matching we use (4.95). Here, as in the $q\bar{q}$ case discussed in section 4.1.2, the on-shell wave function renormalization factor is unity to all orders in perturbation theory, $\sqrt{Z_{g,\mathrm{PDF}}} = 1$. This holds in dimensional regularization, which we use to treat IR and UV divergences, since the loop corrections are scaleless. The situation is the same for the $\sqrt{Z_{g,c}}$ factor on the left-hand side of the matching equation. The calculation the one-loop accurate collinear functions for the $q\bar{q}$-channel carried out in section 4.1.2 presents a higher degree of technical difficulty than the computation of diagrams contributing to the $\mathcal{O}(\alpha_s)$ corrections to $G_{\xi q}(n_+p; \omega_1)$ due to a higher number of contributing terms and presence of momentum derivatives. For this reason, we skip here the details of the computation and rather present the results for individual diagrams which form the one-loop accurate $\langle q_b^+(k)|\mathcal{T}^{\mathfrak{c}}_{\gamma f}(n_+q)|g^B(p)\rangle$ matrix element on the left-hand side of the matching equation (4.91). In order to keep the expressions as concise as possible, we again make use of the short-hand notation for the momentum-dependent loop factor $\mathfrak{K}$ in (4.56) and the finite combination of Γ functions $\mathfrak{f}$ in (4.57).
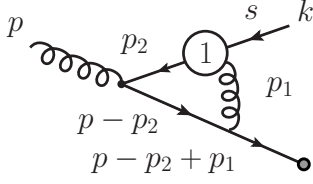
Figure 4.15: *Diagram corresponding to equation* (4.101).
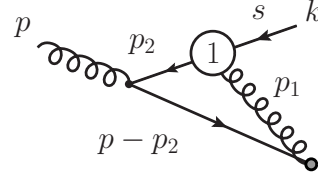
Figure 4.16: *Diagram corresponding to equation* (4.102).

The first diagram we consider is shown in figure 4.13. Performing the loop integral yields the following result

$$\langle q_b^+(k)|\mathcal{T}_{\gamma f}^{\mathfrak{c}}(n_+q)|g^B(p)\rangle_{\text{fig4.13}} = -(2\pi)\frac{\alpha_s}{4\pi}g_s\,\mathbf{T}_{fb}^B\,C_F\,\mathfrak{K}[\mu]\,\mathfrak{f}[\epsilon]$$
$$\times\,\delta(n_+q - n_+p)\frac{1}{\epsilon}(1-\epsilon)\frac{1}{(n_-k)}\left(\frac{\not{n}_-}{2}\gamma_{\perp\eta}\right)_{\gamma\alpha}v_\alpha(k)\epsilon_\perp^\eta(p)\,. \quad (4.99)$$

For the diagram in figure 4.13 we find

$$\langle q_b^+(k)|\mathcal{T}_{\gamma f}^{\mathfrak{c}}(n_+q)|g^B(p)\rangle_{\text{fig4.13}} = 2(2\pi)\frac{\alpha_s}{4\pi}g_s\mathbf{T}_{fb}^B\,C_F\,\mathfrak{K}[\mu]\,\mathfrak{f}[\epsilon]$$
$$\times\,\delta(n_+q - n_+p)\frac{1}{\epsilon^2}(1-\epsilon)\frac{1}{(n_-k)}\left(\frac{\not{n}_-}{2}\gamma_{\perp\eta}\right)_{\gamma\alpha}v_\alpha(k)\epsilon_\perp^\eta(p)\,, \quad (4.100)$$

which is the result for $\langle q_b^+(k)|\mathcal{T}_{\gamma f}^{\mathfrak{c}}(n_+q)|g^B(p)\rangle_{\text{fig4.13}}$ in (4.99) multiplied by a factor of $(-2/\epsilon)$, similarly to the relation between $\langle g^K(k)|\mathcal{T}_{\gamma f}^{\mathfrak{a},1g}(n_+q)|q(p)_e\rangle_{\text{fig4.8}}$ and $\langle g^K(k)|\mathcal{T}_{\gamma f}^{\mathfrak{a},1g}(n_+q)|q(p)_e\rangle_{\text{fig4.9}}$ in the $q\bar{q}$ case. Next, we consider the diagram in figure 4.15 for which we find

$$\langle q_b^+(k)|\mathcal{T}_{\gamma f}^{\mathfrak{c}}(n_+q)|g^B(p)\rangle_{\text{fig4.15}} = -(2\pi)\frac{\alpha_s}{4\pi}g_s\mathbf{T}_{fb}^B\left(C_F - \frac{1}{2}C_A\right)\mathfrak{K}[\mu]\,\mathfrak{f}[\epsilon]\,\delta(n_+q - n_+p)$$
$$\times\frac{1}{\epsilon^2}\left(\frac{(2-5\epsilon+3\epsilon^2-2\epsilon^3)}{(1-\epsilon)}\right)\frac{1}{n_-k}\left(\frac{\not{n}_-}{2}\gamma_\perp^\rho\right)_{\gamma\alpha}v_\alpha(k)\epsilon_\perp^\eta(p)\,. \quad (4.101)$$

The diagram in figure 4.16 is zero due to a vanishing contraction of Lorentz structures

$$\langle q_b^+(k)|\mathcal{T}_{\gamma f}^{\mathfrak{c}}(n_+q)|g^B(p)\rangle_{\text{fig4.16}} = 0\,. \quad (4.102)$$

The result for the diagram in figure 4.17 is

$$\langle q_b^+(k)|\mathcal{T}_{\gamma f}^{\mathfrak{c}}(n_+q)|g^B(p)\rangle_{\text{fig4.17}} = -(2\pi)\frac{\alpha_s}{4\pi}g_s\mathbf{T}_{fb}^B\,C_A\,\mathfrak{K}[\mu]\,\mathfrak{f}[\epsilon]\delta(n_+q - n_+p)$$
$$\times\frac{1}{2\epsilon^2}\frac{1}{(1-\epsilon)}\left(2-6\epsilon+4\epsilon^2\right)\frac{1}{(n_-k)}\left(\frac{\not{n}_-}{2}\gamma_{\perp\eta}\right)_{\gamma\alpha}v_\alpha(k)\epsilon_\perp^\eta(p)\,, \quad (4.103)$$

whereas for the one in figure 4.18 we find

$$\langle q_b^+(k)|\mathcal{T}_{\gamma f}^{\mathfrak{c}}(n_+q)|g^B(p)\rangle_{\text{fig4.18}} = -(2\pi)\frac{\alpha_s}{4\pi}g_s\mathbf{T}_{fb}^B\,C_A\,\mathfrak{K}[\mu]\,\mathfrak{f}[\epsilon]\delta(n_+q - n_+p)$$
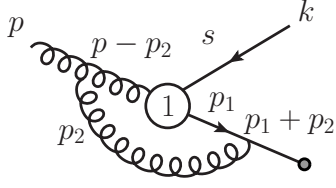
Figure 4.17: *Diagram corresponding to equation (4.103).*

Figure 4.18: *Diagram corresponding to equation (4.104).*

Figure 4.19: *Diagram corresponding to equation (4.105).*
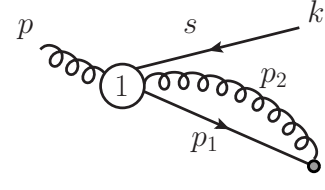
Figure 4.20: *Diagram corresponding to equation (4.106).*

$$\times \frac{1}{2\epsilon^2}\left(2 - 3\epsilon\right)\frac{1}{n_-k}\left(\frac{\slashed{n}_-}{2}\gamma_{\perp\eta}\right)_{\gamma\alpha} v_\alpha(k)\epsilon_\perp^\eta(p)\,. \tag{4.104}$$

The calculation of the diagram in figure 4.19 yields

$$
\begin{aligned}
\langle q_b^+(k)|\mathcal{T}_{\gamma f}^{\mathfrak{c}}(n_+q)|g^B(p)\rangle_{\text{fig4.19}} &= 2(2\pi)\frac{\alpha_s}{4\pi}g_s\mathbf{T}_{fb}^B\left(C_F - \frac{1}{2}C_A\right)\mathfrak{K}[\mu]\,\mathfrak{f}[\epsilon] \\
&\times \delta(n_+q - n_+p)\frac{1}{\epsilon^2}(1 - \epsilon)\frac{1}{(n_-k)}\left(\frac{\slashed{n}_-}{2}\gamma_{\perp\eta}\right)_{\gamma\alpha} v_\alpha(k)\epsilon_\perp^\eta(p)\,,
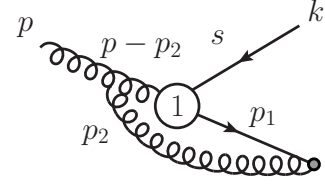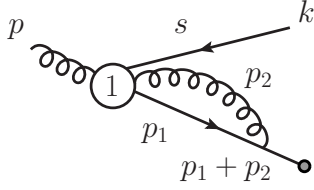\end{aligned} \tag{4.105}
$$

and lastly

$$\langle q_b^+(k)|\mathcal{T}_{\gamma f}^{\mathfrak{c}}(n_+q)|g^B(p)\rangle_{\text{fig4.20}} = 0\,. \tag{4.106}$$

Moreover, the diagram in figure 4.21 does not contribute as the collinear loop does not have a scale. We now perform a summation of all of the contributing diagrams, and write down the result for the matrix element on the left-hand side of the matching equation (4.91) at one-loop level. We denote it by $\langle q_b^+(k)|\mathcal{T}_{\gamma f}^{\mathfrak{c}}(n_+q)|g^B(p)\rangle^{(1)}$, for which we find

$$
\begin{aligned}
\langle q_b^+(k)|\mathcal{T}_{\gamma f}^{\mathfrak{c}}(n_+q)|g^B(p)\rangle^{(1)} &= (2\pi)\frac{\alpha_s}{4\pi}\,g_s\,\mathbf{T}_{fb}^B\,\mathfrak{K}[\mu]\,\mathfrak{f}[\epsilon]\delta(n_+q - n_+p) \\
&\times \frac{1}{\epsilon^2(1 - \epsilon)}\left(C_F\left(2 - 4\epsilon + 3\epsilon^2 + \epsilon^3\right) - C_A\left(2 - 5\epsilon + 3\epsilon^2 + \epsilon^3\right)\right) \\
&\times \frac{1}{(n_-k)}\left(\frac{\slashed{n}_-}{2}\gamma_{\perp\eta}\right)_{\gamma\alpha} v_\alpha(k)\epsilon_\perp^\eta(p)\,. \tag{4.107}
\end{aligned}
$$
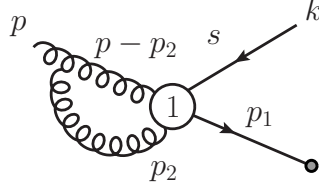
Figure 4.21: *Scaless diagram which does not contribute to the collinear function result.*

We now match this result to the right-hand side of (4.95), from which we extract the perturbative matching coefficient, the collinear function, at one-loop order

$$
\begin{aligned}
G^{\eta,B\,(1)}_{\xi q;\gamma\alpha,fb}\left(n_+q, n_+p;\omega_1\right) &= -\frac{\alpha_s}{4\pi}\,\mathbf{T}^B_{fb}\,\left(\frac{(n_+p)\omega_1}{\mu^2}\right)^{-\epsilon}\delta(n_+q - n_+p) \\
&\times \frac{1}{\epsilon^2(1-\epsilon)}\left(C_F\left(2 - 4\epsilon + 3\epsilon^2 + \epsilon^3\right) - C_A\left(2 - 5\epsilon + 3\epsilon^2 + \epsilon^3\right)\right) \\
&\times \frac{e^{\epsilon\gamma_E}\Gamma[1+\epsilon]\Gamma[1-\epsilon]^2}{\Gamma[2-2\epsilon]}\left(\frac{\slashed{n}_-}{2}\gamma^\eta_\perp\right)_{\gamma\alpha}.
\end{aligned}
\tag{4.108}
$$

This is the $\mathcal{O}(\alpha_s)$ correction to the tree-level collinear function presented in (4.97). The result in (4.108) is valid to all orders in ϵ. Expanding in $\epsilon = (4-d)/2$ yields the following expression

$$
\begin{aligned}
G^{\eta,B\,(1)}_{\xi q;\gamma\alpha,fb}\left(n_+q, n_+p;\omega_1\right) &= -\frac{\alpha_s}{4\pi}\,\mathbf{T}^B_{fb}\,\delta(n_+q - n_+p)\left(\frac{\slashed{n}_-}{2}\gamma^\eta_\perp\right)_{\gamma\alpha} \\
&\times \Bigg\{ C_F\left(\frac{2}{\epsilon^2} - \frac{2}{\epsilon}\left(\ln\left(\frac{n_+p\,\omega_1}{\mu^2}\right) - 1\right) + \ln^2\left(\frac{n_+p\,\omega_1}{\mu^2}\right) - 2\ln\left(\frac{n_+p\,\omega_1}{\mu^2}\right) - \frac{\pi^2}{6} + 5\right) \\
&-C_A\left(\frac{2}{\epsilon^2} - \frac{1}{\epsilon}\left(2\ln\left(\frac{n_+p\,\omega_1}{\mu^2}\right) - 1\right) + \ln^2\left(\frac{n_+p\,\omega_1}{\mu^2}\right) - \ln\left(\frac{n_+p\,\omega_1}{\mu^2}\right) - \frac{\pi^2}{6} + 2\right)\Bigg\} \\
&+\mathcal{O}(\epsilon).
\end{aligned}
\tag{4.109}
$$

It is interesting to compare the above result for the collinear function appearing in the $g\bar{q}$-channel to the collinear functions in the $q\bar{q}$-channel, which have been given in their expanded form in equations (4.85) and (4.88). We note that here, in contrast to $J_1^{(1)}$ and $J_6^{(1)}$, the collinear function $G^{(1)}_{\xi q}$ exhibits $1/\epsilon^2$ poles, and finite logarithms $\alpha\ln^2(n_+p\,\omega_1/\mu^2)$. At cross-section level, as we show in section 8.5, these correspond to leading logarithmic contributions appearing in the collinear sector. This fact complicates the adaptation of the resummation treatment developed for the $q\bar{q}$-channel to the off-diagonal $g\bar{q}$-channel. We provide additional details in chapter 8.5. It is noteworthy that the leading pole structure in the above equation is proportional to $C_F - C_A$, this structure appears in several instances where divergent convolution integrals are encountered [58, 59, 66, 134, 135].

4.3 Discussion

The study of an amplitude with a next-to-soft emission has a long history beginning with the Low-Burnett-Kroll [96, 97] formula in QED and the extension to also include the soft gluon emission from jets [130]. The way in which next-to-soft LBK amplitude is reproduced within SCET was discussed in [136, 137]. The calculation of the collinear functions at the one-loop level presented above forms part of the generalisation of the LBK formula to the one-loop order. The complete next-to-leading power, one-loop amplitude is provided in appendix. B.2. The amplitude presented there includes terms which vanish at the cross-section level, due to the interference with the complex-conjugated tree-level amplitude. The result does not display any suggestive structure, and indeed, to our knowledge there is no simple representation of the one-loop result in terms of the angular momentum operator that would generalise the well-known expression of the tree-level next-to-soft amplitude.

The diagrammatic approach has been applied in the past to study the next-to-soft emission at the one-loop order in amplitudes with a colourless final state [36, 37, 39]. In these investigations, the concept of a "radiative jet function" [130] is used to describe the soft emission from jets. Ultimately, the NLP SCET formalism presented here must capture the same physics, however some conceptual differences are present. The most important one, is that the radiative jet function, as is given in equation (2.12) of [37], is not a single scale object. This is in stark contrast to the collinear functions defined in (3.42). We can see this fact in the result for the one-loop radiative jet function given in equation (3.3) of [37]. In addition to the collinear contributions, one must include subtraction terms which correct for the overlap of the radiative jet function with the soft function. The NLP SCET formalism does not encounter such complications, which makes the effective field theory framework more suitable for resummation using renormalization group techniques. We discuss this further in chapter 8. Despite the complications outlines above, NLP resummation for the Drell-Yan process near threshold has been achieved using diagrammatic techniques at LL accuracy [42]. This is possible due to the fact that the radiative jet or collinear functions do not contribute beyond the tree level at this accuracy [40].

In order to compare our collinear functions with results for the radiative jet function given in [37], it is necessary to multiply our collinear functions with their corresponding soft structures, since the radiatieve jet functions contain both collinear and soft contributions. For this reason, it is most convenient to compare the radiative jet function in [36, 37] with our results for the soft emission amplitude at NLP calculated within SCET and given in appendix B.2. We focus on the contributions given in equations (B.11), (B.12), (B.24), and (B.25). After expanding in ϵ, these expressions are compared with $J_{\mu,F}^{(1)}$ and $J_{\mu,A}^{(1)}$ presented in [37]. We find agreement for all terms,[1] except for contributions (B.24) and (B.25) proportional to $n_-^\rho/(n_- l)$. Given that our calculation gives the full amplitude with the emission of a soft gluon, we conclude that the radiative jet function in [36, 37] does not reproduce the complete amplitude, although the missing terms do not contribute to the matrix element squared at next-to-leading power. It appears that contributions

---

[1] Noting the typo in (3.3) of [37] where one must replace $(-2p \cdot k)^{-\epsilon} \to (2p \cdot k)^{-\epsilon}$ and a overall minus sign error in one-loop results given in [36].

similar to those from the $J^{A0,A1}$ and $J^{A0,B1}$ SCET currents are needed in the radiative jet function formalism. Recent progress in QED has been reported in [138].

5

Drell-Yan: NLP soft functions

We have presented the factorisation formulas for the Drell-Yan partonic cross-section beyond leading power in the $q\bar{q}$ and $g\bar{q}$ channels in equations (3.60) and (3.107) respectively. In the subsequent discussion and exploration of these results thus far, we have focused on the amplitude level collinear functions which are the new objects appearing in the factorisation formulas at subleading powers. However, objects which deserve further attention in their own right are the generalised soft functions, defined at general subleading powers in equations (3.61) and (3.108) for the diagonal and off-diagonal channels respectively. We explore the structure of the next-to-leading power versions of the generalised soft functions in this section.

We observe that in contrast to the leading power soft function, the generalised soft functions contain explicit insertions of soft gauge fields $\mathcal{B}^+$ and soft matter fields q^+. The leading power soft function, which appears in equation (3.29), is a vacuum matrix element of the time-ordered product of Wilson lines only. Wilson lines can be set to unity at the lowest order in the α_s expansion. Thus the leading power soft function is non-zero already at $\mathcal{O}(\alpha_s^0)$, interchangeably referred to here as the leading order and the tree-level contribution. Since the generalised soft functions contain explicit insertions of soft gauge fields, the lowest order at which the next-to-leading power soft functions in equations (3.83) – (3.87) and (3.114) start to contribute is $\mathcal{O}(\alpha_s)$. This is referred to here as the next-to-leading order contribution, despite the fact that a non-zero result at $\mathcal{O}(\alpha_s^0)$ does not exist for these soft functions.

The results for the next-to-leading power soft functions calculated here will be used further in chapters 7 and 8. First in chapter 7, we will use the full information determined with the fixed-order calculation of soft functions in order to obtain results for the Drell-Yan cross-section up to $\mathcal{O}(\alpha_s^2)$, including finite terms. Then, in chapter 8, we will use the information about coefficients of the leading poles in the ϵ expansion in order to construct anomalous dimensions which govern the scale evolution of the soft functions and obtain results for the leading logarithmic contributions to all orders in perturbation theory.

We begin with the diagonal channel of the Drell-Yan process in section 5.1 and focus on the off-diagonal $g\bar{q}$-channel in section 5.2.

5.1   Quark-antiquark channel

There are two types of soft contributions to the factorisation formula for the diagonal $q\bar{q}$-channel as discussed in section 3.2.2. Namely, the generalised soft functions which contribute to the dynamical part, denoted by $\Delta_{\mathrm{NLP}}^{dyn}(z)$ and given in (3.81), and the kinematic soft functions which capture power corrections to the phase space and which are expressed in terms of the leading power soft function $S_{\mathrm{DY}}(\Omega)$ given in equation (3.29). The soft functions which contribute to the dynamical part of the factorisation formula are listed in equations (3.83) – (3.87). We consider these in section 5.1.1. The kinematic soft functions are defined in equations (3.77) – (3.79) and these in turn are considered in section 5.1.2.

5.1.1   Generalised soft functions

In total, there are five possible generalised soft functions which contribute to the Drell-Yan cross-section at next-to-leading power. As mentioned above, these are listed in equations (3.83) – (3.87). However, only one soft function, namely S_1 in (3.83), begins at $\mathcal{O}(\alpha_s)$. The remaining soft functions contain at least two explicit insertions of soft gauge or soft quark fields and therefore begin at $\mathcal{O}(\alpha_s^2)$. The complete calculation of the next-to-next-to-leading order next-to-leading power soft functions is rather involved, in particular, the most challenging part is the calculation of the two real emission contributions to the soft functions. With this in mind, we separate our discussion into two parts. First, in this section, we focus on the calculation of the contributions to the soft functions at next-to-leading order and the real-virtual part of next-to-next-to-leading order contributions. Second, we dedicate chapter 6 to a technical discussion regarding the calculation of the real-real part of the soft functions at next-to-next-to-leading order.

As mentioned above, this section focuses on the calculation of the contributions to the S_1 soft function which is the only soft function beginning at $\mathcal{O}(\alpha_s)$. This soft function is defined in equation (3.83), but for convenience we write down the operatorial definition of this object here once more. The S_1 soft function is given by

$$S_1(\Omega;\omega) = \int \frac{dx^0}{4\pi}\, e^{i\Omega\,x^0/2} \int \frac{dz_-}{2\pi}\, e^{-i\omega z_-} S_1(x_0; z_-)\,, \tag{5.1}$$

with

$$S_1(x^0; z_-) \;=\; \frac{1}{N_c}\,\mathrm{Tr}\langle 0|\bar{\mathbf{T}}\left[Y_+^\dagger(x^0)Y_-(x^0)\right]\mathbf{T}\left(\left[Y_-^\dagger(0)Y_+(0)\right]\frac{i\partial_\perp^\nu}{in_-\partial}\mathcal{B}_{\nu_\perp}^+\,(z_-)\right)|0\rangle\,. \tag{5.2}$$

The soft function is an object defined at the cross-section level. We insert a complete set of states between $\bar{\mathbf{T}}$ and $\mathbf{T}$, and use the momentum operator to translate the fields in the anti-time-ordered piece which, by performing the dx^0 integral, gives rise to an energy conserving delta function

$$S_1(\Omega,\omega) \;=\; \sum_{X_s}\int \frac{d(n_+z)}{4\pi}\, e^{-i\omega\,n_+z/2}\,\delta(\Omega - 2E_{X_s}) \tag{5.3}$$

$$\times \frac{1}{N_c}\mathrm{Tr}\langle 0|\bar{\mathbf{T}}\left[Y_+^\dagger(0)Y_-(0)\right]|X_s\rangle\,\langle X_s|\mathbf{T}\left(\left[Y_-^\dagger(0)Y_+(0)\right]\frac{i\partial_\perp^\nu}{in_-\partial}\mathcal{B}_{\nu_\perp}^+(z_-)\right)|0\rangle\,,$$

where E_{X_s} is the total energy of the soft partons entering the final state. Writing the soft function in this way we see that it is of the amplitude squared form. The final state $\langle X_s|$ is general here, and we begin with the calculation of this object at $\mathcal{O}(\alpha_s)$, where the final state is composed of a single soft gluon, before considering higher order corrections in the α_s expansion.

S_1 at next-to-leading order

In order to yield a non-vanishing result, at the lowest order in α_s, the soft parton emission must be produced by the soft gauge field $\mathcal{B}_{\nu_\perp}^+$ in the time-ordered product piece and be absorbed by one of the Wilson lines in the anti-time-ordered piece of (5.3). We depict this situation in the diagram in figure 5.1. The virtual diagrams are scaleless and vanish in dimensional regularization.

We now proceed to obtain the $\mathcal{O}(\alpha_s)$ result for S_1 by calculating directly from the matrix element definition in (5.3). With the help of the expression for the emission of a single soft gluon from the soft building block in equation (4.10), we can write down the result for a single soft gluon emission from the amplitude side of equation (5.3). We have the following

$$\langle g^A(k)|\mathbf{T}\left(Y_-^\dagger(0)Y_+(0)\frac{i\partial_\perp^\nu}{in_-\partial}\mathcal{B}_{\nu_\perp}^+(z_-)\right)|0\rangle = \mathbf{T}^A\frac{g_s}{(n_-k)}\left[k_\perp^\eta - \frac{k_\perp^2}{(n_-k)}n_-^\eta\right]\epsilon_\eta^*(k)\,e^{iz_-k}, \quad (5.4)$$

where X_s is chosen to be a single gluon $g(k)^A$ with momentum k and the adjoint colour index A. The soft Wilson lines $\left[Y_-^\dagger(0)Y_+(0)\right]$ are set to unity at this order. We draw attention to the e^{iz_-k} factor associated with the single soft gluon emission from the soft building block at position z_-. This factor will combine with $e^{-i\omega\,n_+z/2}$ in (5.3) giving rise to a $\delta(\omega - n_-k)$ term.

According to (5.3), the above expression for the amplitude must be interfered with the expression for the conjugate amplitude which is a leading power object containing only the soft Wilson lines. For an incoming single soft gluon with momentum k and adjoint colour index B we have

$$\langle 0|\bar{\mathbf{T}}\left[Y_+^\dagger(0)Y_-(0)\right]|g^B(k)\rangle \quad = \quad g_s\frac{1}{n_+k}\mathbf{T}^B n_+^\eta\epsilon_\eta(k) - g_s\frac{1}{n_-k}\mathbf{T}^B\,n_-^\eta\epsilon_\eta(k). \quad (5.5)$$

The amplitude and the conjugate amplitude are combined according to the expression in equation (5.3). Then, in order to obtain S_1 at $\mathcal{O}(\alpha_s)$, it remains to calculate the following integral

$$S_1^{(1)}(\Omega, \omega) \quad = \quad 2g_s^2 C_F \int \frac{d^dk}{(2\pi)^d}\left(-2\pi\delta(k^2)\theta(k^0)\right)\delta(\Omega - n_-k - n_+k)$$

$$\times\delta(\omega - n_-k)\frac{1}{n_+k}\left(-\frac{k_\perp^2}{(n_-k)^2}\right), \quad (5.6)$$

where we have dealt with the colour dependence using the colour algebra rules in appendix A.4, and the overall factor of 2 comes from the contraction of light-like vectors, $n_+ \cdot n_- = 2$. The reminder of the calculation follows the standard procedure of writing
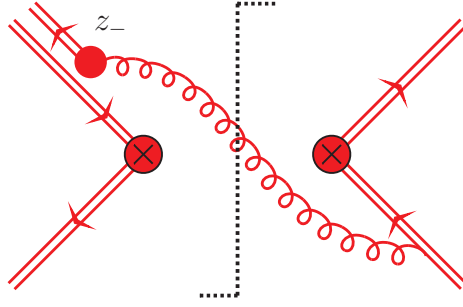
Figure 5.1: *The $\mathcal{O}(\alpha_s)$ contribution to the S_1 NLP soft function in equation* (5.3). *The double red lines are soft Wilson lines and the large red dot represents an explicit insertion of the gauge field $\mathcal{B}^+$ at position z_-. A direct calculation of the matrix elements in equation* (5.3) *gives the result written in* (5.7).

the integral measure in components, integrating over the angular dependence, and using the on-shell delta function to fix the transverse integral. Finally, the $d(n_+k)$ and $d(n_-k)$ integrals are fixed using the two remaining delta functions. This short calculation gives the following result

$$S_1^{(1)}\left(\Omega,\omega\right) = \frac{\alpha_s C_F}{2\pi} \frac{\mu^{2\epsilon}e^{\epsilon\gamma_E}}{\Gamma[1-\epsilon]} \frac{1}{\omega^{1+\epsilon}} \frac{1}{(\Omega-\omega)^\epsilon}\, \theta(\omega)\theta(\Omega-\omega)\ . \tag{5.7}$$

The θ-functions enter this result due to a careful evaluation of the loop integral using the delta functions in (5.6).

   In the single soft gluon emission case presented here it is not a difficult task to calculate the S_1 soft function directly from its matrix element definition. However, for certain contributions in the double real emission case, discussed in chapter 6, we find it convenient to perform the calculation using the next-to-leading power momentum-space Feynman rules. We now briefly discuss the equivalence.

   The NLP momentum-space Feynman rules are straightforwardly applied to calculate SCET amplitudes. The main idea behind using the NLP Feynman rules to calculate soft functions is the fact that for the relevant soft functions, the tree-level hard and collinear functions are simple multiplicative factors. Therefore, there exists a simple correspondence between the diagrams with soft emissions obtained using the NLP Feynman rules and the actual soft functions. This correspondence is demonstrated here using the $\mathcal{O}(\alpha_s)$ S_1 calculation as an example.

   Consider the single soft gluon emission amplitude shown in the left-most diagram of figure 5.2, the result for this diagram obtained using the II piece of the Feynman rule in equation (2.91) is

$$\text{Fig.}\,5.2_{\text{II}}[\text{left}] = \bar{v}_{\bar{c}}(l)\, i\gamma_\perp^\rho g_s \mathbf{T}^A \left[\frac{k_\perp^2 n_{-\nu}}{(n_+p)(n_-k)^2} - \frac{k_{\perp\nu}}{(n_+p)(n_-k)}\right] u_c(p)\epsilon^{*\nu}(k). \tag{5.8}$$

The soft structure here already resembles the corresponding matrix element expression in equation (5.4). Next, we strip off the pieces associated with the incoming anticollinear antiquark and collinear quark, the hard interaction vertex, and the relevant tree-level collinear function which is given in (4.19). We must also include the factor e^{iz_-k}, since it
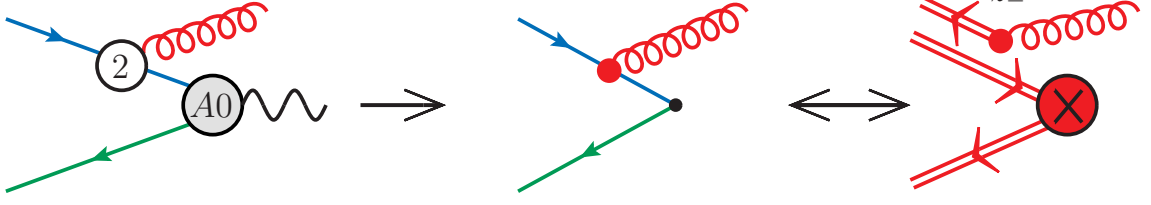
Figure 5.2: *A pictorial representation of the discussion below equation* (5.8)*. Starting from the left-hand side, in the first diagram we depict a SCET amplitude with one power suppressed soft gluon emission calculated using the II piece of the NLP Feynman rule in equation* (2.91)*. The diagram in the middle represents a related quantity, but with the collinear, anticollinear, and vector current factors stripped off. Since all these factors are not included, the middle diagram retains only the information about soft dependence and hence, it is in one-to-one correspondence with the single soft gluon matrix element of the soft building block* $\frac{i\partial_\perp^\mu}{in_-\partial}\mathcal{B}_{\mu\perp}^+$ *given in equation* (5.4) *and represented pictorially in the right-most diagram.*

is known that the power suppressed soft gluon emission occurs at position z_-. The result of this procedure is represented by the middle diagram in figure 5.2. Writing down the expression,

$$\text{Fig.}\,5.2_{\text{II}}[\text{middle}] = g_s\mathbf{T}^A\left[-\frac{k_\perp^2 n_{-\nu}}{(n_-k)^2} + \frac{k_{\perp\nu}}{(n_-k)}\right]\epsilon^{*\nu}(k)\,e^{iz_-k}, \tag{5.9}$$

we see that it is in one-to-one correspondence with the expression for the matrix element in equation (5.4), which is represented by the right-most diagram in figure 5.2.

We apply the same procedure for the conjugate amplitude, now using the leading power Feynman rules in the top line of (2.90), which give rise to eikonal vertices. The resulting expression is in one-to-one correspondence with the expression in (5.5) obtained directly from matrix elements of soft Wilson lines.

Following on from the above considerations regarding the amplitude expressions, we deduce that the calculation of the soft functions, defined at cross-section level, can be performed using diagrams such as one in figure 5.3. We label the expression for the diagram in figure 5.3, obtained using NLP Feynman rules with appropriate factors stripped off as described above, by $S_1^{(1)}(\Omega,\omega)_{fig:5.3}$. This labelling denotes the fact that this contribution to the $S_1^{(1)}$ soft function is calculated using the diagram in figure 5.3. Explicitly, we find the following

$$S_1^{(1)}(\Omega,\omega)_{fig:5.3} = 2\,g_s^2\,C_F\int\frac{d^dk}{(2\pi)^d}\left(-2\pi\delta(k^2)\theta(k^0)\right)\delta(\Omega - n_-k - n_+k)$$

$$\times\delta(\omega - n_-k)\frac{1}{n_+k}\left(-\frac{k_\perp^2}{(n_-k)^2}\right), \tag{5.10}$$

which, as expected, is equivalent to (5.6). Therefore, after performing the integral, we obtain the same result as in equation (5.7). There is little computational gain in the example presented here, however, as mentioned above, we find this way of performing the
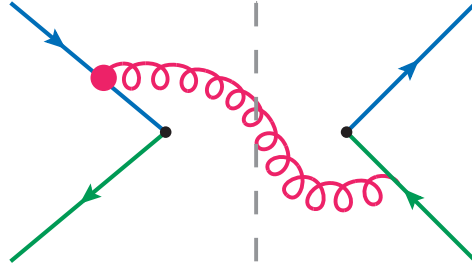
Figure 5.3:   *Diagram depicting an $\mathcal{O}(\alpha_s)$ contribution to the S_1 soft function understood to be evaluated using NLP Feynman rules but with collinear, anticollinear, and vector current pieces stripped off as described below equation (5.8). This diagram is in one-to-one correspondence with the diagram in figure 5.1.*

calculation useful for the case of next-to-next-to-leading order computation discussed in chapter 6.

In the process of finding the result for $S_1^{(1)}(\Omega, \omega)$ in (5.7) we have kept the d-dimensional dependence at every step in the calculation and not expanded in ϵ. This result will be needed to obtain the fixed-order results for the cross-section presented in chapter 7. However, for purposes of resummation discussed in chapter 8, we expand the above result in ϵ which yields the following expression

$$S_1^{(1)}(\Omega, \omega) = \frac{\alpha_s C_F}{2\pi} \left\{ \theta(\Omega)\delta(\omega)\left(-\frac{1}{\epsilon} + \ln\frac{\Omega^2}{\mu^2}\right) + \left[\frac{1}{\omega}\right]_+ \theta(\omega)\theta(\Omega - \omega) \right\}, \qquad (5.11)$$

where the plus distribution is defined as

$$\int_0^\Omega d\omega \, \frac{f(\omega)}{[\omega]_+} = \int_0^\Omega d\omega \, \frac{f(\omega) - f(0)}{\omega}, \qquad (5.12)$$

and where $f(\omega)$ is well behaved at the end point $\omega = 0$. The expansion of (5.7) given in equation (5.11) has already been presented in [40].[1]

Next-to-next-to-leading order: real-virtual contributions

As mentioned above, the calculation of the soft functions at $\mathcal{O}(\alpha_s^2)$ is split into two parts. Here we consider the so-called real-virtual contributions. This refers to the situation where one soft gluon crosses the cut, as was already the case in the NLO diagrams in figures 5.1 and 5.3, and there is one soft virtual loop present. "Soft virtual loop" means that the momentum flowing in the loop has a soft scaling and the loop is on either side of the cut. In chapter 6, we present the calculation of real-real contributions to the $\mathcal{O}(\alpha_s^2)$ soft functions which corresponds to two soft partons crossing the cut and no virtual loops. There is no virtual-virtual contribution to the soft functions as this set up leads to scaleless integrals which are zero in dimensional regularization.

Starting from $\mathcal{O}(\alpha_s^2)$, in addition to the S_1 soft function in equation (3.83), the soft functions $S_2 - S_5$ in equations (3.84) – (3.87) can receive contributions. From the explicit

---

[1]We have adapted the name of the soft function to the current notation, in [40] the same object is denoted by $S_{2\xi}$.

calculation we find that only the S_1 soft function receives a non-vanishing contribution of the real-virtual type. Therefore, in the reminder of this section we discuss only the S_1 soft function. The soft functions $S_2 - S_5$ receive real-real contributions at $\mathcal{O}(\alpha_s^2)$ and so we discuss them, along with real-real contribution to S_1, in chapter 6.

S_1 **real-virtual**

As discussed, one of the pieces of the S_1 soft function at next-to-next-to-leading order is the one-real, one-virtual contribution. The relevant diagrams are shown in figure 5.4.

The calculation is split into two steps. We first perform the virtual soft loop integrals at amplitude level. This is needed for the NLP amplitudes in the top row of figure 5.4 and for leading power amplitude on the conjugate side on the bottom row of the same figure. Then, we interfere the resulting expressions with either the leading power tree-level result for the conjugate amplitude for the diagrams in the top row, or the NLP tree-level amplitude for the bottom diagram. Lastly, we integrate over the soft radiation momentum with the constraint on the total soft energy which gives rise to the scale Ω, as was the case above for the NLO diagram in figure 5.1.

We find the following result for the one-real, one-virtual contribution to the two-loop S_1 soft function

$$
\begin{aligned}
S_1^{(2)1r1v}(\Omega, \omega) \;\; = \;\; & -4 \, \frac{\alpha_s^2}{(4\pi)^2} \, C_F \, C_A \left(-\frac{\omega^2(\Omega - \omega)^2}{\mu^4} \right)^{-\epsilon} \frac{1}{\omega} \\
& \times \frac{1}{\epsilon^2} \frac{e^{2\epsilon\gamma_E} \, \Gamma[1 - \epsilon]^2}{\Gamma[1 - 2\epsilon]} \Gamma[1 + \epsilon]^2 \, \theta(\Omega - \omega)\theta(\omega).
\end{aligned} \tag{5.13}
$$

The superscript $1r1v$ reminds us that this contribution to the next-to-next-to-leading order $S_1^{(2)}$ soft function is due to the one-real, one-virtual soft gluon contribution. The integrals encountered in the NLO and the $1r1v$ NNLO calculation were similar to the well-known leading power case and calculable by hand despite the additional dependence on ω which is absent at leading power. The calculation of the real-real contributions to the soft functions requires more sophisticated methods and will be discussed in chapter 6. However, we first switch focus from the generalised soft functions to the investigation of the next-to-leading power corrections to the phase-space itself, captured by the kinematic soft functions.

5.1.2 Kinematic soft functions

The all order kinematic soft function definitions can be found in equations (3.77), (3.78), and (3.79). We write these here once more for convenience

$$
S_{K1}(\Omega) \;\; = \;\; \frac{\partial}{\partial\Omega} \partial_{\vec{x}}^2 S_{\text{DY}}(\Omega, \vec{x})|_{\vec{x}=0} , \tag{5.14}
$$

$$
S_{K2}(\Omega) \;\; = \;\; \frac{3}{4} \, \Omega^2 \frac{\partial}{\partial\Omega} S_{\text{DY}}(\Omega, \vec{x})|_{\vec{x}=0} , \tag{5.15}
$$

$$
S_{K3}(\Omega) \;\; = \;\; \Omega \, S_{\text{DY}}(\Omega, \vec{x})|_{\vec{x}=0} , \tag{5.16}
$$
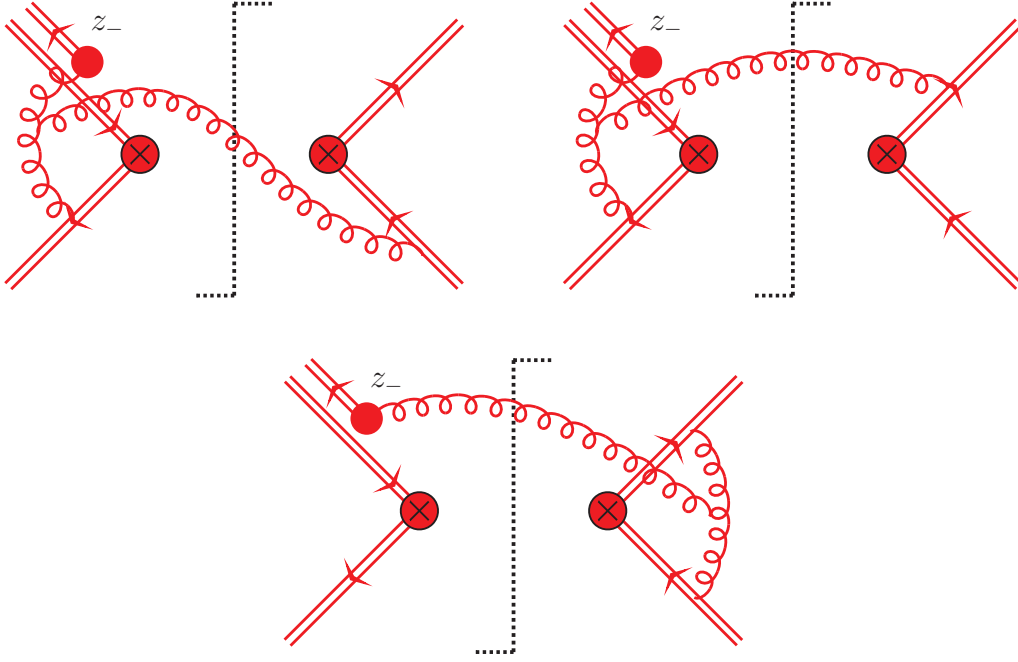
Figure 5.4: *The one-real, one-virtual contributions to the S_1 NLP soft function defined in equation (5.2). These diagrams form a part of the full $\mathcal{O}(\alpha_s^2)$ result for S_1. Expression obtained through calculation of these diagrams is given in (5.13). We note that the diagram on the right-hand side in the top line, where the soft gluon crossing the cut attaches to the soft Wilson line on the collinear side, gives a vanishing result due to contraction of the corresponding Lorentz structures.*

where $S_{\text{DY}}(\Omega, \vec{x})$ is the leading power soft function given in (3.29) with the position argument generalised to contain $\vec{x}$ dependence. The derivatives $\partial_{\vec{x}}^2$ in (5.14) are understood to be evaluated prior to setting $\vec{x} = 0$.

In this section, we compute the next-to-leading order and next-to-next-to-leading order contributions to the next-to-leading power kinematic soft functions $S_{K1}(\Omega)$, $S_{K2}(\Omega)$, and $S_{K3}(\Omega)$.

Next-to-leading order

We begin by considering the next-to-leading order contributions to the kinematic soft functions. It is of course paramount that the derivatives in equations (5.14) and (5.15) are taken prior to setting the position argument $\vec{x} = 0$. Therefore, we require the NLO position-space leading power soft function with the full x dependence. We use the result in equation (30) of [139]. It is given by

$$
\begin{aligned}
S_{\text{DY}}(x) \;\; = \;\; & 1 + \frac{\alpha_s}{\pi} C_F \frac{\Gamma[1-\epsilon]}{\epsilon^2} \left(-\frac{1}{4} n_- x \, n_+ x \, \mu^2 \, e^{\gamma_E} \right)^\epsilon \\
& \times {}_2F_1\left(-\epsilon, -\epsilon; 1-\epsilon; \frac{-x_\perp^2}{n_- x \, n_+ x} \right) + \mathcal{O}(\alpha_s^2).
\end{aligned}
\tag{5.17}
$$

We first perform the required derivatives in position space, set the argument $\vec{x} = 0$, and Fourier transform the result with respect to x^0 back into momentum space for which we use the definition

$$S_{\text{DY}}(\Omega) = \int_{-\infty}^{\infty} \frac{dx_0}{(4\pi)} e^{i\Omega x^0/2} S_{\text{DY}}(x_0) .$$
(5.18)

We begin with the most cumbersome contribution $S_{K1}(\Omega)$. To make taking the spatial derivatives easier, we split this contribution into transverse, $\perp$, piece and the piece along a third direction (or $\hat{z}$, in $(\hat{x}, \hat{y}, \hat{z})$ coordinate space, with $\hat{x}, \hat{y}$ belonging to $\perp$) as follows

$$S_{K1}(\Omega) = S_{K1}^3(\Omega) + S_{K1}^\perp(\Omega).$$
(5.19)

We begin with the $S_{K1}^3(\Omega)$ piece, at next-to-leading order it is given by

$$S_{K1}^{3\,(1)}(\Omega) = \frac{\partial}{\partial\Omega} \partial_3^2 S_{\text{DY}}^{(1)}(\Omega, \vec{x})|_{\vec{x}=0} .$$
(5.20)

Starting from the full x dependent soft function, for which we find the expression in (5.17), and taking the ∂_3 derivatives leads us to

$$S_{K1}^{3\,(1)}(\Omega) = \frac{\partial}{\partial\Omega} \int \frac{dx_0}{4\pi} e^{ix_0\Omega/2} \left(\frac{\alpha_s}{\pi} C_F \frac{\mu^{2\epsilon} e^{\epsilon\gamma_E} \Gamma[1-\epsilon]}{\epsilon^2} \left[-2\epsilon \left(-\frac{1}{4}x_0^2 \right)^\epsilon \frac{1}{x_0^2} \right] \right)$$

$$= \frac{\partial}{\partial\Omega} \frac{\alpha_s}{\pi} C_F \frac{e^{\epsilon\gamma_E} \Gamma[1-\epsilon]}{\epsilon^2 \, \Gamma[-2\epsilon]} \mu^{2\epsilon} 2\epsilon \frac{-\Omega^{1-2\epsilon}}{8\epsilon - 16\epsilon^2}$$

$$= -\frac{\alpha_s}{\pi} C_F \frac{e^{\epsilon\gamma_E} \Gamma[1-\epsilon]}{\epsilon^2 \, \Gamma[-2\epsilon]} \mu^{2\epsilon} \frac{\Omega^{-2\epsilon}}{4}$$

$$= \frac{\alpha_s}{2\pi} C_F \left(\frac{1}{\epsilon} + 2\ln\left(\frac{\mu}{\Omega}\right) + \epsilon\left(2\ln^2\left(\frac{\mu}{\Omega}\right) - \frac{1}{4}\pi^2 \right) + \mathcal{O}(\epsilon^2) \right),$$
(5.21)

where in the last step we have expanded in ϵ. Next, we consider the second piece making up the $S_{K1}(\Omega)$ term in equation (5.19). Namely, we focus on $S_{K1}^\perp(\Omega)$ piece. At NLO it is given by

$$S_{K1}^{\perp\,(1)}(\Omega) = \frac{\partial}{\partial\Omega} \partial_\perp^2 S_{\text{DY}}^{(1)}(\Omega, \vec{x})|_{\vec{x}=0} .$$
(5.22)

Substituting the expression in (5.17) and taking the $\partial_\perp$ derivatives we arrive at the following

$$S_{K1}^{\perp\,(1)}(\Omega) = -\frac{\partial}{\partial\Omega} \int \frac{dx_0}{4\pi} e^{ix_0\Omega/2} \frac{\alpha_s}{\pi} C_F \frac{\Gamma[1-\epsilon]}{\epsilon^2} \left(-\frac{1}{4}x_0^2 \mu^2 \, e^{\gamma_E} \right)^\epsilon \frac{-4\,\epsilon^2}{x_0^2}$$

$$= -\frac{\partial}{\partial\Omega} \frac{\alpha_s}{\pi} C_F \frac{e^{\epsilon\gamma_E} \Gamma[1-\epsilon]}{\epsilon^2 \, \Gamma[-2\epsilon]} \mu^{2\epsilon} \frac{4\epsilon^2 \, (-\Omega^{1-2\epsilon})}{8\epsilon \, (1-2\epsilon)}$$

$$= \frac{\alpha_s}{2\pi} C_F \left(-2 - 4\epsilon\ln\left(\frac{\mu}{\Omega}\right) + \mathcal{O}\left(\epsilon^2\right) \right)$$
(5.23)

where in the last step we have also expanded in ϵ.

The soft kinematic corrections $S_{K2}(\Omega)$ and $S_{K3}(\Omega)$ in equations (5.15) and (5.16) are simpler to obtain as they do not involve a derivative of the position argument. Hence, we can set $\vec{x} = 0$ from the beginning, Fourier transform the soft function to momentum space using (5.18), and perform the $\partial/\partial\Omega$ derivatives where necessary, before expanding in ϵ. For $S_{K2}(\Omega)$, up to $\mathcal{O}(\alpha_s)$ we find

$$
\begin{aligned}
S_{K2} &= \frac{\alpha_s C_F}{2\pi}\left(\frac{3}{\epsilon} + 6\ln\left(\frac{\mu}{\Omega}\right) + 6\right. \\
&\left. + \epsilon\left(+6\ln^2\left(\frac{\mu}{\Omega}\right) + 12\ln\left(\frac{\mu}{\Omega}\right) - \frac{3\pi^2}{4}\right) + \mathcal{O}\left(\epsilon^2\right)\right) + \mathcal{O}(\alpha_s^2).
\end{aligned}
\tag{5.24}
$$

The third kinematic soft correction also starts at $\mathcal{O}(\alpha_s)$ despite not being built from derivatives acting on the leading power soft function. The $\mathcal{O}(\alpha_s^0)$ term vanishes as $S_{\mathrm{DY}} = \delta(\Omega) + \mathcal{O}(\alpha_s)$, so the leading order contribution is set to zero and we find for $S_{K3}(\Omega)$ the following result

$$
S_{K3}(\Omega) = \frac{\alpha_s C_F}{2\pi}\left(-\frac{4}{\epsilon} - 8\ln\left(\frac{\mu}{\Omega}\right) + \epsilon\left(-8\ln^2\left(\frac{\mu}{\Omega}\right) + \pi^2\right) + \mathcal{O}\left(\epsilon^2\right)\right) + \mathcal{O}(\alpha_s^2).
\tag{5.25}
$$

In (5.24) and (5.25) we have again expanded in ϵ for illustration purposes, however, full ϵ dependence is known.

Next-to-next-to-leading order

The calculation of the next-to-next-to-leading order contributions to the kinematic soft functions follows the same steps as the next-to-leading order calculation above. We now require the $\mathcal{O}(\alpha_s^2)$ corrections to equation (5.17). This result can be found in equation (35) of [139].

Since the computation follows the same steps, but requires handling of much larger expressions, we skip the details and directly present the NNLO results for the kinematic soft functions. We find

$$
\begin{aligned}
S_{K1}^{3,(2)}(\Omega) &= \frac{\alpha_s^2}{\pi^2}C_F^2\left(\frac{1}{2\epsilon^3} + \frac{2}{\epsilon^2}\ln\left(\frac{\mu}{\Omega}\right) + \frac{1}{\epsilon}\left(4\ln^2\left(\frac{\mu}{\Omega}\right) - \frac{7\pi^2}{12}\right)\right. \\
&\left. + \frac{16}{3}\ln^3\left(\frac{\mu}{\Omega}\right) - \frac{7\pi^2}{3}\ln\left(\frac{\mu}{\Omega}\right) - \frac{31\zeta(3)}{3}\right) \\
&+ \frac{\alpha_s^2}{\pi^2}C_F C_A\left(\frac{11}{48\epsilon^2} + \frac{1}{\epsilon}\left(\frac{11}{12}\ln\left(\frac{\mu}{\Omega}\right) - \frac{\pi^2}{48} + \frac{67}{144}\right)\right. \\
&\left. + \frac{11}{6}\ln^2\left(\frac{\mu}{\Omega}\right) - \frac{1}{12}\pi^2\ln\left(\frac{\mu}{\Omega}\right) + \frac{67}{36}\ln\left(\frac{\mu}{\Omega}\right) - \frac{7\zeta(3)}{8} + \frac{101}{108} - \frac{77\pi^2}{288}\right) \\
&+ \frac{\alpha_s^2}{\pi^2}C_F n_f\left(-\frac{1}{24\epsilon^2} - \frac{1}{\epsilon}\left(\frac{1}{6}\ln\left(\frac{\mu}{\Omega}\right) + \frac{5}{72}\right)\right. \\
&\left. - \frac{1}{3}\ln^2\left(\frac{\mu}{\Omega}\right) - \frac{5}{18}\ln\left(\frac{\mu}{\Omega}\right) + \frac{7\pi^2}{144} - \frac{7}{54}\right),
\end{aligned}
\tag{5.26}
$$

$$S_{K1}^{\perp\,(2)}(\Omega) \;=\; \frac{\alpha_s^2}{\pi^2}C_F^2\left(-\frac{1}{\epsilon^2}-8\ln^2\left(\frac{\mu}{\Omega}\right)-\frac{4}{\epsilon}\ln\left(\frac{\mu}{\Omega}\right)+\frac{7\pi^2}{6}\right)$$

$$+\frac{\alpha_s^2}{\pi^2}C_FC_A\left(-\frac{11}{12\epsilon}-\frac{11}{3}\ln\left(\frac{\mu}{\Omega}\right)+\frac{\pi^2}{12}-\frac{41}{18}\right)$$

$$+\frac{\alpha_s^2}{\pi^2}C_Fn_f\left(\frac{1}{6\epsilon}+\frac{2}{3}\ln\left(\frac{\mu}{\Omega}\right)+\frac{4}{9}\right), \tag{5.27}$$

$$S_{K2}^{(2)}(\Omega) \;=\; \frac{\alpha_s^2}{\pi^2}C_F^2\left(\frac{3}{2\epsilon^3}+\frac{1}{\epsilon^2}\left(6\ln\left(\frac{\mu}{\Omega}\right)+6\right)+\frac{1}{\epsilon}\left(12\ln^2\left(\frac{\mu}{\Omega}\right)+24\ln\left(\frac{\mu}{\Omega}\right)-\frac{7\pi^2}{4}\right)\right.$$

$$\left.+16\ln^3\left(\frac{\mu}{\Omega}\right)+48\ln^2\left(\frac{\mu}{\Omega}\right)-7\pi^2\ln\left(\frac{\mu}{\Omega}\right)-31\zeta(3)-7\pi^2\right)$$

$$+\frac{\alpha_s^2}{\pi^2}C_FC_A\left(\frac{11}{16\epsilon^2}+\frac{1}{\epsilon}\left(\frac{11}{4}\ln\left(\frac{\mu}{\Omega}\right)-\frac{\pi^2}{16}+\frac{199}{48}\right)\right.$$

$$\left.+\frac{11}{2}\ln^2\left(\frac{\mu}{\Omega}\right)-\frac{1}{4}\pi^2\ln\left(\frac{\mu}{\Omega}\right)+\frac{199}{12}\ln\left(\frac{\mu}{\Omega}\right)-\frac{21\zeta(3)}{8}-\frac{101\pi^2}{96}+\frac{151}{18}\right)$$

$$+\frac{\alpha_s^2}{\pi^2}C_Fn_f\left(-\frac{1}{8\epsilon^2}-\frac{1}{\epsilon}\left(\frac{1}{2}\ln\left(\frac{\mu}{\Omega}\right)+\frac{17}{24}\right)\right.$$

$$\left.-\ln^2\left(\frac{\mu}{\Omega}\right)-\frac{17}{6}\ln\left(\frac{\mu}{\Omega}\right)+\frac{7\pi^2}{48}-\frac{11}{9}\right), \tag{5.28}$$

and

$$S_{K3}^{(2)}(\Omega) \;=\; \frac{\alpha_s^2}{\pi^2}C_F^2\left(-\frac{2}{\epsilon^3}-\frac{8}{\epsilon^2}\ln\left(\frac{\mu}{\Omega}\right)+\frac{1}{\epsilon}\left(\frac{7\pi^2}{3}-16\ln^2\left(\frac{\mu}{\Omega}\right)\right)\right.$$

$$\left.-\frac{1}{3}64\ln^3\left(\frac{\mu}{\Omega}\right)+\frac{28\pi^2}{3}\ln\left(\frac{\mu}{\Omega}\right)+\frac{124\zeta(3)}{3}\right)$$

$$+\frac{\alpha_s^2}{\pi^2}C_FC_A\left(-\frac{11}{12\epsilon^2}+\frac{1}{\epsilon}\left(-\frac{11}{3}\ln\left(\frac{\mu}{\Omega}\right)+\frac{\pi^2}{12}-\frac{67}{36}\right)\right.$$

$$\left.-\frac{22}{3}\ln^2\left(\frac{\mu}{\Omega}\right)+\frac{1}{3}\pi^2\ln\left(\frac{\mu}{\Omega}\right)-\frac{67}{9}\ln\left(\frac{\mu}{\Omega}\right)+\frac{7\zeta(3)}{2}+\frac{77\pi^2}{72}-\frac{101}{27}\right)$$

$$+\frac{\alpha_s^2}{\pi^2}C_Fn_f\left(\frac{1}{6\epsilon^2}+\frac{1}{\epsilon}\left(\frac{2}{3}\ln\left(\frac{\mu}{\Omega}\right)+\frac{5}{18}\right)\right.$$

$$\left.+\frac{4}{3}\ln^2\left(\frac{\mu}{\Omega}\right)+\frac{10}{9}\ln\left(\frac{\mu}{\Omega}\right)+\frac{14}{27}-\frac{7\pi^2}{36}\right). \tag{5.29}$$

These results will be used in section 7.1.2 where we present the full next-to-next-to-leading order cross-section. Specifically, see equation (7.30) for prescription how kinematic functions enter the result for the Drell-Yan process at $\mathcal{O}(\alpha_s^2)$.
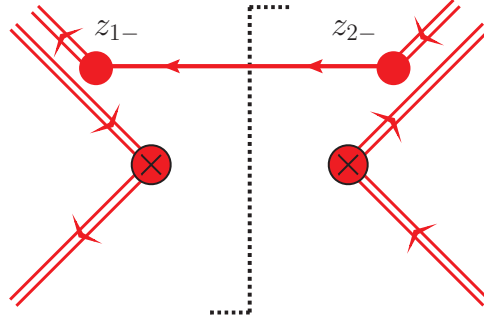
Figure 5.5: *Momentum-space representation of the $\mathcal{O}(\alpha_s)$ contribution to the soft function relevant in the off-diagonal channel, $S(\Omega, \omega_1, \omega_2)$ in (5.30). Positions z_{1-} and z_{2-} denote the insertions of the power suppressed Lagrangian terms, which include the soft quark fields, in time-ordered product operators. Conjugate variables are ω_1 and ω_2 respectively.*

5.2 Gluon-antiquark channel

Due to the inherent power suppressed nature of the off-diagonal channel of the Drell-Yan process the total number of possible soft contributions is smaller than in the diagonal channel. Indeed, as we have seen in section 3.3, there are no kinematic power corrections, since the soft radiation must contain a soft quark field which is included through a time-ordered product insertion of the $\mathcal{L}_{\xi q}^{(1)}$ Lagrangian. Hence, an $\mathcal{O}(\lambda)$ suppression is already provided. This is in contrast to the diagonal channel where the soft emissions can be composed of Wilson line soft gluons only, in which case there is room for power corrections to the phase-space.

The only soft function contributing at next-to-leading power is given in equation (3.114), which we state here once more for convenience

$$
\begin{aligned}
S_{g\bar{q}}(\Omega, \omega_1, \omega_2) \;\; = \;\; & \int \frac{dx^0}{4\pi} \int \frac{dz_{1-}}{2\pi} \int \frac{dz_{2-}}{2\pi} e^{-i\omega_1 z_{1-}} e^{+i\omega_2 z_{2-}} e^{i\,\Omega x^0/2} \\[2mm]
& \times \frac{1}{C_F\, C_A} \langle 0| \bar{\mathbf{T}} \Big(\frac{g_s}{in_-\partial_{z_2}} \bar{q}_+(x^0 + z_{2-})\, \mathbf{T}^A \left\{ Y_+^\dagger(x^0) Y_-(x^0) \right\} \Big) \\[2mm]
& \times \frac{\slashed{n}_-}{4} \mathbf{T}\Big(\left\{ Y_-^\dagger(0) Y_+(0) \right\} \mathbf{T}^A \frac{g_s}{in_-\partial_{z_1}} q_+(z_{1-}) \Big) |0\rangle .
\end{aligned}
\tag{5.30}
$$

Similar to the NLP soft functions in the diagonal channel, it begins to contribute at $\mathcal{O}(\alpha_s)$. The momentum-space diagram is presented in figure 5.5. An explicit calculation reveals that the $S_{g\bar{q}}(\Omega, \omega_1, \omega_2)$ soft function is given by the following expression

$$
\begin{aligned}
S_{g\bar{q}}(\Omega, \omega_1, \omega_2) \;\; = \;\; & \frac{\alpha_s}{4\pi} \mu^{2\epsilon} \frac{1}{\omega_1^{1+\epsilon}} \frac{1}{(\Omega - \omega_1)^\epsilon}\, \theta(\Omega - \omega_1)\, \theta(\omega_1)\, \delta(\omega_1 - \omega_2) \frac{e^{\epsilon \gamma_E}}{\Gamma[1-\epsilon]} \\[2mm]
& + \mathcal{O}(\alpha_s^2).
\end{aligned}
\tag{5.31}
$$

We use this result within the factorisation formula, given in equation (3.113), in section 7.2 in order to arrive at the next-to-leading order contribution to the cross-section from the $g\bar{q}$-channel of the Drell-Yan process.

6

Real-real contributions to the NLP soft functions

In the previous chapter we have discussed the calculation of the next-to-leading order S_1 soft function, and its one-real, one-virtual contribution at the next-to-next-to-leading order. To complete the investigation of the next-to-leading power soft functions up to next-to-next-to-leading order in α_s, we now present the calculation of their real-real corrections. These corrections have a rich structure in their own right, one which proves to be far more non-trivial than the one-virtual one-real contribution at the same order in the perturbative expansion in the coupling. We explore the details of the calculation in this chapter.

6.1 Introduction

According to the next-to-leading power factorisation theorem in equation (3.81), there exist five next-to-leading power soft functions. These are listed in equations (3.83) – (3.87) and the contributions to each one will be discussed here.

The layout of this chapter is as follows. We first describe the organisation of the calculation in terms of the matrix elements and diagrams which contribute to the respective next-to-leading power soft functions. We find that many terms appear in the integrands of the contributing expressions, leading to a significant number of two-loop integrals to perform. Due to this fact, we employ integration-by-parts (IBP) techniques to reduce the magnitude of the calculation to the necessary so-called "master" integrals [140, 141]. We give a brief introduction to IBP techniques and how they are applied to the calculation of real emissions. In section 6.4 we calculate the master integrals appearing in the expressions for the soft functions at $\mathcal{O}(\alpha_s^2)$. While some of the master integrals can be calculated directly, a subset proves to be composed of integrand structures which require the application of more advances integration techniques, such as the differential equations method [142]. We outline this procedure in section 6.4.1. The results for the soft functions are shown in section 6.5.

The final results for the soft functions at $\mathcal{O}(\alpha_s^2)$ are checked through their substitution into the next-to-leading power factorisation theorem in section 7.1.2 of the next chapter. There, we perform the convolution of the soft functions with the relevant collinear functions and compare to the expressions obtained with the expansion-by-regions method at the cross-section level.

6.2   Organisation of the calculation

As we have seen for the S_1 soft function at the next-to-leading order, the soft building blocks making up the soft functions contain a dependence on the z_- component of the position of the insertion of a particular subleading power Lagrangian term in a time-ordered product (two positions z_{1-} and z_{2-} for the case of two $\mathcal{O}(\lambda)$ insertions). The conjugate variable in momentum-space is the ω variable (two variables, ω_1 and ω_2, for the double insertions).

Explicitly, the soft matrix elements, such as for example

$$\langle g^K(k)|\frac{i\partial_\perp^\nu}{in_-\partial}\mathcal{B}_{\nu_\perp}^+\,(z_-)\,|0\rangle \;\; = \;\; \mathbf{T}^K\,\frac{g_s}{(n_-k)}\left[k_\perp^\eta - \frac{k_\perp^2}{(n_-k)}n_-^\eta\right]\epsilon_\eta^*(k)\,e^{iz_-k}\,, \tag{6.1}$$

depend on the e^{iz_-k} factor which combined with the dz_- integral in definition of the momentum-space soft function in equation (3.82) yields a $\delta(\omega - n_-k)$ term, where k is the total momentum emitted from the soft building block. We have already encountered this specific example in equation (5.6) for the case of the S_1 soft function at next-to-leading order.

We note that the exact form of the ω dependent delta functions appearing in the integrals describing the power suppressed soft functions depends on the total soft momentum emitted from the soft building blocks at position z_- (z_{1-} and z_{2-} in case of two $\mathcal{O}(\lambda)$ insertions). The momenta of soft outgoing partons from the power suppressed building blocks are labelled by k_i, where i counts the number of the partons emitted. For example, if only a single gluon emission originates from the next-to-leading power soft building block, the delta function in the corresponding integral will be $\delta(\omega - n_-k_1)$. However, if instead two gluons are emitted, then the relevant constraint appearing in the corresponding integrals will be $\delta(\omega - n_-k_1 - n_-k_2)$, and so on for more emissions. Due to this fact, in the presentation below, we separate the calculation of the relevant integrals as defined by their dependence on the ω dependent delta function structure.

Before we discuss the calculations of the relevant integrals appearing in the real-real contributions to the soft functions, we briefly describe how the calculation is organised. As we have noted, there are five next-to-leading power soft functions which could contribute at this order. We begin by outlining how the expressions for the relevant soft functions were constructed at $\mathcal{O}(\alpha_s^2)$.

The S_1 soft function is discussed in section 6.2.1 and the S_3 soft function in section 6.2.2. Both of these soft functions were calculated directly from their matrix element definitions. We give all the necessary expressions in the relevant sections below. The S_2 soft function vanishes at $\mathcal{O}(\alpha_s^2)$ therefore we do not purse it further here. In chapter 5, we have described how the NLP Feynman rules can be used to directly obtain expressions for soft functions in momentum-space. We use this method for the calculation of S_4 and S_5 soft functions for which further details are provided in section 6.2.3.

6.2.1 S_1 soft function

We begin with S_1 and follow the strategy used in chapter 5 for the calculation of its next-to-leading order correction. Here, we present considerations at the next order in

perturbation theory. Hence, instead of the $\langle X_s |$ state in equation (5.3) being made up of a single gluon, it now contains two partons. It follows that, instead of the single gluon emission matrix element given in equation (5.4), we require expressions for matrix elements with two external partons. These partons can be soft gluons, quarks, and ghosts, since we work in Feynman gauge. We label the momenta of the emitted partons k_1 and k_2 for concreteness. Note that here, not all soft emissions must come from the power suppressed building block $\frac{i\partial_\perp^\mu}{in_-\partial}\mathcal{B}_{\mu_\perp}^+(z_-)$, soft emissions can also originate from the soft Wilson lines present in the soft matrix element due to the decoupling transformation applied to the leading power SCET current (these Wilson lines are already present at leading power). We give explicit expressions and discuss the origin of every term below.

The two real-real soft gluon emission matrix element for the S_1 soft function is given by

$$
\langle g^{K_1}(k_1)g^{K_2}(k_2)|\mathbf{T}\left[Y_-^\dagger(0)Y_+(0)\frac{i\partial_\perp^\mu}{in_-\partial}\mathcal{B}_{\mu_\perp}^+(z_-)\right]|0\rangle \;=\;
$$

$$
g_s^2\mathbf{T}^{K_2}\,\mathbf{T}^{K_1}\frac{1}{(n_-k_1)}\frac{n_-^{\eta_2}}{(n_-k_2)}\left[k_{1\perp}^{\eta_1}-\frac{k_{1\perp}^2}{(n_-k_1)}n_-^{\eta_1}\right]\epsilon_{\eta_1}^*(k_1)\epsilon_{\eta_2}^*(k_2)\,e^{iz_-k_1}
$$

$$
+g_s^2\mathbf{T}^{K_1}\,\mathbf{T}^{K_2}\frac{1}{(n_-k_2)}\frac{n_-^{\eta_1}}{(n_-k_1)}\left[k_{2\perp}^{\eta_2}-\frac{k_{2\perp}^2}{(n_-k_2)}n_-^{\eta_2}\right]\epsilon_{\eta_1}^*(k_1)\epsilon_{\eta_2}^*(k_2)\,e^{iz_-k_2}
$$

$$
-g_s^2\mathbf{T}^{K_2}\,\mathbf{T}^{K_1}\frac{1}{(n_-k_1)}\frac{n_+^{\eta_2}}{(n_+k_2)}\left[k_{1\perp}^{\eta_1}-\frac{k_{1\perp}^2}{(n_-k_1)}n_-^{\eta_1}\right]\epsilon_{\eta_1}^*(k_1)\epsilon_{\eta_2}^*(k_2)\,e^{iz_-k_1}
$$

$$
-g_s^2\mathbf{T}^{K_1}\,\mathbf{T}^{K_2}\frac{1}{(n_-k_2)}\frac{n_+^{\eta_1}}{(n_+k_1)}\left[k_{2\perp}^{\eta_2}-\frac{k_{2\perp}^2}{(n_-k_2)}n_-^{\eta_2}\right]\epsilon_{\eta_1}^*(k_1)\epsilon_{\eta_2}^*(k_2)\,e^{iz_-k_2}
$$

$$
+g_s^2\,if^{K_1K_2K}\mathbf{T}^K\frac{1}{n_-(k_1+k_2)}\left(-\frac{(k_{1\perp}^{\eta_2}+k_{2\perp}^{\eta_2})\,n_-^{\eta_1}}{(n_-k_1)}+\frac{(k_{1\perp}^{\eta_1}+k_{2\perp}^{\eta_1})\,n_-^{\eta_2}}{(n_-k_2)}\right.
$$

$$
-\frac{n_-^{\eta_1}n_-^{\eta_2}}{n_-(k_1+k_2)(n_-k_1)(n_-k_2)}\left[(n_-k_1)\left(k_{1\perp}^2+k_{1\perp}\cdot k_{2\perp}\right)\right.
$$

$$
\left.\left.-(n_-k_2)\left(k_{2\perp}\cdot k_{1\perp}+k_{2\perp}^2\right)\right]\right)\epsilon_{\eta_1}^*(k_1)\epsilon_{\eta_2}^*(k_2)\,e^{iz_-(k_1+k_2)}
$$

$$
+g_s^2if^{K_1K_2K}\mathbf{T}^K\frac{1}{(n_-(k_1+k_2))^2}\frac{1}{(k_1+k_2)^2}\left(\left[n_-^{\eta_1}(2k_1+k_2)^{\eta_2}\right.\right.
$$

$$
\left.-n_-^{\eta_2}(k_1+2k_2)^{\eta_1}-g^{\eta_2\eta_1}(n_-(k_1-k_2))\right](k_{1\perp}+k_{2\perp})^2
$$

$$
+\left[(k_{1\perp}^{\eta_1}+k_{2\perp}^{\eta_1})(-2k_1-k_2)^{\eta_2}+(k_{1\perp}^{\eta_2}+k_{2\perp}^{\eta_2})(k_1+2k_2)^{\eta_1}\right.
$$

$$
\left.\left.+g^{\eta_2\eta_1}\left(k_{1\perp}^2-k_{2\perp}^2\right)\right](n_-(k_1+k_2))\right)\epsilon_{\eta_1}^*(k_1)\epsilon_{\eta_2}^*(k_2)\,e^{iz_-(k_1+k_2)}. \tag{6.2}
$$

We take a moment to describe the terms appearing in the above expression. The first four lines correspond to a single gluon being emitted from the explicit soft building block $\frac{i\partial_\perp^\mu}{in_-\partial}\mathcal{B}_{\mu_\perp}^+(z_-)$ and the second gluon being emitted from one of the Wilson lines, either

$Y_+(0)$ or $Y_-^\dagger(0)$. Therefore, these contributions are proportional to the $e^{iz_-k_1}$ or $e^{iz_-k_2}$ phase factor, depending on whether the emitted power suppressed soft gluon carries soft momentum k_1 or k_2. We sum over all possibilities.

In the following three lines, we encounter the contribution which describes both of the soft gluons originating from the soft gauge field $\mathcal{B}_{\mu_\perp}^+(z_-)$. In this case the Wilson lines which multiply the soft building block are set to unity. This contribution is proportional to $e^{iz_-(k_1+k_2)}$, since both of the emissions originate from the power suppressed building block at the position z_-^μ.

The last four lines of the expression is equation (6.2) correspond to the case where a single soft gluon with a total momentum $k_1 + k_2$ is emitted from the soft gauge field $\mathcal{B}_{\mu_\perp}^+(z_-)$ and which subsequently splits into two final state gluons with momenta k_1 and k_2. As for the previous contribution, these terms are proportional to $e^{iz_-(k_1+k_2)}$.

Naturally, we must consider all possible soft states which cross the cut in (5.3). In addition to the matrix element with two gluons given above, we must also consider the cases where two soft quarks and two ghosts cross the cut. Both of these terms are similar to the contribution of the single soft gluon emitted from $\mathcal{B}_{\mu_\perp}^+(z_-)$ which then splits into two gluons, as given in the last three lines of the $\langle g^{K_1}(k_1)g^{K_2}(k_2)|\mathbf{T}\left[Y_-^\dagger(0)Y_+(0)\frac{i\partial_\perp^\mu}{in_-\partial}\mathcal{B}_{\mu_\perp}^+(z_-)\right]|0\rangle$ matrix element above. Instead of splitting into two gluons, the single gluon emitted from $\mathcal{B}_{\mu_\perp}^+(z_-)$ can also split into a quark-antiquark pair, and also into a pair of ghosts. The individual partons carry away momenta k_1 and k_2. These matrix elements are also proportional to $e^{iz_-(k_1+k_2)}$. Explicitly, we require

$$
\begin{aligned}
\langle q(k_1)\bar{q}(k_2)|\mathbf{T}\left[Y_-^\dagger(0)Y_+(0)\frac{i\partial_\perp^\mu}{in_-\partial}\mathcal{B}_{\mu_\perp}^+(z_-)\right]|0\rangle \;=\;& g_s^2\frac{1}{(n_-(k_1+k_2))^2}\mathbf{T}^B \\
&\times\left(n_-(k_1+k_2)(k_{1\perp\nu}+k_{2\perp\nu})-(k_{1\perp}+k_{2\perp})^2 n_{-\nu}\right) \\
&\times\frac{1}{(k_1+k_2)^2}\bar{u}(k_1)\mathbf{T}^B\gamma^\nu v(k_2)\,e^{iz_-(k_1+k_2)}
\end{aligned}
\tag{6.3}
$$

and

$$
\begin{aligned}
\langle c^{K_1}(k_1)\bar{c}^{K_2}(k_2)|\mathbf{T}\left[Y_-^\dagger(0)Y_+(0)\frac{i\partial_\perp^\mu}{in_-\partial}\mathcal{B}_{\mu_\perp}^+(z_-)\right]|0\rangle \;=\;& g_s^2\frac{1}{(n_-(k_1+k_2))^2}if^{K_1BK_2}\mathbf{T}^B \\
&\times\left(n_-(k_1+k_2)(k_{1\perp\nu}+k_{2\perp\nu})-(k_{1\perp}+k_{2\perp})^2 n_{-\nu}\right) \\
&\times\frac{1}{(k_1+k_2)^2}k_1^\nu\,e^{iz_-(k_1+k_2)}\,.
\end{aligned}
\tag{6.4}
$$

Next, according to (5.3), the above amplitudes need to be interfered with the leading power amplitudes on the conjugate side of the cut. Hence, we require the expression for absorption of two partons by two Wilson lines. First, for two incoming gluons we have the following

$$
\begin{aligned}
\langle 0|\bar{\mathbf{T}}\left[Y_+^\dagger(0)Y_-(0)\right]|g^{K_1}(k_1)g^{K_2}(k_2)\rangle \;=\;& \\
g_s^2\,n_-^{\eta_1}n_-^{\eta_2}\left(\frac{1}{n_-k_2}\frac{1}{n_-(k_1+k_2)}\mathbf{T}^{K_2}\,\mathbf{T}^{K_1}\right.& \left.+\frac{1}{n_-k_1}\frac{1}{n_-(k_1+k_2)}\mathbf{T}^{K_1}\,\mathbf{T}^{K_2}\right)\epsilon_{\eta_1}(k_1)\epsilon_{\eta_2}(k_2)
\end{aligned}
$$

$$+g_s^2\, n_+^{\eta_1} n_+^{\eta_2} \left(\frac{1}{n_+k_2}\frac{1}{n_+(k_1+k_2)}\mathbf{T}^{K_1}\mathbf{T}^{K_2} + \frac{1}{n_+k_1}\frac{1}{n_+(k_1+k_2)}\mathbf{T}^{K_2}\mathbf{T}^{K_1} \right)\epsilon_{\eta_1}(k_1)\epsilon_{\eta_2}(k_2)$$

$$+g_s^2\, \left(-n_-^{\eta_1} n_+^{\eta_2}\frac{1}{n_-k_1}\frac{1}{n_+k_2}\mathbf{T}^{K_1}\mathbf{T}^{K_2} - n_+^{\eta_1} n_-^{\eta_2}\frac{1}{n_+k_1}\frac{1}{n_-k_2}\mathbf{T}^{K_2}\mathbf{T}^{K_1} \right)\epsilon_{\eta_1}(k_1)\epsilon_{\eta_2}(k_2)$$

$$-g_s^2\left(i\, f^{K_1 K_2 K}\,\mathbf{T}^K \right)\frac{1}{n_-(k_1+k_2)}\frac{1}{(k_1+k_2)^2}$$

$$\times\left(-n_-^{\eta_1}(2k_1+k_2)^{\eta_2} + g^{\eta_1\eta_2}\, n_-(k_1-k_2) + n_-^{\eta_2}(2k_2+k_1)^{\eta_1} \right)\epsilon_{\eta_1}(k_1)\epsilon_{\eta_2}(k_2)$$

$$+g_s^2\left(i\, f^{K_1 K_2 K}\,\mathbf{T}^K \right)\frac{1}{n_+(k_1+k_2)}\frac{1}{(k_1+k_2)^2}$$

$$\times\left(-n_+^{\eta_1}(2k_1+k_2)^{\eta_2} + g^{\eta_1\eta_2}\, n_+(k_1-k_2) + n_+^{\eta_2}(2k_2+k_1)^{\eta_1} \right)\epsilon_{\eta_1}(k_1)\epsilon_{\eta_2}(k_2). \quad (6.5)$$

The top two lines describe the capture of two emitted gluons directly by the $Y_+^\dagger(0)$ and $Y_-(0)$ Wilson lines respectively. The third line, describes the capture of one of the soft gluons by $Y_+^\dagger(0)$ and the other by $Y_-(0)$. The following two lines describe two soft gluons combining into a single one via a triple gluon vertex. The gluon formed by the incoming two is then captured by the $Y_+^\dagger(0)$ Wilson line. In the last two lines we have a corresponding term where the formed gluon is captured by $Y_-(0)$ Wilson line.

Similarly to the last four lines of the expression in (6.5), where two gluons combine to a single one which is subsequently captured by the Wilson lines, we have non vanishing leading power matrix elements with soft quarks and soft ghosts. These partons again interact with a single soft gluon which then is captured by one of the Wilson lines. Explicitly, the relevant expressions are

$$\langle 0|\bar{\mathbf{T}}\left[Y_+^\dagger(0)Y_-(0) \right]|q(k_1)\bar{q}(k_2)\rangle = g_s^2\,\mathbf{T}^A\frac{1}{(k_1+k_2)^2}$$

$$\times\left(-\frac{n_{+\nu}}{n_+(k_1+k_2)} + \frac{n_{-\nu}}{n_-(k_1+k_2)} \right)\bar{v}(k_2)\mathbf{T}^A\gamma^\nu u(k_1) \quad (6.6)$$

and

$$\langle 0|\bar{\mathbf{T}}\left[Y_+^\dagger(0)Y_-(0) \right]|c^{K_1}(k_1)\bar{c}^{K_2}(k_2)\rangle = g_s^2 i f^{K_1 K_2 A}\,\mathbf{T}^A$$

$$\times\left(\frac{n_+k_2}{n_+(k_1+k_2)} - \frac{n_-k_2}{n_-(k_1+k_2)} \right)\frac{1}{(k_1+k_2)^2}. \quad (6.7)$$

Now we are in possession of all the necessary two parton matrix elements. In the next step of the calculation, these are combined according to (5.3) in the same way as at the next-to-leading order. We do not provide the full interfered expressions here, simply due to their size. Indeed, to render the calculation practically viable, we employ IBP relations to reduce the calculation to the minimal set of master integrals which need to be computed. In section 6.3 we motivate and describe this procedure on a specific example and provide the expressions for S_1 in terms of the master integrals. As can be seen by the appearance of both $e^{iz_-k_1}$ and $e^{iz_-(k_1+k_2)}$ factors in the matrix element expression in (6.2), the S_1 soft function is described by integrals with $\delta(\omega - n_-k_1)$ and $\delta(\omega - n_-k_1 - n_-k_2)$ constraints. We denote the contributions to the real-real S_1 soft functions due to integrals with a
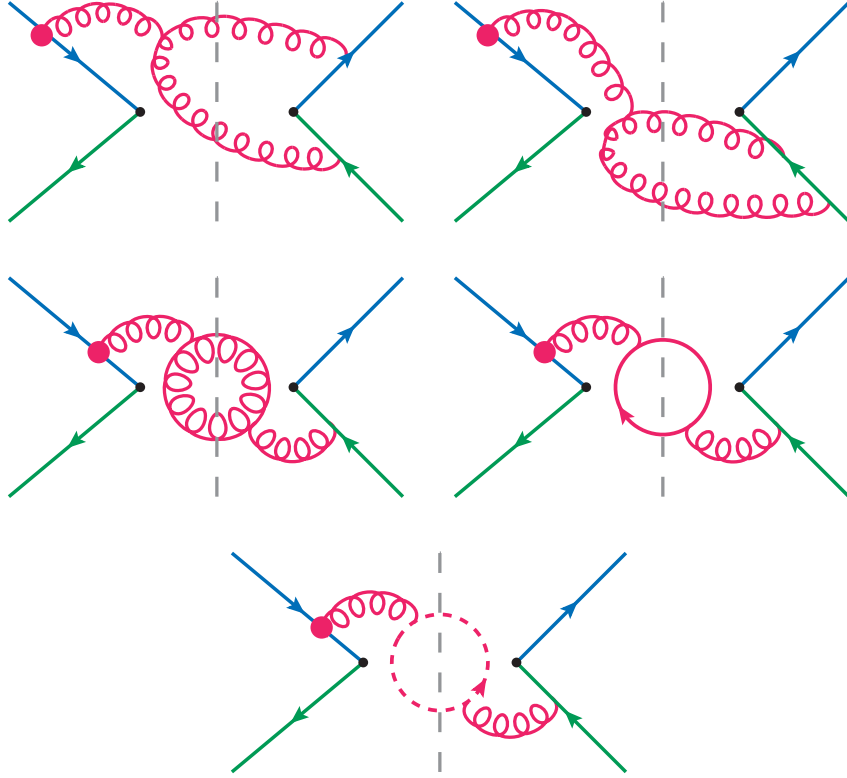
Figure 6.1:　*Sample diagrams showing a subset of the contributing expressions after the interference of the next-to-leading power matrix elements with their leading power counterparts. Not all contributions are depicted here.*

$\delta(\omega - n_- k_1)$ constraint by $S_1^{(2)2r0v}(\Omega, \omega)^{\delta(\omega - n_- k_1)}$. The relevant expressions are presented in section 6.3.1. Similarly, the contributions to the real-real S_1 soft function made from integrals with a $\delta(\omega - n_- k_1 - n_- k_2)$ constraint, are labelled by $S_1^{(2)2r0v}(\Omega, \omega)^{\delta(\omega - n_- k_1 - n_- k_2)}$ and given in section 6.3.2.

　　Thus far, we have only provided analytic expressions for the objects which we calculate, however, we find it instructive to also show the contributions as diagrams which survive the interference of the matrix elements. We provide a small subset of the contributions in figure 6.1. These diagrams are meant to help to visualise the above discussion, but are not exhaustive. For example, we can identify the left diagram in the top row of figure 6.1 as the part of the matrix element in (6.2) which describes single soft power suppressed gluon emission from the soft building block that splits into two gluons, interfered with the third line of the leading power matrix element in (6.5).

6.2.2　S_3 soft function

We now turn our attention to the S_3 soft function defined in (3.85). We write this soft function here again for convenience, with the position of the Wilson lines translated as in (5.3) for the S_1 soft function

$$S_3(\Omega, \omega) \;=\; \sum_{X_s} \int \frac{d(n_+ z)}{4\pi} \, e^{-i\omega\, n_+ z/2} \, \delta(\Omega - 2E_{X_s}) \frac{1}{N_c} \mathrm{Tr}\langle 0| \bar{\mathbf{T}} \left[Y_+^\dagger(0) Y_-(0) \right] |X_s\rangle$$
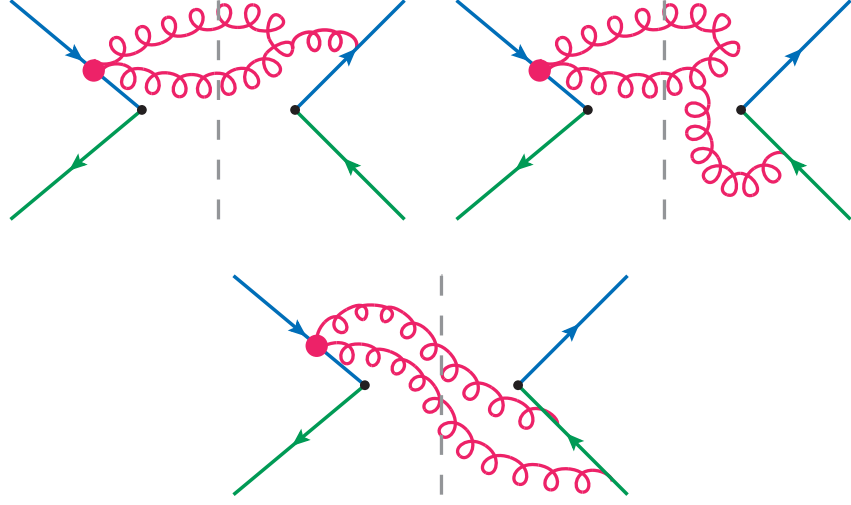
Figure 6.2: *The cross-section level diagrams for the S_3 soft function. Both of the soft gluons are emitted from the power suppressed soft building block represented here by the red dot.*

$$\times \langle X_s | \mathbf{T} \left(\left[Y_-^\dagger(0) Y_+(0) \right] \frac{1}{(in_- \partial)^2} \left[\mathcal{B}^{+\,\mu_\perp}(z_-), \left[in_- \partial \mathcal{B}_{\mu_\perp}^+(z_-) \right] \right] \right) |0\rangle. \quad (6.8)$$

We have already given the necessary expression for the leading power matrix element in section 6.2.1 above. The power suppressed soft building block characterising S_3 contains two explicit $\mathcal{B}^+$ fields, hence at $\mathcal{O}(\alpha_s^2)$ the state $\langle X_s |$ must contain two soft gluons. The result we require is

$$\langle g^{K_1}(k_1) g^{K_2}(k_2) | \mathbf{T} \left(\left[Y_-^\dagger(0) Y_+(0) \right] \frac{1}{(in_- \partial)^2} \left[\mathcal{B}^{+\,\mu_\perp}(z_-), \left[in_- \partial \mathcal{B}_{\mu_\perp}^+(z_-) \right] \right] \right) |0\rangle$$

$$= g_s^2 i f^{K_1 K_2 K} \mathbf{T}^K \frac{1}{(n_-(k_1 + k_2))^2} \left[(n_- k_1 - n_- k_2) g_\perp^{\eta_1 \eta_2} \right.$$

$$+ \frac{(n_- k_2)}{(n_- k_1)} k_{1\perp}^{\eta_2} n_-^{\eta_1} - \frac{(n_- k_1)}{(n_- k_2)} k_{2\perp}^{\eta_1} n_-^{\eta_2} + k_{2\perp}^{\eta_1} n_-^{\eta_2} - k_{1\perp}^{\eta_2} n_-^{\eta_1}$$

$$- \left. \left(\frac{k_{1\perp} \cdot k_{2\perp}}{n_- k_1} - \frac{k_{1\perp} \cdot k_{2\perp}}{n_- k_2} \right) n_-^{\eta_1} n_-^{\eta_2} \right] \epsilon_{\eta_1}^*(k_1) \epsilon_{\eta_2}^*(k_2) e^{iz_-(k_1 + k_2)}. \quad (6.9)$$

This expression is much simpler than the S_1 counterpart in (6.2) due to the fact that Wilson lines here can be set to unity as the emission of soft gluons must occur from the $\mathcal{B}^+$ fields.

Since the expression in (6.9) is only proportional to the $e^{iz_-(k_1+k_2)}$ factor, the ω dependent delta function in the relevant integrals yielding S_3 is $\delta(\omega - n_- k_1 - n_- k_2)$. We provide the representation of the interference in (6.8) in terms of diagrams in figure 6.1 and the reduced cross-section level expression in section 6.3.2.
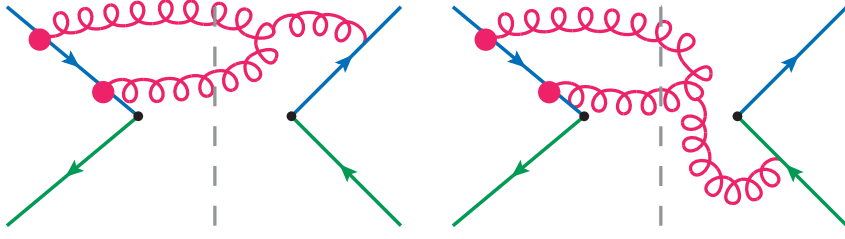
Figure 6.3:   *Diagrams with $\mathcal{O}(\lambda)$ power suppressed interactions inserted at two different positions z_{1-} and z_{2-}. These diagrams contain insertions of the $\mathcal{L}_\xi^{(1)}$ Lagrangian and contribute to the S_4 soft function defined in equation (3.86). The corresponding two loop integrals contain $\delta(\omega_1 - n_- k_1)\delta(\omega_2 - n_- k_2)$ constraints.*
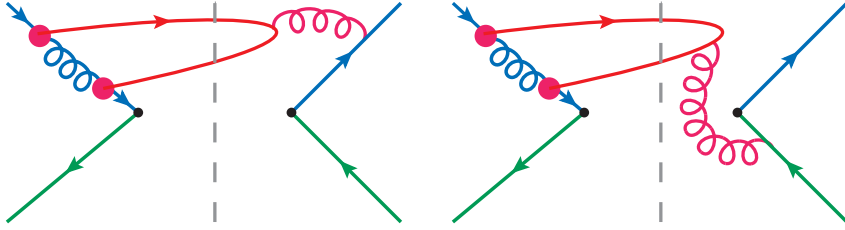
Figure 6.4:   *Similarly to figure 6.3, these diagrams contain two $\mathcal{O}(\lambda)$ power suppressed interactions at two different positions z_{1-} and z_{2-}. However, here we consider two insertions of the $\mathcal{L}_{\xi q}^{(1)}$ Lagrangian with two soft quarks travelling across the cut. These diagrams correspond to the soft function S_5 in equation (3.87). The relevant integrals contain $\delta(\omega_1 - n_- k_1)\delta(\omega_2 - n_- k_2)$ constraints in the integrands.*

6.2.3 S_4 and S_5 soft functions

Lastly, we consider the contributions to the soft functions S_4 and S_5 in equations (3.86) and (3.87) respectively. These soft functions contain two $\mathcal{O}(\lambda)$ power suppressed insertions at two different positions. Therefore, the corresponding soft matrix elements are proportional to $e^{iz_{1-}k_1}\, e^{iz_{2-}k_2}$, which gives rise to the $\delta(\omega_1 - n_- k_1)\delta(\omega_2 - n_- k_2)$ dependence of the integrals which appear for these contributions. In contrast to the calculation of the S_1 and S_3 soft functions, we calculate the contributions to S_4 and S_5 using the momentum-space NLP Feynman rules since the collinear functions in chapter 4 were already obtained by stripping off the corresponding soft dependence from the NLP Feynman diagrams.

The diagrams contributing to the S_4 soft function are shown in figure 6.3 and the diagrams relevant for S_5 can be found in figure 6.4. In both of these figures, the red dots correspond to a $\mathcal{O}(\lambda)$ suppressed interaction, in contrast to the previous figures where the power suppressed interactions are at $\mathcal{O}(\lambda^2)$.

As we have found in chapter 4, the tree-level collinear functions corresponding to these soft functions are rather complicated objects with many open indices. Specifically, the relevant equations are (4.24) and (4.26) for collinear functions $J_{4;\gamma\beta,fb}^{\mu\nu,AB\,(0)}$ and $J_{5;\gamma\sigma\lambda\beta}^{fk_1k_2e\,(0)}$ respectively. Since we perform this investigation at fixed α_s order and only require the collinear functions at tree-level accuracy, we can redefine the collinear functions to be much simpler multiplicative factors and absorb the remaining pieces into the soft functions which we calculate using the next-to-leading power Feynman rules.

To be precise, in the following we recast the $J_{4;\gamma\beta,fb}^{\mu\nu,AB\,(0)}$ and $J_{5;\gamma\sigma\lambda\beta}^{fk_1k_2e\,(0)}$ collinear functions as

$$J_{4;\gamma\beta,fb}^{\mu\nu,AB\,(0)} \to J_4 = \frac{1}{n_+p}, \tag{6.10}$$

and

$$J_{5;\gamma\sigma\lambda\beta}^{fk_1k_2e\,(0)} \to J_5 = \frac{1}{n_+p}, \tag{6.11}$$

which implicitly defines the corresponding soft functions.

One more remark is necessary regarding the S_5 soft function with two insertions of the $\mathcal{L}_{\xi q}$ term of the next-to-leading power Lagrangian. This soft function has open Dirac indices which connect to the spin structure describing the Drell-Yan current and PDFs, namely the $\left[\left(\frac{\not n_-}{4}\right)\gamma_{\perp\rho}\left(\frac{\not n_+}{4}\right)\gamma_\perp^\rho\right]_{\beta\gamma}$ factor in the first line of the factorisation theorem given in equation (3.81). To simplify the calculations, we move this factor inside of the soft function forming a trace over the terms which contain a Dirac structure.

6.3   Reduction of the integrals

As explained above, we organise the calculation according to the deduced ω, (ω_1, ω_2), dependent delta function structure present in the two-loop integrals describing the $\mathcal{O}(\alpha_s^2)$ NLP soft functions.

The two loop integrals involve integrating over the radiated soft momentum, which as mentioned we labelled k_1 and k_2. Therefore, naturally, the delta functions discussed above do not appear in the final answer for the soft functions, but rather are present in the integrands of the relevant integrals and serve to identify the n_-k_i components of the momentum with the soft variable ω_i. The delta functions help us to organise the calculation, as it is naturally separated into three families of integrals each with integrand dependence on one of the above delta functions. Therefore, in the following subsections we separate the contributions according to the delta function structure which appears in the master integrals.

The matrix elements and diagrams contributing to the next-to-next-to-leading order soft functions are given above. As explained, due to the size of the expressions, we do not provide here the raw corresponding expressions obtained by combining the pieces presented above. In fact, in order to render the calculation itself manageable, we employ the IBP integral reduction technique. This technique is widely used in multi-loop Feynman integral calculations and we briefly describe the key principles below.

Just before we jump into this discussion, we motivate the need of employing these IBP techniques on a specific example of a diagram appearing in our calculation. Namely, we consider the gluon-gluon cut gluon bubble diagram shown in figure 6.1 and draw again for convenience in figure 6.5. This diagram is formed by the last three lines of the matrix element expression given in (6.2) interfered with the last two lines of (6.5). Writing down the cross-section level expression for this term in momentum space yields the following result

$$S_1^{(2)}\left(\Omega,\omega\right)_{fig:6.5} = \frac{1}{2}g_s^4 C_F C_A \int \frac{d^dk_1}{(2\pi)^d}\int \frac{d^dk_2}{(2\pi)^d}\left(-2\pi\delta(k_1^2)\theta(k_1^0)\right)\left(-2\pi\delta(k_2^2)\theta(k_2^0)\right)$$
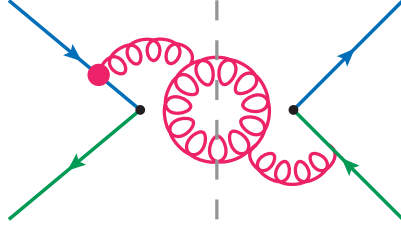
Figure 6.5: *One of the diagrams in figure 6.1 contributing to the S_1 soft function. We present it here again singled out for the purpose an example of integration-by-parts relations. The expression for this diagram obtained using next-to-leading power Feynman rules is given in equation* (6.12).

$$
\times \delta(\Omega - n_- k_1 - n_+ k_1 - n_- k_2 - n_+ k_2)\delta(\omega - n_- k_1 - n_- k_2)
$$

$$
\times \left(- \frac{1}{n_+(k_1+k_2)} \frac{1}{(k_1+k_2)^4} \frac{1}{(n_-(k_1+k_2))^2} \right)
$$

$$
\times \left\{ (k_{1\perp} + k_{2\perp})^2 \left[-4(k_1+k_2)^2 + n_-(2k_1+k_2)n_+(k_1+2k_2) \right. \right.
$$

$$
\left. + n_+(2k_1+k_2)n_-(k_1-k_2) \right] - n_-(k_1+k_2)\left[n_+(k_1+2k_2)\left(2k_{1\perp}^2 \right. \right.
$$

$$
\left. \left. + 3k_{1\perp} \cdot k_{2\perp} + k_{2\perp}^2 \right) + n_+(2k_1+k_2)\left(k_{1\perp}^2 - k_{2\perp}^2 \right) \right]
$$

$$
+ n_+(k_1-k_2)\left[(1-d)n_-(k_1-k_2)\left(k_{1\perp} + k_{2\perp} \right)^2 + n_-(k_1+k_2)\left(k_{2\perp}^2 \right. \right.
$$

$$
\left. \left. - k_{1\perp}^2 + d\left(k_{1\perp}^2 - k_{2\perp}^2 \right) \right) \right] + (k_{1\perp} + k_{2\perp})^2 \left[n_-(2k_2+k_1)n_+(2k_1+k_2) \right.
$$

$$
\left. - 4(k_1+k_2)^2 - n_+(k_1+2k_2)n_-(k_1-k_2) \right]
$$

$$
+ n_-(k_1+k_2)\left[- n_+(2k_1+k_2)\left(k_{1\perp}^2 + 3k_{1\perp} \cdot k_{2\perp} + 2k_{2\perp}^2 \right) \right.
$$

$$
\left. \left. + n_+(k_1+2k_2)\left(k_{1\perp}^2 - k_{2\perp}^2 \right) \right] \right\}, \tag{6.12}
$$

where the $1/2$ in the first line is a symmetry factor for the diagram, and we have already performed the colour trace yielding the $C_F C_A$ factor. The subscript on $S_1^{(2)}(\Omega, \omega)_{fig:6.5}$ denotes the fact that this expression is the contribution to the $S_1^{(2)}$ soft function due to matrix element terms represented by figure 6.5.

The usefulness of reduction techniques can be seen by comparing the above large expression to the result in equation (6.13) below, which gives the result for the same diagram but now in terms of a reduced set of integrals. In fact, it turns out that only one master integral needs to be computed. After reduction we find

$$
S_1^{(2)}(\Omega, \omega)_{fig:6.5} = C_F C_A \frac{(1-\epsilon)(19-12\epsilon)}{2\epsilon(3-2\epsilon)\,\omega^2\,(\Omega-\omega)}\, I_6 \,. \tag{6.13}
$$

The expression for I_6 is given in equation (6.30). This is the only integral which needs to

be computed in practice in order to find a result for the diagram in figure 6.5.

The diagram in figure 6.5 contains two triple gluon interactions, hence it is one of the terms with one of the most complicated numerator structures in the calculation. However, we find that application of IBP relations also simplifies the calculation of the remaining contributions.

Having showcased the appeal of reduction techniques to our calculation, we now explain the principles on a simpler example. The IBP method begins with the realisation that in dimensional regularization the integral of a total derivative vanishes

$$\int d^d k_1 \ldots d^d k_l \, \frac{\partial}{\partial k_i^\mu} \, \frac{v^\mu}{D_1^{n_1} \ldots D_k^{n_k}} = 0, \tag{6.14}$$

which produces linear relations between the integrals [140, 141]. In the above equation, k_i are loop momenta, D_i are propagators raised to some power n_i, and v^μ is an arbitrary vector. The idea is that IBP identities can be applied systematically to yield algebraic relations between the numerous integrals that are present in a calculation, which reduces the number of integrals that have to be calculated. One of the most successful IBP reduction methods in the Laporta algorithm [143] which is implemented in many computer programs which automatise the IBP reduction. In the end, we are left with a smallest set of integrals which have to be computed and these integrals are the so-called "master" integrals.

For concreteness, let us consider a simple example of a single loop massless triangle diagram, that is, containing three propagators which are raised to arbitrary powers α, β, and γ. We define

$$A_{\alpha\beta\gamma} = \int \frac{d^d k}{(2\pi)^d} \, \frac{1}{D_1^\alpha \, D_2^\beta \, D_3^\gamma} \tag{6.15}$$

with external momenta $p_1^2 = p_2^2 = 0$ and $p_3^2 = s$ and the propagators given by

$$D_1 = k^2, \qquad D_2 = (k + p_1)^2, \qquad D_3 = (k + p_1 + p_2)^2. \tag{6.16}$$

The IBP identities yield the following relations between the integrals $A_{\alpha\beta\gamma}$

$$(d - 4)A_{111} - A_{102} - A_{201} = 0, \tag{6.17}$$

$$s \, A_{102} + (d - 3)A_{101} = 0, \tag{6.18}$$

$$s \, A_{201} + (d - 3)A_{101} = 0. \tag{6.19}$$

Therefore, we see that in order to obtain a result for the triangle diagram with three propagators, A_{111}, the integral which actually has to be performed is a simpler bubble diagram with only two propagators, and that the A_{111} integral is related to the simpler integral through

$$A_{111} = \frac{-2(d - 3)}{s \, (d - 4)} \, A_{101} \,. \tag{6.20}$$

The IBP reduction techniques were developed for calculation of higher loop virtual diagrams in QCD. Hence, most publicly available codes cannot be blindly applied out of the

box. Indeed, there are two complications with which we must deal in order to apply these techniques to the calculation of the two-loop soft functions at hand. Firstly, the calculation in SCET contains linear propagators originating from Wilson lines, see section 2.1. And secondly, this is not a two-loop virtual calculation, but rather a calculation of two real emitted partons, therefore we must deal with phase-space constraints. A number of publicly available packages can overcome these obstacles and be applied our problem. We chose to use the `LiteRed` package [144, 145] to perform the integral reduction. Regarding the first issue, `LiteRed` simply allows for construction of linear propagators. As for the second issue, the delta functions constraining the phase-space can be handled using an internal function in `LiteRed` which enables us to implement cut propagators. This method relies on reverse unitarity [146]. Reverse unitarity allows us to write the phase-space integrals as loop integrals, by identifying the phase-space constraining delta functions with the difference of propagators as dictated by the equation

$$\frac{1}{k^2 + i\delta} - \frac{1}{k^2 - i\delta} = -2\pi\, i\, \delta\left(k^2\right)\ . \tag{6.21}$$

There are two remarks to make regarding this implementation. First, we note that some codes used for reduction of integrals such as `FIRE` [147] and `REDUZE` [148] do not distinguish between different $i\delta$ prescriptions which can yield spurious contributions. However, we have applied the cut propagator command in `LiteRed` which behaves as expected. Secondly, we note that virtual loop integrals do not have $\theta(k_1^0)$ like constraints on the energy of the partons crossing the cut. This fact is not problematic, as it has been shown that application of IBP reduction algorithms and application of cuts commutes [146]. Hence, we can apply the reduction techniques to arrive at a set of master integrals, and compute them with the appropriate constraints. For example, see the $\theta(k_1^0)\theta(k_2^0)$ structure in (6.23).

With this, we are now in a position to present the results for matrix elements and the expressions for the diagrams shown in the above figures in terms of the small set of eight master integrals. We separate the presentation of these results into three sections, according to the ω dependent delta function structure in the corresponding master integrals.

6.3.1 $\delta(\omega - n_- k_1)$

We begin with the reduced expressions for the contributions to the S_1 soft function which are characterised by a single soft gluon emission from the power suppressed soft building block and another from one of the soft Wilson lines, as explained in section 6.2.1. The below expression is obtained by interfering the top four lines of equation (6.2) with (6.5), and reducing the result to a set of master integrals. We find

$$
\begin{aligned}
S_1^{(2)2r0v}(\Omega, \omega)^{\delta(\omega - n_- k_1)} \;=\; & C_F^2 \frac{8\left(2 - 9\epsilon + 9\epsilon^2\right)}{\epsilon^2\, \omega\, (\Omega - \omega)^2}\, \mathrm{I}_1 \\[2mm]
& + C_F C_A \Bigg[\frac{(2 - 3\epsilon)\left(-4\Omega + \epsilon\left(\omega + 19\Omega\right) + 4\epsilon^2\left(\omega - 7\Omega\right) - 16\epsilon^3(\omega - \Omega)\right)}{\epsilon^2(1 - 2\epsilon)\, \omega\, \Omega\, (\Omega - \omega)^2}\, \mathrm{I}_1 \\[2mm]
& - \frac{(1 - 4\epsilon^2)}{\epsilon\, \omega\, \Omega}\mathrm{I}_2 + \frac{\left(3\Omega - 10\epsilon\, \Omega + 16\epsilon^2(\omega + \Omega)\right)}{2(1 - 2\epsilon)\, \omega\, \Omega}\mathrm{I}_3
\end{aligned}
$$

$$+\frac{(\Omega - 3\omega)}{2\omega} I_4 + \Omega I_5 \Bigg],$$
(6.22)

where the master integrals I_i appearing in the above expression are given by

$$I_1 = g_s^4 \int \frac{d^d k_1}{(2\pi)^d} \int \frac{d^d k_2}{(2\pi)^d} \left(-2\pi\delta(k_1^2)\theta(k_1^0) \right) \left(-2\pi\delta(k_2^2)\theta(k_2^0) \right)$$
$$\times \delta(\Omega - n_- k_1 - n_+ k_1 - n_- k_2 - n_+ k_2)\delta(\omega - n_- k_1),$$
(6.23)

$$I_2 = g_s^4 \int \frac{d^d k_1}{(2\pi)^d} \int \frac{d^d k_2}{(2\pi)^d} \left(-2\pi\delta(k_1^2)\theta(k_1^0) \right) \left(-2\pi\delta(k_2^2)\theta(k_2^0) \right)$$
$$\times \frac{1}{(n_-(k_1+k_2))}\delta(\Omega - n_- k_1 - n_+ k_1 - n_- k_2 - n_+ k_2)\delta(\omega - n_- k_1),$$
(6.24)

$$I_3 = g_s^4 \int \frac{d^d k_1}{(2\pi)^d} \int \frac{d^d k_2}{(2\pi)^d} \left(-2\pi\delta(k_1^2)\theta(k_1^0) \right) \left(-2\pi\delta(k_2^2)\theta(k_2^0) \right)$$
$$\times \frac{1}{(k_1+k_2)^2}\delta(\Omega - n_- k_1 - n_+ k_1 - n_- k_2 - n_+ k_2)\delta(\omega - n_- k_1),$$
(6.25)

$$I_4 = g_s^4 \int \frac{d^d k_1}{(2\pi)^d} \int \frac{d^d k_2}{(2\pi)^d} \left(-2\pi\delta(k_1^2)\theta(k_1^0) \right) \left(-2\pi\delta(k_2^2)\theta(k_2^0) \right) \frac{1}{(n_+ k_2)}$$
$$\times \frac{1}{(k_1+k_2)^2}\delta(\Omega - n_- k_1 - n_+ k_1 - n_- k_2 - n_+ k_2)\delta(\omega - n_- k_1),$$
(6.26)

$$I_5 = g_s^4 \int \frac{d^d k_1}{(2\pi)^d} \int \frac{d^d k_2}{(2\pi)^d} \left(-2\pi\delta(k_1^2)\theta(k_1^0) \right) \left(-2\pi\delta(k_2^2)\theta(k_2^0) \right) \frac{1}{(n_+ k_2)} \frac{1}{(k_1+k_2)^2}$$
$$\times \frac{1}{(n_-(k_1+k_2))}\delta(\Omega - n_- k_1 - n_+ k_1 - n_- k_2 - n_+ k_2)\delta(\omega - n_- k_1).$$
(6.27)

We see explicitly now the dependence on $\delta(\omega - n_- k_1)$. The calculation of these master integrals and the corresponding results are provided in section 6.4.1.

6.3.2 $\delta(\omega - n_- k_1 - n_- k_2)$

We now give the reduced expressions for contributions to S_1 and S_3 which depend on master integrals with a $\delta(\omega - n_- k_1 - n_- k_2)$ constraint. For S_1, this contribution does not only include the interference of $e^{iz_-\cdot(k_1+k_2)}$ proportional terms in (6.2) with the leading power two gluon matrix element in (6.5), but rather, in addition, the soft quark and soft ghost contributions in the matrix elements in (6.3) and (6.4).

The expression for S_3 is obtained by interfering (6.8) with (6.5). We do not label the S_3 soft function with a $\delta(\omega - n_- k_1 - n_- k_2)$ superscript as this is its only contribution.

Most of the terms forming the S_1 soft function give rise to $C_F C_A$ colour structure, with the exception of the piece where the soft gluon splits into a soft quark-antiquark pair which is proportional to $C_F n_f$ where n_f is the number of flavours. Concretely, we find

$$S_1^{(2)2r0v}(\Omega,\omega)^{\delta(\omega-n_-k_1-n_-k_2)} = C_F C_A \left[\frac{9 - 20\epsilon + 12\epsilon^2 - 2\epsilon^3}{\epsilon^2 (3 - 2\epsilon)\omega^2(\Omega - \omega)} I_6 + (\Omega - \omega)I_7 \right]$$

$$- C_F \, n_f \, \frac{4(1 - \epsilon)^2}{\epsilon \, (3 - 2\epsilon)\omega^2(\Omega - \omega)} \, I_6 \,, \tag{6.28}$$

where we see that two new master integrals I_6 and I_7 appear. These are given in equations (6.30) and (6.31) respectively. For the S_3 soft function we find

$$S_3^{(2)}(\Omega,\omega) = C_F C_A \frac{2(1 - \epsilon)}{(3 - 2\epsilon)\omega^2(\Omega - \omega)} I_6 \,. \tag{6.29}$$

The two new master integrals appearing in the above expressions are given by

$$I_6 = g_s^4 \int \frac{d^d k_1}{(2\pi)^d} \int \frac{d^d k_2}{(2\pi)^d} \left(- 2\pi\delta(k_1^2)\theta(k_1^0) \right) \left(- 2\pi\delta(k_2^2)\theta(k_2^0) \right)$$

$$\times \delta(\Omega - n_-k_1 - n_+k_1 - n_-k_2 - n_+k_2)\delta(\omega - n_-k_1 - n_-k_2) \tag{6.30}$$

and

$$I_7 = g_s^4 \int \frac{d^d k_1}{(2\pi)^d} \int \frac{d^d k_2}{(2\pi)^d} \left(- 2\pi\delta(k_1^2)\theta(k_1^0) \right) \left(- 2\pi\delta(k_2^2)\theta(k_2^0) \right) \frac{1}{(k_1 + k_2)^2} \frac{1}{(n_+k_2)}$$

$$\times \frac{1}{(n_-k_1)}\delta(\Omega - n_-k_1 - n_+k_1 - n_-k_2 - n_+k_2)\delta(\omega - n_-k_1 - n_-k_2) \,. \tag{6.31}$$

We see that the I_6 master integral in equation (6.30) is very similar to the I_1 master integral in equation (6.23). They both do not contain any propagators, and hence, are simply integrals over phase-space only. The sole difference is the $\delta(\omega - n_-k_1)$ term in I_1, which is replaced by $\delta(\omega - n_-k_1 - n_-k_2)$ in I_6. The master integral I_7 in equation (6.31) contains a new propagator structure on top of the change in the argument of the $\delta(\omega - n_-k_1 - n_-k_2)$ delta function.

6.3.3 $\delta(\omega_1 - n_-k_1)\delta(\omega_2 - n_-k_2)$

Lastly, we present the results for the diagrams in figures 6.3 and 6.4 which correspond to contributions to the S_4 and S_5 soft functions. As explained above in section 6.2.3, we have redefined the collinear functions for these objects, such that the collinear functions are rendered to be simple multiplicative factors and the complicated ω_1, ω_2 dependence is contained within the soft functions only.

We again find a new master integral, due to the fact that the power suppressed emissions in these diagrams occurs at two different positions z_{1-} and z_{2-} which gives rise to the $\delta(\omega_1 - n_-k_1)\delta(\omega_2 - n_-k_2)$ dependence of the necessary soft integrals.

For the diagrams in figure 6.3 we find

$$S_4^{(2)}(\Omega,\omega_1,\omega_2) = -C_F C_A \frac{2(1 - \epsilon)\omega_2(\omega_1 - \omega_2)}{(\omega_1 + \omega_2)^4(\Omega - \omega_1 - \omega_2)} I_8 \,. \tag{6.32}$$

The soft quark contributions due to $\mathcal{L}_{\xi q}^{(1)}$ Lagrangian insertions in the diagrams in figure 6.4 yields the following expression

$$S_5^{(2)}(\Omega, \omega_1, \omega_2) = \left(C_F^2 - \frac{1}{2}C_F C_A\right) \frac{8(-1 + \epsilon)\omega_2}{(\omega_1 + \omega_2)^3(\Omega - \omega_1 - \omega_2)} I_8, \tag{6.33}$$

with the relevant master integral given by

$$\begin{aligned}
I_8 &= g_s^4 \int \frac{d^d k_1}{(2\pi)^d} \int \frac{d^d k_2}{(2\pi)^d} \left(-2\pi\delta(k_1^2)\theta(k_1^0)\right)\left(-2\pi\delta(k_2^2)\theta(k_2^0)\right) \\
&\quad \times \delta(\Omega - n_- k_1 - n_+ k_1 - n_- k_2 - n_+ k_2)\delta(\omega_1 - n_- k_1)\delta(\omega_2 - n_- k_2).
\end{aligned} \tag{6.34}$$

Similarly to the I_1 and I_6 master integrals given in equations (6.23) and (6.30) respectively, the I_8 master integral does not contain any propagator structure and differs to aforementioned integrals only through the dependence on the ω of the delta function.

6.4 Master integrals

Having obtained the expressions for the two-loop soft functions in terms of a set of master integrals, it now remains only to calculate the master integrals themselves. We do not present full calculation of every master integral as some are lengthy and tedious to write down, but are in general rather straightforward to solve. Instead, we will present one example of an uncomplicated integral, and further describe how the trickier master integrals were calculated. The presentation, as above, is again divided according to the $\delta(\omega - n_- k_1)$, $\delta(\omega - n_- k_1 - n_- k_2)$, and $\delta(\omega_1 - n_- k_1)\delta(\omega_2 - n_- k_2)$ dependence appearing in each master integral.

6.4.1 $\delta(\omega - n_- k_1)$

We begin with the set of master integrals $I_1 - I_5$ given in equations (6.23) – (6.27). As we go down the list, the master integrals get progressively more complicated through the appearance of additional propagators.

Indeed, the leading power soft functions have been previously calculated to a high loop accuracy and for many processes. One could envisage that it is possible to apply similar methods to the next-to-leading power calculation presented here. However, a glace at the complicated structure of the results given below already suggests the additional non-trivial complexity is present in the master integrals containing a constraint on the $n_- k_i$ components of the soft momentum.

The calculation is differential in one more variable than at leading power, which can be seen as having one more scale in the problem. The more scales appear in a calculation the more involved it becomes. The identification of one of the components of loop integration momentum with ω places it on a different footing to the other components. We find that this greatly complicates the calculation of some of the master integrals, in particular I_3, I_4, and I_5. We can see this indirectly, for example, by considering a set of diagrams computed in SCET using the NLP Feynman rules *without* the $\delta(\omega - n_- k_1)$ constraint (equivalent to calculation using the expansion-by-regions method). This set up simply corresponds to the

$J \otimes S$ contribution to the factorisation theorem after the $d\omega$ integral has been performed. In this case, only two master integrals appear in the whole calculation, hinting at the reduced complexity[1]. This would be a perfectly acceptable way to proceed if our aim was to simply reproduce the next-to-next-to-leading order cross-section. However, here we wish to obtain information about the soft functions themselves. Therefore, we must retain the dependence on the ω_i variables.

We begin by outlining the calculation of the I_1 given in equation (6.23). First, the integral is written in components

$$
\begin{aligned}
I_1 \;=\;& g_s^4 \frac{1}{(4\pi)^2} \int_0^\infty d(n_+k_1)d(n_-k_1)d(n_+k_2)d(n_-k_2) \\
&\times \int \frac{d^{d-2}k_{1\perp}}{(2\pi)^{d-2}} \int \frac{d^{d-2}k_{2\perp}}{(2\pi)^{d-2}} \; \delta\Big((n_-k_1)(n_+k_1)+k_{1\perp}^2\Big)\delta\Big((n_-k_2)(n_+k_2)+k_{2\perp}^2\Big) \\
&\times \; \delta(\Omega - n_-k_1 - n_+k_1 - n_-k_2 - n_+k_2)\delta(\omega - n_-k_1)
\end{aligned}
\tag{6.35}
$$

Next, we perform the angular integrals. Followed by the $dk_{1\perp}dk_{2\perp}$ using the $\delta\big((n_-k_1)(n_+k_1)+k_{1\perp}^2\big)$ and $\delta\big((n_-k_2)(n_+k_2)+k_{2\perp}^2\big)$ delta functions. Additionally, setting the dimension to $d = 4 - 2\epsilon$ yields the following expression

$$
\begin{aligned}
I_1 \;=\;& g_s^4 \frac{1}{(4\pi)^2} \int_0^\infty d(n_+k_1)d(n_-k_1)d(n_+k_2)d(n_-k_2) \frac{1}{\Gamma[1-\epsilon]^2} \frac{1}{(4\pi)^{2-2\epsilon}} \Big(n_-k_1 n_+k_1\Big)^{-\epsilon} \\
&\times \Big(n_-k_2 n_+k_2\Big)^{-\epsilon} \; \delta(\Omega - n_-k_1 - n_+k_1 - n_-k_2 - n_+k_2)\delta(\omega - n_-k_1)
\end{aligned}
\tag{6.36}
$$

Next we perform the dn_+k_1 and dn_-k_1 integrals using the two remaining delta functions, the leftover theta functions set the upper limits on the last two integrals. These can be performed using equation (A.2). The final result for I_1 in equation (6.23) is

$$
I_1 = \frac{\alpha_s^2}{(4\pi)^2} \frac{\mu^{4\epsilon}}{\omega^\epsilon} (\Omega - \omega)^{2-3\epsilon} \frac{e^{2\epsilon\gamma_E}\Gamma[1-\epsilon]}{\Gamma[3-3\epsilon]} \; \theta(\Omega - \omega)\,\theta(\omega)\,.
\tag{6.37}
$$

The remaining integrals are more difficult to calculate directly. However, we found that they form a system of coupled differential equations which enables us to obtain the necessary results. To be precise, by implicitly defining a dimensionless variable, $\omega = r\,\Omega$, we found the following relation between the master integrals I_1 and I_2, and master integrals I_1 and I_3

$$
\left(\frac{\mu}{\Omega}\right)^{-4\epsilon} \Omega^{-1} \frac{d}{dr} I_2 \;=\; \frac{(2-3\epsilon)}{(r-1)r} I_1 - \frac{2\epsilon}{r} I_2,
\tag{6.38}
$$

$$
\left(\frac{\mu}{\Omega}\right)^{-4\epsilon} \frac{d}{dr} I_3 \;=\; \frac{(2-9\epsilon(1-\epsilon))}{\epsilon(r-1)^2 r} I_1 - \frac{2\epsilon}{r} I_3\,.
\tag{6.39}
$$

Next, we find that I_4 is related to I_1 and I_3 through the following differential equation linking all three

$$
\left(\frac{\mu}{\Omega}\right)^{-4\epsilon} \Omega \frac{d}{dr} I_4 \;=\; \frac{(2-9\epsilon(1-\epsilon))}{\epsilon(r-1)^3 r} I_1 + \frac{2\epsilon}{(r-1)r} I_3 - \frac{(1+4\epsilon)}{(r-1)} I_4\,.
\tag{6.40}
$$

---

[1]For a direct example see the discussion below equation (6.56).

Lastly, the differential equation for I_5 links together the I_1, I_3, and I_4 master integrals. It is given by

$$\left(\frac{\mu}{\Omega}\right)^{-4\epsilon} \Omega^2 \frac{d}{dr} I_5 = \frac{(2 - 9\epsilon(1 - \epsilon))}{\epsilon(r-1)^3 r} I_1 + \frac{2\epsilon}{(r-1)r} I_3 - \frac{1 + 4\epsilon}{(r-1)r} I_4 - \frac{(1+2\epsilon)}{r} I_5 . \quad (6.41)$$

We see that we can solve the above system of differential equations iteratively. The first two equations in (6.38) and (6.39) enable us to obtain I_2 and I_3 from the knowledge about I_1 which is solved above and the result given in equation (6.37). Then, since we have obtained result for I_1 and I_3, we can solve the next differential equation in (6.40) for I_4. Similarly, once we have knowledge of I_4 through a solution of (6.40), we can solve for I_5 in (6.41).

Naturally, each of the solutions of the differential equations in (6.38) – (6.41) will be correct up to an ϵ dependent constant, which we must fix through an appropriate choice of boundary conditions. We can obtain the necessary boundary conditions by solving the integrals I_2 – I_5 in equations (6.24) – (6.27) without the $\delta(\omega - n_- k_1)$ constraint. Or, equivalently, solving $\int_0^\Omega d\omega\, I_i$ for $i = 2, \ldots, 5$, which formally eliminates the $\delta(\omega - n_- k_1)$. We refer to these results as *inclusive* versions of I_2 – I_5. Without the additional constraint on ω (or equivalently r) the integrals are not difficult, and we find

$$\int_0^\Omega d\omega\, I_2 = \frac{\alpha_s^2}{(4\pi)^2} \Omega^2 \left(\frac{\mu}{\Omega}\right)^{4\epsilon} \frac{1}{(1 - 2\epsilon)} \frac{e^{2\epsilon \gamma_E} \Gamma[1 - \epsilon]^2}{\Gamma[2 - 4\epsilon]} , \quad (6.42)$$

$$\int_0^\Omega d\omega\, I_3 = -\frac{\alpha_s^2}{(4\pi)^2} \Omega \left(\frac{\mu}{\Omega}\right)^{4\epsilon} \frac{2}{\epsilon} \frac{e^{2\epsilon \gamma_E} \Gamma[1 - \epsilon]^2}{\Gamma[3 - 4\epsilon]} , \quad (6.43)$$

$$\int_0^\Omega d\omega\, I_4 = -\frac{\alpha_s^2}{(4\pi)^2} \left(\frac{\mu}{\Omega}\right)^{4\epsilon} \frac{1}{2\epsilon^3} \frac{e^{2\epsilon \gamma_E} \Gamma[1 - \epsilon]^2}{\Gamma[1 - 4\epsilon]} , \quad (6.44)$$

$$\int_0^\Omega d\omega\, I_5 = -\frac{\alpha_s^2}{(4\pi)^2} \frac{1}{\Omega} \left(\frac{\mu}{\Omega}\right)^{4\epsilon} \frac{1}{\epsilon^3} \frac{e^{2\epsilon \gamma_E} \Gamma[1 - \epsilon]^2}{\Gamma[1 - 4\epsilon]} . \quad (6.45)$$

The reason why this is useful is that the results for integrals I_2 – I_5 found through solutions of the above differential equations must correspond to the above respective inclusive results after the $d\omega$ (dr) integral has been performed over the former. For example, solving the differential equation in (6.38) for I_2 yields the following result

$$I_2 = \frac{\alpha_s^2}{(4\pi)^2} \Omega \left(\frac{\mu}{\Omega}\right)^{4\epsilon} r^{-\epsilon} \frac{(-2 + 3\epsilon)e^{2\epsilon \gamma_E} \Gamma[1 - \epsilon]}{\epsilon\, \Gamma[3 - 3\epsilon]} \,_2F_1\left(\epsilon, -1 + 3\epsilon; 1 + \epsilon; r\right) + r^{-2\epsilon} c_1, \quad (6.46)$$

where c_1 is a constant of integration still to be determined. As described above, we fix it by integrating (6.46) with respect to r and matching to the inclusive result in (6.42). We find the following

$$\begin{aligned}
I_2 &= \frac{\alpha_s^2}{(4\pi)^2} \Omega \left(\frac{\mu}{\Omega}\right)^{4\epsilon} \frac{(2 - 3\epsilon)\, e^{2\,\epsilon\, \gamma_E}\, \Gamma[1 - \epsilon]}{\epsilon\, \Gamma[3 - 3\epsilon]} \,\theta(1 - r)\,\theta(r) \\
&\quad \times \left(r^{-2\epsilon} \frac{\Gamma[2 - 3\epsilon]\Gamma[1 + \epsilon]}{\Gamma[2 - 2\epsilon]} - r^{-\epsilon} \,_2F_1\left(\epsilon, -1 + 3\epsilon; 1 + \epsilon; r\right)\right) . \quad (6.47)
\end{aligned}$$

Having calculated I_2, we have all the ingredients necessary to solve the differential equation in (6.39) for I_3. Using (6.43) as a boundary condition after a further $d\omega \, (dr)$ integration yields the final result

$$
\begin{aligned}
I_3 \quad &= \quad \frac{\alpha_s^2}{(4\pi)^2} \left(\frac{\mu}{\Omega}\right)^{4\epsilon} \frac{e^{2\epsilon\gamma_E}}{\epsilon^2} \frac{\Gamma[1-\epsilon]\Gamma[1+\epsilon]}{\Gamma[1-3\epsilon]\Gamma[1-2\epsilon]} \theta(1-r)\,\theta(r) \\
&\quad \times \left(-r^{-2\epsilon}\Gamma[1-3\epsilon] + r^{-\epsilon}\frac{\Gamma[1-2\epsilon]}{\Gamma[1+\epsilon]} \,_2F_1\left(\epsilon, 3\epsilon; 1+\epsilon; r\right)\right).
\end{aligned}
\tag{6.48}
$$

Next, by solving the differential equation in (6.40) we find the following result for the master integral I_4. The result is

$$
\begin{aligned}
I_4 \quad &= \quad -\frac{\alpha_s^2}{(4\pi)^2}\Omega^{-1} \left(\frac{\mu}{\Omega}\right)^{4\epsilon} \frac{1}{(1-r)^{1+4\epsilon}} \frac{e^{2\epsilon\gamma_E}\Gamma[1-\epsilon]}{\epsilon^2}\theta(1-r)\theta(r)\left(\frac{\Gamma[1-\epsilon]\Gamma[1+\epsilon]}{\Gamma[1-3\epsilon]}\right. \\
&\quad + \frac{\epsilon}{\Gamma[1-3\epsilon]}\left(B_{1-r}(1+\epsilon, -\epsilon) + B_r(-\epsilon, 1+\epsilon)\right) + \frac{\Gamma[1+\epsilon]}{\Gamma[-2\epsilon]}B_r(-2\epsilon, 1+4\epsilon) \\
&\quad \left. -\frac{3}{\Gamma[1-3\epsilon]}\left(\frac{1}{r}-1\right)^\epsilon \,_3F_2\left(1, -\epsilon, 1+3\epsilon; 1-\epsilon, 1+\epsilon; \frac{r}{r-1}\right)\right),
\end{aligned}
\tag{6.49}
$$

where the incomplete Beta functions are defined by

$$
B_z(a,b) = \int_0^z u^{a-1}(1-u)^{b-1}\,du
\tag{6.50}
$$

in contrast to the complete Beta function with upper integral limit of 1 as shown in equation (A.2). For later convenience we also implicitly define $\bar{I}_4$ which corresponds to the terms in the parenthesis of equation (6.49), explicitly

$$
I_4 \quad = \quad -\frac{\alpha_s^2}{(4\pi)^2}\Omega^{-1}\left(\frac{\mu}{\Omega}\right)^{4\epsilon}(1-r)^{-1-4\epsilon}\frac{e^{2\epsilon\gamma_E}\Gamma[1-\epsilon]}{\epsilon^2}\theta(1-r)\theta(r)\bar{I}_4\,.
\tag{6.51}
$$

Lastly, we solve equation (6.41) for I_5. A complete d-dimensional result turns out to be too complicated to obtain here. Therefore, we resort to isolating the problematic limits of $r \to 0$ and $r \to 1$ and evaluating those pieces in d-dimensions, and expanding the rest. We find

$$
\begin{aligned}
I_5 \quad &= \quad \frac{\alpha_s^2}{(4\pi)^2}\Omega^{-2}\left(\frac{\mu}{\Omega}\right)^{4\epsilon}\theta(1-r)\theta(r) \\
&\quad \times \left(-\frac{1}{2\epsilon^3}\left(\delta(1-r) + \delta(r)\right) + \frac{1}{\epsilon^2}\left(2\left[\frac{1}{1-r}\right]_+ + \left[\frac{1}{r}\right]_+\right)\right. \\
&\quad + \frac{1}{12\epsilon}\left(\pi^2\left(5\delta(1-r) - \delta(r)\right) - 24\left(4\left[\frac{\ln(1-r)}{1-r}\right]_+ + \left[\frac{\ln(r)}{r}\right]_+\right)\right) \\
&\quad \left. -\frac{48}{r}\ln(1-r) - \frac{12}{(1-r)}\ln(r)\right)
\end{aligned}
$$

$$+\frac{\zeta(3)}{3}\Big(28\delta(1-r)-5\delta(r)\Big)-\frac{5\pi^2}{3}\left[\frac{1}{1-r}\right]_+ +\frac{\pi^2}{6}\left[\frac{1}{r}\right]_+$$

$$+4\left(8\left[\frac{\ln^2(1-r)}{1-r}\right]_+ +\left[\frac{\ln^2(r)}{r}\right]_+\right)+\frac{(6-7r)}{(r-1)r}\mathrm{Li}_2(r)+\frac{\pi^2}{6(r-1)}$$

$$+\frac{8}{r}\ln^2(1-r)+\frac{1}{2(r-1)}\ln^2(r)-\frac{2(r+1)}{r(r-1)}\ln(r)\ln(1-r)+\mathcal{O}(\epsilon)\bigg).\quad(6.52)$$

As for I_4, we implicitly define $\bar{I}_5$ as

$$I_5(r)\quad=\quad\frac{\alpha_s^2}{(4\pi)^2}\Omega^{-2}\left(\frac{\mu}{\Omega}\right)^{4\epsilon}\theta(1-r)\theta(r)\,\bar{I}_5\,.\qquad(6.53)$$

This concludes the presentation of the results of master integrals with a $\delta(\omega-n_-k_1)$ constraint.

6.4.2 $\delta(\omega-n_-k_1-n_-k_2)$

In this section we present the results for the master integrals I_6 and I_7 which are needed in equations (6.28) and (6.29).

The calculation of the master integral I_6 defined in equation (6.30) follows the same steps as the calculation of I_1 presented between equations (6.35) and (6.37) except for the fact that the $\delta(\omega-n_-k_1)$ function in equation (6.35) is replaced by $\delta(\omega-n_-k_1-n_-k_2)$. We find the following result

$$I_6\quad=\quad\frac{\alpha_s^2}{(4\pi)^2}\,\mu^{4\epsilon}\omega^{1-2\epsilon}(\Omega-\omega)^{1-2\epsilon}\frac{e^{2\epsilon\gamma_E}\,\Gamma[1-\epsilon]^2}{\Gamma[2-2\epsilon]^2}\,\theta(\Omega-\omega)\,\theta(\omega).\qquad(6.54)$$

Next, we consider the I_7 master integral defined in equation (6.31). This integral contains a more intricate propagator structure and for this reason we consider it in greater detail here.

We begin the calculation by inserting the identity $1=\int d^d Q\,\delta^{(d)}(Q-k_1-k_2)$ into equation (6.31) and changing the order of integration. Then we have

$$I_7\quad=\quad g_s^4\frac{1}{(2\pi)^{2d-2}}\int d^d Q\,\frac{1}{Q^2}\,\delta(\Omega-n_-Q-n_+Q)\,\delta(\omega-n_-Q)\qquad(6.55)$$

$$\times\int d^d k_1\int d^d k_2\,\Big(\delta(k_1^2)\theta(k_1^0)\Big)\Big(\delta(k_2^2)\theta(k_2^0)\Big)\,\frac{1}{(n_-k_1)}\frac{1}{(n_+k_2)}\,\delta^{(d)}(Q-k_1-k_2)\,.$$

Now, we use an auxiliary integral from [149] to write down the result for the double integral in the second line of the above expression. We find

$$I_7\quad=\quad g_s^4\frac{1}{(2\pi)^{2d-2}}\int d^d Q\,\frac{1}{Q^2}\,\delta(\Omega-n_-Q-n_+Q)\,\delta(\omega-n_-Q)\qquad(6.56)$$

$$\times\pi^{1-\epsilon}\,\frac{\Gamma[-\epsilon]}{\Gamma[1-2\epsilon]}\,(n_-Q\,n_+Q)^{\epsilon}\,(Q_T)^{-2-2\epsilon}\,\big(Q^2\big)^{-\epsilon}\,{}_2F_1\left(-\epsilon,-\epsilon,1-\epsilon,\frac{Q^2}{n_+Q n_-Q}\right).$$

As a side remark, the corresponding step in the calculation of I_3, I_4 and I_5 is precisely where the direct integration is too complicated, as the $\delta(\omega - n_- k_1)$ piece must remain in the $d^d k_1 \, d^d k_2$ integrals unlike here, where we could factor out the $\delta(\omega - n_- Q)$ outside of the $d^d k_1 \, d^d k_2$ integrals. Concretely, the issue is that the auxiliary integrals are usually performed in a special frame and later related to the general result using Lorentz invariance. The issue we encountered is that the presence of the $\delta(\omega - n_- k_1)$ term singles out the $n_- k_1$ component. This makes the calculation more difficult in two ways. Firstly, the auxiliary integrals themselves become complicated, and second, their results reach beyond the $_2F_1$ hypergeometric function in equation (6.56), such that further manipulation is hindered.

Returning to the integral of I_7 at hand, decomposing the $d^d Q$ integral into components the calculation from here follows along similar lines to I_1. We utilise the two remaining delta functions and finally arrive at

$$
I_7 \;=\; \frac{\alpha_s^2}{(4\pi)^2} \frac{\mu^{4\epsilon}}{\omega^{1+2\epsilon}(\Omega - \omega)^{1+2\epsilon}} \, \theta(\Omega - \omega) \, \theta(\omega)
$$
$$
\times \frac{2 \, e^{2\epsilon\gamma_E}}{\Gamma[1-\epsilon]} \frac{\Gamma[-\epsilon]^2}{\Gamma[1-2\epsilon]} \frac{\Gamma[-2\epsilon]}{\Gamma[-3\epsilon]} \, {}_3F_2\left(-\epsilon, -\epsilon, -\epsilon; -3\epsilon, 1-\epsilon; 1\right), \qquad (6.57)
$$

where $_3F_2\left(\{-\epsilon, -\epsilon, -\epsilon\}, \{-3\epsilon, 1-\epsilon\}, 1\right)$ is a hypergeometric function.

6.4.3 $\quad \delta(\omega_1 - n_- k_1)\delta(\omega_2 - n_- k_2)$

Lastly, we present the result for the master integral I_8 defined in equation (6.34). This calculation is straightforwardly related to the calculation of I_1 which is obtained starting from equation (6.30). Considering a similar expression with an additional delta function, namely $\delta(\omega_2 - n_- k_2)$, yields the following result

$$
I_8 = \frac{\alpha_s^2}{(4\pi)^2} \frac{\mu^{4\epsilon}}{\omega_1^\epsilon \, \omega_2^\epsilon}(\Omega - \omega_1 - \omega_2)^{1-2\epsilon} \frac{e^{2\epsilon\gamma_E}}{\Gamma[2-2\epsilon]} \, \theta(\Omega - \omega_1 - \omega_2)\theta(\omega_1)\theta(\omega_2). \qquad (6.58)
$$

With this, we conclude the presentation of the results of the master integrals. We are now in possession of all the ingredients necessary to write down the next-to-next-to-leading order soft functions.

6.5   Results

We now collect the results presented in the above sections to arrive at the final results for the real-real contributions to the soft functions.

First, we provide the result for the S_1 soft function. The result is written in terms of the dimensionless variable r defined by $r = \omega/\Omega$. By summing the contribution dependent on integrals with a $\delta(\omega - n_- k_1)$ constraint in (6.22) and the expression in (6.28) with master integrals containing a $\delta(\omega - n_- k_1 - n_- k_2)$ term, and inserting the relevant master integral results from the section above, we find

$$
S_1^{(2)2r0v}(\Omega, r) = 8 \frac{\alpha_s^2}{(4\pi)^2} C_F^2 \frac{1}{\Omega} \left(\frac{\Omega}{\mu}\right)^{-4\epsilon} r^{-1-\epsilon} \left(1 - r\right)^{-3\epsilon} \frac{1}{\epsilon^2} \frac{e^{2\epsilon\gamma_E}\Gamma[1-\epsilon]}{\Gamma[1-3\epsilon]} \theta(1-r)\theta(r)
$$

$$-4\frac{\alpha_s^2}{(4\pi)^2}C_F\,n_f\frac{1}{\Omega}\left(\frac{\Omega}{\mu}\right)^{-4\epsilon}r^{-1-2\epsilon}(1-r)^{-2\epsilon}\frac{(1-\epsilon)^2}{\epsilon(3-2\epsilon)}\frac{e^{2\epsilon\gamma_E}\Gamma[1-\epsilon]^2}{\Gamma[2-2\epsilon]^2}\theta(1-r)\theta(r)$$

$$+\frac{\alpha_s^2}{(4\pi)^2}C_FC_A\frac{1}{\Omega}\left(\frac{\Omega}{\mu}\right)^{-4\epsilon}\Bigg[\frac{(2-3\epsilon)\,(-4+\epsilon\,(r+19)+4\epsilon^2\,(r-7)+16\epsilon^3(1-r))}{\epsilon^2(1-2\epsilon)}$$

$$\times r^{-1-\epsilon}(1-r)^{-3\epsilon}\frac{e^{2\epsilon\gamma_E}\,\Gamma[1-\epsilon]}{\Gamma[3-3\epsilon]}$$

$$+\frac{(9-20\epsilon+12\epsilon^2-2\epsilon^3)}{\epsilon^2\,(3-2\epsilon)}r^{-1-2\epsilon}(1-r)^{-2\epsilon}\frac{e^{2\epsilon\gamma_E}\,\Gamma[1-\epsilon]^2}{\Gamma[2-2\epsilon]^2}$$

$$+r^{-1-2\epsilon}(1-r)^{-2\epsilon}\frac{2\,e^{2\epsilon\gamma_E}}{\epsilon^2}\frac{\Gamma[1-\epsilon]}{\Gamma[1-2\epsilon]}\frac{\Gamma[-2\epsilon]}{\Gamma[-3\epsilon]}\,{}_3F_2\left(-\epsilon,-\epsilon,-\epsilon;-3\epsilon,1-\epsilon;1\right)$$

$$-\frac{(1-4\epsilon^2)(2-3\epsilon)\,e^{2\epsilon\gamma_E}\,\Gamma[1-\epsilon]}{\epsilon^2\,\Gamma[3-3\epsilon]}$$

$$\times\left(r^{-1-2\epsilon}\frac{\Gamma[2-3\epsilon]\Gamma[1+\epsilon]}{\Gamma[2-2\epsilon]}-r^{-1-\epsilon}\,{}_2F_1\left(\epsilon,-1+3\epsilon;1+\epsilon;r\right)\right)$$

$$+\frac{(3-10\epsilon+16\epsilon^2(1+r))\,e^{2\epsilon\gamma_E}\,\Gamma[1-\epsilon]}{2(1-2\epsilon)}\frac{}{\epsilon^2\,\Gamma[1-3\epsilon]}$$

$$\times\left(-r^{-1-2\epsilon}\frac{\Gamma[1-3\epsilon]\Gamma[1+\epsilon]}{\Gamma[1-2\epsilon]}+r^{-1-\epsilon}\,{}_2F_1\left(\epsilon,3\epsilon;1+\epsilon;r\right)\right)$$

$$-\frac{(1-3r)}{2r}(1-r)^{-1-4\epsilon}\frac{1}{\epsilon^2}e^{2\epsilon\gamma_E}\,\Gamma[1-\epsilon]\,\bar{\mathrm{I}}_4+\bar{\mathrm{I}}_5\Bigg]\theta(1-r)\theta(r)\,.\tag{6.59}$$

Next, we provide the result for the two-loop contribution to the S_3 soft function by inserting the master integral in (6.54) into equation (6.29) arriving at the following final expression

$$S_3^{(2)}(\Omega,\omega)=2\frac{\alpha_s^2}{(4\pi)^2}C_FC_A\left(\frac{\omega^2(\Omega-\omega)^2}{\mu^4}\right)^{-\epsilon}\frac{1}{\omega}\frac{(1-\epsilon)}{(3-2\epsilon)}\frac{e^{2\epsilon\gamma_E}\,\Gamma[1-\epsilon]^2}{\Gamma[2-2\epsilon]^2}\theta(\Omega-\omega)\theta(\omega),\tag{6.60}$$

where we have kept the dimensionful convolution variable ω. Similarly, inserting the master integral into the reduced expression in (6.32) we find the final result for the S_4 soft function to be

$$S_4^{(2)}(\Omega,\omega_1,\omega_2)\;=\;-\frac{\alpha_s^2}{(4\pi)^2}C_FC_A\left(\frac{\omega_1\,\omega_2(\Omega-\omega_1-\omega_2)^2}{\mu^4}\right)^{-\epsilon}\frac{2(1-\epsilon)\omega_2(\omega_1-\omega_2)}{(\omega_1+\omega_2)^4}$$

$$\times\frac{e^{2\epsilon\gamma_E}}{\Gamma[2-2\epsilon]}\;\theta(\Omega-\omega_1-\omega_2)\theta(\omega_1)\theta(\omega_2)\tag{6.61}$$

and the result for the S_5 soft function is

$$S_5^{(2)}(\Omega,\omega_1,\omega_2)\;=\;-\frac{\alpha_s^2}{(4\pi)^2}\left(C_F^2-\frac{1}{2}C_FC_A\right)\left(\frac{\omega_1\,\omega_2(\Omega-\omega_1-\omega_2)^2}{\mu^4}\right)^{-\epsilon}\frac{8(1-\epsilon)\omega_2}{(\omega_1+\omega_2)^3}$$

$$\times \frac{e^{2\epsilon\gamma_E}}{\Gamma[2 - 2\epsilon]} \, \theta(\Omega - \omega_1 - \omega_2)\theta(\omega_1)\theta(\omega_2) \,. \tag{6.62}$$

The above two-loop results are verified in the next chapter. By insertion into the relevant parts of the factorisation formula, combining with the corresponding collinear functions, and integrating over the convolution variables ω, ω_1, and ω_2 as appropriate find the correct contributions at the next-to-next-to-leading order at the cross-section level. Explicit details are presented in the chapter below.

<div style="text-align: center; font-size: 3em;">7</div>

Drell-Yan: fixed-order results

In this chapter we combine the results for collinear functions calculated in chapter 4 with the fixed order results for the generalised subleading-power soft functions presented in chapters 5 and 6, and the leading power hard function. This is done according to the factorisation formulas derived in chapter 3. For the purposes of this chapter we continue to work with regularized objects and perform the convolutions between the soft and collinear functions in d-dimensions. With the results obtained in this way, we verify the validity of the bare next-to-leading power factorisation formulas derived in chapter 3. This is achieved through a direct comparison against the next-to-leading power results for partonic Drell-Yan process at NLO and NNLO in α_s [31, 35, 36, 37, 116, 150] calculated by a direct evaluation of the QCD diagrams and using the expansion-by-regions method [89].

7.1 Quark-antiquark channel

The expansion of the next-to-leading power factorisation formula for the $q\bar{q}$-channel in equation (3.81) at fixed α_s and α_s^2 orders has been performed in section 3.2.3. We make use of these expansions below.

7.1.1 Next-to-leading order

The NLO accurate factorisation formula is given in equation (3.91). The tree-level collinear function given in (4.19) and the tree-level hard matching coefficient, $H^{(0)}(Q^2) = 1$, have already been implemented. We find only the one dynamical contribution to the cross-section. This is because the next-to-leading power soft functions begin at lowest $\mathcal{O}(\alpha_s)$. The result for the relevant one-loop soft function is given in (5.7). At NLO we then find for the cross-section

$$\Delta_{\mathrm{NLP}}^{dyn\,(1)}(z) \;\; = \;\; -4\frac{\alpha_s}{2\pi}C_F\frac{\mu^{2\epsilon}e^{\epsilon\gamma_E}}{\Gamma[1-\epsilon]}\int_0^\Omega d\omega\,\frac{1}{\omega^{1+\epsilon}}\frac{1}{(\Omega-\omega)^\epsilon}\;. \tag{7.1}$$

Performing now the convolution integral over ω yields the following result at next-to-leading order in α_s

$$\Delta_{\mathrm{NLP}}^{dyn\,(1)}(z) \;\; = \;\; \frac{\alpha_s}{4\pi}C_F\frac{8}{\epsilon}(1-2\epsilon)\frac{\mu^{2\epsilon}}{\Omega^{2\epsilon}}\frac{e^{\epsilon\gamma_E}\Gamma[1-\epsilon]}{\Gamma[2-2\epsilon]}\;. \tag{7.2}$$

Expanding this result in ϵ, we arrive at

$$\Delta_{\text{NLP}}^{dyn\,(1)}(z) \;=\; \frac{\alpha_s}{4\pi}C_F\left(\frac{8}{\epsilon} - 16\ln(1-z) - \epsilon\left(2\pi^2 - 16\ln^2(1-z)\right) + \mathcal{O}(\epsilon^2)\right), \quad (7.3)$$

where we set the renormalization scale $\mu = Q$.

In addition to the dynamic contribution to the next-to-leading power cross-section, we must also consider the kinematic corrections at this order in α_s, namely the $\Delta_{\text{NLP}}^{kin\,(1)}(z)$ term. This contribution is given by the sum of $\Delta_{\text{NLP}}^{K1}(\Omega)$, $\Delta_{\text{NLP}}^{K2}(\Omega)$, and $\Delta_{\text{NLP}}^{K3}(\Omega)$ defined in equations (3.73), (3.74), and (3.75) respectively. The fourth kinematic correction $\Delta_{\text{NLP}}^{K4}(\Omega)$ in equation (3.76) does not contribute as the derivative of the tree-level hard function vanishes. The listed kinematic corrections require the input of the kinematic soft functions S_{K1}, S_{K2}, and S_{K3} the results for which at next-to-leading order are given in equations (5.21), (5.23), (5.24), and (5.25). Since all of the kinematic soft functions begin to contribute at $\mathcal{O}(\alpha_s)$, we only require the tree-level hard function contribution $H^{(0)} = 1$ to each piece of the cross-section. Combining together the relevant pieces, we arrive at the following results

$$\Delta_{\text{NLP}}^{K1\,(1)}(z) \;=\; \frac{\alpha_s\,C_F}{2\pi}\left(\frac{1}{\epsilon} + 2\ln\left(\frac{\mu}{\Omega}\right) - 2 + \epsilon\left(2\ln^2\left(\frac{\mu}{\Omega}\right) - 4\ln\left(\frac{\mu}{\Omega}\right) - \frac{\pi^2}{4}\right) + \mathcal{O}(\epsilon^2)\right)$$

$$\stackrel{\mu=Q}{=} \frac{\alpha_s\,C_F}{2\pi}\left(\frac{1}{\epsilon} - 2\ln(1-z) - 2 + \epsilon\left(2\ln^2(1-z) + 4\ln(1-z) - \frac{\pi^2}{4}\right) + \mathcal{O}(\epsilon^2)\right), \quad (7.4)$$

for the first kinematic correction in (3.73). For the second in (3.74) we find

$$\Delta_{\text{NLP}}^{K2\,(1)}(\Omega) \;=\; \frac{\alpha_s\,C_F}{2\pi}\left(\frac{3}{\epsilon} + 6\ln\left(\frac{\mu}{\Omega}\right) + 6 + 3\epsilon\left(2\ln^2\left(\frac{\mu}{\Omega}\right) + 4\ln\left(\frac{\mu}{\Omega}\right) - \frac{\pi^2}{4}\right) + \mathcal{O}(\epsilon^2)\right)$$

$$\stackrel{\mu=Q}{=} \frac{\alpha_s\,C_F}{2\pi}\left(\frac{3}{\epsilon} - 6\ln(1-z) + 6 + 3\epsilon\left(2\ln^2(1-z) - 4\ln(1-z) - \frac{\pi^2}{4}\right) + \mathcal{O}(\epsilon^2)\right). \quad (7.5)$$

Lastly, for the third in (3.75) we have

$$\Delta_{\text{NLP}}^{K3\,(1)}(z) \;=\; \frac{\alpha_s\,C_F}{2\pi}\left(-\frac{4}{\epsilon} - 8\ln\left(\frac{\mu}{\Omega}\right) + \epsilon\left(-8\ln^2\left(\frac{\mu}{\Omega}\right) + \pi^2\right) + \mathcal{O}(\epsilon^2)\right)$$

$$\stackrel{\mu=Q}{=} \frac{\alpha_s\,C_F}{2\pi}\left(-\frac{4}{\epsilon} + 8\ln(1-z) + \epsilon\left(-8\ln^2(1-z) + \pi^2\right) + \mathcal{O}(\epsilon^2)\right). \quad (7.6)$$

Upon summation of the above results, for the total contribution due to kinematic corrections at next-to-leading order we find

$$\Delta_{\text{NLP}}^{kin\,(1)}(z) = \frac{\alpha_s\,C_F}{4\pi}\left(8 - \epsilon\,16\ln(1-z)\right). \quad (7.7)$$

Results for next-to-leading power contributions to the Drell-Yan cross-section at NLO have been previously reported in [35] within a diagrammatic approach. In this approach the power-suppressed soft radiation is taken into account by generalised next-to-soft Wilson lines. Our dynamical result, $\Delta_{\text{NLP}}^{dyn\,(1)}(z)$ in equation (7.3), is in agreement with

the corresponding expression in equation (6.17) of [35]. The kinematic correction result obtained here, $\Delta_{\rm NLP}^{kin\,(1)}(z)$ in equation (7.7), is confirmed by the corresponding result in equation (6.13) of [35]. In the diagrammatic approach, this contribution arises as a phase space power correction to the leading power matrix element. We can also compare to results in literature the sum of $\Delta_{\rm NLP}^{dyn\,(1)}(z)$ and $\Delta_{\rm NLP}^{kin\,(1)}(z)$ in equations (7.3) and (7.7) respectively. We must first apply subtractions originating from PDF renormalization to the total result, after which we can compare with the next-to-leading order next-to-leading power result given in equation (B.29) of [116] with which we find agreement.

7.1.2 Next-to-next-to-leading order

In section 3.2.3 we have discussed the three possible types of dynamical next-to-leading power contributions to the cross-section appearing at next-to-next-to-leading order. Namely, we have the collinear, hard, and soft contributions. The simplified expressions for each of these can be found in equations (3.95), (3.96), and (3.94), respectively. The aim of this section is to combine the ingredients computed in previous chapters in order to obtain the explicit results for the collinear, hard, and soft contributions and check these against the results existing in literature. Moreover, a complete result for the one-loop next-to-leading power Drell-Yan amplitude with one real soft emission is presented in appendix B.2

We also present the kinematic contribution to the NNLO Drell-Yan next-to-leading power cross-section, making use of the results for kinematic soft functions in section 5.1.2.

Collinear contribution

We begin with the contribution which includes the one-loop collinear function results obtained in chapter 4. We have already simplified the expression describing this contribution using the tree-level result for the hard function. This result can be found in equation (3.95), and we write it here again for convenience

$$\Delta_{\rm NLP-coll}^{dyn\,(2)}(z) \;=\; 4Q \int d\omega \, J_{1,1}^{(1)}(x_a\,n_+p_A;\omega)\, S_1^{(1)}(\Omega;\omega)\,. \tag{7.8}$$

We see that the one-loop collinear function is combined with the corresponding NLO soft function. It is also noteworthy that only the $J_{1,1}^{(1)}$ can in principle contribute here. This is because the $J_{1,2}^{(1)}$ piece of the collinear function multiplies a delta-function derivative term (see the decomposition in (3.89)). After partial integration this derivative acts on the hard function which at tree level is a constant and so this term cannot feature in (7.8). Moreover, we found in (4.86) that $J_{1,2}^{(1)} = 0$. The expression for the $J_{1,1}^{(1)}(x_a\,n_+p_A;\omega)$ one-loop collinear function which does enter the expression in (7.8) can be found in equation (4.84) with colour generator and Dirac-index Kronecker-symbol removed.

As we have stressed above, in order to obtain the NNLO fixed-order result we do not expand neither the collinear nor the soft function in ϵ. Rather, we keep the d-dimensional expression of the collinear function and perform the last integral over the convolution variable ω while also using the d-dimensional soft function which is given in equation (5.7). We find

$$\Delta_{\rm NLP-coll}^{dyn\,(2)}(z) \;=\; 8\frac{\alpha_s^2}{(4\pi)^2}\left(\frac{Q\,\Omega^3}{\mu^4}\right)^{-\epsilon} \frac{e^{2\epsilon\gamma_E}\Gamma[1+\epsilon]\Gamma[1-\epsilon]^2\Gamma[1-2\epsilon]}{\Gamma[1-3\epsilon]\Gamma[3-2\epsilon]}$$

$$\times \left(-C_F^2 \frac{1}{\epsilon^2}(4 - 7\epsilon - \epsilon^2) + C_F C_A \frac{(5 - 8\epsilon - \epsilon^2)}{\epsilon(1 + \epsilon)} \right). \tag{7.9}$$

Only now, *after* this convolution is performed, we expand the resulting expression in ϵ. We set the soft scale to $\Omega = Q(1 - z)$ and $\mu = Q$. The sequence of above steps yields

$$
\begin{aligned}
\Delta_{\text{NLP}-\text{coll}}^{dyn\,(2)}(z) \;=\; & \frac{\alpha_s^2}{(4\pi)^2} \Bigg(C_F^2 \bigg(-\frac{16}{\epsilon^2} + \frac{48\ln(1 - z) - 20}{\epsilon} \\
& + \Big(-72\ln^2(1 - z) + 60\ln(1 - z) + 8\pi^2 - 24 \Big) + \mathcal{O}(\epsilon) \bigg) \\
& + C_A C_F \left(\frac{20}{\epsilon} - (60\ln(1 - z) - 8) + \mathcal{O}(\epsilon) \right) \Bigg).
\end{aligned}
\tag{7.10}
$$

We draw attention to the fact that no leading logarithmic contributions, which are of the form $\alpha_s^2 \ln^3(1 - z)$, are present in the collinear contribution to the Drell-Yan cross-section. The highest encountered logarithmic power in the finite terms in the second line of the above equation is at the next-to-leading logarithmic accuracy. Namely, it is proportional to $\alpha_s^2 \ln^2(1 - z)$.

Studies regarding virtual collinear radiation at one-loop level with an emission of a soft gluon have been reported in literature, see for example [31] which is carried out within the expansion-by-regions method [89], and [36, 37] performed within a diagrammatic approach. The information regarding effects due to presence of collinear loops is contained within the so-called "radiative jet function" [130]. We can compare the C_F^2 term given in (7.10) against the corresponding contribution found in equations (13), (14) of [31] and equation (4.22) of [36], where only the abelian contribution is considered. We find agreement with those results, although these references drop all contributions which are proportional to transcendental numbers, such as π^2. A corresponding result for the second colour structure, $C_A C_F$, which appears in our result in equation (7.10) does not separately exist in the literature. It is provided in a sum with the hard and soft contributions which we consider next.

Hard contribution

Here we consider the contribution to the Drell-Yan cross-section which is made up of the one-loop hard function, the tree-level collinear functions, and the one-loop soft function. Unlike in the case of the collinear contribution considered above, the piece of the tree-level collinear function attached to the derivative-delta function gives a non-vanishing result. This is because the hard matching coefficient is momentum-dependent beyond tree level.

The formula for the cross-section simplified to this case is given in equation (3.96). We state it again here for convenience

$$\Delta_{\text{NLP}-\text{hard}}^{dyn\,(2)}(z) = -4\,(1 - \epsilon)\,H^{(1)}(Q^2) \int d\omega\, S_1^{(1)}\,(\Omega;\,\omega\,). \tag{7.11}$$

In order to obtain this expression we have already utilised the results for the collinear functions at tree level. The necessary one-loop soft function can be found in equation (5.7).

The one-loop hard function $H = |C^{A0,A0}|^2$ up to finite order in ϵ expansion is given above in equation (2.59). With these results at hand, we perform the $d\omega$ integration in (7.11) over the d-dimensional expression for the soft function, we set $\mu = Q$, and only then expand in ϵ which leads to the following result

$$
\begin{aligned}
\Delta^{dyn\,(2)}_{\mathrm{NLP-hard}}(z) &= \frac{\alpha_s^2 C_F^2}{(4\pi)^2}\Bigg(-\frac{32}{\epsilon^3} + \frac{64\ln(1-z) - 16}{\epsilon^2} \\
&\quad + \frac{-64\ln^2(1-z) + 32\ln(1-z) + \frac{80}{3}\left(\pi^2 - 3\right)}{\epsilon} \\
&\quad - \frac{8}{3}\Big(-16\ln^3(1-z) + 12\ln^2(1-z) + 20\left(\pi^2 - 3\right)\ln(1-z) \\
&\quad - 56\zeta(3) - 5\pi^2 + 48 \Big) + \mathcal{O}(\epsilon)\Bigg),
\end{aligned}
\tag{7.12}
$$

where $\zeta(3)$ is a Riemann zeta value. Unlike in the collinear contribution to the next-to-leading power cross-section, leading logarithmic contributions are present in this expression. These terms are proportional to $\alpha_s^2 \ln^3(1-z)$. This implies that the hard function must be resummed to capture all leading logarithmic contributions to all orders in perturbation theory. This was achieved in [40] and is considered below in chapter 8.

The result for $\Delta^{dyn\,(2)}_{\mathrm{NLP-hard}}$ in (7.12) can be compared against a result obtained by making use of the expansion-by-regions method for an amplitude with one hard one-loop and one real soft gluon emission. This expression has been presented in equation (12) of [31], and is in agreement with our result in (7.12).[1] In the diagrammatic approach [36, 37], the hard contribution presented here in equation (7.12) originates from the dressing of the non-radiative amplitude with one real soft gluon emission, as dictated by the LBK theorem.

Soft contribution

We now turn our attention to the soft contribution to the cross-section. Here we provide both the one-real, one-virtual contribution to the cross-section and the double real contributions due to several soft functions. In section 5.1.1, we have obtained the one-real, one-virtual result for the S_1 soft function. In principle, other soft functions could contribute to this part of the NNLO cross-section as can be seen in equation (3.94). However, remarkably, only one soft structure, the one corresponding to the S_1 soft function, contributes. This is explored in more detail in appendix B.2.3. Since only the S_1 soft function and its corresponding tree-level soft function contribute to this piece of the NNLO cross-section, the simplified factorisation formula has the following form

$$
\Delta^{dyn\,(2)1r1v}_{\mathrm{NLP-soft}}(z) = 4Q\,H^{(0)}(Q^2)\int d\omega\, J^{(0)}_{1,1}\left(x_a(n_+ p_A);\omega\right) S^{(2)1r1v}_1(\Omega,\omega).
\tag{7.13}
$$

We now make use of the one-real, one-virtual result for the S_1 next-to-leading power soft function, $S^{(2)1r1v}_1(\Omega,\omega)$, written in equation (5.13), along with the corresponding tree-level

---

[1]The following typo has to be accounted for in [31]: in equation (12) the $\left[1 + 4\log(1-z)\right]/\epsilon^2$ should in fact be $\left[-1 + 4\log(1-z)\right]/\epsilon^2$.

collinear function given in equation (4.19). Combining the expressions as dictated by (7.13), integrating over ω, and only then expanding in ϵ and setting $\mu = Q$ yields

$$\Delta^{dyn\,(2)1r1v}_{\text{NLP}-\text{soft}}(z) = \frac{\alpha_s^2}{(4\pi)^2} C_F C_A \left(-\frac{8}{\epsilon^3} + \frac{32\ln(1-z)}{\epsilon^2} - \frac{64\ln^2(1-z)}{\epsilon} + \frac{28\pi^2}{3\epsilon} \right.$$
$$\left. +\frac{256}{3}\ln^3(1-z) - \frac{112}{3}\pi^2\ln(1-z) + \frac{448\zeta(3)}{3} + \mathcal{O}(\epsilon) \right). \qquad (7.14)$$

It is not straightforward to compare this result directly with literature, as the non-abelian $C_F C_A$ term of the one-real, one-virtual contribution has been reported in a sum with the collinear pieces, kinematic corrections, and other soft contributions (see equation (4.6) of [37]). The result in equation (7.14) has been checked against the soft region of the one-real, one-virtual correction within the expansion-by-regions method [150].

In section 6.5, we have presented the ω dependent real-real results for the S_1, S_3, S_4, and S_5 next-to-leading power soft functions. We now consider the contribution of these terms to the Drell-Yan cross-section.

We first focus on the C_F^2 part of the S_1 soft function, this contribution is given in the top line of the result in equation (6.59). Making the variable transformation $r = \omega/\Omega$, the relevant part of the factorisation formula is given by

$$\Delta^{dyn\,(2)2r0v}_{\text{NLP}-\text{soft},S_{1,C_F^2}}(z) = 4\,Q\,\Omega\,H^{(0)}(Q^2) \int dr J^{(0)}_{1,1}\left(x_a(n_+ p_A);\omega\right) S^{(2)2r0v}_{1,C_F^2}(\Omega, r), \qquad (7.15)$$

where $S^{(2)2r0v}_{1,C_F^2}$ denotes the C_F^2 proportional terms of $S^{(2)2r0v}_1$ in (6.59). Inserting the result for the $S^{(2)2r0v}_{1,C_F^2}(\Omega, r)$ soft function and the tree-level collinear function from (4.19), and then integrating over the convolution variable dr in d-dimensions yields

$$\Delta^{dyn\,(2)2r0v}_{\text{NLP}-\text{soft},S_{1,C_F^2}}(z) = 32\frac{\alpha_s^2}{(4\pi)^2}C_F^2\left(\frac{\Omega^4}{\mu^4}\right)^{-\epsilon}\frac{1}{\epsilon^3}\frac{e^{2\epsilon\gamma_E}\Gamma[1-\epsilon]^2}{\Gamma[1-4\epsilon]}. \qquad (7.16)$$

Setting the soft scale to $\Omega = Q(1-z)$, the scale $\mu = Q$, and finally expanding in ϵ we find the following expression

$$\Delta^{dyn\,(2)2r0v}_{\text{NLP}-\text{soft},S_{1,C_F^2}}(z) = \frac{\alpha_s^2}{(4\pi)^2}C_F^2\left(\frac{32}{\epsilon^3} - \frac{128}{\epsilon^2}\ln(1-z) + \frac{256}{\epsilon}\ln^2(1-z) - \frac{112\pi^2}{3\epsilon} \right.$$
$$\left. +\frac{32}{3}\left(-32\ln^3(1-z) + 14\pi^2\ln(1-z) - 62\zeta(3)\right) + \mathcal{O}\left(\epsilon\right)\right). \qquad (7.17)$$

This result can be checked against equation (5.2) in [37]. However, care must be taken as the result presented there includes also the leading power contribution to the double real emission which we must subtract, and the transcendental pieces have been dropped. Additionally, the above result is in agreement with the calculation of next-to-leading power real-real emission using the expansion-by-regions method [150].

Similarly to the above considerations, we can insert into the factorisation theorem the piece of $S^{(2)2r0v}_1$ proportional to $C_F n_f$ which we label by $S^{(2)2r0v}_{1,C_F n_f}$. The relevant result can be found in the second line of (6.59). The contribution to the Drell-Yan cross-section is

$$\Delta^{dyn\,(2)2r0v}_{\text{NLP}-\text{soft},S_{1,C_F n_f}}(z) = -8\frac{\alpha_s^2}{(4\pi)^2}C_F n_f\left(\frac{\Omega^4}{\mu^4}\right)^{-\epsilon}\frac{1}{\epsilon^2}\frac{1}{(1-2\epsilon)^2(3-2\epsilon)}\frac{e^{2\epsilon\gamma_E}\Gamma[2-\epsilon]^2}{\Gamma[1-4\epsilon]}. \qquad (7.18)$$

The above result still contains d - dimensional information, we now set the soft scale to $\Omega = Q(1-z)$, the scale $\mu = Q$. Then, expanding in ϵ yields

$$\Delta^{dyn\,(2)2r0v}_{\mathrm{NLP-soft},S_{1,C_F n_f}}(z) = \frac{\alpha_s^2}{(4\pi)^2} C_F n_f \left(-\frac{8}{3\epsilon^2} - \frac{32}{9\epsilon}(3\ln(1-z)-2) \right.$$
$$\left. + \frac{4}{27}\left(-144\ln^2(1-z) + 21\pi^2 + 192\ln(1-z) - 122\right) + \mathcal{O}\left(\epsilon\right) \right). (7.19)$$

This is the only $C_F n_f$ proportional contribution to the cross-section. Our result obtained through calculation of objects appearing in the factorisation formula and presented in (7.19) has been verified by a calculation of QCD diagrams using the expansion-by-regions method [150].

Lastly for the S_1 soft function, we must consider the $C_F C_A$ proportional pieces in (6.59). This contribution is labelled by $S^{(2)2r0v}_{1,C_F C_A}$. Inserting this piece into an analogue of (7.15), we find[2]

$$\Delta^{dyn\,(2)2r0v}_{\mathrm{NLP-soft},S_{1,C_F C_A}}(z) = -4\frac{\alpha_s^2}{(4\pi)^2} C_F C_A \left(\frac{\Omega^4}{\mu^4}\right)^{-\epsilon} \frac{e^{2\epsilon\gamma_E}\Gamma[1-\epsilon]^2}{\epsilon^3(1-2\epsilon)^2\Gamma[1-4\epsilon]} \qquad (7.20)$$
$$\times \left(\frac{(3-25\epsilon+50\epsilon^2-23\epsilon^3)}{(3-2\epsilon)} - \frac{3\Gamma[2-2\epsilon]^2}{\Gamma[1-\epsilon]\Gamma[1-3\epsilon]}\,{}_3F_2(-\epsilon,-\epsilon,-\epsilon;1-\epsilon,-3\epsilon;1)\right).$$

The hypergeometric functions in the d - dimensional result must be carefully expanded, this can be accomplished the using `HypExp` package [151], which yields

$$\Delta^{dyn\,(2)2r0v}_{\mathrm{NLP-soft},S_{1,C_F C_A}}(z) = \frac{\alpha_s^2}{(4\pi)^2} C_F C_A \left(\frac{8}{\epsilon^3} - \frac{4}{3\epsilon^2}(24\ln(1-z)-11)\right.$$
$$-\frac{16}{9\epsilon}\left(-36\ln^2(1-z) + 33\ln(1-z) + 6\pi^2 - 16\right)$$
$$-\frac{256}{3}\ln^3(1-z) + \frac{352}{3}\ln^2(1-z) + \frac{128}{3}\pi^2\ln(1-z)$$
$$\left.-\frac{1024}{9}\ln(1-z) - \frac{616\zeta(3)}{3} - \frac{154\pi^2}{9} + \frac{1484}{27} + \mathcal{O}(\epsilon)\right). \qquad (7.21)$$

An interesting observation is that leading logarithmic contributions of form $\alpha_s^2 \ln^3(1-z)$ appearing here are exactly cancelled by the one-real one-virtual contributions for the S_1 soft function in (7.14), such that there are no leading logarithmic contributions proportional to the $C_F C_A$ colour structure in the cross-section.

The $C_F C_A$ result for the cross-section due to S_1 cannot a priori be directly compared against an expansion-by-regions calculation, as the latter is organised by collecting together

---

[2]We note that this result is d-dimensional, whereas I_5 above was obtained only in ϵ expansion. This is because we have performed the reduction without an additional ω dependent delta function for terms that produce the tricky ω dependent master integrals, we then checked that they agree in the ϵ expansion, and used these expressions instead of the expanded integrals after the dr integration. This means that our inclusive result is more general than what is available in the literature, as it has complete d-dimensional dependence. We are only able to compare the results for the cross-section order by order in ϵ.

all diagrams with the same final state, for example real-real gluon emission. However, in the SCET calculation these contributions are separated between S_1, S_3, and S_4 soft functions. Hence, we can only compare the $C_F C_A$ proportional pieces in the cross-section after considering also the contributions to the cross-section due to S_3 and S_4.

We begin with S_3. The relevant piece of factorisation formula is

$$\Delta^{dyn\,(2)2r0v}_{\mathrm{NLP-soft},S_3}(z) = 4\,Q\,H^{(0)}(Q^2)\ \int d\omega\, J^{(0)}_{3,1}\left(x_a(n_+ p_A);\omega\right) S^{(2)}_3\left(\Omega,\omega\right). \tag{7.22}$$

Inserting now the result in (6.60) and integrating over the convolution variable yields the following expression

$$\Delta^{dyn\,(2)2r0v}_{\mathrm{NLP-soft},S_3}(z) = 4\,\frac{\alpha_s^2}{(4\pi)^2}\,C_F C_A\left(\frac{\Omega^4}{\mu^4}\right)^{-\epsilon}\frac{1}{\epsilon}\frac{(1-\epsilon)}{(1-2\epsilon)^2(3-2\epsilon)}\frac{e^{2\epsilon\gamma_E}\Gamma[1-\epsilon]^2}{\Gamma[1-4\epsilon]}. \tag{7.23}$$

Next, setting the soft scale to $\Omega = Q(1-z)$, and the scale $\mu = Q$, we expand in ϵ and arrive at

$$\Delta^{dyn\,(2)2r0v}_{\mathrm{NLP-soft},S_3}(z)\ =\ \frac{\alpha_s^2}{(4\pi)^2}\,C_F C_A\left(\frac{4}{3\epsilon}-\frac{4}{9}\left(12\ln(1-z)-11\right)+\mathcal{O}\left(\epsilon\right)\right). \tag{7.24}$$

Now, we consider the S_4 soft function contribution. The adapted factorisation formula, with the scalar collinear function in (6.10), is

$$\Delta^{dyn\,(2)2r0v}_{\mathrm{NLP-soft},S_4}(z) = 4\,Q\,H^{(0)}(Q^2)\ \int d\omega_1 d\omega_2\, J^{(0)}_4\left(x_a(n_+ p_A)\right) S^{(2)}_4\left(\Omega,\omega_1,\omega_2\right). \tag{7.25}$$

Inserting (6.61) and performing the convolution integrals yields

$$\Delta^{dyn\,(2)2r0v}_{\mathrm{NLP-soft},S_4}(z) = -4\,\frac{\alpha_s^2}{(4\pi)^2}\,C_F C_A\left(\frac{\Omega^4}{\mu^4}\right)^{-\epsilon}\frac{1}{\epsilon}\frac{(1-\epsilon)}{(1-2\epsilon)^2(3-2\epsilon)}\frac{e^{2\epsilon\gamma_E}\Gamma[1-\epsilon]^2}{\Gamma[1-4\epsilon]}, \tag{7.26}$$

which is identical to $\Delta^{dyn\,(2)2r0v}_{\mathrm{NLP-soft},S_3}(z)$ in (7.23) up to a minus sign, such that the two cancel each other in the expression for the full Drell-Yan cross-section at this order.

With this observation, it becomes apparent that we can in fact directly compare the result for the $C_F C_A$ proportional cross-section due to the S_1 soft function contribution against the calculation employing the expansion-by-regions method. Indeed, the result in (7.21) is reproduced by sum of expanded QCD diagrams with two radiated soft gluons and two radiated soft ghosts [150].

Last, we consider the contribution the Drell-Yan cross-section due to the S_5 NNLO soft function with two insertions of the $\mathcal{L}_{\xi q}$ terms of the next-to-leading power Lagrangian. As explained in section 6.2.3, the spin trace in (3.81) has already been performed and is included in the soft function, therefore the factorisation formula we must consider here is

$$\Delta^{dyn\,(2)2r0v}_{\mathrm{NLP-soft},S_5}(z) = 4\,Q\,H^{(0)}(Q^2)\ \int d\omega_1 d\omega_2\, J^{(0)}_5\left(x_a(n_+ p_A)\right) S^{(2)}_5\left(\Omega,\omega_1,\omega_2\right), \tag{7.27}$$

with the soft function given by (6.62) and the scalar collinear function by (6.11). Performing the integrals, we arrive at

$$\Delta^{dyn\,(2)2r0v}_{\mathrm{NLP-soft},S_5}(z) = 8\,\frac{\alpha_s^2}{(4\pi)^2}\,\left(C_F^2-\frac{1}{2}C_F C_A\right)\left(\frac{\Omega^4}{\mu^4}\right)^{-\epsilon}\frac{(1-\epsilon)}{\epsilon(1-2\epsilon)^2}\frac{e^{2\epsilon\gamma_E}\Gamma[1-\epsilon]^2}{\Gamma[1-4\epsilon]}. \tag{7.28}$$

Setting $\mu = Q$ and expanding this result

$$\Delta_{\mathrm{NLP-soft},S_5}^{dyn\,(2)2r0v}(z) = \frac{\alpha_s^2}{(4\pi)^2}\left(C_F^2 - \frac{1}{2}C_F C_A\right)\left(\frac{8}{\epsilon} - 32\ln(1-z) + 24 + \mathcal{O}(\epsilon)\right), \quad (7.29)$$

we find agreement with the calculation using the expansion-by-regions method [150].

A concluding remark regarding the soft functions beginning at α_s^2, namely S_3, S_4, and S_5, is in order. We can see from the results of expansion in ϵ for these soft functions in (7.24) and (7.29), that they do not contribute leading logarithmic terms to the cross-section. This confirms an assumption made in [40]. Specifically, this confirms that there is no logarithmically enhanced off diagonal mixing of these soft functions with the single gluon soft function, hence, they do not contribute leading logarithmic terms to the cross-section.

Kinematic contribution

Lastly, we consider the NNLO contribution to the next-to-leading power Drell-Yan cross-section due to kinematic corrections which are listed in equations (3.73)–(3.76). Considering the perturbative expansion of each of the contributing objects, the total kinematic correction at NNLO is given by

$$\Delta_{\mathrm{NLP}}^{kin\,(2)}(z) = H'^{(1)}\!\left(Q^2\right)Q^2\,S_{K3}^{(1)}(\Omega) + \sum_i\left[H^{(1)}\!\left(Q^2\right)S_{Ki}^{(1)}(\Omega) + H^{(0)}\!\left(Q^2\right)S_{Ki}^{(2)}(\Omega)\right]. \quad (7.30)$$

The required one-loop hard function is written in equation (2.59) and the one-loop kinematic soft functions are listed in equations (5.21), (5.23), (5.24), and (5.25). We also now need the two-loop kinematic soft functions. The results for these objects are listed in equations (5.26) – (5.29). Combining these elements together, we find

$$\begin{aligned}
\Delta_{\mathrm{NLP}}^{kin\,(2)}(z) \;=\; \frac{\alpha_s^2}{(4\pi)^2}\Bigg[& C_F^2\bigg(\frac{16}{\epsilon^2} - \frac{192\ln(1-z) + 96}{\epsilon} + 512\ln^2(1-z) \\
& + 192\ln(1-z) - 40\pi^2 - 256\bigg) + C_F C_A\bigg(\frac{88}{3\epsilon} - \frac{352\ln(1-z)}{3} \\
& - \frac{8\pi^2}{3} + \frac{476}{9}\bigg) + C_F n_f\bigg(-\frac{16}{3\epsilon} + \frac{64\ln(1-z)}{3} - \frac{56}{9}\bigg)\Bigg]. \quad (7.31)
\end{aligned}$$

We observe that there are no leading logarithmic contributions in the NLP cross-section due to kinematic corrections.

The corrections due to integration over leading power matrix elements with the phase space expanded to next-to-leading power, which corresponds to the kinematic corrections, has been previously considered within the expansion-by-regions or the diagrammatic approach. However, an expression which could directly be compared to (7.31) has not been provided explicitly. It forms a part of equation (4.6) and (5.2) in [37], but it cannot be disentangled from the contribution due to the next-to-leading power matrix element. Therefore, we compare (7.31) to a calculation using the expansion-by-regions method in which the leading power matrix elements describing double-real, and one-real, one-virtual emissions is integrated over the phase space which is expanded to next-to-leading power [150]. We find agreement.

7.1.3   Next-to-next-to-next-to-leading order

The current perturbative knowledge about the ingredients making up the NLP factorisation formula in (3.81) does not allow us to verify it completely at N³LO. However, partial results can be obtained. For example, in the N³LO expansion of (3.81) there exists a contribution due to one-loop collinear functions convoluted with their respective two-loop soft functions. Interestingly, there exist published results which allow us to check one such contribution. Namely, in [32] the expansion-by-regions method is used to compute one-virtual two-real gluon emission contribution to the Drell-Yan cross-section at threshold. Part of this calculation is the contribution due to a collinear virtual loop, with two soft gluons radiated. The analogue in SCET is precisely the combination of one-loop collinear functions with two-loop soft functions. In [32], the C_F^3 proportional pieces of the cross-section are presented. In the NLP SCET framework, we can reproduce this result since only the S_1 soft function contains a C_F^2 term that originates from the cut two-soft gluon contribution (there is a C_F^2 contribution in S_5, however this is due to soft quarks in the final state and the authors of [32] do not consider such contributions) and its corresponding collinear function at one-loop carries terms proportional to C_F. Therefore, we now focus on the following part of the factorisation formula expanded to the third order in the coupling constant

$$\Delta_{\mathrm{NLP-coll},\, C_F^3}^{dyn\,(3)}(z) \;=\; 4Q \int d\omega \, J_{1,1}^{(1)}(x_a\, n_+ p_A; \omega)\, S_{1,C_F^2}^{(2)}(\Omega; \omega)\,. \tag{7.32}$$

For the one-loop collinear function we use the C_F part of the result given in (4.84) after the colour generator and Dirac-index Kronecker-symbol are removed. The relevant two-loop soft function is given in the top line of (6.59). For concreteness, we write it again in terms of the variable ω here

$$S_{1,C_F^2}^{(2)2r0v}(\Omega, \omega) = 8\frac{\alpha_s^2}{(4\pi)^2}\, C_F^2 \left(\frac{\omega\, (\Omega - \omega)^3}{\mu^4}\right)^{-\epsilon} \frac{1}{\omega}\, \frac{1}{\epsilon^2}\, \frac{e^{2\epsilon\gamma_E}\Gamma[1-\epsilon]}{\Gamma[1-3\epsilon]}\theta(\Omega-\omega)\theta(\omega). \tag{7.33}$$

We perform the convolution according to (7.32) and arrive at the following d-dimensional result

$$\begin{aligned}\Delta_{\mathrm{NLP-coll},\, C_F^3}^{dyn\,(3)}(z) \;=\;& 32\frac{\alpha_s^3}{(4\pi)^3}C_F^3 \left(\frac{Q\,\Omega^5}{\mu^4}\right)^{-\epsilon} \frac{1}{\epsilon^4}(-4 + 7\epsilon + \epsilon^2) \\ & \times \frac{e^{3\epsilon\gamma_E}\Gamma[1+\epsilon]\Gamma[1-\epsilon]^2\Gamma[1-2\epsilon]}{\Gamma[1-5\epsilon]\Gamma[3-2\epsilon]}.\end{aligned} \tag{7.34}$$

Setting $\Omega = Q(1-z)$ and $\mu = Q$, and expanding in ϵ we find

$$\begin{aligned}\Delta_{\mathrm{NLP-coll},\, C_F^3}^{dyn\,(3)}(z) \;=\;& \frac{\alpha_s^3}{(4\pi)^3}C_F^3 \left(-\frac{64}{\epsilon^4} + \frac{80(4\ln(1-z)-1)}{\epsilon^3} + \frac{16}{\epsilon^2}\left(-50\ln^2(1-z)\right.\right. \\ & \left. + 25\ln(1-z) + 7\pi^2 - 6\right) + \frac{1}{\epsilon}\left(\frac{4000}{3}\ln^3(1-z) - 1000\ln^2(1-z)\right. \\ & \left.\left. -560\pi^2\ln(1-z) + 480\ln(1-z) + 2624\zeta(3) + 140\pi^2 - 128\right)\right.\end{aligned}$$

$$-\frac{5000}{3}\ln^4(1-z)+\frac{5000}{3}\ln^3(1-z)+1400\pi^2\ln^2(1-z)$$

$$-1200\ln^2(1-z)-700\pi^2\ln(1-z)+640\ln(1-z)$$

$$+\zeta(3)(3280-13120\ln(1-z))+\frac{62\pi^4}{5}+168\pi^2-192\Bigg).\qquad(7.35)$$

The finite constant terms are not quoted in [32]. However, aside from the finite constant terms, our expanded result in (7.35) agrees with equation (45) of [32] after the latter is multiplied by a factor of two, to account for the anticollinear contribution.

Similarly to the C_F^2 contribution to the soft functions, the colour structure $C_F n_f$ appears only in the S_1 soft function, see second line of (6.59). This enables us to make a prediction for contributions to the N³LO cross-section due to a collinear virtual loop and two real-parton emission proportional to $C_F^2 n_f$ and $C_F C_A n_f$. We consider

$$\Delta^{dyn\,(3)}_{\mathrm{NLP-coll},\,(C_F,C_A)C_F n_f}(z) = 4Q\int d\omega\, J^{(1)}_{1,1}(x_a\,n_+ p_A;\omega)\, S^{(2)}_{1,C_F n_f}(\Omega;\omega),\qquad(7.36)$$

where, as before, we use equation (4.84) for the one-loop collinear function. We write here again the $C_F n_f$ proportional contribution to S_1 from the second line in equation (6.59). We have in terms of the ω variable

$$S^{(2)}_{1,C_F n_f}(\Omega,\omega) = -4\frac{\alpha_s^2}{(4\pi)^2}C_F\,n_f\left(\frac{\omega^2(\Omega-\omega)^2}{\mu^4}\right)^{-\epsilon}\frac{1}{\omega}\frac{(1-\epsilon)^2}{\epsilon(3-2\epsilon)}$$

$$\times\frac{e^{2\epsilon\gamma_E}\Gamma[1-\epsilon]^2}{\Gamma[2-2\epsilon]^2}\theta(\Omega-\omega)\theta(\omega).\qquad(7.37)$$

We again obtain a d-dimensional result. Then, setting $\Omega = Q(1-z)$ and $\mu = Q$, we expand in ϵ and find the following expression

$$\Delta^{dyn\,(3)}_{\mathrm{NLP-coll},\,(C_F,C_A)C_F n_f}(z) = \frac{\alpha_s^3}{(4\pi)^3}\Bigg(C_F^2 n_f\bigg(\frac{64}{9\epsilon^3}-\frac{16(60\ln(1-z)-47)}{27\epsilon^2}$$

$$-\frac{16}{81\epsilon}\Big(-450\ln^2(1-z)+705\ln(1-z)+57\pi^2-418\Big)$$

$$+\Big(-\frac{4000}{27}\ln^3(1-z)+\frac{9400}{27}\ln^2(1-z)+\frac{1520}{27}\pi^2\ln(1-z)$$

$$-\frac{33440}{81}\ln(1-z)-\frac{2368\zeta(3)}{9}-\frac{3572\pi^2}{81}+\frac{53552}{243}\Big)\bigg)$$

$$+C_F C_A n_f\bigg(-\frac{80}{9\epsilon^2}+\frac{16(75\ln(1-z)-46)}{27\epsilon}$$

$$+\frac{20}{81}\Big(-450\ln^2(1-z)+552\ln(1-z)+57\pi^2-340\Big)\bigg)\Bigg).\ (7.38)$$

7.2 Gluon-antiquark channel

In this section we focus on the fixed-order results we can obtain in the off-diagonal channel of the Drell-Yan process. The next-to-leading power factorisation formula is written in equation (3.113). Since this channel does not contain a leading power contribution, the structure at NLP is somewhat simpler than the one encountered in the diagonal channel and the number of contributing terms is smaller.

The generalised soft function with soft quark insertions relevant for this channel starts at $\mathcal{O}(\alpha_s)$ and the result is given in equation (5.31). Therefore, to obtain the cross-section result at $\mathcal{O}(\alpha_s)$ we must combine the soft function with just the tree-level results for the hard and collinear functions according to the next-to-leading order accurate factorisation formula

$$
\begin{aligned}
\Delta_{g\bar{q}}^{(1)}(z) \;=\;& 4H^{(0)}(Q^2) \int d\omega_1\, d\omega_2 \\
& \times G_{\xi q}^{*(0)}(x_a n_+ p_A; \omega_2) G_{\xi q}^{(0)}(x_a n_+ p_A; \omega_1) S_{g\bar{q}}^{(1)}(\Omega, \omega_1, \omega_2)\,.
\end{aligned}
\tag{7.39}
$$

The hard function $H^{(0)}(Q^2)$ is the same as at leading power and the necessary result is given in equation (2.59). The tree-level result for the collinear function is given in (4.98). Collecting together all the individual ingredients, performing the integrals over convolution variables ω_1 and ω_2, then expanding in ϵ, yields

$$
\Delta_{g\bar{q}}^{(1)}(z) \;=\; \frac{\alpha_s}{4\pi}\left(-\frac{1}{\epsilon} + 2\ln(1-z) - 2\ln\left(\frac{\mu}{Q}\right)\right)\,.
\tag{7.40}
$$

This result was compared against a calculation performed using the expansion-by-regions method [150] and we find agreement. After the $1/\epsilon$ pole is subtracted using PDF renormalization we can also compare this result with equation (B.37) of [116] again finding agreement.

Part IV

Resummation at next-to-leading power

8

Drell-Yan: resummation at next-to-leading power

Resummation is a powerful concept, not only supplementing fixed-order computations and increasing the predictive power of theoretical calculations, but in certain cases simply making the predictions possible. Factorisation theorems form the basis for resummation by segregating physical effects manifest at different energy scales into objects which naturally exist at the respective relevant scales. In dimensional regularization, each of these objects may contain divergences. Renormalization renders each object finite separately and introduces spurious scale dependence into each object, however the physical observable cannot depend on this scale. One then derives renormalization group equations which govern the evolution of each piece in the factorisation formula. By solving the renormalization group equations, we can obtain results to all orders in α_s.

We have thus far derived formal d-dimensional factorisation theorems for the $q\bar{q}$ and $g\bar{q}$-channels of the Drell-Yan process in the threshold regime in chapter 3 and validated their correctness at next-to-next-to-leading fixed perturbative order in chapter 7. In this section, we make a conceptual leap from performing calculations at fixed orders in α_s to obtaining results valid to all orders in perturbation theory. This includes shifting the outlook on the role of the factorisation theorems. Up to this point, we have presented formal results containing regularized quantities. For the purpose of resummation, we adopt the more traditional understanding, where each object in the factorisation formula is separately renormalized. The analysis presented here is based on the published work [65]. We focus on the leading logarithmic resummation carried out in the $q\bar{q}$-channel. Issues related to convolutions between collinear and soft functions complicate resummation beyond leading logarithmic accuracy in the $q\bar{q}$-channel and already at the leading logarithmic level in the $g\bar{q}$-channel. In section 8.5 we showcase these issues using the collinear functions results from chapter 4.

8.1 Factorisation formula: leading logarithmic accuracy

In equation (3.81) we have presented the all order next-to-leading power factorisation formula for the $q\bar{q}$-channel of the Drell-Yan process at threshold. Indeed, we saw in

chapter 7 that the fixed-order results found in literature can be reproduced by bringing together the expressions for the objects appearing in the factorisation formula, each one computed to the appropriate accuracy, and performing the convolution integrals in d-dimensions. In particular, not only the leading logarithms at NNLO, $\alpha_s^2 \ln^3(1-z)$, were correctly obtained in the results given in section 7.1.2, but also the subleading logarithms, $\alpha_s^2 \ln^2(1-z)$, and $\alpha_s^2 \ln(1-z)$, along with the constant terms. Since the aim of the considerations presented in this section is to calculate the resummed result at next-to-leading power at the leading logarithmic accuracy, we must first determine which are the relevant contributing pieces in the total sum of five contributions found in equation (3.81).

We first stress that in this section, as mentioned above, we move from the formal d-dimensional treatment of factorisation presented in chapter 3 towards the more common view of factorisation formulas. Here, the objects appearing in the formulas are renormalized and no longer exhibit divergences. The dimension is understood to be set to $d = 4$. Concretely, this implies that all the factors in the factorisation formula in (3.81) depend on μ. This includes the partonic cross-section on the left-hand side of equation (3.81). The scale dependence cancels upon convolution of the partonic cross-section with the parton distribution functions. Each of the factors, the hard, collinear, and soft functions, appearing in (3.81) depend on one characteristic scale. We chose the renormalization scale μ to be of the order of the collinear scale, $\mathcal{O}(Q\lambda)$. With the scale $\mu \sim Q\lambda$ there are no large logarithms in the collinear functions at any order in perturbation theory. However, the large logarithms of $(1-z)$ are contained in the hard and soft functions. We sum these logarithms to all orders in α_s at the leading logarithmic accuracy.

The leading logarithmic series at next-to-leading power is given by the $\alpha_s^n \ln^{2n-1}(1-z)$ terms. The soft functions which appear in the next-to-leading power factorisation formula in (3.81), and are given in equations (3.83) – (3.87), begin contributing at $\mathcal{O}(\alpha_s)$ or higher. This is due to the fact that the generalised soft functions contain explicit insertions of $\mathcal{B}^+$ or q^+ soft building blocks and therefore involve at least one soft parton radiated into the final state. A leading logarithmic contribution at next-to-leading power is generated at one-loop accuracy only if the soft function at one-loop contains a $\alpha_s \ln(1-z)$ term and the corresponding collinear function starts at $\mathcal{O}(\alpha_s^0)$. For the purpose of leading logarithmic resummation, the terms for which the relevant collinear functions do not have a tree-level contribution can be dropped. At next-to-leading power, we have already found that the only hard current which contributes is the leading power hard current. This hard current does contain a tree-level contribution. Considering the list of next-to-leading power soft functions in equations (3.83) – (3.87) we find that for leading logarithmic resummation, only the contributions from operators with a single soft gluon are necessary. The reason for this is that the soft functions with an insertion of soft building blocks which begin with the emission of two soft gluons start at $\mathcal{O}(\alpha_s^2)$. These soft functions could in principle contribute to the leading logarithmic series at next-to-leading power if the $\mathcal{O}(\alpha_s^2)$ contribution would contain a $\alpha_s^2 \ln^3(1-z)$ term. Such a term could arise, if the one-loop mixing with a one-gluon soft function is logarithmically enhanced. However, logarithmic enhancements of the cusp anomalous dimension of this type are not known for off-diagonal operator mixing. We also assume that the logarithmically enhanced mixing of this type is absent in this case. By this reasoning the soft functions S_2 and S_3 in equations (3.84) and

(3.85) respectively are excluded. Soft functions which are induced by the double insertion of $\mathcal{L}_\xi^{(1)}$ and the double insertion of $\mathcal{L}_{\xi q}^{(1)}$ also start at $\mathcal{O}(\alpha_s^2)$. This fact also excludes the possibility of leading logarithmic contributions arising from such soft functions by the same reasoning as above. Therefore, we can drop soft functions S_4 and S_5 in equations (3.86) and (3.87) respectively.

Considering the list of soft functions appearing at next-to-leading power given in equations (3.83) – (3.87) we arrive at the conclusion that the only soft function which contains a leading logarithmic contribution at next-to-leading power is the first soft function in the list, namely S_1 given in equation (3.83). We remind the reader that there exists one more soft function, S_6, which starts at $\mathcal{O}(\alpha_s)$ with a single soft gluon emission. The S_6 soft function is given in equation (3.88). However, we have excluded its contribution to all orders in perturbation theory due to parity conservation in QCD as detailed below equation (3.88).

Following the above considerations, we now write down the dynamical next-to-leading power factorisation formula at leading logarithmic accuracy, starting from the general next-to-leading power formula in equation (3.81). We find

$$\Delta_{\text{NLP}-\text{LL}}^{dyn}(z) \;\; = \;\; 4\,H(Q^2,\mu_c)\,Q \int d\omega\, J_{1,1}^{(0)}\left(x_a n_+ p_A; \omega, \mu_c\right)\,S_1(Q(1-z);\omega,\mu_c). \quad (8.1)$$

A few explanations regarding the simplifications performed in arriving at such a simple expression are in order.

In the above formula, we have explicitly written the scale dependence of the hard, collinear, and soft functions. As we have explained earlier in the text, the H and S_1 functions are evolved from the hard, $\mu_h \sim Q$, and soft, $\mu_s \sim Q(1-z)$, scales to a common collinear scale, $\mu_c \sim Q\sqrt{1-z}$.

We have made use of the collinear function decomposition into parts multiplying a collinear momentum delta function, $\delta(n_+ p - x_a n_+ p_A)$, and its derivative, $\frac{\partial}{\partial(n_+p)}\delta(n_+ p - x_a n_+ p_A)$, as given in (3.89). Only the term proportional to $\delta(n_+p - x_a n_+ p_A)$, the $J_{1,1}$ piece, appears in (8.1). This is due to the fact that the leading logarithmic series is generated by contributions for which the hard function starts at tree level. However, we know that the tree-level hard function is momentum independent. Therefore, the derivative contained in the collinear function, multiplying the $J_{1,2}$ piece, evaluates to zero once it is integrated by parts to act on the tree-level hard function and hence cannot contribute to the leading logarithms.

At this point, one makes use of the collinear momentum delta function which multiplies the $J_{1,1}$ term to trivially evaluate the $d(n_+p)$ integral in (3.81). Moreover, we have combined the Kronecker delta $\delta_{\gamma\beta}$ in the decomposition of the collinear function in (3.89) with the $\left[\left(\frac{\not{n}_-}{4}\right)\gamma_{\perp\rho}\left(\frac{\not{n}_+}{4}\right)\gamma_\perp^\rho\right]_{\beta\gamma}$ spin structure in (3.81). This yields a trace over the spin structures which evaluates to $-(1-\epsilon)$. Additionally, since we no longer need the contributions to the collinear functions which are associated with derivatives on collinear momentum delta functions and with this we do not have to distinguish between the momentum derivatives acting on either the C or C^* hard matching coefficients, the h.c. piece in (3.81) simply contributes a factor of two to the cross-section in (8.1).

The last simplification on which we wish to comment is with regards to the argument of the hard function. The hard function which we obtain in (3.81) is given by $H(\hat{s}) =$

$|C^{A0,A0}(x_a n_+ p_A, x_b n_- p_B)|^2$. However, in (8.1) we keep only the $H(Q^2)$ piece. This is the leading power contribution which is the only necessary piece here due to the fact that the power suppression here is provided by time-ordered product insertions of the subleading-power Lagrangian terms.

8.2 Soft functions and kinematic corrections

The lowest-ordered solution for the soft function appearing in the leading logarithmic factorisation formula in (8.1) is given in (5.7). The expansion of this result in ϵ, presented in (5.11), shows that already at the lowest order in the α_s expansion the soft function S_1 contains a divergence. This divergence is interpreted as mixing of the S_1 soft function into the S_{x_0} soft function [40], which in turn is defined as

$$S_{x_0}(\Omega) = \int \frac{dx^0}{4\pi} e^{ix^0 \Omega/2} \frac{-2i}{x^0 - i\varepsilon} \frac{1}{N_c} \text{Tr} \langle 0| \bar{\mathbf{T}} \left[Y_+^\dagger(x^0) Y_-(x^0) \right] \mathbf{T} \left[Y_-^\dagger(0) Y_+(0) \right] |0\rangle. \qquad (8.2)$$

This object is related to the leading power soft function, that is given in equation (3.30), by a factor of $-2i/x^0$. This factor provides a $\mathcal{O}(\lambda^2)$ power suppression and leads to the appearance of the theta function, $\theta(\Omega)$, in the tree-level result for this auxiliary soft function, $S_{x_0}(\Omega) = \theta(\Omega) + \mathcal{O}(\alpha_s)$, that is needed to cancel the divergence in (5.11). At leading power, the introduction of such auxiliary soft functions is not necessary, as the soft function in (3.30) is not divergent at tree level. Hence, the appearance of such a soft function beyond leading power could seem peculiar. However, we note that similar functions with collinear fields were needed in the renormalization of subleading gluon jet functions [152]. Moreover, the S_{x_0} soft function in (8.2) is the position-space and Drell-Yan process equivalent of the "θ-soft functions" which were introduced in [54] for the treatment of thrust distribution at subleading-power .

The soft functions are renormalized by writing

$$S_A(\Omega, \omega_i)|_{\text{ren}} = \sum_B \int d\Omega' \int d\omega'_j \, Z_{AB}(\Omega, \omega_i; \Omega', \omega'_j) \, S_B(\Omega', \omega'_j)|_{\text{bare}} \qquad (8.3)$$

where ω_i, ω'_j denote sets, that could possibly be empty, of continuous variables which parameterise the non-locality of the soft functions. This is in addition to the dependence of the particular soft function on Ω. The number of arguments ω_i could be different than the number of arguments ω'_j. The integration in (8.3) is over all ω'_j that the bare soft function depends on. If the dependence of the soft function is only on Ω, then the integration $\int d\omega'_j$ is omitted. Focusing now on the case at hand, the S_1 soft function satisfies

$$\begin{aligned}
S_1(\Omega, \omega)|_{\text{ren}} &= \int d\Omega' \int d\omega' \, Z_{1,1}(\Omega, \omega; \Omega', \omega') \, S_1(\Omega', \omega')|_{\text{bare}} \\
&+ \int d\Omega' \, Z_{1,0}(\Omega, \omega; \Omega') \, S_{x_0}(\Omega')|_{\text{bare}}
\end{aligned} \qquad (8.4)$$

with

$$Z_{1,1}(\Omega, \omega; \Omega, \omega') = \delta(\Omega - \Omega')\delta(\omega - \omega') + \mathcal{O}(\alpha_s), \qquad (8.5)$$

$$Z_{1,0}(\Omega, \omega; \Omega') = \frac{\alpha_s C_F}{2\pi} \frac{1}{\epsilon} \delta(\Omega - \Omega') \delta(\omega) + \mathcal{O}(\alpha_s^2). \tag{8.6}$$

The first term on the right-hand side of (8.4) is known as the "diagonal term". The term in the second line of (8.4) is called the "mixing term" and it subtracts the divergent part of the diagonal term present in the first line. This procedure results in a finite, renormalized soft function at $\mathcal{O}(\alpha_s)$.

The complete one-loop anomalous dimension matrix for the above soft functions required for LL resummation at next-to-leading power is derived in appendix A.2 of [40].

A priori, one could also expect that the kinematic soft functions, $S_{K1}(\Omega)$, $S_{K2}(\Omega)$, and $S_{K3}(\Omega)$ defined in equations (3.77), (3.78), and (3.79) respectively, could also contribute to leading logarithms at next-to-leading power. Each of the three soft functions $S_{Ki}(\Omega)$ vanishes at tree-level order, $\mathcal{O}(\alpha_s^0)$. However, they all mix into $S_{x_0}(\Omega)$ through a $1/\epsilon$ pole at $\mathcal{O}(\alpha_s)$. The one-loop order results for the three kinematic soft functions are separately divergent, and each produces a next-to-leading power leading logarithmic contribution at $\mathcal{O}(\alpha_s)$. Concretely, in section 5.1.2 we have explicitly calculated the kinematic soft functions contributions and found the following results

$$S_{K1}(\Omega) = \frac{\alpha_s C_F}{2\pi} \left(\frac{1}{\epsilon} + 2 \ln \frac{\mu}{\Omega} - 2 \right) \theta(\Omega) + \mathcal{O}(\alpha_s^2), \tag{8.7}$$

$$S_{K2}(\Omega) = \frac{\alpha_s C_F}{2\pi} \left(\frac{3}{\epsilon} + 6 \ln \frac{\mu}{\Omega} + 6 \right) \theta(\Omega) + \mathcal{O}(\alpha_s^2), \tag{8.8}$$

$$S_{K3}(\Omega) = \frac{\alpha_s C_F}{2\pi} \left(-\frac{4}{\epsilon} - 8 \ln \frac{\mu}{\Omega} \right) \theta(\Omega) + \mathcal{O}(\alpha_s^2). \tag{8.9}$$

However, we note that when these contributions are summed, the divergences cancel and the contribution of all three kinematic corrections taken together is finite

$$\sum_{i=1}^{3} S_{Ki}(\Omega) = 2 \frac{\alpha_s C_F}{\pi} \theta(\Omega). \tag{8.10}$$

Therefore, these three kinematic soft functions do not contribute to the series of leading logarithms in the Drell-Yan cross-section. The kinematic soft functions all come from the same $S_0(x)$, hence the diagonal renormalization of all three kinematic soft functions involves the same cusp anomalous dimension. The general structure of the renormalization group equation then ensures that the cancellation of the leading logarithmic contributions coming from the kinematic soft functions in the Drell-Yan partonic cross-section $\Delta_{q\bar{q}}(z)$ (however, not $\hat{\sigma}_{q\bar{q}}(z)$ as S_{K3} does not exist for $\hat{\sigma}_{q\bar{q}}(z)$) holds to all orders in α_s, see appendix A.1 of [40] for more details.

Lastly, additional power corrections do arise from expanding the hard matching coefficient $H(\hat{s}) = H(Q^2) + Q^2(1-z)H'(Q^2) + \mathcal{O}(\lambda^4)$, as is described by equation (3.76). However, similarly to the first three kinematic corrections, these terms do not give leading logarithmic contributions at next-to-leading power. The reason for this occurrence is the fact that the tree-level leading power soft function is given by $\delta(1-z)$. This delta function sets the $\mathcal{O}(\alpha_s \ln(1-z))$ term, which $H'(Q^2)$ starts with, to zero. Any further term which comes from the product of $(1-z)H'(Q^2)$ with the leading power soft function can at most contribute at the next-to-leading logarithmic accuracy.

To summarise, we have shown how there are no leading logarithmic contributions to the Drell-Yan partonic cross-section coming from the kinematic correction part $\Delta_{\text{NLP}}^{kin}(z)$. Therefore, resummation at leading logarithmic accuracy at next-to-leading power is achieved by obtaining all order results for the objects appearing in the dynamic contribution to the partonic cross-section $\Delta_{\text{NLP}-\text{LL}}^{dyn}(z)$ given in equation (8.1). We focus on this next.

8.3   Resummation

The necessary ingredients are now in place for us to sum the leading logarithms at next-to-leading power to all order in perturbation theory. The logarithms in the cross-section originate from ratio of scales which are present in the process. Here, we use the renormalization group equations (RGEs) for the hard and soft functions to sum the logarithms. This is done by evolving the hard function from the hard scale $\mu_h \sim Q$ and the soft functions from the soft scale $\mu_s \sim Q(1-z)$ to a common collinear scale, $\mu_c \sim Q\sqrt{1-z}$. We chose μ_c to be of the order of the collinear scale for convenience, this way no large logarithms appear in the collinear function and we do not require the RGE of the collinear function. We focus on the expansion of the quantity $\Delta(z) = \hat{\sigma}(z)/z$ as is customary in the literature. Moreover, this simplifies the discussion since, as we have explained above, the kinematic corrections cancel at leading logarithmic accuracy for $\Delta(z)$, which, on the other hand, is not the case for $\hat{\sigma}(z)$.

We have found in section 3.2.2 that only the leading power J^{A0} hard current contributes to the Drell-Yan cross-section at next-to-leading power. Therefore the RGE for the hard matching function $H(Q^2, \mu)$ is given by

$$\frac{d}{d \ln \mu} H(Q^2, \mu) = \left(2\Gamma_{\text{cusp}} \ln \frac{Q^2}{\mu^2} + 2\gamma \right) H(Q^2, \mu), \qquad (8.11)$$

which follows from the anomalous dimension of the leading power SCET J^{A0} operator. It is known that the time-ordered products formed by insertions of subleading power Lagrangian terms with the J^{A0} operator do not mix into subleading power currents [87]. This is in agreement with the fact that the power-suppressed current operators, such as J^{A1} and J^{B1}, do not appear in the next-to-leading power factorisation formula at leading logarithmic accuracy. In fact, as we have pointed out, we have found that the subleading power currents do not contribute at any logarithmic accuracy at next-to-leading power.

The anomalous dimensions are given by

$$\Gamma_{\text{cusp}} = \frac{\alpha_s}{\pi} C_F + \mathcal{O}(\alpha_s^2), \qquad \gamma = -\frac{3}{2}\frac{\alpha_s}{\pi} C_F + \mathcal{O}(\alpha_s^2). \qquad (8.12)$$

We denote the $\overline{\text{MS}}$ QCD coupling at the scale μ by α_s. The general solution to the RGE for the hard matching function in equation (8.11) reads

$$H(Q^2, \mu) = \exp\left[4S(\mu_h, \mu) - 2a_\gamma(\mu_h, \mu)\right] \left(\frac{Q^2}{\mu_h^2}\right)^{-2a_\Gamma(\mu_h, \mu)} H(Q^2, \mu_h), \qquad (8.13)$$

where [24]

$$S(\nu, \mu) = -\int_{\alpha_s(\nu)}^{\alpha_s(\mu)} d\alpha \, \frac{\Gamma_{\text{cusp}}(\alpha)}{\beta(\alpha)} \int_{\alpha_s(\nu)}^{\alpha} \frac{d\alpha'}{\beta(\alpha')}, \tag{8.14}$$

$$a_\Gamma(\nu, \mu) = -\int_{\alpha_s(\nu)}^{\alpha_s(\mu)} d\alpha \, \frac{\Gamma_{\text{cusp}}(\alpha)}{\beta(\alpha)}, \qquad a_\gamma(\nu, \mu) = -\int_{\alpha_s(\nu)}^{\alpha_s(\mu)} d\alpha \, \frac{\gamma(\alpha)}{\beta(\alpha)}. \tag{8.15}$$

Up to leading logarithmic accuracy, we can set a_Γ and a_γ to zero, and evaluate $S(\nu, \mu)$ with the one-loop approximation to the cusp anomalous dimension and the beta function given by

$$\beta(\alpha_s) = \frac{d}{d\ln\mu}\alpha_s = -2\frac{\beta_0\alpha_s^2}{4\pi} + \mathcal{O}(\alpha_s^3), \qquad \beta_0 = \frac{11}{3}N_c - \frac{2}{3}n_f. \tag{8.16}$$

These approximations give the following result

$$S^{\text{LL}}(\nu, \mu) = \frac{C_F}{\beta_0^2}\frac{4\pi}{\alpha_s(\nu)}\left(1 - \frac{\alpha_s(\nu)}{\alpha_s(\mu)} + \ln\frac{\alpha_s(\nu)}{\alpha_s(\mu)}\right). \tag{8.17}$$

As we have described above, the S_1 soft function mixes into the S_{x_0} soft function. Therefore, to evolve S_1 it is necessary to solve the coupled system of RGEs derived in appendix A.2 of [40]

$$\frac{d}{d\ln\mu}\begin{pmatrix} S_1(\Omega, \omega) \\ S_{x_0}(\Omega) \end{pmatrix} = \frac{\alpha_s}{\pi}\begin{pmatrix} 4C_F\ln\dfrac{\mu}{\mu_s} & -C_F\delta(\omega) \\ 0 & 4C_F\ln\dfrac{\mu}{\mu_s} \end{pmatrix}\begin{pmatrix} S_1(\Omega, \omega) \\ S_{x^0}(\Omega) \end{pmatrix}. \tag{8.18}$$

The scale μ_s here is an arbitrary soft scale $\mathcal{O}(Q(1-z))$. A general solution for a coupled system of equations of this type has been derived in appendix A.1 of [40]. We make use of this solution to write down the final expression for the S_1 soft function at leading logarithmic accuracy

$$S_1^{\text{LL}}(\Omega, \omega, \mu) = \frac{2C_F}{\beta_0}\ln\frac{\alpha_s(\mu)}{\alpha_s(\mu_s)}\exp\left[-4S^{\text{LL}}(\mu_s, \mu)\right]\theta(\Omega)\delta(\omega). \tag{8.19}$$

Here, the scale μ can be chosen freely, and does not necessarily have to be of order of the soft scale $Q(1-z)$. If that is the case, the solution then sums the large leading logarithms $\ln(\mu/\mu_s)$ to all orders in perturbation theory.

The expressions for the solved RGEs for the hard and soft functions can now be used to evaluate the next-to-leading power partonic cross-section which is given by its dynamical contribution in (8.1). All the quantities are evaluated at the collinear scale as indicated in (8.1). Inserting the tree-level result for the collinear function given in equation (4.19), $J_{1,1}^{(0)}(x_a n_+ p_A; \omega, \mu_c) = -1/(x_a n_+ p_A)$, and using $x_a n_+ p_A = Q + \mathcal{O}(Q(1-z))$ we arrive at the following formula

$$\Delta_{\text{NLP}-\text{LL}}^{dyn}(z) = -4\,H(Q^2, \mu_c)\int d\omega\, S_1(Q(1-z); \omega, \mu_c). \tag{8.20}$$

We now insert into the above formula the leading logarithmic solutions for the hard $H(Q^2, \mu)$ and soft $S_1(\Omega, \omega, \mu)$ functions, given in (8.13), (8.19) respectively. This procedure yields

$$\Delta^{dyn}_{\text{NLP}-\text{LL}}(z) = -\exp\left[4S^{\text{LL}}(\mu_h, \mu_c) - 4S^{\text{LL}}(\mu_s, \mu_c)\right] \times \frac{8C_F}{\beta_0} \ln\frac{\alpha_s(\mu_c)}{\alpha_s(\mu_s)} \theta(1-z), \quad (8.21)$$

where we also used $H(Q^2, \mu_h) = 1 + \mathcal{O}(\alpha_s)$. The scales appearing above can be set to $\mu_h = Q$, $\mu_s = Q(1-z)$, and $\mu_c = Q\sqrt{1-z}$ up to next-to-leading logarithmic corrections.

At this point, we draw attention to the fact that the result in equation (8.21) is not in its most general form. This is because it implies that the factorisation scale μ in the PDFs must be set to the collinear scale given by $\mu_c = Q\sqrt{1-z}$. However, the scale dependence in (8.21) can be restored to an arbitrary scale μ using the evolution equation for the partonic cross-section

$$\frac{d}{d\ln\mu}\hat{\sigma}_{ab}(z, \mu) = -\sum_c \int_z^1 dx \left(P_{ca}(x)\hat{\sigma}_{cb}\left(\frac{z}{x}, \mu\right) + P_{cb}(x)\hat{\sigma}_{ac}\left(\frac{z}{x}, \mu\right)\right), \quad (8.22)$$

where the objects P_{xy} are the Altarelli-Parisi splitting kernels. The details of this analysis are presented in [40]. The important point is that in the end, the functional form of the result in (8.21) remains the same and the only change is to replace the collinear scale μ_c by an arbitrary scale μ. For concreteness, we find

$$\Delta^{dyn}_{\text{NLP}-\text{LL}}(z, \mu) = \exp\left[4S^{\text{LL}}(\mu_h, \mu) - 4S^{\text{LL}}(\mu_s, \mu)\right] \times \frac{-8C_F}{\beta_0} \ln\frac{\alpha_s(\mu)}{\alpha_s(\mu_s)} \theta(1-z). (8.23)$$

This result for the summed next-to-leading power leading logarithms is one of main results presented here.

We make one more observation regarding the above result. Since the form of (8.21) and (8.23) is identical, we deduce that the collinear function cannot contain leading logarithms when it is evaluated at an arbitrary scale μ which is different from the collinear scale μ_c. This fact can be verified by inspecting the one-loop collinear function result in (4.85). Indeed, no leading logarithmic $\alpha_s \ln^2$ term is present in that expression which validates the assumptions made in the derivation of the resummed result.

8.4   Fixed-order expansion

The next step in our analysis involves the expansion in α_s of the resummed next-to-leading power cross-section obtained in the section above. This is done in order to check our result against known expressions obtained with fixed-order calculations of the partonic cross-section, and to give explicit new results that go beyond the ones at fixed α_s.

In order to produce the fixed-order logarithms from our result in (8.23), we expand the ratios of the running strong coupling into a series in $\alpha_s(\mu)$ and logarithms. At leading logarithmic accuracy, the following approximations can be made

$$S^{\text{LL}}(\mu_1, \mu_2) = -\frac{\alpha_s C_F}{2\pi} \ln^2\frac{\mu_2}{\mu_1}, \qquad \frac{1}{\beta_0} \ln\frac{\alpha_s(\mu_1)}{\alpha_s(\mu_2)} = \frac{\alpha_s}{2\pi} \ln\frac{\mu_2}{\mu_1}. \qquad (8.24)$$

We do not indicate the exact scale of α_s on the right-hand sides of the above equations, since the precise value of this scale dependence is a NLL effect. With μ taken to be the free renormalization and factorisation scale, the next-to-leading power cross-section in (8.23) then reduces to

$$\Delta_{\text{NLP}-\text{LL}}^{dyn}(z,\mu) = \exp\left[-2\frac{\alpha_s C_F}{\pi}\ln^2\frac{\mu}{\mu_h}\right]\exp\left[+2\frac{\alpha_s C_F}{\pi}\ln^2\frac{\mu}{\mu_s}\right]$$
$$\times(-4)\frac{\alpha_s C_F}{\pi}\ln\frac{\mu_s}{\mu}\,\theta(1-z)\,. \tag{8.25}$$

It is an interesting observation that the two exponential terms cancel to leading logarithmic accuracy for the special choice of the scale $\mu = \mu_c$. Then the next-to-leading power leading logarithmic series becomes very simple

$$\Delta_{\text{NLP}}^{\text{LL}}(z,\mu_c) = -2\frac{\alpha_s C_F}{\pi}\ln(1-z)\,\theta(1-z)\,. \tag{8.26}$$

However, we also provide results for arbitrary scale μ. We expand (8.25) along with setting $\mu_h = Q$ and $\mu_s = Q(1-z)$. For brevity, we also define $L_\mu = \ln(\mu/Q)$. We then find for the expansion of (8.25)

$$\Delta_{\text{NLP}-\text{LL}}^{dyn}(z,\mu) = -\theta(1-z)\left\{4C_F\frac{\alpha_s}{\pi}\left[\ln(1-z)-L_\mu\right]\right.$$
$$+8C_F^2\left(\frac{\alpha_s}{\pi}\right)^2\left[\ln^3(1-z)-3L_\mu\ln^2(1-z)+2L_\mu^2\ln(1-z)\right]$$
$$+8C_F^3\left(\frac{\alpha_s}{\pi}\right)^3\left[\ln^5(1-z)-5L_\mu\ln^4(1-z)+8L_\mu^2\ln^3(1-z)-4L_\mu^3\ln^2(1-z)\right]$$
$$+\frac{16}{3}C_F^4\left(\frac{\alpha_s}{\pi}\right)^4\left[\ln^7(1-z)-7L_\mu\ln^6(1-z)+18L_\mu^2\ln^5(1-z)-20L_\mu^3\ln^4(1-z)\right.$$
$$\left.+8L_\mu^4\ln^3(1-z)\right]$$
$$+\frac{8}{3}C_F^5\left(\frac{\alpha_s}{\pi}\right)^5\left[\ln^9(1-z)-9L_\mu\ln^8(1-z)+32L_\mu^2\ln^7(1-z)-56L_\mu^3\ln^6(1-z)\right.$$
$$\left.\left.+48L_\mu^4\ln^5(1-z)-16L_\mu^5\ln^4(1-z)\right]\right\}+\mathcal{O}(\alpha_s^6\times(\log)^{11})\,, \tag{8.27}$$

where $(\log)^{11}$ stands for any combination of the two logarithms, L_μ and $\ln^5(1-z)$, to the 11th power.

We now detail how our expanded leading logarithmic results at next-to-leading power can be compared to those existing in the literature. We begin with the first two lines of (8.27), these can be compared to known exact results in [116]. For reference, our $\Delta(z,\mu)$ corresponds to $\Delta_{ij}(x,Q^2,M^2)$ in the notation of [116], where $ij=q\bar{q}$, $x=z$, and the hard scale is given by $M=\mu$. To be more precise, the $\mathcal{O}(\alpha_s)$ result in the first line of (8.27) is in agreement with equation (B.29) of [116] and the $\mathcal{O}(\alpha_s^2)$ terms in the second line of (8.27) are in agreement with those in equation (B.31) found in [116]. The agreement is up to subleading terms in the expansion in logarithms, as our resummed expression captures the leading logarithmic contributions. Next, our $\mathcal{O}(\alpha_s^3)$ term confirms the conjecture

[153, 154] that the leading logarithm at this order is given through the inclusion of the next-to-leading power term in the Altarelli-Parisi splitting kernels within the standard leading power resummation formalism. The $\mathcal{O}(\alpha_s^3)$ and $\mathcal{O}(\alpha_s^4)$ terms with $L_\mu = 0$ have already been given in equations (B.4) and (B.5) of [155]. These results were based on the observation that the "physical evolution kernels", which govern the scale dependence of a given quantity in terms of the quantity itself, exhibit only single logarithms in the threshold region, as $z \to 1$, to the respective order in the strong coupling expansion. Our direct derivation using factorisation and RGE methods also agrees with these expressions.

The $\mathcal{O}(\alpha_s^5)$ term in the last two lines of (8.27) is a new result. Moreover, the expansion to any desired order can be easily obtained from (8.25).

8.5   Resummation beyond LL at NLP

By construction, the purpose of a factorisation theorem is to serve as a stepping stone towards the ultimate goal of obtaining results valid to all orders in perturbation theory. As we have demonstrated above, resummation can be achieved via renormalization group evolution techniques once the contributions to the cross-section are separated into single scale objects. It is often the case that the soft-collinear factorisation involves convolutions $C \otimes F$ of hard with collinear functions, as occurs for example in deep-inelastic scattering and in the relation between PDFs and partonic cross-sections. Soft-collinear factorisation can also involve convolutions $J \otimes S$ of jet and soft functions, as is the case for radiation from jets in the final state. In the process of resummation, each object is renormalized separately from the others. In dimensional regularization, the poles are subtracted and we solve a renormalization group equation for the renormalized factor which can also have the form of a convolution. The summation of large logarithms is then achieved through scale evolution of one of the objects from its own characteristic scale, to the characteristic scale of the other object. The last step in the procedure is to perform the convolution between the two factors.

It is clear that a necessary requirement in this procedure is that the final convolution between the renormalized objects is itself well defined in four dimensions, without the need for any extra regularization. However, as we show in what follows, it has been observed [65] that the final convolution integral between the soft and collinear functions in the next-to-leading power factorisation formula for the Drell-Yan process is not well defined. Issues arise at next-to-leading logarithmic accuracy in the diagonal $q\bar{q}$-channel, and are already manifest at the leading logarithmic accuracy in the off-diagonal $g\bar{q}$-channel. In a perturbative setting, the endpoint-divergent convolution integrals have been reported in the study of the exclusive decay $B \to \chi_{cJ}K$ [156] and in the study of non-local power corrections to the inclusive radiative decay $B \to X_s\gamma$ [157].

In order to pin point the issue here, we focus on the functional form of the collinear and soft functions appearing at NNLO in the one-loop collinear times one-loop soft term in the factorisation formula written in (3.95). We first consider the diagonal $q\bar{q}$-channel and use the one-loop collinear function result, $J_{1,1}^{(1)}$, given in equation (4.84) along with the soft function taken from equation (5.7). Stripping off the factors which do not depend on the convolution variable ω, the final convolution integral between the soft and collinear

functions reads

$$
\int_0^{\Omega} d\omega \underbrace{\left(n_+ p\,\omega\right)^{-\epsilon}}_{\text{collinear piece}} \underbrace{\frac{1}{\omega^{1+\epsilon}} \frac{1}{(\Omega - \omega)^{\epsilon}}}_{\text{soft piece}} \;. \tag{8.28}
$$

Evidently, the integral can be well defined using a regularization prescription such as dimensional regularization in which we keep exact ϵ dependence. Indeed, in chapter 7 we have obtained and reproduced the fixed-order NNLO next-to-leading power results by performing the $d\omega$ convolution integral in d-dimensions. However, as outlined above, this procedure is unsatisfactory from the point of view of resummation, in which the parts originating in the collinear function, $(n_+ p\,\omega)^{-\epsilon}$, and the parts originating in the soft function, $\omega^{-1-\epsilon}\,(\Omega - \omega)^{-\epsilon}$, are treated independently. Following the renormalization procedure, we must first expand each in ϵ to subtract the divergent parts and define renormalized functions. It is at the point of expansion in ϵ that we encounter a complication if the procedure is applied to (8.28). We see that the expansion in ϵ of the $1/\omega^{1+\epsilon}$ factor in the soft piece yields the standard plus distribution, whereas the expansion of $\omega^{-\epsilon}$ factor in the collinear piece gives rise to a logarithmic contribution. In combination with each other, these contributions lead to a divergent integral $\int d\omega\,\delta(\omega)\ln(\omega)$ and other ill-defined integrals.

We can expose the issue in a more explicit manner by making use of the ϵ-expanded one-loop collinear function which can be found in (4.85) and the ϵ-expanded one-loop soft function given in equation (5.11). We write both of these results again below for convenience. For the collinear function we have

$$
J_{1,1}^{(1)}\left(n_+ p;\,\omega\right) \;=\; \frac{\alpha_s}{4\pi}\frac{1}{(n_+ p)}\left(C_F\left(\frac{4}{\epsilon} + 5 - 4\ln\left(\frac{n_+ p\,\omega}{\mu^2}\right)\right) - 5\,C_A\right) \;+\; \mathcal{O}(\epsilon)\,, \tag{8.29}
$$

and

$$
S_1^{(1)}\left(\Omega, \omega\right) = \frac{\alpha_s C_F}{4\pi}\left(2\,\delta(\omega)\,\theta(\Omega)\left(-\frac{1}{\epsilon} + \ln\left(\Omega^2/\mu^2\right)\right) + 2\left[\frac{1}{\omega}\right]_+ \theta(\omega)\theta(\Omega - \omega)\right) \tag{8.30}
$$

for the soft function. We now use these expanded expressions as ingredients in (3.95) and perform the final convolution integral in the variable ω. We then find the following expression

$$
\Delta_{\text{NLP}-\text{coll}}^{dyn\,(2)}(z) \;=\; \frac{\alpha_s^2}{(4\pi)^2}\left(C_F^2\left(-\frac{32}{\epsilon^2} - \frac{8}{\epsilon}\left[5 - 8\ln(1-z) - 4\int d\omega\,\delta(\omega)\ln\left(\frac{\omega}{Q}\right)\right]\right)\right.
$$
$$
\left. + C_A C_F\,\frac{40}{\epsilon} + \mathcal{O}(\epsilon^0)\right) \tag{8.31}
$$

where we have set the scale $\mu = Q$ as in chapter 7 and have only displayed the pole terms in ϵ.

We discover two ways in which this result is problematic. The first clear point of failure we have raised in the discussion above, namely the fact that one the terms which contains a $1/\epsilon$ divergence is completely ill-defined as the ϵ pole is multiplied by the divergent

integral $\int d\omega\, \delta(\omega)\ln(\omega)$. Second, less obvious issue, is that the coefficients of the C_F^2/ϵ^2 and $C_F C_A/\epsilon$ pole terms, which are not themselves divergent, are different from the correct result given in equation (7.10). We recall that the result in equation (7.10) was obtained by performing the convolution in d-dimensions and only *after* expanding the resultant expression in ϵ.

It may seem possible that the issue could be resolved by moving factors of ω between the soft and collinear functions. Indeed, it is possible to move integer ω powers from the collinear to the soft functions by changing the power of $1/in_-\partial$ factor in the definition of the soft function. However, this does not solve the issue to all orders in perturbation theory, as factors of $\omega^{-n\epsilon}$ tied to the collinear function will always appear at the n-th order in the strong coupling expansion.

The above analysis clearly shows that it is not possible to calculate the next-to-leading power logarithms of $(1-z)$ correctly to arbitrary logarithmic accuracy using the standard renormalization methods and convolutions defined in four dimensions. This situation is in stark contrast to the leading power case, where the extension of the resummation to any logarithmic order is a technical challenge of obtaining results for the relevant ingredients at high loop orders. However, although it is not possible to sum the logarithms of $(1-z)$ in Drell-Yan production to arbitrary accuracy, it is possible to sum the leading logarithms in the $q\bar{q}$-channel [40], as we have shown in section 8.3. It is also possible to sum the leading logarithms in the diagonal gg-channel in Higgs production via gluon fusion [41], which will be explored in chapter 9. The summation of leading logarithms in these channels is possible as only the tree-level collinear functions are required and the loop corrections to the collinear functions do not themselves contribute to the leading logarithmic series. This fact is manifest in equation (8.29), the highest logarithm appearing is $\alpha_s \ln\left(n_+ p\,\omega/\mu^2\right)$, which contributes only at the next-to-leading logarithmic level to the cross-section. For this reason the ill-defined convolution prevents the extension of the resummation formalism beyond the leading logarithmic series in the diagonal channel. We see that the convolution itself is divergent and a subtraction procedure is needed. The convolution contributes to the next-to-leading logarithms, which implies that these cannot be fully obtained from individual renormalization group equations for the collinear and soft functions.

With the above considerations in mind, we could attempt to find an all order expression for the Drell-Yan cross-section at threshold in the off-diagonal $g\bar{q}$-channel. However, we find that the complications regarding the ill-defined convolution which hamper the resummation at next-to-leading logarithmic accuracy in the diagonal $q\bar{q}$-channel, already play a role at the leading logarithmic accuracy in the off-diagonal channel. Indeed, the issue becomes transparent when we consider the result for the one-loop collinear function in the $g\bar{q}$-channel given in equation (4.109), which we write here again for convenience

$$
\begin{aligned}
G_{\xi q}^{(1)}\left(n_+ p; \omega\right) \;=\; & -\frac{\alpha_s}{4\pi}\Bigg\{ C_F\bigg[\frac{2}{\epsilon^2} - \frac{2}{\epsilon}\left(\ln\left(\frac{n_+ p\,\omega}{\mu^2}\right) - 1\right) + \ln^2\left(\frac{n_+ p\,\omega}{\mu^2}\right) \\
& -2\ln\left(\frac{n_+ p\,\omega}{\mu^2}\right) - \frac{\pi^2}{6} + 5\bigg] - C_A\bigg[\frac{2}{\epsilon^2} - \frac{1}{\epsilon}\left(2\ln\left(\frac{n_+ p\,\omega}{\mu^2}\right) - 1\right) \\
& + \ln^2\left(\frac{n_+ p\,\omega}{\mu^2}\right) - \ln\left(\frac{n_+ p\,\omega}{\mu^2}\right) - \frac{\pi^2}{6} + 2\bigg]\Bigg\} + \mathcal{O}(\epsilon)\,.
\end{aligned}
\tag{8.32}
$$

We see that in this expression there appear terms of order $\alpha_s \ln^2 (n_+ p\,\omega/\mu^2)$, as opposed to only terms of order $\alpha_s \ln (n_+ p\,\omega/\mu^2)$ in the result for the one-loop collinear function for the $q\bar{q}$-channel in (8.29). The $\alpha_s \ln^2 (n_+ p\,\omega/\mu^2)$ terms from the collinear function contribute to the leading logarithmic series in the $g\bar{q}$-channel and spoil the resummation already at this accuracy.

Despite the issues regarding the use of factorisation formulas for resummation, the next-to-leading power factorisation formulas for the $q\bar{q}$-channel and the $g\bar{q}$-channel derived in this work consistently factorise the different momentum scales appearing in the Drell-Yan process at the level of regularized matrix elements of the collinear and soft operators. For this reason these justifiably are valid factorisation formulas.

This concludes our specific example regarding the emergence of divergent convolutions in the Drell-Yan production at threshold. However, the appearance of endpoint divergent convolutions is ubiquitous in next-to-leading power investigations and an active area of research. Recently, leading logarithms at next-to-leading power in the off-diagonal parton-scattering channel $q + \phi^*$ in deep-inelastic scattering were resummed using d-dimensional consistency relations and refactorisation techniques [66]. These expressions are in agreement with earlier results obtained using diagrammatic techniques [134, 158, 159] and confirm the curious appearance of Bernoulli numbers in the quark-gluon splitting function. Another type of divergent convolution integrals with the hard matching coefficients is discussed in [88]. The endpoint contributions in event shapes were studied in [135], and factorisation at subleading power, treatment of endpoint divergences, and next-to-leading logarithmic resummation in $h \to \gamma\gamma$ decay were recently reported [56, 57, 62].

9

Higgs production: resummation at next-to-leading power

In the previous chapters we have presented in detail the effective field theory framework for threshold resummation at next-to-leading power. Thus far, we have concentrated on the case study of the Drell-Yan process in the diagonal and off-diagonal channels. In this chapter we broaden the scope of our investigations and implement within the next-to-leading power framework the process of Higgs production via gluon-gluon fusion at threshold.

The Higgs boson was the last piece of the Standard Model to be discovered, however, questions about its nature such as the coupling to other particles and shape of potential are still currently studied. It should then not be surprising that also on the side of theoretical computations the Higgs production cross-section has attracted substantial attention [160, 161, 162, 163]. In the fixed order perturbation theory it is known at N³LO in the heavy-top approximation [12, 164, 165, 166, 167] and the leading power threshold resummation is at the N³LL accuracy [23, 25, 168, 169, 170, 171]. As such, it is one of the most precisely computed observables in hadron-hadron collisions to date.

With these considerations in mind, it is clear that the Higgs production via gluon-gluon fusion is important to study both due to its phenomenological relevance and as a test ground for application of new theoretical methods. Hence, we dedicate this chapter to the discussion of the next-to-leading power factorisation and resummation for the Higgs production process in the threshold regime. The analysis presented here largely follows the one presented in the previous chapters for the case of virtual photon production, therefore to avoid repetition we will focus on the similarities and differences between these two processes. In addition to the analytic considerations, in the last section of this chapter we explore the numerical contribution due to the next-to-leading power leading logarithms and find that it is not negligible compared to the numerical size of the leading power terms. Bulk of the considerations presented in this chapter have been published in [41].

The outline of this chapter is as follows. In section 9.1 we follow section 3.2 and derive the next-to-leading power factorisation formula for single Higgs production in gluon-gluon fusion. A notable difference to the derivation presented in section 3.2 is that here we target the leading logarithmic contributions for the outset. In section 9.2 we first perform the resummation of the next-to-leading power leading logarithms via renormalization group evolution of the hard, soft, and collinear functions and later expand the obtained

expression for the resummed result in the strong coupling constant, α_s. The latter serves as a check of our final all-order expression through a comparison against the fixed-order results found in literature. Lastly, section 9.3 contains the details of the numerical study regarding the contribution of the next-to-leading power leading logarithms to the threshold Higgs production cross-section.

9.1 Factorisation at next-to-leading power

We begin with the derivation of the next-to-leading power factorisation formula for Higgs production in gluon-gluon fusion at the leading logarithmic accuracy. To this end, we consider the following process

$$A(p_A) + B(p_B) \to \mathrm{H}(q) + X, \tag{9.1}$$

where $A(p_A)$, $B(p_B)$ denote the incoming protons with momenta p_A and p_B, $\mathrm{H}(q)$ is the Higgs boson produced in the collision between the two protons with momentum q, and X describes the unobserved QCD final state. The hadronic cross-section for the process described here is given by

$$\sigma = \frac{\alpha_s^2}{576\pi v^2} \sum_{a,b} \int_0^1 dx_a \int_0^1 dx_b \, f_{a/A}(x_a) f_{b/B}(x_b) \, \hat{\sigma}_{ab}(z). \tag{9.2}$$

Similarly to the corresponding equation for the Drell-Yan process given in (3.27), the $f_{i/I}(x_i)$ here are the parton distribution functions. Higgs vacuum expectation value is denoted by v and its value is given by $v^2 = 1/(\sqrt{2}G_F)$, where G_F is the Fermi constant. As in the Drell-Yan analysis in preceding chapters, the strong coupling constant without a scale argument, α_s, denotes to the strong coupling constant at the $\overline{\mathrm{MS}}$ scale μ. In the work presented here, only the diagonal gg-channel of Higgs production is considered. Therefore the indices a, b can be dropped in what follows.

The production of a Higgs boson in gluon-gluon fusion in mediated by a top quark loop, through which the Higgs boson and the gluons are coupled. As depicted by the first arrow in the diagram in figure 9.1, we work in the heavy-top-quark mass limit $m_t \gg m_H$, in which the coupling of the Higgs boson to the pair of gluons is given by the following effective Lagrangian term

$$\mathcal{L}_{\mathrm{eff}} = C_t\left(m_t,\,\mu\right) \frac{\alpha_s}{12\pi} \frac{H}{v} F_{\mu\nu}^A F^{\mu\nu A}. \tag{9.3}$$

The matching coefficient $C_t\left(m_t,\,\mu\right)$ is

$$C_t\left(m_t,\,\mu\right) = 1 + \frac{\alpha_s}{4\pi}(5C_A - 3C_F) + \mathcal{O}(\alpha_s^2)\,. \tag{9.4}$$

In the same fashion as in our Drell-Yan analysis, the partonic cross-section denoted by $\hat{\sigma} \equiv \hat{\sigma}_{gg}$ is also a function of the dimensionless variable $z = m_H^2/\hat{s}$. The invariant mass Q^2 is replaced by m_H^2 from the Drell-Yan case, however the partonic centre-of-mass energy squared remains identical, $\hat{s} = x_a x_b s$. The incoming gluon momenta are given by
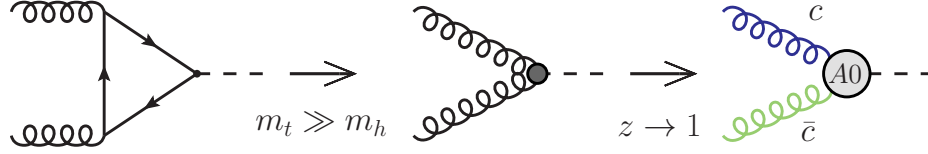
Figure 9.1: *The progression of the effective field theory description. In the first step, we assume that the mass of the top quark is much larger than the mass of the Higgs boson, and so it is integrated out. In the second step, we consider the kinematics in the threshold $z \to 1$ regime, for which SCET is the appropriate framework.*

$p_a^\mu = x_a \sqrt{s} n_-^\mu / 2$ and $p_b^\mu = x_b \sqrt{s} n_+^\mu / 2$ where the variables x_a and x_b measure the momentum fractions of the gluons in their respective hadrons.

As in the Drell-Yan resummation, presented in chapter 8, the aim here is to sum the next-to-leading power *leading logarithms* in the series $\sum_{n=1}^{\infty} \sum_{m=0}^{2n-1} d_{nm} \ln^m(1-z)$. The starting point for our analysis is the cross-section for Higgs production which is written as follows

$$\sigma = \frac{1}{2s} \int \frac{d^3\vec{q}}{(2\pi)^3 2E_q} \sum_X |\langle HX|AB\rangle|^2 (2\pi)^4 \delta^{(4)}(p_A + p_B - q - p_X). \tag{9.5}$$

The squared matrix element is itself given by the following expression in terms of the QCD fields

$$\sum_X |\langle HX|AB\rangle|^2 = \frac{\alpha_s^2(\mu)\, C_t^2(m_t, \mu)}{144\pi^2 v^2}$$
$$\times \sum_X \langle AB| \big[F_{\rho\sigma}^{A'} F^{\rho\sigma A'} \big](0)|X\rangle \langle X| \big[F_{\mu\nu}^A F^{\mu\nu A} \big](0)|AB\rangle. \tag{9.6}$$

Following the discussion on the construction of N-jet operator basis in section 2.4.1, the QCD operator here, namely $F_{\mu\nu}^A F^{\mu\nu A}$, is matched onto the SCET operators. Only one operator is needed at leading power, which we give here for concreteness

$$F_{\mu\nu}^A F^{\mu\nu A}(0) = \int dt \, d\bar{t} \, \widetilde{C}^{A0}(t, \bar{t})\, J^{A0}(t, \bar{t}), \tag{9.7}$$

where

$$J^{A0}(t, \bar{t}) = 2g_{\mu\nu}\, n_- \partial \mathcal{A}_{\bar{c}\perp}^{\nu A}(\bar{t}n_-)\, n_+ \partial \mathcal{A}_{c\perp}^{\mu A}(tn_+), \tag{9.8}$$

$$C^{A0}(n_+p, n_-\bar{p}) = \int dt \, d\bar{t}\, e^{-i(n_+p)t - i(n_-\bar{p})\bar{t}}\, \widetilde{C}^{A0}(t, \bar{t}). \tag{9.9}$$

The $\mathcal{A}_{c\perp}^\mu$ field is the collinear-gauge-invariant transverse collinear gluon building block of SCET given in equation (2.49). As we have shown in the rightmost diagram of figure 9.1, this leading power operator sources a collinear and an anticollinear field. The operator is non-local along the respective light-ray directions and the derivatives acting on the collinear and anticollinear fields correspond to their respective large momentum components. The hard matching coefficient in equation (9.7) in position space is given by $\widetilde{C}^{A0}(t, \bar{t}) = \delta(t)\delta(\bar{t}) + \mathcal{O}(\alpha_s)$ which in momentum space takes the form $C^{A0}(n_+p, n_-\bar{p}) = 1 + \mathcal{O}(\alpha_s)$ according to the Fourier transform in equation (9.9).

At subleading powers in position-space SCET, the matching equation relating the hard gluon-gluon-Higgs vertex to the SCET operator in (9.7) must be extended to include operators of the J^{An}, J^{Bn}, $J^{Cn}\ldots$ – type, where we have at least one $n > 0$. This subleading power basis was described in section 2.4.1 based on the construction developed in [86, 87, 88].

The discussion regarding the appearance of *collinear functions* first at next-to-leading power presented in section 3.1.2 applies also to the case at hand. The central objects are again the time-ordered product insertions of the subleading power Lagrangian terms which induce a collinear scale in the threshold loops. Similarly to the $q\bar{q} \to \gamma^*$ investigation, the leading logarithms in the dynamical part of the cross-section for Higgs production come from the time-ordered product of the leading power SCET current J^{A0} with the $\mathcal{O}(\lambda^2)$ Lagrangian terms. For concreteness, we write such time-ordered product operator here again

$$J_{A0,j}^{T2}(t,\bar{t}) = i \int d^4z\, \mathbf{T}\Big[J_{A0}(t,\bar{t})\, \mathcal{L}_j^{(2)}(z)\Big]. \tag{9.10}$$

As before, the index j labels the various terms in the next-to-leading power Lagrangian $\mathcal{L}^{(2)}(z)$ given in [73]. In practice, we add the operator in (9.10) to (9.7) which, once we consider the appropriate matrix element, extends the accuracy of the amplitude to contain the next-to-leading power leading logarithmic terms.

In the next step, the decoupling transformation [71] is used to separate the soft and collinear sectors of the leading power Lagrangian. Here, the required field redefinition is one where the adjoint soft Wilson lines $\mathcal{Y}_+$ ($\mathcal{Y}_-$), defined below, multiply the (anti)collinear gluon fields. The $\mathcal{Y}_+$ ($\mathcal{Y}_-$) are given by

$$\mathcal{Y}_{\pm}^{AB}(x) = \mathbf{P}\exp\left\{g_s \int_{-\infty}^0 ds\, f^{ABC}\, n_{\mp} A_s^C(x + sn_{\mp})\right\}. \tag{9.11}$$

In the derivation of the factorisation theorem, we make use of the decoupled (anti)collinear fields. In terms of these fields, the leading power hard matching current in (9.8) takes the form

$$J^{A0}(t,\bar{t}) = 2g_{\mu\nu}\,\mathcal{Y}_-^{AC}(0)\, n_-\partial\mathcal{A}_{\bar{c}\perp}^{\nu C}(\bar{t}n_-)\,\mathcal{Y}_+^{AD}(0)\, n_+\partial\mathcal{A}_{c\perp}^{\mu D}(tn_+)\,. \tag{9.12}$$

As is the case for the hard matching current, we use the decoupled collinear fields and the soft-gluon building blocks, given in equation (2.105), to rewrite the subleading power interaction Lagrangian. The relevant analysis was presented in section 2.4.3 and the complete Yang-Mills Lagrangian is written in appendix A.1.

In contrast to the derivation presented for Drell-Yan production at threshold, here we do not derive the next-to-leading power factorisation theorem to arbitrary logarithmic accuracy before restricting to the leading logarithmic contributions in order to perform resummation. Rather, we identify the terms in the Yang-Mills SCET Lagrangian which contribute to the leading logarithmic series from the outset. These interaction terms are $\mathcal{L}_{1\mathrm{YM}}^{(2)}$ and $\mathcal{L}_{2\mathrm{YM}}^{(2)}$ in the Yang-Mills Lagrangian given in equation (A.1). We write these again here for convenience

$$\mathcal{L}_{1\mathrm{YM}}^{(2)} = -\frac{1}{2g_s^2}\,\mathrm{tr}\left(\Big[n_+\partial\,\mathcal{A}_{\nu\perp}^c\Big]\Big[n_-x\,in_-\partial\,n_+\mathcal{B}^+,\,\mathcal{A}_c^{\nu\perp}\Big]\right) \tag{9.13}$$

and

$$\mathcal{L}_{2\text{YM}}^{(2)} = -\frac{1}{2g_s^2} \, \text{tr} \left(\left[n_+\partial \, \mathcal{A}_{\nu_\perp}^c \right] \left[x_\perp^\rho x_{\perp\omega} \left[\partial^\omega, \, in_-\partial \, \mathcal{B}_\rho^+ \right], \, \mathcal{A}_c^{\nu_\perp} \right] \right).$$ (9.14)

As in the Drell-Yan analysis, the inclusion of the Lagrangian insertions as interaction terms in the amplitude calculation leads to a surplus of threshold (anti)collinear fields with a virtuality too large to be radiated into the final state in the threshold kinematics, $m_H^2(1-z) \gg \Lambda^2$. This brings about the need for the introduction of the main new feature in subleading power factorisation theorems, namely the collinear functions [40, 65]. Discussed at length in section 3.1.2, the collinear functions are defined as the perturbative matching coefficients in the relation between the threshold (anti)collinear fields and the $(\bar{c})c$-PDF collinear fields (with virtuality Λ^2), in the presence of the soft fields (with virtuality $m_H^2(1-z)^2$).

The soft fields appearing in the Lagrangian terms $\mathcal{L}_{1\text{YM}}^{(2)}$ and $\mathcal{L}_{2\text{YM}}^{(2)}$, given in equations (9.13) and (9.14) respectively, can be written in terms of the same soft building block by an application the equation-of motion identity in equation (3.46). Therefore, despite two Lagrangian terms contributing to the Higgs production cross-section at next-to-leading power, only one collinear function appears. This collinear function has the following operatorial definition

$$i \int d^4z \, \mathbf{T} \left[n_+\partial \mathcal{A}_{c\perp\mu}^Y(tn_+) \left(\mathcal{L}_{1\text{YM}}^{(2)}(z) + \mathcal{L}_{2\text{YM}}^{(2)}(z) \right) \right]$$
$$= 2\pi \int du \int \frac{d(n_+z)}{2} \, \widetilde{J}_{\text{YM}\,\mu\rho}^{YBC} \left(t, u; \frac{n_+z}{2} \right) \mathcal{A}_{c\perp}^{C\rho, \, \text{PDF}}(un_+) \frac{\partial_\perp^\omega}{in_-\partial} \mathcal{B}_{\omega_\perp}^{+B}(z_-).$$ (9.15)

Note the difference between the definition given here for the Yang-Mills collinear function and one given in equation (3.66) for Drell-Yan. In addition to the trivial change of the χ_c to $\mathcal{A}_{c\perp}$, the soft building block is defined without the imaginary i factor. By exchanging with n_+ and n_- we define a similar anticollinear function relevant for the anticollinear gluon field.

In the calculation of the Higgs production amplitude we use Fourier transforms of the gluon field and the collinear function. The inverse Fourier transform of the gluon field has been written in (3.98). For clarity, here we use

$$\hat{\mathcal{A}}_{c\perp\mu}^{C, \, \text{PDF}}(n_+p) = \int du \, e^{i(n_+p)u} \mathcal{A}_{c\perp\mu}^{C, \, \text{PDF}}(un_+),$$ (9.16)

for the collinear gluon field. For the Yang-Mills collinear function, we use the following relation

$$J_{\text{YM}\,\mu\rho}^{YBC}(n_+p, n_+p'; \omega) = \int dt \, e^{i(n_+p)t} \int du \, e^{-i(n_+p')u}$$
$$\times \int \frac{d(n_+z)}{2} \, e^{i\omega(n_+z)/2} \, \widetilde{J}_{\text{YM}\,\mu\rho}^{YBC} \left(t, u; \frac{n_+z}{2} \right).$$ (9.17)

The Yang-Mills collinear function arising due to the insertions of the above Lagangain terms starts to contribute at $\mathcal{O}(\alpha_s^0)$. We find for this lowest order result the following expression in momentum space

$$J_{\text{YM}\,\mu\rho}^{YBC}(n_+p, n_+p'; \omega) = -2i \, T_R \, f^{YBC} \, g_{\perp\mu\rho} \left[2 - 2n_+p' \frac{\partial}{\partial n_+p} \right] \delta(n_+p - n_+p')$$ (9.18)

where $T_R = 1/2$. The contribution to this result from the $\mathcal{L}_{1YM}^{(2)}$ Lagrangian insertion is $\left(1 - 2n_+ p' \frac{\partial}{\partial n_+ p}\right)$, and the $\mathcal{L}_{2YM}^{(2)}$ Lagrangian insertion contributes the remaining 1. As for the leading logarithmic resummation in the Drell-Yan process at threshold, here we also only require the lowest order, tree-level, expression for the collinear function.

We are now in possession of all the ingredients needed to write the factorised form of the next-to-leading power contribution to the matrix element $\langle X | [F_{\mu\nu}^A F^{\mu\nu A}](0) | AB \rangle$ which is a part of the expression given in equation (9.6). Using the fact that the final state $\langle X |$ is made up of threshold-soft and $(\bar{c})c$-PDF states, and decomposes as $\langle X | = \langle X_s | \otimes \langle X_{c,\text{PDF}} | \otimes \langle X_{\bar{c},\text{PDF}} |$, we have

$$
\begin{aligned}
\langle X | \left[F_{\mu\nu}^A F^{\mu\nu A} \right](0) | A(p_A) B(p_B) \rangle_{\text{NLP}} &= -2i \int \frac{dn_+ p \, dn_- \bar{p}}{2\pi \, 2\pi} g^{\mu\nu} \, C^{A0}(n_+ p, n_- \bar{p}) \\
&\times \int dn_- p_b \, \delta(n_- \bar{p} - n_- p_b) \, n_- p_b \, \langle X_{\bar{c}\text{PDF}} | \hat{\mathcal{A}}_{\bar{c}\perp\nu}^{X,\,\text{PDF}}(n_- p_b) | B(p_B) \rangle \\
&\times \int dn_+ p_a \, \langle X_{c\text{PDF}} | \hat{\mathcal{A}}_{c\perp}^{C\rho,\,\text{PDF}}(n_+ p_a) | A(p_A) \rangle \int \frac{d\omega}{4\pi} J_{\text{YM}\,\mu\rho}^{YBC}(n_+ p, n_+ p_a; \omega) \\
&\times \int d(n_+ z) \, e^{-i\omega(n_+ z)/2} \, \langle X_s | \mathbf{T} \left[\mathcal{Y}_-^{AX}(0) \mathcal{Y}_+^{AY}(0) \frac{\partial_\perp^\omega}{in_- \partial} \mathcal{B}_{\omega_\perp}^{+B}(z_-) \right] | 0 \rangle + \bar{c}\text{-term}.
\end{aligned}
\tag{9.19}
$$

We focus on the Yang-Mills NLP collinear function given in equation (9.18) and notice the presence of the derivative which acts on the collinear-momentum conserving delta function in the square bracket. This derivative is integrated by parts in (9.19) such that it is acting on the rest of the matrix element. The only $n_+ p$ dependent term in (9.19) is the short-distance hard matching coefficient $C^{A0}(n_+ p, n_- \bar{p})$ which has the tree-level value $C^{A0}(n_+ p, n_- \bar{p}) = 1 + \mathcal{O}(\alpha_s)$ as noted below equation (9.9). Since for the resummation of leading logarithmic series we do not requite the $\mathcal{O}(\alpha_s)$ momentum dependent contributions to $C^{A0}(n_+ p, n_- \bar{p})$, the derivative term in (9.18) can be dropped. In the next step, we simply extract the momentum, colour, and Lorentz structure of $J_{\mu\rho}^{YBC}(n_+ p, n_+ p'; \omega)$ and substitute

$$
J_{\text{YM}\,\mu\rho}^{YBC}(n_+ p, n_+ p_a; \omega) \;\to\; if^{YBC} \, g_{\perp\mu\rho} \, J_{\text{YM}}(n_+ p_a; \omega) \, \delta(n_+ p - n_+ p_a)
\tag{9.20}
$$

in (9.19). At lowest order, the scalar collinear function $J_{\text{YM}}^{(0)}(n_+ p_a; \omega)$ has the following value

$$
J_{\text{YM}}^{(0)}(n_+ p_a; \omega) = -4T_R = -2.
\tag{9.21}
$$

Inserting also this result into the expression for the next-to-leading power matrix element in (9.19) we get

$$
\begin{aligned}
\langle X | \left[F_{\mu\nu}^A F^{\mu\nu A} \right](0) | A(p_A) B(p_B) \rangle_{\text{NLP}} &= 2 \int \frac{dn_+ p_a \, dn_- p_b}{2\pi \, 2\pi} g^{\mu\nu} \, C^{A0}(n_+ p_a, n_- p_b) \\
&\times n_- p_b \, \langle X_{\bar{c}\text{PDF}} | \hat{\mathcal{A}}_{\bar{c}\perp\nu}^{X,\,\text{PDF}}(n_- p_b) | B(p_B) \rangle \, \langle X_{c\text{PDF}} | \hat{\mathcal{A}}_{c\perp\mu}^{C,\,\text{PDF}}(n_+ p_a) | A(p_A) \rangle \\
&\times \int \frac{d\omega}{4\pi} J_{\text{YM}}(n_+ p_a; \omega) \int d(n_+ z) \, e^{-i\omega(n_+ z)/2} \\
&\times \langle X_s | \mathbf{T} \left[\mathcal{Y}_-^{AX}(0) \mathcal{Y}_+^{AY}(0) f^{YBC} \frac{\partial_\perp^\omega}{in_- \partial} \mathcal{B}_{\omega_\perp}^{+B}(z_-) \right] | 0 \rangle + \bar{c}\text{-term}.
\end{aligned}
\tag{9.22}
$$

This equation can be compared with (3.56) for the Drell-Yan production case. We note that the expressions are very similar once we account for the fact that Higgs production entails gluonic initial states, instead of a quark-antiquark pair, and that only a single collinear function remains at leading logarithmic accuracy.

The next step of the calculation involves squaring the matrix element which yields the factorised expression for the cross-section in equations (9.5) and (9.6). Gluon parton distribution functions are obtained by summing over the $(\bar{c})c$-PDF final state as in the case of the derivation of the factorisation formula in the $g\bar{q}$-channel of the Drell-Yan process in section 3.3. The d-dimensional expression is given in equation (3.105), however here we require

$$\left\langle A(p_A)\big|\mathcal{A}_{c\perp\rho'}^{A',\,\text{PDF}}(x+u'n_+)\mathcal{A}_{c\perp\rho}^{A,\,\text{PDF}}(un_+)\big|A(p_A)\right\rangle = -\frac{g_{\perp\rho\rho'}}{2}\frac{\delta^{AA'}}{N_c^2-1}$$
$$\times \int_0^1 \frac{dx_a}{x_a}\, f_{g/A}(x_a)\, e^{ix_a(x+u'n_+ - un_+)\cdot p_A}\,. \qquad (9.23)$$

The sum over the final state soft radiation gives the next-to-leading power soft function $S_{\text{YM}}(\Omega,\omega)$ which we define below.

We then perform the integration over n_+p_a, n_-p_b and strip off the gluon parton distribution functions. This leads us to the expression for the partonic cross-section, as defined in equation (9.2), that accurate to next-to-leading power in the threshold expansion. Including also the leading power term, and prior to performing any expansion in the phase space, we find

$$\hat{\sigma}(z) = \frac{8C_t^2(m_t)}{N_c^2-1}\,\hat{s}H(\hat{s})\int\frac{d^3\vec{q}}{(2\pi)^3\,2\sqrt{m_H^2+\vec{q}^{\,2}}}\frac{1}{2\pi}\int d^4x\, e^{i(x_ap_A+x_bp_B-q)\cdot x}$$
$$\times\left\{\widetilde{S}_0(x)-\frac{2}{\sqrt{\hat{s}}}\int d\omega\, J_{\text{YM}}(x_an_+p_A;\omega)\,\widetilde{S}_{\text{YM}}(x,\omega)+\bar{c}\text{-term}\right\}. \qquad (9.24)$$

The hard function $H(\hat{s},\mu_h)$ here, is given by

$$H(\hat{s},\mu_h) = |C^{A0}(-\hat{s})|^2\,. \qquad (9.25)$$

As only the J^{A0} hard matching current plays a role in the factorisation up to next-to-leading power, this hard function is the same for the leading power and next-to-leading power term.

Th leading power position-space soft function that is defined as the vacuum expectation value of adjoint Wilson lines and with the position argument generalised to $x^0 \to x^\mu = (x^0, \vec{x})$ is denoted in (9.24) by $\widetilde{S}_0(x)$. The Fourier transform of $\widetilde{S}_0(x)$ with respect to x^0 will be written as $S_0(\Omega, \vec{x})$, such that $S_{\text{H}}(\Omega) = S_0(\Omega, \vec{0})$. The next-to-leading power soft function is represented by $\widetilde{S}_{\text{YM}}(x,\omega)$. It is defined as the Fourier transform

$$\widetilde{S}_{\text{YM}}(x,\omega) = \int\frac{d(n_+z)}{4\pi}\,e^{-i\omega(n_+z)/2}\frac{1}{N_c^2-1}\,\langle 0|\widetilde{\mathcal{S}}_{\text{YM}}(x,z_-)|0\rangle\,, \qquad (9.26)$$

of the vacuum matrix element of the following operator, with an explicit insertion of the soft building block

$$\widetilde{\mathcal{S}}_{\text{YM}}(x,z_-) = \bar{\mathbf{T}}\Big[\mathcal{Y}_+^{A'C}(x)\mathcal{Y}_-^{A'X}(x)\Big]\mathbf{T}\Big[\mathcal{Y}_-^{AX}(0)\mathcal{Y}_+^{AY}(0)\,f^{YBC}\,\frac{\partial_\perp^\sigma}{in_-\partial}\mathcal{B}_{\sigma_\perp}^{+B}(z_-)\Big]. \qquad (9.27)$$

The Fourier transform of the next-to-leading power soft function $\widetilde{S}_{\text{YM}}(x, \omega)_{|\vec{x}=0}$ with respect to x^0 will be denoted as $S_{\text{YM}}(\Omega, \omega)$. We also note that the factor of two which multiplies the $J_{\text{YM}} \otimes \widetilde{S}_{\text{YM}}$ term in the second line of (9.24) comes from two identical next-to-leading power terms in the square of the amplitude.

As we have described in section 3.2.2, in addition to the so-called dynamic next-to-leading power corrections, there exist kinematic power corrections. These arise from the expansion of the first line of (9.24) and the combination of the next-to-leading power terms from this expansion with the generalised leading power soft function $\widetilde{S}_0(x)$. The relevant equations in the centre-of-mass frame are the same as for Drell-Yan production in (3.25) and (3.26). Moreover, as is conventionally done we consider the partonic cross-section rescaled by a factor of $1/z$,

$$\Delta(z) = \frac{\hat{\sigma}(z)}{z}, \tag{9.28}$$

as we have done for the Drell-Yan case. The kinematic corrections for Higgs production cross-section are obtained in the same way as for the Drell-Yan production. Hence we do not repeat the analysis of section 3.2.2. We do note however, that a difference arises due to an extra factor of $\hat{s} = m_H^2/z$ in (9.24), which is not present in γ^* production. This factor comes about from the derivatives corresponding to large momentum components in the current operator written in equation (9.8). The extra $\hat{s}$ factor here can be regarded as an additional contribution to the third type of kinematic correction in equation (3.71). We recall that the original $K3$ arises due to the $1/z$ factor (9.28). This implies that the third soft kinematic function, $S_{K3}(\Omega)$, given in (3.79) (and (8.9) at its lowest order) is twice as large. Therefore, in the sum of all the kinematic corrections, we no longer find a complete cancellation of the leading logarithmic terms. Instead, the Higgs production cross-section valid up to next-to-leading power has the following form

$$
\begin{aligned}
\Delta(z) \;=\; & \frac{8 C_t^2(m_t)}{N_c^2 - 1}\, m_H\, H(m_H^2) \bigg\{ S_{\text{H}}(m_H(1-z)) + \frac{1}{m_H} S_K(m_H(1-z)) \\
& - \frac{2}{m_H} \int d\omega\, J_{\text{YM}}(x_a n_+ p_A; \omega)\, S_{\text{YM}}(m_H(1-z), \omega) + \bar{c}\text{-term} \bigg\},
\end{aligned} \tag{9.29}
$$

where the sum of kinematic soft functions is now

$$S_K(\Omega) = \frac{\alpha_s C_A}{2\pi} \left(-8 \ln \frac{\mu}{\Omega} + 4 \right) \theta(\Omega) + \mathcal{O}(\alpha_s^2). \tag{9.30}$$

Hence, we find that, in contrast to the Drell-Yan case, the kinematic corrections *do* contribute to the next-to-leading power leading logarithmic series in the Higgs production cross-section at threshold.

9.2   Resummation

As in section 8.3, the resummation of the next-to-leading power leading logarithms in Higgs production is achieved via evolution of scale-dependent functions in (9.29) to a common collinear scale $\mu_c \sim m_H\sqrt{1-z}$ using renormalization group equations. A difference regarding the scale evolution in Higgs production with respect to the analysis performed

for the Drell-Yan process appears due to the *ggH* vertex given by the effective Lagrangian in equation (9.3). We see the presence of an additional short-distance coefficient $C_t(m_t)$ which appears both for the leading and next-to-leading power contributions. At a generic scale μ, the C_t coefficient has the value (see, for example [168])

$$C_t(m_t, \mu) = \frac{\beta\big(\alpha_s(\mu)\big)}{\alpha_s^2(\mu)} \frac{\alpha_s^2(\mu_t)}{\beta\big(\alpha_s(\mu_t)\big)} C_t(m_t, \mu_t). \tag{9.31}$$

The initial condition at the scale $\mu_t \sim m_t$ is given by $C_t(m_t, \mu_t)$ and where

$$\beta(\alpha_s) = \frac{d}{d\ln\mu}\alpha_s = -2\frac{\beta_0\alpha_s^2}{4\pi} + \mathcal{O}(\alpha_s^3), \qquad \beta_0 = \frac{11}{3}N_c - \frac{2}{3}n_f. \tag{9.32}$$

The evolution of the hard function $H(m_H^2)$ from the hard scale, $\mu_h \sim m_H$, to the collinear scale, $\mu_c \sim m_H(1-z)^{1/2}$, is almost the same as for the case of Drell-Yan production. The only difference in the hard RGE between the two processes is the relevant colour factor. Therefore, for Higgs production up to leading logarithmic accuracy we simply change $C_F \to C_A$ in (8.13) and (8.17). Concretely, here we need

$$H(m_H^2, \mu) = \exp\left[4S^{\mathrm{LL}}(\mu_h, \mu)\right] H(m_H^2, \mu_h) \tag{9.33}$$

with

$$S^{\mathrm{LL}}(\nu, \mu) = \frac{C_A}{\beta_0^2} \frac{4\pi}{\alpha_s(\nu)} \left(1 - \frac{\alpha_s(\nu)}{\alpha_s(\mu)} + \ln\frac{\alpha_s(\nu)}{\alpha_s(\mu)}\right). \tag{9.34}$$

Finally, it remains for us to consider the evolution of the next-to-leading power soft function and the contribution from the kinematic corrections. The generalised soft function required for Higgs production, written here in equations (9.26) and (9.27), has the same form as one encountered in the γ^* production discussed in section 8.2. We note that the difference between the two cases is the appearance of Wilson lines in the adjoint rather than fundamental representation. The evolution of the soft function is again from the soft scale, $\mu_s \sim m_H(1-z)$, to the collinear scale, $\mu_c \sim m_H(1-z)^{1/2}$. Similarly as for the hard function case, the structure of the RGE for the soft function necessary for resummation at leading logarithmic accuracy and the $\mathcal{O}(\alpha_s)$ result for the soft function is the same as for the Drell-Yan case in section 8.2 up to the exchange of the colour factor $C_F \to C_A$.

The NLP soft function in Higgs production is divergent at its lowest contributing order and mixes into a new type of soft function defined here, analogously to $S_{x_0}(\Omega)$ in equation (8.2), as follows

$$S_{x_0}^{\mathrm{ad}}(\Omega) = \int \frac{dx^0}{4\pi} e^{ix^0\Omega/2} \frac{-2i}{x^0 - i\varepsilon} \frac{1}{N_c^2 - 1} \langle 0| \bar{\mathbf{T}}\left[\mathcal{Y}_+^{A'Y}(x^0)\mathcal{Y}_-^{A'X}(x^0)\right] \mathbf{T}\left[\mathcal{Y}_-^{AX}(0)\mathcal{Y}_+^{AY}(0)\right]|0\rangle. \tag{9.35}$$

The soft function $S_{x_0}^{\mathrm{ad}}(\Omega)$ is adjoint-representation equivalent to $S_{x_0}(\Omega)$ and the leading logarithmic series is generated in the mixing between the NLP soft function $\widetilde{S}_{\mathrm{YM}}(x,\omega)$ and $S_{x_0}^{\mathrm{ad}}(\Omega)$.

We do not repeat the discussion of the renormalization of these soft functions here which was carried out in section 8.2, it suffices to state that the relevant RGE system is

given by

$$\frac{d}{d\ln\mu}\begin{pmatrix} S_{\mathrm{YM}}(\Omega,\omega) \\ S_{x_0}^{\mathrm{ad}}(\Omega) \end{pmatrix} = \frac{\alpha_s}{\pi}\begin{pmatrix} 4C_A\ln\dfrac{\mu}{\mu_s} & C_A\delta(\omega) \\ 0 & 4C_A\ln\dfrac{\mu}{\mu_s} \end{pmatrix}\begin{pmatrix} S_{\mathrm{YM}}(\Omega,\omega) \\ S_{x^0}^{\mathrm{ad}}(\Omega) \end{pmatrix}. \qquad (9.36)$$

The scale μ_s is an arbitrary soft scale of order $m_H(1-z)$. As we have discussed, in Higgs production the kinematic corrections also give rise to the leading logarithmic series. Therefore we must also consider the evolution of S_{K}, for which we find

$$\frac{d}{d\ln\mu}\begin{pmatrix} S_{\mathrm{K}}(\Omega) \\ S_{x_0}^{\mathrm{ad}}(\Omega) \end{pmatrix} = \frac{\alpha_s}{\pi}\begin{pmatrix} 4C_A\ln\dfrac{\mu}{\mu_s} & -4C_A \\ 0 & 4C_A\ln\dfrac{\mu}{\mu_s} \end{pmatrix}\begin{pmatrix} S_{\mathrm{K}}(\Omega) \\ S_{x^0}^{\mathrm{ad}}(\Omega) \end{pmatrix}. \qquad (9.37)$$

A general solution for a system of RGEs of this type is given in appendix A of [40]. We then obtain the following leading logarithmic solution for the two relevant soft functions

$$S_{\mathrm{K}}^{\mathrm{LL}}(\Omega,\mu) = \frac{8C_A}{\beta_0}\ln\frac{\alpha_s(\mu)}{\alpha_s(\mu_s)}\exp\left[-4S^{\mathrm{LL}}(\mu_s,\mu)\right]\theta(\Omega), \qquad (9.38)$$

$$S_{\mathrm{YM}}^{\mathrm{LL}}(\Omega,\omega,\mu) = -\frac{2C_A}{\beta_0}\ln\frac{\alpha_s(\mu)}{\alpha_s(\mu_s)}\exp\left[-4S^{\mathrm{LL}}(\mu_s,\mu)\right]\theta(\Omega)\delta(\omega). \qquad (9.39)$$

We are now in possession of all the necessary ingredients making up (9.29). Since we evolve to the collinear scale, the collinear function does not contain large logarithms and we can use the tree-level result in equation (9.21) and arrive at

$$\begin{aligned} \Delta(z,\mu_c) &= \frac{\alpha_s^2(\mu_c)}{\alpha_s^2(\mu)}C_t^2(m_t,\mu_c)\,H(m_H^2,\mu_c)\left\{m_H\,S_{\mathrm{H}}\Big(m_H(1-z),\mu_c\Big) + S_{\mathrm{K}}^{\mathrm{LL}}(\Omega,\mu_c)\right. \\ &\quad \left. +8\int d\omega\,S_{\mathrm{YM}}^{\mathrm{LL}}\Big(m_H(1-z),\omega,\mu_c\Big)\right\} \end{aligned} \qquad (9.40)$$

in terms of the hard and soft functions evolved to the collinear scale. We have inserted the factor $\alpha_s^2(\mu_c)/\alpha_s^2(\mu)$ multiplying $C_t^2(m_t,\mu_c)$ in order to compensate for the factor of $\alpha_s^2(\mu)$ that is not included in $\Delta(z,\mu_c)$ but which does appear in the hadronic cross-section given in (9.2). Another simplification is the appearance of a factor of two multiplying the second line of (9.40) which arises due to the $\bar{c}$-term in (9.29) that gives a next-to-leading power contribution identical the collinear one which we explicitly considered here.

It is also notable that the equation for $\Delta(z,\mu_c)$ in (9.40) is written by assuming that we do not distinguish between the scale of the effective Higss-gluon-gluon coupling and the SCET factorisation scale. This in turn implies that the SCET anomalous dimension which describes the evolution of the hard function $H(m_H^2,\mu)$ must contain a contribution from the anomalous dimension of the HFF operator. In this way, the evolution of $C_t^2(m_t,\mu)$ below the hard scale is compensated for. In a conceptually clearer treatment the two appearing scales would be distinguished, as is the case for example in the discussion of tensor quark currents in [172]. However, the final result presented in equation (9.41) is nonetheless identical in both cases.

We continue by inserting the resummed soft functions in equations (9.38) and (9.39) into the expression for the cross-section (9.40), we arrive at

$$\Delta^{\mathrm{LL}}(z,\mu_c) = \Delta_{\mathrm{LP}}^{\mathrm{LL}}(z,\mu_c) - \frac{\alpha_s^2(\mu_c)}{\alpha_s^2(\mu)} \left[\frac{\beta\big(\alpha_s(\mu_c)\big)}{\alpha_s^2(\mu_c)} \frac{\alpha_s^2(\mu_t)}{\beta\big(\alpha_s(\mu_t)\big)} \right]^2 C_t^2(m_t,\mu_t)$$

$$\times \exp\left[4S^{\mathrm{LL}}(\mu_h,\mu_c) - 4S^{\mathrm{LL}}(\mu_s,\mu_c)\right] \frac{8C_A}{\beta_0} \ln\frac{\alpha_s(\mu_c)}{\alpha_s(\mu_s)} \theta(1-z), \quad (9.41)$$

where we have also used $H(m_H^2,\mu_h) = 1 + \mathcal{O}(\alpha_s)$.

This final resummed result for the Higgs production cross-section can be compared with the corresponding result for the Drell-Yan case given in equation (8.21). We see that despite the differences in the derivation between the two processes, in particular regarding the contribution from kinematic corrections to the leading logarithms in Higgs production, remarkably the combination of kinematic contributions and the NLP soft function conspire to give final results which are identical up to the exchange of the colour factors C_F and C_A.

The main differences between the $q\bar{q}$-channel in Drell-Yan production and the diagonal channel in Higgs production via gluon-gluon fusion at threshold boil down to two points. Firstly, there is a factor of two difference in the tree-level collinear function due to two the Lagrangian terms in (9.13) and (9.14). Secondly, the aforementioned contribution from the kinematic corrections. Both of these differences are related to the presence of the derivatives in the operator in equation (9.8), and eventually they cancel to give the expression in (9.41).

The term $\Delta_{\mathrm{LP}}^{\mathrm{LL}}(z)$ in the final result in equation (9.41) is the leading logarithmic contribution to the *leading* power partonic cross-section. In the present formalism it can be found in [168]. We are free to set the hard, soft, and collinear scales to $\mu_h = m_H$, $\mu_s = m_H(1-z)$, and $\mu_c = m_H\sqrt{1-z}$ respectively, since the differences in the precise choices enter only beyond the leading logarithmic accuracy. However, the result in (9.41) is not in its most general form. This is because in the derivation of the partonic cross-section we have set the factorisation scale μ to the collinear scale $\mu_c = m_H\sqrt{1-z}$, which implies that the factorisation scale in parton distribution functions is set to the collinear $\mu_c = m_H\sqrt{1-z}$ scale. Using the scale invariance of the hadronic cross-section, the result can be translated to an arbitrary scale μ, as detailed in [40]. We find that the functional form of the result for the resummed partonic cross-section at a arbitrary scale μ is the same as the functional form of the result at the collinear scale μ_c. Similar to the Drell-Yan production, here the collinear function cannot contribute at the leading logarithmic accuracy when it is evaluated at a scale μ different from μ_c. We have for the resummed partonic cross-section

$$\Delta_{\mathrm{NLP}}^{\mathrm{LL}}(z,\mu) = \left[\frac{\beta\big(\alpha_s(\mu)\big)}{\alpha_s^2(\mu)} \frac{\alpha_s^2(\mu_t)}{\beta\big(\alpha_s(\mu_t)\big)} \right]^2 C_t^2(m_t,\mu_t)$$

$$\times \exp\left[4S^{\mathrm{LL}}(\mu_h,\mu) - 4S^{\mathrm{LL}}(\mu_s,\mu)\right] \frac{-8C_A}{\beta_0} \ln\frac{\alpha_s(\mu)}{\alpha_s(\mu_s)} \theta(1-z). \quad (9.42)$$

The scale of the parton luminosity which is multiplying the partonic cross-section $\Delta_{\mathrm{NLP}}^{\mathrm{LL}}(z,\mu)$

is independent of z. The threshold logarithms of $(1-z)$ arise from setting the scale $\mu_s \sim m_H(1-z)$.

Having obtained the main result of this section, that is the resummed next-to-leading power leading logarithms in Higgs production in gluon-gluon fusion in (9.42), we proceed to expand it in the strong coupling such that we can compare with existing results obtained at fixed order in perturbation theory. The factors $\left[\beta\big(\alpha_s(\mu)\big)/\alpha_s^2(\mu)\,\alpha_s^2(\mu_t)/\beta\big(\alpha_s(\mu_t)\big)\right]^2$ and $C_t^2(m_t, \mu_t)$ can be omitted here since they are both equal to unity at $\mathcal{O}(\alpha_s^0)$ and do not contribute to the leading logarithmic series at higher orders. This means that the expansion of the result in equation (9.42) to fixed order in α_s is the same, up to the exchange of colour factor $C_F \to C_A$, as the expansion we have found for the Drell-Yan case in the $q\bar{q} \to \gamma^*$ production channel given in equation (8.27). We keep the scale μ arbitrary, and set $\mu_h = m_H$ and $\mu_s = m_H(1-z)$, we then obtain the following expression for the expansion

$$
\begin{aligned}
\Delta_{\mathrm{NLP}}^{\mathrm{LL}}(z,\mu) \;=\; & -\theta(1-z)\left\{4C_A\frac{\alpha_s}{\pi}\left[\ln(1-z)-L_\mu\right]\right. \\
& +8C_A^2\left(\frac{\alpha_s}{\pi}\right)^2\left[\ln^3(1-z)-3L_\mu\ln^2(1-z)+2L_\mu^2\ln(1-z)\right] \\
& +8C_A^3\left(\frac{\alpha_s}{\pi}\right)^3\left[\ln^5(1-z)-5L_\mu\ln^4(1-z)+8L_\mu^2\ln^3(1-z)-4L_\mu^3\ln^2(1-z)\right] \\
& +\frac{16}{3}C_A^4\left(\frac{\alpha_s}{\pi}\right)^4\left[\ln^7(1-z)-7L_\mu\ln^6(1-z)+18L_\mu^2\ln^5(1-z)-20L_\mu^3\ln^4(1-z)\right. \\
& \left.\hspace{4cm}+8L_\mu^4\ln^3(1-z)\right] \\
& +\frac{8}{3}C_A^5\left(\frac{\alpha_s}{\pi}\right)^5\left[\ln^9(1-z)-9L_\mu\ln^8(1-z)+32L_\mu^2\ln^7(1-z)-56L_\mu^3\ln^6(1-z)\right. \\
& \left.\left.\hspace{4cm}+48L_\mu^4\ln^5(1-z)-16L_\mu^5\ln^4(1-z)\right]\right\}+\mathcal{O}(\alpha_s^6\times(\log)^{11})\,.
\end{aligned}
$$
(9.43)

In the above we have defined the abbreviation $L_\mu = \ln(\mu/m_H)$, and as before in equation (8.27), the $(\log)^{11}$ takes the place of any combination of the two logarithms to the 11th power.

Our result in equation (9.43) is checked in the following ways. The exact calculation [173] and the "physical evolution kernels" method [155] provide the N^{3}LO terms. The relevant equations are in particular equation (2.12) in [173] and equation (B.2) in [155]. We find agreement between these references and (9.43) at this order. Moreover, the N^{4}LO expression is provided in equation (B.3) of [155]. The relevant terms in equation (9.43) are in agreement with this result. The N^{5}LO contribution in the last two lines of equation (9.42) constitute a new result and an expression at any order in α_s can be obtained by expanding (9.42) without much effort. Our derivation of (9.42) justifies the methods of [153, 154] which account for the next-to-leading power leading logarithms by implementing the Altarelli-Parisi splitting kernels up to next-to-leading power accuracy within the standard leading power resummation formalism.

9.3 Numerical analysis

As mentioned in the introduction of this chapter, Higgs production in gluon-gluon fusion is a phenomenologically relevant process for the LHC. It is therefore interesting to study the numerical impact of the next-to-leading power leading logarithms on the resummed cross-section which thus far could only formally include the leading power contributions, albeit to a very high logarithmic accuracy. Hence, in this section, we numerically explore the next-to-leading power resummed Higgs production cross-section in the large top mass approximation. We take the centre-of-mass energy at the LHC as $\sqrt{s} = 13\,\text{TeV}$, and use as the mass of the Higgs $m_H = 125\,\text{GeV}$. The cross-section can be written in the following way

$$\sigma = \frac{\alpha_s^2(\mu)\,m_H^2}{576\pi\,v^2 s} \int_\tau^1 \frac{dz}{z}\,\mathcal{L}\left(\frac{\tau}{z},\mu\right)\Delta(z,\mu). \tag{9.44}$$

The $\Delta(z,\mu)$ piece is the partonic cross-section rescaled by a factor of $1/z$ as we have defined in equation (9.28) and the term $\mathcal{L}(\tau/z,\mu)$ is known as the luminosity function which involves the parton distribution functions. Concretely, $\mathcal{L}(\tau/z,\mu)$ is defined in the following way

$$\mathcal{L}(y,\mu) = \int_y^1 \frac{dx}{x}\,f_{g/A}(x,\mu)f_{g/B}\left(\frac{y}{x},\mu\right). \tag{9.45}$$

For the numerical evaluation we make use of the PDF4LHC15nnlo30 PDF sets [174, 175, 176, 177, 178]. In section 9.2 we have computed the next-to-leading power leading logarithmic contributions to $\Delta(z,\mu)$ in equation (9.44). However, in the numerical study we additionally consider the resummed leading power cross-section at next-to-next-to-leading logarithmic accuracy. The size of these contributions will serve as a comparison against the corresponding contributions due to next-to-leading power corrections. The leading power resummed cross-section is provided in equations (30) and (31) of [168]. The leading power result is composed of a hard and soft functions at one loop order, the anomalous dimension Γ_{cusp} taken up to and including the third loop order, and the remaining anomalous dimensions enter at the two loop order. See for example the Table 1 of [24].

The formula for the resummed cross-section at next-to-leading power in (9.42) is a function of the scales μ_t, μ_h, μ_c, μ_s, and the arbitrary factorisation scale μ. The scale μ_t is chosen to be $\mu_t = 173.1\,\text{GeV}$ and we set $\mu_h = \mu = m_H$. Moreover, as part of our analysis we consider the scale of μ_h to be set to $\mu_h^2 = -m_H^2 - i\epsilon$ (the $-i\epsilon$ is implied in what follows below). This choice for μ_h includes factors of π^2 in the resummation. These factors of π^2 are associated with logarithmic contributions which are evaluated with a time-like momentum transfer [168]. As we have already discussed, at leading logarithmic accuracy, the next-to-leading power cross-section in equation (9.42) does not explicitly depend on the collinear scale, μ_c, and we do not consider it in the following.

Setting of the soft scale requires some careful attention. In section 9.2 we have applied a parametric choice for the soft scale. Namely, we set it to $\mu_s = m_H(1-z)$ and have obtained the result expanded to fixed-order with this choice. However, as is well-known at leading power, such a choice is not admissible in the evaluation of the *resummed* cross-section due to the Landau pole. We explore this further in Table 9.1 and shortly discuss below. Instead of applying the parametric $\mu_s = m_H(1-z)$ choice for the soft scale, we set the

(pb)	$\sigma^{\mathrm{LL}}_{\mathrm{LP}}$			$\sigma^{\mathrm{LL}}_{\mathrm{NLP}}$		
	$\mu_s = m_H(1-z)$ $\mu_h^2 = m_H^2$	$\mu_s = \mu_s^{\mathrm{dyn}}$ $\mu_h^2 = m_H^2$	$\mu_s = \mu_s^{\mathrm{dyn}}$ $\mu_h^2 = -m_H^2$	$\mu_s = m_H(1-z)$ $\mu_h^2 = m_H^2$	$\mu_s = \mu_s^{\mathrm{dyn}}$ $\mu_h^2 = m_H^2$	$\mu_s = \mu_s^{\mathrm{dyn}}$ $\mu_h^2 = -m_H^2$
$\mathcal{O}\left(\alpha_s^0\right)$	12.94	12.94	12.94	–	–	–
$\mathcal{O}\left(\alpha_s\right)$	4.70	1.95	8.82	4.35	3.57	3.57
$\mathcal{O}\left(\alpha_s^2\right)$	6.49	1.72	4.58	7.50	1.38	3.28
$\mathcal{O}\left(\alpha_s^3\right)$	15.35	1.03	2.49	18.67	0.35	1.58
$\mathcal{O}\left(\alpha_s^4\right)$	51.09	0.61	1.45	62.97	0.07	0.52
$\mathcal{O}\left(\alpha_s^5\right)$	217.53	0.36	0.87	269.10	0.01	0.13
$\mathcal{O}\left(\alpha_s^6\right)$	1111.56	0.22	0.52	1376.45	0.002	0.03

Table 9.1: *Comparison of the LL contributions to the Higgs production cross section in gluon fusion expanded in powers of α_s for various choices of the soft and hard scales, and for LP and NLP, respectively. For the naive choice $\mu_s = m_H(1-z)$ the series does not converge at LP and neither at NLP, while higher-order contributions decrease rapidly when using the dynamical soft scale $\mu_s = \mu_s^{\mathrm{dyn}}$. Furthermore, we distinguish the case in which $\mu_h^2 = m_H^2$ and $\mu_h^2 = -m_H^2$.*

soft scale dynamically [179] for which we use

$$\mu_s^{\mathrm{dyn}} = \frac{Q}{\bar{s}_1(\tau)}, \quad \bar{s}_1(\tau) \equiv -e^{\gamma_E} \frac{d \ln \mathcal{L}(y, \mu)}{d \ln y}\bigg|_{y=\tau}. \tag{9.46}$$

For the value of the Higgs mass set at $m_H = 125\,\mathrm{GeV}$ and the centre-of-mass energy at $\sqrt{s} = 13\,\mathrm{TeV}$ as given at the beginning of the section, for the dynamically set soft scale we find $\mu_s^{\mathrm{dyn}} \simeq 38\,\mathrm{GeV}$. An alternative way of performing the resummation is to transform to Mellin space [180, 181], this can be regarded as implicitly setting an effective soft scale. However, in this case we cannot keep the soft scale independent from the rest of the scales which appear in the formula. Therefore, we choose to implement the dynamic soft scale setting procedure and as part of the analysis we explore the effect of changing the value of the soft scale μ_s. The relevant plots are given in figures 9.2 and 9.3.

We focus now on the results presented in Table 9.1. In this table, we give the values of the contributions to the cross-section at each order in α_s after having perturbatively expanded the resummed formula. The goal of this investigation is to ensure that our choice for the soft scale is indeed suitable. In order to arrive at the numerical values shown in Table 9.1, we have evaluated both the leading and next-to-leading power results at the leading logarithmic accuracy. The coefficient $C_t^2(m_t, \mu_t)$ and its evolution factor, which is given in the first line of equation (9.42), are both set to unity. The running coupling constant is taken at one loop. From the second and fifth column in Table 9.1, it is clear that setting the soft scale to its parametric value of $\mu_s = m_H(1-z)$ is problematic. The series is numerically divergent at the leading and next-to-leading power as expected. From the third and sixth column in Table 9.1 we see that for the dynamically set soft scale, $\mu_s = \mu_s^{\mathrm{dyn}}$, the higher order contributions in α_s become suppressed. This behaviour indicates that the expansion of the series is perturbatively convergent as required. We see that this is the case for both the leading and next-to-leading power contributions. In

the fourth and seventh column of Table 9.1, we also present the numerical values for the expanded result found for the case where the hard scale is set to $\mu_h^2 = -m_H^2$. The different choice of the hard scale does not cause the convergence of the perturbative expansion of the leading logarithmic terms to break down. However, we do note that the rate of convergence appears too slow as at any fixed α_s order for $\mu_s = \mu_s^{\mathrm{dyn}}$, the value for the cross-section is larger for the scale choice $\mu_h^2 = -m_H^2$ when compared with the value obtained for $\mu_h^2 = m_H^2$.

We now shift the focus of the investigation to consider the all order effects. Within our numerical study, we find it instructive to consider a generalised version of the resummed leading logarithmic next-to-leading power cross-section presented in (9.42). To this end, we consider $\Delta_{\mathrm{NLP}}^{\mathrm{LL}}(z, \mu)$ modified to the following form

$$\Delta_{\mathrm{NLP}}^{\mathrm{LL}}(z, \mu) = \left[\frac{\beta\big(\alpha_s(\mu)\big)}{\alpha_s^2(\mu)} \frac{\alpha_s^2(\mu_t)}{\beta\big(\alpha_s(\mu_t)\big)}\right]^2 C_t^2(m_t, \mu_t) \exp\left[4C_A\big(S^{\mathrm{LL}}(\mu_h, \mu) - S^{\mathrm{LL}}(\mu_s, \mu)\big)\right]$$
$$\times \left[S_{\mathrm{NLP}}\big(m_H(1-z), \mu_s\big) - \frac{8C_A}{\beta_0} \ln \frac{\alpha_s(\mu)}{\alpha_s(\mu_s)} S_{x0}^{\mathrm{ad}}\big(m_H(1-z), \mu_s\big)\right]. \quad (9.47)$$

The term $S_{\mathrm{NLP}}\big(m_H(1-z), \mu_s\big)$ takes care of the initial condition of the evolution equations given in (9.36) and (9.37) for the sum of the next-to-leading power soft function and the kinematic soft function in equation (9.40) evaluated at the soft scale

$$S_{\mathrm{NLP}}\big(m_H(1-z), \mu_s\big) = S_{\mathrm{K}}\big(m_H(1-z), \mu_s\big) - 8 \int d\omega\, S_{\mathrm{YM}}\big(m_H(1-z), \omega, \mu_s\big). \quad (9.48)$$

In the following analysis, we choose to investigate two separate initial conditions. At the soft scale, we can have

$$\begin{aligned} &\text{A)} \quad S_{\mathrm{NLP}}\big(m_H(1-z), \mu_s\big) = 0, \\ &\text{B)} \quad S_{\mathrm{NLP}}\big(m_H(1-z), \mu_s\big) = -4C_A \frac{\alpha_s(\mu_s)}{2\pi} \ln \frac{m_H^2(1-z)^2}{\mu_s^2}, \end{aligned} \quad (9.49)$$

together with $S_{x0}^{\mathrm{ad}}\big(m_H(1-z), \mu_s\big) = 1$. The two initial conditions are equivalent at leading logarithmic accuracy. We have used the choice labelled by A in the original derivation above and it reproduces the result shown in equation (9.42). On the other hand, the choice B ensures that the logarithmic part of the next-to-leading power next-to-leading order contribution is included for every value of the soft scale μ_s.

To arrive at numerical values for the resummed next-to-leading power result, we use the expression for $C_t^2(m_t, \mu_t)$ in equation (9.47) at the two loop accuracy. This ingredient can be found in equation (12) of [168]. Moreover, we use the three-loop β-function for α_s. These considerations yield $C_t^2(m_t, \mu = m_H) \simeq 1.22$ for C_t which has been evolved to the factorisation scale. For concreteness, the evolved C_t is given by the product of the first two factors on the right-hand side of equation (9.47). The numerical result for the leading power cross-section is obtained through the implementation of [168]. Here the C_t is required at the soft scale. The value of C_t at the soft scale is found to be $C_t^2(m_t, \mu = \mu_s) \simeq 1.80$.

The numerical results for the resummed leading logarithmic next-to-leading power cross-section are presented in Table 9.2. We give the results for the two schemes discussed

σ (pb)	$\mu_s = \mu_s^{\mathrm{dyn}}$	
	$\mu_h^2 = m_H^2$	$\mu_h^2 = -m_H^2$
$\sigma_{\mathrm{LP}}^{\mathrm{NNLL}}$	24.12	28.04
$\sigma_{\mathrm{LP}}^{\mathrm{NNLO}}$	28.93	
$\sigma_{\mathrm{LP}}^{\mathrm{N^3LO}}$	29.24	
$\sigma_{\mathrm{NLP}}^{\mathrm{LL}}$ (A)	7.18	12.76
$\sigma_{\mathrm{NLP}}^{\mathrm{LL}}$ (B)	8.82	15.68
$\sigma_{\mathrm{non\,LP}}^{\mathrm{NNLO}}$	11.90	
$\sigma_{\mathrm{non\,LP}}^{\mathrm{N^3LO}}$	16.27	
$\sigma_{\mathrm{LP}}^{\mathrm{NNLL}} + \sigma_{\mathrm{NLP}}^{\mathrm{LL}}$ (A)	31.30	40.80
$\sigma_{\mathrm{LP}}^{\mathrm{NNLL}} + \sigma_{\mathrm{NLP}}^{\mathrm{LL}}$ (B)	32.94	43.72
σ^{NNLO}	40.82	
$\sigma^{\mathrm{N^3LO}}$	45.52	

Table 9.2: *Resummed Higgs production cross section in gluon fusion at LP with NNLL, and at NLP with LL accuracy. For NLP we present the result for the two cases defined in (9.49). For comparison, we also show the fixed-order results for gluon fusion at NNLO and N³LO based on the* iHixs *code [182]. In addition, we distinguish the LP contribution and the difference between the full result and LP contribution (denoted by non LP) for the fixed-order results.*

above, A and B in (9.49), and we compare the obtained values to the NNLL leading power result. Additionally, we have included the fixed order results at NNLO and N³LO. These were calculated using the iHixs code [182]. We discover that the leading logarithmic next-to-leading power correction is sizeable and its value can be as large as 40% of the value of the resummed NNLL leading power cross-section. We also find that the resummation of π^2 enhanced terms is numerically important. This effect formally reaches beyond the leading logarithmic accuracy, however, its inclusion in the combined result for the NNLL LP + LL NLP resummed cross-section yields a final result that is comparable to the N³LO result [166, 12].

Lastly, we present a study of the dependence of the resummed leading and next-to-leading power cross-section on the soft scale μ_s. The relevant plots are given in figures 9.2 and 9.3. We first note that the next-to-leading power cross-section is more sensitive to the choice of μ_s compared to the leading power cross-section. This is within our expectations, as only the leading logarithmic terms are available for the next-to-leading power cross-section, compared to NNLL accurate expressions available for the LP cross-section. Although the sensitivity to the soft scale μ_s for the next-to-leading power cross-section is sizable, the values of the cross-section computed for the two initial conditions A and B in (9.49) overlap in the region close to $\mu_s = \mu_s^{\mathrm{dyn}}$. For $\mu_h^2 = m_H^2$ the combination of the leading and next-to-leading power cross-sections exhibits a smaller sensitivity to the soft scale μ_s.
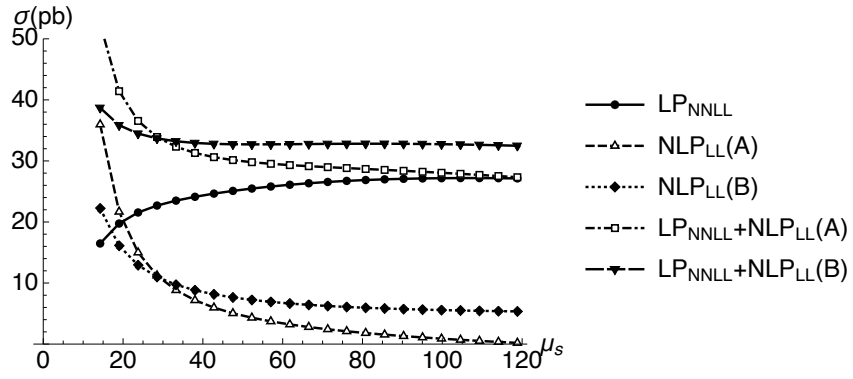
Figure 9.2: *Dependence of the NNLL LP and LL NLP resummed Higgs production cross section on the soft scale μ_s, for $\mu_h^2 = m_H^2$. For NLP we present the result for the two cases defined in (9.49).*
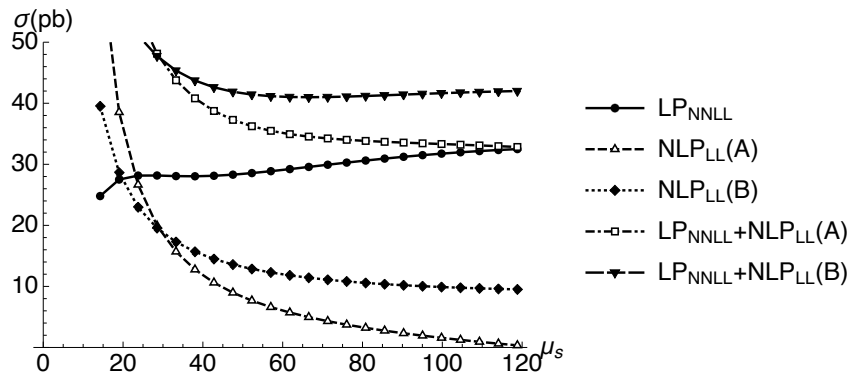
Figure 9.3: *Same information as in figure 9.2, however using $\mu_h^2 = -m_H^2$ for the hard scale.*

Part V

Conclusions

10

Summary and outlook

At the core of the work presented here stands the investigation of elementary scattering processes at subleading powers using soft collinear effective field theory. We have largely focused on the Drell-Yan process near the threshold $z \to 1$ limit, where large double logarithms of $(1-z)$ develop and must be resummed to all orders in perturbation theory. Resummation at leading power has been well understood for some time, and can be performed at high logarithmic accuracy in the effective field theory framework using renormalization group equation techniques. However, resummation of subleading power terms is a relatively recent development. It has been achieved for the threshold Drell-Yan process in [40] and for event shapes in [54] within the last three years. As the details presented in this work attest to, the step between a description of processes at leading power and at the next-to-leading power is more of a leap. As we have seen for the Drell-Yan process, new objects, the amplitude level NLP collinear functions, emerge in the factorisation formula, and endpoint divergent convolutions hinder a straightforward application of standard renormalization group methods to sum large logarithms to all orders in the strong coupling. Except for special cases, such as the leading logarithmic terms described here.

A broad understanding of the subleading power corrections can advance the accuracy of phenomenological predictions for various processes. However, the benefits of the first next-to-leading power investigations are already clear, as these studies help us to learn about the intricate structure of gauge theories beyond the leading power regime. Subleading power investigations can have a positive impact in many contexts. For example, our results can be helpful in bootstrapping procedures. These techniques aim to derive quantities of interest, such as cross-sections, by starting with a general ansätze and constraining them using information from singular limits of QCD. Knowledge about infrared limits of QCD beyond the leading power regime is therefore desirable for such considerations. In other contexts, the subleading power corrections have helped to improve subtraction techniques [47]. Moreover, the emergent issues, such as the divergent convolution problem and collinear colour non-conservation (the leading pole structure proportional to $C_F - C_A$ as discussed in section 4.2.2), are interesting to study from the point of view of advancing our knowledge about quantum field theories in a very broad sense. In particular, due to the fact that the appearance of endpoint divergent convolutions is so ubiquitous beyond leading power. Much recent progress has been made in this area of study, including application of consistency relations and refactorisation to perform resummation [66, 56, 57].

In the $h \to \gamma\gamma$ process, the NLP resummation has been achieved at NLL [61, 62]. A subleading power four dimensional factorisation formula for the Drell-Yan process at threshold remains elusive. The considerations presented in this work provide a firm formal grounding, with a factorisation formula which applies to bare regularized quantities, and the new relevant ingredients such as the NLP collinear functions and generalised soft functions computed to an accuracy in α_s which enables us to verify the factorisation formula up to next-to-next-to-leading order, and partly even at N^{3}LO.

The analysis presented here is carried out within the position-space formulation of SCET. In chapter 2, we have introduced the next-to-leading power SCET framework, and kept the discussion largely general for N energetic directions in a given process. This part highlights the important aspects of NLP SCET. However, the interested reader is directed to original publications for details [86, 87, 88, 137].

The main contents of this work begin with Part II and the derivation of the formal all order factorisation formulas for the diagonal and off-diagonal channels of the Drell-Yan process at threshold presented in chapter 3. These formulas are then specialised to next-to-leading power and the objects which appear in the factorisation formulas at this accuracy are listed.

Then, in Part III we present the details of the technical calculations carried out to obtain results for the objects appearing in the factorisation formulas at fixed orders in perturbation theory. First, in chapter 4 we compute the amplitude level NLP collinear functions to one-loop accuracy. These are important new ingredients, which only emerge at subleading powers. Through the explicit one-loop calculation we confirmed the fact that no leading logarithms are present in the relevant collinear functions. This knowledge is subsequently used in chapter 8 in order to achieve leading logarithmic resummation for the Drell-Yan process at threshold.

Chapters 5 and 6 contain fixed order calculations of the generalised soft functions. These objects are functions of two scales and their calculations up to next-to-next-to-leading order in α_s prove to be far from trivial. In particular, the real-real soft parton emission contributions considered in chapter 6 require us to employ advanced techniques developed for high order loop calculations.

By combining together the d - dimensional results for the collinear and soft functions, obtained in chapters 4, and 5 and 6 respectively, in chapter 7 we verify the correctness of the factorisation formulas for bare regularized objects up to next-to-next-to-leading order in perturbation theory. Partial N^{3}LO results are presented in section 7.1.3.

With the fixed-order investigations concluded, we continue on to Part IV which consists of two chapters discussing the leading logarithmic resummation for the Drell-Yan and Higgs production processes. We begin with the Drell-Yan process at threshold in chapter 8, where we first restrict the factorisation formulas to include only the leading logarithmic terms, before setting up renormalization group equations and solving them. This yields results valid to all orders in perturbation theory. Higgs production via gluon-gluon fusion is investigated in chapter 9. Here, we first derive the leading logarithmic factorisation formula and later proceed with similar steps to the Drell-Yan resummation also arriving at all order results. Our result proves that, to all orders in the strong coupling constant, the leading logarithmic terms at next-to-leading power are identical to those obtained for the threshold expansion of the Drell-Yan process in the $q\bar{q}$ channel up to an exchange of

the colour factor, $C_F \to C_A$.

Lastly, based on an explicit example, we discussed issues in the extension of the resummation formalism within the standard paradigm of SCET due to the divergent convolutions. As we have already mentioned above, this is an active field of research, with new results appearing recently.

The next-to-leading power investigations of relevant collider processes is a captivating field of research with plenty of developments still to be made. With the detailed calculations, discussions, examples, and new results presented here, we hope that this work is a useful resource in future investigations.

Part VI

Appendices

A

A.1 YM subleading SCET Lagrangian

The subleading-power gluon self-interaction terms of the soft-collinear Yang-Mills Lagrangian [73] expressed in terms of the collinear and soft gauge-invariant fields are given by

$$\mathcal{L}_{1\text{YM}}^{(1)} = -\frac{1}{g_s^2}\text{tr}\Big(\big[n_+\partial\,\mathcal{A}_{\nu_\perp}^c\big]\big[x_\perp^\rho\,in_-\partial\,\mathcal{B}_\rho^+,\mathcal{A}_c^{\nu_\perp}\big]\Big),$$

$$\mathcal{L}_{2\text{YM}}^{(1)} = -\frac{1}{g_s^2}\text{tr}\Big(\big[n_+\partial\,\mathcal{A}_c^{\nu_\perp}\big]in_-\partial\,\mathcal{B}_{\nu_\perp}^+\Big),$$

$$\mathcal{L}_{1\text{YM}}^{(2)} = -\frac{1}{2g_s^2}\text{tr}\Big(\big[n_+\partial\,\mathcal{A}_{\nu_\perp}^c\big]\big[n_-x\,in_-\partial\,n_+\mathcal{B}^+,\mathcal{A}_c^{\nu_\perp}\big]\Big),$$

$$\mathcal{L}_{2\text{YM}}^{(2)} = -\frac{1}{2g_s^2}\text{tr}\Big(\big[n_+\partial\,\mathcal{A}_{\nu_\perp}^c\big]\big[x_\perp^\rho x_{\perp\omega}\big[\partial^\omega,\,in_-\partial\,\mathcal{B}_\rho^+\big],\mathcal{A}_c^{\nu_\perp}\big]\Big),$$

$$\mathcal{L}_{3\text{YM}}^{(2)} = -\frac{1}{2g_s^2}\text{tr}\Big(\big[n_+\partial\,\mathcal{A}_{\nu_\perp}^c\big]\big[x_\perp^\rho x_{\perp\omega}\big[\mathcal{B}_+^\omega,n_-\partial\,\mathcal{B}_\rho^+\big],\mathcal{A}_c^{\nu_\perp}\big]\Big),$$

$$\mathcal{L}_{4\text{YM}}^{(2)} = -\frac{1}{2g_s^2}\text{tr}\Big(\big[n_+\partial\,\mathcal{A}_{\nu_\perp}^c\big]\big[x_\perp^\rho\big[i\partial_\rho\mathcal{B}_{\nu_\perp}^+ - i\partial_{\nu_\perp}\mathcal{B}_\rho^+\big],n_-\mathcal{A}_c\big]\Big),$$

$$\mathcal{L}_{5\text{YM}}^{(2)} = -\frac{1}{2g_s^2}\text{tr}\Big(\big[n_+\partial\,\mathcal{A}_{\nu_\perp}^c\big]\big[x_\perp^\rho\big[\mathcal{B}_\rho^+,\mathcal{B}_{\nu_\perp}^+\big],n_-\mathcal{A}_c\big]\Big),$$

$$\mathcal{L}_{6\text{YM}}^{(2)} = -\frac{1}{g_s^2}\text{tr}\Big(\big[i\partial^{\mu_\perp}\mathcal{A}_c^{\nu_\perp} - i\partial^{\nu_\perp}\mathcal{A}_c^{\mu_\perp}\big]\big[ix_\perp^\rho\big[i\partial_\rho\mathcal{B}_{\mu_\perp}^+ - i\partial_{\mu_\perp}\mathcal{B}_\rho^+\big],\mathcal{A}_{\nu_\perp}^c\big]\Big),$$

$$\mathcal{L}_{7\text{YM}}^{(2)} = -\frac{1}{g_s^2}\text{tr}\Big(\big[\mathcal{A}_c^{\mu_\perp},\mathcal{A}_c^{\nu_\perp}\big]\big[ix_\perp^\rho\big[i\partial_\rho\mathcal{B}_{\mu_\perp}^+ - i\partial_{\mu_\perp}\mathcal{B}_\rho^+\big],\mathcal{A}_{\nu_\perp}^c\big]\Big),$$

$$\mathcal{L}_{8\text{YM}}^{(2)} = -\frac{1}{g_s^2}\text{tr}\Big(\big[i\partial^{\mu_\perp}\mathcal{A}_c^{\nu_\perp} - i\partial^{\nu_\perp}\mathcal{A}_c^{\mu_\perp}\big]\big[ix_\perp^\rho\big[\mathcal{B}_\rho^+,\mathcal{B}_{\mu_\perp}^+\big],\mathcal{A}_{\nu_\perp}^c\big]\Big),$$

$$\mathcal{L}_{9\text{YM}}^{(2)} = -\frac{1}{g_s^2}\text{tr}\Big(\big[\mathcal{A}_c^{\mu_\perp},\mathcal{A}_c^{\nu_\perp}\big]\big[ix_\perp^\rho\big[\mathcal{B}_\rho^+,\mathcal{B}_{\mu_\perp}^+\big],\mathcal{A}_{\nu_\perp}^c\big]\Big),$$

$$\mathcal{L}_{10\text{YM}}^{(2)} = -\frac{1}{2g_s^2}\text{tr}\Big(\big[n_+\partial\,n_-\mathcal{A}^c\big]n_-\partial\,n_+\mathcal{B}^+\Big),$$

$$\mathcal{L}_{11\text{YM}}^{(2)} = \frac{1}{g_s^2}\text{tr}\Big(\big(i\partial^{\mu_\perp}\mathcal{A}_c^{\nu_\perp} - i\partial^{\nu_\perp}\mathcal{A}_c^{\mu_\perp}\big)\big(i\partial_{\mu_\perp}\mathcal{B}_{\nu_\perp}^+ - i\partial_{\nu_\perp}\mathcal{B}_{\mu_\perp}^+\big)\Big),$$

$$
\begin{aligned}
\mathcal{L}^{(2)}_{12\text{YM}} &= \frac{1}{g_s^2}\text{tr}\left(\left[\mathcal{A}^{\mu_\perp}_c, \mathcal{A}^{\nu_\perp}_c\right]\left(i\partial_{\mu_\perp}\mathcal{B}^+_{\nu_\perp} - i\partial_{\nu_\perp}\mathcal{B}^+_{\mu_\perp}\right)\right), \\
\mathcal{L}^{(2)}_{13\text{YM}} &= \frac{1}{g_s^2}\text{tr}\left(\left(i\partial^{\mu_\perp}\mathcal{A}^{\nu_\perp}_c - i\partial^{\nu_\perp}\mathcal{A}^{\mu_\perp}_c\right)\left[\mathcal{B}^+_{\mu_\perp}, \mathcal{B}^+_{\nu_\perp}\right]\right), \\
\mathcal{L}^{(2)}_{14\text{YM}} &= \frac{1}{g_s^2}\text{tr}\left(\left[\mathcal{A}^{\mu_\perp}_c, \mathcal{A}^{\nu_\perp}_c\right]\left[\mathcal{B}^+_{\mu_\perp}, \mathcal{B}^+_{\nu_\perp}\right]\right), \\
\mathcal{L}^{(2)}_{15\text{YM}} &= -\frac{1}{g_s^2}\text{tr}\left(\left[n_+\partial\,\mathcal{A}^{\nu_\perp}_c\right]x_{\perp\sigma}\left[\partial^\sigma, n_-\partial B^+_{\nu_\perp}\right]\right), \\
\mathcal{L}^{(2)}_{16\text{YM}} &= \frac{1}{g_s^2}\text{tr}\left(\left[n_+\partial\,\mathcal{A}^{\nu_\perp}_c\right]x_{\perp\sigma}\left[iB^\sigma_+, n_-\partial B^+_{\nu_\perp}\right]\right).
\end{aligned}
\tag{A.1}
$$

A.2   Useful formulas for Feynman integration

The integral representation of the Beta function has the following form

$$
B(r,s) = \int_0^1 dt\, t^{r-1}(1-t)^{s-1} = \frac{\Gamma[r]\Gamma[s]}{\Gamma[r+s]}.
\tag{A.2}
$$

We can also write the Beta function in terms of an integral from 0 to ∞, rather than the lower limit of 0 and upper limit of 1. The formula reads

$$
B(r,s) = \int_0^\infty dx\, \frac{x^{r-1}}{(1+x)^{r+s}} = \frac{\Gamma[r]\Gamma[s]}{\Gamma[r+s]}.
\tag{A.3}
$$

We can show this by performing the following substitution $x = \frac{y}{1-y}$ in (A.3), which with further manipulations then leads to

$$
\begin{aligned}
\int_0^\infty dx\, \frac{x^{r-1}}{(1+x)^{r+s}} &= \int_0^1 dy\, \frac{1}{(1-y)^2}\frac{y^{r-1}}{(1-y)^{r-1}}\frac{1}{\left(1+\frac{y}{1-y}\right)^{r+s}} \\
&= \int_0^1 dy\, \frac{y^{r-1}}{(1-y)^{r+1}}(1-y)^{r+s} = \int_0^1 dy\, y^{r-1}(1-y)^{s-1}.
\end{aligned}
\tag{A.4}
$$

After the last step we arrive at the integral representation of the Beta function as given in (A.2). The $_2F_1$ hypergeometric function has the following integral representation

$$
_2F_1(a,b,c,x) = \frac{\Gamma[c]}{\Gamma[b]\Gamma[c-b]}\int_0^1 dz\, z^{b-1}(1-z)^{c-b-1}(1-zx)^{-a}
\tag{A.5}
$$

For the evaluation of Feynman integrals the following parametrisation often appears in SCET calculations

$$
\frac{1}{a^n b^m} = \frac{\Gamma[n+m]}{\Gamma[n]\Gamma[m]}\int_0^\infty dy\, \frac{y^{m-1}}{(a+yb)^{n+m}}
\tag{A.6}
$$

The above is proved using (A.3) and rescalling of variable $y = (a/b)y'$. One can also see that using (A.6) twice, the following holds for more than two propagators

$$
\frac{1}{a^n b^m c^p} = \frac{\Gamma[n+m+p]}{\Gamma[n]\Gamma[m]\Gamma[p]}\int_0^\infty dy \int_0^\infty dx\, \frac{y^{m-1}x^{p-1}}{(a+yb+xc)^{n+m+p}}
\tag{A.7}
$$

Euclidean-space integral results

$$\int \frac{d^d l_E}{(2\pi)^d} \frac{1}{\left(l_E^2 + M^2\right)^n} = \frac{1}{(4\pi)^{d/2}} \frac{\Gamma[n - \frac{d}{2}]}{\Gamma[n]} \left(M^2\right)^{\frac{d}{2} - n} \tag{A.8}$$

$$\int \frac{d^d l_E}{(2\pi)^d} \frac{l_E^2}{\left(l_E^2 + M^2\right)^n} = \frac{1}{(4\pi)^{d/2}} \frac{d}{2} \frac{\Gamma[n - \frac{d}{2} - 1]}{\Gamma[n]} \left(M^2\right)^{\frac{d}{2} + 1 - n} \tag{A.9}$$

Minkowski-space integral results

$$\int \frac{d^d l}{(2\pi)^d} \frac{1}{\left(l^2 - M^2\right)^n} = \frac{(-1)^n i}{(4\pi)^{d/2}} \frac{\Gamma[n - \frac{d}{2}]}{\Gamma[n]} \left(M^2\right)^{\frac{d}{2} - n} \tag{A.10}$$

$$\int \frac{d^d l}{(2\pi)^d} \frac{l^2}{\left(l^2 - M^2\right)^n} = \frac{(-1)^{n-1} i}{(4\pi)^{d/2}} \frac{d}{2} \frac{\Gamma[n - \frac{d}{2} - 1]}{\Gamma[n]} \left(M^2\right)^{\frac{d}{2} + 1 - n} \tag{A.11}$$

$$\int \frac{d^d l}{(2\pi)^d} \frac{l^\mu l^\nu}{\left(l^2 - M^2\right)^n} = \frac{(-1)^{n-1} i}{(4\pi)^{d/2}} \frac{g^{\mu\nu}}{2} \frac{\Gamma[n - \frac{d}{2} - 1]}{\Gamma[n]} \left(M^2\right)^{\frac{d}{2} + 1 - n} \tag{A.12}$$

$$\int \frac{d^d l}{(2\pi)^d} \frac{l^\mu l^\nu l^\rho l^\sigma}{\left(l^2 - M^2\right)^n} = \frac{(-1)^n i}{(4\pi)^{d/2}} \frac{\Gamma[n - \frac{d}{2} - 2]}{\Gamma[n]} \left(M^2\right)^{\frac{d}{2} + 2 - n}$$

$$\times \frac{1}{4} \Big[g^{\mu\nu} g^{\rho\sigma} + g^{\mu\rho} g^{\nu\sigma} + g^{\mu\sigma} g^{\nu\rho} \Big] \tag{A.13}$$

These integrals are ubiquitous in loop integrals in quantum field theories, see for example [183], and are stated here for ease of use.

A.3   Useful spinor relations

As in the main text, we decompose the metric

$$g^{\mu\nu} = n_+^\mu \frac{n_-^\nu}{2} + n_-^\mu \frac{n_+^\nu}{2} + g_\perp^{\mu\nu}. \tag{A.14}$$

This is consistent as

$$p^\nu = p_\mu g^{\mu\nu} = p_\mu n_+^\mu \frac{n_-^\nu}{2} + p_\mu n_-^\mu \frac{n_+^\nu}{2} + p_\mu g_\perp^{\mu\nu} = (n_+ p) \frac{n_-^\nu}{2} + (n_- p) \frac{n_+^\nu}{2} + p_\perp^\nu. \tag{A.15}$$

The following holds

$$\{\gamma_\perp^\mu, \gamma_\perp^\nu\} = 2 g_\perp^{\mu\nu}. \tag{A.16}$$

We prove it here. First write

$$\gamma_\perp^\mu = \gamma^\mu - \slashed{n}_+ \frac{n_-^\mu}{2} - \slashed{n}_- \frac{n_+^\mu}{2}, \tag{A.17}$$

so we have

$$\{\gamma_\perp^\mu, \gamma_\perp^\nu\} = \{\gamma^\mu - \slashed{n}_+ \frac{n_-^\mu}{2} - \slashed{n}_- \frac{n_+^\mu}{2}, \gamma^\nu - \slashed{n}_+ \frac{n_-^\nu}{2} - \slashed{n}_- \frac{n_+^\nu}{2}\}$$

$$
\begin{aligned}
=\;& \{\gamma^\mu,\gamma^\nu\} - \{\gamma^\mu,\slashed{n}_+\}\frac{n_-^\nu}{2} - \{\gamma^\mu,\slashed{n}_-\}\frac{n_+^\nu}{2} - \frac{n_-^\mu}{2}\{\slashed{n}_+,\gamma^\nu\} + \frac{n_-^\mu}{2}\{\slashed{n}_+,\slashed{n}_+\}\frac{n_-^\nu}{2} \\
& + \frac{n_-^\mu}{2}\{\slashed{n}_+,\slashed{n}_-\}\frac{n_+^\nu}{2} - \frac{n_+^\mu}{2}\{\slashed{n}_-,\gamma^\nu\} + \frac{n_+^\mu}{2}\{\slashed{n}_-,\slashed{n}_+\}\frac{n_-^\nu}{2} + \frac{n_+^\mu}{2}\{\slashed{n}_-,\slashed{n}_-\}\frac{n_+^\nu}{2} \\
=\;& 2g^{\mu\nu} - \{\gamma^\mu,\gamma^\eta\}n_{+\eta}\frac{n_-^\nu}{2} - \{\gamma^\mu,\gamma^\eta\}n_{-\eta}\frac{n_+^\nu}{2} - \frac{n_-^\mu}{2}n_{+\eta}\{\gamma^\eta,\gamma^\nu\} + 0 \\
& + \frac{n_-^\mu}{2}\{\slashed{n}_+,\slashed{n}_-\}\frac{n_+^\nu}{2} - \frac{n_+^\mu}{2}\{\slashed{n}_-,\gamma^\nu\} + \frac{n_+^\mu}{2}\{\slashed{n}_-,\slashed{n}_+\}\frac{n_-^\nu}{2} \\
=\;& 2g^{\mu\nu} - n_+^\mu n_-^\nu - n_-^\mu n_+^\nu - n_-^\mu n_+^\nu + n_-^\mu n_+^\nu - n_+^\mu n_-^\nu + n_+^\mu n_-^\nu \\
=\;& 2g^{\mu\nu} - n_+^\mu n_-^\nu - n_-^\mu n_+^\nu \\
=\;& 2g_\perp^{\mu\nu} \,.
\end{aligned}
\tag{A.18}
$$

Using (A.14) in the last line. Then also

$$
\{\gamma_\perp^\mu,\gamma_{\perp\mu}\} = 2d - 2 - 2 = 4(1-\epsilon) \implies \gamma_\perp^2 = 2(1-\epsilon)\,,
\tag{A.19}
$$

$$
\gamma_\perp^2 = d - 2\,.
\tag{A.20}
$$

For a spinor

$$
\gamma^\mu\gamma^\nu\gamma_\mu = -\gamma^\nu\gamma^\mu\gamma_\mu + 2\gamma^\nu = (2-d)\gamma^\nu\,.
\tag{A.21}
$$

For perpendicular spinors

$$
\gamma_\perp^\mu\gamma_\perp^\nu\gamma_{\mu\perp} = -\gamma_\perp^\nu\gamma_\perp^\mu\gamma_{\mu\perp} + 2\gamma_\perp^\nu = -\gamma_\perp^\nu(d-2) + 2\gamma_\perp^\nu = (4-d)\gamma_\perp^\nu\,,
\tag{A.22}
$$

using (A.20). Another useful result is

$$
\gamma_\perp^\mu\gamma_\perp^\nu\gamma_\perp^\delta\gamma_{\mu\perp} = -\gamma_\perp^\nu\gamma_\perp^\mu\gamma_\perp^\delta\gamma_{\mu\perp} + 2g_\perp^{\nu\mu}\gamma_\perp^\delta\gamma_{\perp\mu} = \gamma_\perp^\nu\gamma_\perp^\delta(d-4) + 2\gamma_\perp^\delta\gamma_\perp^\nu = \gamma_\perp^\nu\gamma_\perp^\delta(d-6) + 4g_\perp^{\delta\nu}\,.
\tag{A.23}
$$

$\Sigma_{\alpha\mu}$ in light cone coordinates .

This quantity appears often in the calculation using the expansion-by-regions method. We writre it here using light-cone components for convenience. $\Sigma_{\alpha\mu}$ is defined as

$$
\Sigma_{\alpha\mu} = \frac{i}{4}\left[\gamma_\alpha,\gamma_\mu\right].
\tag{A.24}
$$

We use (A.17)

$$
\Sigma_{\alpha\mu} = \frac{i}{4}\left[\slashed{n}_+\frac{n_{-\alpha}}{2} + \slashed{n}_-\frac{n_{+\alpha}}{2} + \gamma_{\perp\alpha}, \slashed{n}_+\frac{n_{-\mu}}{2} + \slashed{n}_-\frac{n_{+\mu}}{2} + \gamma_{\perp\mu}\right],
\tag{A.25}
$$

$$
\begin{aligned}
\Sigma_{\alpha\mu} =\;& \frac{i}{4}\Bigg\{\left(\slashed{n}_+\frac{n_{-\alpha}}{2} + \slashed{n}_-\frac{n_{+\alpha}}{2} + \gamma_{\perp\alpha}\right)\left(\slashed{n}_+\frac{n_{-\mu}}{2} + \slashed{n}_-\frac{n_{+\mu}}{2} + \gamma_{\perp\mu}\right) \\
& - \left(\slashed{n}_+\frac{n_{-\mu}}{2} + \slashed{n}_-\frac{n_{+\mu}}{2} + \gamma_{\perp\mu}\right)\left(\slashed{n}_+\frac{n_{-\alpha}}{2} + \slashed{n}_-\frac{n_{+\alpha}}{2} + \gamma_{\perp\alpha}\right)\Bigg\}.
\end{aligned}
\tag{A.26}
$$

Then we have

$$
\Sigma_{\alpha\mu} = \frac{i}{4}\Bigg\{\left(\slashed{n}_-\frac{n_{+\alpha}}{2}\slashed{n}_+\frac{n_{-\mu}}{2} + \gamma_{\perp\alpha}\slashed{n}_+\frac{n_{-\mu}}{2} + \slashed{n}_+\frac{n_{-\alpha}}{2}\slashed{n}_-\frac{n_{+\mu}}{2}\right.
$$

$$+\gamma_{\perp\alpha}\slashed{n}_- \frac{n_{+\mu}}{2} + \slashed{n}_+ \frac{n_{-\alpha}}{2}\gamma_{\perp\mu} + \slashed{n}_- \frac{n_{+\alpha}}{2}\gamma_{\perp\mu} + \gamma_{\perp\alpha}\gamma_{\perp\mu}\Big)$$
$$-\Big(\slashed{n}_- \frac{n_{+\mu}}{2}\slashed{n}_+ \frac{n_{-\alpha}}{2} + \gamma_{\perp\mu}\slashed{n}_+ \frac{n_{-\alpha}}{2} + \slashed{n}_+ \frac{n_{-\mu}}{2}\slashed{n}_- \frac{n_{+\alpha}}{2}$$
$$+\gamma_{\perp\mu}\slashed{n}_- \frac{n_{+\alpha}}{2} + \slashed{n}_+ \frac{n_{-\mu}}{2}\gamma_{\perp\alpha} + \slashed{n}_- \frac{n_{+\mu}}{2}\gamma_{\perp\alpha} + \gamma_{\perp\mu}\gamma_{\perp\alpha}\Big)\Big\}. \tag{A.27}$$

Now we make use of the fact that $\{\slashed{n}_+, \gamma_\perp^\nu\} = 0$ and $\{\slashed{n}_+, \slashed{n}_-\} = 4$ Then

$$\Sigma_{\alpha\mu} = \frac{i}{4}\Big\{\Big(-\slashed{n}_+\slashed{n}_- n_{+\alpha}\frac{n_{-\mu}}{2} + \gamma_{\perp\alpha}\slashed{n}_+ n_{-\mu} + \slashed{n}_+\slashed{n}_- n_{-\alpha}\frac{n_{+\mu}}{2} + \gamma_{\perp\alpha}\slashed{n}_- n_{+\mu}$$
$$+\slashed{n}_+\gamma_{\perp\mu}n_{-\alpha} + \slashed{n}_-\gamma_{\perp\mu}n_{+\alpha} + [\gamma_{\perp\alpha},\gamma_{\perp\mu}]\Big) - \Big(n_{-\alpha}n_{+\mu} - n_{+\alpha}n_{-\mu}\Big)\Big\} \tag{A.28}$$

Only now we specialise to the case where on the right-hand side we have a collinear spinor χ_c. All the terms with $\slashed{n}_-$ on the rightmost of the expression vanish.

$$\Sigma_{\alpha\mu}u_c(p) = \frac{i}{4}\Big\{\gamma_{\perp\alpha}\slashed{n}_+ n_{-\mu} + \slashed{n}_+\gamma_{\perp\mu}n_{-\alpha} + [\gamma_{\perp\alpha},\gamma_{\perp\mu}] - n_{-\alpha}n_{+\mu} + n_{+\alpha}n_{-\mu}\Big\}u_c(p). \tag{A.29}$$

Here on the left-hand side we assume that there is a generic spinor structure and not a $\gamma_\perp^\rho$. This is why the $\slashed{n}_-$ can survive here. We write $\gamma_{\perp\alpha}$ in terms of the full γ_α

$$\Sigma_{\alpha\mu}u_c(p) = \frac{i}{4}\Big\{\Big(\gamma_\alpha - \slashed{n}_+\frac{n_{-\alpha}}{2} - \slashed{n}_-\frac{n_{+\alpha}}{2}\Big)\slashed{n}_+ n_{-\mu} - n_{-\alpha}\gamma_{\perp\mu}\slashed{n}_+ + [\gamma_{\perp\alpha},\gamma_{\perp\mu}]$$
$$-n_{-\alpha}n_{+\mu} + n_{+\alpha}n_{-\mu}\Big\}u_c(p) \tag{A.30}$$

Then

$$\Sigma_{\alpha\mu}u_c(p) = \frac{i}{4}\Big\{n_{-\mu}\gamma_\alpha\slashed{n}_+ - n_{-\mu}\slashed{n}_-\frac{n_{+\alpha}}{2}\slashed{n}_+ - n_{-\alpha}\gamma_{\perp\mu}\slashed{n}_+ + [\gamma_{\perp\alpha},\gamma_{\perp\mu}]$$
$$-n_{-\alpha}n_{+\mu} + n_{+\alpha}n_{-\mu}\Big\}u_c(p) \tag{A.31}$$

Using $\{\slashed{n}_+, \slashed{n}_-\} = 4$ we can move $\slashed{n}_-$ to the right in the second term which means that we can annihilate it with u_c. Then we have

$$\frac{i}{4}\Big[\gamma_\alpha,\gamma_\mu\Big]u_c(p) = \frac{i}{4}\Big\{n_{-\mu}\gamma_\alpha\slashed{n}_+ - n_{-\alpha}\gamma_{\perp\mu}\slashed{n}_+ + [\gamma_{\perp\alpha},\gamma_{\perp\mu}] - n_{-\alpha}n_{+\mu} - n_{+\alpha}n_{-\mu}\Big\}u_c(p). \tag{A.32}$$

We next take k^α and ϵ^μ. Then we have from above (rearranging for $[\gamma_{\perp\alpha},\gamma_{\perp\mu}]$)

$$[\gamma_{\perp\alpha},\gamma_{\perp\mu}] = \Big[\gamma_\alpha,\gamma_\mu\Big] - n_{-\mu}\gamma_\alpha\slashed{n}_+ + n_{-\alpha}\gamma_{\perp\mu}\slashed{n}_+ + n_{-\alpha}n_{+\mu} + n_{+\alpha}n_{-\mu} \tag{A.33}$$

$$[\slashed{k}_\perp,\slashed{\epsilon}_\perp] = \Big[\slashed{k},\slashed{\epsilon}\Big] - (n_-\epsilon)\slashed{k}\slashed{n}_+ + (n_-k)\slashed{\epsilon}_\perp\slashed{n}_+ + (n_-k)(n_+\epsilon) + (n_+k)(n_-\epsilon) \tag{A.34}$$

However, for the comparison of SCET DY computation to the expansion-by-regions method the most useful would be equation (A.29), since we can immediately combine this expression with $\Gamma^\rho = \gamma^\rho$ which appears to the left of this expression. For example

$$\gamma^\rho\Sigma_{\alpha\mu}u_c(p) = \frac{i}{4}\gamma^\rho\Big\{\gamma_{\perp\alpha}\slashed{n}_+ n_{-\mu} + \slashed{n}_+\gamma_{\perp\mu}n_{-\alpha} + [\gamma_{\perp\alpha},\gamma_{\perp\mu}] - n_{-\alpha}n_{+\mu} + n_{+\alpha}n_{-\mu}\Big\}u_c(p). \tag{A.35}$$

The last three terms will pick out only the $\gamma_\perp^\rho$ component because of the spinors $\bar{v}_{\bar{c}}$ and u_c and their projection operators. Hence now we focus on the first two terms with a $\not{n}_+$ spinor appearing

$$\left(\not{n}_- \frac{n_+^\rho}{2} + \not{n}_+ \frac{n_-^\rho}{2} + \gamma_\perp^\rho \right) \left\{ -\not{n}_+ \gamma_{\perp\alpha} n_{-\mu} + \not{n}_+ \gamma_{\perp\mu} n_{-\alpha} \right\} \tag{A.36}$$

Now, $\not{n}_+ \not{n}_+ = 0$ and $\bar{v}_{\bar{c}} \gamma_\perp^\rho \not{n}_+ = 0$. We find that only one term yields a non-zero result

$$\left(\not{n}_- \frac{n_+^\rho}{2} \right) \left\{ -\not{n}_+ \gamma_{\perp\alpha} n_{-\mu} + \not{n}_+ \gamma_{\perp\mu} n_{-\alpha} \right\} \tag{A.37}$$

Then forming projection operators and acting on $\bar{v}_{\bar{c}}$ we have

$$\left\{ -2 n_+^\rho \gamma_{\perp\alpha} n_{-\mu} + 2 n_+^\rho \gamma_{\perp\mu} n_{-\alpha} \right\} \tag{A.38}$$

These are the terms not proportional to $\gamma_\perp^\rho$ coming from $\gamma^\rho \Sigma_{\alpha\mu}$, the three terms which are proportional to $\gamma_\perp^\rho$ are the last three terms in (A.35).

A.4   Colour identities

We define a basis of colour generators $\mathbf{T}_i^A$ which are matrices which act in colour space on the colour index of the i-th parton [184] (for an example see equation (H.2) of [79]). We use the notation $\mathbf{T}_i^A \mathbf{T}_j^A = \mathbf{T}_i \cdot \mathbf{T}_j$. We have

$$f^{ABC} f^{ABD} = C_A \delta^{CD}, \tag{A.39}$$

where C_A is the Casimir of the adjoint representation.

$$\begin{aligned} \mathbf{T}_1^A \mathbf{T}_1^B \mathbf{T}_1^A &= \mathbf{T}_1^A \mathbf{T}_1^A \mathbf{T}_1^B + i \mathbf{T}_1^A f^{BAC} \mathbf{T}_1^C \\ &= C_F \mathbf{T}_1^B + \frac{1}{2} i^2 f^{BAC} f^{ACD} \mathbf{T}_1^D = \left(C_F - \frac{1}{2} C_A \right) \mathbf{T}_1^B \end{aligned} \tag{A.40}$$

where we have used the fact that we can always write

$$2 \mathbf{T}^A \mathbf{T}^B = \left[\mathbf{T}^A, \mathbf{T}^B \right] + \left\{ \mathbf{T}^A, \mathbf{T}^B \right\} \tag{A.41}$$

and that the symmetric part of $\mathbf{T}^A \mathbf{T}^B$ is zero when contracted with the fully anti-symmetric structure constant f^{BAC}.

A.5   List of useful integrals

In this appendix we collect solutions to the integrals appearing in various Feynman diagrams encountered in the collinear function calculation in the Drell-Yan process. All the integrals were calculated using contour and Feynman parametrisation methods, and checked using reduction techniques. Note that the results presented here are not valid for general kinematics. We assume that the collinear momentum p^μ carries only its large

component $p^\mu = (n_+ p) \frac{n_-^\mu}{2}$ and is on-shell, $p^2 = 0$. Moreover, external the soft momentum $k_+^\mu = (n_- k) \frac{n_+^\mu}{2} = k_+ \frac{n_+^\mu}{2}$ as only the $(n_- k)$ component of the soft momentum survives in soft-collinear interactions due to multipole expansion.

$$g_s^2 \int \frac{d^d q}{(2\pi)^d} \frac{1}{q^2 (p - k_+ - q)^2} = \frac{i\alpha_s}{(4\pi)} \left[\frac{(n_+ p)(n_- k)}{\mu^2} \right]^{-\epsilon} \frac{e^{\epsilon\gamma_E} \Gamma[\epsilon] \Gamma[1 - \epsilon]^2}{\Gamma[2 - 2\epsilon]} \tag{A.42}$$

$$g_s^2 \int \frac{d^d q}{(2\pi)^d} \frac{1}{q^2} \frac{q_\perp^\sigma q_\perp^\eta}{(p - k_+ - q)^4} = \frac{i\alpha_s}{(4\pi)} \left[\frac{(n_+ p)(n_- k)}{\mu^2} \right]^{-\epsilon} \frac{g_\perp^{\sigma\eta}}{4}$$
$$\times \frac{e^{\epsilon\gamma_E} \Gamma[\epsilon] \Gamma[1 - \epsilon]^2}{\Gamma[2 - 2\epsilon]} \tag{A.43}$$

$$g_s^2 \int \frac{d^d q}{(2\pi)^d} \frac{1}{q^2} \frac{\left(q_\perp^\sigma q_\perp^\alpha \right)}{(p - k_+ - q)^6} = \frac{-i\alpha_s}{(4\pi)} \left[\frac{(n_- k)(n_+ p)}{\mu^2} \right]^{-\epsilon} \frac{1}{(n_- k)(n_+ p)}$$
$$\times \frac{g_\perp^{\sigma\alpha}}{4} \frac{e^{\epsilon\gamma_E} \Gamma[1 + \epsilon] \Gamma[-\epsilon] \Gamma[2 - \epsilon]}{\Gamma[2 - 2\epsilon]} \tag{A.44}$$

$$g_s^2 \int \frac{d^d q}{(2\pi)^d} \frac{1}{q^2} \frac{1}{(p - k_+ - q)^2} \frac{q_\perp^2}{(n_+ (p - q))} = \frac{i\alpha_s}{(4\pi)} \left[\frac{(n_+ p)(n_- k)}{\mu^2} \right]^{-\epsilon} (n_- k)$$
$$\times \frac{1}{2} \frac{e^{\epsilon\gamma_E} \Gamma[\epsilon] \Gamma[1 - \epsilon]^2}{\Gamma[2 - 2\epsilon]} \tag{A.45}$$

$$g_s^2 \int \frac{d^d q}{(2\pi)^d} \frac{1}{q^2} \frac{1}{(p - k_+ - q)^2} \frac{\gamma_{\perp\mu} \slashed{q}_\perp \slashed{q}_\perp \gamma_\perp^\mu}{(n_+ (p - q))^2} = \frac{i\alpha_s}{(4\pi)} \left[\frac{(n_+ p)(n_- k)}{\mu^2} \right]^{-\epsilon} \frac{(n_- k)}{(n_+ p)}$$
$$\times 2(1 - \epsilon) \frac{e^{\epsilon\gamma_E} \Gamma[-\epsilon] \Gamma[2 - \epsilon] \Gamma[\epsilon]}{\Gamma[2 - 2\epsilon]} \tag{A.46}$$

$$g_s^2 \int \frac{d^d q}{(2\pi)^d} \frac{1}{(p - k_+ - q)^4} \frac{1}{q^2} \frac{\gamma_{\perp\mu} \slashed{q}_\perp \slashed{q}_\perp \gamma_\perp^\mu}{(n_+ (p - q))} = \frac{i\alpha_s}{(4\pi)} \left[\frac{(n_+ p)(n_- k)}{\mu^2} \right]^{-\epsilon} \frac{1}{(n_+ p)}$$
$$\times 2(1 - \epsilon)^2 \frac{e^{\epsilon\gamma_E} \Gamma[-\epsilon] \Gamma[2 - \epsilon] \Gamma[\epsilon]}{\Gamma[2 - 2\epsilon]} \tag{A.47}$$

$$g_s^2 \int \frac{d^d q}{(2\pi)^d} \frac{1}{q^2} \frac{1}{(p - k_+ - q)^4} \frac{q_\perp^\sigma q_\perp^\eta}{(n_+ (p - q))} = \frac{i\alpha_s}{(4\pi)} \left[\frac{(n_+ p)(n_- k)}{\mu^2} \right]^{-\epsilon} \frac{1}{(n_+ p)}$$
$$\times \frac{g_\perp^{\sigma\eta}}{2} \frac{e^{\epsilon\gamma_E} \Gamma[-\epsilon] \Gamma[2 - \epsilon] \Gamma[\epsilon]}{\Gamma[2 - 2\epsilon]} \tag{A.48}$$

$$g_s^2 \int \frac{d^d q}{(2\pi)^d} \frac{1}{(p - k_+ - q)^6} \frac{1}{q^2} \frac{\left(q_\perp^\sigma q_\perp^\alpha \right) q_\perp^2}{(n_+ (p - q))} = \frac{i\alpha_s}{(4\pi)} \left[\frac{(n_+ p)(n_- k)}{\mu^2} \right]^{-\epsilon} \frac{1}{(n_+ p)}$$

$$\times g_\perp^{\sigma\alpha} \frac{(2-\epsilon)}{4} \frac{e^{\epsilon\gamma_E}\Gamma[-\epsilon]\Gamma[3-\epsilon]\Gamma[\epsilon]}{\Gamma[3-2\epsilon]} \qquad (A.49)$$

$$g_s^2 \int \frac{d^d q}{(2\pi)^d} \frac{1}{q^2} \frac{(n_-(k+q))}{(p-k_+-q)^4} \frac{\gamma_{\perp\mu}\slashed{q}_\perp\slashed{q}_\perp\gamma_\perp^\mu}{(n_+(p-q))} = \frac{i\alpha_s}{(4\pi)} \left[\frac{(n_+p)(n_-k)}{\mu^2}\right]^{-\epsilon} \frac{(n_-k)}{(n_+p)}$$
$$\times \left(2-2\epsilon+\epsilon^2\right) \frac{e^{\epsilon\gamma_E}\Gamma[\epsilon]\Gamma[-\epsilon]\Gamma[2-\epsilon]}{\Gamma[2-2\epsilon]} \qquad (A.50)$$

$$g_s^2 \int \frac{d^d q}{(2\pi)^d} \frac{1}{q^2} \frac{(n_-(k-q))}{(p-k_+-q)^4} \frac{\gamma_{\perp\mu}\slashed{q}_\perp\slashed{q}_\perp\gamma_\perp^\mu}{(n_+(p-q))} = \frac{i\alpha_s}{(4\pi)} \left[\frac{(n_+p)(n_-k)}{\mu^2}\right]^{-\epsilon} \frac{(n_-k)}{(n_+p)}$$
$$\times \left(2-6\epsilon+3\epsilon^2\right) \frac{e^{\epsilon\gamma_E}\Gamma[\epsilon]\Gamma[-\epsilon]\Gamma[2-\epsilon]}{\Gamma[2-2\epsilon]} \quad (A.51)$$

$$g_s^2 \int \frac{d^d q}{(2\pi)^d} \frac{1}{q^2} \frac{1}{(p-k_+-q)^4} \frac{q_\perp^\sigma q_\perp^\eta (n_+q)}{(n_+(p-q))} = \frac{i\alpha_s}{(4\pi)} \left[\frac{(n_+p)(n_-k)}{\mu^2}\right]^{-\epsilon}$$
$$\times \frac{g_\perp^{\sigma\eta}}{2} \frac{e^{\epsilon\gamma_E}\Gamma[-\epsilon]\Gamma[3-\epsilon]\Gamma[\epsilon]}{\Gamma[3-2\epsilon]} \quad (A.52)$$

$$g_s^2 \int \frac{d^d q}{(2\pi)^d} \frac{1}{q^2} \frac{1}{(p-k_+-q)^2} \frac{1}{(n_+(p-q))} = \frac{i\alpha_s}{(4\pi)} \left[\frac{(n_+p)(n_-k)}{\mu^2}\right]^{-\epsilon} \frac{1}{(n_+p)}$$
$$\times \frac{e^{\epsilon\gamma_E}\Gamma[-\epsilon]\Gamma[1-\epsilon]\Gamma[\epsilon]}{\Gamma[1-2\epsilon]} \qquad (A.53)$$

$$g_s^2 \int \frac{d^d q}{(2\pi)^d} \frac{1}{q^2} \frac{1}{(p-k_+-q)^2} (n_+q) = \frac{i\alpha_s}{(4\pi)} \left[\frac{(n_+p)(n_-k)}{\mu^2}\right]^{-\epsilon} (n_+p)$$
$$\times \frac{e^{\epsilon\gamma_E}\Gamma[1-\epsilon]\Gamma[2-\epsilon]}{\Gamma[3-2\epsilon]}\Gamma[\epsilon] \qquad (A.54)$$

$$g_s^2 \int \frac{d^d q}{(2\pi)^d} \frac{1}{(n_+q)} \frac{1}{q^2} \frac{1}{(p-k_+-q)^2} = \frac{i\alpha_s}{(4\pi)} \left[\frac{(n_+p)(n_-k)}{\mu^2}\right]^{-\epsilon} \frac{1}{(n_+p)}$$
$$\times \frac{e^{\epsilon\gamma_E}\Gamma[1-\epsilon]\Gamma[-\epsilon]\Gamma[\epsilon]}{\Gamma[1-2\epsilon]} \qquad (A.55)$$

$$g_s^2 \int \frac{d^d q}{(2\pi)^d} \frac{1}{(n_+q)} \frac{1}{q^2} \frac{(n_-(k+q))}{(p-k_+-q)^4} = -\frac{i\alpha_s}{(4\pi)} \left[\frac{(n_+p)(n_-k)}{\mu^2}\right]^{-\epsilon} \frac{1}{(n_+p)^2}$$
$$\times (1+\epsilon) \frac{e^{\epsilon\gamma_E}\Gamma[\epsilon]\Gamma[1-\epsilon]\Gamma[-\epsilon]}{\Gamma[1-2\epsilon]} \qquad (A.56)$$

$$g_s^2 \int \frac{d^d q}{(2\pi)^d} \frac{1}{q^2} \frac{1}{(n_+ q)} \frac{1}{(p - k_+ - q)^4} = -\frac{i\alpha_s}{(4\pi)} \left[\frac{(n_+ p)(n_- k)}{\mu^2} \right]^{-\epsilon} \frac{1}{(n_+ p)^2 (n_- k)}$$
$$\times \frac{e^{\epsilon \gamma_E} \Gamma[1 + \epsilon] \Gamma[-\epsilon] \Gamma[-\epsilon]}{\Gamma[-2\epsilon]} \tag{A.57}$$

$$g_s^2 \int \frac{d^d q}{(2\pi)^d} \frac{1}{q^2} \frac{(n_-(k + q))}{(p - k_+ - q)^4} = -\frac{i\alpha_s}{(4\pi)} \left[\frac{(n_+ p)(n_- k)}{\mu^2} \right]^{-\epsilon} \frac{1}{(n_+ p)}$$
$$\times \frac{e^{\epsilon \gamma_E} \Gamma[1 + \epsilon] \Gamma[1 - \epsilon]^2}{\Gamma[2 - 2\epsilon]} \tag{A.58}$$

$$g_s^2 \int \frac{d^d q}{(2\pi)^d} \frac{1}{q^2} \frac{1}{(p - k_+ - q)^4} = \frac{i\alpha_s}{(4\pi)} \left[\frac{(n_+ p)(n_- k)}{\mu^2} \right]^{-\epsilon} \frac{1}{(n_- k)(n_+ p)}$$
$$\times \frac{e^{\epsilon \gamma_E} \Gamma[\epsilon] \Gamma[1 - \epsilon] \Gamma[1 - \epsilon]}{\Gamma[1 - 2\epsilon]} \tag{A.59}$$

$$g_s^2 \int \frac{d^d q}{(2\pi)^d} \frac{1}{q^2} \frac{1}{(n_+ q)} \frac{\left(q_\perp^\sigma q_\perp^\eta\right)}{(p - k_+ - q)^4} = \frac{i\alpha_s}{(4\pi)} \left[\frac{(n_+ p)(n_- k)}{\mu^2} \right]^{-\epsilon} \frac{1}{(n_+ p)}$$
$$\times \frac{g_\perp^{\sigma\eta}}{2} \frac{e^{\epsilon \gamma_E} \Gamma[1 - \epsilon] \Gamma[1 - \epsilon] \Gamma[\epsilon]}{\Gamma[2 - 2\epsilon]} \tag{A.60}$$

$$g_s^2 \int \frac{d^d q}{(2\pi)^d} \frac{1}{q^2} \frac{1}{(n_+ q)} \frac{\left(q_\perp^\sigma q_\perp^\alpha\right)}{(p - k_+ - q)^6} = -\frac{i\alpha_s}{(4\pi)} \left[\frac{(n_+ p)(n_- k)}{\mu^2} \right]^{-\epsilon} \frac{1}{(n_+ p)^2 (n_- k)}$$
$$\times \frac{g_\perp^{\sigma\alpha}}{4} \frac{e^{\epsilon \gamma_E} \Gamma[1 - \epsilon] \Gamma[-\epsilon] \Gamma[1 + \epsilon]}{\Gamma[1 - 2\epsilon]} \tag{A.61}$$

$$g_s^2 \int \frac{d^d q}{(2\pi)^d} \frac{1}{(n_+ q)} \frac{1}{q^2} \frac{(n_+(p - q))}{(p - k_+ - q)^2} = \frac{i\alpha_s}{(4\pi)} \left[\frac{(n_+ p)(n_- k)}{\mu^2} \right]^{-\epsilon}$$
$$\times (1 - \epsilon) \frac{e^{\epsilon \gamma_E} \Gamma[\epsilon] \Gamma[-\epsilon] \Gamma[1 - \epsilon]}{\Gamma[2 - 2\epsilon]} \tag{A.62}$$

$$g_s^2 \int \frac{d^d q}{(2\pi)^d} \frac{1}{(p - k_+ - q)^2} \frac{1}{(p - q)^2} \frac{q_\perp^2}{(n_+(p - q))} \frac{1}{q^2} = \frac{i\alpha e^{\epsilon \gamma_E}}{(4\pi)} \left[\frac{(n_+ p)(n_- k)}{\mu^2} \right]^{-\epsilon} \frac{1}{(n_+ p)}$$
$$\times \frac{\Gamma[\epsilon] \Gamma[-\epsilon] \Gamma[2 - \epsilon]}{\Gamma[2 - 2\epsilon]} \tag{A.63}$$

$$g_s^2 \int \frac{d^d q}{(2\pi)^d} \frac{1}{(p - k_+ - q)^2} \frac{1}{(p - q)^2} \frac{q_\perp^\eta q_\perp^\delta}{(n_+(p - q))} \frac{1}{q^2} = \frac{i\alpha_s}{(4\pi)} \left[\frac{(n_+ p)(n_- k)}{\mu^2} \right]^{-\epsilon} \frac{1}{(n_+ p)}$$

$$\times \frac{g_\perp^{\eta\delta}}{2} \frac{e^{\epsilon\gamma_E}\Gamma[\epsilon]\Gamma[-\epsilon]\Gamma[1-\epsilon]}{\Gamma[2-2\epsilon]} \quad (A.64)$$

$$g_s^2 \int \frac{d^d q}{(2\pi)^d} \frac{q_\perp^2}{(p-k_+-q)^4} \frac{1}{(p-q)^2} \frac{1}{q^2} = \frac{i\alpha_s}{(4\pi)} \left[\frac{(n_+p)(n_-k)}{\mu^2}\right]^{-\epsilon} \frac{1}{(n_-k)(n_+p)}$$
$$\times \frac{e^{\epsilon\gamma_E}\Gamma[\epsilon]\Gamma[1-\epsilon]\Gamma[2-\epsilon]}{\Gamma[2-2\epsilon]} \quad (A.65)$$

$$g_s^2 \int \frac{d^d q}{(2\pi)^d} \frac{q_\perp^2 (n_-q)}{(p-k_+-q)^4} \frac{1}{(p-q)^2} \frac{1}{q^2} = -\frac{i\alpha_s}{(4\pi)} \left[\frac{(n_+p)(n_-k)}{\mu^2}\right]^{-\epsilon} \frac{1}{(n_+p)}$$
$$\times \frac{1}{2} \frac{e^{\epsilon\gamma_E}\Gamma[\epsilon]\Gamma[2-\epsilon]\Gamma[1-\epsilon]}{\Gamma[2-2\epsilon]} \quad (A.66)$$

$$g_s^2 \int \frac{d^d q}{(2\pi)^d} \frac{q_\perp^2}{(p-k_+-q)^2} \frac{1}{(p-q)^2} \frac{1}{q^2} = \frac{i\alpha_s}{(4\pi)} \left[\frac{(n_+p)(n_-k)}{\mu^2}\right]^{-\epsilon}$$
$$\times \frac{e^{\epsilon\gamma_E}\Gamma[1-\epsilon]\Gamma[1-\epsilon]\Gamma[\epsilon]}{2\Gamma[2-2\epsilon]} \quad (A.67)$$

$$g_s^2 \int \frac{d^d q}{(2\pi)^d} \frac{q_\perp^\alpha q_\perp^\eta}{(p-k_+-q)^2} \frac{1}{(p-q)^2} \frac{1}{q^2} = \frac{i\alpha_s}{(4\pi)} \left[\frac{(n_+p)(n_-k)}{\mu^2}\right]^{-\epsilon}$$
$$\times \frac{g_\perp^{\alpha\eta}}{2} \frac{e^{\epsilon\gamma_E}\Gamma[\epsilon]\Gamma[1-\epsilon]\Gamma[1-\epsilon]}{\Gamma[3-2\epsilon]} \quad (A.68)$$

$$g_s^2 \int \frac{d^d q}{(2\pi)^d} \frac{1}{(p-k_+-q)^2} \frac{1}{(p-q)^2} \frac{1}{q^2} = \frac{i\alpha_s}{(4\pi)} \left[\frac{(n_+p)(n_-k)}{\mu^2}\right]^{-\epsilon} \frac{1}{(n_-k)(n_+p)}$$
$$\times (1-2\epsilon) \frac{e^{\epsilon\gamma_E}\Gamma[\epsilon]\Gamma[-\epsilon]\Gamma[1-\epsilon]}{\Gamma[2-2\epsilon]} \quad (A.69)$$

$$g_s^2 \int \frac{d^d q}{(2\pi)^d} \frac{q_\perp^\alpha q_\perp^\eta}{(p-k_+-q)^4} \frac{1}{(p-q)^2} \frac{1}{q^2} = \frac{i\alpha_s}{(4\pi)} \left[\frac{(n_+p)(n_-k)}{\mu^2}\right]^{-\epsilon} \frac{1}{(n_+p)(n_-k)}$$
$$\times \frac{g_\perp^{\alpha\eta}}{2} \frac{e^{\epsilon\gamma_E}\Gamma[\epsilon]\Gamma[1-\epsilon]\Gamma[1-\epsilon]}{\Gamma[2-2\epsilon]} \quad (A.70)$$

$$g_s^2 \int \frac{d^d q}{(2\pi)^d} \frac{(n_+q)q_\perp^\alpha q_\perp^\eta}{(p-k_+-q)^4} \frac{1}{(p-q)^2} \frac{1}{q^2} = \frac{i\alpha_s}{(4\pi)} \left[\frac{(n_+p)(n_-k)}{\mu^2}\right]^{-\epsilon} \frac{1}{(n_-k)}$$
$$\times \frac{g_\perp^{\alpha\eta}}{2} (2-\epsilon) \frac{e^{\epsilon\gamma_E}\Gamma[\epsilon]\Gamma[1-\epsilon]\Gamma[1-\epsilon]}{\Gamma[3-2\epsilon]} \quad (A.71)$$

$$g_s^2 \int \frac{d^d q}{(2\pi)^d} q_\perp^2 q_\perp^\alpha q_\perp^\sigma \frac{1}{(p - k_+ - q)^6} \frac{1}{(p - q)^2} \frac{1}{q^2} = \frac{i\alpha_s}{(4\pi)} \left[\frac{(n_+ p)(n_- k)}{\mu^2} \right]^{-\epsilon} \frac{1}{(n_+ p)(n_- k)}$$
$$\times (2 - \epsilon) g_\perp^{\alpha\sigma} \frac{1}{8} \frac{e^{\epsilon\gamma_E} \Gamma[\epsilon] \Gamma[1 - \epsilon] \Gamma[1 - \epsilon]}{\Gamma[2 - 2\epsilon]} \quad \text{(A.72)}$$

$$g_s^2 \int \frac{d^d q}{(2\pi)^d} \frac{q_\perp^\sigma q_\perp^\delta q_\perp^2}{(p - k_+ - q)^4} \frac{1}{(p - q)^2} \frac{1}{(n_+(p - q))} \frac{1}{q^2} = \frac{i\alpha_s}{(4\pi)} \left[\frac{(n_+ p)(n_- k)}{\mu^2} \right]^{-\epsilon} \frac{1}{(n_+ p)}$$
$$\times \frac{(\epsilon - 2) g_\perp^{\sigma\delta}}{4\epsilon} \frac{e^{\epsilon\gamma_E} \Gamma[\epsilon] \Gamma[1 - \epsilon] \Gamma[1 - \epsilon]}{\Gamma[2 - 2\epsilon]} \quad \text{(A.73)}$$

$$g_s^2 \int \frac{d^d q}{(2\pi)^d} \frac{1}{(p - k_+ - q)^2} \frac{1}{(p - q)^2} \frac{1}{q^2} \frac{1}{(n_+ q)} = \frac{i\alpha_s}{(4\pi)} \left[\frac{(n_+ p)(n_- k)}{\mu^2} \right]^{-\epsilon} \frac{1}{(n_- k)(n_+ p)^2}$$
$$\times 2(1 - 2\epsilon) \frac{e^{\epsilon\gamma_E} \Gamma[\epsilon] \Gamma[-\epsilon] \Gamma[1 - \epsilon]}{\Gamma[2 - 2\epsilon]} \quad \text{(A.74)}$$

$$g_s^2 \int \frac{d^d q}{(2\pi)^d} \frac{(n_- q)}{(p - k_+ - q)^4} \frac{1}{(p - q)^2} \frac{1}{q^2} \frac{1}{(n_+ q)} = \frac{i\alpha_s}{(4\pi)} \left[\frac{(n_+ p)(n_- k)}{\mu^2} \right]^{-\epsilon} \frac{1}{(n_- k)(n_+ p)^3}$$
$$\times (-2)(1 - 2\epsilon) \frac{e^{\epsilon\gamma_E} \Gamma[\epsilon] \Gamma[1 - \epsilon] \Gamma[1 - \epsilon]}{\Gamma[2 - 2\epsilon]} \quad \text{(A.75)}$$

$$g_s^2 \int \frac{d^d q}{(2\pi)^d} \frac{1}{(p - k_+ - q)^4} \frac{1}{(p - q)^2} \frac{1}{q^2} \frac{1}{(n_+ q)} = -\frac{i\alpha_s}{(4\pi)} \left[\frac{(n_+ p)(n_- k)}{\mu^2} \right]^{-\epsilon} \frac{1}{(n_- k)^2 (n_+ p)^3}$$
$$\times 2(1 + 2\epsilon)(1 - 2\epsilon) \frac{e^{\epsilon\gamma_E} \Gamma[\epsilon] \Gamma[-\epsilon] \Gamma[1 - \epsilon]}{\Gamma[2 - 2\epsilon]} \quad \text{(A.76)}$$

$$g_s^2 \int \frac{d^d q}{(2\pi)^d} \frac{1}{(p - k_+ - q)^4} \frac{1}{(p - q)^2} \frac{1}{q^2} = \frac{i\alpha_s}{(4\pi)} \left[\frac{(n_+ p)(n_- k)}{\mu^2} \right]^{-\epsilon} \frac{1}{(n_- k)^2 (n_+ p)^2}$$
$$\times 2(1 - 2\epsilon) \frac{e^{\epsilon\gamma_E} \Gamma[\epsilon] \Gamma[1 - \epsilon]^2}{\Gamma[2 - 2\epsilon]} \quad \text{(A.77)}$$

$$g_s^2 \int \frac{d^d q}{(2\pi)^d} \frac{(n_+ q)}{(p - k_+ - q)^4} \frac{1}{(p - q)^2} \frac{1}{q^2} = \frac{i\alpha_s}{(4\pi)} \left[\frac{(n_+ p)(n_- k)}{\mu^2} \right]^{-\epsilon} \frac{1}{(n_- k)^2 (n_+ p)}$$
$$\times (1 - 2\epsilon)(1 - \epsilon) \frac{e^{\epsilon\gamma_E} \Gamma[\epsilon] \Gamma[-\epsilon] \Gamma[1 - \epsilon]}{\Gamma[2 - 2\epsilon]} \quad \text{(A.78)}$$

$$g_s^2 \int \frac{d^d q}{(2\pi)^d} \frac{(n_- q)}{(p - k_+ - q)^4} \frac{1}{(p - q)^2} \frac{1}{q^2} = \frac{i\alpha_s}{(4\pi)} \left[\frac{(n_+ p)(n_- k)}{\mu^2} \right]^{-\epsilon} \frac{1}{(n_+ p)^2 (n_- k)}$$

$$\times (1 - 2\epsilon) \frac{e^{\epsilon \gamma_E} \Gamma[1 + \epsilon] \Gamma[-\epsilon] \Gamma[1 - \epsilon]}{\Gamma[2 - 2\epsilon]} \qquad (A.79)$$

$$g_s^2 \int \frac{d^d q}{(2\pi)^d} \frac{(n_+ q)(n_- q)}{(p - k_+ - q)^4} \frac{1}{(p - q)^2} \frac{1}{q^2} = \frac{i\alpha_s}{(4\pi)} \left[\frac{(n_+ p)(n_- k)}{\mu^2} \right]^{-\epsilon} \frac{1}{(n_- k)(n_+ p)}$$
$$\times (1 - \epsilon) \frac{e^{\epsilon \gamma_E} \Gamma[1 + \epsilon] \Gamma[-\epsilon] \Gamma[1 - \epsilon]}{\Gamma[2 - 2\epsilon]} \qquad (A.80)$$

$$g_s^2 \int \frac{d^d q}{(2\pi)^d} \frac{1}{(n_+ q)} \frac{1}{(p - k_+ - q)^2} \frac{(n_+(p - q))^2}{(p - q)^2} \frac{1}{q^2} = \frac{i\alpha_s}{(4\pi)} \left[\frac{(n_+ p)(n_- k)}{\mu^2} \right]^{-\epsilon} \frac{1}{(n_- k)}$$
$$\times \frac{(-1 + \epsilon)}{\epsilon} \frac{e^{\epsilon \gamma_E} \Gamma[\epsilon] \Gamma[1 - \epsilon]^2}{\Gamma[2 - 2\epsilon]} \qquad (A.81)$$

$$g_s^2 \int \frac{d^d q}{(2\pi)^d} \frac{(n_+(p - q))}{(q - k_+)^2} \frac{q_\perp^2}{(n_+ q)^2} \frac{1}{(p - q)^2} \frac{1}{q^2} = \frac{i\alpha_s}{(4\pi)} \left[\frac{(n_+ p)(n_- k)}{\mu^2} \right]^{-\epsilon} \frac{1}{(n_+ p)}$$
$$\times \frac{1}{\epsilon(1 + \epsilon)} \frac{e^{\epsilon \gamma_E} \Gamma[\epsilon] \Gamma[1 - \epsilon] \Gamma[3 - \epsilon]}{\Gamma[2 - 2\epsilon]} \qquad (A.82)$$

$$g_s^2 \int \frac{d^d q}{(2\pi)^d} \frac{(n_-(q - k))}{(q - k_+)^4} \frac{q_\perp^2}{(n_+ q)} \frac{(n_+(p - q))}{(p - q)^2} \frac{1}{q^2} = \frac{i\alpha_s}{(4\pi)} \left[\frac{(n_+ p)(n_- k)}{\mu^2} \right]^{-\epsilon} \frac{1}{(n_+ p)}$$
$$\times \frac{(1 - \epsilon)}{2(\epsilon + 1)} \frac{e^{\epsilon \gamma_E} \Gamma[\epsilon] \Gamma[3 - \epsilon] \Gamma[-\epsilon]}{\Gamma[2 - 2\epsilon]} \qquad (A.83)$$

$$g_s^2 \int \frac{d^d q}{(2\pi)^d} \frac{(n_-(q - k))}{(q - k_+)^4} \frac{q_\perp^2}{(p - q)^2} \frac{1}{q^2} = -\frac{i\alpha_s}{(4\pi)} \left[\frac{(n_+ p)(n_- k)}{\mu^2} \right]^{-\epsilon} \frac{1}{(n_+ p)}$$
$$\times \frac{1}{2} \frac{e^{\epsilon \gamma_E} \Gamma[\epsilon] \Gamma[2 - \epsilon] \Gamma[1 - \epsilon]}{\Gamma[2 - 2\epsilon]} \qquad (A.84)$$

$$g_s^2 \int \frac{d^d q}{(2\pi)^d} \frac{(n_-(q - k))}{(q - k_+)^4} \frac{q_\perp^2}{(n_+(p - q))} \frac{(n_+ q)}{(p - q)^2} \frac{1}{q^2} = \frac{i\alpha_s}{(4\pi)} \left[\frac{(n_+ p)(n_- k)}{\mu^2} \right]^{-\epsilon} \frac{1}{(n_+ p)}$$
$$\times \frac{(1 + \epsilon)}{2} \frac{e^{\epsilon \gamma_E} \Gamma[\epsilon] \Gamma[1 - \epsilon]^2}{\Gamma[2 - 2\epsilon]} \qquad (A.85)$$

$$g_s^2 \int \frac{d^d q}{(2\pi)^d} \frac{q_\perp^2}{(n_+(p - q))} \frac{1}{(q - k_+)^2} \frac{1}{(p - q)^2} \frac{1}{q^2} = \frac{i\alpha_s}{(4\pi)} \left[\frac{(n_+ p)(n_- k)}{\mu^2} \right]^{-\epsilon} \frac{1}{(n_+ p)}$$
$$\times \frac{e^{\epsilon \gamma_E} \Gamma[\epsilon] \Gamma[1 - \epsilon]^2}{\Gamma[2 - 2\epsilon]} \qquad (A.86)$$

$$g_s^2 \int \frac{d^d q}{(2\pi)^d} \frac{1}{(q-k_+)^4} \frac{1}{(p-q)^2} \frac{1}{q^2} q_\perp^\lambda q_\perp^\eta = \frac{i\alpha_s}{(4\pi)} \left[\frac{(n_-k)(n_+p)}{\mu^2} \right]^{-\epsilon} \frac{1}{(n_-k)(n_+p)}$$
$$\times \frac{g_\perp^{\lambda\eta}}{2} \frac{e^{\epsilon\gamma_E} \Gamma[\epsilon] \Gamma[1-\epsilon]^2}{\Gamma[2-2\epsilon]} \quad\quad (A.87)$$

$$g_s^2 \int \frac{d^d q}{(2\pi)^d} \frac{1}{(q-k_+)^4} \frac{1}{(p-q)^2} \frac{1}{q^2} \frac{q_\perp^\lambda q_\perp^\eta}{(n_+q)} = \frac{i\alpha_s}{(4\pi)} \left[\frac{(n_-k)(n_+p)}{\mu^2} \right]^{-\epsilon} \frac{1}{(n_-k)(n_+p)^2}$$
$$\times \frac{g_\perp^{\lambda\eta}}{2} \frac{1}{(1+\epsilon)} \frac{e^{\epsilon\gamma_E} \Gamma[1+\epsilon] \Gamma[-\epsilon] \Gamma[1-\epsilon]}{\Gamma[1-2\epsilon]} \quad (A.88)$$

$$g_s^2 \int \frac{d^d q}{(2\pi)^d} \frac{1}{(q-k_+)^2} \frac{1}{(p-q)^2} \frac{1}{q^2} q_\perp^2 \frac{1}{(n_+q)} = \frac{i\alpha_s}{(4\pi)} \left[\frac{(n_-k)(n_+p)}{\mu^2} \right]^{-\epsilon} \frac{1}{(n_+p)}$$
$$\times \frac{e^{\epsilon\gamma_E} \Gamma[\epsilon] \Gamma[-\epsilon] \Gamma[2-\epsilon]}{\Gamma[2-2\epsilon]} \quad\quad (A.89)$$

$$g_s^2 \int \frac{d^d q}{(2\pi)^d} \frac{1}{(q-k_+)^2} \frac{1}{(p-q)^2} \frac{1}{q^2} \frac{q_\perp^2 (n_+q)}{(n_+(p-q))} = \frac{i\alpha_s}{(4\pi)} \left[\frac{(n_+p)(n_-k)}{\mu^2} \right]^{-\epsilon}$$
$$\times \frac{1}{2} \frac{e^{\epsilon\gamma_E} \Gamma[\epsilon] \Gamma[1-\epsilon]^2}{\Gamma[2-2\epsilon]} \quad\quad (A.90)$$

$$g_s^2 \int \frac{d^d q}{(2\pi)^d} \frac{1}{(q-k_+)^4} \frac{1}{(p-q)^2} \frac{1}{q^2} \frac{q_\perp^2 (n_+q)}{(n_+(p-q))} = -\frac{i\alpha_s e^{\epsilon\gamma_E}}{(4\pi)} \left[\frac{(n_+p)(n_-k)}{\mu^2} \right]^{-\epsilon} \frac{1}{(n_+p)(n_-k)}$$
$$\times \frac{\Gamma[1+\epsilon] \Gamma[1-\epsilon]^2}{\Gamma[2-2\epsilon]} \quad\quad (A.91)$$

$$g_s^2 \int \frac{d^d q}{(2\pi)^d} \frac{1}{(q-k_+)^6} \frac{q_\perp^\alpha q_\perp^\lambda q_\perp^2}{(p-q)^2} \frac{1}{q^2} \frac{1}{(n_+q)} = \frac{i\alpha_s}{(4\pi)} \left[\frac{(n_-k)(n_+p)}{\mu^2} \right]^{-\epsilon} \frac{1}{(n_-k)(n_+p)^2}$$
$$\times \frac{(2-\epsilon) g_\perp^{\alpha\lambda}}{4(1+\epsilon)} \frac{e^{\epsilon\gamma_E} \Gamma[1+\epsilon] \Gamma[-\epsilon] \Gamma[2-\epsilon]}{\Gamma[2-2\epsilon]} \quad (A.92)$$

$$g_s^2 \int \frac{d^d q}{(2\pi)^d} \frac{1}{(q-k_+)^2} \frac{1}{(n_+q)} (n_+(p-q)) \frac{1}{(p-q)^2} = \frac{i\alpha_s}{(4\pi)} \left[\frac{(n_+p)(n_-k)}{\mu^2} \right]^{-\epsilon}$$
$$\times \frac{e^{\epsilon\gamma_E} \Gamma[\epsilon] \Gamma[-\epsilon] \Gamma[2-\epsilon]}{\Gamma[2-2\epsilon]} \quad\quad (A.93)$$

$$g_s^2 \int \frac{d^d q}{(2\pi)^d} \frac{1}{(q-k_+)^2} (n_+(p-q)) \frac{1}{(p-q)^2} \frac{1}{q^2} = \frac{i\alpha_s}{(4\pi)} \left[\frac{(n_+p)(n_-k)}{\mu^2} \right]^{-\epsilon} \frac{1}{(n_-k)}$$

$$\times \frac{e^{\epsilon\gamma_E}\Gamma[\epsilon]\Gamma[-\epsilon]\Gamma[2-\epsilon]}{\Gamma[2-2\epsilon]} \qquad (A.94)$$

$$g_s^2 \int \frac{d^dq}{(2\pi)^d} \frac{(n_-(q-k))}{(q-k_+)^2}(n_+(p-q))\frac{1}{(p-q)^2}\frac{1}{q^2} = -\frac{i\alpha_s}{(4\pi)}\left[\frac{(n_+p)(n_-k)}{\mu^2}\right]^{-\epsilon}$$
$$\times \frac{1}{2}(2-\epsilon)\frac{e^{\epsilon\gamma_E}\Gamma[\epsilon]\Gamma[1-\epsilon]\Gamma[-\epsilon]}{\Gamma[2-2\epsilon]} \qquad (A.95)$$

$$g_s^2 \int \frac{d^dq}{(2\pi)^d} \frac{1}{(q-k_+)^2}\frac{q_\perp^\eta q_\perp^\lambda}{(n_+q)}\frac{1}{(p-q)^2}\frac{1}{q^2} = \frac{i\alpha_s}{(4\pi)}\left[\frac{(n_-k)(n_+p)}{\mu^2}\right]^{-\epsilon}\frac{1}{(n_+p)}$$
$$\times \frac{g_\perp^{\lambda\eta}}{2}\frac{e^{\epsilon\gamma_E}\Gamma[\epsilon]\Gamma[-\epsilon]\Gamma[1-\epsilon]}{\Gamma[2-2\epsilon]} \qquad (A.96)$$

$$g_s^2 \int \frac{d^dq}{(2\pi)^d} \frac{1}{(q-k_+)^2}q_\perp^\eta q_\perp^\lambda\frac{1}{(p-q)^2}\frac{1}{q^2} = \frac{i\alpha_s}{(4\pi)}\left[\frac{(n_-k)(n_+p)}{\mu^2}\right]^{-\epsilon}$$
$$\times \frac{g_\perp^{\lambda\eta}}{2}\frac{e^{\epsilon\gamma_E}\Gamma[\epsilon]\Gamma[1-\epsilon]^2}{\Gamma[3-2\epsilon]} \qquad (A.97)$$

$$g_s^2 \int \frac{d^dq}{(2\pi)^d} \frac{1}{(q-k_+)^4}\frac{q_\perp^\kappa q_\perp^\lambda(n_-q)}{(n_+q)}\frac{1}{(p-q)^2}\frac{1}{q^2} = \frac{i\alpha_s}{(4\pi)}\left[\frac{(n_-k)(n_+p)}{\mu^2}\right]^{-\epsilon}\frac{1}{(n_+p)^2}$$
$$\times \frac{g_\perp^{\kappa\lambda}}{2}\frac{e^{\epsilon\gamma_E}\Gamma[\epsilon]\Gamma[-\epsilon]\Gamma[2-\epsilon]}{\Gamma[2-2\epsilon]} \qquad (A.98)$$

$$g_s^2 \int \frac{d^dq}{(2\pi)^d} \frac{(n_-q)q_\perp^\kappa q_\perp^\lambda}{(q-k_+)^4}\frac{1}{(p-q)^2}\frac{1}{q^2} = \frac{i\alpha_s}{(4\pi)}\left[\frac{(n_-k)(n_+p)}{\mu^2}\right]^{-\epsilon}\frac{1}{(n_+p)}$$
$$\times \frac{g_\perp^{\kappa\lambda}}{4}\frac{e^{\epsilon\gamma_E}\Gamma[\epsilon]\Gamma[1-\epsilon]^2}{\Gamma[2-2\epsilon]} \qquad (A.99)$$

$$g_s^2 \int \frac{d^dq}{(2\pi)^d} \frac{1}{(q-k_+)^4}\frac{1}{(n_+(p-q))}q_\perp^\kappa q_\perp^\lambda q_\perp^2\frac{1}{(p-q)^2}\frac{1}{q^2} = \frac{i\alpha_s}{(4\pi)}\left[\frac{(n_+p)(n_-k)}{\mu^2}\right]^{-\epsilon}\frac{1}{(n_+p)}$$
$$\times \frac{g_\perp^{\kappa\lambda}}{4}\frac{e^{\epsilon\gamma_E}\Gamma[\epsilon]\Gamma[1-\epsilon]^2}{\Gamma[2-2\epsilon]} \qquad (A.100)$$

$$g_s^2 \int \frac{d^dq}{(2\pi)^d} \frac{(n_+(p-q))}{(p-q)^2}\frac{1}{q^2}\frac{1}{(q-k_+)^2}\frac{1}{n_+q} = -\frac{i\alpha_s}{(4\pi)}\left[\frac{(n_+p)(n_-k)}{\mu^2}\right]^{-\epsilon}\frac{1}{(n_-k)(n_+p)}$$
$$\times \frac{(1-\epsilon)(1-2\epsilon)}{(1+\epsilon)}\frac{e^{\epsilon\gamma_E}\Gamma[\epsilon]\Gamma[-\epsilon]\Gamma[1-\epsilon]}{\Gamma[2-2\epsilon]} \qquad (A.101)$$

$$g_s^2 \int \frac{d^dq}{(2\pi)^d} \frac{(n_+(p-q))}{(p-q)^2} \frac{1}{q^2} q_\perp^2 \frac{1}{(q-k_+)^2} \frac{1}{n_+q} = -\frac{i\alpha_s}{(4\pi)} \left[\frac{(n_+p)(n_-k)}{\mu^2} \right]^{-\epsilon}$$
$$\times \frac{(2-\epsilon)}{2\epsilon} \frac{e^{\epsilon\gamma_E}\Gamma[\epsilon]\Gamma[1-\epsilon]^2}{\Gamma[2-2\epsilon]} \quad \text{(A.102)}$$

$$g_s^2 \int \frac{d^dq}{(2\pi)^d} \frac{(n_+(p-q))}{(p-q)^2} \frac{1}{q^2} q_\perp^2 \frac{1}{(q-k_+)^4} \frac{1}{n_+q} = -\frac{i\alpha_s}{(4\pi)} \left[\frac{(n_+p)(n_-k)}{\mu^2} \right]^{-\epsilon} \frac{1}{(n_-k)(n_+p)}$$
$$\times \frac{(2-\epsilon)(1-\epsilon)}{(1+\epsilon)} \frac{e^{\epsilon\gamma_E}\Gamma[\epsilon]\Gamma[1-\epsilon]^2}{\Gamma[2-2\epsilon]} \quad \text{(A.103)}$$

$$g_s^2 \int \frac{d^dq}{(2\pi)^d} \frac{(n_+(p-q))}{(p-q)^2} \frac{1}{q^2} \frac{q_\perp^\lambda q_\perp^\eta}{(q-k_+)^4} \frac{1}{n_+q} = -\frac{i\alpha_s}{(4\pi)} \left[\frac{(n_+p)(n_-k)}{\mu^2} \right]^{-\epsilon} \frac{1}{(n_-k)(n_+p)}$$
$$\times \frac{(2-\epsilon)g_\perp^{\eta\lambda}}{2(1+\epsilon)} \frac{e^{\epsilon\gamma_E}\Gamma[\epsilon]\Gamma[1-\epsilon]^2}{\Gamma[2-2\epsilon]} \quad \text{(A.104)}$$

$$g_s^2 \int \frac{d^dq}{(2\pi)^d} \frac{(n_+(p-q))}{(p-q)^2} \frac{1}{q^2} \frac{q_\perp^2 q_\perp^\eta q_\perp^\lambda}{(q-k_+)^6} \frac{1}{n_+q} = -\frac{i\alpha_s}{(4\pi)} \left[\frac{(n_+p)(n_-k)}{\mu^2} \right]^{-\epsilon} \frac{1}{(n_-k)(n_+p)}$$
$$\times \frac{g_\perp^{\eta\lambda}(3-\epsilon)(2-\epsilon)}{8(1+\epsilon)} \frac{e^{\epsilon\gamma_E}\Gamma[\epsilon]\Gamma[1-\epsilon]^2}{\Gamma[2-2\epsilon]} \quad \text{(A.105)}$$

$$g_s^2 \int \frac{d^dq}{(2\pi)^d} \frac{1}{(p-q)^2} \frac{1}{q^2} \frac{q_\perp^2 q_\perp^\eta q_\perp^\lambda}{(q-k_+)^6} = \frac{i\alpha_s}{(4\pi)} \left[\frac{(n_+p)(n_-k)}{\mu^2} \right]^{-\epsilon} \frac{1}{(n_-k)(n_+p)}$$
$$\times \frac{(2-\epsilon)g_\perp^{\eta\lambda}}{8} \frac{e^{\epsilon\gamma_E}\Gamma[\epsilon]\Gamma[1-\epsilon]^2}{\Gamma[2-2\epsilon]} \quad \text{(A.106)}$$

$$g_s^2 \int \frac{d^dq}{(2\pi)^d} \frac{1}{(q-k_+)^4} \frac{1}{(p-q)^2} \frac{1}{q^2}(n_+q)q_\perp^2 = -\frac{i\alpha_s}{(4\pi)} \left[\frac{(n_-k)(n_+p)}{\mu^2} \right]^{-\epsilon} \frac{1}{(n_-k)}$$
$$\times \frac{\epsilon}{2} \frac{e^{\epsilon\gamma_E}\Gamma[\epsilon]\Gamma[1-\epsilon]^2}{\Gamma[2-2\epsilon]} \quad \text{(A.107)}$$

$$g_s^2 \int \frac{d^dq}{(2\pi)^d} \frac{1}{(q-k_+)^4} \frac{1}{(p-q)^2} \frac{1}{q^2}(n_+q)q_\perp^\alpha q_\perp^\eta = -\frac{i\alpha_s}{(4\pi)} \left[\frac{(n_-k)(n_+p)}{\mu^2} \right]^{-\epsilon} \frac{1}{(n_-k)}$$
$$\times \frac{\epsilon\, g_\perp^{\alpha\eta}}{4(1-\epsilon)} \frac{e^{\epsilon\gamma_E}\Gamma[\epsilon]\Gamma[1-\epsilon]^2}{\Gamma[2-2\epsilon]} \quad \text{(A.108)}$$

$$g_s^2 \int \frac{d^dq}{(2\pi)^d} \frac{1}{(n_+q)} \frac{q_\perp^\alpha q_\perp^\sigma}{(p-k_+-q)^6} \frac{(n_+(p-q))^2}{(p-q)^2} \frac{1}{q^2} = \frac{i\alpha_s}{(4\pi)} \left[\frac{(n_+p)(n_-k)}{\mu^2} \right]^{-\epsilon} \frac{1}{(n_-k)^2(n_+p)}$$
$$\times \frac{\epsilon(1+\epsilon)g_\perp^{\alpha\sigma}}{4(1-\epsilon)} \frac{e^{\epsilon\gamma_E}\Gamma[\epsilon]\Gamma[1-\epsilon]^2}{\Gamma[2-2\epsilon]} \quad \text{(A.109)}$$

B

B.1   Drell-Yan: LP collinear-loop diagram calculation

In the main text, in equations (3.15) – (3.20), we have provided results for the calculation of the leading power amplitude with one collinear loop and one soft real emission. The relevant diagrams are presented in figure 3.5.

Here we calculate the first representative diagram as an example. This is a standard leading power computation with eikonal vertices included here for completeness. The incoming collinear momentum is on-shell and carries only the large component, $p^\mu = (n_+p)\frac{n_-^\mu}{2}$.

The amplitude for diagram a in figure 3.5 is given by

$$
\mathcal{M}_a^{\text{LP}} = \bar{v}_{\bar{c}}(l)i\gamma_\perp^\rho \frac{i(n_+p_1)}{p_1^2}\frac{\slashed{n}_-}{2}\int \frac{d^dq}{(2\pi)^d}\, ig_s\mathbf{T}^A C_\mu(p_1, p_1-q)\frac{\slashed{n}_+}{2}\frac{i(n_+(p_1-q))}{(p_1-q)^2}\frac{\slashed{n}_-}{2}
$$

$$
\times ig_s\mathbf{T}^A C^\mu(p_1-q, p_1)\frac{\slashed{n}_+}{2}\frac{i(n_+p_1)}{p_1^2}\frac{\slashed{n}_-}{2}\, ig_s\mathbf{T}^B\frac{\slashed{n}_+}{2}n_{-\nu}\frac{-i}{q^2}\, u_c(p) \qquad \text{(B.1)}
$$

Momentum conservation at the soft-collinear vertex can be imposed immediately. Hence $p_1^\mu = p^\mu - k_+^\mu$ is set and yields

$$
C^\mu(p_1, p_1-q) = C^\mu(p-k_+, p-k_+-q) = n_-^\mu - \gamma_\perp^\mu \frac{\slashed{q}_\perp}{(n_+(p-q))} \qquad \text{(B.2)}
$$

since k_+^μ and p^μ do not have perpendicular to direction of motion components. Similarly

$$
C^\mu(p_1-q, p_1) = C^\mu(p-k_+-q, p-k_+) = n_-^\mu - \frac{\slashed{q}_\perp}{(n_+(p-q))}\gamma_\perp^\mu \qquad \text{(B.3)}
$$

Substituting these into the expression, using Feynman parametrisation, completing the square in the denominator, and shifting the integration momentum $q \to l$ gives

$$
\mathcal{M}_a^{\text{LP}} = -\bar{v}_{\bar{c}}g_s^3\gamma_\perp^\rho C_F\mathbf{T}^B\frac{2n_{-\nu}}{(n_-k)^2}\int \frac{d^dl}{(2\pi)^d}\int_0^\infty dx_1 dx_2 \frac{\gamma_{\mu\perp}\slashed{l}_\perp\slashed{l}_\perp\gamma_\perp^\mu}{(1+x_1)^3}\left\{l^2 - M^2\right\}^{-3}u_c, \quad \text{(B.4)}
$$

where $M^2 = \left[\frac{x_1(n_+p)(n_-k)}{(1+x_1)^2} - \frac{x_2(n_+p)}{(1+x_1)^2}\right]$. We can perform the integral in (B.4) directly using result (A.12). Then substituting again for M^2, simplifying the expression and rescaling

the integration variables gives

$$
\begin{aligned}
\mathcal{M}_a^{\mathrm{LP}} &= 2n_{-\nu}\bar{v}_{\bar{c}}(l)\frac{ig_s\alpha_s}{4\pi}\gamma_\perp^\rho\frac{C_F\mathbf{T}^B e^{\epsilon\gamma_E}}{(n_-k)}\left[\frac{(n_+p)(n_-k)}{\mu^2}\right]^{-\epsilon}\Gamma[\epsilon](1-\epsilon)^2 \\
&\quad \times \int_0^\infty dx_1 \int_0^\infty dx_2 \frac{x_1^{1-\epsilon}}{(1+x_1)^{3-2\epsilon}}\left(1+x_2\right)^{-\epsilon}u_c(p).
\end{aligned}
\tag{B.5}
$$

Using (A.3) we obtain

$$
\mathcal{M}_a^{\mathrm{LP}} = -\bar{v}_{\bar{c}}(l)i\gamma_\perp^\rho\frac{\alpha_s}{4\pi}g_s\mathbf{T}^B C_F\frac{n_{-\nu}}{(n_-k)}\left[\frac{(n_+p)(n_-k)}{\mu^2}\right]^{-\epsilon}\frac{(1-\epsilon)}{\epsilon}\mathfrak{f}[\epsilon]u_c(p),
\tag{B.6}
$$

where, as defined in the main text in (3.21),

$$
\mathfrak{f}[\epsilon] \equiv \frac{e^{\epsilon\gamma_E}\Gamma[1+\epsilon]\Gamma[1-\epsilon]^2}{\Gamma[2-2\epsilon]}.
\tag{B.7}
$$

B.2 Drell-Yan: NLP amplitude results

In the main body of the text we focused on the factorisation formula at the cross-section level. As a by-product of the computation of the collinear functions, which are amplitude-level objects, we also calculated the power-suppressed one-loop one-soft emission DY amplitude, which we summarise here. The results below, computed directly in SCET, are in agreement with results obtained by applying the expansion-by-regions method to the same quantity [150].

We consider the following operator, which is the right-hand side of (3.47) without the soft current J_s:

$$
\sum_{m_1,m_2} \int \{dt_k\}\{d\bar{t}_{\bar{k}}\}\,\widetilde{C}^{m_1,m_2}\left(\{t_k\},\{\bar{t}_{\bar{k}}\}\right) J_\rho^{m_1,m_2}\left(\{t_k\},\{\bar{t}_{\bar{k}}\}\right)
\tag{B.8}
$$

where

$$
J_\rho^{m_1,m_2}\left(\{t_k\},\{\bar{t}_{\bar{k}}\}\right) = J_{\bar{c}}^{m_1}(\{\bar{t}_{\bar{k}}\})\,\Gamma_\rho^{m_1,m_2}\,J_c^{m_2}\left(\{t_k\}\right)
\tag{B.9}
$$

as in (3.48). The variables appearing in this expression are defined in section 3.2.1, and the sum is performed over the different power-suppressed currents in the N-jet SCET operator matched to the QCD current.

Below we focus solely on the case in which the power suppression is in the collinear sector, thereby setting $m_1 = A0$, and allow for structures which give power-suppression up to $\mathcal{O}(\lambda^2)$ (NLP). Specifically, we consider the time-ordered product of $J_\rho^{m_1,m_2}$ with subleading-power Lagrangian insertions between an emitted soft gluon $\langle g^K(k)|$, and an incoming collinear quark and anticollinear antiquark, $|q(p)\,\bar{q}(l)\rangle$. This defines the amplitude

$$
\mathcal{M}_\rho^K = \langle g^K(k)|\sum_m \int \{dt_k\}\,d\bar{t}\,\widetilde{C}^{A0,m}\left(\{t_k\},\bar{t}\right)\,J_\rho^{A0,m}\left(\{t_k\},\bar{t}\right)|q(p)\,\bar{q}(l)\rangle,
\tag{B.10}
$$
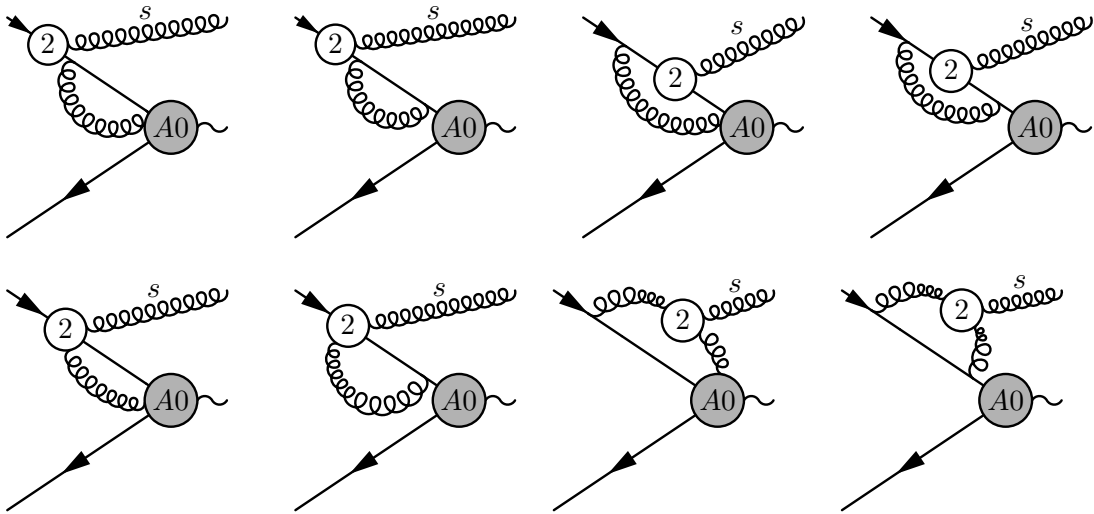
Figure B.1: *One-loop collinear diagrams with one soft gluon emission. Only the LP current, A0, is used here. Power suppression is provided by the time-ordered product insertion of $\mathcal{L}^{(2)}$ Lagrangian terms. The collinear gluon in the loop attaches either to the collinear quark or the collinear Wilson line of the χ_c field, which is a part of the A0 current. Note the difference in the drawing of the diagrams in those in figure 4.3: here we included the anticollinear leg and hard current.*

that we calculate at the one-loop order. Concretely, we consider only the time-ordered products of the collinear operator part $J_c^{m_2}$ in (B.9) with subleading-power soft-collinear (not: soft-anticollinear) Lagrangian insertions. The complete result for the amplitude is obtained by subtracting from the contributions given below the corresponding ones with n_+ and n_- interchanged.

In the following sections we present the different contributions to this object. Partial results found when the virtual loop is collinear (soft) carry a subscript c (s), $\mathcal{M}_c$ ($\mathcal{M}_s$). The NLO contributions from the one-loop hard matching coefficient are marked with h, $\mathcal{M}_h$. Moreover, we further split the results according to the polarisation of the off-shell DY photon γ^* produced by the vector current, that is, we separate the amplitude into the terms proportional to $\gamma_{\perp\rho}$, $n_{+\rho}$, and $n_{-\rho}$. Notice that the $\gamma_{\perp\rho}$ structure appears due to the leading power current in (3.11), while $n_{\pm\rho}$ terms arise from the power-suppressed $A1$ and $B1$ currents in (3.62) and (3.63), respectively.

B.2.1 Collinear loop: $\gamma_{\perp\rho}$

We begin with the results for the set of diagrams in which the virtual loop has collinear momentum scaling and the virtual photon created by the vector current has a transverse ρ index. In (B.10) this means taking the LP current, and index m spans over time-ordered product insertions of the $\mathcal{L}^{(2)}$ Lagrangian. The equations below are in fact related to the results presented in (4.83) and originate from the calculation of the diagrams shown in figure B.1.

We separate the resulting expression into the amplitude with colour factor C_F and C_A. The former receives contributions from the diagrams in the top line of figure B.1, the latter from those in the bottom line and the non-abelian part of the last two diagrams in

the top line. We find

$$
\begin{aligned}
\mathcal{M}_{c,C_F}^{\gamma_\perp \rho K} &= \bar{v}_{\bar{c}}(l)\gamma_\perp^\rho \frac{ig_s\alpha_s}{4\pi}\left[\frac{(n_+p)(n_-k)}{\mu^2}\right]^{-\epsilon}\frac{C_F\mathbf{T}^K}{(n_+p)(n_-k)}\frac{e^{\epsilon\gamma_E}\Gamma[1+\epsilon]\Gamma[1-\epsilon]^2}{(1+\epsilon)(1-\epsilon)\Gamma[2-2\epsilon]} \\
&\times \left\{(n_+k)n_{-\nu}\left(\frac{3}{\epsilon}-4-7\epsilon\right)+[\not{k}_\perp,\gamma_{\perp\nu}]\frac{1}{2}\left(1-\epsilon^2\right)\right. \tag{B.11} \\
&\left. + k_{\perp\nu}\left(\frac{2}{\epsilon}-5-6\epsilon+\epsilon^2\right)+(n_-k)n_{+\nu}\left(-\frac{1}{\epsilon}-1+\epsilon+\epsilon^2\right)\right\}u_c(p)\epsilon^{*\nu}(k)\,,
\end{aligned}
$$

$$
\begin{aligned}
\mathcal{M}_{c,C_A}^{\gamma_\perp \rho K} &= \bar{v}_{\bar{c}}(l)\gamma_\perp^\rho \frac{ig_s\alpha_s}{4\pi}\left[\frac{(n_+p)(n_-k)}{\mu^2}\right]^{-\epsilon}\frac{C_A\mathbf{T}^K}{(n_+p)(n_-k)}\frac{e^{\epsilon\gamma_E}\Gamma[1+\epsilon]\Gamma[1-\epsilon]^2}{(1+\epsilon)(1-\epsilon)\Gamma[2-2\epsilon]} \\
&\times \left\{(n_+k)n_{-\nu}\frac{1}{2}\left(-\frac{1}{\epsilon^2}-\frac{1}{\epsilon}-2+11\epsilon+\epsilon^2\right)+[\not{k}_\perp,\gamma_{\perp\nu}]\frac{1}{2}\left(-1+\epsilon^2\right)\right. \tag{B.12} \\
&\left. + k_{\perp\nu}\left(-\frac{1}{\epsilon^2}-\frac{1}{\epsilon}+3+3\epsilon\right)+(n_-k)n_{+\nu}\frac{1}{2}\left(-\frac{1}{\epsilon^2}-\frac{1}{\epsilon}+8-5\epsilon-\epsilon^2\right)\right\}u_c(p)\epsilon^{*\nu}(k)\,.
\end{aligned}
$$

In this appendix, we use the on-shell condition $k^2=0$ to rewrite $k_\perp^2=-(n_-k)(n_+k)$, but we do not impose the transversality relation (4.14). Notice that in (B.12) there are still $1/\epsilon^2$ poles. These only cancel once soft structures are combined as described in the main text.

For completeness, we now give the individual contributions due to Lagrangian insertions which make up the results in the above two equations. The on-shell condition and the trasversality relation have *not* been used to obtain these

$$
\begin{aligned}
\mathcal{M}_{c,J^{A0}\mathcal{L}_{1\xi}^{(2)}}^{\rho K} &= \bar{v}_{\bar{c}}(l)\,\gamma_\perp^\rho\frac{ig_s\alpha_s}{4\pi}\left(\frac{(n_+p)(n_-k)}{\mu^2}\right)^{-\epsilon}\frac{\mathbf{T}^K}{(n_+p)}\left(C_F\left(-\frac{2}{\epsilon}-2\right)+C_A\left(-\frac{3}{\epsilon}+6-\epsilon\right)\right) \\
&\times \frac{e^{\epsilon\gamma_E}\Gamma[1+\epsilon]\,\Gamma[1-\epsilon]^2}{2\Gamma[2-2\epsilon]}\left(n_+^\nu-n_-^\nu\frac{(n_+k)}{(n_-k)}\right)u_c(p)\epsilon_\nu^*(k)\,, \tag{B.13}
\end{aligned}
$$

$$
\begin{aligned}
\mathcal{M}_{c,J^{A0}\mathcal{L}_{2\xi}^{(2)}}^{\rho K} &= \bar{v}_{\bar{c}}(l)\,\gamma_\perp^\rho\frac{ig_s\alpha_s}{4\pi}\left(\frac{(n_+p)(n_-k)}{\mu^2}\right)^{-\epsilon}\frac{\mathbf{T}^K}{(n_+p)}\frac{e^{\epsilon\gamma_E}\Gamma[1+\epsilon]\Gamma[1-\epsilon]^2}{2(1-\epsilon)\Gamma[2-2\epsilon]} \tag{B.14} \\
&\times \left(C_F\left(\frac{4}{\epsilon}-14+2\epsilon\right)+C_A\left(-\frac{4}{\epsilon^2}+\frac{3}{\epsilon}+10-6\epsilon+\epsilon^2\right)\right)\left(\frac{k_\perp^\nu}{(n_-k)}-\frac{k_\perp^2 n_-^\nu}{(n_-k)^2}\right)u_c(p)\epsilon_\nu^*(k)\,,
\end{aligned}
$$

$$
\begin{aligned}
\mathcal{M}_{c,J^{A0}\mathcal{L}_{1YM}^{(2)}}^{\rho K} &= \bar{v}_{\bar{c}}(l)\,\gamma_\perp^\rho\frac{ig_s\alpha_s}{4\pi}\left(\frac{(n_+p)(n_-k)}{\mu^2}\right)^{-\epsilon}\frac{\mathbf{T}^K}{(n_+p)}C_A\left(-\frac{2}{\epsilon}+5-4\epsilon+\epsilon^2\right) \\
&\times \frac{e^{\epsilon\gamma_E}\Gamma[1+\epsilon]\Gamma[1-\epsilon]^2}{2(1+\epsilon)\Gamma[2-2\epsilon]}\left(n_+^\nu-\frac{(n_+k)}{(n_-k)}n_-^\nu\right)u_c(p)\epsilon_\nu^*(k)\,, \quad \text{(B.15)}
\end{aligned}
$$

$$
\mathcal{M}_{c,J^{A0}\mathcal{L}_{2YM}^{(2)}}^{\rho K} = \bar{v}_{\bar{c}}(l)\,\gamma_\perp^\rho\frac{ig_s\alpha_s}{4\pi}\left(\frac{(n_+p)(n_-k)}{\mu^2}\right)^{-\epsilon}\frac{\mathbf{T}^K}{(n_+p)}C_A\left(\frac{4}{\epsilon^2}-\frac{5}{\epsilon}-2-4\epsilon+\epsilon^2\right)
$$

$$\times \frac{e^{\epsilon\gamma_E}\Gamma[1+\epsilon]\Gamma[1-\epsilon]^2}{2(1+\epsilon)\Gamma[2-2\epsilon]} \left(\frac{k_{\perp\nu}}{(n_-k)} - \frac{k_\perp^2}{(n_-k)^2}n_{-\nu} \right) u_c(p)\,\epsilon_\nu^*(k)\,, \quad \text{(B.16)}$$

$$\mathcal{M}^{\rho\,K}_{c,J^{A0}\mathcal{L}^{(2)}_{10\text{YM}}} = \bar{v}_{\bar c}(l)\,\gamma_\perp^\rho \frac{ig_s\alpha_s}{4\pi} \left(\frac{(n_+p)(n_-k)}{\mu^2} \right)^{-\epsilon} \frac{\mathbf{T}^K}{(n_+p)} C_A \left(-\frac{1}{\epsilon^2} + \frac{3}{\epsilon} - 2 \right)$$
$$\times \frac{e^{\epsilon\gamma_E}\Gamma[1+\epsilon]\Gamma[1-\epsilon]^2}{2(1+\epsilon)\Gamma[2-2\epsilon]} \left(n_+^\nu - \frac{(n_+k)}{(n_-k)}n_-^\nu \right) u_c(p)\epsilon_\nu^*(k)\,, \quad \text{(B.17)}$$

$$\mathcal{M}^{\rho\,K}_{c,J^{A0}\mathcal{L}^{(2)}_{15\text{YM}}} = \frac{ig_s\alpha_s}{4\pi} \left(\frac{(n_+p)(n_-k)}{\mu^2} \right)^{-\epsilon} \frac{\mathbf{T}^K}{(n_+p)} C_A \left(-\frac{2}{\epsilon^2} + \frac{6}{\epsilon} - 4 \right)$$
$$\times \frac{e^{\epsilon\gamma_E}\Gamma[1+\epsilon]\Gamma[1-\epsilon]^2}{2(1+\epsilon)\Gamma[2-2\epsilon]} \left(\frac{k_{\perp\nu}}{(n_-k)} - \frac{k_\perp^2}{(n_-k)^2}n_{-\nu} \right) u_c(p)\,\epsilon_\nu^*(k)\,. \quad \text{(B.18)}$$

$$\mathcal{M}^{\rho\,K}_{c,J^{A0}\mathcal{L}^{(2)}_{4\xi}} = \bar{v}_{\bar c}(l)\,\gamma_\perp^\rho \frac{ig_s\alpha_s}{4\pi} \left(\frac{(n_+p)(n_-k)}{\mu^2} \right)^{-\epsilon} \frac{\mathbf{T}^K}{(n_+p)(n_-k)} [\slashed{k}_\perp, \gamma_{\perp\nu}]$$
$$\times \left(2C_F - C_A \left(\frac{4}{\epsilon^2} - \frac{5}{\epsilon} + 2 \right) \right) \frac{e^{\epsilon\gamma_E}\Gamma[1+\epsilon]\Gamma[1-\epsilon]^2}{4\,\Gamma[2-2\epsilon]} u_c(p)\epsilon^{*\nu}(k)\,, \quad \text{(B.19)}$$

$$\mathcal{M}^{\rho\,K}_{c,J^{A0}\mathcal{L}^{(2)}_{4+6\text{YM}}} = \bar{v}_{\bar c}(l)\,\gamma_\perp^\rho \frac{ig_s\alpha_s}{4\pi} \left(\frac{(n_+p)(n_-k)}{\mu^2} \right)^{-\epsilon} \frac{\mathbf{T}^K}{(n_+p)(n_-k)} [\slashed{k}_\perp, \gamma_{\perp\nu}]$$
$$\times C_A \left(-\frac{3}{4\epsilon} \right) \frac{e^{\epsilon\gamma_E}\Gamma[1+\epsilon]\Gamma[1-\epsilon]^2}{\Gamma[2-2\epsilon]} u_c(p)\epsilon^{*\nu}(k)\,, \quad \text{(B.20)}$$

$$\mathcal{M}^{\rho\,K}_{c,J^{A0}\mathcal{L}^{(2)}_{11+12\text{YM}}} = \bar{v}_{\bar c}(l)\,\gamma_\perp^\rho \frac{ig_s\alpha_s}{4\pi} \left(\frac{(n_+p)(n_-k)}{\mu^2} \right)^{-\epsilon} \frac{\mathbf{T}^K}{(n_+p)(n_-k)} [\slashed{k}_\perp, \gamma_{\perp\nu}]$$
$$\times C_A \left(\frac{1}{\epsilon^2} - \frac{1}{2\epsilon} \right) \frac{e^{\epsilon\gamma_E}\Gamma[1+\epsilon]\Gamma[1-\epsilon]^2}{\Gamma[2-2\epsilon]} u_c(p)\epsilon^{*\nu}(k)\,, \quad \text{(B.21)}$$

From the above results, we see the importance of defining the collinear functions as coefficients of particular soft structures. For example, $\mathcal{M}^{\rho\,K}_{c,J^{A0}\mathcal{L}^{(2)}_{2\xi}}$ in (B.14) is related to the one-loop correction to the collinear function for the insertion of the $\mathcal{L}^{(2)}_{2\xi}$ Lagrangian term. Only the corresponding tree-level piece is needed for LL resummation. However, the one-loop correction contains $1/\epsilon^2$ poles proportional to the C_A colour factor, as can be seen in (B.14). Hence, using only this piece as the contribution to the collinear function which is needed for LL resummation would lead to incorrect results. Rather, the correct objects to consider are the coefficients of particular soft structures, for which the problematic poles cancel once the contributions due to different Lagrangian insertions are combined.

Finally, we combine the above results according to the momentum dependent structures. We focus on equations (B.13) – (B.18). These correspond to the Lagrangian insertions with $n_+ \mathcal{B}^+$ and $\frac{\partial^\mu}{i n_- \partial} \mathcal{B}^+_\mu$ soft building blocks. Summing (B.19) – (B.21) gives the results in (B.11) and (B.12) directly. We stress that here we still work without using the on-shell and transversality relations. First we have

$$
\mathcal{M}^{\rho\,K}_{c,J^{A0}\mathcal{L}^{(2)}_{1\xi}} + \mathcal{M}^{\rho\,K}_{c,J^{A0}\mathcal{L}^{(2)}_{1\mathrm{YM}}} + \mathcal{M}^{\rho\,K}_{c,J^{A0}\mathcal{L}^{(2)}_{10\mathrm{YM}}} = \bar{v}_{\bar{c}}(l)\,\gamma^\rho_\perp \frac{ig_s\alpha_s}{4\pi}\left(\frac{(n_+p)(n_-k)}{\mu^2}\right)^{-\epsilon} \frac{\mathbf{T}^K}{(n_+p)}
$$

$$
\times \left(C_F\left(-\frac{2}{\epsilon}-4-2\epsilon\right)+C_A\left(-\frac{1}{\epsilon^2}-\frac{2}{\epsilon}+\epsilon+6\right)\right)
$$

$$
\times \frac{e^{\epsilon\gamma_E}\Gamma[1+\epsilon]\,\Gamma[1-\epsilon]^2}{2(1+\epsilon)\Gamma[2-2\epsilon]}\left(n^\nu_+ - n^\nu_-\frac{(n_+k)}{(n_-k)}\right)u_c(p)\epsilon^*_\nu(k)\,, \tag{B.22}
$$

$$
\mathcal{M}^{\rho\,K}_{c,J^{A0}\mathcal{L}^{(2)}_{2\xi}} + \mathcal{M}^{\rho\,K}_{c,J^{A0}\mathcal{L}^{(2)}_{2\mathrm{YM}}} + \mathcal{M}^{\rho\,K}_{c,J^{A0}\mathcal{L}^{(2)}_{15\mathrm{YM}}} = \bar{v}_{\bar{c}}(l)\,\gamma^\rho_\perp \frac{ig_s\alpha_s}{4\pi}\left(\frac{(n_+p)(n_-k)}{\mu^2}\right)^{-\epsilon} \frac{\mathbf{T}^K}{(n_+p)}
$$

$$
\times \left(C_F\left(\frac{4}{\epsilon}-10-12\epsilon+2\epsilon^2\right)+C_A\left(-\frac{2}{\epsilon^2}-\frac{2}{\epsilon}+6\epsilon+6\right)\right)
$$

$$
\times \frac{e^{\epsilon\gamma_E}\Gamma[1+\epsilon]\Gamma[1-\epsilon]^2}{2(1-\epsilon)(1+\epsilon)\Gamma[2-2\epsilon]}\left(\frac{k^\nu_\perp}{(n_-k)} - \frac{k^2_\perp n^\nu_-}{(n_-k)^2}\right)u_c(p)\epsilon^*_\nu(k)\,, \tag{B.23}
$$

We see that the $1/\epsilon^2$ poles do not cancel for the collinear function corresponding to the $n_+\mathcal{B}^+$ soft structure in equation (B.22), nor for the collinear function proportional to $\frac{\partial^\mu_\perp}{i n_- \partial}\mathcal{B}^+_\mu$ which can be extracted from (B.23). Indeed, these are not independent soft structures. The $1/\epsilon^2$ poles only cancel after the seemingly different collinear functions are combined using the equation-of-motion relation as done in the main text, or explicitly at this level using $\left[n^\nu_+ - \frac{n_+k}{n_-k}n^\nu_-\right]\epsilon^*_\nu(k) = -2\left[\frac{k^\nu_\perp}{(n_-k)} - \frac{k^2_\perp}{(n_-k)^2}n^\nu_-\right]\epsilon^*_\nu(k)$. Here is manifest a subtle, yet critical point in a consistent definition of the collinear functions.
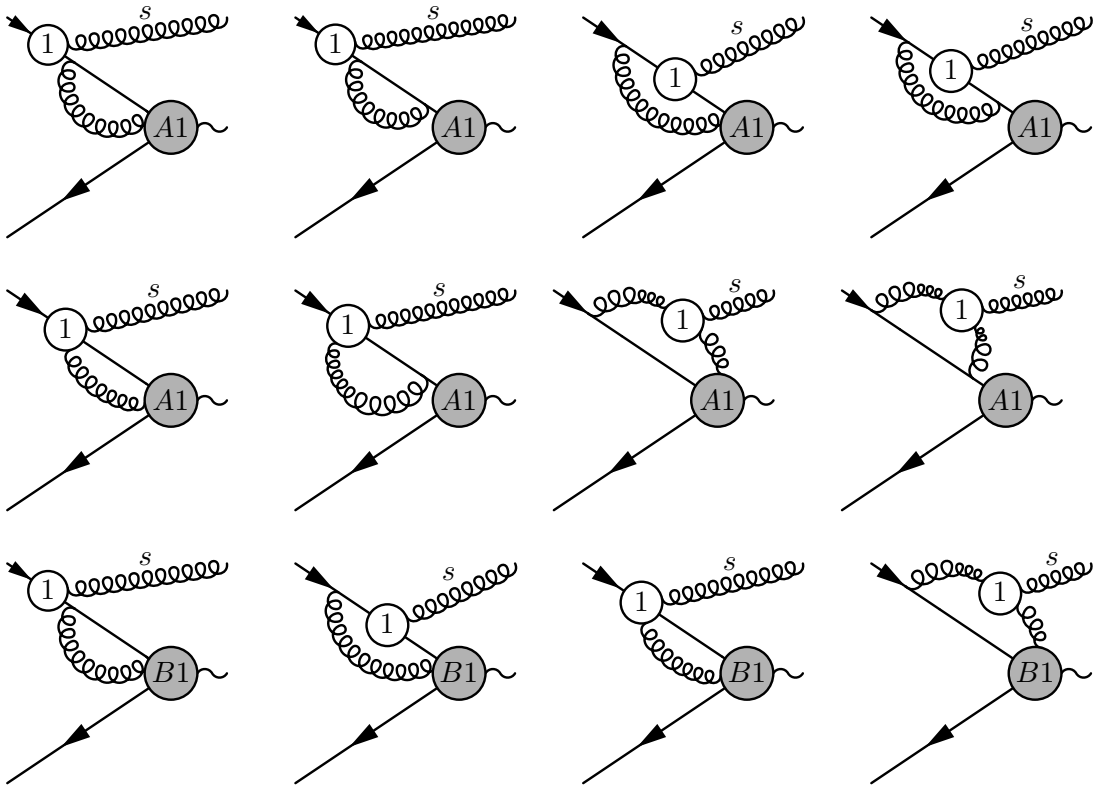
B.2.2 Collinear loop: n^ρ_- and n^ρ_+

These contributions are due to time-ordered products of the power-suppressed hard currents defined in (3.62) and (3.63) with $\mathcal{L}^{(1)}$ Lagrangian insertions. The corresponding diagrams are shown in figure B.2. Separating the two colour structures, we find

$$
\mathcal{M}^{n_\pm\rho\,K}_{c,C_F} = \bar{v}_{\bar{c}}(l)\left(\frac{n^\rho_-}{n_-l}-\frac{n^\rho_+}{n_+p}\right)\frac{ig_s\alpha_s}{4\pi}\left[\frac{(n_+p)(n_-k)}{\mu^2}\right]^{-\epsilon}C_F\mathbf{T}^K\frac{e^{\epsilon\gamma_E}\Gamma[1+\epsilon]\Gamma[1-\epsilon]^2}{(1+\epsilon)(1-\epsilon)\Gamma[2-2\epsilon]}
$$

$$
\times \left(\gamma_{\perp\nu}-\frac{\slashed{k}_\perp n_{-\nu}}{(n_-k)}\right)\left(1+2\epsilon+\epsilon^2\right)u_c(p)\epsilon^{*\nu}(k)\,, \tag{B.24}
$$

$$
\mathcal{M}^{n_\pm\rho\,K}_{c,C_A} = \bar{v}_{\bar{c}}(l)\left(\frac{n^\rho_-}{n_-l}-\frac{n^\rho_+}{n_+p}\right)\frac{ig_s\alpha_s}{4\pi}\left[\frac{(n_+p)(n_-k)}{\mu^2}\right]^{-\epsilon}C_A\mathbf{T}^K\frac{e^{\epsilon\gamma_E}\Gamma[1+\epsilon]\Gamma[1-\epsilon]^2}{(1+\epsilon)(1-\epsilon)\Gamma[2-2\epsilon]}
$$

$$
\times \left(\gamma_{\perp\nu}-\frac{\slashed{k}_\perp n_{-\nu}}{(n_-k)}\right)\left(\frac{1}{\epsilon}-2\,\epsilon-\epsilon^2\right)u_c(p)\epsilon^{*\nu}(k)\,. \tag{B.25}
$$

Figure B.2: *Collinear one-loop diagrams with one soft gluon emission. The $\mathcal{O}(\lambda^1)$ power-suppressed currents $A1$ and $B1$ defined in (3.62) and (3.63), respectively, are used here. The collinear virtual gluon must attach to the $B1$ current, because of the additional $\mathcal{A}_{c\perp}$ gluon field present in this subleading current.*

B.2.3 Soft loop: $\gamma_{\perp\rho}$

In this section we present the result for the soft one-virtual, one-real soft gluon amplitude proportional to $\gamma_{\perp\rho}$. Only one SCET diagram, shown in figure B.3, is needed to reproduce the corresponding virtual-real contribution from the expansion-by-regions method. Hence only non-abelian contributions arise here and we find

$$
\begin{aligned}
\mathcal{M}_{s,C_A}^{\gamma_{\perp\rho}\,K} &= \bar{v}_{\bar{c}}(l)\,\gamma_\perp^\rho\,\frac{ig_s\alpha_s}{4\pi}\left(\frac{-(n_-k)(n_+k)}{\mu^2}\right)^{-\epsilon}\frac{C_A\mathbf{T}^K}{(n_+p)(n_-k)}\frac{e^{\epsilon\gamma_E}\Gamma[1+\epsilon]^2\Gamma[1-\epsilon]^3}{\Gamma[2-2\epsilon]}\\
&\quad\times\left(n_+k\,n_{-\nu}+k_{\perp\nu}+\frac{1}{2}[\not{k}_\perp,\gamma_{\perp\nu}]\right)\left(\frac{1}{\epsilon^2}-\frac{2}{\epsilon}\right)u_c(p)\epsilon^{*\nu}(k)\,.
\end{aligned}
\tag{B.26}
$$

Details on the vanishing of numerous other a priori possible diagrams are provided in figures B.4 and B.5. Note that the latter figure also includes diagrams that represent insertions of both, the collinear (on the upper leg) and anticollinear (on the lower leg) subleading soft-collinear interactions, when $a = b = 1$. However, as all these terms vanish, there is a unique separation of contributions from collinear Lagrangian insertions and from anticollinear Lagrangian insertions. In (B.26) we have given the $a = 2, b = 0$ contribution from the last diagram in figure B.5, while the $a = 0, b = 2$ anticollinear one is obtained by exchanging $n_+ \leftrightarrow n_-$. We further note that the absence of a contribution of the second diagram in figure B.5, containing a power-suppressed two-soft gluon vertex, implies
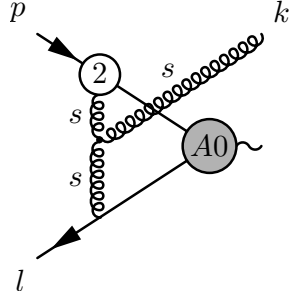
Figure B.3: *The only diagram relevant to the one virtual, one-real contribution to the two-loop soft function. Here the power suppression is placed on the collinear leg as indicated by the $\mathcal{O}(\lambda^2)$ vertex.*

the statement made in section 7.1.2 that only the single soft-gluon structures with their corresponding soft functions S_1, S_6 contribute at NNLO, of which only S_1 is relevant at cross-section level as explained in the main text.

B.2.4 Soft loop: n_+^ρ

The relevant diagram is again the topology of figure B.3. However, since one power of λ is used up by the power-suppressed current, at the soft-collinear vertex we now insert the $\mathcal{L}^{(1)}$ term from the SCET Lagrangian.

The $J^{A0,B1}$ current cannot give a contribution here since it produces a collinear gluon, that cannot be contracted to form a soft loop.

The diagrams shown in figures B.4 and B.5 are also present here. The only change is that the LP hard current is replaced by $J^{A0,A1}$ and the sum of $a + b\,(+\,c) = 1$ only. Once again only the last diagram in figure B.5 does not vanish, and we find
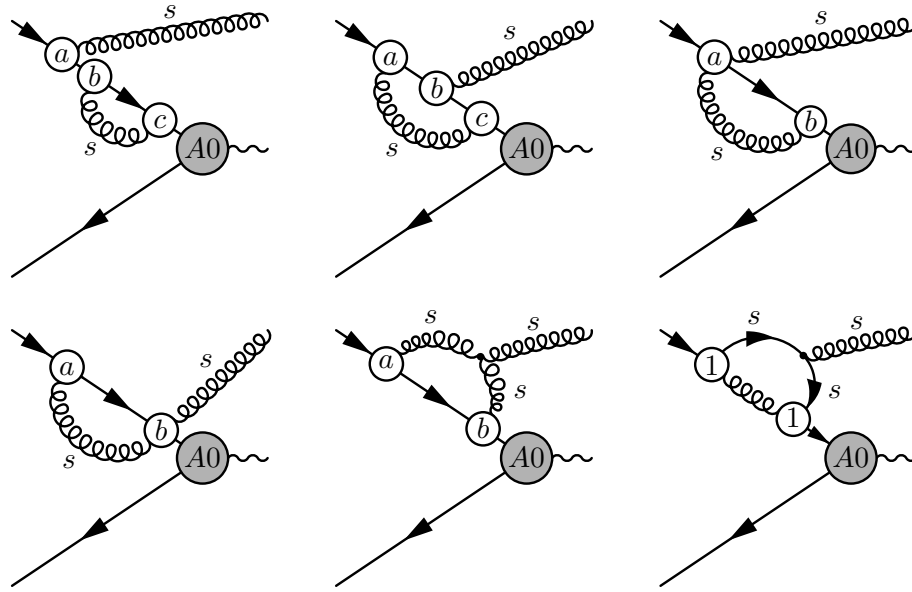
$$
\begin{aligned}
\mathcal{M}_{s,C_A}^{n_+\rho K} &= \bar{v}_{\bar{c}}(l)\, n_+^\rho\, \frac{ig_s\alpha_s}{4\pi} \left(\frac{-(n_-k)(n_+k)}{\mu^2} \right)^{-\epsilon} \frac{C_A \mathbf{T}^K}{(n_+p)} \frac{e^{\epsilon\gamma_E}\Gamma[1+\epsilon]^2\,\Gamma[1-\epsilon]^3}{\Gamma[2-2\epsilon]} \\
&\quad \times \left[\gamma_{\perp\nu} \frac{1}{\epsilon^2} + \frac{k_{\perp\nu}\slashed{k}_\perp}{(n_-k)(n_+k)} \frac{1}{\epsilon^2} + \left(\frac{n_{+\nu}}{(n_+k)} - \frac{n_{-\nu}}{(n_-k)} \right) \slashed{k}_\perp \left(\frac{1}{2\epsilon^2} - \frac{1}{\epsilon} \right) \right] u_c(p)\epsilon^{*\nu}(k)\,.
\end{aligned}
\tag{B.27}
$$

There is no term proportional to n_-^ρ.

B.2.5 Hard loop: $\gamma_{\perp\rho}$

As discussed in the main text, there exists also a contribution to the NLO NLP amplitude from the one-loop hard matching coefficient $C^{A0,A0}$ given in (2.58). We obtain

$$
\begin{aligned}
\mathcal{M}_{h,C_F}^{\gamma_{\perp}\rho K} &= \bar{v}_{\bar{c}}(l)\, \gamma_\perp^\rho\, \frac{ig_s\alpha_s}{4\pi} \left(\frac{-(n_-l)(n_+p)}{\mu^2} \right)^{-\epsilon} \frac{C_F \mathbf{T}^K}{(n_+p)(n_-k)} \\
&\quad \times \left((n_+k)n_{-\nu}\left(\frac{2}{\epsilon^2} + \frac{1}{\epsilon} + 5 - \frac{\pi^2}{6} \right) + \left[\slashed{k}_\perp, \gamma_{\perp\nu} \right]\left(\frac{1}{\epsilon^2} + \frac{3}{2\epsilon} - \frac{\pi^2}{12} + 4 \right) \right.
\end{aligned}
\tag{B.28}
$$

Figure B.4: *Diagrams with one soft emitted gluon and one soft loop. Since all the diagrams here include the LP $J^{A0,A0}$ current, the $\mathcal{O}(\lambda^2)$ power suppression must be provided by Lagrangian insertions. This means using all possible insertions such that $a + b\,(+c) = 2$ at the indicated vertices. Out of the 20 possibilities, many vanish immediately due to contractions which yield $n_\pm^2 = n_\pm \cdot \gamma_\perp = 0$ or propagators which give zero due to the vanishing external transverse momentum. The remaining integrals, where the integrand does not immediately vanish, are either scaleless or vanish by Cauchy's theorem, because all propagator poles lie in one half of the complex momentum plane.*

$$+ k_{\perp\nu}\left(\frac{2}{\epsilon^2} + \frac{3}{\epsilon} - \frac{\pi^2}{6} + 8\right) + (n_-k)n_{+\nu}\left(\frac{2}{\epsilon} + 3\right) + \mathcal{O}(\epsilon)\Bigg)\, u_c(p)\epsilon^{*\nu}(k)\,,$$

and $\mathcal{M}^{\gamma_\perp\rho\,K}_{h,C_A} = 0$.

B.2.6   Hard loop: n_+^ρ

This contribution comes from the one-loop correction to the matching coefficient $C^{A0,A1}$ of the $J^{A0,A1}$ current together with an insertion of the $\mathcal{O}(\lambda)$ piece of quark SCET Lagrangian. $C^{A0,A1}$ is related to $C^{A0,A0}$ by reparametrisation invariance [102]. With the definition (3.62) the relation reads $C^{A0,A1} = -1/(n_+p)\, C^{A0,A0}$. We then find

$$\mathcal{M}^{n_+\rho\,K}_{h,C_F} = \bar{v}_{\bar{c}}(l)\, n_+^\rho\, \frac{ig_s\alpha_s}{4\pi}\left(\frac{-(n_-l)(n_+p)}{\mu^2}\right)^{-\epsilon} \frac{C_F \mathbf{T}^K}{(n_+p)(n_-k)}\left(\not{k}_\perp n_{-\nu} - (n_-k)\gamma_{\perp\nu}\right)$$

$$\times \left(-\frac{2}{\epsilon^2} - \frac{3}{\epsilon} - 8 + \frac{\pi^2}{6} + \mathcal{O}(\epsilon)\right) u_c(p)\epsilon^{*\nu}(k)\,. \tag{B.29}$$

There is no term proportional to n_-^ρ.
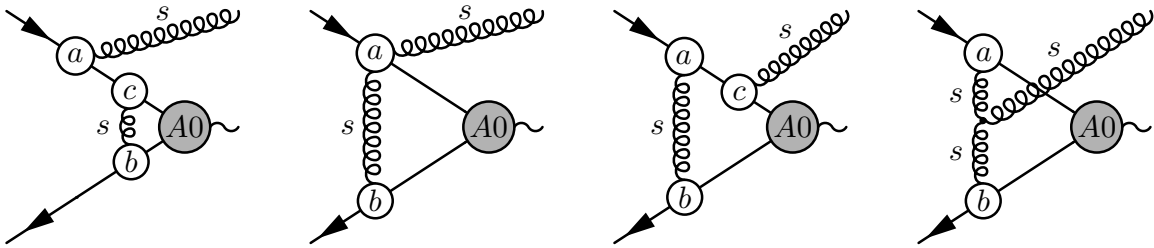
Figure B.5: *Soft one-loop diagrams with one emitted soft gluon. As in the previous figure, only the LP current is present in these diagrams, however now the virtual soft gluon connects the collinear and anticollinear legs. Lagrangian insertions must again be chosen such that $a + b\,(+\,c) = 2$. Note that all diagrams with $b = 1$ vanish, since a single leg cannot carry a $\mathcal{O}(\lambda)$ suppression as explained in section 3.2.2. Only the last diagram with $a = 2$ or $b = 2$ gives a non-vanishing result. The others are either scaleless or vanish after momentum conservation is imposed.*

C

One-soft-particle reducible contributions

The results for tree-level collinear functions corresponding to double soft gluon structures presented in section 4.1.1 contain contributions from one-soft-particle reducible diagrams. The reasons for including these terms are stated in the main text, however, a technical discussion is missing. In this appendix, we fill this gap.

Let us begin with reiterating the need for the inclusion of contributions due to one-soft-particle reducible diagrams in these collinear functions.

The main point for the necessary inclusion of the one-soft-particle reducible diagrams corresponding to a $\mathcal{L}_{1\xi}^{(2)}$ insertion as part of the contribution to the collinear functions with two soft partons is that in the derivation of the factorisation formula we have eliminated the $n_+\mathcal{B}^+$ soft structure from the basis using the equation-of-motion relation in equation (3.46). We see in the equation-of-motion relation in (3.46) that the $n_+\mathcal{B}^+$ structure can be written in terms of the single gluon structure $\frac{i\partial_\perp^\mu}{in_-\partial}\mathcal{B}_{\mu\perp}^+(z_-)$, but also the two parton soft structures. The one-soft-particle-reducible diagrams must reproduce precisely those contributions.

In other words, had we not eliminated the $n_+\mathcal{B}^+$ soft gluon building block from the basis of possible soft structures, we would not need to consider one-soft-particle-reducible diagrams from a $\mathcal{L}_{1\xi}^{(2)}$ insertion. The main point is that identical contribution to the amplitude must be produced in both basis. We show that this is the case here, by carefully computing the relevant collinear functions.

We begin by targeting the J_3 collinear function, so the starting point is the matching equation and we choose the external state to contain gluons. The soft structures $\mathfrak{s}_{6;\mu\nu}^A$, $\mathfrak{s}_{2,fb}$, and $\mathfrak{s}_{4,\mu\nu}^{AB}$ are not affected by the equation-of-motion relations, so we do not include them in the analysis here to avoid unnecessary clutter.

The matching is performed at operator level. Let us first consider the matrix element of the operators with a single soft gluon final state. The right hand side of the matching equation is

$$
\langle g^K(k)|\mathcal{T}_{\gamma f}(n_+q)|q(p)_q\rangle = 2\pi \int \frac{dn_+p_a}{2\pi} du\, e^{i\,(n_+p_a)\,u} \int \frac{d\omega}{2\pi} \int dz_-\, e^{-i\,\omega\,z_-}
$$

$$
\times \left(J_{1;\gamma\beta,fb}^A\left(n_+q, n_+p_a; \omega\right) \langle 0|\chi_{c,\beta b}^{\mathrm{PDF}}(un_+)|q(p)_q\rangle \langle g(k)^K|\mathfrak{s}_1^A(z_-)|0\rangle \right.
$$

$$+ J_{3;\gamma\beta}\left(n_+q, n_+p_a; \omega\right) \langle 0|\chi^{\mathrm{PDF}}_{c,\beta b}(un_+)|q(p)_q\rangle \langle g(k)^K|\mathfrak{s}_{3,fb}(z_-)|0\rangle\Big). \qquad \text{(C.1)}$$

With a single soft gluon, the analysis is identical to the one performed in the main text. Only the $\langle g(k)^K|\mathfrak{s}_1^A(z_-)|0\rangle$ contribution is non-vanishing, and by comparing to the left-hand side obtained by calculation using the NLP Feynman rules, we can immediately write down the collinear function

$$J^{K(0)}_{1;\gamma\beta,fq}(n_+q, n_+p; \omega) \;=\; \mathbf{T}^K_{fq}\delta_{\beta\gamma}\left(-\frac{1}{n_+p}\delta(n_+q - n_+p) + 2\frac{\partial}{\partial n_+q}\delta(n_+q - n_+p)\right). \quad \text{(C.2)}$$

Now, since the matching equation is an operator relation, we can choose a different external state to perform the matching. Since we target the J_3 and J_4 collinear functions, we choose a two soft gluon external state. The right-hand side of the matching equation is then

$$\langle g^{K_1}(k_1)g^{K_2}(k_2)|\mathcal{T}_{\gamma f}(n_+q)|q(p)_q\rangle \;=\; 2\pi\int\frac{dn_+p_a}{2\pi}du\,e^{i\,(n_+p_a)\,u}\int\frac{d\omega}{2\pi}\int dz_-\,e^{-i\,\omega\,z_-}$$

$$\times\left(\, J^A_{1;\gamma\beta,fb}\left(n_+q, n_+p_a; \omega\right) \langle 0|\chi^{\mathrm{PDF}}_{c,\beta b}(un_+)|q(p)_q\rangle \langle g^{K_1}(k_1)g^{K_2}(k_2)|\mathfrak{s}_1^A(z_-)|0\rangle\right.$$

$$\left.+ J_{3;\gamma\beta,}\left(n_+q, n_+p_a; \omega\right) \langle 0|\chi^{\mathrm{PDF}}_{c,\beta b}(un_+)|q(p)_q\rangle \langle g^{K_1}(k_1)g^{K_2}(k_2)|\mathfrak{s}_{3,fb}(z_-)|0\rangle\right), \quad \text{(C.3)}$$

where, for concreteness,

$$\mathfrak{s}_{3,fb}(z_-) = \frac{1}{(in_-\partial)^2}\left[\mathcal{B}^{+\,\mu_\perp,}(z_-), \left[in_-\partial\mathcal{B}^{+;}_{\mu_\perp}(z_-)\right]\right]_{fb}. \qquad \text{(C.4)}$$

The two soft gluon matrix element of this operator has been already given in equation (6.9). Here, we chose the gluon to be transversely polarised to eliminate Wilson line contributions for transparency

$$\langle g^{K_1}_\perp(k_1)g^{K_2}_\perp(k_2)|\frac{1}{(in_-\partial)^2}\left[\mathcal{B}^{+\,\mu_\perp}(z_-), \left[in_-\partial\mathcal{B}^+_{\mu_\perp}(z_-)\right]\right]_{fb}|0\rangle \;=\; \qquad \text{(C.5)}$$

$$\frac{1}{(n_-(k_1+k_2))^2}g_s^2(if^{K_1K_2B}\mathbf{T}^B_{fb})\left[(n_-k_1 - n_-k_2)g_\perp^{\eta_1\eta_2}\right]e^{i(k_1+k_2)z_-}\epsilon^*_{\perp\eta_1}(k_1)\epsilon^*_{\perp\eta_2}(k_2).$$

For the soft structure which begins with a single gluon emission, the two soft gluon matrix element is given by

$$\langle g^{K_1}_\perp(k_1)g^{K_2}_\perp(k_2)|\mathfrak{s}_1^A(z_-)|0\rangle \;=\; \frac{g_s}{n_-(k_1+k_2)}\left[(k_{1\perp}^\eta + k_{2\perp}^\eta) - \frac{(k_{1\perp}+k_{2\perp})^2}{(n_-(k_1+k_2))}n_-^\eta\right]$$

$$\times\frac{-i}{(k_1+k_2)^2}\epsilon^*_{\perp\nu_1}(k_1)\epsilon^*_{\perp\nu_2}(k_2)g_s f^{K_1K_2A} \qquad\qquad \text{(C.6)}$$

$$(g^{\nu_1\eta}(2k_1+k_2)^{\nu_2} - g^{\eta\nu_2}(k_1+2k_2)^{\nu_1} + g^{\nu_1\nu_2}(k_2-k_1)^\eta)\,e^{iz_-(k_1+k_2)} \qquad .$$

We put this together according to (C.3) and perform the integrals. We arrive at

$$\langle g^{K_1}_\perp(k_1)g^{K_2}_\perp(k_2)|\mathcal{T}_{\gamma f}(n_+q)|q(p)_q\rangle \;=\;$$
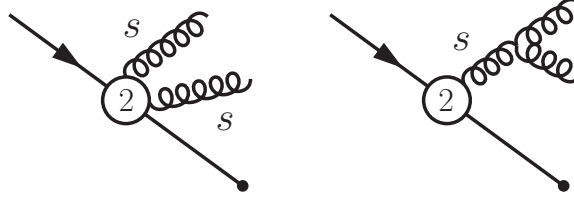
Figure C.1: *Possible SCET diagrams with two gluon external states required for the calculation of J_3 collinear function.*

$$\times 2\pi J^A_{1;\gamma\beta,fq}\left(n_+q, n_+p; n_-(k_1+k_2)\right) u_{c,\beta}(p)\, \frac{g_s}{n_-(k_1+k_2)}\left[(k^\eta_{1\perp}+k^\eta_{2\perp}) - \frac{(k_{1\perp}+k_{2\perp})^2}{(n_-(k_1+k_2))}n^\eta_-\right]$$

$$\times\frac{-i}{(k_1+k_2)^2}\,\epsilon^*_{\perp\nu_1}(k_1)\epsilon^*_{\perp\nu_2}(k_2)g_s f^{K_1K_2A}\left(g^{\nu_1\eta}(2k_1+k_2)^{\nu_2} - g^{\eta\nu_2}(k_1+2k_2)^{\nu_1} + g^{\nu_1\nu_2}(k_2-k_1)^\eta\right)$$

$$+2\pi J_{3;\gamma\beta}\left(n_+q, n_+p; n_-(k_1+k_2)\right) u_{c,\beta}(p)\frac{1}{(n_-(k_1+k_2))^2}g_s^2(if^{K_1K_2B}\mathbf{T}^B_{fq})$$

$$\times\left[(n_-k_1 - n_-k_2)g^{\eta_1\eta_2}_\perp\right]\epsilon^*_{\perp\eta_1}(k_1)\epsilon^*_{\perp\eta_2}(k_2) \tag{C.7}$$

From the single external soft gluon matrix element calculation, we already have the J_1 collinear function, hence we now substitute the result from (C.2) and we arrive at

$$\langle g^{K_1}_\perp(k_1)g^{K_2}_\perp(k_2)|\mathcal{T}_{\gamma f}(n_+q)|q(p)_q\rangle \quad =$$

$$\times 2\pi\,\mathbf{T}^A_{fq}\delta_{\beta\gamma}\left(-\frac{1}{n_+p}\delta(n_+q-n_+p) + 2\frac{\partial}{\partial n_+q}\delta(n_+q-n_+p)\right)u_{c,\beta}(p)$$

$$\times\frac{g_s}{n_-(k_1+k_2)}\left[(k^\eta_{1\perp}+k^\eta_{2\perp}) - \frac{(k_{1\perp}+k_{2\perp})^2}{(n_-(k_1+k_2))}n^\eta_-\right]$$

$$\times\frac{-i}{(k_1+k_2)^2}\,\epsilon^*_{\perp\nu_1}(k_1)\epsilon^*_{\perp\nu_2}(k_2)g_s f^{K_1K_2A}$$

$$\times\left(g^{\nu_1\eta}(2k_1+k_2)^{\nu_2} - g^{\eta\nu_2}(k_1+2k_2)^{\nu_1} + g^{\nu_1\nu_2}(k_2-k_1)^\eta\right)$$

$$+2\pi J_{3;\gamma\beta}\left(n_+q, n_+p; n_-(k_1+k_2)\right) u_{c,\beta}(p)\frac{1}{(n_-(k_1+k_2))^2}g_s^2(if^{K_1K_2B}\mathbf{T}^B_{fq})$$

$$\times\left[(n_-k_1 - n_-k_2)g^{\eta_1\eta_2}_\perp\right]\epsilon^*_{\perp\eta_1}(k_1)\epsilon^*_{\perp\eta_2}(k_2) \tag{C.8}$$

At this point, the only undetermined piece on the right-hand side of the matching equation is the collinear function J_3.

Therefore, we next proceed to compute the left-hand side of the matching equation by computing the relevant SCET diagrams, shown in figure C.1. We have two objectives. Firstly, we check that the structures corresponding to J_1 are reproduced. Secondly, the leftover pieces will be identified with J_3.

After a short calculation using the NLP Feynman rules, we arrive at

$$\langle g^{K_1}_\perp(k_1)g^{K_2}_\perp(k_2)|\mathcal{T}_{\gamma f}(n_+q)|q(p)_q\rangle \quad = \quad 2\pi\left(-\frac{1}{(n_+p)}\delta(n_+q-n_+p) + 2\frac{\partial}{\partial n_+q}\delta(n_+q-n_+p)\right)$$

$$\times g_s^2 \, i f^{K_1 K_2 B} \mathbf{T}_{fb}^B \frac{1}{(n_-(k_1 + k_2))^2}$$

$$\times \Big((n_- k_1) - (n_- k_2) \Big) g_\perp^{\nu_1 \nu_2} \, u_{c,\gamma}(p) \epsilon_{\perp \nu_1}^*(k_1) \epsilon_{\perp \nu_2}^*(k_2)$$

$$+ 2\pi \left(-\frac{1}{(n_+ p)} \delta(n_+ q - n_+ p) + 2 \frac{\partial}{\partial n_+ q} \delta(n_+ q - n_+ p) \right)$$

$$\times \frac{1}{(n_-(k_1 + k_2))} \, g_s \mathbf{T}_{fb}^B \, \epsilon_{\perp \nu_1}^*(k_1) \epsilon_{\perp \nu_2}^*(k_2) \left((k_{1\perp \nu} + k_{2\perp \nu}) - \frac{(k_{1\perp} + k_{2\perp})^2}{(n_-(k_1 + k_2))} n_{-\nu} \right) u_{c,\gamma}(p)$$

$$\times \frac{-i}{(k_1 + k_2)^2} g_s f^{K_1 K_2 B} \left(g^{\nu \nu_2} (-k_1 - 2k_2)^{\nu_1} + g^{\nu_2 \nu_1} (k_2 - k_1)^\nu + g^{\nu_1 \nu} (2k_1 + k_2)^{\nu_2} \right). \quad \text{(C.9)}$$

In order to facilitate the comparison against the right-hand side of the matching equation presented in (C.8), we have marked the last three lines of the above equation in green. These pieces correspond to J_1 and its soft structure, as can be seen in the top four lines of (C.8). We see that these pieces are in agreement, which achieves our first objective.

Lastly, we can extract the collinear function J_3 which contains a piece originating from a $\mathcal{L}_{3\xi}^{(2)}$ insertion, and another from the $n_+\mathcal{B}$ one-soft-particle reducible diagram. Moreover, we see that it is indeed the same as collinear function J_1 after the colour generator has been moved to the soft function. We find

$$J_{3,\gamma\beta} = \delta_{\gamma\beta} \left(-\frac{1}{(n_+ p)} \delta(n_+ q - n_+ p) + 2 \frac{\partial}{\partial n_+ q} \delta(n_+ q - n_+ p) \right). \quad \text{(C.10)}$$

The second term in the above equation originates from the one-soft-particle reducible diagram due to $\mathcal{L}_{1\xi}^{(2)}$ insertion. We see that it contains the derivative on the momentum conserving delta function which only appears in the NLP Feynman rules from the $\mathcal{L}_{1\xi}^{(2)}$ Lagrangian term.

Before we continue, we show that in fact we can obtain this result at the operatorial level directly from the equation of motion.

In the following we wish to focus on the piece coming from $\mathcal{L}_{1\xi}^{(2)}$, which we label the matrix element with in the subscript. We have

$$\langle g^K(k) | \mathcal{T}_{\gamma f}^{1g}(n_+ q) | q(p)_q \rangle_{\mathcal{L}_{1\xi}^{(2)}} = -2\pi \frac{g_s}{(n_- k)} \mathbf{T}_{fq}^K \left[(n_- k) n_+^\eta - (n_+ k) n_-^\eta \right] \epsilon^*(k)_\eta \, u_{c,\gamma}(p)$$

$$\times \left(\frac{\partial}{\partial n_+ q} \delta(n_+ q - n_+ p) \right). \quad \text{(C.11)}$$

We write the soft structure in matrix element form using

$$\langle g^K(k) | n_+^\nu \mathcal{B}_\nu^+ (z_-) | 0 \rangle = \mathbf{T}^K \frac{g_s}{(n_- k)} \left[(n_- k) n_+^\eta - (n_+ k) n_-^\eta \right] \epsilon_\eta^*(k) \, e^{iz_- k}, \quad \text{(C.12)}$$

we have

$$\langle g^K(k) | \mathcal{T}_{\gamma f}^{1g}(n_+ q) | q(p)_q \rangle_{\mathcal{L}_{1\xi}^{(2)}} = -2\pi \langle g^K(k) | n_+ \mathcal{B}_{fq}^+(z_-) | 0 \rangle \, e^{-iz_- k} \, u_{c,\gamma}(p)$$

$$\times \left(\frac{\partial}{\partial n_+ q} \delta(n_+ q - n_+ p) \right) \quad \text{(C.13)}$$

Now using the equation of motion for the n_+ component of the soft field, including the two-gluon term

$$\langle g^K(k)|\mathcal{T}_{\gamma f}^{1g}(n_+q)|q(p)_q\rangle_{\mathcal{L}_{1\xi}^{(2)}} = -2\pi\,\langle g^K(k)| - 2\frac{i\partial_\perp^\mu}{in_-\partial}\mathcal{B}_{\mu_\perp,fq}^+(z_-)$$

$$-2\frac{1}{(in_-\partial)^2}\left[\mathcal{B}^{+\,\mu_\perp}(z_-),\left[in_-\partial\mathcal{B}_{\mu_\perp}^+(z_-)\right]\right]_{fq}|0\rangle\,e^{-iz_-k}$$

$$\times\,u_{c,\gamma}(p)\left(\frac{\partial}{\partial n_+q}\delta(n_+q - n_+p)\right) \tag{C.14}$$

Now, we can see that the first term in the above equation gives the one-gluon soft structure, which we have presented in equation ((4.16)). We have set $\sqrt{Z_{q,c}}|_{\text{tree}} = 1$.

We now focus on the two gluon term. We need to input the result from (C.5). Now there are two gluons, momentum in the exponential is $k = k_1 + k_2$.

$$\langle g^K(k)|\mathcal{T}_{\gamma f}^{1g}(n_+q)|q(p)_q\rangle_{\mathcal{L}_{1\xi}^{(2)}} = 2\,(2\pi)\,\langle g^K(k)|\frac{1}{(in_-\partial)^2}\left[\mathcal{B}^{+\,\mu_\perp}(z_-),\left[in_-\partial\mathcal{B}_{\mu_\perp}^+(z_-)\right]\right]_{fq}|0\rangle\,e^{-iz_-k}$$

$$\times\,u_{c,\gamma}(p)\left(\frac{\partial}{\partial n_+q}\delta(n_+q - n_+p)\right) \tag{C.15}$$

where we actually need to take a two gluon state which is for $\perp$ gluons from (C.5). Hence, we have

$$\langle g_\perp^{K_1}(k_1)g_\perp^{K_2}(k_2)|\mathcal{T}_{\gamma f}^{1g}(n_+q)|q(p)_q\rangle_{\mathcal{L}_{1\xi}^{(2)}} = 2\pi\,\frac{1}{(n_-(k_1+k_2))^2}g_s^2(if^{K_1K_2B}\mathbf{T}_{fq}^B) \tag{C.16}$$

$$\times\left[(n_-k_1 - n_-k_2)g_\perp^{\eta_1\eta_2}\right]\epsilon_{\eta_1}^*(k_1)\epsilon_{\eta_2}^*(k_2)\,u_{c,\gamma}(p)\left(2\frac{\partial}{\partial n_+q}\delta(n_+q - n_+p)\right).$$

This can now be compared to the right-hand side of the matching equation, and directly extract the $J_{3,2}$ contribution. This result agrees with the above one-soft-particle reducible SCET diagrams computation.

In the following, we repeat the discussion above, however, now instead of the soft gluons, we choose soft quarks in the external state. This way we can find all contributions to the J_5 collinear function, including contributions due to one-soft-particle reducible diagrams. The required right-hand side of the matching equation is

$$\langle g^K(k)|\mathcal{T}_{\gamma f}(n_+q)|q(p)_q\rangle = 2\pi\int\frac{dn_+p_a}{2\pi}du\,e^{i\,(n_+p_a)\,u}\int\frac{d\omega}{2\pi}\int dz_-\,e^{-i\,\omega\,z_-}$$

$$\times\left(J_{1;\gamma\beta,fb}^A\,(n_+q, n_+p_a;\omega)\,\langle 0|\chi_{c,\beta b}^{\text{PDF}}(un_+)|q(p)_q\rangle\,\langle g^K(k)|\mathfrak{s}_1^A(z_-)|0\rangle\right.$$

$$+\left(\int\frac{d\omega_2}{2\pi}\int dz_{2-}\,e^{-i\,\omega_2\,z_{2-}}\right)J_{5;\gamma\sigma\lambda\beta}^{fghb}\,(n_+q, n_+p_a;\omega,\omega_2)\,\langle 0|\chi_{c,\beta b}^{\text{PDF}}(un_+)|q(p)_q\rangle$$

$$\left.\times\langle g^K(k)|\mathfrak{s}_{5;\sigma\lambda,gh}(z_-, z_{2-})|0\rangle\right), \tag{C.17}$$

Matrix element for the single soft gluon emission is evaluated as before, with only the $\mathfrak{s}_1^A$ contributing. Inserting it and performing the integrals we obtain for the right-hand side of

the matching equation

$$\langle g^K(k)|\mathcal{T}_{\gamma f}^{1g}(n_+q)|q(p)_q\rangle = 2\pi \frac{g_s}{(n_-k)}\left(J_{1;\gamma\beta,fq}^K(n_+q,n_+p;n_-k)\left[k_\perp^\eta - \frac{k_\perp^2}{(n_-k)}n_-^\eta\right]\right)$$
$$\times u_{c,\beta}(p)\epsilon_\eta^*(k)\,. \tag{C.18}$$

The left-hand side is computed using the NLP Feynman rules, and after comparing the two sides of the matching equation we arrive at the familiar collinear function

$$J_{1;\gamma\beta,fq}^{K(0)}(n_+q,n_+p;\omega) = \mathbf{T}_{fq}^K\delta_{\beta\gamma}\left(-\frac{1}{n_+p}\delta(n_+q-n_+p)+2\frac{\partial}{\partial n_+q}\delta(n_+q-n_+p)\right), \tag{C.19}$$

which is the same as in (C.2). Now, we consider the two soft quark external state.

$$\langle q(k_1)\bar{q}(k_2)|\mathcal{T}_{\gamma f}(n_+q)|q(p)_q\rangle = 2\pi\int\frac{dn_+p_a}{2\pi}du\,e^{i\,(n_+p_a)\,u}\int\frac{d\omega}{2\pi}\int dz_-\,e^{-i\omega\,z_-}$$
$$\times\left(J_{1;\gamma\beta,fb}^A(n_+q,n_+p_a;\omega)\,\langle 0|\chi_{c,\beta b}^{\mathrm{PDF}}(un_+)|q(p)_q\rangle\,\langle q(k_1)\bar{q}(k_2)|\mathfrak{s}_1^A(z_-)|0\rangle\right.$$
$$+\left(\int\frac{d\omega_2}{2\pi}\int dz_{2-}\,e^{-i\omega_2\,z_{2-}}\right)J_{5;\gamma\sigma\lambda\beta}^{fghb}(n_+q,n_+p_a;\omega,\omega_2)\,\langle 0|\chi_{c,\beta b}^{\mathrm{PDF}}(un_+)|q(p)_q\rangle$$
$$\left.\times\langle q(k_1)\bar{q}(k_2)|\mathfrak{s}_{5;\sigma\lambda,gh}(z_-,z_{2-})|0\rangle\right), \tag{C.20}$$

Next, substituting into the equations
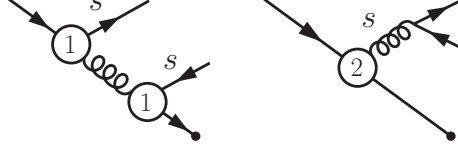
$$\langle q(k_1)\bar{q}(k_2)|\mathfrak{s}_1^A(z_-)|0\rangle = \frac{g_s}{n_-(k_1+k_2)}\left[(k_{1\perp}^\eta+k_{2\perp}^\eta)-\frac{(k_{1\perp}+k_{2\perp})^2}{(n_-(k_1+k_2))}n_-^\eta\right]$$
$$\times\frac{1}{(k_1+k_2)^2}\bar{u}(k_1)g_s\mathbf{T}^A\gamma^\eta v(k_2)\,e^{iz_-(k_1+k_2)}, \tag{C.21}$$

and

$$\langle q_{k_1}(k_1)\bar{q}_{k_2}(k_2)|\mathfrak{s}_{5;\sigma\lambda,gh}(z_-,z_{2-})|0\rangle = g_s^2\frac{1}{(n_-k_1)}\frac{1}{(n_-k_2)}$$
$$\times\bar{u}_\lambda(k_1)\,\delta_{k_1 h}v_\sigma(k_2)\delta_{k_2 g}\,e^{iz_{2-}k_1}\,e^{iz_-k_2}, \tag{C.22}$$

and performing the integrals gives the right-hand side of the matching equation

$$\langle q(k_1)\bar{q}(k_2)|\mathcal{T}_{\gamma f}(n_+q)|q(p)_q\rangle =$$

$$2\pi\,J_{1;\gamma\beta,fq}^A(n_+q,n_+p;n_-(k_1+k_2))\,u_{c,\beta}(p)\,\frac{g_s}{n_-(k_1+k_2)}$$

$$\times\left[(k_{1\perp}^\eta+k_{2\perp}^\eta)-\frac{(k_{1\perp}+k_{2\perp})^2}{(n_-(k_1+k_2))}n_-^\eta\right]\frac{1}{(k_1+k_2)^2}\bar{u}(k_1)g_s\mathbf{T}^A\gamma^\eta v(k_2)$$

$$+2\pi\,J_{5;\gamma\sigma\lambda\beta}^{fk_2k_1q}(n_+q,n_+p;n_-k_2,n_-k_1)\,u_{c,\beta}(p)\,g_s^2\frac{1}{(n_-k_1)}\frac{1}{(n_-k_2)}\bar{u}_\lambda(k_1)\,v_\sigma(k_2) \tag{C.23}$$

Figure C.2: *Diagrams contributing to the matching of the two soft quark collinear functions. Soft lines are labelled with an "s". For the one-soft-particle reducible diagram, the internal gluon originates from the $n_+\mathcal{B}^+$ term in $\mathcal{L}^{(2)}$.*

The left-hand side of the matching equation is obtained by calculation of diagrams in figure C.2 using the NLP Feynman rules

$$
\langle q(k_1)\bar{q}(k_2)|\mathcal{T}_{\gamma f}(n_+q)|q(p)_q\rangle = 2\pi \frac{g_s}{n_-(k_1+k_2)}\mathbf{T}_{fq}^K\left[(k_{1\perp}^\eta + k_{2\perp}^\eta) - \frac{(k_{1\perp}+k_{2\perp})^2}{(n_-(k_1+k_2))}n_-^\eta\right]
$$

$$
\times\left(-\frac{1}{n_+p}\delta(n_+q - n_+p)\right)u_{c,\gamma}(p)\frac{1}{(k_1+k_2)^2}\bar{u}(k_1)g_s\mathbf{T}^K\gamma^\eta v(k_2)
$$

$$
-2\pi \frac{g_s}{(n_-(k_1+k_2))}\mathbf{T}_{fq}^K\left[2(k_1^\eta + k_2^\eta) - 2(k_{1\perp}^\eta + k_{2\perp}^\eta)\right.
$$

$$
\left.-2\frac{(k_1+k_2)^2}{n_-(k_1+k_2)}n_-^\eta + 2\frac{(k_{1\perp}+k_{2\perp})^2}{n_-(k_1+k_2)}n_-^\eta\right]u_{c,\gamma}(p)
$$

$$
\times\left(\frac{\partial}{\partial n_+q}\delta(n_+q - n_+p)\right)\times\frac{1}{(k_1+k_2)^2}\bar{u}(k_1)g_s\mathbf{T}^K\gamma^\eta v(k_2)
$$

$$
-2\pi\,\delta(n_+q - n_+p)g_s^2\frac{1}{n_+p}\frac{1}{(n_-(k_1+k_2))}\frac{1}{n_-k_1}\mathbf{T}_{f\,k_2}^A\frac{\slashed{n}_{-\gamma\eta}}{2}\gamma_{\perp,\eta\sigma}^\mu\,v_{s\sigma}(k_2)
$$

$$
\times\bar{u}_{s\lambda}(k_1)\,\gamma_{\perp,\lambda\beta,\mu}\mathbf{T}_{k_1\,q}^A\,u_{c,\beta}(p)\,. \tag{C.24}
$$

We can compare this with the right-hand side result (C.23) after substituting collinear functions from (C.19). We see that there are terms proportional to $\mathfrak{s}_1$ structure are reproduced. The leftover terms are identified with the J_5 collinear function, which is the remaining degree of freedom in the matching procedure. In the following equation, we have kept only the terms from the diagram calculation which were not obtained due to J_1 contributions

$$
\langle q(k_1)\bar{q}(k_2)|\mathcal{T}_{\gamma f}(n_+q)|q(p)_q\rangle_{\text{extra}} = 2\pi \frac{g_s}{(n_-(k_1+k_2))}\mathbf{T}_{fq}^K\left[-(k_1^\eta + k_2^\eta) + \frac{(k_1+k_2)^2}{n_-(k_1+k_2)}n_-^\eta\right]
$$

$$
\times\left(2\frac{\partial}{\partial n_+q}\delta(n_+q - n_+p)\right)u_{c,\gamma}(p)\frac{1}{(k_1+k_2)^2}\bar{u}(k_1)g_s\mathbf{T}^K\gamma^\eta v(k_2)
$$

$$
-2\pi\,\delta(n_+q - n_+p)g_s^2\frac{1}{n_+p}\frac{1}{(n_-(k_1+k_2))}\frac{1}{n_-k_1}\mathbf{T}_{f\,k_2}^A\frac{\slashed{n}_{-\gamma\eta}}{2}\gamma_{\perp,\eta\sigma}^\mu\,v_{s\sigma}(k_2)
$$

$$\times \bar{u}_{s\lambda}(k_1)\, \gamma_{\perp,\lambda\beta,\mu}\, \mathbf{T}^A_{k_1 q}\, u_{c,\beta}(p)\,. \tag{C.25}$$

The first term in the top line cancels using Dirac equation for the soft spinor $\slashed{k}_2 v(k_2) = 0$. The bottom two lines correspond to the contributions due to two $\mathcal{O}(\lambda)$ insertions of the Lagrangian terms with soft quarks. This leaves us with one extra term in the top line where the propagator cancels and this one corresponds precisely to the double soft quark term from the equation of motion relation for the $n_+\mathcal{B}$ field. Simplifying, we have

$$
\begin{aligned}
\langle q(k_1)\bar{q}(k_2)|\mathcal{T}_{\gamma f}(n_+q)|q(p)_q\rangle_{rem} \;=\;& 2\pi\, \mathbf{T}^K_{fq}\left(2\frac{\partial}{\partial n_+q}\delta(n_+q - n_+p)\right) u_{c,\gamma}(p) \\[2mm]
& \times \frac{g_s}{(n_-(k_1+k_2))^2} n_-^\eta\, \bar{u}_s(k_1) g_s \mathbf{T}^K \gamma^\eta v_s(k_2) \\[2mm]
& -2\pi\, \delta(n_+q - n_+p) g_s^2 \frac{1}{n_+p}\frac{1}{(n_-(k_1+k_2))}\frac{1}{n_-k_1}\mathbf{T}^A_{f\,k_2}\frac{\slashed{n}_{-\gamma\eta}}{2}\gamma^\mu_{\perp,\eta\sigma}\, v_{s\sigma}(k_2) \\[2mm]
& \times \bar{u}_{s\lambda}(k_1)\, \gamma_{\perp,\lambda\beta,\mu}\, \mathbf{T}^A_{k_1 q}\, u_{c,\beta}(p)\,.
\end{aligned}
\tag{C.26}
$$

Now matching the above left-hand side to the right-hand side of the matching equation in (C.23), excluding the J_1 proportional terms, namely

$$
\begin{aligned}
\langle q(k_1)\bar{q}(k_2)|\mathcal{T}_{\gamma f}(n_+q)|q(p)_q\rangle \;=\;& 2\pi\, J^{fk_2 k_1 q}_{5;\gamma\sigma\lambda\beta}\,(n_+q, n_+p;\, n_-k_2,\, n_-k_1)\, u_{c,\beta}(p) \\[2mm]
& \times g_s^2 \frac{1}{(n_-k_1)}\frac{1}{(n_-k_2)}\bar{u}_\lambda(k_1)\, v_\sigma(k_2)
\end{aligned}
\tag{C.27}
$$

Then we have

$$
\begin{aligned}
J^{fk_2 k_1 q}_{5;\gamma\sigma\lambda\beta}\,(n_+q, n_+p;\, n_-k_2,\, n_-k_1) \;=\;& \mathbf{T}^K_{fq}\mathbf{T}^K_{k_1 k_2}\left(2\frac{\partial}{\partial n_+q}\delta(n_+q - n_+p)\right) \\[2mm]
& \times \delta_{\gamma\beta}\frac{1}{(n_-(k_1+k_2))^2}(n_-k_1)(n_-k_2)\slashed{n}_{-\lambda\sigma} \\[2mm]
& -\mathbf{T}^A_{f\,k_2}\mathbf{T}^A_{k_1 q}\frac{1}{n_+p}\frac{1}{(n_-(k_1+k_2))}n_-k_2\frac{\slashed{n}_{-\gamma\eta}}{2}\gamma^\mu_{\perp,\eta\sigma}\,\gamma_{\perp,\lambda\beta,\mu}\,.
\end{aligned}
\tag{C.28}
$$

We also obtain the derivative piece of the collinear function directly from (4.13) at the operator level using the equation-of-motion relation as done between equations (C.11) and (C.16) above

$$
\begin{aligned}
\mathcal{T}^{1g}_{\gamma f}(n_+q)_{\mathcal{L}^{(2)}_{1\xi}} \;=\;& -2\pi\left\{ -2\frac{i\partial^\mu_\perp}{in_-\partial}\mathcal{B}^+_{\mu_\perp}(z_-) \right. \\[2mm]
& -2\frac{1}{(in_-\partial)^2}\left[\mathcal{B}^{+\,\mu_\perp}(z_-),\left[in_-\partial\mathcal{B}^+_{\mu_\perp}(z_-)\right]\right] \\[2mm]
& \left. -2\frac{g_s^2}{(in_-\partial)^2}\mathbf{T}^K\,\bar{q}_+(z_-)\,\mathbf{T}^K\slashed{n}_- q_+(z_-)\right\} \\[2mm]
& \times \chi_{c,\gamma}\left(\frac{\partial}{\partial n_+q}\delta(n_+q - n_+p)\right)\,.
\end{aligned}
\tag{C.29}
$$

The top two terms we have discussed previously, and the last one with soft quarks is the one-soft-particle reducible contribution to the J_5 collinear function.

Bibliography

[1] S. Glashow, *Partial Symmetries of Weak Interactions*, *Nucl. Phys.* **22** (1961) 579–588.

[2] S. Weinberg, *A Model of Leptons*, *Phys. Rev. Lett.* **19** (1967) 1264–1266.

[3] A. Salam, *Weak and Electromagnetic Interactions*, *Conf. Proc. C* **680519** (1968) 367–377.

[4] G. 't Hooft and M. Veltman, *Regularization and Renormalization of Gauge Fields*, *Nucl. Phys. B* **44** (1972) 189–213.

[5] ATLAS collaboration, G. Aad et al., *Observation of a new particle in the search for the Standard Model Higgs boson with the ATLAS detector at the LHC*, *Phys. Lett. B* **716** (2012) 1–29, [1207.7214].

[6] CMS collaboration, S. Chatrchyan et al., *Observation of a New Boson at a Mass of 125 GeV with the CMS Experiment at the LHC*, *Phys. Lett. B* **716** (2012) 30–61, [1207.7235].

[7] O. Brüning and L. Rossi, eds., *The High Luminosity Large Hadron Collider: the new machine for illuminating the mysteries of Universe*, vol. 24. 2015, 10.1142/9581.

[8] D. J. Gross and F. Wilczek, *Ultraviolet Behavior of Nonabelian Gauge Theories*, *Phys. Rev. Lett.* **30** (1973) 1343–1346.

[9] H. Politzer, *Reliable Perturbative Results for Strong Interactions?*, *Phys. Rev. Lett.* **30** (1973) 1346–1349.

[10] Particle Data Group collaboration, P. A. Zyla et al., *Review of Particle Physics*, *PTEP* **2020** (2020) 083C01.

[11] C. Anastasiou, C. Duhr, F. Dulat, F. Herzog and B. Mistlberger, *Higgs Boson Gluon-Fusion Production in QCD at Three Loops*, *Phys. Rev. Lett.* **114** (2015) 212001, [1503.06056].

[12] B. Mistlberger, *Higgs boson production at hadron colliders at N^3LO in QCD*, *JHEP* **05** (2018) 028, [1802.00833].

[13] F. A. Dreyer and A. Karlberg, *Vector-Boson Fusion Higgs Production at Three Loops in QCD*, *Phys. Rev. Lett.* **117** (2016) 072001, [1606.00840].

[14] C. Duhr, F. Dulat and B. Mistlberger, *Drell-Yan Cross Section to Third Order in the Strong Coupling Constant*, *Phys. Rev. Lett.* **125** (2020) 172001, [2001.07717].

[15] C. Duhr, F. Dulat and B. Mistlberger, *Charged current Drell-Yan production at N³LO, JHEP* **11** (2020) 143, [2007.13313].

[16] F. Caola, A. Von Manteuffel and L. Tancredi, *Diphoton Amplitudes in Three-Loop Quantum Chromodynamics, Phys. Rev. Lett.* **126** (2021) 112004, [2011.13946].

[17] S. Amoroso et al., *Les Houches 2019: Physics at TeV Colliders: Standard Model Working Group Report*, in *11th Les Houches Workshop on Physics at TeV Colliders: PhysTeV Les Houches*, 3, 2020, 2003.01700.

[18] G. Heinrich, *Collider Physics at the Precision Frontier*, 2009.00516.

[19] J. C. Collins, D. E. Soper and G. F. Sterman, *Factorization for Short Distance Hadron - Hadron Scattering, Nucl. Phys.* **B261** (1985) 104–142.

[20] G. Sterman, *Summation of Large Corrections to Short Distance Hadronic Cross-Sections, Nucl. Phys.* **B281** (1987) 310.

[21] S. Catani and L. Trentadue, *Resummation of the QCD Perturbative Series for Hard Processes, Nucl. Phys.* **B327** (1989) 323–352.

[22] A. Idilbi and X.-d. Ji, *Threshold resummation for Drell-Yan process in soft-collinear effective theory, Phys. Rev.* **D72** (2005) 054016, [hep-ph/0501006].

[23] A. Idilbi, X.-d. Ji and F. Yuan, *Resummation of threshold logarithms in effective field theory for DIS, Drell-Yan and Higgs production, Nucl. Phys.* **B753** (2006) 42–68, [hep-ph/0605068].

[24] T. Becher, M. Neubert and G. Xu, *Dynamical Threshold Enhancement and Resummation in Drell- Yan Production, JHEP* **07** (2008) 030, [0710.0680].

[25] S. Moch and A. Vogt, *Higher-order soft corrections to lepton pair and Higgs boson production, Phys. Lett.* **B631** (2005) 48–57, [hep-ph/0508265].

[26] S. Moch, J. A. M. Vermaseren and A. Vogt, *Higher-order corrections in threshold resummation, Nucl. Phys.* **B726** (2005) 317–335, [hep-ph/0506288].

[27] T. Becher, M. Neubert and B. D. Pecjak, *Factorization and Momentum-Space Resummation in Deep-Inelastic Scattering, JHEP* **01** (2007) 076, [hep-ph/0607228].

[28] W. Bizon, A. Gehrmann-De Ridder, T. Gehrmann, N. Glover, A. Huss, P. F. Monni et al., *The transverse momentum spectrum of weak gauge bosons at N^3 LL + NNLO, Eur. Phys. J. C* **79** (2019) 868, [1905.05171].

[29] S. Dawson, P. Jaiswal, Y. Li, H. Ramani and M. Zeng, *Resummation of jet veto logarithms at N^3LL_a + NNLO for W^+W^- production at the LHC, Phys. Rev. D* **94** (2016) 114014, [1606.01034].

[30] A. H. Hoang, D. W. Kolodrubetz, V. Mateu and I. W. Stewart, *Precise determination of α_s from the C-parameter distribution, Phys. Rev. D* **91** (2015) 094018, [1501.04111].

[31] D. Bonocore, E. Laenen, L. Magnea, L. Vernazza and C. D. White, *The method of regions and next-to-soft corrections in Drell-Yan production*, *Phys. Lett.* **B742** (2015) 375–382, [`1410.6406`].

[32] N. Bahjat-Abbas, J. Sinninghe Damsté, L. Vernazza and C. D. White, *On next-to-leading power threshold corrections in Drell-Yan production at N³LO*, *JHEP* **10** (2018) 144, [`1807.09246`].

[33] E. Laenen, L. Magnea and G. Stavenga, *On next-to-eikonal corrections to threshold resummation for the Drell-Yan and DIS cross sections*, *Phys. Lett.* **B669** (2008) 173–179, [`0807.4412`].

[34] E. Laenen, G. Stavenga and C. D. White, *Path integral approach to eikonal and next-to-eikonal exponentiation*, *JHEP* **03** (2009) 054, [`0811.2067`].

[35] E. Laenen, L. Magnea, G. Stavenga and C. D. White, *Next-to-eikonal corrections to soft gluon radiation: a diagrammatic approach*, *JHEP* **01** (2011) 141, [`1010.1860`].

[36] D. Bonocore, E. Laenen, L. Magnea, S. Melville, L. Vernazza and C. D. White, *A factorization approach to next-to-leading-power threshold logarithms*, *JHEP* **06** (2015) 008, [`1503.05156`].

[37] D. Bonocore, E. Laenen, L. Magnea, L. Vernazza and C. D. White, *Non-abelian factorisation for next-to-leading-power threshold logarithms*, *JHEP* **12** (2016) 121, [`1610.06842`].

[38] C. White, *Diagrammatic insights into next-to-soft corrections*, *Phys. Lett. B* **737** (2014) 216–222, [`1406.7184`].

[39] V. Del Duca, E. Laenen, L. Magnea, L. Vernazza and C. D. White, *Universality of next-to-leading power threshold effects for colourless final states in hadronic collisions*, *JHEP* **11** (2017) 057, [`1706.04018`].

[40] M. Beneke, A. Broggio, M. Garny, S. Jaskiewicz, R. Szafron, L. Vernazza et al., *Leading-logarithmic threshold resummation of the Drell-Yan process at next-to-leading power*, *JHEP* **03** (2019) 043, [`1809.10631`].

[41] M. Beneke, M. Garny, S. Jaskiewicz, R. Szafron, L. Vernazza and J. Wang, *Leading-logarithmic threshold resummation of Higgs production in gluon fusion at next-to-leading power*, *JHEP* **01** (2020) 094, [`1910.12685`].

[42] N. Bahjat-Abbas, D. Bonocore, J. Sinninghe Damsté, E. Laenen, L. Magnea, L. Vernazza et al., *Diagrammatic resummation of leading-logarithmic threshold effects at next-to-leading power*, *JHEP* **11** (2019) 002, [`1905.13710`].

[43] A. H. Ajjath, P. Mukherjee and V. Ravindran, *On next to soft corrections to Drell-Yan and Higgs Boson productions*, `2006.06726`.

[44] R. Boughezal, X. Liu and F. Petriello, *Power Corrections in the N-jettiness Subtraction Scheme*, *JHEP* **03** (2017) 160, [`1612.02911`].

[45] I. Moult, L. Rothen, I. W. Stewart, F. J. Tackmann and H. X. Zhu, *Subleading Power Corrections for N-Jettiness Subtractions*, *Phys. Rev.* **D95** (2017) 074023, [1612.00450].

[46] I. Moult, L. Rothen, I. W. Stewart, F. J. Tackmann and H. X. Zhu, *N -jettiness subtractions for $gg \to H$ at subleading power*, *Phys. Rev.* **D97** (2018) 014013, [1710.03227].

[47] M. A. Ebert, I. Moult, I. W. Stewart, F. J. Tackmann, G. Vita and H. X. Zhu, *Power Corrections for N-Jettiness Subtractions at $\mathcal{O}(\alpha_s)$*, *JHEP* **12** (2018) 084, [1807.10764].

[48] R. Boughezal, A. Isgró and F. Petriello, *Next-to-leading-logarithmic power corrections for N-jettiness subtraction in color-singlet production*, *Phys. Rev.* **D97** (2018) 076006, [1802.00456].

[49] R. Boughezal, A. Isgró and F. Petriello, *Next-to-leading power corrections to $V + 1$ jet production in N-jettiness subtraction*, *Phys. Rev.* **D101** (2020) 016005, [1907.12213].

[50] M. A. Ebert, I. Moult, I. W. Stewart, F. J. Tackmann, G. Vita and H. X. Zhu, *Subleading power rapidity divergences and power corrections for q_T*, *JHEP* **04** (2019) 123, [1812.08189].

[51] L. Cieri, C. Oleari and M. Rocco, *Higher-order power corrections in a transverse-momentum cut for colour-singlet production at NLO*, *Eur. Phys. J.* **C79** (2019) 852, [1906.09044].

[52] M. A. Ebert, J. K. L. Michel, I. W. Stewart and F. J. Tackmann, *Drell-Yan q_T Resummation of Fiducial Power Corrections at N^3LL*, *JHEP* **04** (2021) 102, [2006.11382].

[53] M. van Beekveld, W. Beenakker, E. Laenen and C. D. White, *Next-to-leading power threshold effects for inclusive and exclusive processes with final state jets*, *JHEP* **03** (2020) 106, [1905.08741].

[54] I. Moult, I. W. Stewart, G. Vita and H. X. Zhu, *First Subleading Power Resummation for Event Shapes*, *JHEP* **08** (2018) 013, [1804.04665].

[55] I. Moult, G. Vita and K. Yan, *Subleading power resummation of rapidity logarithms: the energy-energy correlator in $\mathcal{N} = 4$ SYM*, *JHEP* **07** (2020) 005, [1912.02188].

[56] Z. L. Liu and M. Neubert, *Factorization at subleading power and endpoint-divergent convolutions in $h \to \gamma\gamma$ decay*, *JHEP* **04** (2020) 033, [1912.08818].

[57] Z. L. Liu, B. Mecaj, M. Neubert and X. Wang, *Factorization at subleading power and endpoint divergences in $h \to \gamma\gamma$ decay. Part II. Renormalization and scale evolution*, *JHEP* **01** (2021) 077, [2009.06779].

[58] T. Liu and A. A. Penin, *High-Energy Limit of QCD beyond the Sudakov Approximation, Phys. Rev. Lett.* **119** (2017) 262001, [1709.01092].

[59] T. Liu and A. Penin, *High-Energy Limit of Mass-Suppressed Amplitudes in Gauge Theories, JHEP* **11** (2018) 158, [1809.04950].

[60] J. Wang, *Resummation of double logarithms in loop-induced processes with effective field theory*, 1912.09920.

[61] C. Anastasiou and A. Penin, *Light Quark Mediated Higgs Boson Threshold Production in the Next-to-Leading Logarithmic Approximation, JHEP* **07** (2020) 195, [2004.03602].

[62] Z. L. Liu, B. Mecaj, M. Neubert and X. Wang, *Factorization at Subleading Power and Endpoint Divergences in Soft-Collinear Effective Theory*, [2009.04456].

[63] M. Beneke, C. Bobeth and R. Szafron, *Enhanced electromagnetic correction to the rare B-meson decay $B_{s,d} \to \mu^+\mu^-$, Phys. Rev. Lett.* **120** (2018) 011801, [1708.09152].

[64] M. Beneke, C. Bobeth and R. Szafron, *Power-enhanced leading-logarithmic QED corrections to $B_q \to \mu^+\mu^-$, JHEP* **10** (2019) 232, [1908.07011].

[65] M. Beneke, A. Broggio, S. Jaskiewicz and L. Vernazza, *Threshold factorization of the Drell-Yan process at next-to-leading power, JHEP* **07** (2020) 078, [1912.01585].

[66] M. Beneke, M. Garny, S. Jaskiewicz, R. Szafron, L. Vernazza and J. Wang, *Large-x resummation of off-diagonal deep-inelastic parton scattering from d-dimensional refactorization, JHEP* **10** (2020) 196, [2008.04943].

[67] S. Jaskiewicz, *Next-to-leading power threshold factorization for Drell-Yan production*, in *Proceedings, 14th International Symposium on Radiative Corrections: Application of Quantum Field Theory to Phenomenology (RADCOR 2019): Avignon, France, September 8-13, 2019*, 2019, 1912.08882, DOI.

[68] A. Broggio, S. Jaskiewicz and L. Vernazza, in preparation.

[69] C. W. Bauer, S. Fleming and M. E. Luke, *Summing Sudakov logarithms in B —> X(s gamma) in effective field theory, Phys. Rev. D* **63** (2000) 014006, [hep-ph/0005275].

[70] C. W. Bauer, S. Fleming, D. Pirjol and I. W. Stewart, *An Effective field theory for collinear and soft gluons: Heavy to light decays, Phys. Rev.* **D63** (2001) 114020, [hep-ph/0011336].

[71] C. W. Bauer, D. Pirjol and I. W. Stewart, *Soft collinear factorization in effective field theory, Phys. Rev.* **D65** (2002) 054022, [hep-ph/0109045].

[72] M. Beneke, A. P. Chapovsky, M. Diehl and T. Feldmann, *Soft collinear effective theory and heavy to light currents beyond leading power, Nucl. Phys.* **B643** (2002) 431–476, [hep-ph/0206152].

[73] M. Beneke and T. Feldmann, *Multipole expanded soft collinear effective theory with non-abelian gauge symmetry, Phys. Lett.* **B553** (2003) 267–276, [`hep-ph/0211358`].

[74] G. P. Korchemsky and G. F. Sterman, *Infrared factorization in inclusive B meson decays, Phys. Lett. B* **340** (1994) 96–108, [`hep-ph/9407344`].

[75] M. Beneke, F. Campanario, T. Mannel and B. D. Pecjak, *Power corrections to $\bar{B} \to X_u \ell \bar{\nu} (X_s \gamma)$ decay spectra in the 'shape-function' region, JHEP* **06** (2005) 071, [`hep-ph/0411395`].

[76] C. W. Bauer and A. V. Manohar, *Shape function effects in B —> X(s) gamma and B —> X(u) l anti-nu decays, Phys. Rev. D* **70** (2004) 034024, [`hep-ph/0312109`].

[77] T. Becher and M. Neubert, *Analysis of Br(anti-B —> X(s gamma)) at NNLO with a cut on photon energy, Phys. Rev. Lett.* **98** (2007) 022003, [`hep-ph/0610067`].

[78] M. Neubert, *Renormalization-group improved calculation of the B —> X(s) gamma branching ratio, Eur. Phys. J. C* **40** (2005) 165–186, [`hep-ph/0408179`].

[79] T. Becher, A. Broggio and A. Ferroglia, *Introduction to Soft-Collinear Effective Theory, Lect. Notes Phys.* **896** (2015) 1–206, [`1410.1892`].

[80] T. Becher, *Soft-Collinear Effective Theory, Les Houches Lect. Notes* **108** (2020) , [`1803.04310`].

[81] T. Cohen, *As Scales Become Separated: Lectures on Effective Field Theory, PoS* **TASI2018** (2019) 011, [`1903.03622`].

[82] M. Neubert, *Renormalization Theory and Effective Field Theories, Les Houches Lect. Notes* **108** (2020) , [`1901.06573`].

[83] M. Beneke, *Lectures at the Helmholtz International Summer School on Heavy Quark Physics, Dubna, Russia,* http://theor.jinr.ru/~hq2005/Lectures/Beneke/Beneke-Dubna-05.pdf , 6 – 16 June 2005.

[84] I. Stewart, *Lectures on the Soft-Collinear Effective Theory,* https://ocw.mit.edu/courses/physics/8-851-effective-field-theory-spring-2013/lecture-notes/MIT8-851S13-scetnotes.pdf , 23 December 2013.

[85] M. D. Schwartz, *Quantum Field Theory and the Standard Model.* Cambridge University Press, 3, 2014.

[86] M. Beneke, M. Garny, R. Szafron and J. Wang, *Anomalous dimension of subleading-power N-jet operators, JHEP* **03** (2018) 001, [`1712.04416`].

[87] M. Beneke, M. Garny, R. Szafron and J. Wang, *Anomalous dimension of subleading-power N-jet operators. Part II, JHEP* **11** (2018) 112, [`1808.04742`].

[88] M. Beneke, M. Garny, R. Szafron and J. Wang, *Violation of the Kluberg-Stern-Zuber theorem in SCET*, *JHEP* **09** (2019) 101, [1907.05463].

[89] M. Beneke and V. A. Smirnov, *Asymptotic expansion of Feynman integrals near threshold*, *Nucl. Phys.* **B522** (1998) 321–344, [hep-ph/9711391].

[90] V. A. Smirnov, *Applied asymptotic expansions in momenta and masses*, *Springer Tracts Mod. Phys.* **177** (2002) 1–262.

[91] M. Srednicki, *Quantum field theory.* Cambridge University Press, 1, 2007.

[92] R. J. Hill and M. Neubert, *Spectator interactions in soft collinear effective theory*, *Nucl. Phys. B* **657** (2003) 229–256, [hep-ph/0211018].

[93] P. Baikov, K. Chetyrkin, A. Smirnov, V. Smirnov and M. Steinhauser, *Quark and gluon form factors to three loops*, *Phys. Rev. Lett.* **102** (2009) 212002, [0902.3519].

[94] T. Gehrmann, E. Glover, T. Huber, N. Ikizlerli and C. Studerus, *The quark and gluon form factors to three loops in QCD through to $O(\epsilon^2)$*, *JHEP* **11** (2010) 102, [1010.4478].

[95] T. Gehrmann, E. W. N. Glover, T. Huber, N. Ikizlerli and C. Studerus, *Calculation of the quark and gluon form factors to three loops in QCD*, *JHEP* **06** (2010) 094, [1004.3653].

[96] F. E. Low, *Bremsstrahlung of very low-energy quanta in elementary particle collisions*, *Phys. Rev.* **110** (1958) 974–977.

[97] T. H. Burnett and N. M. Kroll, *Extension of the low soft photon theorem*, *Phys. Rev. Lett.* **20** (1968) 86.

[98] R. J. Hill, T. Becher, S. J. Lee and M. Neubert, *Sudakov resummation for subleading SCET currents and heavy-to-light form-factors*, *JHEP* **07** (2004) 081, [hep-ph/0404217].

[99] M. Beneke and D. Yang, *Heavy-to-light B meson form-factors at large recoil energy: Spectator-scattering corrections*, *Nucl. Phys.* **B736** (2006) 34–81, [hep-ph/0508250].

[100] S. M. Freedman and R. Goerke, *Renormalization of Subleading Dijet Operators in Soft-Collinear Effective Theory*, *Phys. Rev.* **D90** (2014) 114010, [1408.6240].

[101] R. Goerke and M. Inglis-Whalen, *Renormalization of dijet operators at order $1/Q^2$ in soft-collinear effective theory*, *JHEP* **05** (2018) 023, [1711.09147].

[102] C. Marcantonini and I. W. Stewart, *Reparameterization Invariant Collinear Operators*, *Phys. Rev.* **D79** (2009) 065028, [0809.1093].

[103] D. W. Kolodrubetz, I. Moult and I. W. Stewart, *Building Blocks for Subleading Helicity Operators*, *JHEP* **05** (2016) 139, [1601.02607].

[104] I. Feige, D. W. Kolodrubetz, I. Moult and I. W. Stewart, *A Complete Basis of Helicity Operators for Subleading Factorization*, *JHEP* **11** (2017) 142, [`1703.03411`].

[105] I. Moult, I. W. Stewart and G. Vita, *A subleading operator basis and matching for $gg \to H$*, *JHEP* **07** (2017) 067, [`1703.03408`].

[106] S. Drell and T. M. Yan, *Massive Lepton Pair Production in Hadron-Hadron Collisions at High-Energies*, *Phys. Rev. Lett.* **25** (1970) 316–320.

[107] J. H. Christenson, G. S. Hicks, L. M. Lederman, P. J. Limon, B. G. Pope and E. Zavattini, *Observation of massive muon pairs in hadron collisions*, *Phys. Rev. Lett.* **25** (Nov, 1970) 1523–1526.

[108] E598 collaboration, J. Aubert et al., *Experimental Observation of a Heavy Particle J*, *Phys. Rev. Lett.* **33** (1974) 1404–1406.

[109] J. E. Augustin, A. M. Boyarski, M. Breidenbach, F. Bulos, J. T. Dakin, G. J. Feldman et al., *Discovery of a narrow resonance in e^+e^- annihilation*, *Phys. Rev. Lett.* **33** (Dec, 1974) 1406–1408.

[110] UA1 collaboration, G. Arnison et al., *Experimental Observation of Isolated Large Transverse Energy Electrons with Associated Missing Energy at s**(1/2) = 540-GeV*, *Phys. Lett. B* **122** (1983) 103–116.

[111] UA1 collaboration, G. Arnison et al., *Experimental Observation of Lepton Pairs of Invariant Mass Around 95-GeV/c**2 at the CERN SPS Collider*, *Phys. Lett. B* **126** (1983) 398–410.

[112] UA2 collaboration, P. Bagnaia et al., *Evidence for $Z^0 \to e^+e^-$ at the CERN $\bar{p}p$ Collider*, *Phys. Lett. B* **129** (1983) 130–140.

[113] UA2 collaboration, M. Banner et al., *Observation of Single Isolated Electrons of High Transverse Momentum in Events with Missing Transverse Energy at the CERN anti-p p Collider*, *Phys. Lett. B* **122** (1983) 476–485.

[114] G. Altarelli, R. Ellis and G. Martinelli, *Leptoproduction and Drell-Yan Processes Beyond the Leading Approximation in Chromodynamics*, *Nucl. Phys. B* **143** (1978) 521.

[115] G. Altarelli, R. Ellis and G. Martinelli, *Large Perturbative Corrections to the Drell-Yan Process in QCD*, *Nucl. Phys. B* **157** (1979) 461–497.

[116] R. Hamberg, W. L. van Neerven and T. Matsuura, *A complete calculation of the order α_s^2 correction to the Drell-Yan K factor*, *Nucl. Phys.* **B359** (1991) 343–405.

[117] T. Matsuura and W. L. van Neerven, *Second Order Logarithmic Corrections to the Drell-Yan Cross-section*, *Z. Phys.* **C38** (1988) 623.

[118] T. Matsuura, S. van der Marck and W. van Neerven, *The Order α_s^2 Contribution to the K Factor of the Drell-Yan Process*, *Phys. Lett. B* **211** (1988) 171–178.

[119] T. Matsuura, S. van der Marck and W. van Neerven, *The Calculation of the Second Order Soft and Virtual Contributions to the Drell-Yan Cross-Section, Nucl. Phys. B* **319** (1989) 570–622.

[120] T. Matsuura, R. Hamberg and W. van Neerven, *The Contribution of the Gluon-gluon Subprocess to the Drell-Yan K Factor, Nucl. Phys. B* **345** (1990) 331–368.

[121] W. van Neerven and E. Zijlstra, *The $O(\alpha_s^2)$ corrected Drell-Yan K factor in the DIS and MS scheme, Nucl. Phys. B* **382** (1992) 11–62.

[122] R. V. Harlander and W. B. Kilgore, *Next-to-next-to-leading order Higgs production at hadron colliders, Phys. Rev. Lett.* **88** (2002) 201801, [`hep-ph/0201206`].

[123] U. Baur, O. Brein, W. Hollik, C. Schappacher and D. Wackeroth, *Electroweak radiative corrections to neutral current Drell-Yan processes at hadron colliders, Phys. Rev. D* **65** (2002) 033007, [`hep-ph/0108274`].

[124] U. Baur, S. Keller and W. Sakumoto, *QED radiative corrections to Z boson production and the forward backward asymmetry at hadron colliders, Phys. Rev. D* **57** (1998) 199–215, [`hep-ph/9707301`].

[125] M. Delto, M. Jaquier, K. Melnikov and R. Röntsch, *Mixed QCD⊗QED corrections to on-shell Z boson production at the LHC, JHEP* **01** (2020) 043, [`1909.08428`].

[126] R. Bonciani, F. Buccioni, N. Rana, I. Triscari and A. Vicini, *NNLO QCD×EW corrections to Z production in the qq̄ channel, Phys. Rev. D* **101** (2020) 031301, [`1911.06200`].

[127] G. Lustermans, J. K. Michel and F. J. Tackmann, *Generalized Threshold Factorization with Full Collinear Dynamics*, `1908.00985`.

[128] G. P. Korchemsky and G. Marchesini, *Resummation of large infrared corrections using Wilson loops, Phys. Lett.* **B313** (1993) 433–440.

[129] G. Falcioni, E. Gardi and C. Milloy, *Relating amplitude and PDF factorisation through Wilson-line geometries, JHEP* **11** (2019) 100, [`1909.00697`].

[130] V. Del Duca, *High-energy Bremsstrahlung Theorems for Soft Photons, Nucl. Phys.* **B345** (1990) 369–388.

[131] S. W. Bosch, M. Neubert and G. Paz, *Subleading shape functions in inclusive B decays, JHEP* **11** (2004) 073, [`hep-ph/0409115`].

[132] K. S. M. Lee and I. W. Stewart, *Factorization for power corrections to $B \to X_s\gamma$ and $B \to X_u\ell\bar{\nu}$, Nucl. Phys.* **B721** (2005) 325–406, [`hep-ph/0409045`].

[133] M. Beneke, P. Falgari and C. Schwinn, *Threshold resummation for pair production of coloured heavy (s)particles at hadron colliders, Nucl. Phys.* **B842** (2011) 414–474, [`1007.5414`].

[134] A. Vogt, *Leading logarithmic large-x resummation of off-diagonal splitting functions and coefficient functions*, *Phys. Lett. B* **691** (2010) 77–81, [`1005.1606`].

[135] I. Moult, I. W. Stewart, G. Vita and H. X. Zhu, *The Soft Quark Sudakov*, *JHEP* **05** (2020) 089, [`1910.14038`].

[136] A. J. Larkoski, D. Neill and I. W. Stewart, *Soft Theorems from Effective Field Theory*, *JHEP* **06** (2015) 077, [`1412.3108`].

[137] M. Beneke, M. Garny, R. Szafron and J. Wang, *Subleading-power N-jet operators and the LBK amplitude in SCET*, *PoS* **RADCOR2017** (2017) 048, [`1712.07462`].

[138] E. Laenen, J. Sinninghe Damsté, L. Vernazza, W. Waalewijn and L. Zoppi, *Towards all-order factorization of QED amplitudes at next-to-leading power*, *Phys. Rev. D* **103** (2021) 034022, [`2008.01736`].

[139] Y. Li, S. Mantry and F. Petriello, *An Exclusive Soft Function for Drell-Yan at Next-to-Next-to-Leading Order*, *Phys. Rev.* **D84** (2011) 094014, [`1105.5171`].

[140] K. G. Chetyrkin and F. V. Tkachov, *Integration by Parts: The Algorithm to Calculate beta Functions in 4 Loops*, *Nucl. Phys. B* **192** (1981) 159–204.

[141] F. V. Tkachov, *A Theorem on Analytical Calculability of Four Loop Renormalization Group Functions*, *Phys. Lett. B* **100** (1981) 65–68.

[142] E. Remiddi, *Differential equations for Feynman graph amplitudes*, *Nuovo Cim. A* **110** (1997) 1435–1452, [`hep-th/9711188`].

[143] S. Laporta, *High precision calculation of multiloop Feynman integrals by difference equations*, *Int. J. Mod. Phys. A* **15** (2000) 5087–5159, [`hep-ph/0102033`].

[144] R. N. Lee, *Presenting LiteRed: a tool for the Loop InTEgrals REDuction*, `1212.2685`.

[145] R. N. Lee, *LiteRed 1.4: a powerful tool for reduction of multiloop integrals*, *J. Phys. Conf. Ser.* **523** (2014) 012059, [`1310.1145`].

[146] C. Anastasiou and K. Melnikov, *Higgs boson production at hadron colliders in NNLO QCD*, *Nucl. Phys. B* **646** (2002) 220–256, [`hep-ph/0207004`].

[147] A. V. Smirnov and F. S. Chuharev, *FIRE6: Feynman Integral REduction with Modular Arithmetic*, *Comput. Phys. Commun.* **247** (2020) 106877, [`1901.07808`].

[148] A. von Manteuffel and C. Studerus, *Reduze 2 - Distributed Feynman Integral Reduction*, `1201.4330`.

[149] T. Becher, G. Bell and S. Marti, *NNLO soft function for electroweak boson production at large transverse momentum*, *JHEP* **04** (2012) 034, [`1201.5572`].

[150] L. Vernazza, private communication.

[151] T. Huber and D. Maitre, *HypExp: A Mathematica package for expanding hypergeometric functions around integer-valued parameters*, *Comput. Phys. Commun.* **175** (2006) 122–144, [`hep-ph/0507094`].

[152] T. Becher and G. Bell, *The gluon jet function at two-loop order*, *Phys. Lett.* **B695** (2011) 252–258, [`1008.1936`].

[153] M. Kramer, E. Laenen and M. Spira, *Soft gluon radiation in Higgs boson production at the LHC*, *Nucl. Phys.* **B511** (1998) 523–549, [`hep-ph/9611272`].

[154] N. Kidonakis, *Collinear and soft gluon corrections to Higgs production at NNNLO*, *Phys. Rev.* **D77** (2008) 053008, [`0711.0142`].

[155] D. de Florian, J. Mazzitelli, S. Moch and A. Vogt, *Approximate N^3LO Higgs-boson production cross section using physical-kernel constraints*, *JHEP* **10** (2014) 176, [`1408.6277`].

[156] M. Beneke and L. Vernazza, $B \to \chi_{cJ}K$ *decays revisited*, *Nucl. Phys. B* **811** (2009) 155–181, [`0810.3575`].

[157] M. Benzke, S. J. Lee, M. Neubert and G. Paz, *Factorization at Subleading Power and Irreducible Uncertainties in* $\bar{B} \to X_s\gamma$ *Decay*, *JHEP* **08** (2010) 099, [`1003.5012`].

[158] A. Almasy, G. Soar and A. Vogt, *Generalized double-logarithmic large-x resummation in inclusive deep-inelastic scattering*, *JHEP* **03** (2011) 030, [`1012.3352`].

[159] A. Vogt, C. Kom, N. Lo Presti, G. Soar, A. Almasy, S. Moch et al., *Progress on double-logarithmic large-x and small-x resummations for (semi-)inclusive hard processes*, *PoS* **LL2012** (2012) 004, [`1212.2932`].

[160] LHC Higgs Cross Section Working Group collaboration, D. de Florian et al., *Handbook of LHC Higgs Cross Sections: 4. Deciphering the Nature of the Higgs Sector*, `1610.07922`.

[161] J. F. Gunion, H. E. Haber, G. L. Kane and S. Dawson, *The Higgs Hunter's Guide*, vol. 80. 2000.

[162] LHC Higgs Cross Section Working Group collaboration, S. Dittmaier et al., *Handbook of LHC Higgs Cross Sections: 1. Inclusive Observables*, `1101.0593`.

[163] S. Dawson et al., *Working Group Report: Higgs Boson*, in *Community Summer Study 2013: Snowmass on the Mississippi*, 10, 2013, `1310.8361`.

[164] C. Anastasiou, C. Duhr, F. Dulat, E. Furlan, T. Gehrmann, F. Herzog et al., *Higgs boson gluon–fusion production at threshold in N^3LO QCD*, *Phys. Lett. B* **737** (2014) 325–328, [`1403.4616`].

[165] C. Anastasiou, C. Duhr, F. Dulat, F. Herzog and B. Mistlberger, *Higgs Boson Gluon-Fusion Production in QCD at Three Loops*, *Phys. Rev. Lett.* **114** (2015) 212001, [1503.06056].

[166] C. Anastasiou, C. Duhr, F. Dulat, E. Furlan, T. Gehrmann, F. Herzog et al., *High precision determination of the gluon fusion Higgs boson cross-section at the LHC*, *JHEP* **05** (2016) 058, [1602.00695].

[167] F. Dulat, B. Mistlberger and A. Pelloni, *Precision predictions at N^3LO for the Higgs boson rapidity distribution at the LHC*, *Phys. Rev.* **D99** (2019) 034004, [1810.09462].

[168] V. Ahrens, T. Becher, M. Neubert and L. L. Yang, *Renormalization-Group Improved Prediction for Higgs Production at Hadron Colliders*, *Eur. Phys. J.* **C62** (2009) 333–353, [0809.4283].

[169] E. Laenen and L. Magnea, *Threshold resummation for electroweak annihilation from DIS data*, *Phys. Lett.* **B632** (2006) 270–276, [hep-ph/0508284].

[170] A. Idilbi, X.-d. Ji, J.-P. Ma and F. Yuan, *Threshold resummation for Higgs production in effective field theory*, *Phys. Rev.* **D73** (2006) 077501, [hep-ph/0509294].

[171] M. Bonvini and S. Marzani, *Resummed Higgs cross section at N^3LL*, *JHEP* **09** (2014) 007, [1405.3654].

[172] G. Bell, M. Beneke, T. Huber and X.-Q. Li, *Heavy-to-light currents at NNLO in SCET and semi-inclusive $\bar{B} \to X_s l^+ l^-$ decay*, *Nucl. Phys.* **B843** (2011) 143–176, [1007.3758].

[173] C. Anastasiou, C. Duhr, F. Dulat, E. Furlan, T. Gehrmann, F. Herzog et al., *Higgs Boson Gluon-Fusion Production Beyond Threshold in N^3LO QCD*, *JHEP* **03** (2015) 091, [1411.3584].

[174] A. Buckley, J. Ferrando, S. Lloyd, K. Nordström, B. Page, M. Rüfenacht et al., *LHAPDF6: parton density access in the LHC precision era*, *Eur. Phys. J.* **C75** (2015) 132, [1412.7420].

[175] J. Butterworth et al., *PDF4LHC recommendations for LHC Run II*, *J. Phys.* **G43** (2016) 023001, [1510.03865].

[176] S. Dulat, T.-J. Hou, J. Gao, M. Guzzi, J. Huston, P. Nadolsky et al., *New parton distribution functions from a global analysis of quantum chromodynamics*, *Phys. Rev.* **D93** (2016) 033006, [1506.07443].

[177] L. A. Harland-Lang, A. D. Martin, P. Motylinski and R. S. Thorne, *Parton distributions in the LHC era: MMHT 2014 PDFs*, *Eur. Phys. J.* **C75** (2015) 204, [1412.3989].

[178] NNPDF collaboration, R. D. Ball et al., *Parton distributions for the LHC Run II*, *JHEP* **04** (2015) 040, [`1410.8849`].

[179] G. Sterman and M. Zeng, *Quantifying Comparisons of Threshold Resummations*, *JHEP* **05** (2014) 132, [`1312.5397`].

[180] S. Catani, M. L. Mangano, P. Nason and L. Trentadue, *The Resummation of Soft Gluon in Hadronic Collisions*, *Nucl. Phys.* **B478** (1996) 273–310, [`hep-ph/9604351`].

[181] S. Moch, J. A. M. Vermaseren and A. Vogt, *The Quark form-factor at higher orders*, *JHEP* **08** (2005) 049, [`hep-ph/0507039`].

[182] F. Dulat, A. Lazopoulos and B. Mistlberger, *iHixs 2 – Inclusive Higgs cross sections*, *Comput. Phys. Commun.* **233** (2018) 243–260, [`1802.00827`].

[183] M. E. Peskin and D. V. Schroeder, *An Introduction to quantum field theory.* Addison-Wesley, Reading, USA, 1995.

[184] S. Catani, *The Singular behavior of QCD amplitudes at two loop order*, *Phys. Lett.* **B427** (1998) 161–171, [`hep-ph/9802439`].

Acknowledgements

I would first like to thank my advisor Prof. Martin Beneke. It is impossible for me to express the extent of my gratitude for his guidance, patience, advice and help in all aspects of my doctoral studies. Thank you for the incredible opportunity to carry out this work together, and for inspiring and teaching me so much.

I am thankful to Prof. Einan Gardi and Prof. Gudrun Heinrich for their continued support and mentorship.

Thank you to all my collaborators: Alessandro Broggio, Mathias Garny, Robert Szafron, Leonardo Vernazza, Jian Wang and Christopher Wever. It has been a pleasure to learn from you and tackle the NLP physics together.

A big special thank you goes out to Robert, who never lost a moment to teach me physics and who is always eager to challenge me to understand better and ask the right questions. Thank you for your time and effort to help me develop. I am very much in your debt.

Thank you to Alessandro for always having the time to answer my questions about your book, for all the advice regarding calculations, and for teaching me new methods.

I would also like to extend another huge thank you to Robert and Basia Szafron for reading my thesis, providing in depth comments, corrections and suggestions. Thank you to Alessandro and Leonardo for comments on chapter 6, and I am grateful to Andreas Mütter for the thesis template.

Thank you to Elke Hutsteiner for always going out your way to help with all the administrative matters and for always providing the biscuits before seminars.

I would also like to mention the rest of T31, Prof. Rikkert Frederix and Prof. Johann Kühn, the postdocs: Philipp, Keri, Hong, Martin, Christoph, Clara, Davide, Ioannis, and fellow doctoral students: Caspar, Kai, Jan, Julian, Patrick, Petter, and Yan-Bing. It has been a great pleasure to spend time with you, have interesting discussions over lunch and in journal clubs. Special thanks to Kai, I enjoyed our coffee breaks and getting to know you. Thank you for all your help.

A big thanks to my office mate Reuven, for help and discussions, and for putting up with all the paper everywhere...

Thanks to my colleagues elsewhere, Calum, Christian, Mikey, and Andres, it is always a pleasure to discuss with you when we meet.

Thank you to Vassi, Amy, Peter, Petter, Kåre, Kai, Juan, Uli, Johanna, Philipp, and all the rest of the TUM family and friends at the Max Planck Institute who made my time in Munich special.

To my brothers Mieszko and Mateusz, thanks for always having my back. Chciałbym również podziękować moim rodzicom i babciom za ich nieustające bezwarunkowe wsparcie. Kocham Was i czekam na pytania.

Let me leave you with a photo of the blackboards on the final day of the *Higgs School for Theoretical Physics* at the University of Edinburgh in May 2016. Prof. Thomas Becher lectured about soft-collinear effective field theory, and you might be able to make out the leading power Drell-Yan process presented on the first board. Captivating as it was, sitting in that room, I would not have believed anyone claiming I would be lucky enough to explore the extension of these formulas in my doctoral studies and have all the great experiences along the way. Thank you to everyone who made it possible.
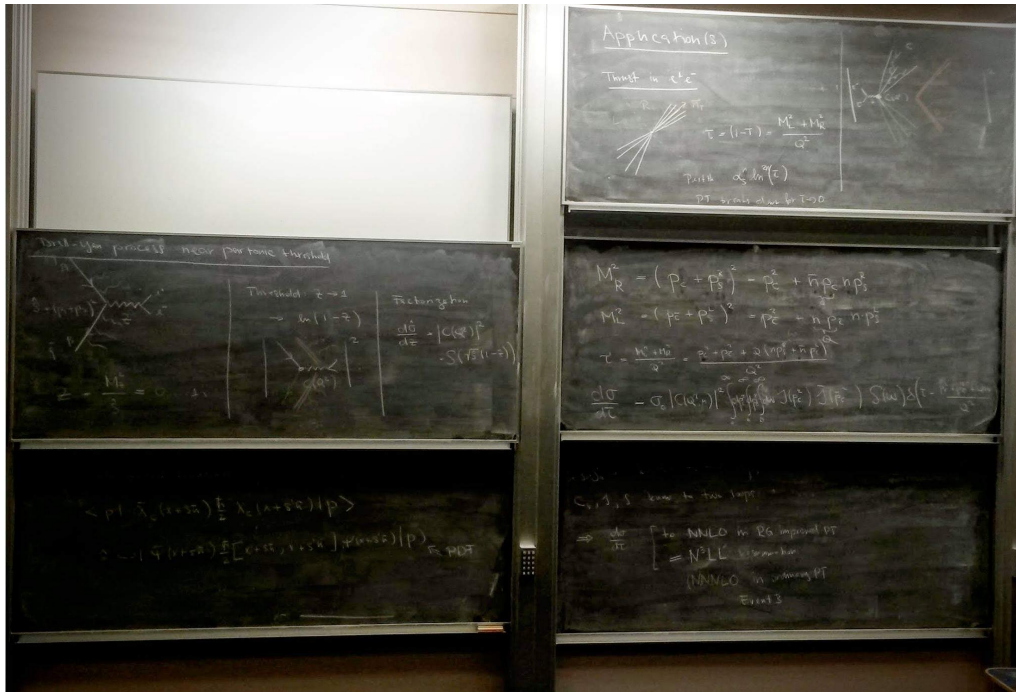
Figure C.3: *Final set of boards of the Higgs School for Theoretical Physics at the University of Edinburgh in May 2016.*